ACKNOWLEDGMENTS

Aside from I, many people have contributed towards the making of this thesis. First, I would like to say a big thank you to my supervisor Alex Whitworth, who has guided me through the ups and downs of this project, and provided invaluable support and encouragement along the way.

Second, I would like to extend a warm thank you to all members of the Whitworth Laboratory, particularly Alvaro and Vinay, for their technical and conceptual advice, as well as many essential tea breaks over the last 4 years.

Third, without the encouragement and support of my Mum (Barbara), Dad (Steve), older sister (Helen) and Grandma (Betty), non of this would have been possible, especially during those initial turbulent years. Many heartfelt thanks to you all.

Finally, I am unable to express how grateful I am to my better half, William, and his mischief of scabby and diseased rats (David Beckham, Michael Owen, Titus Bramble, Little Piglet and Lucky Carl (aka Snaky Steve)). Every evening, this gang of miscreants gave me a much-needed rest from the trials and tribulations of academic life, forcing me to turn my attention towards feeding, bathing and exercising my small furry family. Many, and continued thanks to you William.

A Whole Genome RNAi Screen to Identify Novel Promoters of PINK1/Parkin-mediated Mitophagy

Thesis submitted in fulfilment of the degree of
Doctor of Philosophy at the
University of Sheffield

by

Rachael Ivatt

Department of Biomedical Science
University of Sheffield

December 2013

CONTENTS

ABSTRACT

The PINK1/Parkin pathway is genetically linked to recessive forms of Parkinson's disease (PD) and plays a central role in the maintenance of mitochondrial homeostasis. Following toxification with the membrane uncoupler CCCP, PINK1, a serine/threonine kinase, becomes stabilised on the outer membrane of damaged mitochondria. This stabilisation is necessary for the translocation of Parkin, an E3-ubiquitin ligase, to mitochondria prior to their removal via mitophagy. In order to identify novel pathway components upstream of Parkin translocation, we performed a genome-wide RNAi screen using *Drosophila* S2R+ cells. Upon completion, we validated primary screen hits with multiple rounds of secondary screening, assessing a range of mitochondrial homeostatic processes. In follow-up screens, corresponding human orthologs were assessed for their ability to influence Parkin translocation and mitophagy in HeLa cells, demonstrating conserved pathway function. Human screen hits selected for in depth analysis included several genes acting in a common lipogenesis pathway. These are the transcription factor and master pathway regulator *SREBF1*, the Skp1-Cul1-F-box E3-ligase protein *FBXW7* and the serine/threonine kinase *GSK3A.* Follow-up analyses of these genes suggest a role for SREBP-dependent lipid synthesis in PINK1/Parkin-mediated mitophagy, likely acting upstream of PINK1. Importantly, *SREBF1* has recently been identified as a risk locus for sporadic forms of PD (Do et al, 2011). Hence, this study reveals a novel mechanistic link between familial- and sporadic causes of PD, with mitochondrial dysfunction at its centre.

ABBREVIATIONS

$[Ca^{2+}]_{IC}$	Intracellular calcium concentration
$\Delta\Psi m$	Mitochondrial membrane potential
AbFM	Antibiotic-free MEM
ATP	Adenosine Tri-Phosphate
CCCP	Carbonyl cyanide m-chlorophenyl hydrazone
CL	Cardiolipin
CNS	Central nervous system
CT	Threshold cycle
DA	Dopamine
DDC	DOPA decarboxylase
ddH_2O	Double-distilled water
DMSO	Dimethly sulfoxide
dsRNA	Double-stranded RNA
EMS	ethyl methanesulfonate
ER	Endoplasmic reticulum
ETC	Electron Transport Chain
FBS	Fetal bovine serum
FOV	Field of view
GD	Gaucher's disease
HeLa	Henrietta Lacks [cells]
IBR	Inbetween RING
IMS	Intermembrane space
$_L$-DOPA	$_L$-3,4-dihydroxyphenylalanine
LB	Luria-Bertani [broth]
MAD	Median absolute deviation
MEF	Mouse embryonic fibroblast [cells]
MEM	Modified Eagle's Media
MIM	Mitochondrial inner membrane
MOM	Mitochondrial outer membrane
MPTP	1-methyl-4-phenyl-1,2,3,6-tetrahydropyridine
mPTP	Mitochondrial permeability transition pore
MTR	MitoTracker Red
MTS	Mitochondrial targeting sequence
NCM	Normal culture medium
PBS	Phosphate Buffered Saline
PD	Parkinson's disease
PE	Phosphatidylethanolamine
RBR	RING-between-RING
RING	Really interesting new gene [domain]
RISC	RNA-induced silencing complex
ROS	Reactive oxygen species
RPE1	Retinal Pigmented Epithelial 1 [cells]
S2R+	Schneider 2 receptor plus [cells]
SAbFM	Serum and antibiotic-free MEM
SFSM	Serum-free Schneider's Medium
siRNA	Small interfering RNA
SM	Schneider's Medium
SNpc	Substantia Nigra pars compacta
SRSF	Sheffield RNAi Screening Facility
SSD	Sterol sensing domain
TH	Tyrosine hydroxylase
TM	Transmembrane
UBL	Ubiquitin-like
UPR	Unfolded protein response
UPS	Ubiquitin-proteasome system
VDRC	Vienna Drosophila RNAi Centre

1. INTRODUCTION

1.1 PARKINSON'S DISEASE

Parkinson's disease (PD) is the second most common neurodegenerative disorder after Alzheimer's disease, affecting 1 in 5000 people, with a mean age of onset of 55 (Dauer and Przedborski, 2003). Incidence of the disease increases dramatically with age, affecting ~1 in 1000 people between the ages of 70 - 79 (Lees et al., 2009). First described by the physician, James Parkinson in 1817 (Parkinson, 2002), Parkinson's disease is a progressive movement disorder, with a mean duration from diagnosis to death of 15 years (Lees et al., 2009). Pathology targets a multitude of neuronal populations of the central nervous system (CNS), including somatomotor, limbic, and autonomic regions (Braak et al., 2004). However, the hallmark lesions are the selective loss of pigmented dopaminergic neurons in the substantia nigra pars compacta (SNpc) of the midbrain (Figure 1.1 A & B), an area involved in fine motor control; and the appearance of proteinaceous inclusions, or Lewy bodies in surviving neurons (Figure 1.1 C). The cumulative loss of neuronal mass in PD manifests itself as a decrease in SNpc pigmentation, and results in a range of characteristic motor symptoms including bradykinesia, muscle rigidity, resting tremor, and postural instability.

Dopamine (DA) is a catecholamine neurotransmitter produced primarily in the midbrain from the amino acid, L-tyrosine. L-tyrosine is first converted into L-3,4-dihydroxyphenylalanine (L-DOPA) by the enzyme tyrosine hydroxylase (TH), before transformation into dopamine by DOPA decarboxylase (DDC). The majority of dopaminergic neurons reside in the ventral mesencephalon, and form four major dopaminergic pathways throughout the central nervous system. Of fundamental importance to PD is the nigrostriatal pathway, originating in the SNpc and extending to the caudate nucleus and putamen, which constitute the striatum (Figure 1.1 A). This pathway controls the initiation and execution of voluntary movement, hence why Parkinson's disease patients present motor dysfunction (Chinta and Andersen, 2005). Patients also experience wide-ranging non-motor symptoms including, but not limited to depression, hallucinations, dementia, sleep disorders, gastrointestinal issues and sensory disturbances (Chaudhuri et al., 2006). Often, symptoms such as olfactory disturbances are noted at early stages (Braak stage 1) of Parkinson's disease, before the classic motor symptoms begin, making these potential diagnostic markers for pre-clinical PD sufferers (Braak et al., 2004).

Diagnosing a patient with Parkinson's disease is difficult, and can only be definitively confirmed following the discovery of Lewy bodies in post-mortem substantia nigra brain tissue. In the living patient, the presence of bradykinesia, plus one or more additional

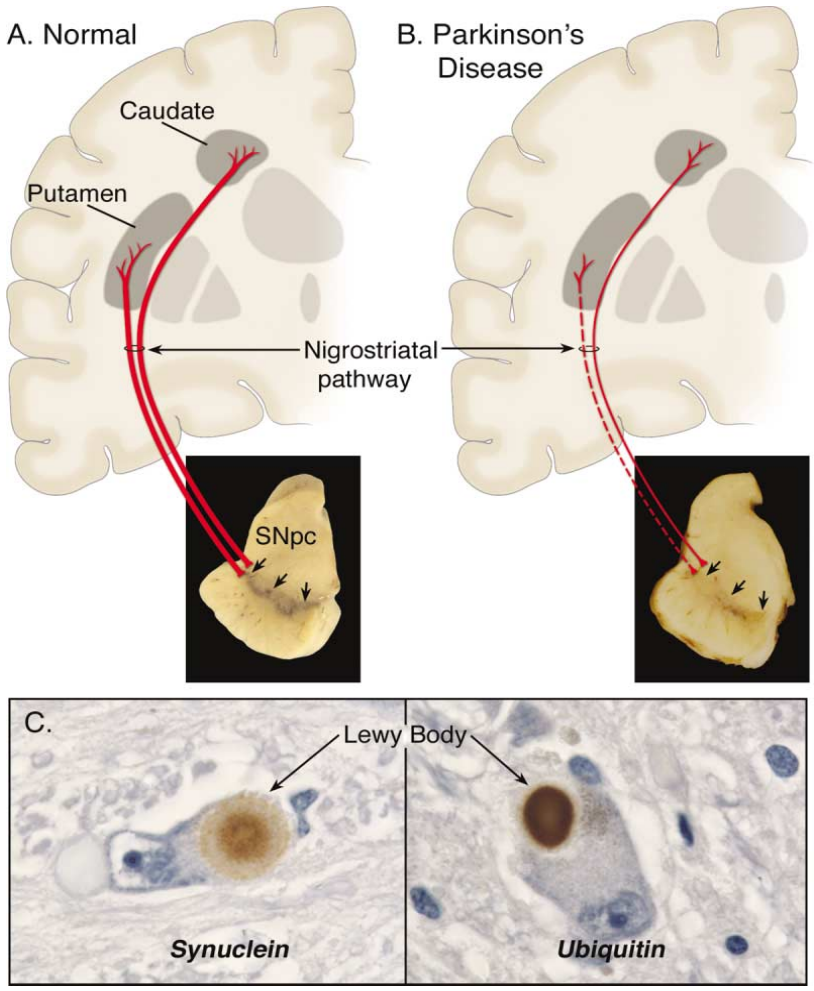

Figure 1.1 Hallmarks of Parkinson's disease. A) Schematic of normal dopaminergic innervation from the Substantia Nigra pars compacta (SNpc) of the midbrain, to the striatum (Putamen and Caudate) via the nigrostriatal pathway (red). Arrows indicate neuromelanin-pigmented dopaminergic neurons of the SNpc. B) Schematic of the Parkinson's disease-state, where arrows indicate a loss of pigmented dopaminergic neurons, resulting in a reduced innervation of the striatum (dashed & thin red line). C) Demonstration of Lewy body pathology in surviving dopaminergic neurons. Immunostaining for α-synuclein and ubiquitin. Figure from Dauer and Przedborski, (2003).

'classic' PD motor symptoms will often lead to a positive diagnosis of Parkinson's disease. Additionally, alleviation of symptoms following treatment with L-DOPA supports this diagnosis. In some cases, a disease with similar symptoms to PD will be termed a 'parkinsonism.' This often relates to cases where the etiology of the syndrome is distinct to that of PD, or where Lewy bodies are absent at autopsy, such is the case with some familial forms of PD (Hardy et al., 2006).

1.2 HALLMARKS OF PARKINSON'S DISEASE

PD pathology is dominated by the loss of neuromelanin-containing neurons of the nigrostriatal dopaminergic pathway, and the presence of proteinaceous inclusions or Lewy bodies in surviving neurons. However, neuronal death and Lewy body pathology

are not confined to SNpc neurons alone, with cells as far reaching as the neocortex being affected at late stages of disease. Despite this promiscuity, significant population losses are restricted to the dopaminergic neurons of the SNpc and the noradrenergic neurons of the locus coeruleus, with a decrease of ~80% as the disease reaches terminal progression (Sulzer, 2007).

1.2.1 NEURODEGENERATION

In 2004, Braak and colleagues split the progression of sporadic PD into 6 stages, by analysing the presence of Lewy bodies in different regions of the brain. They found that in pre-clinical stages, Lewy bodies first appear in the brainstem, moving up into the substantia nigra and on to the neocortex in late stages of the disease. Usually, at Braak stages 3 and 4 the disease becomes symptomatic, by which time ~70% of the SNpc dopaminergic neurons are lost (Braak et al., 2004).

1.2.2 SELECTIVE VULNERABILITY OF DOPAMINERGIC NEURONS

A topic of ongoing discussion in the PD field is the reason/s behind the largely dopamine-specific neuronal loss. The loss of these neurons is undoubtedly the cause of motor symptoms observed in PD sufferers, as these are greatly ameliorated by treatment with L-DOPA. Many theories regarding the cause of selective DA neuron loss in PD have been proposed, including an increase in oxidative stress following the metabolism of DA itself. Here, cytoplasmic DA is readily oxidised, causing increased production of reactive oxygen species (ROS), and resulting in nucleic acid, protein and lipid damage (Sulzer and Zecca, 2000). However, there are some discrepancies with this argument, notably that L-DOPA, the gold-standard treatment for PD, does not negatively affect symptoms or progression of the disease (Fahn et al., 2004). Additionally, PD-related cell death is not exclusively limited to DA-containing neurons, indicating that DA-metabolism cannot be the sole cause of PD.

Alternatively, the architecture of vulnerable PD neurons may contribute to their selective loss. Here, dopaminergic neurons exhibit extremely long, unmyleinated axons, requiring them to endure slow, myelin-free action potentials over huge axonal distances. Additionally each neuron is required to innervate a plethora of targets via ~370,000 synapses (Braak et al., 2004). Such energy-intensive characteristics, together with the vast number of energy-reliant synapses at axon termini, place a great burden upon the mitochondrial population (Surmeier et al., 2010). Therefore another putative source of selective vulnerability is an elevation of intracellular ROS from

overworked mitochondria, combined with a chronic energy deficit. Notably, elevated lipid peroxidation has been detected in postmortem brain tissue from PD patients, confirming the incidence of increased oxidative stress (Jenner et al., 1992).

Other theories are built around the unusual 'pace making' behavior of SNpc neurons (Grace and Bunney, 1983), whereby action potentials are fired regularly, in the absence of external stimuli. The reason for this is thought to be in maintaining a constant supply of DA to the striatal region of the brain. However, chronic neuronal depolarisation via calcium influx carries high-energy costs to the cell. This calcium must be pumped back across the plasma membrane via ATP hydrolysis, or buffered by the endoplasmic reticulum (ER) and mitochondria, to maintain low cytoplasmic concentrations. However, mitochondrial calcium buffering causes the mitochondrial membrane potential ($\Delta\Psi m$) to collapse, thereby halting ATP production and producing a potentially fatal energy deficit (Chan et al., 2009). Additionally, increases in intracellular calcium stimulate DA production (Sutoo et al., 1989), perhaps contributing to DA oxidation and cell damage, as discussed previously.

Whether the cause of selective dopaminergic vulnerability is one, or a combination of the theories outlined above remains to be elucidated. However, it is likely to arise from both the oxidative damage of cellular components and mitochondrial dysfunction, to levels beyond that which the cell can cope with. This coincides with an increased risk of PD with aging, as cellular damage increases over time.

1.2.3 LEWY BODIES

Together with dopaminergic neurodegeneration, the second hallmark of PD is the occurrence of widespread intraneuronal proteinaceous inclusions or Lewy bodies. Typically 15 μm in diameter, Lewy bodies have a characteristic structure with a dense hyaline core and an outer halo of radiating fibrils (Figure 1.1 C). They are found intraneuronally, in multiple locations of the PD brain, displaying a characteristic and predictable topography as the disease progresses (Braak et al., 2004). Typically, they are found in both sporadic and familial forms of PD; but are notably absent in a small number of familial PD patients, including most cases of *parkin* and *PINK1*-related autosomal recessive PD (Hardy, 2010; Klein and Westenberger, 2012).

The major component of Lewy bodies is the pre-synaptic protein, α-synuclein (Spillantini et al., 1997), together with ubiquitin and other cellular lipids and proteins. In health, α-synuclein is thought to play a role in synaptic plasticity (George et al., 1995),

however in both familial and sporadic forms of PD it is believed to aggregate into small cytotoxic protofibrils capable of forming intracellular pore-like structures. These structures are proposed to initiate permeabilisation of intracellular organelles, ultimately leading to neuronal death (Lashuel et al., 2002; Volles and Lansbury, 2002). Lewy bodies are therefore considered to be the byproduct of a protective mechanism, whereby cytotoxic protofibrils are aggregated into fibrillar masses for proteolytic removal (Conway et al., 2001; Volles and Lansbury, 2003). Of note, DA has been shown to inhibit the formation of aggregated α-synuclein inclusions from the cytotoxic protofibrils, again implicating DA in the mechanism of pathology (Conway et al., 2001).

1.2.4 PRION THEORY OF PARKINSON'S DISEASE PROGRESSION

An emerging theory for PD progression is the spread of α-synuclein throughout the brain in a prion-like fashion. Key to this theory is the observation that Lewy bodies are not only found in surviving midbrain dopaminergic neurons, but also in more peripheral, non-dopaminergic cell types. Braak and colleagues have proposed that Lewy bodies first appear in the medulla oblongata and olfactory bulb of the brainstem at a pre-clinical stage of PD, before ascending to the SN, and on to regions such as the neocortex as the disease progresses (Braak et al., 2003). Evidence for a non-cell-autonomous prion-like spreading of α-synuclein came from the observation that embryonic grafts in the brains of PD suffers contained Lewy bodies a number of years post-transplantation (Kordower et al., 2008; Li et al., 2008). This suggested that Lewy pathology may propagate from cell to cell over time. In support of this, recent evidence has shown that a proportion of newly-synthesised monomeric and aggregated α-synuclein is packaging into vesicles and exocytosed from SH-SY5Y neuroblastoma cells (Lee et al., 2005). Additionally, fibrillar α-synuclein can undergo endocytosis, followed by the formation of insoluble inclusions in axons and cell bodies of primary neurons (Volpicelli-Daley et al., 2011). Taken together, these studies demonstrate the ability of α-synuclein to leave host cells, and enter unaffected cells, supporting the idea of neural Lewy body transmission. However, it remains to be elucidated whether the presence of alpha-synuclein aggregates are the cause of neuronal death in PD, or a harmless byproduct of a cell-protective process; and why neuronal death is observed even in the absence of Lewy bodies.

1.3 TREATMENT OF PARKINSON'S DISEASE

Currently, the neurodegeneration observed in PD patients cannot be prevented or cured by pharmacological intervention. The gold standard treatment, L-DOPA, acts to replace the lost dopamine following SNpc neurodegeneration, hence alleviating the associated symptoms. Most patients are responsive to this treatment, seeing a great improvement in associated motor symptoms over a 3-month period. However, extended L-DOPA treatment is not without issues. Many patients experience extrapyramidal, involuntary movements or dyskinesias after chronic treatment periods. During these times, a substitution of dopamine agonists or monoamine oxidase B inhibitors (an enzyme involved in the breakdown of DA) can be used instead of L-DOPA, although the efficacy is usually lower (Lees et al., 2009). For advanced patients suffering from severe L-DOPA side effects, an alternative, surgical intervention called 'deep brain stimulation' in the subthalamic nucleus has shown great clinical benefits (Rascol et al., 2011). This method involves the implantation of a pacemaker producing high frequency electrical stimulation to the brain, through which normal midbrain activity is restored.

One of the issues with treating PD patients is that often, at the time of clinical diagnosis ~70% of SNpc neurons have already been lost (Lesage and Brice, 2009). By this stage, the disease has progressed beyond the point of preventive measures. Future research is likely to focus on replacement of lost neurons through grafts and stem cell therapies. However, to date, these approaches have either failed to produce significant beneficial results, or presented worrying side effects such as the presence of Lewy bodies in embryonic grafts, as mentioned previously (Rascol et al., 2011).

1.4 ETIOLOGY OF PARKINSON'S DISEASE

Approximately 90% of PD cases are 'sporadic', with no known genetic or environmental cause. However, the remaining 10% of disease sufferers have a clear monogenetic inheritance. These genetic cases have experienced intense study since the discovery of the first disease-related gene, *SNCA*, encoding *α-synuclein,* in 1996 (Polymeropoulos et al., 1996; Polymeropoulos et al., 1997). Insights gained from studying monogenic PD cases are hoped to enhance our understanding of common sporadic PD, with the ultimate goal of developing more effective treatments and even pre-clinical tests for the disease. Importantly, recent work indicates that 'sporadic' PD cases often carry genetic risk variants of monogenic PD genes including *α-synuclein,* and more commonly *LRRK2,* highlighting a crossover between the two disease groups.

1.4.1 ENVIRONMENTAL RISK FACTORS

A number of non-genetic risk factors have been linked to the occurrence of PD via epidemiology studies. However, most of these risk factors are yet to be supported by sufficient evidence to define them as 'causal' to disease development (Kieburtz and Wunderle, 2013). Two exceptions are 'age' and 'gender', both of which consistently confer risk; with PD being more common in aged males (Bower et al., 1999; Van Den Eeden et al., 2003).

A number of chemicals have been linked to the development of parkinsonian syndromes, with the most famous example being the administration of MPTP in a group of American drug-users. Here, the MPTP metabolite, MPP+ was found to induce a severe, parkinsonian syndrome via mitochondrial complex I inhibition, a matter of weeks following exposure (Langston et al., 1983). This case offered clear evidence that environmental determinates have the potential to play a role in PD etiology. Additionally, toxin-induced animal models of PD implicate common pesticides such as paraquat and rotenone as putative causal factors of parkinsonian neuropathology (Betarbet et al., 2000; Norris et al., 2007; Thiruchelvam et al., 2003). Both compounds share similarities with MPTP. For example, the herbicide and redox-cycling compound paraquat has a similar chemical structure to MPTP; and rotenone, an insecticide and fish poison, acts as a mitochondrial complex I inhibitor. Importantly, both pesticides have been implicated as causative factors in the development of sporadic PD in case-control studies (Costello et al., 2009; Tanner et al., 2011). Additionally, epidemiology studies have identified a link between rural living and Parkinson's disease risk. Aspects investigated included pesticide exposure, well-water consumption and connections to farming. However, the strongest risk factor was again, pesticide-related (Gorell et al., 1998; Hancock et al., 2008).

Other environmental factors able to modify the risk of PD development are dose-dependent exposure to tobacco, through cigarette smoking (Allam et al., 2004; Hernan et al., 2001) and caffeine, through coffee drinking (Ascherio et al., 2004; Hernan et al., 2002), both of which have been shown to reduce disease incidence.

Despite the identification of a number of potential environmental risk factors, much of the data are inconclusive or have an unexplained relationship to PD. In recent history, focus has turned away from environmental, and towards genetic risk factors of PD, some of which are now being identified as contributing towards sporadic forms of the disease.

1.4.2 GENETIC RISK FACTORS

Besides the large proportion of sporadic PD sufferers, a small number of familial PD cases with monogenic inheritance have been identified; often associated with features atypical of sporadic PD, such as early onset, slow disease progression and the absence of Lewy bodies. To date, 18 genetic regions or 'loci' have been found to have a putative link to Parkinsonian syndromes (Table 1.1), of which 8 are unequivocally associated with PD (Lesage and Brice, 2012). This association has established a clear genetic component to at least a small proportion (~10%) of PD cases. Thus far, characterisation of these loci has greatly increased our understanding of the molecular pathways thought to play a role in common PD (Klein and Westenberger, 2012)

Of the 8 confirmed PD loci, four genes are responsible for autosomal dominant forms of PD, and four for autosomal recessive PD. Within the autosomal dominant group, *PARK1&4/SNCA* (Farrer et al., 1999; Polymeropoulos et al., 1996; Polymeropoulos et al., 1997) and *PARK8/LRRK2* (Funayama et al., 2002; Paisan-Ruiz et al., 2004), have been studied in great depth; whereas *PARK17/VPS35* (Vilarino-Guell et al., 2011; Zimprich et al., 2011) and *PARK18/EIF4G1* (Chartier-Harlin et al., 2011), have only recently been identified. Interestingly, in addition to the familial link, both *SNCA* and *LRRK2* variants are strongly implicated as causative risk factors of sporadic PD (Ahn et al., 2008; Paisan-Ruiz et al., 2008; Troiano et al., 2008).

Of the four confirmed autosomal recessive genes, *PARK2/parkin* (Kitada et al., 1998), *PARK6/PINK1* (Valente et al., 2004a) and *PARK7/DJ1* (Bonifati et al., 2003b) produce an early onset form of Parkinsonism, often lacking Lewy bodies, and *PARK9/ATP13A2* produces an atypical form of PD called Kufor-Rakeb syndrome (Ramirez et al., 2006). Again, heterozygous mutations in *Parkin*, *PINK1*, and *DJ1* are suggested to increase the risk of late onset PD in combination with additional unknown factors (Choi et al., 2006; Klein et al., 2007).

1.4.3 PARKINSON'S DISEASE-CAUSING GENE LOCI

The 18 genetic loci identified as causal or susceptibility factors for familial Parkinson's disease have each been assigned a '*PARK1-18'* annotation, numbered according to their date of discovery (Table 1.1). These include a mixture of autosomal dominant and recessive monogenic modes of inheritance, plus a handful of loci with an unknown mechanism of inheritance. The causative PD genes within a number of the *PARK* loci have been identified, whereas others remain elusive. These PD loci and genes have

Symbol	Gene locus	Disorder	Inheritance	Gene	Mode of identification
PARK1	4q21-22	EOPD	AD	*SNCA*	Linkage analysis
PARK2	6q25.2-a27	EOPD	AR	*parkin*	Linkage analysis
PARK3	2p13	Classical PD	AD	Unknown	Linkage analysis
PARK4	4q21-q23	EOPD	AD	*SNCA*	Linkage analysis
PARK5	4p13	Classical PD	AD	*UCHL1*	Functional candidate gene approach
PARK6	1p35-p36	EOPD	AR	*PINK1*	Linkage analysis
PARK7	1p36	EOPD	AR	*DJ-1*	Linkage analysis
PARK8	12q12	Classical PD	AD	*LRRK2*	Linkage analysis
PARK9	1p36	Kufor-Rakeb syndrome; atypical PD with dementia, spasticity, and supranuclear gaze palsy	AR	*ATP13A2*	Linkage analysis
PARK10	1p32	Classical PD	Risk factor	Unknown	Linkage analysis
PARK11	2q36-27	Late-onset PD	AD	Unknown, not *GIGYF2*	Linkage analysis
PARK12	Xq21-q25	Classical PD	Risk factor	Unknown	Linkage analysis
PARK13	2p12	Classical PD	AD or risk factor	*HTRA2*	Candidate gene approach
PARK14	22q13.1	Early-onset, dystonia-parkinsonism	AR	*PLA2G6*	Linkage analysis (homozygosity mapping)
PARK15	22q12-q13	Early-onset, parkinsonian-pyramidal syndrome	AR	*FBXO7*	Linkage analysis
PARK16	1q32	Classical PD	Risk factor	Unknown	Genome-wide association studies
PARK17	16q11.2	Classical PD	AD	*VPS35*	Exome sequencing
PARK18	3q27.1	Classical PD	AD	*EIF4G1*	Linkage analysis

AD - autosomal dominant, AR - autosomal recessive, EOPD - early-onset Parkinson's disease

Table 1.1 *PARK*-designated PD-related loci. Table of *PARK* loci from *PARK1-PARK18* (symbol), together with the chromosomal position (Gene locus), equivalent disorder, form of inheritance, known causal gene and the mode of loci identification. Table adapted from Klein and Westenberger, (2012).

been identified via gene mapping approaches, such as linkage studies and genome wide association studies, plus candidate gene methodologies (Klein and Westenberger, 2012). In this section, literature regarding the most well-studied PD genes will be reviewed in brief.

1.4.4 AUTOSOMAL DOMINANT FAMILIAL PARKINSON'S DISEASE

1.4.4.1 *PARK1/4 - ALPHA-SYNUCLEIN (SNCA)*

SNCA, encoding the protein α-synuclein, was the first familial Parkinson's disease gene identified, more than 15 years ago (Polymeropoulos et al., 1996; Polymeropoulos et al., 1997). Only four pathogenic point mutations have been identified in *SNCA*, all of which are rare and follow an autosomal dominant pattern of inheritance (Berg et al., 2005; Proukakis et al., 2013). *SNCA*-related PD cases show earlier onset than sporadic PD, with additional, non-parkinsonian symptoms including cognitive decline. As well as causing monogenic PD, *SNCA* risk alleles have been found to significantly contribute to the development of sporadic PD, strengthening the link between familial and sporadic disease etiologies (Lesage and Brice, 2012). In addition to *SNCA* mutations, a number of gene duplication and triplication cases have been found to

cause PD, with disease severity and onset occurring in a dose-dependent manner (Fuchs et al., 2007; Ibanez et al., 2004; Singleton et al., 2003).

α-synuclein is a soluble protein with undefined structure, found in association with synaptic vesicles in the presynapsis of CNS neurons (George, 2002). The normal function of α-synuclein is not fully elucidated, however evidence indicates that it may be involved in synaptic transmission via the regulation of vesicular release (Bellani et al., 2010). However, both wild-type, and particularly mutant forms of α-synuclein can form stable β-sheet structures which are the building blocks for toxic, soluble oligomers, and insoluble filaments making up Lewy bodies (Bertoncini et al., 2005; Conway et al., 2000). Importantly, in PD patients, α-synuclein is the major component of Lewy bodies (Spillantini et al., 1997), indicating a toxic gain of function role for this protein.

1.4.4.2 *PARK 8 - LEUCINE-RICH REPEAT KINASE 2 (LRRK2)*

The second confirmed autosomal dominant form of PD is that resulting from mutations in *leucine-rich repeat kinase 2 (LRRK2)* (Funayama et al., 2002; Paisan-Ruiz et al., 2004; Zimprich et al., 2004). Mutations in this gene are the most prolific known genetic cause of PD, accounting for ~7% of all familial cases (Mata et al., 2006), with the common G2019S variant alone accounting for ~4% of familial cases, and contributing to ~1% of sporadic cases (Xiong et al., 2012). *LRRK2*-related PD is similar in onset, pathogenesis, and progression to sporadic forms of the disease, setting it aside from *PARK* loci with atypical features, such as *PARK2/parkin* (Healy et al., 2008).

LRRK2 is a very large gene, more than 9 kilobases in size and comprising 51 exons. The multidomain protein includes a series of leucine rich repeats in the N-terminus, a ROC (Ras of complex proteins) GTPase domain, a COR (C-terminal of ROC) regulatory domain and a kinase domain. With the exception of the leucine rich repeats, all aforementioned domains contain pathogenic mutations. However, the most common mutation, G2019S, resides in the kinase domain of the protein, implicating its importance in the development of PD (Xiong et al., 2012). Despite *LRRK2* being the most prevalent disease-causing gene, little is known about the exact wild-type function of the protein. However, analysis of LRRK2 protein domains indicates a participation in protein-protein interactions via its scaffold domains, and a role in pathway signaling via its kinase and GTPase domains (Kumar and Cookson, 2011). Additionally, LRRK2 has been found to associate with a range of intracellular membranes including the mitochondrial outer membrane (MOM) and autophagic vesicles. However, the

significance of this it not yet understood (Alegre-Abarrategui et al., 2009; Biskup et al., 2006).

1.4.5 AUTOSOMAL RECESSIVE FAMILIAL PARKINSON'S DISEASE

1.4.5.1 *PARK2 - PARKIN*

The *PARK2* locus was first identified in 1997, in 11 consanguineous families displaying an autosomal recessive parkinsonian disease with early onset (typically <40 years) (Matsumine et al., 1997). Later, using positional cloning, the causative gene at the *PARK2* locus was identified and named '*parkin*' (Kitada et al., 1998). Parkin is the most prevalent cause of autosomal recessive Parkinson's disease, and accounts for ~50% of early onset cases under 45 and more than 70% of cases under 20 (Lucking et al., 2000). However, despite this high frequency of mutation in early onset cases, *parkin* only accounts for approximately 1 - 2% of the total number of PD cases (Hardy, 2010). The parkinsonian syndrome conferred by *parkin* mutation is similar to sporadic PD, aside from the early age of onset, slow disease progression, and often, but not always a lack of Lewy body pathology (Farrer et al., 2001; Pramstaller et al., 2005; Takahashi et al., 1994). Despite this, classic PD motor symptoms are often present, together with a good response to L-DOPA therapy. Perturbations in the *parkin* gene include point mutations and exon rearrangements, and arise as either homozygous, or compound heterozygous mutations (Farrer et al., 2001; Lucking et al., 2000). Additionally, heterozygous *parkin* mutations have been identified in subjects with later onset PD, closely phenocopying sporadic forms of the disease. This suggests that there could also be a link between single *parkin* mutations, haploinsufficiency and sporadic PD risk (West et al., 2002).

parkin encodes a 464-amino acid E3-ubiquitin protein ligase, capable of autoubiquitination and subsequent degradation (Shimura et al., 2000; Zhang et al., 2000). The protein contains an N-terminal ubiquitin-like (UBL) domain, a RING0 domain, and a C-terminal RING-between-RING (RBR) domain, consisting of two RING finger domains surrounding an inbetween RING (IBR) domain (Figure 1.2, Chaugule et al., 2011; Hristova et al., 2009). Pathogenic point mutations and rearrangements span to entirety of the protein (Walden and Martinez-Torres, 2012), including the RBR domain; responsible for protein interactions and E3-ligase activity (Beasley et al., 2007) and the UBL domain; believed to inhibit the autoubiquitination of the RBR domain (Figure 1.2, Chaugule et al., 2011).

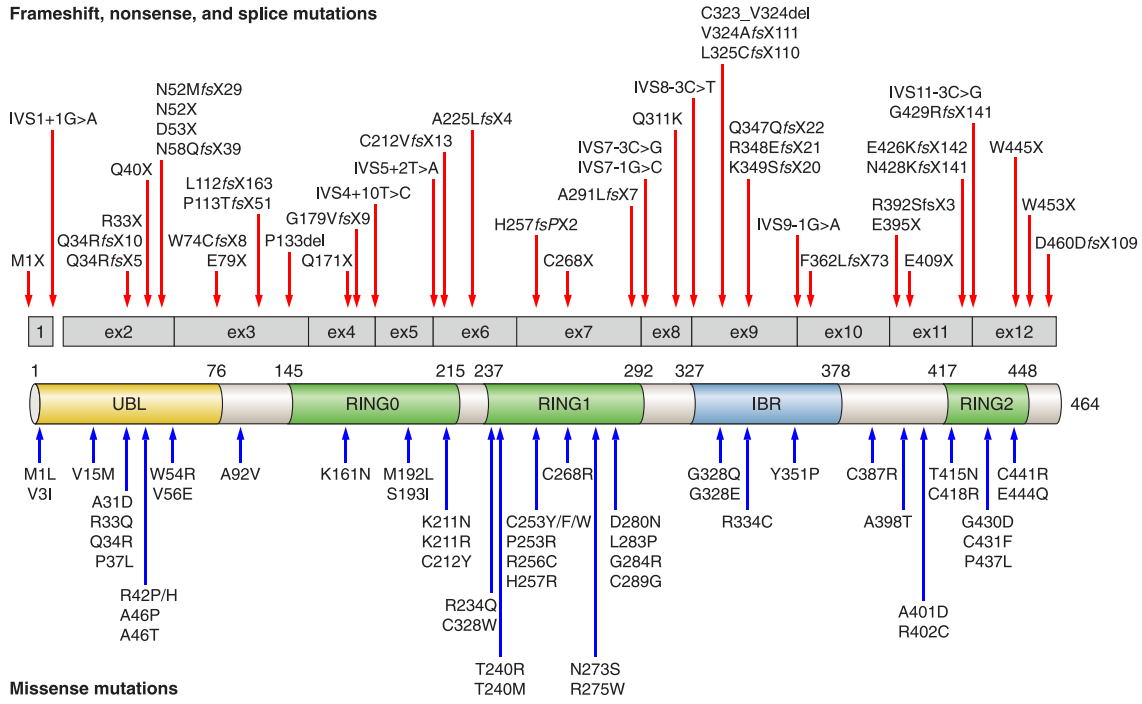

Figure 1.2 Schematic representation of *parkin* transcript and protein, with associated PD mutations. *parkin* transcript, made up of 12 exons is represented in grey. Equivalent Parkin protein is shown below, with functional domains highlighted (UBL domain in yellow, RING domains in green, IBR domain in blue). PD-related point mutations are indicated by arrows; with frameshift, nonsense and splice mutations represented by red arrows, and missense mutations represented by blue arrows. Figure from Corti et al., (2011).

Within the E3-ligase family, there are RING-E3 ligases and HECT-E3 ligases, with the mode of ubiquitin ligation being the distinguishing feature. Recent reports have indicated that Parkin may act as a RING/HECT hybrid, whereby interaction with the E2-conjugating enzyme occurs via the RING1 domain, and transfer of a thioester-linked ubiquitin moiety occurs via an active cysteine in the RING2 domain (Lazarou et al., 2013; Wenzel et al., 2011). The significance of this discovery in the context of the PINK1/Parkin-pathway will become apparent in later sections.

E3-ubiquitin ligases act together with E1-activating and E2-conjugating enzymes to add ubiquitin moieties to specific target proteins. This modification can affect a number of different outcomes, but commonly leads to either proteasomal degradation of the target protein, or the stimulation of intracellular signaling cascades (Pickart and Fushman, 2004). Parkin is known to be involved in poly-, mono- and multimono-ubiquitination events (Hampe et al., 2006; Moore et al., 2008; Olzmann et al., 2007), conferring alternative outcomes in a protein specific manner. Parkin has a number of known substrates (Table 1.2), including an apparent enrichment for mitochondria-linked

Table 1 Putative Parkin substrates, the pathways involved, techniques used to identify the substrate, and accumulation in patient brains or Parkin-null mice

(tag+)Substrate	Method of identification	Parkin	Biological pathway	Accumulation	References
cMyc-SEPT5 (CdCrel-1)	Yeast 2-hybrid, full-length Parkin as bait	Endogenous and cMyc-Parkin	Synaptic function	Nd	Zhang et al., 2000
cMyc-Synphilin-1	Found in Lewy body-like inclusion	FLAG-Parkin	Unclear, but may play a role in neurodegeneration	No	Chung et al., 2001, Lim et al., 2005
αSP22	Co-IP from frontal cortex of normal brain tissue	Endogenous	Unclear	Yes[a]	Shimura et al., 2001
cMyc-SEPT4 (CDCrel-2)[b]	Yeast 2-hybrid, full-length Parkin as bait	cMyc-Parkin	Synaptic function	Yes	Choi et al., 2003
FLAG-Pael-R	Yeast 2-hybrid, full-length Parkin as bait	Endogenous and GST-Parkin	Unknown	Yes	Imai et al., 2001, Yang et al., 2003
Cyclin E	Pull downs using Parkin to IP	FLAG-Parkin	Cell cycle control	Yes[c]	Staropoli et al., 2003
cMyc-p38/JTV-1	Yeast 2-hybrid, Parkin 135–290 as bait	HA-Parkin	Protein biosynthesis	Yes[d]	Corti et al., 2003, Ko et al., 2005
GFP-synaptotagmin XI	Yeast 2-hybrid, full-length Parkin as bait	HA-Parkin	Synaptic function	No	Huynh et al., 2003
α/β-tubulin	Yeast 2-hybrid, full-length Parkin as bait	FLAG-Parkin	Cytoskeleton	No	Ren et al., 2003
GST-polyQ proteins	Co-localisation with model proteins	FLAG-Parkin	Neurotoxicity	No	Tsai et al., 2003
FLAG-dopamine transporter	N/A	Untagged-Parkin	Neurotransmission	No	Jiang et al., 2004
HA-SIM2 (single-minded 2)	N/A	FLAG-Parkin	Transcription	No	Okui et al., 2005
cMyc-FBP1	Interaction with AIMP2	cMyc-Parkin	Transcription	Yes	Ko et al., 2006
His-Eps15#	Ubiquitination performed in vitro and in cells	GST/FLAG-Parkin	Endocytosis	No	Fallon et al., 2006
GFP-RanBP2	Yeast 2-hybrid, full-length Parkin as bait	cMyc-Parkin	Nuclear import/SUMOylation	No	Um et al., 2006
FLAG-IKKγ and FLAG-TRAF2	Co-transfection and co-immunoprecipitation	Untagged-Parkin	NF-κB signalling	No	Henn et al., 2007
PICK1 and cMyc-PICK1[b]	GST pulldowns from mouse synaptosomes	GST/FLAG-Parkin	Synaptic function	No	Joch et al., 2007
DJ-1(L166P mutant)	N/A	Endogenous	Neurotoxicity	No	Olzmann et al., 2007
3xFLAG-PDCD2-1	Yeast 2-hybrid, Parkin 1-238 used as bait	Endogenous and cMyc-Parkin	Apoptosis/cell proliferation	Yes	Fukae et al., 2009
EGFP-Bcl-2[b]	GST pulldowns from HEK293 cells	GST/FLAG-Parkin	Anti-apoptosis	No	Chen et al., 2010
VDAC1/p62-SQTM1	N/A	FLAG-Parkin	Autophagy/Mitophagy	No	Geisler et al., 2010
FLAG-Mitofusins 1 and 2	N/A	Endogenous	Mitochondrial fusion	No	Ziviani et al., 2010
cMyc-Drp1	N/A	GFP-Parkin	Mitochondrial fission	No	Wang et al., 2011
FLAG-PARIS	Yeast 2-hybrid, full-length Parkin as bait	cMyc-or His-Parkin	Transcription	Yes	Shin et al., 2011
MIRO	N/A	YFP-Parkin	Mitochondrial function	No	Wang et al., 2011

Table 1.2 Putative Parkin substrates. Table representing putative Parkin substrates, their method of substrate identification, the form of Parkin used in the study, the biological pathways involved if known, and whether substrate accumulation is observed in PD patient brains or Parkin-null mice (Nd – not determined). Figure from Walden and Martinez-Torres et al., (2012).

proteins including Mitofusin 1 and 2, VDAC1, Miro and PARIS (Walden and Martinez-Torres, 2012), suggesting a role for Parkin in the regulation of the mitochondrial proteasome.

1.4.5.2 *PARK6 - PTEN-INDUCED KINASE 1 (PINK1)*

PINK1 was originally identified as a putative tumour suppressor, acting in the Phosphatase and tensin homolog (PTEN) pathway (Matsushima-Nishiu et al., 2001). This was later found to be a spurious connection (Unoki and Nakamura, 2001), but left behind the legacy of the name, *PTEN-Inducted Kinase 1* or *PINK1*. Since these studies, the *PARK6* locus and corresponding gene, *PINK1*, were identified as the second autosomal recessive region linked to early onset familial Parkinson's disease (Valente et al., 2004a; Valente et al., 2001). Mutations in *PINK1* produce symptoms synonymous with those observed in *parkin*-linked PD (Gasser et al., 2011), and are the second most common cause of recessive PD, accounting for between 1 - 9% of cases (Thomas and Beal, 2007). Perturbations in *PINK1* are extensive across the whole gene, and include missense mutations, exon rearrangements and truncations (Figure 1.3, Hatano et al., 2004; Valente et al., 2004a). Like with *parkin*, homozygous and compound heterozygous *PINK1* mutations have been attributed to familial PD, most notably clustering around, and within the C-terminal kinase, highlighting the significance of this domain in pathogenicity (Hatano et al., 2004; Sim et al., 2006). In support of this, analysis of PINK1-autophosphorylation of disease-relevant mutants G309D and L347P, saw a significant reduction in kinase activity, suggesting the cause of *PINK1*-related PD to be due to a loss of phosphorylation events (Beilina et al., 2005).

In addition to familial PD, heterozygous *PINK1* mutations have been suggested to contribute towards increased sporadic PD risk with later onset (Valente et al., 2004b). Interestingly, one case of digenic inheritance has been recorded where heterozygous mutations in *PINK1* and *DJ-1* (see section 1.4.5.3) were found to be the cause of a novel, autosomal recessive form of PD (Tang et al., 2006). This may suggest cooperation between *PINK1* and *DJ-1* in cellular protection.

PINK1 encodes a 581-amino acid protein kinase, localised to the mitochondria and comprising of an N-terminal mitochondrial targeting sequence (MTS), a hydrophobic transmembrane (TM) domain, a large C-terminal serine/threonine kinase, and a putative regulatory C-terminal portion (Figure 1.3, Silvestri et al., 2005; Sim et al., 2006; Valente et al., 2004a). Wild-type, but not pathologically mutated *PINK1* confers

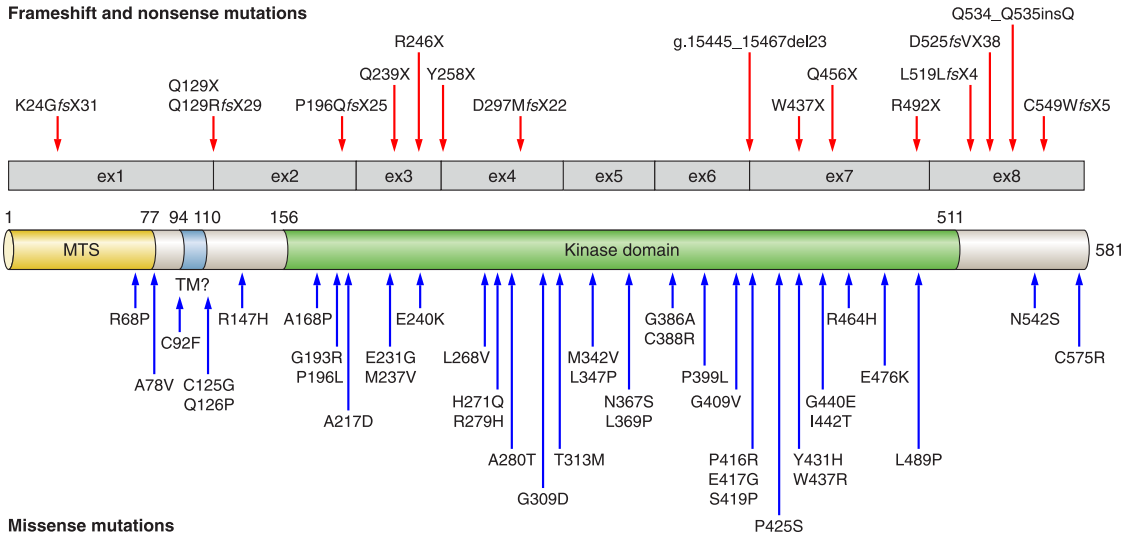

Figure 1.3 Schematic representation of *PINK1* transcript and protein, with associated PD mutations. *PINK1* transcript, made up of 8 exons is represented in grey. Equivalent PINK1 protein is shown below, with functional domains highlighted (MTS domain in yellow, TM domain in blue, kinase domain in green). PD-related point mutations are indicated by arrows; with frameshift and nonsense mutations represented by red arrows, and missense mutations represented by blue arrows. Figure from Corti et al.,(2011).

cellular protection in cultured dopaminergic neurons following toxic insult (Petit et al., 2005; Valente et al., 2004a), whereas *PINK1* siRNA reduces cell viability; an effect further exacerbated by complex I inhibition (Deng et al., 2005). The protective effect of *PINK1* has been attributed to its serine/threonine kinase domain (Sim et al., 2006), a claim supported by data whereby the kinase domain of PINK1 alone was sufficient to prevent MPTP-induced cell death (Haque et al., 2008). Therefore *PINK1* is likely conferring cellular protection via the phosphorylation of target substrates.

Until recently, the sub-cellular and sub-mitochondrial localisations of PINK1 have been the subject of long-standing debate within the field. This confusion can be partly attributed to 1) difficulties in detection due to the rapid turnover of processed isoforms, 2) the motile nature of the PINK1 lifecycle, 3) the re-distribution of PINK1 under conditions of cellular stress and 4) poor antibodies resulting in most studies being performed in overexpression systems. As alluded to, PINK1 exists as a number of isoforms, enduring several proteolytic events during its lifetime. Under basal conditions, following translation, the 63 kDa full-length ‘precursor’ PINK1 protein (PINK1-FL) is targeted to the mitochondria via its N-terminal MTS domain (Valente et al., 2004a). The MTS alone is responsible for this mitochondrial localisation, as a MTS-fusion with ECFP is sufficient for organelle specificity (Silvestri et al., 2005). Like most proteins with a mitochondrial presequence, once at the mitochondrial surface, PINK1 is imported into the intermembrane space (IMS) and then the mitochondrial inner membrane (MIM) via the translocase pore complexes, TOM and TIMM23 respectively

(Jin and Youle, 2012; Neupert and Herrmann, 2007). A 'stop transfer' sequence in the TM domain of PINK1 halts import, preventing release into the mitochondrial matrix, and embedding PINK1 laterally in the MIM (Jin and Youle, 2012; Lin and Kang, 2010; Neupert and Herrmann, 2007; Zhou et al., 2008). Here, the matrix protease, mitochondrial processing peptidase (MPP), is responsible for the removal of the MTS domain from the N-terminus, producing a protein of ~60 kDa (Greene et al., 2012). Following MTS cleavage, PARL, an intramembrane protease in the MIM, is responsible for a second cleavage event in the TM domain at A103 (Deas et al., 2011; Jin et al., 2010; Meissner et al., 2011; Whitworth et al., 2008), releasing a short, 52 kDa PINK1 isoform into the cytoplasm (Yamano and Youle, 2013). Following PARL-dependent cleavage, the exposed N-terminus phenylalanine (F) acts as a type-2 degradation signal or degron (Sriram et al., 2011), leading to N-end rule pathway proteolysis via UBR1, UBR2 and UBR4 E3-ubiqutin ligases (Figure 1.4). The activation of the cytoplasmic N-end rule pathway allows for the rapid turnover of the 52 kDa isoform of PINK1 (Yamano and Youle, 2013).

Aside from PINK1 autophosphorylation (Nakajima et al., 2003), at least five proteins are putatively phosphorylated in a PINK1-dependent manner; all of which reside in, or are associated with mitochondria. The first identified PINK1 substrate was the IMS chaperone, TNF-associated receptor 1 (TRAP1). Here, kinase assays demonstrated that PINK1 directly phosphorylates TRAP1 both *in vitro* and *in vivo*; and this event is increased in the presence of the oxidative stressor, hydrogen peroxide. This phosphorylation was proposed to inhibit the release of the pro-apoptotic protein, cytochrome C, through the mitochondrial permeability transition pore (mPTP), hence performing an anti-apoptotic cell-protective function (Pridgeon et al., 2007).

In the same year, another mitochondrial protein, High Temperature requirement A2 (HtrA2), was identified as a putative PINK1 substrate (Plun-Favreau et al., 2007). HtrA2 is an IMS serine protease involved in the induction of apoptotic cell death upon release into the cytoplasm (Suzuki et al., 2001). In 2005, *HtrA2* was assigned to the locus '*PARK13*', due to its involvement in a parkinsonian-like syndrome (Plun-Favreau et al., 2007; Strauss et al., 2005). However, this association could not be replicated, casting doubt over the involvement of this protein in disease etiology (Simon-Sanchez and Singleton, 2008). Nevertheless, HtrA2 has been shown to bind to PINK1, and become phosphorylated in a PINK1-dependent manner under conditions of cellular stress (Plun-Favreau et al., 2007).

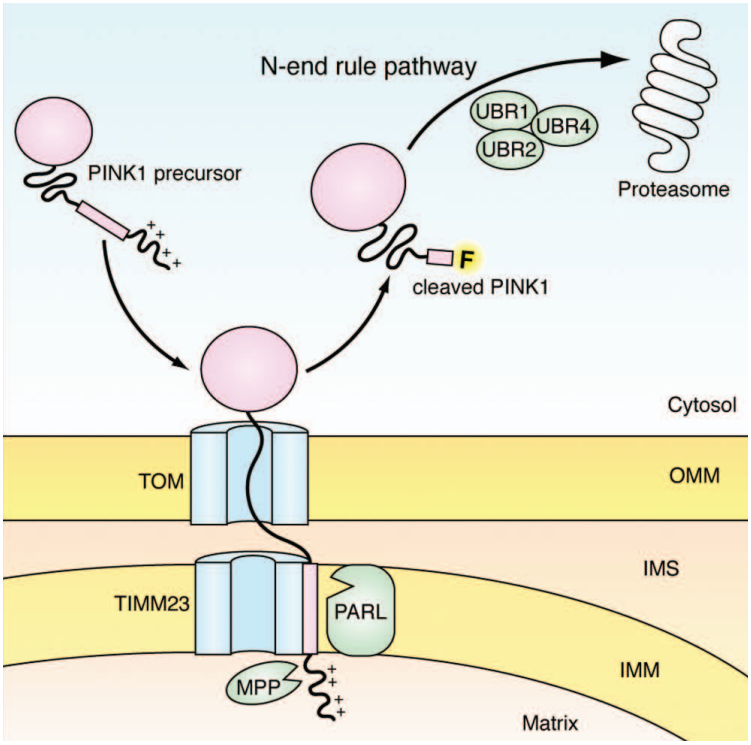

Figure 1.4 PINK1 proteolytic turnover under basal conditions. Schematic representation of PINK1 import into mitochondria via the TOM and TIMM23 complexes, subsequent cleavage events via MPP and PARL, and release into the cytosol for proteolytic N-end rule degradation via the proteasome. OMM – outer mitochondrial membrane, IMM – inner mitochondrial membrane, IMS – intermembrane space. Figure adapted from Yamano et al.,(2013).

Two further substrates of PINK1 are the MOM GTPases, Mitofusin 2 (Mfn2), involved in mitochondrial fusion (Chen and Dorn, 2013), and Miro, involved in mitochondrial transport (Wang et al., 2011). Here, coordinated PINK1-dependent phosphorylation and subsequent Parkin-dependent ubiquitination triggers the removal of these proteins from dysfunctional mitochondria via the proteasomal degradation pathway. Together, these events are suggested to sequester and isolate failing mitochondria prior to removal from the cell; a subject covered in greater detail in later sections.

Finally, using an *in vitro* bacterial system, Kondapalli and colleagues recently screened 17 proteins including previously reported PINK1 interactors and genes residing at the *PARK* loci, with a view to reproduce, and/or identify new PINK1 substrates. Where the phosphorylation of TRAP1, HtrA2, Miro and Mfn2 could not be replicated, a novel PINK1-dependent phosphorylation was observed in the UBL domain of Parkin. This *in vitro* phosphorylation event was recapitulated in a mammalian system, where the phosphorylation site was identified as Ser^{65} (Kondapalli et al., 2012). As discussed later, these data have greatly enhanced our understanding of how PINK1 and Parkin interact with each other in a common pathway.

1.4.5.3. *PARK 7 - DAISUKE-JUNKO-1 (DJ-1)*

Daisuke-Junko-1 (DJ-1), the third autosomal recessive gene to be linked to early onset PD, was found to be responsible for *PARK7*-linked PD cases in 2003 (Bonifati et al., 2003a; Bonifati et al., 2003b; van Duijn et al., 2001). Point mutations and exon deletions in *DJ-1* are very rare, accounting for less than 1% of all monogenic forms of PD (Pankratz et al., 2006).

First described as an oncogene, DJ-1 is ubiquitously expressed, and localises mostly in the cytosol, with trace amounts detectable in mitochondrial and nuclear fractions (Canet-Aviles et al., 2004; Miller et al., 2003; Nagakubo et al., 1997). The expression of DJ-1 is increased in the presence of ROS accumulation, suggesting a possible anti-oxidant role for this protein (Mitsumoto and Nakagawa, 2001). Further evidence for an anti-oxidant role came from SH-SY5Y human neuroblastoma cells, after the application of the oxidative stressor hydrogen peroxide. Here, wild type, but not PD-linked pathogenic variants of DJ-1 underwent oxidation, prior to promoting the elimination of hydrogen peroxide from these cells. This elimination protected cells from ROS-induced cell death, hence highlighting the cytoprotective function of DJ-1 (Taira et al., 2004).

In PD brain tissue, there is an increase in DJ-1 oxidation compared to control samples, indicating increased levels of oxidative stress in the diseased state (Bandopadhyay et al., 2004). DJ-1 oxidation was also observed in M17 neuroblastoma cells, following the application of the ROS-producing herbicide, paraquat. Here, paraquat triggered oxidised DJ-1 to translocate from the cytoplasm to the MOM (Canet-Aviles et al., 2004) via the mitochondrial chaperone, Grp75 (Li et al., 2005). Importantly, mice carrying a *DJ-1* deficiency have heightened sensitivity to oxidative stressors such as MPTP, leading to the demise of dopaminergic neurons (Kim et al., 2005). Taken together these data suggest that DJ-1 is a potent anti-oxidant and neuroprotectant, which scavenges cells for neurotoxic compounds, and neutralises their effect. It also highlights an interaction with mitochondria, once again implicating these organelles in the etiology of PD.

1.4.6 GENETIC SUCEPTABILITY TO SPORADIC PD

Monogenic forms of PD account for only a small fraction of the total number of PD cases. In such cases, a clear pattern of Mendelian inheritance is often apparent, whereby the gene mutation alone is responsible for the development of the disease. However, in sporadic cases, the cause of disease development is likely to be a

combination of multiple genetic risk variants, perhaps with an environmental risk element. Early efforts to identify polymorphisms of genes involved in sporadic PD took a candidate gene approach, whereby monogenic PD genes, and genes associated with other neurodegenerative diseases were analysed. Subsequently, a small number of these genes has been confirmed following modern, meta-analysis techniques. For example, both *SNCA* (Kruger et al., 1999; Tan et al., 2004) and *LRRK2* (Bonifati, 2007; Mata et al., 2005) polymorphisms, as well as *microtubule-associated protein tau (MAPT)* polymorphisms (Golbe et al., 2001; Healy et al., 2004), the gene closely linked to Alzheimer's disease pathology, were found to be linked to sporadic PD. Additionally, *SNCA* mutations and multiplications associated with monogenic PD have been identified in some apparently 'sporadic' cases, suggesting either reduced penetrance or the occurrence of *de novo* mutation in the population (Lesage and Brice, 2009; Lesage and Brice, 2012).

Another common risk factor for sporadic PD, particularly in the Ashkenazi Jew population, is the presence of heterozygous mutations in the lysosomal enzyme, *glucocerebrosidase (GBA)* (Lesage et al., 2011; Sidransky et al., 2009). In the case of homozygous mutations, *GBA* causes a recessive lysosomal storage disease called Gaucher's disease (GD), characterized by the deposition of lipids within the cell. Importantly, it was observed that together with clinical features including anaemia, liver and spleen enlargement, and diminishing platelet numbers, GD patients occasionally display parkinsonian-like symptoms, with the presence of Lewy bodies (Tayebi et al., 2003). This observation prompted investigation into a putative link between the two syndromes. Of interest, a disproportionate number of relatives of GD-sufferers develop PD, suggesting increased risk in heterozygous carriers of *GBA* mutations (Goker-Alpan et al., 2004). This was confirmed following a large number of worldwide, single- and multi-centre collaborative approaches, where the prevalence of PD in people with heterozygous *GBA* mutations was 5-fold higher than the control group (Sidransky and Lopez, 2012; Sidransky et al., 2009). How these mutations confer the disease is still unknown, but may be related to disrupted lysosomal degradation pathways, and accumulation of dysfunctional cellular components.

Genome-wide association studies (GWAS) are a relatively recent technique, which analyse a vast number of genetic markers or single nucleotide polymorphisms (SNPs) to identify common disease risk variants. The benefit of this approach is the ability to compare thousands of disease-specific samples against thousands of control samples, allowing the identification of very rare variants with a mild or moderate effect. Such polymorphisms would be likely missed, or fall out of significance in the smaller-scale

genetic linkage techniques, which employ much smaller sample numbers (Hardy and Singleton, 2009). Using this approach, *SNCA, LRRK2* and *MAPT* polymorphisms have been strongly implicated as conferring risk for the development of sporadic PD (Satake et al., 2009; Simon-Sanchez et al., 2009). Additionally, *GBA* has also been identified as a risk factor, together with a number of *de novo* regions including *HLA, GAK* and *SREBF1* (Do et al., 2011; Liu et al., 2011; Nalls et al., 2011).

With the first 'mega-meta-analyses' now underway (J. Hardy, personal correspondence), increasing numbers of case-group samples enable GWAS techniques to become even more powerful. This should act to increase confidence in the strength of previously discovered risk loci, whilst removing spurious results.

1.5 MITOCHONDRIA AND PARKINSON'S DISEASE

A number of theories have been put forward regarding the etiology of Parkinson's disease. These include aberrant build-up and aggregation of proteins, oxidative damage and mitochondrial dysfunction. One emerging theory centres on the 'mitochondrial dysfunction' model of PD, supported by an increasing body of evidence from an array of sources. Mitochondria are double membrane-bound organelles responsible for oxidative respiration; the major source of cellular energy or adenosine triphosphate (ATP). Alongside energy production, mitochondria also provide a calcium buffering facility, play a central role in a range of catabolic and anabolic processes such as fatty acid β-oxidation, and are responsible for the initiation of the apoptosis cascade via the release of cytochrome c and other pro-apoptotic proteins. Mitochondrial respiratory complexes are responsible for generating high levels of reactive oxygen species (ROS) via the synthesis of superoxide anions; a byproduct of the electron transport chain. Not only do cellular ROS cause general cellular damage to proteins and lipids, it specifically damages mitochondria themselves, probably due to their close proximity to the ROS source. Due to this, mitochondria require tightly controlled anti-oxidant mechanisms in order to prevent a build-up of damaged components.

Healthy mitochondria, able to overcome adverse oxidative environments can be easily distinguished from those that have succumbed to damage, through the maintenance of their mitochondrial electrochemical membrane potential ($\Delta\Psi m$). This potential is produced by the electron transport chain (ETC), via the pumping of protons from the matrix to the IMS as electrons flow between the respiratory complexes. This differential

electrochemical gradient across the MIM leads to ATP production via oxidative phosphorylation, as protons re-enter the matrix through ATP-Synthase. However, when mitochondrial damage reaches a critical threshold, the electron transport chain no longer maintains efficient electron transfer, leading to the collapse of the electrochemical gradient. This occurrence is commonly used to assess the health of a mitochondrial population, and taken as a marker for mitochondrial dysfunction. Importantly, ROS can cause mitochondrial damage leading to the loss of $\Delta\Psi m$, demonstrating how both oxidative damage and mitochondrial dysfunction theories of PD could be closely linked to one another.

Mitochondria were first implicated in PD following the onset of Parkinsonian symptoms in drug users exposed to the ETC complex I inhibitor, MPTP (Langston et al., 1983). The supposed outcome of this complex I inhibition was the uncoupling of the ETC, leading to an energy deficit, increased ROS production and eventual cell death. As a result of these cases, analysis of respiratory complexes in brain and blood samples of PD patients highlighted a marked decrease in mitochondrial complex I activity (Janetzky et al., 1994; Mann et al., 1992; Mizuno et al., 1989; Parker et al., 1989; Schapira et al., 1990), as well as a higher burden of somatic mtDNA mutations, compared to control samples (Bender et al., 2006). As mtDNA encodes 13 respiratory complex genes, this increase in mtDNA point mutations and deletions is likely to reduce the efficiency of oxidative respiration, perhaps accounting for the observed decrease in complex I activity in PD patients. To add further weight to the mitochondrial model of PD, epidemiology studies identified a link between exposure to pesticides, such as the complex I inhibitor rotenone, and the development of sporadic PD (Gorell et al., 1998; Tanner et al., 2011). Importantly, in animal models of Parkinson's disease, both MPTP and rotenone closely recapitulate pathological and clinical hallmarks of PD, including dopaminergic neuron loss and Lewy body pathology (Betarbet et al., 2000; Langston et al., 1984).

Mitochondrial involvement in PD etiology was strengthened following the observation that the monogenic autosomal recessive PD genes, *parkin, PINK1* and *DJ-1*, all localise to mitochondria under basal or stress-induced conditions (Canet-Aviles et al., 2004; Miller et al., 2003; Narendra et al., 2008; Valente et al., 2004a). Analysis of *parkin*- and *PINK1*-null animals has greatly enhanced our understanding of how dysregulation of mitochondrial homeostasis may contribute to disease pathology. First, *parkin*-null *Drosophila melanogaster* models were found to have shortened life-spans, severe motor dysfunction, progressive myofibril degeneration with abnormal wing posture, dopaminergic neuron loss and swollen mitochondria with irregular cristae

(Greene et al., 2003; Pesah et al., 2004; Whitworth et al., 2005). As well as demonstrating the reproducibility of human disease phenotypes in an invertebrate model, these studies provided clear evidence for mitochondrial involvement in disease pathology. Further evidence for a mitochondrial role came from cellular studies, where apoptosis was induced by ceramide; an endogenous lipid which assembles into pores in the MOM allowing the release of pro-apoptotic IMS proteins (Siskind, 2005). Here, Parkin overexpression prevented ceramide-induced cell death by slowing mitochondrial swelling and the consequent release of cytochrome c (Darios et al., 2003). Importantly, *parkin*-null mice also exhibited deficits in mitochondrial respiratory complex subunits, despite maintaining apparently normal mitochondrial architecture and dopaminergic neuron numbers (Goldberg et al., 2003; Palacino et al., 2004). One possible reason for a lack of dopaminergic neuron degradation in the *parkin*-null mouse model is the initiation of early compensatory events, such as the upregulation of protective and/or redundant genes, which shield aged animals against PD pathology (Dawson et al., 2010). In support of this, conditional knockout (KO) of *parkin* in adult mice avoids developmental compensatory effects, resulting in significant and progressive DA neuron loss (Shin et al., 2011).

Second, *PINK1*-null and *PINK1* RNAi-expressing *Drosophila* exhibit equivalent phenotypes to the *parkin*-null fly model, again displaying swollen mitochondria, with abnormal cristae and a concomitant reduction in ATP production (Clark et al., 2006; Park et al., 2006; Yang et al., 2006). Importantly, overexpression of wild type, but not C-terminally truncated *PINK1* rescued the aberrant phenotypes described (Yang et al., 2006), highlighting the importance of the kinase domain in PINK1 cellular protection. Furthermore, data from primary patient fibroblasts carrying homozygous *PINK1* mutations showed reduced complex I activity coupled with increased oxidative damage (Hoepken et al., 2007). However, where *PINK1*-null mice displayed progressive mitochondrial dysfunction together with a mild locomotor defect, neuronal degeneration and Lewy body pathology were absent following post mortem analysis (Gautier et al., 2008; Gispert et al., 2009; Kitada et al., 2007), again, possibly due to compensatory mechanisms.

Finally, whilst data from *DJ-1*-deficient animal models have been inconsistent, a recent study reported locomotor defects and progressive mitochondrial dysfunction, together with decreased ATP-production in aged *DJ-1*-null mice and *Drosophila* (Hao et al., 2010). These data again highlight the mitochondrial theme running through *PARK* loci gene function.

Taken together, these data offer an overwhelming body of evidence indicating the central involvement of aberrant mitochondrial homeostasis in the etiology of PD. Whether the observed mitochondrial defects are the cause or effect of disease sequelae remains an open question. However, given that mitochondrial swelling in *Drosophila PINK1*- and *parkin*-mutants is a relatively early pathogenic event, this indicates that mitochondrial dysfunction could be the primary cause of disease (Clark et al., 2006; Greene et al., 2003; Whitworth et al., 2005).

1.5.1 THE PINK1/PARKIN-PATHWAY

Following the observation that both *parkin*- and *PINK1*-null *Drosophila* models carry near-identical pathological phenotypes, it was suggested that these genes might act in a common molecular pathway. In agreement with this, double knockout *Drosophila* models lacking both *PINK1* and *parkin* developed comparable disease phenotypes to those observed in the single mutants, consistent with an involvement in a mutual linear pathway. Additionally, overexpression of *parkin* in a *PINK1*-null background ameliorated mutant phenotypes; a finding that was not true for the reverse. Taken together these data indicate that *PINK1* acts upstream of *parkin* in the same linear pathway, hereafter called the PINK1/Parkin-pathway (Clark et al., 2006; Park et al., 2006; Yang et al., 2006; Yang et al., 2008). These studies represent a significant discovery in the field, as it was the first demonstration that genes attributed to *PARK* loci acted together in a common pathway with a clear function. Such a finding greatly strengthened the reputation of the mitochondrial theory of disease, and prompted increased interest in the study of recessive PD genes.

Importantly, data from *Drosophila* studies were substantiated by studies in human cells, whereby *PINK1* deficiency resulted in a fall in $\Delta\Psi m$ and a change in mitochondrial morphology, the latter of which was rescued by *parkin* overexpression (Exner et al., 2007). This placed mammalian *PINK1* upstream of *parkin* in a common pathway, confirming previous data from *Drosophila* models.

1.5.2 MITOCHONDRIAL DYNAMICS

Rather than existing as discrete, individual organelles, mitochondria form a dynamic, ever-changing network throughout the cytoplasm of the cell. Mitochondria utilise fusion, fragmentation (fission) and trafficking machinery in order to alter their shape, size and position within the cell. Each of these events depend upon the energy requirements of distinct subcellular locations, as well as the overall health of the mitochondria

themselves. The core proteins involved in mitochondrial fusion and fission are dynamin-like GTPases, comprehensively studied in yeast and mammalian systems, and found to be highly conserved across species. In a mammalian setting, mitochondrial fusion is mediated by two MOM GTPases, *mitofusin 1* and *mitofusin 2* (*MFN1/MFN2*), which catalyse fusion of the outer membrane; and *optic atrophy 1* (*OPA1*), a MIM GTPase that facilitates fusion of the inner membrane. Mitochondrial fission is performed principally by *dynamin-related protein 1* (*DRP1*), a cytosolic GTPase which forms a constrictive ring at the MOM, possibly following mitochondrial recruitment by *fission 1* (*FIS1*), a tail anchored MOM protein (Westermann, 2010). When the mitochondrial morphology balance is tipped towards increased fusion, the mitochondrial network adopts an interconnected 'string-like' appearance. In contrast, when the morphology balance is tipped towards fission, mitochondria adopt a more punctate 'dot-like' appearance.

1.5.2.1 Mitochondrial Dynamics and Disease

Mutations in pro-fusion genes have been attributed to two distinct progressive neuropathies. Heterozygous *MFN2* mutations produce a peripheral axonal sensorimotor neuropathy known as Charcot-Marie-Tooth disease, type 2a, characterised by distal muscle weakness and wasting (Zuchner et al., 2004). Also, heterozygous mutations in *OPA1* cause autosomal dominant optic atrophy type 1, a disease leading to the loss of visual acuity and blindness via optic nerve deterioration (Delettre et al., 2000). Additionally, despite the lack of a known disease caused by core fission genes, a heterozygous mutation in pro-fission *DRP1* has been reported to cause neonatal lethality with neurological features (Waterham et al., 2007). Taken together these data highlight the importance of a careful balance between mitochondrial fission and fusion for the maintenance of cell health.

The first suggestion of a PINK1/Parkin-involvement in mitochondrial dynamics came from the observation that mitochondria from *PINK1*- and *parkin*-null *Drosophila* exhibit an abnormal, enlarged morphology in flight muscle and testes (Clark et al., 2006; Greene et al., 2003; Park et al., 2006; Yang et al., 2006). Leading on from this, groups studying the role of the PINK1/Parkin-pathway scrutinised the effects of altering fission and fusion gene dosage on *Drosophila PINK1 (dPINK1)*- and *parkin (dparkin)*-null phenotypes. Here, functional rescue of climbing and flight defects, muscle degeneration with abnormal wing posture, DA reduction and aberrant mitochondrial morphology were observed following increased *dDrp1,* or reduced *dOpa1 or dmfn* gene dosage (Deng et al., 2008; Poole et al., 2008; Yang et al., 2008). Additionally,

quantification of mitochondrial morphology phenotypes in cultured *Drosophila* DA neurons and S2R+ cells showed an increase in punctate mitochondria following *PINK1* and/or *parkin* overexpression, and an increase in tubular mitochondria following *PINK1* and/or *parkin* RNAi silencing (Yang et al., 2008; Ziviani et al., 2010). Finally, overexpression of *PINK1* in the *Drosophila* visual system produced toxicity resulting in a 'rough eye' phenotype. However, increased mitochondrial fusion, or decreased mitochondrial fission ameliorated this phenotype; whilst the opposite manipulation caused an exacerbation (Poole et al., 2008). Taken together, these data indicated that *Drosophila PINK1* and *parkin* promote fission and/or inhibit fusion.

Whilst the morphological data from *Drosophila* models are relatively clear-cut, the same cannot be said for mammalian cell systems. In general, it is agreed that *PINK1* and *parkin* can influence mitochondrial morphology, however the mode of influence is a matter of dispute. In contrast to *Drosophila* data, *PINK1* siRNA knockdown in cultured human SH-SY5Y and HeLa cells has been shown to evoke excess mitochondrial fragmentation (Dagda et al., 2009; Exner et al., 2007). One explanation for the disparity could be that compensatory mechanisms are in place to account for the loss of key genes in more complex systems. For example, reduced expression of pro-fission *PINK1* may result in excess fission as alternative genes take on the role. In a less complex system such as *Drosophila*, these compensatory mechanisms may not exist, resulting in an excessively fused mitochondrial network, as observed. Nevertheless, this opposing phenotype is not always observed in mammalian cell types. For example, in agreement with *Drosophila* data, COS-7 fibroblast cells and rat dopaminergic and hippocampal neurons exhibited punctate, fragmented mitochondria following overexpression-, and tubular, fused mitochondria following siRNA-silencing of *PINK1* and/or *parkin* (Yang et al., 2008; Yu et al., 2011). In complete contrast to the above studies, one group reported a total lack of mitochondrial morphology defects in *PINK1*-null *Drosophila* neuromuscular junctions and mouse fibroblasts (Morais et al., 2009). Taken together, these data imply a cell-specific response to *PINK1* and *parkin* gene loss. It has been suggested that transformed cell-lines such as HeLa cells may behave differently to post-mitotic cells such as neurons, due to differences in cell-cycle input and a greater reliance upon glycolysis, perhaps accounting for these discrepancies (Yu et al., 2011)

1.5.2.2 Functions of Mitochondrial Dynamics

Establishing the purpose of a highly dynamic mitochondrial network, and how it benefits cellular health is fundamental to understanding the role of the PINK1/Parkin-

pathway. Critically, new mitochondria are not synthesised *de novo;* rather they are brought about by the expansion of existing organelles. For this, mtDNA multiplication and increased synthesis of nuclear- and mitochondrial-encoded proteins and lipids must occur. With this expansion, concomitant mitochondrial fission creates a greater number of solitary mitochondria, which relocate to serve different areas of the cell (Westermann, 2010). This biogenesis is crucial for maintaining a complete and healthy network of mitochondria, particularly following the elimination of dysfunctional mitochondria from the cell (see later sections).

Another function of mitochondrial dynamics is the ability of individual mitochondria to fuse with the network and initiate matrix content mixing. This mixing has been demonstrated elegantly through the use of mitochondrial matrix-targeted photoactivatable GFP (Twig et al., 2008a). Here, a small portion of the mitochondrial population was laser-activated, producing isolated GFP fluorescence. However, after 45 minutes, homogenous distribution of GFP was observed across the entire mitochondrial population. The purpose of this content mixing is thought to be in the maintenance of mitochondrial network health via the replenishment, repair and complementation of intact mitochondrial components, together with the removal of dysfunctional factors (Youle and van der Bliek, 2012). In support of this, fusion-deficient *MFN1/2* double knock-out and OPA1-RNAi expressing mouse embryonic fibroblasts (MEFs) produce a heterogeneous mitochondrial population, with some organelles exhibiting a well-maintained $\Delta\Psi m$, and others showing either diminished or lost $\Delta\Psi m$ (Chen et al., 2005). As the $\Delta\Psi m$ status is typically regarded as a read-out for mitochondrial health, a lack of fusion, and subsequent content mixing therefore produces a mixed population of healthy and dysfunctional organelles. In support of this, another study showed that prevention of fusion led to a significant decrease in the ATP-producing capacity of mitochondria (Liu et al., 2009). In part, this is likely due to the instability and loss of respiratory-complex encoding mtDNA, as documented in optic atrophy type 1 patients with heterozygous *OPA1* mutations (Amati-Bonneau et al., 2008; Hudson et al., 2008).

Mitochondrial dynamics are also important for the segregation of damaged mitochondrial components for removal from the network. This relies upon mitochondrial fission in order to isolate less active mitochondria from the network. Here, fission is likely a permissive event, allowing solitary mitochondria exhibiting a sustained reduction in $\Delta\Psi m$, to become separated from the healthy mitochondrial population (Figure 1.5). Importantly, these mitochondria lose their capacity to re-fuse with

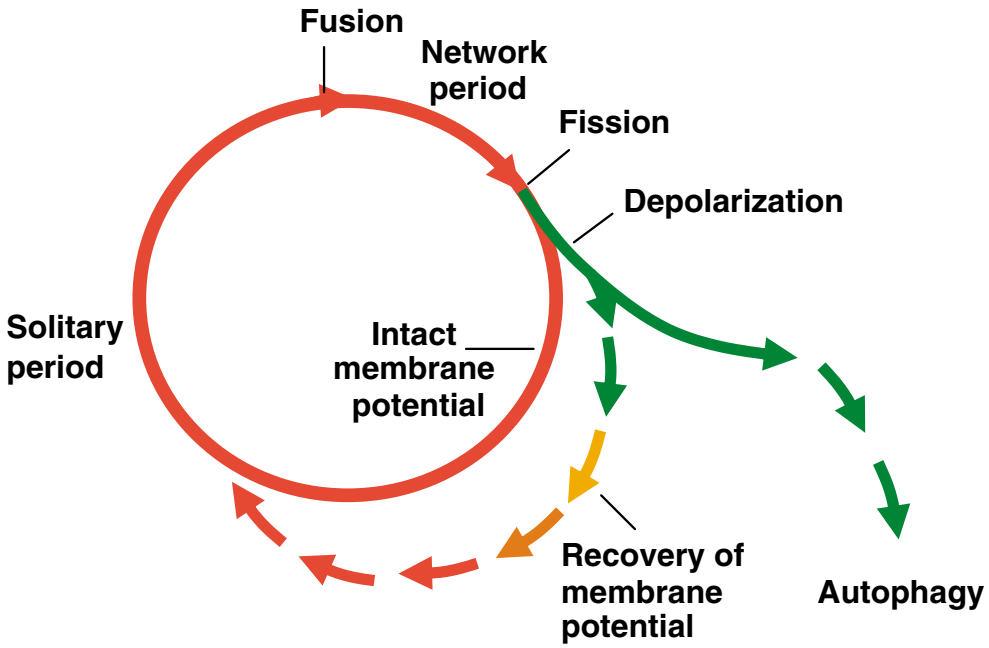

Figure 1.5 Mitochondrial fission as a pre-requisite for mitophagy. Schematic of the mitochondrial life-cycle whereby mitochondria exist as 'solitary' post-fission organelles, or 'networked' post-fusion organelles. The fusion period is brief, and leads quickly to a fission event, whereby heterogeneous daughter mitochondria with hypo- or hyperpolarised membranes are produced. Those in a hyperpolarised state will remain able to re-fuse with the network (red line), whereas those in a hypo-polarised state will lose their fusion ability (green line) and become directed down the degradative autophagy route. In some circumstances, mitochondria are able to recover their $\Delta\Psi m$, allowing them to re-join the healthy mitochondrial population, hence avoiding degradation (arrows). Image from Twig et al., (2008b).

neighbouring mitochondria, probably through the loss of pro-fusion factors OPA1 (Twig et al., 2008a) and Mitofusin (Ziviani and Whitworth, 2010), allowing efficient segregation for degradation via the macroautophagy route. This process is known as mitochondrial autophagy or 'mitophagy', and involves the packaging of dysfunctional mitochondria in a double-membrane autophagosome, before fusion with the lysosome for hydrolytic degradation.

Distinct from the process of mitophagy is the recent discovery of mitochondria-derived vesicles (MDVs), which package specific cargo into small ~100 nm vesicles for delivery to peroxisomal (Neuspiel et al., 2008) and lysosomal (Soubannier et al., 2012) pathways. This process is DRP1-independent, indicating a dynamic process distinct from that of the core morphology genes. The role of MDVs is believed to be in the removal of ROS-damaged mitochondrial proteins and lipids, in order to maintain a healthy network. Such quality control measures are proposed to occur prior to widespread network fragmentation, and independently of mitophagy, supposedly acting as a first-line defence in the event of increased oxidative stress (Neuspiel et al., 2008; Soubannier et al., 2012)

Finally, another proposed function of mitochondrial dynamics is the division of mitochondria for efficient transport and spatial re-distribution to locations of high-energy demand. This intracellular transport is particularly important in very large cells such a neurons, where the cell body and synapses, both of which expend large amounts of energy, can be separated by tens of centimetres or more in humans. In this respect, individual, fragmented mitochondria are much more amenable to transport than a fused and interconnected mitochondrial network. In support of this, primary neuronal culture from *DRP1*-null mice showed a lack of mitochondria in cell termini such as synapses and dendrites, and an accumulation in the cell body (Ishihara et al., 2009). Thus, for motor proteins to efficiently deliver their cargo, mitochondria must undergo some degree of fission.

With both mitochondrial fission and fusion performing crucial and distinct roles in the maintenance of a healthy mitochondrial population, a tightly regulated balance between the two processes is key. It is conceivable that an aberrant shift in either direction could produce cellular pathologies with devastating consequences, as demonstrated by section 1.5.2.1.

1.5.3 MITOCHONDRIAL TRAFFICKING

Mitochondria, particularly those in cells such as neurons, with a large size and high-energy demand, must be delivered to areas of ATP-requirement, such as synapses, for efficient energy provision. Here, mitochondria are essential for the production of ATP required for the repolarisation of the plasma membrane, as well as the buffering of high intracellular calcium ($[Ca^{2+}]_{IC}$) levels (Schwarz, 2013). Mitochondrial components have short half-lives in the order of days to weeks (Lipsky and Pedersen, 1981; Vincow et al., 2013), therefore requiring continuous mitochondrial trafficking and replenishment. Here, a constant supply of healthy mitochondria with intact membrane potentials are brought to the synapses, coupled with the retrotransport of damaged mitochondria to the cell body for recycling (Miller and Sheetz, 2004). For mitochondria to be transported in anterograde (away from the cell body) and retrograde (towards the cell body) directions, the motor proteins kinesin and dynein are employed respectively, to taxi organelles along microtubule tracks.

For the linkage of mitochondria to microtubules, motor proteins must interact with both mitochondrial and cytoplasmic adapter proteins. The core proteins involved in anterograde mitochondrial transport are the heavy chain of kinesin (*KHC*) (Tanaka et al., 1998), the cytoplasmic adapter *milton* (Stowers et al., 2002), and the MOM GTPase

Miro (Guo et al., 2005). *milton* was first discovered in *Drosophila* following an EMS screen, which identified defective synaptic transmission in *milton* mutant animals. This defective physiology was attributed to the absence of axonal and synaptic mitochondria, despite the presence of somal mitochondria. This aberrant distribution phenotype was caused by defective, mitochondria-specific transport; a claim substantiated by the association of Milton with both mitochondria and the anterograde mitochondrial motor protein, KHC (Stowers et al., 2002). This association implied that Milton acts as an adapter protein, bridging the gap between mitochondria and microtubule-associated motor proteins.

Following the discovery of Milton, a third protein was found to be involved in the mitochondrial transport complex. This was the mitochondrial GTPase Miro, initially discovered in *Drosophila* models whereby EMS-induced mutation produced comparable mitochondrial distribution defects as those observed in *milton* mutants (Guo et al., 2005). Importantly, Milton and Miro were found to physically interact with each other, suggesting that Miro may act as an anchor-point for Milton at the mitochondrial surface (Glater et al., 2006). As well as anterograde transport, *milton* and *miro* have also been shown to play a role in dynein-related retrograde transport (van Spronsen et al., 2013). Here the two mammalian *milton* orthologs, *TRAK1* and *TRAK2,* show differential motor protein preference, determining the direction of mitochondrial transport.

The crucial question is how the mitochondrial motility complex coordinates the movement of mitochondria. The structure of Miro has provided valuable insight into how mitochondrial movements may be regulated by this complex. First, Miro contains a C-terminal transmembrane domain, which inserts into the MOM, providing an anchor for Milton to bind. Second, the amino-portion of the protein, which faces the cytoplasm, comprises two GTPase domains, flanking two EF-hand calcium-sensing domains (Reis et al., 2009). One of the known intracellular signals influencing the progression of mitochondria is a change in local $[Ca^{2+}]_{IC}$; where high $[Ca^{2+}]_{IC}$ blocks mitochondrial transport. Increases in $[Ca^{2+}]_{IC}$ are often found at energy-intensive synapses, or areas of the cell where the local ATP-provision and mitochondrial calcium buffering abilities are deficient. Therefore, incoming mitochondria are able to accumulate in these areas, rectifying the deficit. This accumulation was found to occur through the calcium sensing EF-hands of Miro. Here, high $[Ca^{2+}]_{IC}$ is suggested to cause a conformational change in Miro, allowing a direct, Milton-independent interaction with the motor domain of KHC. This interaction causes the dissociation of KHC from the microtubules, hence reversibly halting progress (Figure 1.6, Wang and Schwarz, 2009).

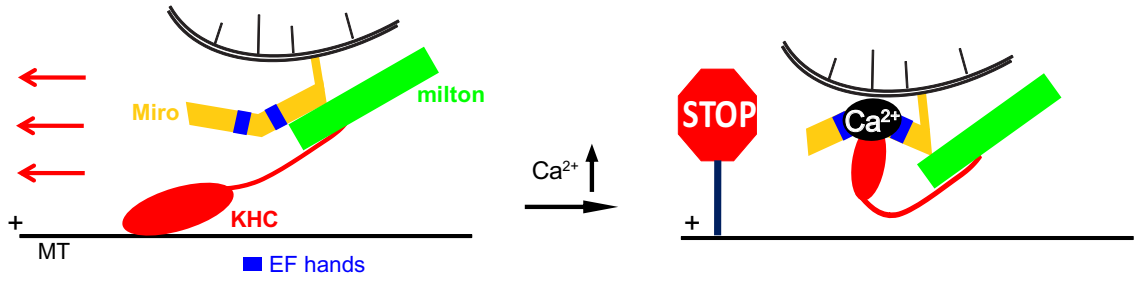

Figure 1.6 Mitochondrial transport and calcium regulation. Schematic representation of mitochondrial anterograde transport in the presence and absence of high intracellular calcium. Mitochondria are linked to the microtubule tracks via the anterograde motor protein kinesin heavy chain (KHC - red), the cytoplasmic adapter protein Milton (green) and the MOM GTPase, Miro (yellow). Transport of mitochondria can be regulated by changes in intracellular calcium levels, whereby high concentrations cause a transient transport block. This transport block is controlled by the calcium sensing EF-hands of Miro (blue), which bind directly to the N-terminal motor domain of KHC, hence disconnecting the complex from the microtubules. Figure from Wang and Schwarz,(2009).

The trafficking of mitochondria is not only essential for efficient cellular energy supply and calcium buffering, but also in the process of mitochondrial fusion, as discussed in earlier sections. Importantly, for fusion to take place, some form of mitochondrial movement must be involved. For example, the inhibition of mitochondrial transport by nocodazole; a microtubule de-polymerisation agent, also prevents mitochondrial fusion and concomitant matrical mixing. This lack of matrix complementation manifests itself as a reduction in oxidative phosphorylation and subsequent ATP production (Liu et al., 2009). These data reinforce the idea that mitochondrial dynamics and spatial distribution are not mutually exclusive processes; with both being fundamental to the maintenance of mitochondrial homeostasis.

1.5.3.1 Mitochondrial Trafficking and the PINK1/Parkin-Pathway

A growing body of evidence has implicated the PINK1/Parkin-pathway in the regulation of intracellular mitochondrial trafficking. This involvement is believed to be a critical step in mitochondrial quality control, functioning to permanently separate dysfunctional organelles from the network as a whole. Therefore the mechanism of trafficking arrest imposed by the PINK1/Parkin-pathway is distinct from that described previously, whereby high $[Ca^{2+}]_{IC}$ produces a reversible pause in transport.

The first indication of a pathway contribution to mitochondrial trafficking came following the discovery that PINK1, Milton and Miro form a complex capable of physical and functional interaction (Weihofen et al., 2009). Interestingly, the overexpression of *PINK1* or *parkin* significantly arrested mitochondrial movement in both anterograde and

retrograde directions (Wang et al., 2011). Additionally, knockdown of trafficking complex components in *Drosophila* rescues *PINK1*-null phenotypes, indicating a clear genetic interaction between these genes (Liu et al., 2012). Importantly, a direct interaction between PINK1, Parkin and Miro results in a PINK1-dependent Miro phosphorylation event, leading to its proteasomal degradation in a Parkin-dependent manner (Figure 1.7, Liu et al., 2012; Wang et al., 2011). Miro degradation results in mitochondrial dissociation from the KHC-linked microtubules, therefore producing stationary mitochondria. All aforementioned processes are increased upon exposure to the mitochondrial uncoupler, CCCP (Carbonyl cyanide m-chlorophenyl hydrazone) (Liu et al., 2012; Wang et al., 2011), indicating that the PINK1/Parkin-pathway inhibits trafficking in order to isolate damaged mitochondria from the mitochondrial network.

To prevent re-fusion with the mitochondrial network, the PINK1/Parkin-pathway must not only prevent trafficking, but also fusion events from occurring. Importantly, a well documented target of Parkin-dependent ubiquitination and proteasomal degradation is the MOM pro-fusion factor Mitofusin (Poole et al., 2010; Tanaka et al., 2010; Ziviani et al., 2010). Interestingly, recent work has reported a physical interaction between Mitofusin and the Milton/Miro complex, as well as disrupted bi-directional mitochondrial transport upon *mitofusin* mutation (Misko et al., 2010). These observations were seemingly distinct from a general defect in mitochondrial fusion, again suggesting interplay between the homeostatic mechanisms governing mitochondrial quality control.

One frequent observation following prolonged CCCP-exposure is the redistribution and aggregation of mitochondria in the perinuclear region of the cell, in a *PINK1* & *parkin*-dependent manner (Vives-Bauza et al., 2010). This mitochondrial perinuclear clustering was dependent upon both microtubules and the retrograde motor protein dynein, and resulted in mitophagy (Lee et al., 2010), indicating that organelle repositioning occurs prior to degradation. This repositioning may occur due to the high concentration of both lysosomes and autophagosomes in the perinucleus of the cell, increasing the efficiency of the degradation process.

1.5.4 THE MITOPHAGY PATHWAY

Determined from evidence amassed over the last 5 years, the overriding theme of the PINK1/Parkin-pathway is the maintenance of mitochondrial homeostasis by the removal of dysfunctional mitochondria. Whole mitochondria are degraded and recycled via the autophagy-lysosomal pathway in a process known as mitophagy. Mitophagy is

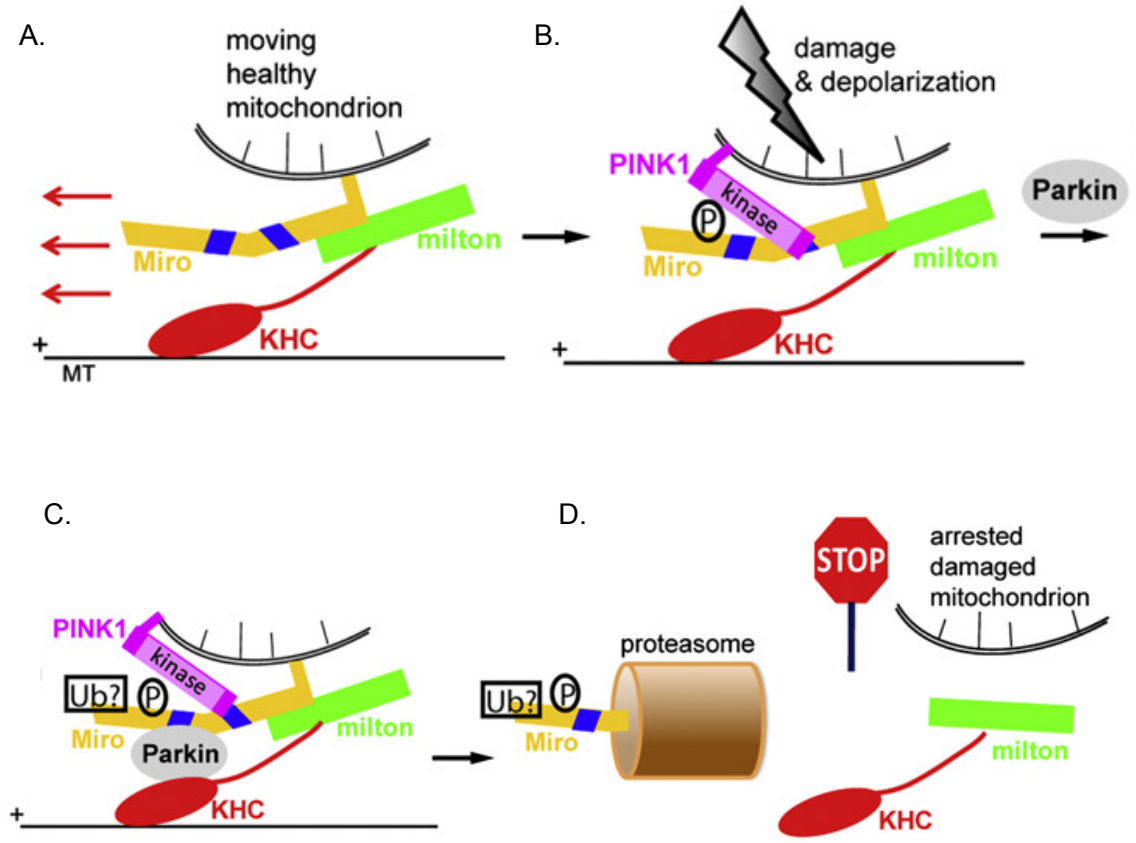

Figure 1.7 PINK1/Parkin-mediated mitochondrial trafficking inhibition, Schematic representation of a permanent trafficking block following irreversible mitochondrial damage. A) Mitochondrial trafficking under basal conditions as in Figure 1.6. B) Irreversible damage caused by a toxic insult such as CCCP application leads to membrane depolarisation and subsequent Miro phosphorylation by PINK1. C) Following this phosphorylation event, Parkin translocates to mitochondria, and Miro is ubiquitinated in a Parkin-dependent manner. D) This ubiquitination results in the proteasomal degradation of Miro and the subsequent arrest of mitochondrial movement along the microtubules. Figure adapted from Wang et al.,(2011).

a form of selective autophagy, which involves the engulfment of cargo in a double membrane vesicle known as an autophagosome, before fusion with the lysosome for hydrolytic degradation. The first demonstration of whole mitochondria contained within double-membrane vacuoles came in 1957 from electron micrographs of neonatal mouse kidneys (Clark, 1957). Since this observation, growing evidence suggests that this engulfment is a selective process with the purpose of eliminating dysfunctional and aged organelles, rather than a non-specific bulk-autophagy event, such as that initiated following starvation.

Relatively little is known about the mechanisms involved in mitophagy, other than the absolute requirement for the core bulk-autophagy machinery (Kanki et al., 2009a). These genes have been given the universal '*autophagy-related gene*' (*ATG*) nomenclature, which currently ranges from *ATG1-34*, and encompasses 15 genes

common to both bulk and selective forms (Kanki et al., 2011). Much of the data regarding the autophagy pathway have come from studies in yeast, where the mitophagy-specific factor *Atg32* has been identified as a possible receptor for cargo recognition genes such as *Atg11* (Kanki et al., 2009b; Okamoto et al., 2009). Surprisingly, despite the high degree of conservation between yeast and mammalian core *ATG* genes, a clear homolog of *Atg32* is lacking in mammals. However, one mitophagy-specific mammalian gene of the MOM, *Nix*, has been identified as a mitophagy receptor in developing reticulocytes (Novak et al., 2010; Sandoval et al., 2008; Schweers et al., 2007). Nevertheless, whether the participation of *Nix* in mitophagy is restricted to reticulocyte maturation, or plays a wider role in the whole organism is currently unclear (Kanki, 2010). Additionally, two studies showed that p62, an autophagy adapter that relocates to CCCP-compromised mitochondria, is essential for mitophagy (Geisler et al., 2010a; Lee et al., 2010). Here it recognises both MOM protein-ubiquitination and the autophagosomal membrane constituent, Atg8/LC3, hence leading to selective degradation of mitochondria. However, conflicting data from a subsequent study found that despite p62-induced mitochondrial aggregation, mitophagy could proceed normally in *p62*-null murine fibroblasts and *p62*-silenced HeLa cells (Narendra et al., 2010a). These data call into question the necessity for p62 in the induction of mitophagy, and may highlight differences in autophagy processes between model systems.

1.5.4.1 Mitophagy and the PINK1/Parkin-Pathway

Despite conflicting evidence surrounding the relationship between p62 and mitophagy, one common theme was the recruitment of p62 following Parkin-dependent ubiquitination of MOM proteins (Geisler et al., 2010a; Narendra et al., 2010a). A seminal study in 2008 revealed a clear and central role for the PINK1/Parkin-pathway in mitophagy (Narendra et al., 2008). Here, endogenous and overexpressed Parkin relocated from a cytoplasmic distribution to a subset of dysfunctional mitochondria following uncoupling with CCCP for 4 hours; a phenomenon that was demonstrated in several cell lines. Critically, prolonged toxification for 12 and 48 hours led first to the perinuclear aggregation of mitochondria, and then global degradation in an autophagy-dependent manner. Importantly, persistent exposure to CCCP failed to induce the autophagy of other cellular organelles such as peroxisomes, indicating that Parkin acts in a selective manner to induce mitophagy (Narendra et al., 2008). Critical to PINK1/Parkin-pathway involvement, all aforementioned processes have been shown to

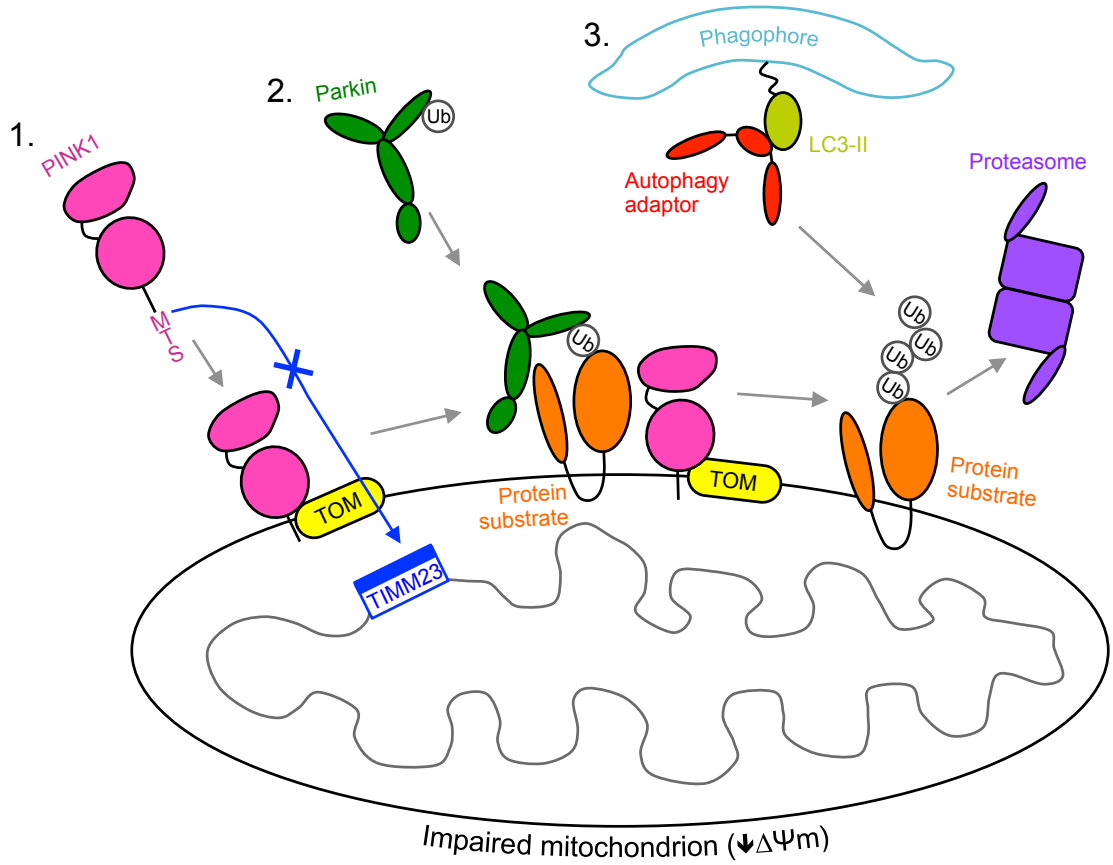

Figure 1.8 PINK1/Parkin-mediated mitophagy. Schematic of PINK1/Parkin-induced mitophagy following the loss of ΔΨm in failing mitochondria. 1) PINK1 is no longer imported into the MIM for proteasomal degradation, but becomes stabilised on the MOM, associated with the TOM complex. 2) Parkin translocates from the cytoplasm to the mitochondria in a PINK1-dependent manner, where it ubiquitinates MOM proteins including Mitofusin and Miro. 3) Ubiquitination of MOM proteins triggers mitophagy via mechanism including their proteasomal degradation and autophagy adapter recruitment. Figure adapted from Narendra et al.,(2012).

require the expression of both *PINK1* and *parkin* to proceed (Geisler et al., 2010b; Matsuda et al., 2010; Narendra et al., 2010b; Vives-Bauza et al., 2010; Ziviani et al., 2010). Specifically, Parkin translocation requires the stabilisation of full-length PINK1 on the MOM of mitochondria with a reduced or lost ΔΨm (Figure 1.8, Matsuda et al., 2010; Narendra et al., 2010b). This ΔΨm-dependent PINK1 stabilisation is proposed to occur through the loss of TOM-mediated protein import, and the consequential absence of PARL-dependent PINK1 cleavage (Jin et al., 2010). Through this, PINK1 is no longer rapidly degraded via the N-end rule pathway (Yamano and Youle, 2013). Once stabilised, PINK1 has been shown to associate with the TOM complex on the outer membrane (Lazarou et al., 2012). Rather than performing a mitophagy-specific function, this association is suggested to allow rapid re-import and degradation of PINK1 in the event of mitochondrial repolarisation, hence preventing mitophagy induction. Exogenous expression of a non-cleavable, MOM-targeted form of PINK1 is able to cause Parkin translocation, indicating that PINK1 MOM stabilisation is not only necessary, but sufficient for this event (Narendra et al., 2010b). Additionally, a kinase-

dead version of PINK1 failed to target Parkin to the mitochondria, highlighting the importance of kinase activity in this process (Geisler et al., 2010b; Matsuda et al., 2010). In agreement, a recent study revealed that Parkin translocation required the autophosphorylation of PINK1 following $\Delta\Psi$m (Okatsu et al., 2012).

Once at the MOM, Parkin is suggested to physically interact with PINK1 (Geisler et al., 2010a; Vives-Bauza et al., 2010) via its kinase domain (Geisler et al., 2010b). Importantly, PINK1 has been shown to activate the ubiquitin ligase activity of Parkin (Kondapalli et al., 2012; Matsuda et al., 2010), through the addition of a phosphate group at the highly conserved Ser^{65} of the UBL domain (Kondapalli et al., 2012; Shiba-Fukushima et al., 2012). How this phosphorylation event activates Parkin is yet to be ascertained. However, reports that the UBL-domain confers autoinhibition of the catalytic RBR domain indicate that phosphorylation may alleviate the negative regulation, perhaps via a conformational change in tertiary protein structure, hence activating Parkin (Chaugule et al., 2011; Trempe et al., 2013). Additionally, as mentioned in previous sections, Parkin has been designated as a HECT/RING-hybrid E3 ligase (Wenzel et al., 2011). A recent study proposed that for Parkin to translocate to mitochondria, stably attach to MOM and activate its ubiquitin ligase activity, PINK1 locally activates Parkin; probably by phosphorylation at Ser^{65}; leading to HECT-independent, RBR-dependent Parkin self-binding. This self-binding causes a 6-fold increase in Parkin-complex size, and was suggested to be a prerequisite for both mitochondrial translocation and the activation of Parkin's HECT-like ubiquitin ligase activity (Lazarou et al., 2013). Such events are responsible for Parkin-dependent ubiquitination of MOM proteins, and for the stable association of Parkin with the outer surface of the mitochondria (Figure 1.9). Interestingly, upon mutation of the cysteine residue responsible for Parkin's HECT-like activity (Cys^{431}), Parkin no longer stably associates with mitochondria, indicating that HECT-domain activation is required for this process (Lazarou et al., 2013).

As well as an absolute dependence on PINK1 for translocation, it has recently been shown that Parkin translocation and subsequent downstream events including mitophagy are influenced by another PD-linked gene, *FBXO7/PARK15* (Burchell et al., 2013). Here following CCCP-treatment, FBXO7, associated with the SCF-complex, relocates to mitochondria in a PINK1-dependent manner, via a putative mitochondrial targeting sequence. Silencing of FBXO7 causes a significant decrease in Parkin translocation, leading to the suggestion that FBXO7 may be involved in chaperoning Parkin to mitochondria. Strikingly, FBXO7 overexpression rescued *parkin*- but not *PINK1*-null *Drosophila* phenotypes, indicating that PINK1 activity is necessary for

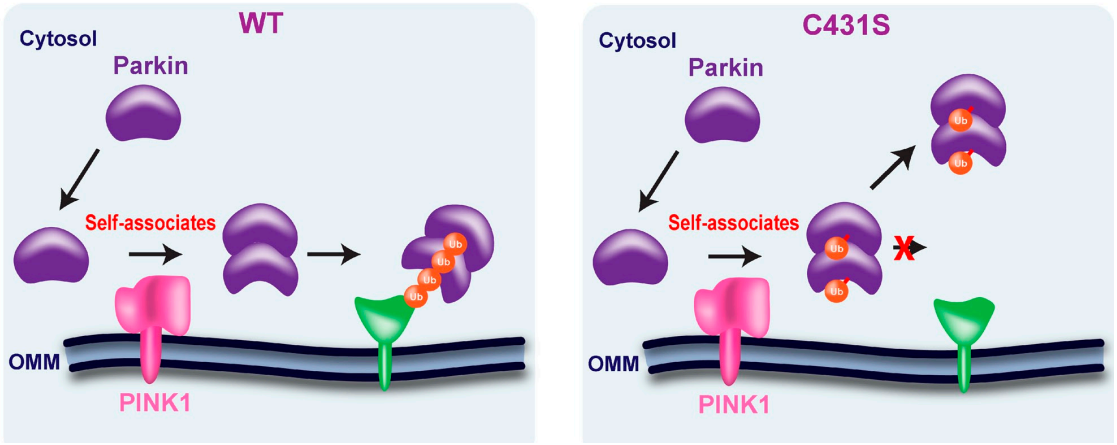

Figure 1.9 Parkin self-association and HECT domain activation. Schematic of Parkin translocation and MOM substrate ubiquitination in wild-type (WT) and mutant (C431S) situations. In wild-type conditions, Parkin self-association is activated by PINK1, which precedes HECT-domain activation, possibly via Ser^{65} phosphorylation, and stable association with the mitochondrial surface via the ubiquitination of MOM substrates. In the mutant situation, Parkin self-association occurs, but stable association with the mitochondrial surface is not observed due to the inactivity of the HECT-domain, and an inability to ubiquitinate target substrates. Figure from Lazarou et al.,(2013).

FBXO7-related function. This finding is supported by a lack of FBXO7-rescue in *PINK1/parkin* double knockout animals. Additionally, the rescue of *parkin*-null phenotypes by FBXO7 overexpression would suggest the involvement of a novel Parkin-redundant E3-ligase in this pathway.

The significance of the Parkin translocation event became clear following the identification of two Parkin substrates, Mitofusin and Miro, both of which reside in the MOM. Following mitochondrial toxification, the MOM pro-fusion factor Mitofusin undergoes Parkin-dependent ubiquitination and subsequent proteasomal degradation, possibly via the ATPase, p97. This process has been demonstrated in *Drosophila*, mammalian and PD-patient fibroblast systems, revealing a high degree of conservation across species (Gegg et al., 2010; Glauser et al., 2011; Poole et al., 2010; Rakovic et al., 2011; Tanaka et al., 2010; Ziviani et al., 2010). Additionally, recent data indicate that the MOM GTPase Miro, involved in trafficking mitochondria along microtubules, also undergoes Parkin-dependent ubiquitination and degradation (Liu et al., 2012). Importantly, this as well as the Parkin-dependent ubiquitination of Mfn2, occurs following a coordinated PINK1-dependent phosphorylation event, demonstrating the degree of built-in regulation in this degradation pathway (Chen and Dorn, 2013; Liu et al., 2012; Wang et al., 2011).

The Parkin-dependent decrease in protein levels of both Mitofusin and Miro following CCCP-treatment is substantial when compared to other reported Parkin substrates such as VDAC1 (Chan et al., 2011). Using a non-biased proteomics approach, Chan

and colleagues showed that both Mitofusin and Miro protein levels decreased, together with a concomitant increase in members of the ubiquitin-proteasome system (UPS). Importantly, as well as UPS induction, adapters of mitophagy including p62 and Atg8/LC3 were enriched on mitochondria, indicating a co-operative role for both systems in the initiation and execution of mitochondrial degradation. In further support, an additional elegant non-biased proteomics study identified both Mitofusin and Miro as Parkin binding partners whose Parkin-dependent ubiquitination states altered under CCCP-toxification conditions (Sarraf et al., 2013). Crucially, to date only Mitofusin and Miro have been shown to be ubiquitinated by endogenous, as well as overexpressed exogenous Parkin (Narendra et al., 2012), highlighting their physiological significance as effectors of the PINK1/Parkin-pathway. As the key role of the pathway appears to be in the maintenance of bioenergetic efficiency via quarantine and removal of unhealthy mitochondria, co-degradation of Mitofusin and Miro prevent transport-dependent re-fusion of failing mitochondria, hence contributing to this function.

Interestingly, Parkin has recently been linked to an increase in mitochondrial biogenesis, by UPS-mediated degradation of PARIS (Shin et al., 2011). In this study, PARIS was found to be a transcriptional repressor of PGC1-α, a transcriptional coactivator involved in mitochondrial biogenesis. Therefore, these data indicate that not only is Parkin involved in the degradation of failing mitochondria, it also plays a putative role in the increased biogenesis of the mitochondrial pool, hence replacing those lost.

To date, the majority of data regarding PINK1/Parkin-mediated mitophagy have originated from studies in cultured cell systems. However, a recent study in *Drosophila* has demonstrated for the first time the occurrence of PINK1/Parkin-mediated mitophagy in an *in vivo* system (Vincow et al., 2013). These data represent a significant advance in our understanding of mitophagy in a physiological context, particularly compared to cancer cell studies where the reliance on mitochondrial oxidative phosphorylation is greatly diminished compared to most post-mitotic tissues.

1.5.5 PINK1/PARKIN-PATHWAY MODEL

In summary of the evidence outlined in previous sections, the PINK1/Parkin-pathway has a clear central role in the maintenance of mitochondrial homeostasis, principally through the mitophagic removal of dysfunctional mitochondria. Under basal conditions, the E3-ubiquitin ligase Parkin remains diffusely localised throughout the cytoplasm, whereas the N-terminal portion of PINK1 is imported into the mitochondria. At the MIM, the MTS is removed by the matrical protease, MPP, followed by the cleavage of the TM domain by the intramembrane protease PARL. This cleavage releases the short

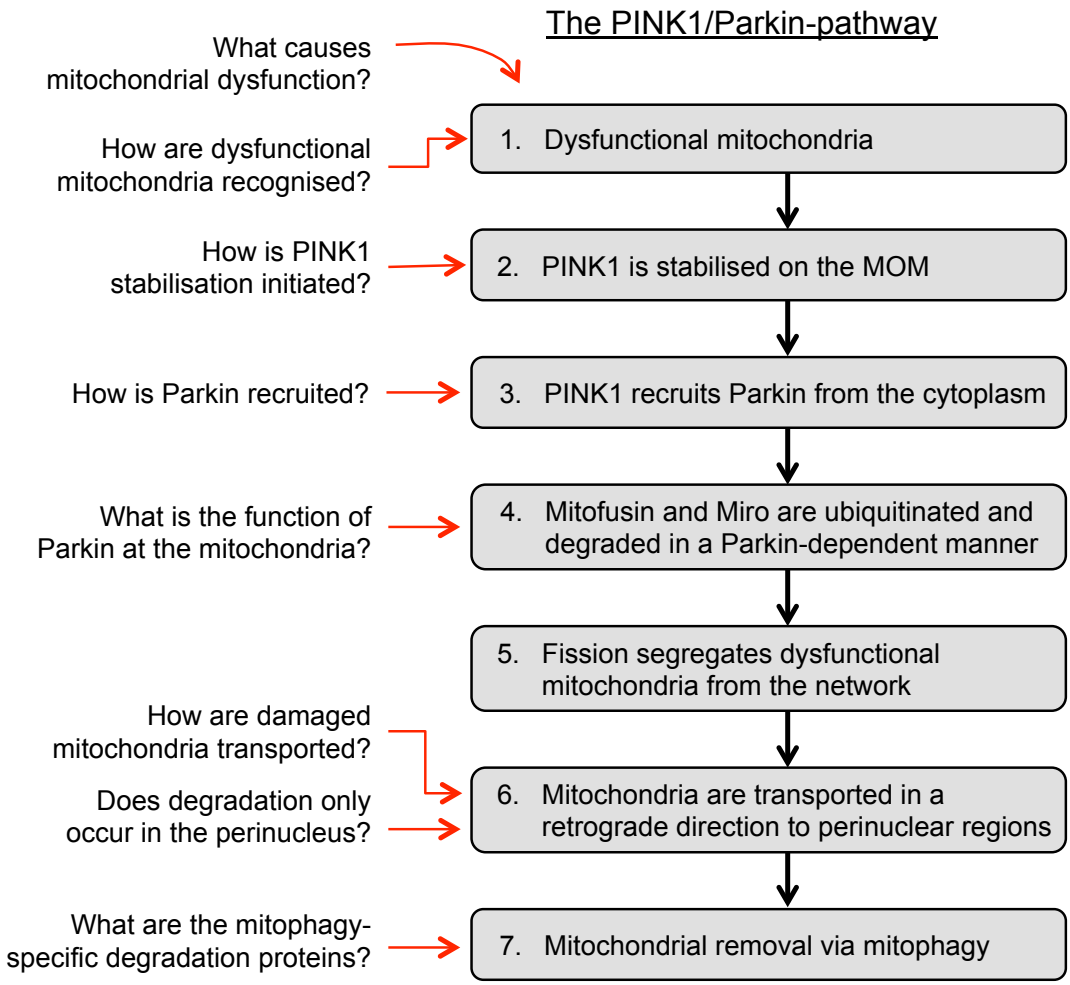

Figure 1.10 PINK1/Parkin-mediated mitophagy. Following mitochondrial membrane depolarisation, dysfunctional mitochondria (1) lose the ability to re-fuse with the healthy mitochondrial network via a down-regulation of OPA1. These mitochondria accumulate full-length PINK1 on their MOM (2), leading to Parkin translocation (3). At the mitochondrial surface, Parkin ubiquitinates a number of MOM substrates including Mitofusin and Miro (4), which are degraded by the proteasome. In the absence of Mitofusin and Miro, dysfunctional mitochondria become isolated via fission (5) and are transported to the juxtanuclear region (6) where mitophagy proceeds (7). Highlighted at each pathway step are mechanistic questions requiring resolution (red arrows).

form of PINK1 into the cytoplasm, where an exposed phenylalanine motif stimulates its proteasomal degradation via the N-end-rule pathway. However, upon mitochondrial damage, such as that inflicted by the application of CCCP, a drop in $\Delta\Psi m$ prevents PINK1 mitochondrial import through the TOM/TIMM23 complexes, blocking the two intramitochondrial cleavage events outlined. PINK1 is stabilised on the MOM, and able to activate the self-association of Parkin, possibly through the phosphorylation of the UBL domain. This acts to alleviate Parkin's autoinhibition, and promotes translocation to the mitochondrial surface. Here, the activation of latent HECT domain activity allows Parkin to stably associate with mitochondria, leading to the poly-ubiquitination of MOM substrates including Mitofusin and Miro. The subsequent UPS-related degradation of these proteins both halts the transport of mitochondria through the cell, as well as inhibiting re-fusion with neighboring mitochondria. Now isolated, dysfunctional

mitochondria undergo mitophagy in a process that is yet to be fully understood, but which may involve the autophagy adapter p62 for cargo selectivity (Figure 1.10, grey).

Despite great advances made in the PINK1/Parkin field over the last 5 years, many outstanding processes require full resolution (Figure 1.10, red arrows). These include the source of mitochondrial damage, and how mitochondrial dysfunction is recognised; the exact mechanism behind PINK1 stabilisation and the mode of Parkin translocation in the absence of a MTS. Additionally, many of the processes downstream of Parkin translocation require clarification including the way in which segregated mitochondria are ultimately eliminated.

1.5.6 CCCP TOXIFICATION IN THE PINK1/PARKIN-FIELD

CCCP is used frequently in the PINK1/Parkin-field, in order to cause a potent toxic insult to the mitochondrial population. Here, CCCP acts as a proton transporter, delivering H^+ ions to the mitochondrial matrix, hence uncoupling the ETC. Through this, CCCP mimics the loss of $\Delta\Psi m$ in unhealthy mitochondria, across the entire cellular population. While this is a harsh cellular insult, and one that is unlikely to occur under physiological conditions, it allows the analysis of processes that may otherwise require the lengthy build-up of toxicity, or occur with such rarity that study is impractical.

1.6 *DROSOPHILA* AS A MODEL ORGANISM

In 1910, Thomas Hunt Morgan first discovered the *Drosophila melanogaster* sex-linked 'white' mutation conferring a change in eye colour from red to white. This discovery paved the way for the use of *Drosophila* as a model organism in the study of genetics, and later development. However, the introduction of ethyl methanesulfonate-induced mutagenesis in the 1960s resulted in a plethora of genetic mutant flies, leading to the discovery of gene function across the breadth of the genome. Importantly, the development of balancer chromosomes in the late 1920s allowed the easy maintenance of gene mutations in heterozygous fly stocks (Bellen et al., 2010).

Despite being an invertebrate model, the study of human disease in *Drosophila* has provided great insight into the mechanisms behind many disorders including the two most prevalent neurodegenerative disorders, Alzheimer's disease and Parkinson's disease. In 2000, the *Drosophila* genome was sequenced revealing ~13,600 genes, which were found the share a high degree of genetic conservation to the human

genome (Adams et al., 2000). Additionally, ~60% of known human disease-causing genes were found to have a clear homolog in *Drosophila*, making this relatively simple organism amenable to manipulation in a human-disease context (Rubin et al., 2000). Also, unlike many murine models of disease, *Drosophila* often recapitulate the symptoms of their human counterparts, perhaps due to a low degree of genetic redundancy compared higher organisms (Guo, 2012). Taken together, these characteristics make *Drosophila* an attractive species for modeling human disease.

With regards to practicalities, *Drosophila* offer many advantages over higher, more complex organisms. Specifically, *Drosophila* produce a large number of offspring, with a short development time of 10 - 12 days. This allows for the generation of large numbers of complex genetic combinations over a relatively short period. Additionally, fly stocks are maintained in small vials, which can be racked and shelved, allowing a great number to be held in a relatively small space. Many genetically divergent *Drosophila* lines can be purchased from a number of central repositories, and for little cost, making genetic studies in *Drosophila* comparatively inexpensive compared to mammalian models. Finally, *Drosophila* offer a great number of excellent genetic tools for the manipulation of pathways at both developmental and adult stages, and in a number of tissues. Specifically, the GAL4/UAS system, developed in 1993, allows gene upregulation and downregulation in the whole fly or specific tissues according to the GAL4 ‘enhancer’ or ‘driver’ employed (Brand and Perrimon, 1993). This system works by crossing two flies, one of which contains the yeast transcriptional activator GAL4, and the other which contains the gene of interest, flanked upstream by the ‘upstream activating sequence’ or ‘UAS’ promoter. This promoter contains five GAL4 binding sites, therefore undergoing transcriptional activation only in tissues expressing the GAL4 protein. In the offspring of these animals, genetic combinations with both GAL4- and UAS-containing alleles will express the gene of interest through the activation of UAS by GAL4 (Figure 1.11). Importantly, the accumulation of a wide range of tissue- and stage-specific GAL4 drivers means that gene expression can be spatially and temporally controlled. Not only is this useful for studying the effects of ectopically expressed genes, it also allows functional studies of genes whose whole-body expression would otherwise be lethal, preventing the easy maintenance of stocks. Additionally, a common practice is to utilise the GAL4/UAS system in the expression of fluorescently tagged proteins, increasing the ease of live-imaging via fluorescence microscopy analysis.

This system is also used to drive RNAi expression, allowing for loss of function analyses. This is useful where a genetic null is lacking, or when the effect of eliminating

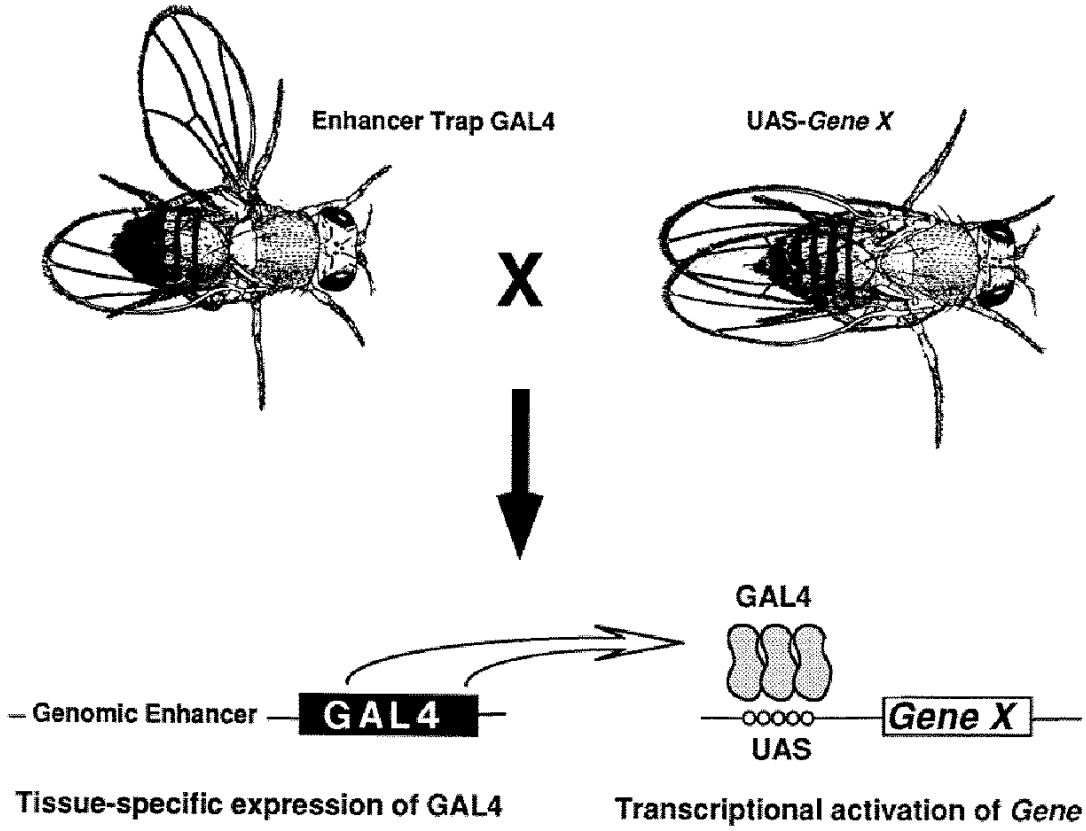

Figure 1.11 GAL4-UAS system in *Drosophila.* Schematic representation of the GAL4/UAS system involved in spatially and temporally regulating exogenous gene expression in *Drosophila.* This technique involves crossing parental flies with either an integrated, tissue specific GAL4 enhancer, or a gene of interest (Gene X) flanked upstream by a UAS promoter. Resultant offspring will express Gene X in tissues where GAL4 is driven. Figure from Brand and Perrimon,(1993).

expression completely causes a severe or fatal phenotype. A number of groups have created *in vivo* RNAi libraries, able to target the vast majority of the *Drosophila* genome (Dietzl et al., 2007; Ni et al., 2009). These RNAi stocks are readily available and provide an excellent tool for large-scale analyses such as genetic screening.

For many years, *Drosophila* have been used in the study of a number of different diseases, particularly those linked to neurological disorders. These include Huntington's disease, Alzheimer's disease, Tauopathies, Parkinson's disease and Prion disease. Whilst these models often lack the full extent of pathology seen in human patients, in many cases neurodegeneration is observed together with aberrant accumulation of disease-relevant proteins and toxic inclusions (Jeibmann and Paulus, 2009). In particular, *Drosophila* models of Parkinson's disease are able to faithfully recreate many of the pathological features of its human counterpart. Specifically, loss of either *dPINK1* or *dparkin* produces a set of phenotypes including DA neuron loss, mitochondrial dysfunction and locomotor difficulties (Clark et al., 2006; Greene et al., 2003; Park et al., 2006; Pesah et al., 2004; Whitworth et al., 2005; Yang et al., 2006).

Importantly, work in *Drosophila* revealed for the first time that PINK1 acts upstream of Parkin in the same linear pathway, with mitochondrial dysfunction central to the pathology (Clark et al., 2006; Deng et al., 2005; Greene et al., 2003; Park et al., 2006; Yang et al., 2006). This discovery has revolutionised the ideas behind the etiology of PD, and steered the field towards mitochondrial biology, rather than the protein accumulation and ROS theories of earlier years.

1.7 HIGH CONTENT RNAi SCREENING

High content RNA interference (RNAi) screening techniques have offered a powerful, unbiased way of identifying novel genes involved in a wide array of different processes. RNAi approaches use synthetic oligonucleotides to 'silence' gene expression, allowing the analysis of 'loss of function' phenotypes. This technique takes advantage of endogenous cellular machineries whose role is to degrade foreign double-stranded RNA (dsRNA) from external sources such as viruses. The mechanism by which RNAi transiently silences genes in a post-transcriptional manner is well defined, and largely conserved across all eukaryotes. Briefly, long dsRNA sequences are broken into small fragments known as small interfering RNA (siRNA), by the RNase enzyme Dicer. These siRNAs are unwound into single-stranded fragments following ATP-hydrolysis, and integrated into the RNA-induced silencing complex (RISC), where target mRNA recognition and Argonaute-dependent degradation takes place (reviewed in Hannon and Rossi, 2004). From an experimental point of view, *Drosophila* cells exposed to exogenous dsRNA sequences efficiently activate this pathway, producing a gene-specific silencing effect. However, in a manner divergent from *Drosophila,* mammalian systems exposed to dsRNA activate a concomitant interferon immune response, leading to non-specific RNA degradation together with a decrease in protein synthesis. In order to circumvent these non-specific effects, it was found that exposure to short, 21 bp siRNA sequences could produce a gene-specific silencing effect in the absence of immune-system activation (Elbashir et al., 2001). Therefore, experiments in *Drosophila* systems typically incorporate long dsRNA sequences, whereas mammalian systems are limited to siRNA sequences.

The ease of RNAi-dependent gene silencing, coupled with the completion of human and *Drosophila* whole-genome sequencing has led to the development of high-throughput RNAi screening techniques for forward-genetic approaches in cultured cell systems. The most frequently utilised cell-types are those derived from *Drosophila* and mammalian systems. Each presents its own advantages and disadvantages. For example, many *Drosophila* cell lines will take up dsRNA without the need for

transfection reagents (Clemens et al., 2000), whereas mammalian cells require siRNA delivery across the plasma membrane. Such delivery not only substantially increases the cost of high-throughput screening, but often causes intracellular toxicity which demands significant optimisation. Additionally the low redundancy of the *Drosophila* genome compared to the human genome can facilitate data interpretation. However, whilst high conservation exists between *Drosophila* and human genomes, divergent pathways and processes do occur, ultimately making human cell systems more relevant in a human-disease setting.

The first *Drosophila* dsRNA library was developed by Norbert Perrimon and colleagues in 2004 (Boutros et al., 2004). This library covers almost every gene in the *Drosophila* genome, and has since undergone complete re-design and modification to reduce off-target effects (Horn et al., 2010). Importantly, these dsRNA sequences have been incorporated into an *in vivo Drosophila* library, allowing easy transition between cell-based and whole-organism analysis.

To date, very few RNAi cell-based screens focusing on PD etiology have been published. Of these, a whole genome RNAi screen in HeLa cells identified the HECT-domain ubiquitin ligase, SMURF1 as playing a role in the promotion of Parkin-dependent mitophagy. Here, SMURF1 is predicted to interact with p62, suggesting a role in selective mitophagy (Orvedahl et al., 2011). Additionally, a recent whole genome screen also in HeLa cells assessed modifiers of Parkin translocation following CCCP-toxification. Here, *ATPase inhibitory factor 1 (ATPIF1*) was identified as an essential factor for Parkin translocation, whose absence led to the reversal of ATP-synthase and the maintenance of the $\Delta\Psi m$ (Lefebvre et al., 2013). Finally, a further HeLa cell screen looking at Parkin translocation identified the glycolysis-related gene, *Hexokinase 2* as important for this process. This finding links the regulation of metabolic pathways to the activation of PINK1/Parkin-mediated mitophagy. As techniques develop and technologies such as high-throughput microscopy and automated data capture improve, we are likely to see many more of these high-throughout approaches in both the PD field and other disciplines.

1.8 AIMS OF THE THESIS

The aim of this thesis is to identify novel promoters of PINK1/Parkin-mediated mitophagy by the means of whole-genome RNAi screening in *Drosophila* S2R+ cells. Specifically, I aim to identify genes acting upstream of Parkin translocation following a

short toxification with CCCP. Predicted hits from this screen would be genes involved in the identification of dysfunctional mitochondria for degradation, as well as those involved in the relocation of Parkin from the cytoplasm to the mitochondrial surface.

Following the completion of the primary whole genome screen, hits will be tested for an ability to influence other aspects of mitochondrial homeostasis in a series of secondary screens. As highlighted, both *PINK1*- and *parkin* deficiency cause a hyperfused mitochondrial network in *Drosophila* systems. Taking advantage of this observation, hits will be assessed for their ability to either phenocopy, or produce an alternative mitochondrial morphology to *PINK1*- or *parkin* loss. Additionally, prior to mitophagy, mitochondria are frequently observed as an aggregated mass in the perinuclear region. Importantly, loss of *PINK1* or *parkin* prevents this phenomenon, with mitochondria remaining diffusely distributed throughout the extent of the cytoplasm. Therefore, hits will be assessed for an ability to prevent perinuclear aggregation following toxification, thus phenocopying the effect observed following *PINK1* and *parkin* silencing. Finally, to ensure that Parkin translocation is dependent on general mitochondrial damage rather than CCCP-specific effects, hits will be assessed for their ability to block paraquat-induced translocation.

Upon completion of secondary screen analysis, a final list of *Drosophila* screening hits will be collated, comprising of genes able to influence a diverse set of mitochondrial homeostatic processes with clear links to the PINK1/Parkin-pathway.

To evaluate the ability of final *Drosophila* hits to influence PINK1/Parkin-mediated mitochondrial quality control in a more complex system, human orthologs will be identified, and screening will switch to a HeLa cell-based system. Here, both CCCP-induced Parkin translocation and mitophagy will be assessed, producing an overall hit list of human genes with a clear influence on both of these processes. After bioinformatic scrutiny, a small number of human hit genes will be selected for low-throughput analysis whereby a functional involvement in the PINK1/Parkin-pathway itself will be tested. For this, both *in vivo Drosophila*, and cell-based biochemical techniques will be employed, in order to elucidate the relationship between hit genes, *PINK1* and *parkin*.

2. MATERIALS AND METHODS

2.1 CELL CULTURE TECHNIQUES

2.1.1 *DROSOPHILA* CELL LINES

For the purpose of *Drosophila melanogaster* whole genome screening, Schneider 2 receptor plus cells (S2R+), an isolate of Schneider 2 cells, were chosen for their increased ability to adhere to culture surfaces (Yanagawa et al, 1998). S2R+ cells were derived from a primary culture of late-stage embryonic tissue and are suggested to be of a macrophage-like lineage (Schneider, 1972). When compared to other available *Drosophila* cell lines. S2R+ cells are ideal for the visualisation of cytoplasmic structures due to their relatively large size (~15 µm diameter) and flattened appearance.

2.1.1.1 Cell culture

Drosophila S2R+ cells have a doubling time of approximately 39 hours, and were grown at 25 ºC in the absence of CO_2. Both S2R+ and Parkin-GFP.S2R+ cell lines were passaged in T75 flasks (Greiner, 658170) every 3 - 4 days, at a ratio of 1:5. Normal culture media (NCM) consisted of Schneider's *Drosophila* Medium 1X liquid with L-Glutamine (SM) (Gibco, 21720-024), 10% fetal bovine serum (FBS) (v/v) (Sigma, F4135) and 1% Penicillin-Streptomycin (v/v) (Sigma, P4333). Media was filtered (Millipore, SCGPU05RE) and stored at 4ºC.

Whole genome screening required the creation of an S2R+ cell line stably expressing pMK33-Parkin-GFP (Parkin-GFP.S2R+). This population was maintained through the addition of 300 µg/ml Hygromycin B (Invitrogen, 10687-010) to NCM.

Cells were routinely maintained to a maximum of 25 - 30 passages. Following this, a fresh aliquot of cells would be defrosted, and aged to a passage number of 2 - 3 before being applied to an experimental scenario.

2.1.1.2 Freezing cell cultures for long-term storage

Cell cultures were expanded and grown to full confluency in T75 flasks. Following manual detachment and re-suspension, cultures were transferred to 15 ml falcons (Starlab, E1415-0800) and pelleted by centrifugation at 1200 rpm. Media was aspirated and cells re-suspended in 1 ml of freezing medium (20% FBS (v/v), 10% Dimethly sulfoxide (DMSO) (v/v) (Sigma, D2650) in SM; filtered). Cultures were transferred to

cryovials (Nalgene, V4757) and placed at -80 ºC for 24 hours in propan-2-ol, before being submerged in liquid nitrogen.

2.1.2 HUMAN CELL LINES

For the purpose of human cell screening and subsequent follow-up data, two human cell lines were implemented: HeLa cells; derived from cervical cancer tissue, and retinal pigment epithelial 1 (RPE1) cells, derived from retinal pigmented epithelium.

HeLa and RPE1 cell lines stably expressing pLVX-Puro-YFP-Parkin were a kind gift from Dr Jon Lane (University of Bristol). They were made using a YFP-Parkin plasmid (Addgene - 23955, Narendra et al, 2008), sub-cloned into pLVX-Puro (Clontech, 632164) and delivered using Lenti-XTM HT Packaging System (Clontech, 632160). Cells were selected using 10 - 15 µg/ml Puromycin (Sigma, P8833) and FACs sorted.

2.1.2.1 Cell culture

Human cells were grown at 37 ºC in 95% air, 5% CO_2. Both HeLa and RPE1 cell lines were passaged in T75 flasks every 3 - 4 days, at a ratio of 1:5. When passaging, all reagents were heated to 37 ºC to avoid cell shock. Existing media was aspirated and cell cultures washed with 5 ml phosphate buffered saline (PBS) (Thermo Scientific, OXBR0014G) to remove traces of serum. 2.5% Trypsin (Gibco, 15090-046) (2 ml per flask) was added and cells returned to the incubator for 10 - 20 minutes. Cells were re-suspended by manual pipetting, and passaged following the addition of 10 ml NCM.

Cells were maintained for a maximum of 25 passages before being replaced by a freshly defrosted aliquot. These were aged to passage number of 2 - 3 before being applied to an experimental scenario.

2.1.2.2 HeLa cells

HeLa cells have a doubling time of 24 hours. Normal culture medium consisted of MEM with HEPES & GlutaMAX™ (Gibco, 42360-032), with 10% FBS (v/v) and 1% Penicillin-Streptomycin (v/v), which was filtered and stored at 4ºC.

2.1.2.3 RPE1 cells

RPE1 cells have a doubling time of 19 hours. Normal culture medium, contained DMEM/Nutrient mixture F-12 Ham (Sigma, D8062), with 10% FBS (v/v) and 1% Penicillin-Streptomycin (v/v), which was filtered and stored at 4ºC.

2.1.2.4 Freezing cell cultures for long-term storage

Cell cultures were frozen following the protocol detailed in 2.1.3. Freezing medium consisted of 50% FBS (v/v) and 10% DMSO (v/v) in the appropriate medium (see above).

2.2 GENE KNOCKDOWN

The following protocols are designed for use in a 12-well format. For other formats, volumes were adjusted according to culture surface area.

2.2.1 GENE SILENCING - *DROSOPHILA* CELLS

dsRNA was seeded at 5 µg per well. Media was aspirated from cells, and replaced with serum-free SM (SFSM). Cells were manually re-suspended and counted using a haemocytometer. 200,000 cells per well were plated in 500 µl of SFSM and incubated at 25 ºC for 1 hour. Following this, 500 µl of 2x FBS-containing media was added, and cells were incubated at 25 ºC for 3 - 4 days.

2.2.2 GENE SILENCING - HUMAN CELLS

A number of siRNA delivery techniques have been implemented in order to optimise knockdown for various cell types. These include Dharmafect1 (Dharmacon, T2001-02), Lipofectamine 2000 (Invitrogen, 11668-027) and Effectene (Qiagen, 301425) transfection reagents. In each case, the transfection protocol was performed according to manufacturers instructions.

Both forward and reverse delivery techniques have been investigated, but largely, reverse transfection was employed. Additionally, a range of siRNA concentrations have been used, from 25 - 100 nM. Following optimisation, a concentration of 25 nM was chosen for screening purposes and follow-up experiments.

2.2.2.1 Reverse transfection

In general, siRNA was seeded in culture plates at a final concentration of 25 nM. Transfection reagents were mixed and incubated with siRNA *in situ*, in serum and antibiotic-free media (SAbFM). Cells were plated directly into culture plates at an appropriate density, in antibiotic-free media (AbFM), and incubated at 37 ºC. Depending on the reagent, media was replaced with NCM 6 - 20 hours post-transfection to reduce cytotoxicity, and plates incubated for a further 3 - 4 days.

2.2.2.2 Forward transfection

In general, cells were seeded in culture plates and incubated overnight in NCM. Transfection reagents and siRNA were mixed in a microcentrifuge tube and incubated according to manufacturers instructions. Existing media was aspirated and replaced with AbFM, and transfection complexes were added drop-wise to culture plates. Depending on the reagent, media was replaced with NCM 6 - 20 hours post-transfection to reduce cytotoxicity, and plates incubated for a further 2 - 3 days.

2.3 PLASMID TRANSFECTION

For both *Drosophila* and human cells, plasmids were delivered using Effectene transfection reagent. Briefly, in a 12-well plate, 0.3 µg of expression plasmid was delivered following the protocols detailed in 2.2.2.1 and 2.2.2.2. Expression of most plasmids could be detected 12 - 24 hours post-transfection.

2.4 HIGH CONTENT RNAi SCREENING

2.4.1 WHOLE GENOME SCREENING - *DROSOPHILA* CELLS

A *Drosophila* whole genome RNAi library was purchased from the Sheffield RNAi Screening Facility (SRSF). This consisted of 18,434 dsRNA amplicons, arrayed in 53 clear-bottomed 384-well plates (PerkinElmer, 60017460). Each well contained 5 µl of dsRNA at a concentration of 50 µg/ml, giving 250 ng of dsRNA per well.

2.4.1.1 Protocol

Prior to screening, eight pre-defined user controls were spiked into columns 9 and 17 of each plate. On the day of screening, plates were defrosted and centrifuged briefly. Parkin-GFP.S2R+ cells, at a density of 6,000 cells per well, were dispensed in 30 µl of SFSM, and plates were incubated at 25 ºC. After 1 hour, 30 µl of 2x FBS-containing media was added, and cells were incubated for a further 3 days. A solution of copper sulphate (final concentration, 500 µM) in SM was added to each well, inducing the expression of Parkin-GFP via the metallothionein promoter. After 16 hours, cells were toxified with Carbonyl cyanide *m*-chlorophenyl hydrazone (CCCP)-containing SM at a final concentration of 10 µM and incubated for a further 2 hours before fixation and nuclear staining with Hoechst-containing formaldehyde. Plates were washed 3x with PBS, sealed and imaged using an ImageXpress Micro widefield high content screening microscope (Molecular Devices).

2.4.1.2 Stock solutions

Copper sulphate: 100 mM Copper (III) Sulphate (Sigma, C1297) in water.
CCCP: 10 mM CCCP (Sigma, C2759) in ethanol.
Formaldehyde solution: 3.7% formaldehyde solution (Sigma, F1635) in PBS with 2 mg/ml Hoechst (Invitrogen, 33342).

2.4.1.3 Equipment

All solutions apart from CCCP-containing SM were dispensed using either a Multidrop Combi Reagent Dispenser or Multidrop 384 Reagent Dispenser (Thermo Scientific, 5840300 & 5840150). CCCP-containing SM was dispensed using a MICROLAB® STAR Liquid Handling robot (Hamilton). Plates were sealed using a PlateLoc® thermal plate sealer (Velocity11) after each protocol step. Following toxification, all liquid aspiration steps were carried out using an ELx405 Select Deep Well Microplate Washer (BioTek). For automated plate imaging, plates were stacked onto an 'Automate.it Scara' system (PAA) and loaded systematically onto the microscope by a robotic arm.

All high-content screening images were acquired using an ImageXpress Micro widefield high content screening microscope (Molecular Devices). The chosen magnification for whole genome screening was 40x (CFI S Plan Fluor ELWD 40X, Nikon), with 9 fields of view (FOV) being acquired per fluorophore, per well. Parkin-

GFP was imaged using a GFP filter cube (1-6300-0450, Molecular Devices) and Hoechst was imaged via a DAPI filter cube (1-6300-0442, Molecular Devices).

2.4.1.4 Data analysis

Microscopy images were analysed automatically using the pre-programmed 'Transfluor' application (Molecular devices). Here, parameters were optimised to enable the detection of puncta between 0.6 – 1 μm in size, and 60 grey levels above local background intensity. From this, each FOV was assigned a corresponding 'mask' image, and value for 'average number of puncta per cell.' Across the 9 FOV, the 'mean number of puncta per cell' was found, producing one value per well. Following analysis of the entire dataset, data were normalised using the 'robust z-score' incorporating the 'median absolute deviation', where a z-score of zero represented the median (Fisher et al, 2012). Primary hits were defined as those with a z-score ≤ -3.

2.4.2 CONFIRMATION SCREENING - *DROSOPHILA* CELLS

The confirmation library was synthesised by matching hit dsRNA amplicons to their unique 'BKN' identifier, allowing stock PCR templates to be located. PCR-picking was automated, using a MICROLAB® STAR Liquid Handling robot. Additional, amplicon templates from the kinome / phosphatome subset library were hand picked and spiked into the appropriate locations within the destination plate. The template library was printed into plates containing the '*in vitro* transcription' reaction outlined in 2.6.1, and dsRNA synthesis could proceed. Upon completion, dsRNA underwent dilution to reduce the possibility of pipetting errors, before being transferred to deep-well mother plates. Here, the stock dsRNAs underwent further dilution to achieve a working concentration of 5 ng/μl, before the printing of multiple copies of the confirmation library.

2.4.2.1 Protocol

The 'confirmation' assay protocol was identical to that outlined in 2.4.1.1, where Parkin-GFP.S2R+ cells were toxified for 2 hours with CCCP (10 μM).

2.4.2.2 Data analysis

Image acquisition and analysis was automated as in 2.4.1.3 and 2.4.1.4. Per confirmation round, a hit amplicon was any dsRNA with an average puncta score within two standard deviations (SD) of the mean of the 'No CCCP' control. Over four rounds

of screening, each time an amplicon appeared in the hit list it was given a score of 1. Upon completion of the four repeat screens, the score from each screening round was totalled, producing an overall 'score' for each dsRNA. If a gene had more than one dsRNA amplicon in any one of the four hit lists, that gene would gain an extra 'multiples score' of 0.5, producing a maximum screen score of 4.5. For a hit to become 'confirmed,' an arbitrary cut-off of 2.5 was defined.

2.4.3 SECONDARY SCREENING - *DROSOPHILA* CELLS

2.4.3.1 Paraquat-induced Parkin translocation

Confirmation library plates were defrosted and briefly centrifuged. 6,000 Parkin-GFP.S2R+ cells per well were plated in SFSM, and incubated for 1 hour at 25 ºC. 2x FBS-containing media was added, and cells incubated for a further 48 hours at 25 ºC. Parkin-GFP expression was induced for 16 hours with 200 µM copper sulphate, before toxification with 10 mM paraquat (Sigma Aldrich, 856177) for 24 hours. Samples were fixed with ice-cold methanol, and processed for imaging. This included the application of 0.2 µg/ml anti-ATP5A (MS507, Mitosciences), 2 µg/ml anti-Alexa Fluor 594 (A-11005, Molecular Probes), and 2 mg/ml Hoechst (Invitrogen, 33342).

Parkin translocation images were acquired as in 2.4.1.3, and data quantified as in 2.4.1.4. The assay was performed in triplicate. Per screening round, a hit amplicon was any dsRNA with a raw puncta score within 2 SD of the mean of the vehicle-treated negative control dsRNA. Over three rounds of screening, each time an amplicon appeared in the hit list, it was given a score of 1. Upon completion of the three screens, the score from each round was totalled, producing an overall 'score' for each dsRNA. Assay hits required a minimum score of 2 out of 3.

2.4.3.2 Mitochondrial morphology analysis

Confirmation library plates were defrosted and briefly centrifuged. 4,000 S2R+ cells per well were plated in SFSM, and incubated for 1 hour at 25 ºC. 2x FBS-containing media was added, and cells incubated for a further 96 hours at 25ºC. Media was then aspirated, and replaced with NCM, containing 150 nM of MitoTracker Red (MTR) (M-7512, Molecular Probes) and Hoechst (2 mg/ml). After an incubation of 15 minutes, media was replaced, and live cells were imaged immediately on the high content screening microscope.

Morphology images were acquired as in 2.4.1.3, using a Texas Red® filter cube (1-6300-0449, Molecular Devices) for MTR detection, and a DAPI filter cube (as in 2.4.1.3) for Hoechst detection. Data were quantified manually using a 4-point morphology scoring system, where 1 = fragmented, 2 = wild-type, 3 = fused and 4 = clumped mitochondria (Pogson et al., manuscript in preparation). Here, each FOV was assigned an overall population score, which was averaged over 9 FOV producing an 'average mitochondrial morphology score' for each dsRNA amplicon. This assay was performed in isolation, with hits defined as any dsRNA with an 'average mitochondrial morphology score' ± 2 SD of the mean of the negative control dsRNA.

2.4.3.3 Mitochondrial perinuclear aggregation

Mitochondrial perinuclear aggregation was assessed using the protocol outlined in 2.4.3.1. Here, perinuclear aggregation images were acquired as in 2.4.1.3 using a Texas Red® filter cube (as in 2.4.3.2) for ATP5A detection, and a DAPI filter cube (as in 2.4.1.3) for Hoechst detection. Per condition, 4 FOV were acquired using a 10x objective (10x Plan Fluor NA 0.30, Nikon). Data were quantified manually using a 3-point scoring system, where 1 = diffuse mitochondria, 2 = mixture of diffuse and aggregated mitochondria and 3 = aggregated mitochondria. Here each FOV was assigned an overall population score, which was averaged over 4 FOV producing an 'average mitochondrial perinuclear aggregation score' for each dsRNA amplicon. This assay was performed in triplicate. Per screening round, a hit amplicon was any dsRNA with a mitochondrial perinuclear aggregation score ± 2 SD of the mean of the paraquat-treated negative control dsRNA. Over three rounds of screening, each time an amplicon appeared in the hit list, it was given a score of 1. Upon completion of the three screens, the score from each round was totalled, producing an overall 'score' for each dsRNA. Assay hits required a minimum score of 2 out of 3.

2.4.4 HUMAN CELL SCREENING

A custom library of human siRNA probes was ordered, comprising a total of 98 siGENOME SMARTpool siRNAs (Dharmacon), including 8 control wells. siRNAs were supplied as 0.1 nmol dry pellets, arrayed over two 96-well plates. Resuspension involved the addition of 50 µl RNase-free water per well, for a final stock concentration of 2 µM. Prior to the addition of water, plates were briefly centrifuged to collect the siRNA pellet at the bottom of each well, and the foil lid sterilised with 70% ethanol. In a laminar flow cabinet, the foil lid was removed and 50 µl of water was added to each well by multi-channel pipette. Plates were then resealed, and placed on an orbital

mixer for 2 hours at room temperature to ensure total resuspension. Six copies of the library were printed into 96-well clear-bottomed assay plates (Greiner, 655090), allowing a final siRNA concentration of 25 nM (1.25 µl/well). Assay plates were barcoded with a plate identifier and placed at -20 ºC until required.

2.4.4.1 Parkin translocation

To assess Parkin translocation, plates were defrosted, and centrifuged briefly. A solution of 'Dharmafect 1' (DF1) transfection reagent (0.2 µl / well) (Dharmacon, T-2001) in SAbFM (18.55 µl / well) was arrayed across assay plates using a multi-channel pipette, and left to complex with the siRNA for 30 minutes at room temperature. 4,000 YFP-Parkin.HeLa cells in 80 µl AbFM were plated per well, and incubated for 24 hours at 37 ºC. Media was replaced with NCM, and plates incubated for a further 72 hours. Media was exchanged for vehicle- or CCCP-containing media (10 µM) for 4 hours, before fixation with ice-cold methanol for 10 minutes. Samples were processed for imaging by the addition of anti-ATP5A, anti-AlexaFluor 594 and Hoechst, as in 2.4.3.1.

Images were captured using the ImageXpress Micro widefield high content screening microscope (Molecular Devices), with a 10x objective (10x Plan Fluor NA 0.30, Nikon). Three channels were acquired using a YFP filter cube (1-6300-0448, Molecular devices) for YFP-Parkin detection, a Texas Red® filter cube (as in 2.4.3.2) for ATP5A detection, and a DAPI filter cube (as in 2.4.1.3) for Hoechst detection. 9 FOV were acquired per well. Each FOV was analysed manually using a five-point system. Here, 0 = dead or low-YFP expressing cells, 1 = < 10% of cells with Parkin translocation, 2 = between 10 - 50% of cells with Parkin translocation, 3 = between 50 - 90% of cells with Parkin translocation, and 4 = > 90% of the cells with Parkin translocation. Over the 9 FOV, the 'average Parkin translocation score' per well was calculated. This assay was performed in triplicate. Per screen, hits were siRNAs with a score ± 3 SD of the mean of the CCCP-treated negative control siRNA. Each time a siRNA appeared in the hit list, it achieved a score of 1. Upon completion of the three screens, the score from each round was totalled, producing an overall 'score' for each siRNA. For a siRNA to be deemed an overall 'hit', a minimum score of 2 out of 3 was required.

2.4.4.2 Mitophagy

Protocol as in 2.4.2.2 but with the following deviations: seed-cell density; 10,000 cells per well, post media-change incubation duration; 48 hours, toxification duration; 24 hours.

Each FOV was analysed manually using a five-point system. Here, 0 = dead or low-YFP expressing cells, 1= a full complement of mitochondria, 2 = an overall reduced mitochondrial signal, 3 = a reduced mitochondrial signal, plus ~ 10% of cells with no mitochondria, and 4 = a reduced mitochondrial signal plus > 20% of cells with no mitochondria. Over the 9 FOV, the 'average mitophagy score' per well was calculated. Hits were defined as in 2.4.4.1.

2.4.5 BIOINFORMATICS

The 'DRSC Interactive Ortholog Prediction Tool' (DIOPT) was used to convert *Drosophila* genes into human orthologs (Hu et al, 2011). Known and predicted protein interactions were assessed using STRING 9.0 ('Search Tool for the Retrieval of Interacting Genes/Proteins') (Jensen et al, 2009). Gene symbol, name and function were acquired from a number of sources including FlyBase, Uniprot and NCBI gene.

2.5 MOLECULAR BIOLOGY - DNA

2.5.1 POLYMERASE CHAIN REACTION (PCR)

General DNA amplification was performed in a 'Mastercycler personal' thermal cycler (Eppendorf) using standard protocols. Either 'Platinum Taq' (Invitrogen, 10966018) or 'Phusion High Fidelity' (Thermo Scientific, F-530) DNA polymerase was employed depending on the assay. Efficiency and fidelity of the PCR reaction was checked using a 'NanoDrop 1000' spectrophotometer (Thermo Scientific), and gel electrophoresis.

Amplification of DNA templates from the 'Sheffield RNAi Screening Facility' (SRSF) for the synthesis of dsRNA required a touchdown PCR protocol, and incorporated 'Reddymix PCR mastermix' (Thermo Scientific, AB-0575) and a standardised set of primers incorporating a T7 tag (uppercase – see section 2.6.1), upstream of a library position-specific primer sequence (lowercase):

TU	TAATACGACTCACTATAGGGtggcgcccctagatg
T1	TAATACGACTCACTATAGGGcgacgcccgctgata
T2	TAATACGACTCACTATAGGGtaggtctagccccgc
T3	TAATACGACTCACTATAGGGcgcatgtagcctgcc
T4	TAATACGACTCACTATAGGGtagcctccctagcgc

2.5.2 TRANSFORMATIONS

Plasmid preparations were expanded using bacterial transformation of 'Library Efficiency® DH5α™ competent cells' (Invitrogen, 18263-012). This process involved incubating 50 µl defrosted competent cells with 1 µl plasmid DNA on wet ice for 30 minutes, before heat shocking at 42 ºC for 45 seconds. The mixture was then returned to ice for 2 minutes, before the addition of 200 µl pre-warmed Luria-Bertani (LB) broth. The transformation was transferred to a shaker, set at 37 ºC, 225 rpm for ~ 60 minutes, before being streaked onto pre-warmed LB agar plates containing the appropriate antibiotic. Plasmid-containing bacterial colonies were grown on LB agar plates for 16 hours at 37 ºC before bacterial expansion in suspension culture.

2.5.3 PLASMID PREPARATION

Following plasmid transformation into bacterial cells, clonal colonies were picked and grown on in mini- or midi-suspension cultures depending on the amount of plasmid required. Small-volume mini-cultures (~5 ml of LB) were purified using the 'QIAprep Spin Miniprep Kit' (Qiagen, 27104), and large-volume midi-cultures (~100 ml of LB) were purified using the 'HiSpeed Plasmid Midi Kit' (Qiagen, 12643). Each format was executed as per the manufacturers instructions. In each case, plasmids were eluted in PCR-grade water (Sigma, W4502) and assessed using gel electrophoresis for product specificity, and NanoDrop spectrophotometry for product concentration.

2.5.4 PLASMIDS UTILISED

Below is a table of all expression plasmids used in this project.

Transgene	Vector	Species	Source
Mitofusin-FLAG	pAct-PPA	*Drosophila*	Elena Ziviani
Mito-GFP	pAct-PPA	*Drosophila*	Elena Ziviani
Parkin-GFP	pMK33	*Drosophila*	Elena Ziviani
PINK1-Myc	pMK33	*Drosophila*	Venus Ho
YFP-Parkin	pEYFP-C1	Human	Richard Youle
PINK1-GFP	pEGFP-N1	Human	Emma Deas

2.6 MOLECULAR BIOLOGY - RNA

2.6.1 GENERATION OF dsRNA

For *Drosophila* gene silencing, dsRNA probes were synthesised. For this, PCR templates flanked by the T7 promoter sequence are utilised. These PCR templates were either synthesised 'in house' or acquired from the SRSF as described in 2.5.1. dsRNA probes were synthesised using an *in vitro* transcription 'MEGAscript' kit (Ambion, AM1334), performed to manufacturers instructions. Following *in vitro* transcription, dsRNA preparations were purified by the addition of 1 µl TURBO DNase for 30 minutes at 37 ºC, followed by 2.1 µl ammonium acetate 'stop solution' and 52.5 µl ethanol. The solution was then placed at -80 ºC for 2 hours to enhance precipitation, followed by centrifugation for 1 hour at 14,000 rpm, 4 ºC. The supernatant was drawn off in a laminar flow hood, and the dsRNA pellet allowed to air dry before resuspension in 100 µl PCR-grade water (Sigma, W4502). The efficiency of the reaction and fidelity of the dsRNA probes were assessed by NanoDrop spectrophotometry and gel electrophoresis.

2.6.2 HUMAN siRNA ACQUISITION

Human siRNAs used throughout this study were acquired from Dharmacon (Thermo Scientific) as siGENOME SMARTpools. For low-throughput analysis, frequently used siRNA probes include control, *PINK1*, *parkin*, *SREBF1* and *FBXW7*. Below are the four siRNA sequences making up the SMARTpool for each gene target.

Product code	Gene Symbol	Gene ID	Gene Accession	GI Number	Sequence
M-004030-02	*PINK1*	65018	NM_032409	112382374	GAAAUCCGACAACAUCCUU
					GAGCAUCGGCCUGCAGUUG
					GGAGCCAUCGCCUAUGAAA
					GCAAAUGUGCUUCAUCUAA
M-003603-00	*parkin*	5071	NM_004562	4758883	GGAGUGCAGUGCCGUAUUU
					UCAAGGAGGUGGUUGCUAA
					UUAAAGAGCUCCAUCACUU
					GUAAAGAAGCGUACCAUGA
M-006891-01	*SREBF1*	6720	NM_004176	52630417	UGACUUCCCUGGCCUAUUU
					ACAUUGAGCUCCUCUCUUG
					GCGCACUGCUGUCCACAAA
					ACACAGACGUGCUCAUGGA
M-004264-02	*FBXW7*	55294	NM_001013415	61743925	GAAAUUGCUUGCUUUAGAU
					GAACUCAAAUCUCCUAAGG
					CAACAACGACGCCGAAUUA
					GGAGUUGUGUGGCGGAUCA

2.6.3 QUANTITATIVE REAL-TIME PCR (qRT-PCR)

2.6.3.1 RNA isolation from cells

Extraction of total RNA from *Drosophila* and mammalian cells involved washing cell cultures briefly in cold PBS, before lysing cells and extracting total RNA using an RNeasy RNA purification kit, (Qiagen, 74104). This protocol was performed to manufacturers instructions.

2.6.3.2 Reverse transcription for cDNA synthesis

cDNA was synthesised from total RNA using 'ProtoScript® II first strand cDNA Synthesis Kit (New England BioLabs, E6560S) according to manufacturers instructions. Here, total RNA concentration was ascertained using spectrophotometry, and equivalent amounts (typically 1 µg) of total RNA underwent reverse transcription for each sample. Following reverse transcription, cDNA synthesis efficiency was tested using spectrophotometry, and samples were adjusted accordingly to ensure equal sample concentrations.

2.6.3.3 qRT-PCR

Quantitative real-time PCR (qRT-PCR) was ultilised to measure relative expression levels of mRNA within cells. Here, mRNA extracted from cultured cells (2.6.3.1) was assessed by cDNA (2.6.3.2) quantification. Each sample was normalised to a 'reference gene,' which maintains a steady expression in all samples under the experimental conditions. Here, the *Drosophila* ribosomal gene, *RpL32*, and the human ribosomal gene, *RNA18S5,* were chosen due to their reproducibility.

The qRT-PCR assay was performed in 96-well PCR plates (Bio Rad, 223-9441) with a reaction volume of 25 µl. The reaction mixture consisted of 1 µl cDNA, 12.5 µl iQ™ SYBR® Green Supermix (Bio Rad, 170-8880), 1.5 µl forward and reverse primers (final concentration, 300 nM) and 8.5 µl PCR-grade water. Plates were sealed (Bio Rad, MSB1001) and briefly centrifuged before being loaded into the MyiQ™ real-time PCR system (Bio Rad, 170-9770). For each condition, samples were assayed in triplicate, and an average value taken.

For gene expression quantification, 'SYBR Green' binds to double-stranded DNA and emits fluorescence. As the qRT-PCR progresses, the intensity of the dye increases

proportionally as the cDNA of interest undergoes multiplication. In the exponential phase, the amount of cDNA should double for each cycle. As the fluorescence reaches a pre-set threshold level, the number of PCR cycles required to reach this point is recorded as the 'threshold cycle' or 'C_T' value for that sample. Using these C_T values, the relative expression ratio between samples can be ascertained.

To achieve a set of C_T values, the qRT-PCR system runs a standard qPCR program:

Step	Name	Temperature	Seconds	
1	Initialisation	95 ºC	180	
2	Denaturation	95 ºC	30	
3	Annealing	60 ºC	30	
4	Extention	72 ºC	30	Real time measurement
5	Repeat steps 2 - 4 (40x)			
6	Melt curve analysis	95 ºC	30	
7		60 ºC	30	
8		55 ºC	10	Melt curve measurement
9	Increase step 8 by 1 ºC until 95 ºC is reached			

The 'melt curve' performed at the end of the qRT-PCR amplification allows analysis of the specificity of the amplification. Here, for each sample, the melt curve should possess just one 'peak' indicating the amplification of just one product. In the case of more than one peak, this may indicate non-specificity, contamination, or primer dimers in the reaction mixture. In this situation, assay optimisation or primer redesign would be the appropriate action.

2.6.3.4 Relative fold-change calculation

To calculate the relative fold change of expression between cDNA samples, the $2^{-\Delta\Delta CT}$ or 'Livak' method is used (Livak & Schmittgen, 2001). Here, for each sample, the average 'threshold cycle' (C_T) value of the 'gene of interest' (GOI) is normalised to the average C_T value of the 'reference gene'. This produces a value known as ΔC_T:

$$\Delta C_T = C_{T\,(GOI)} - C_{T\,(Reference\ gene)}$$

Once each sample is normalised to the reference gene, the experimental samples (e.g. *PINK1* siRNA-treated cells) must be normalised to the control sample (e.g. control siRNA-treated cells). This produces a value known as $\Delta\Delta C_T$:

$$\Delta\Delta C_T = \Delta C_{T\,(Experimental\ sample)} - \Delta C_{T\,(Control\ sample)}$$

Finally, to produce a normalised expression ratio between experimental and control samples, $2^{-\Delta\Delta CT}$ is calculated for each value. Here, the control sample is equal to 1, with experimental samples representing relative expression levels.

2.6.3.5 qRT-PCR primers

Below is a table of all qRT-PCR primers utilised in this project.

Gene	Species	Forward primer	Reverse primer	Amplicon size
RpL32	*Drosophila*	GCCGCTTCAAGGGACAGTATCTG	AAACGCGGTTCTGCATGAG	144 bp
PINK1	*Drosophila*	CAACATCCTCAATCCCAACC	TCTTAGTGGTCAGCGAAAGG	158 bp
RNA18S5	Human	CAGCCACCCGAGATTGAGCA	TAGTAGCGACGGGCGGTGTG	252 bp
PINK1	Human	GCCGGACGCTGTTCCTCGTT	TGGACACCTCTGGGGCCATC	327 bp
parkin	Human	CACACTGACAGCAGGAAGGA	AGGGGCCTTTGCAATACA	91 bp
FBXW7	Human	GGGCACCAGTCGTTAACAAG	GTCACAGCACTCTGATGCTTG	149 bp
SREBF1	Human	CGTGCTGGGCACCGAGAGC	GGCCGTGTGACTGGCTCACC	138 bp

2.7 WESTERN BLOT

2.7.1 REAGENTS

All reagents are purchased from Sigma-Aldrich, unless otherwise stated.

RIPA Buffer (filtered)

- 50 mM Tris-HCL
- 150 mM sodium chloride (NaCl)

Lysis buffer (7 ml)

- RIPA buffer - 6188 µl
- 1% Triton X
- 10% Glycerol
- 2 mM ethylene glycol tetraacetic acid (EGTA)
- 1 mM magnesium chloride ($MgCl_2$)
- 50 µM MG-132
- 1x Protease inhibitor cocktail (Roche, 11836170001)
- 10 mM N-Ethylmaleimide (NEM)

4x SDS Sample Buffer

- 240 mM Tris-HCl pH 6.8

- 8% Sodium dodecyl sulphate (SDS)
- 40% Glycerol
- 1% β-mercaptoethanol
- 0.008% Bromophenol Blue

2.7.2 CELL LYSIS

Cells cultured in a 12-well plate were placed on an ice-block, washed briefly in cold PBS and lysed in 200 µl fresh lysis buffer (see 2.7.1). The cell monolayer was dislodged with a pipette tip and resuspended in the lysis buffer by repeat pipetting, before transfer to a microcentrifuge tube.

2.7.3 PROTEIN QUANTIFICATION

To quantify the amount of protein in each cell lysate, Bradford reagent (Sigma, B6916) was mixed with double distilled water (ddH_2O) at a ratio of 1:1. 1 µl of lysis buffer alone (control) or cell lysate was mixed with 1 ml Bradford solution, and incubated at room temperature for between 5 – 60 minutes. Samples were transferred to cuvettes (Sarstedt, 67.742) and analysed by spectrophotometry (Eppendorf BioPhotometer) at 595 nm.

2.7.4 SDS PAGE

Cell lysates were heated with 1x sodium dodecyl sulphate (SDS) sample buffer (see section 2.7.1) at 94 ºC for 10 minutes to remove secondary and tertiary structures. Samples were centrifuged briefly and placed on ice.

Polyacrylamide gels were hand-cast to the appropriate concentration using a Bio-Rad Mini-PROTEAN® Tetra Handcast System, to manufacturers instructions. Gels were mounted in electrophoresis chambers, and 1x Tris/Glycine/SDS (TGS) running buffer (Bio-Rad, 161-0772) added. Protein samples were loaded at quantities ranging between 30 - 100 µg / lane, plus one lane of protein standard (5 µl) for monitoring protein molecular weight (Bio-Rad, 161-0373). Gels were run at 60 V through the stacking gel, and 190 V through the resolving gel until the protein of interest lay roughly halfway down the gel.

Upon completion of gel electrophoresis, gels were removed from the running chamber and placed in 1x Tris/Glycine (TG) transfer buffer (Bio-Rad, 161-0771) containing 20% methanol. Simultaneously, membranes were activated in methanol (PVDF only) and

placed in transfer buffer (PVDF and nitrocellulose). Gels and membranes remained in transfer buffer for 5 - 10 minutes, allowing equilibration. To transfer proteins from the polyacrylamide gel to the membrane (PVDF - Bio-Rad 162-0177, nitrocellulose – Amersham RPN3032D), a transfer cassette 'sandwich' was constructed, consisting of two outer fibre pads, flanking two pieces of filter paper. This construction ensured that the gel and membrane were in close contact at the centre of the sandwich allowing efficient transfer. The transfer cassette was loaded into the transfer chamber together with an ice block and sufficient transfer buffer. The transfer was performed at 300 mA for 2 hours.

Upon completion of protein transfer, the membrane was removed from the cassette and assessed for efficient transfer through analysis of the protein standard or Ponceau S staining (Sigma, P7170) for 5 minutes. The membrane was then placed on an orbital shaker, and blocked at room temperature or 4 ºC for 2 – 24 hours in 5% milk powder in PBST or TBST, depending on the assay. Following blocking, the membrane was sealed into a polythene bag together with the primary antibody, at room temperature or 4 ºC for 1 – 24 hours on a rotating platform. Membranes were washed thoroughly in PBST or TBST for 1 - 2 hours before exposure to the secondary horseradish peroxidase (HRP)-conjugated antibody, for 0.5 – 2 hours. Following a further washing step, membranes were exposed using an enhanced chemiluminescence (ECL) system (Amersham, RPN2232). Here, membranes were incubated with ECL for 10 – 120 seconds, before exposure to a light-sensitive photographic sheet (Amersham, 28-9068-44) for 1 second to 10 minutes depending on the intensity of the chemiluminescence signal. Here, chemiluminescence arises when the enzyme, HRP and hydrogen peroxide oxidise the chemiluminescent substrate, luminol, causing it to emit light proportional to the amount of HRP present. Photographic films were developed using an automatic film developer.

2.7.5 DATA ANALYSES

Western blot films are quantified using the ImageJ plugin 'Gels.' Here, films are scanned, straightened, and opened in ImageJ. Using the rectangular selection tool, protein bands are selected, and the relative density of each protein lane is given. This is normalised to the relative density of the corresponding loading control, producing values of the relative protein amounts in each lane. These data are then plotted in a column graph, producing a graphical quantification of the qualitative western blot image.

2.7.6 ANTIBODIES

All antibodies were diluted in blocking buffer prior to incubation. Detailed are the antibodies used during western blotting in this study, together with the favoured dilution buffer.

Antibody type	Name	Source	Product code	Dilution	Buffer	Host animal
Primary	DYKDDDDK-Tag (FLAG)	Cell Signaling Technologies	2368	1 in 1,000	PBST	Rabbit
Primary	ATP5A	Mitosciences	MS507	1 in 10,000	PBST	Mouse
Primary	LC3	Sigma-Aldrich	L8918	1 in 1,000	TBST	Rabbit
Primary	SREBP1 (2A4)	Santa Cruz	sc-13551	1 in 200	TBST	Mouse
Primary	SREBP1 (2A4)	BD Biosciences	557036	1 in 1,000	TBST	Mouse
Primary	Actin	Millipore	MAB1501	1 in 5,000	PBST	Mouse
Primary	Tubulin	Sigma	T 9026	1 in 10,000	PBST	Mouse
Secondary	HRP-conjugate Anti-Mouse	Abcam	ab6789	1 in 5,000	PBST	Goat
Secondary	HRP-conjugate Anti-Rabbit	Molecular probes	G21234	1 in 5,000	PBST	Goat

2.7.7 ASSESSING GENERAL AUTOPHAGY VIA LC3 LIPIDATION

General autophagy was assessed by the analysis of endogenous LC3 lipidation following starvation. HeLa cells were exposed to 25 nM siRNA as indicated, and incubated for 4 days. Media was replaced with either fresh media (U – untreated), HBSS (Invitrogen, 24020) (S – starvation), 20 nM bafilomycin A_1-containing media (Sigma, B1793) (B – Bafilomycin A_1) or 20 nM bafilomycin A_1-containing HBSS (S&B – starvation and Bafilomycin A_1) for 2 hours. Protein samples were collected and endogenous LC3 analysed using SDS-PAGE. Immunoblots were quantified using ImageJ. Assays were performed in triplicate, and the mean ‘LC3-II / total LC3’ ratio was calculated per sample.

2.8 FLUORESCENCE MICROSCOPY

2.8.1 SAMPLE PREPARATION

For immunofluorescence techniques, cells were cultured on circular coverslips in 12-well plates or 8-well chamber slides (BD Bioscience, 354118). Upon assay completion, media was aspirated, cells were washed briefly in cold PBS, and fixed / permeabilised in ice-cold methanol for 10 minutes. Cells were placed on an orbital shaker, and blocked for 30 minutes in a solution of 1% bovine serum albumin (BSA) in PBS. Following this, primary antibodies in blocking buffer were applied for 1-2 hours at room temperature. Cells were washed 3 x 10 minutes in PBST, before the addition of the secondary antibody in blocking buffer for 1 - 2 hours at room temperature. Cells underwent 3 further PBS-washing steps for 10 minutes each, before the addition of the

nuclear stain, Hoechst, for 10 minutes. Following a final wash step, samples were mounted for imaging using MOWIOL mounting media.

For live cell imaging, cells were cultured on 8-well live imaging trays (Ibidi, 80826). Cells were treated with fluorescent dyes i*n situ*, allowing direct imaging with an inverted microscope.

2.8.2 MICROSCOPES

In this study, three microscopes have been utilised, with a variety of objectives as detailed in figure legends.

2.8.2.1 Deltavision RT Deconvolution widefield microscope

The Deltavision widefield microscope (Applied Precision, Inc. Washington) was used for early low-throughput assay development work. The two objectives used were a 60x Plan Apo NA 1.42 objective (Olympus) and a 100x U Plan S Apo NA 1.40 objective (Olympus). The following filter blocks were employed to visualise fluorescence: 360/457 (DAPI), 490/528 (GFP), 500/535 (YFP), and 555/617 (Alexa Fluor 594).

2.8.2.2 Olympus FV1000 Fluoview confocal microscope

The Olympus FV1000 Fluoview confocal system (Olympus corporation) was used for the majority of the low-throughput data analysis. In all assays, the objective of choice was a 60x Plan Apo NA 1.42 (Nikon) with 2x digital zoom as indicated. Here, 405, 488, 514 and 534 laser lines were used to visualise DAPI, GFP, YFP and Alexa Fluor 594 respectively.

2.8.2.3 ImageXpress Micro high content widefield microscope

For all high-throughput work, an ImageXpress Micro widefield high content screening microscope (Molecular Devices) was employed. For *Drosophila* whole genome screening and the majority of *Drosophila* follow-up screens, a 40x S Plan Fluor NA 0.60 ELWD objective (Nikon) was utilised. In addition, a small number of *Drosophila* follow-up screens and all human screening protocols required the use of a 10x Plan Fluor NA 0.30 objective (Nikon). A range of fluorescence filter cubes was used over the screening process including DAPI (1-6300-0442, Molecular Devices), GFP (1-6300-

0450, Molecular Devices), YFP (1-6300-0448, Molecular devices) and Texas Red® (1-6300-0449, Molecular Devices).

2.8.3 ANTIBODIES AND DYES

The following antibodies and cellular dyes were used in fluorescence microscopy assays throughout this study as indicated.

Antibody / Dye	Name	Source	Product code	Dilution	Host animal
Primary	ATP5A	Mitosciences	MS507	1 in 5,000	Mouse
Primary	c-Myc (9E10)	Santa Cruz	sc-40	1 in 50	Mouse
Primary	GFP	Abcam	ab6556	1 in 1,000	Rabbit
Secondary	Alexa Fluor® 594 Anti-Mouse	Molecular probes	A-11005	1 in 400	Goat
Secondary	Alexa Fluor® 488 Anti-Rabbit	Molecular probes	A-11008	1 in 400	Goat
Dye	Hoechst 33342	Molecular probes	H3570	2 µg/ml	-
Dye	MitoTracker® Red CMXRos	Molecular probes	M7512	50 - 150 nM	-
Dye	TMRM	Molecular probes	T-668	50 nM	-

2.9 FLUORESCENCE ASSAYS

2.9.1 PARKIN TRANSLOCATION RESCUE WITH LIPIDS

In chapter 6, fluorescence microscopy is used to assess YFP-Parkin translocation in YFP-Parkin.HeLa cells. Here, control, *PINK1* and *SREBF1* siRNA was applied for 3 days, before priming cells with various concentrations of lipids for 24 hours. Following lipid priming, cells were treated with 10 µM CCCP for 4 hours, fixed and processed for imaging as in 2.8.1.

Lipids used in these assays are detailed below.

Lipid	Source	Product code	Dilution factor
Fatty Acid Supplement (aqueous mixture)	Sigma	F7050	1 in 2,000 ('High') 1 in 4,000 ('Low')
SyntheChol™ Supplement (synthetic cholesterol)	Sigma	S5442	1 in 100 ('Very High') 1 in 250 ('High') 1 in 500 ('Low')
Cardiolipin Solution (bovine heart)	Sigma	C1649	1 in 1,000
Phosphatidylethanolamine Solution (soybean)	Sigma	60660	1 in 1,000

2.9.2 ASSESSING ΔΨm WITH TMRM

2.9.2.1 Reagents

Tetramethylrhodamine, Methyl Ester (TMRM) – Molecular Probes, T668
Stock solution - 100 µM (in DMSO)

Assay Buffer (pH 7.8)

- 80 mM sodium chloride (NaCl)
- 75 mM potassium chloride (KCl)
- 25 mM D-Glucose
- 25 mM HEPES

2.9.2.2 ΔΨm analysis

To analyse the integrity of the ΔΨm in HeLa cells following siRNA silencing of *PINK1*, *SREBF1* and *FBXW7*, the cationic dye Tetramethylrhodamine methyl ester (TMRM) was utilised. Assays were carried out in opaque 96-well plates (Corning, CLS3362) containing siRNA at a final concentration of 25 nM. Each siRNA was assessed in the presence of vehicle or CCCP, with 5 wells of each condition per plate. Additionally, plate controls comprised siRNA- and cell-free wells in the presence of vehicle or CCCP.

The siRNA-silencing protocol was comparable to that detailed in section 2.4.2. Briefly, probes were complexed to the siRNA-delivery reagent, DF1 for 30 minutes at room temperature. Each well received 6,000 HeLa cells, before an incubation period of 24 hours at 37 ºC. Media was replaced to reduce the risk of transfection-reagent toxicity, followed by a further incubation of 24 hours. Media was aspirated and replaced with either vehicle or CCCP-containing media (10 µM) for 1 hour. Media was aspirated, and cells washed with pre-warmed 'assay buffer.' Cells were then incubated with assay buffer containing 50 nM TMRM for 30 minutes at 37 ºC. Plates were washed 3x in vehicle- or CCCP-containing assay buffer, before fluorescence quantification using a Mithras LB940 plate reader. Here, TMRM fluorescence was detected at 580 nm, quantifying the output as relative fluorescence units (RFU).

To determine the final data, average RFU data from 'cell-free' wells for vehicle- and CCCP-treated portions of the plate were subtracted from equivalent experimental data points to account for background. Additionally, each well was normalised according to

cell number, determined by the addition of the DNA-binding dye, CyQuant (Molecular Devices, C35007). Here, CCCP-containing assay buffer was applied across the entire plate to allow all remaining TMRM to diffuse away. Then, per well, 30 µl 1x CyQuant was incubated for a period of 1 hour at 37 ºC. CyQuant fluorescence was detected at 530 nm by a Varioskan Flash plate reader (Thermo Scientific), quantifying the output as relative fluorescence units (RFU). Following cell number normalisation, average RFU values across 5 repeat wells were calculated for each condition. The dataset underwent a final normalisation step, to 'control siRNA, vehicle.' Four assays were performed and an overall average for each condition produced.

2.9.3 PINK1 STABILISATION FOLLOWING CCCP-TREATMENT

HeLa cells were treated with control, *PINK1, FBXW7* or *SREBF1* siRNA (25 nM) as in 2.4.2. After 2 days, PINK1-GFP was transfected as in section 2.3, and cells were incubated for a further 16 hours before being treated with vehicle- or CCCP-containing media for 1 hour. Samples were fixed with ice-cold methanol and processed for imaging. Here, anti-ATP5A and anti-GFP primary antibodies were applied for the visualisation of mitochondria and enhanced detection of native PINK1-GFP. Secondary antibodies were anti-AlexaFluor 594 (mouse) and anti-AlexaFluor 488 (rabbit).

2.9.4 CHEMICAL INHIBITION OF THE SREBP-PATHWAY

The SREBP-pathway was chemically blocked by the addition of genistein (Sigma, G6649), prepared in DMSO and used over a range of concentrations from 10 – 100 µM. Here, YFP-Parkin.HeLa cells were exposed to varying concentrations of genistein-containing NCM for 24 hours prior to toxification with 10 µM CCCP for 4 hours. Cells were fixed and processed for imaging.

2.10 *DROSOPHILA* GENETICS

2.10.1 *DROSOPHILA* HUSBANDRY

All *Drosophila* stocks were maintained in cotton wool-stoppered plastic vials containing cornmeal agar media and bakers yeast. When placed at 18 ºC, the *Drosophila* life cycle persists for approximately 40 days. Each stock had at least three copies, which were flipped cyclically into fresh tubes every 2 weeks. To select flies of the correct genotype for crosses, stocks were tipped out onto CO_2 anaesthesia stations. Crosses

generally consisted of 8 males and 10 - 12 virgin females, which were incubated at 25 ºC allowing the appearance of larvae after ~3 days. Under most conditions, adults began to eclose from pupal cases 10 days after placing the cross in the incubator. Parental flies were flipped into fresh vials every three days, to increase longevity and egg-laying potential.

2.10.2. *DROSOPHILA* LINES

Below are the fly stocks used to create the *Drosophila* genotypes utilised in this study.

Stock name	Genotype	Stock ID	Source
Control RNAi	w;P(UAS-RH4-RNAi)	v46919	VDRC
HLH106 RNAI (1)	w[1118]; P{GD4360}v37641	v37641	VDRC
HLH106 RNAi (2)	w[1118]; P{GD4360}v37640	v37640	VDRC
ago RNAi	yv; agoTRiP(4005)	31501	TRiP
sgg RNAi	P{KK108994}VIE-260B	v101538	VDRC
park^{25}	w;park^{25}/TM6B	-	Greene et al., 2003
UAS-ago	UAS-ago/TM3	-	Mortimer and Moberg 2007
UAS-agoΔF	UAS-agoΔF/TM6B	-	Mortimer and Moberg 2007
ago^{1}	ago^{1}FRT80/TM6B	-	Moberg et al., 2001
ago^{3}	ago^{3}FRT80/TM6B	-	Moberg et al., 2001
UAS-HLH106	w[*]; P{w[+mC]=UAS-HLH106.K}2/CyO; HLH106[189]/TM6B, Tb[1)	38396	Bloomington
UAS-HLH106ΔC	y[1] w[*]; P{w[+mC]=UAS-HLH106.1-452}2/CyO; HLH106[189]/TM6B, Tb[1]	41018	Bloomington
Act5C-GAL4	w;P(Act5C-GAL4)/CyO	25374	Bloomington
da-GAL4	w;P(da-GAL4)	8641	Bloomington

2.10.3 CLIMBING ASSAY

Adult flies aged between 0 - 3 days were sorted according to their genotype and transferred to empty plastic tubes at a maximum density of 25 flies per tube. Tubes were placed with the climbing apparatus for 1 - 2 hours prior to assay commencement, to allow acclimatisation. Following acclimatisation, a single fly-containing tube was inserted into position 1 of the climbing apparatus, consisting of six lower tubes and six upper tubes in a counter-current arrangement. For each tube set, flies were given 10 seconds to climb upwards from the lower tube to the upper tube. After 10 seconds, flies that reached the upper tube were transferred into the adjacent tube set. This process was repeated five times, giving flies the chance to arrive at the final tube set. Upon assay completion, the number of flies residing in each of the tubes were counted, and scored relative to their position within the climbing apparatus. From this, a ‘climbing index’ was calculated for the cohort, and normalised to the control group.

2.10.4 FLIGHT ASSAY

Flies tested for climbing in 2.10.3 were transferred to food-containing tubes and left to acclimatise with the flight apparatus for ~ 1 hour. Following acclimatisation, flight ability was tested using a 1 litre-measuring cylinder, lined with a sticky grease-coated acetate sheet. Flies were gently but firmly dropped through a plastic funnel into the cylinder. Those able to initiate flight would fly out and up, becoming stuck to the acetate sheet. The position with which flies would become stuck depended on the speed with which the flight reflex was initiated. To quantify this, the acetate sheet was carefully removed from the cylinder, and sandwiched to an additional acetate 'score sheet' divided into 4 portions. The number of flies residing in each portion of the scoring sheet were counted, and given a score relative to their position. From this, a 'flight index' was calculated for the cohort, and normalised to the control group.

3. WHOLE GENOME RNAi SCREEN

3.1 BACKGROUND

3.1.1 PINK1/PARKIN-PATHWAY

Following the discovery that the PD-related genes *PINK1* and *parkin* were acting in a common pathway (Clark et al, 2006; Park et al, 2006; Yang et al, 2006), research has focused on ascertaining the role of the pathway in a cellular context. A large body of evidence built up over the last few years indicates a central importance in the maintenance of mitochondrial homeostasis, encompassing aspects of mitochondrial morphology, transport and clearance.

Of particular interest to this project is the selective elimination of dysfunctional mitochondria from the cell via mitophagy. The current model involves the PINK1-dependent translocation of Parkin from the cytoplasm to a subset of failing mitochondria, followed by their selective removal via the autophagy-lysosomal pathway (Narendra et al, 2008). To date, a number of additional genes have been shown to play a role in the PINK1/Parkin-pathway, including *mitofusin*, encoding a MOM GTPase involved in mitochondrial fusion (Gegg et al, 2010; Poole et al, 2010; Tanaka et al, 2010; Ziviani et al, 2010), and *miro*, encoding a MOM GTPase involved in mitochondrial trafficking (Liu et al, 2012; Wang et al, 2011). However, there are many unanswered questions regarding the mechanism by which dysfunctional mitochondria are identified and flagged up for degradation by the PINK1/Parkin-pathway (Figure 1.10).

3.2 HYPOTHESES AND AIMS

The initial aim of this project was to perform a cell-based whole genome RNAi screen in order to identify novel promoters of PINK1/Parkin-mediated mitophagy. Specifically, the screening assay was developed in *Drosophila* S2R+ cells, and focused on the identification of genes acting upstream of Parkin translocation following mitochondrial depolarisation with the protonophore carbonyl cyanide 3-chlorophenylhydrazone (CCCP). The intended outcome of this screen was to produce a list of robust hit genes causing a decrease in Parkin translocation following silencing. Hence, these genes are potentially involved in the translocation event itself, or signaling events upstream, such as damage recognition and pathway initiation

3.2.1. *DROSOPHILA* AS A SCREENING MODEL

There are a number of advantages of using *Drosophila* cells as a model for high-throughput screening assays. First, the *Drosophila* genome has a very low level of redundancy compared to mammalian genomes (Beckingham et al, 2005). This feature is likely to reduce the number of false negative events and decrease the complexity of data analyses following screening. Second, *Drosophila* cells readily take up dsRNA when applied in serum-free media, eliminating the need for transfection. This greatly reduces costs and eliminates the toxic side effects of transfection reagents, which would otherwise require consideration during assay optimisation. Finally, with the 'Sheffield RNAi Screening Facility' (SRSF) on our doorstep, the reagents, equipment and support necessary for carrying out a screen in *Drosophila* cells are readily available. Importantly, the *Drosophila* RNAi library held in the SRSF contains identical dsRNA sequences to those used to make an *in vivo Drosophila* RNAi library (VDRC KK library), allowing easy transition from a cellular to a whole-organism system.

3.2.1.1 *Drosophila* dsRNA library

The available *Drosophila* dsRNA library is the Heidelberg 2 (HD2.0), second-generation library developed by the Boutros laboratory using NEXT-RNAi software. This software is designed to avoid areas of low-complexity and reduce the number of potential off-target effects (Boutros et al, 2004; Horn et al, 2010).

The mechanism by which dsRNA transiently silences genes in a post-transcriptional manner is well defined in *Drosophila*. Briefly, cells are bathed in FBS-free media containing the gene-specific dsRNA probe. This probe is taken up by the cell and broken into a number of 22mer, double-stranded siRNA fragments by the RNase enzyme Dicer. These siRNAs are unwound into single-stranded fragments following ATP-hydrolysis, and integrated into the RNA-induced silencing complex (RISC), where target mRNA recognition and Argonaute-dependent degradation takes (reviewed in Hannon & Rossi, 2004).

The HD2.0 library itself contains dsRNA probes ranging in size from 81 – 800 bp, covering ~98.8% of the *Drosophila* transcriptome. Within the library, there are 18,434 dsRNA probes targeting 15,177 coding and non-coding genes, thus in some cases there are two or more dsRNAs targeting the same gene. Additionally, dsRNA design is such that every known isoform of a gene is silenced by a single dsRNA, ensuring full knockdown of target gene expression.

3.2.2 SCREENING OVERVIEW

In order to successfully perform a whole genome screen, a clear screening strategy must be in place. In our case, a screening workflow guided the project from the initial biological question of 'Which genes act upstream of Parkin translocation?; through to hit selection and low-throughput analysis (Figure 3.1).

To ensure success, significant effort was committed to developing a robust and reproducible assay. Following assay development, the quality of the assay was assessed through a series of 'pilot' screens using small sub-set libraries, before undertaking the whole genome screen itself. Following completion of the whole genome screen, hits were confirmed in several rounds of re-screening. This acted to remove false positives from the dataset, and produced a final primary hit list of genes. Taking these hit genes, a number of secondary screening assays were performed looking at different of aspects of mitochondrial homeostasis. Collating these data produced an overall list of genes able to influence a range of mitochondria-related processes. To validate these genes in a system with greater genetic complexity, corresponding human orthologs of hits were assessed in the context of Parkin translocation and mitophagy using a HeLa cell line. This culminated in a final list of genes showing strong cross-species effects. With the help of bioinformatics, a small number of interesting hits were selected for low-throughput analysis.

3.3 ASSAY DEVELOPMENT

3.3.1 VALIDATING THE *DROSOPHILA* S2R+ CELL MODEL

The majority of recent work on PINK1/Parkin-mediated mitophagy has been carried out in mammalian cell systems. The initial challenge of this project was to recapitulate the well-defined steps of the PINK1/Parkin-pathway in a *Drosophila* cell system, thus validating S2R+ cells as a viable model. These steps included the dissipation of the mitochondrial membrane potential ($\Delta\Psi m$) following toxification with CCCP, the stabilisation of PINK1 on the MOM, the translocation of Parkin to mitochondria and the clearance of damaged mitochondria via mitophagy.

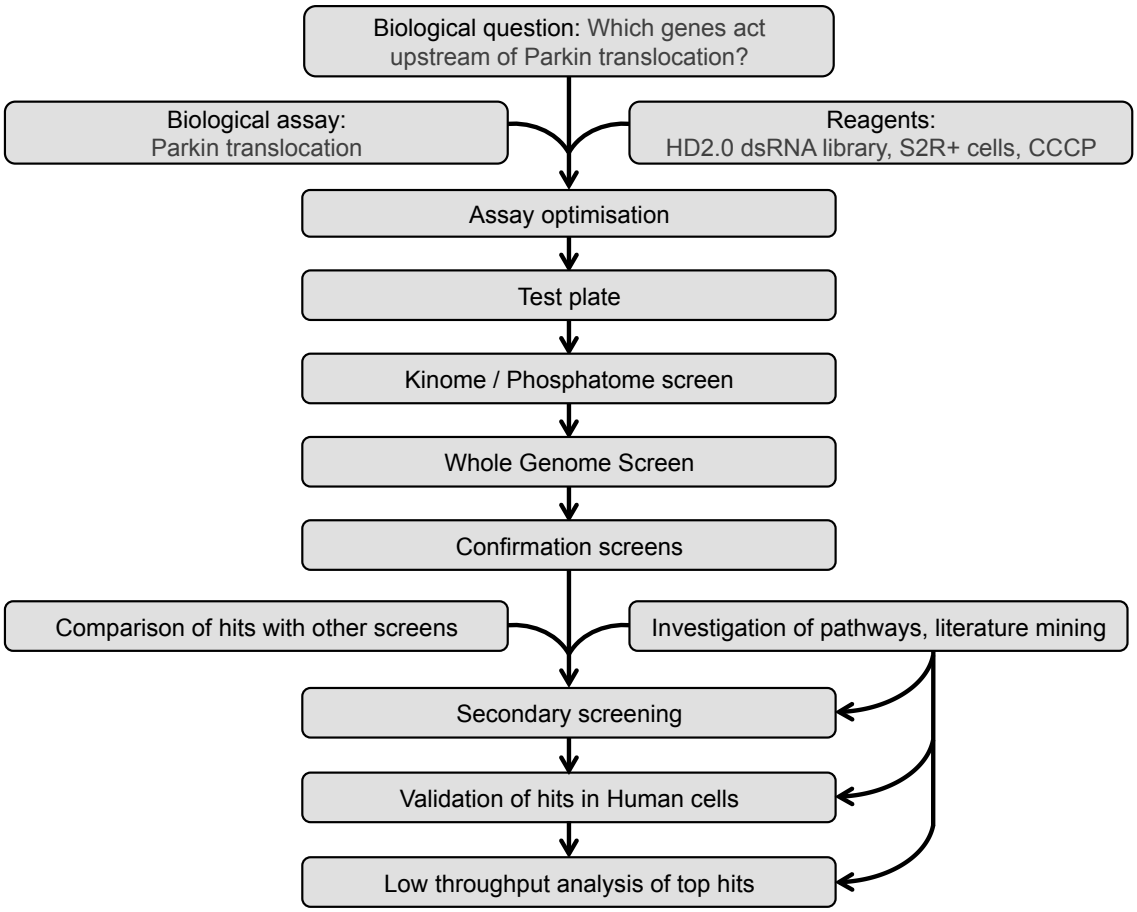

Figure 3.1. Screening Overview. Schematic representation of the screening process from the initial biological question through to the low-throughput analysis of the top screening hits. The biological assay involved the analysis of CCCP-induced Parkin translocation following gene silencing, with a focus on dsRNA amplicons causing a significant reduction in Parkin-GFP puncta number. The reagents used included the HD2.0 dsRNA library developed by Michael Boutros and colleagues (Boutros et al, 2004; Horn et al, 2010), a stable S2R+ cell line overexpressing Parkin-GFP, and CCCP to induce the translocation event. Following thorough assay optimisation, a number of subset screens were performed (test plates & kinome / phosphatome) prior to the whole genome screen. Screen hits were confirmed in several rounds of re-screening, before being scrutinised for their ability to influence other aspects of mitochondrial homeostasis in secondary screening assays. Next, overall *Drosophila* hits were converted to their human orthologs, and HeLa-cell screening was undertaken, for validation in a mammalian system. From the point of *Drosophila* gene confirmation screening, hit lists were analysed for an involvement in common pathways using bio-informatics, as well as being compared to other published screening data. This assisted in the selection of a small number of genes for low-throughput analysis following screening completion.

3.3.1.1 Dissipation of the mitochondrial membrane potential

CCCP is a diffusible protonophore, able to induce rapid dissipation of the $\Delta\Psi m$. As an amphipathic, weak acid, protonated $CCCP^+$ freely diffuses across the mitochondrial membrane. Here, it rapidly dissociates from H^+, and exits the mitochondria as an anion. As a consequence, this increase in H^+ ions in the mitochondrial matrix causes the $\Delta\Psi m$ to discharge, hence uncoupling the mitochondrial ETC. Whilst CCCP is present in culture media, this process will cycle continuously, maintaining mitochondrial uncoupling and blocking the production of ATP.

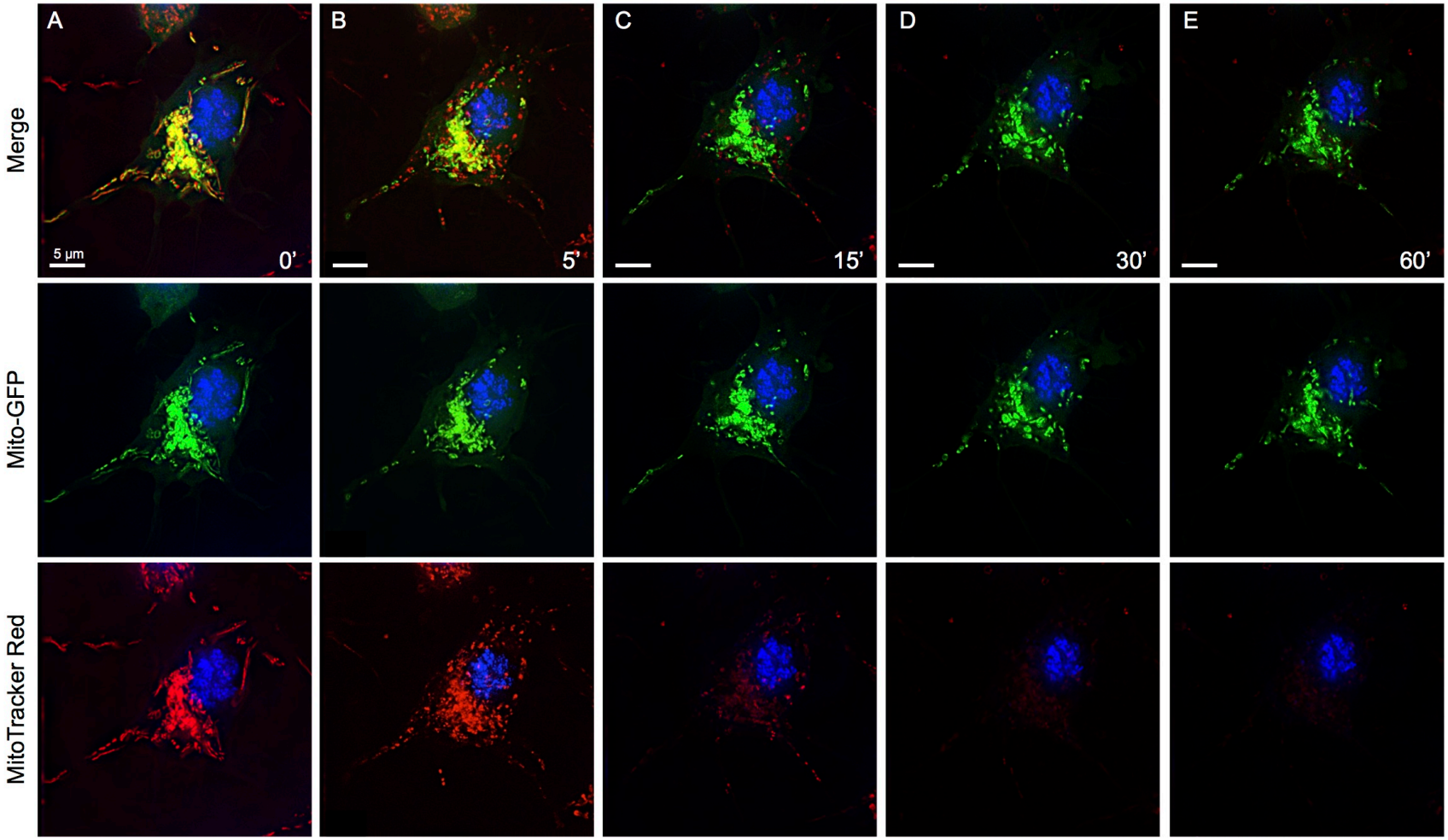

Figure 3.2. Mitochondrial membrane potential dissipation following CCCP toxification. S2R+ cells were transiently transfected with Mito-GFP (mitochondria – green), and treated with 50 nM MitoTracker Red - MTR (mitochondria – red) and Hoechst (nucleus – blue) for 30 minutes prior to imaging. Live cells were imaged before CCCP application (A) and after the addition of 10 µM CCCP over a 60 minute period (B, C, D & E). Images were acquired using a Deltavision RT system with a 100x objective, scale bar: 5 µm.

To demonstrate the effect of CCCP in S2R+ cells, cells were subjected to CCCP treatment and imaged live over a period of 60 minutes. The status of the $\Delta\Psi m$ was measured using the potentiometric mitochondrial dye, MitoTracker Red (MTR). Prior to toxification, MTR co-localises with Mito-GFP, signifying a mitochondrial network with an intact $\Delta\Psi m$ (Figure 3.2 A). This co-localisation is reduced after 5 minutes of CCCP toxification (Figure 3.2 B) and lost after 15 minutes of CCCP toxification (Figure 3.2 C). After 30 & 60 minutes of CCCP toxification, the MTR signal is lost entirely (Figure 3.2 D & E). These data demonstrate the rapid and successful collapse of the $\Delta\Psi m$ following CCCP treatment in S2R+ cells. Importantly, the induction of mitochondrial fragmentation following CCCP toxification is also observed (Figure 3.2 B - E), as reported previously (Ishihara et al, 2003; Legros et al, 2002), further strengthening the similarities between *Drosophila* and mammalian cell systems.

3.3.1.2 PINK1 stabilisation

Under basal conditions, mammalian PINK1 is cleaved by the mitochondrial proteases MPP and PARL (Deas et al, 2011; Greene et al, 2012; Jin et al, 2010; Meissner et al, 2011; Whitworth et al, 2008), before rapid proteasomal degradation via the N-end rule pathway (Yamano & Youle, 2013). When overexpressed, a very low level of diffusely localised PINK1 is observed in the cytoplasm. However, after a short CCCP toxification, PINK1 levels increase, and it becomes stabilised on the MOM (Matsuda et al, 2010; Narendra et al, 2010b). To assess this phenomenon in S2R+ cells, PINK1-myc was overexpressed in the absence or presence of CCCP. In contrast to human cells, under basal conditions, PINK1-myc colocalises with the mitochondrial marker Mito-GFP, rather than adopting a diffuse cytoplasmic localisation (Figure 3.3 A & A'). However, upon CCCP treatment PINK1-myc no longer fully co-localises with Mito-GFP; now decorating an area around the periphery of the marker (Figure 3.3 B & B'). This observation is in agreement with mammalian data whereby CCCP causes PINK1 to become stabilised on the MOM. However, the disparity observed prior to toxification indicates a difference in the dynamic turnover of *Drosophila* PINK1 (dPINK1). Perhaps in S2R+ cells, dPINK1 is not degraded as rapidly as in mammalian cells, allowing the existence of a stable fraction in the inner compartments of mitochondria. In support of this suggestion, both full-length and processed dPINK1 isoforms are readily detectable in whole *Drosophila* lysates (Whitworth et al, 2008).

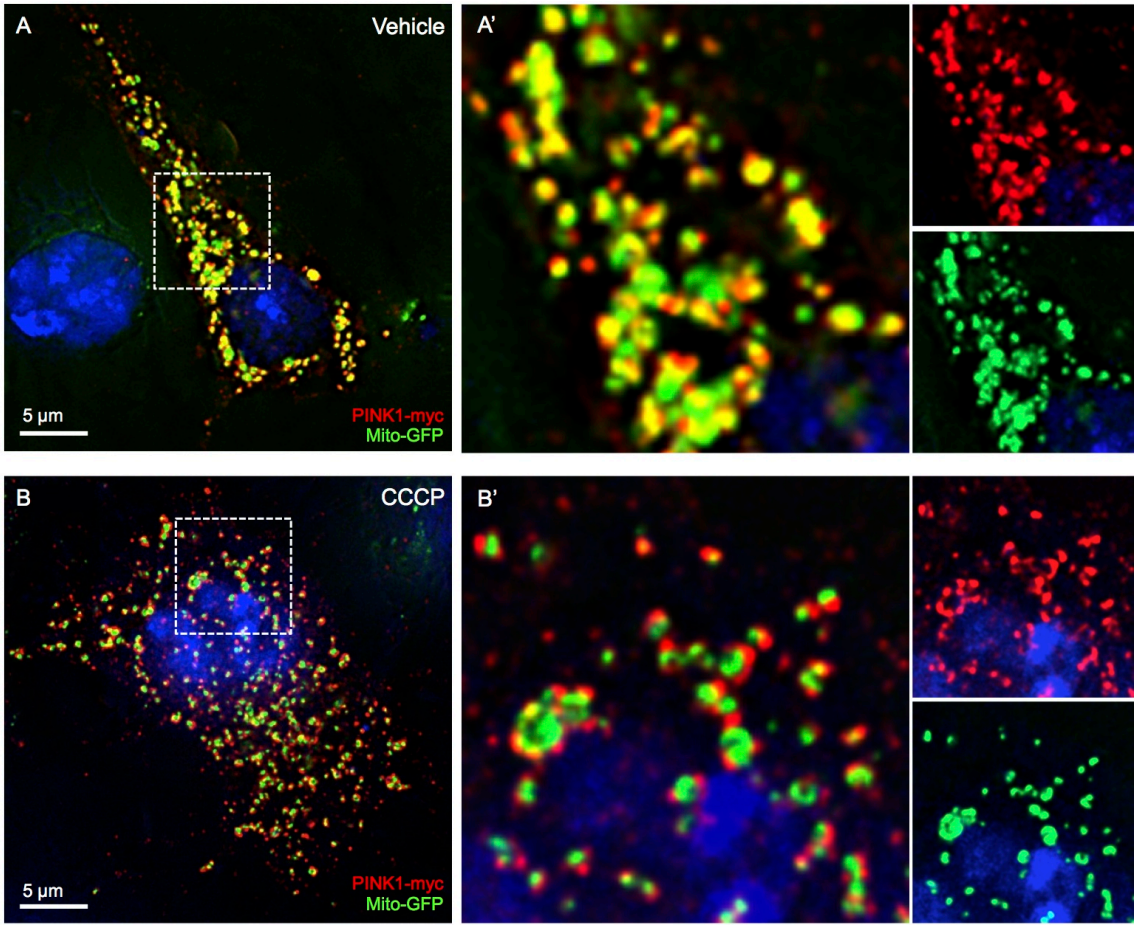

Figure 3.3. dPINK1 stabilisation following CCCP toxification. S2R+ cells were transiently transfected with PINK1-myc. Following the addition of vehicle (A & A') or CCCP (B & B') for 4 hours, cells were fixed and processed for imaging. Mitochondria (Mito-GFP – green) and PINK1-myc (red) are represented. Images were acquired using a Deltavision RT system with a 100x objective. Boxed areas represent images in A' & B'. Scale bar: 5 µm.

3.3.1.3 Parkin translocation and mitophagy

In mammalian cells, following CCCP-induced PINK1 stabilisation on the MOM, Parkin is recruited to those mitochondria in a PINK1-dependent fashion. To demonstrate this translocation event, S2R+ cells were transiently transfected with Parkin-GFP and subjected to either vehicle- or CCCP-toxification for a period of 2 hours. In vehicle-treated cells, *Drosophila* Parkin (dParkin) distribution is largely cytoplasmic, with only ~30% of cells exhibiting any degree of Parkin-GFP puncta (Figure 3.4 A & B). This observation is in agreement with published mammalian data whereby endogenous Parkin was shown to colocalise with a subset of mitochondria in the absence of toxification, albeit infrequently (Narendra et al, 2008). However, in CCCP-treated S2R+ cells, Parkin-GFP formed numerous punctate structures; which colocalise with the mitochondrial marker ATP5A; in ~80% of the population (Figure 3.4 A & B). Like in mammalian cells, these data confirm the occurrence of dParkin translocation in S2R+ cells following CCCP toxification. However, whilst dParkin clearly co-localises with a

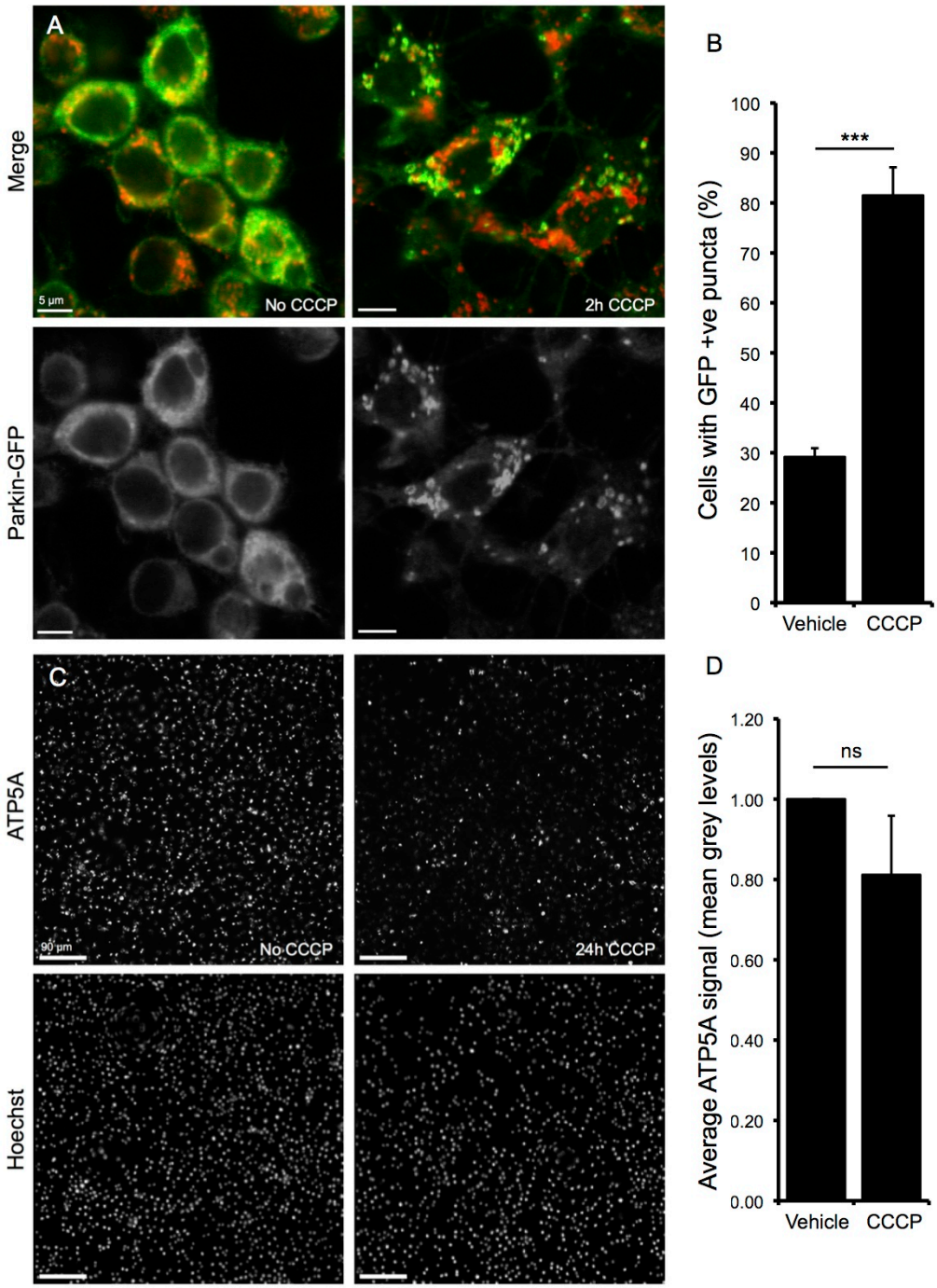

Figure 3.4. dParkin translocation and mitophagy following CCCP toxification. Parkin-GFP.S2R+ cells were toxified for 2 hours (A & B) or 24 hours (C & D) with 10 µM CCCP. (A) Following a 2-hour CCCP toxification, Parkin-GFP (green) translocates from the cytoplasm to mitochondria (ATP5A – red). This effect has been analysed by eye and quantified in (B) as the percentage of cells with Parkin-GFP +ve puncta. Data from three biological repeats, with at least 6 FOV per condition, per assay. Error bars represent standard deviation, ***P<0.001 (Student's T-test). (C) Following a 24-hour CCCP toxification, a marked decrease in the mitochondrial marker, ATP5A can be observed. Cells were counterstained with Hoechst nucleic acid dye. The decrease in ATP5A signal was quantified in (D) as the 'average ATP5A signal' in mean grey levels (ImageJ). Data from two biological repeats with at least 3 FOV per condition, per assay. Error bars represent standard deviation. No significance (ns) was found between toxified and non-toxified conditions (Student's T-test). Images were acquired using an Olympus FV1000 confocal system with a 60x objective (A) or a Deltavision RT system with a 10x objective (C). Scale bars as indicated.

subset of mitochondria here, a proportion of the mitochondrial network remains dParkin-free following toxification (Figure 3.4 A). The reason for this is unclear, but may be due to a heterogeneous response of the mitochondrial network to the CCCP challenge. For example, mitochondria exhibiting prior damage are likely to suffer a large drop in $\Delta\Psi m$ following CCCP toxification, resulting in significant activation of the PINK1/parkin-pathway. In contrast, healthy mitochondria with a full complement of intact components may more easily maintain their $\Delta\Psi m$, hence avoiding dParkin translocation and the activation of mitophagy. In the mammalian field, whilst many studies show complete colocalisation between Parkin and mitochondria following CCCP application (Geisler et al, 2010; Narendra et al, 2010a; Okatsu et al, 2010; Rakovic et al, 2011; Tanaka et al, 2010; Vives-Bauza et al, 2010), others have a phenotype similar to that observed here (Narendra et al, 2008; Narendra et al, 2010b; Van Laar et al, 2011). Importantly, there is good correlation between Parkin-GFP translocation in S2R+ cells, and endogenous Parkin translocation in HEK293 cells and cultured rat neurons (Narendra et al, 2008; Van Laar et al, 2011), perhaps highlighting the physiological relevance of the observed distribution.

Sustained CCCP toxification for 24 hours has been shown to lead to the loss of mitochondria from the cell via mitophagy (Narendra et al, 2008). The severity of the phenotype is very much cell-type specific, and has been shown to vary greatly in mammalian-derived cell lines. For example, primary neurons, which rely heavily upon oxidative phosphorylation for their energy production undergo mitophagy much less readily than glycolytic, cancer-derived HeLa cells (Gusdon & Chu, 2011). This suggests that cells with a greater reliance upon the mitochondrial network for ATP synthesis are less likely to permit mitophagy than those whose energy may be sourced by alternative routes. In S2R+ cells, persistent CCCP toxification for 24 hours does not appear to cause a complete loss of mitochondrial markers as shown in HeLa cells, but can lead to a marked reduction in the ATP5A signal (Figure 3.4 C & D). This demonstrates the ability of S2R+ cells to alter their mitochondrial proteome following toxification. However, this reduction in ATP5A signal has proved variable between experiments, and is therefore not a reliable occurrence in this cell-type under the tested conditions. Because of this variability, combined treatments of CCCP with autophagy inhibitors such as Bafilomycin A_1 were unable to show definitively that the reduction in ATP5A signal was due to mitophagy. Despite this, published data in S2R+ cells have shown that CCCP-induced ATP5A signal reduction is dependent upon autophagy- but not proteasomal-related genes (Ziviani et al, 2010).

3.3.2 SCALING-UP FOR HIGH-THROUGHPUT SCREENING

Having validated *Drosophila* S2R+ cells as a suitable model for the assessment of PINK1/Parkin-related processes, the next challenge was to scale-up the dParkin translocation assay into the 384-well plate format used for whole-genome primary screening.

3.3.2.1 dParkin translocation

For the primary screen, the chosen image-based assay assesses the translocation of Parkin-GFP to the MOM following CCCP toxification. The output of the screen is the quantification of the number of Parkin-GFP positive 'dots' or 'puncta' that are formed as a consequence of this toxification. This feature of the PINK1/Parkin-pathway was selected for screening due to the simple nature of the assay, making it amenable to high-throughput usage, and the reproducibility of the observed effect. The advantage of assessing dParkin itself is the increased likelihood of capturing PINK1/Parkin-specific hits, perhaps compared with a broader, mitochondrial degradation assay. In contrast, the disadvantage of focusing on an early pathway step is the limited number of positive screen controls. For example, the only known gene required for Parkin translocation in a mammalian setting is *PINK1*. However, when considering these points, the advantages offered by this screening scenario were perceived to outweigh the negative aspects, deeming it a viable assay for primary screening.

3.3.2.2 Genes of interest

The primary screening assay has the potential to identify genes causing both a decrease and an increase in dParkin translocation following CCCP toxification. For the scope of this project, data analyses focuses on genes causing a decrease in dParkin translocation when silenced. One motive for concentrating on this group is to identify genes phenocopying the loss of *dPINK1*. Such genes are potentially pathway agonists, acting upstream or downstream of dPINK1. In contrast, hits increasing translocation would represent pathway antagonists. Both gene groups are equally interesting, however, an increase in dParkin translocation may potentially arise from non-specific cellular toxicity as well as PINK1/Parkin-related processes. As a consequence, it will be difficult to uncouple these two root causes, in order to determine pathway-specific genes.

3.3.2.3 Reagents

To simplify the screening protocol and maximise data capture, it was considered advantageous to produce an S2R+ cell line, stably overexpressing pMK33.Parkin-GFP (Parkin-GFP.S2R+). For this, a copper-inducible plasmid containing *Drosophila* Parkin-GFP and a Hygromycin B resistant cassette was transiently transfected into S2R+ cells. Following selection with 300 µg/ml Hygromycin B for three weeks, virtually the entire population of cells expressed GFP at variable levels (Figure 3.5) Unlike mammalian cell lines which will grow readily at very low cell densities, *Drosophila* cell cultures often undergo widespread cell death if the population drops below optimum density. Because of this, producing clonal S2R+ cell lines is near impossible. However, despite our Parkin-GFP.S2R+ line being of a non-clonal origin, visual assessment found the vast majority of cells to stably express Parkin-GFP at largely comparable levels, circumventing this issue.

3.3.2.4 Screening protocol

The basic screening protocol entailed seeding 6,000 Parkin-GFP.S2R+ cells suspended in 30 µl serum-free Schneider's medium (SFSM), in 384-well plates arrayed with pre-printed dsRNA probes. Whilst in SFSM, the cells readily take up the dsRNA, and gene silencing begins. After 1 hour, equal volumes (30 µl) of 2x FBS-containing Schneider's media are added to screening plates, and cells are incubated at 25 ºC for 72 hours. Parkin-GFP expression is induced by the addition of copper sulphate to a final concentration of 500 µM, and cells are incubated for a further 16 hours. Media is aspirated and replaced with vehicle- or CCCP-containing media at a final concentration of 10 µM for 2 hours. Cells are fixed for 10 minutes in Hoechst-containing formaldehyde, washed once in PBS, and stacked for automated imaging using an 'Automate.it Scara' robotic loader (PAA) and 'ImageXpress Micro' high content microscope (Molecular Devices). Per well, 9 fields of view (FOV) and 2 fluorescent channels (GFP and DAPI) are captured using a 40x objective. Here, the chosen number of images per well provided enough cell-data to build a detailed overview of the entire population, and the degree of magnification allowed for the resolution of Parkin-GFP puncta.

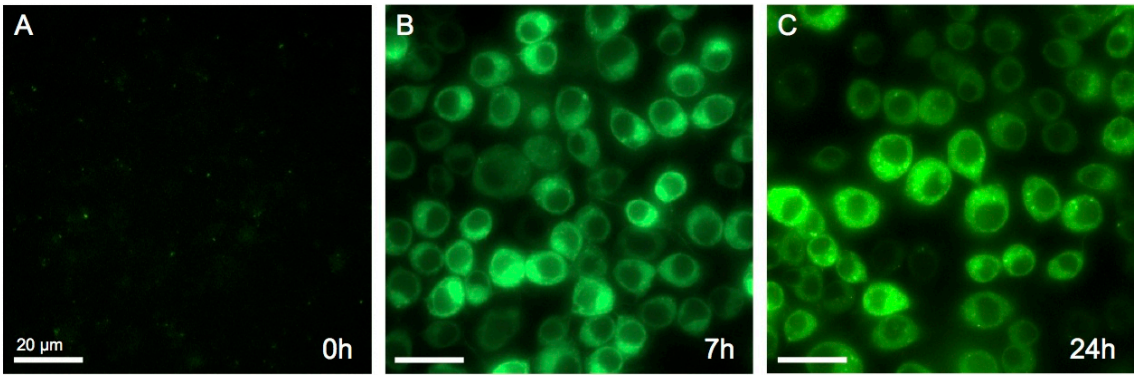

Figure 3.5. Time course of Parkin-GFP expression induction with copper sulphate. Cells were imaged live at various time points following the addition of copper sulphate solution (500 µM). (A) At 0 hours very little GFP expression was observed. (B) By 7 hours and (C) 24 hours of copper sulphate induction, virtually the entire population expressed Parkin-GFP at high levels. Images captured on a Deltavision RT system with a 40x objective. Scale bar: 20 µm.

3.3.3 ASSAY OPTIMISATION

3.3.3.1 Automating data analyses

The *Drosophila* whole genome screen library comprises 53x 384-well plates, totalling 20,352 individual wells for data collection. Due to the scale of the screen, it was necessary to automate image analysis using a pre-programmed application called 'Transfluor' (Molecular Devices). Transfluor works by quantifying the number of user-defined objects within specified parameters in a FOV. For example, in the context of the primary screen, the chosen output was the 'total number of GFP puncta' in an image, normalised to cell (nuclei) number, and averaged across the 9 FOV. This gave a measure of the 'average number of GFP puncta per cell' for a given condition. To produce this quantification, the 'Transfluor' algorithm took the original micrograph image (Figure 3.6 A) and created a 'mask' (Figure 3.6 A' & A'') whereby objects such as nuclei (grey) and puncta (white) were identified. Together with the mask image, quantification data for each FOV was logged in a data file accessible via Microsoft Excel.

Transfluor allows the user to specify object parameters within a FOV including minimum and maximum object size (µm), and the minimum intensity above local background (grey levels). Due to the influence of background fluorescence, such parameters required careful adjustment in order to produce optimum settings for the assay. The objectives for optimising these parameters were first, to achieve the greatest separation between vehicle- and CCCP-treated cells and second, to produce the most accurate 'mask' representation of the original image. Having tested a range of

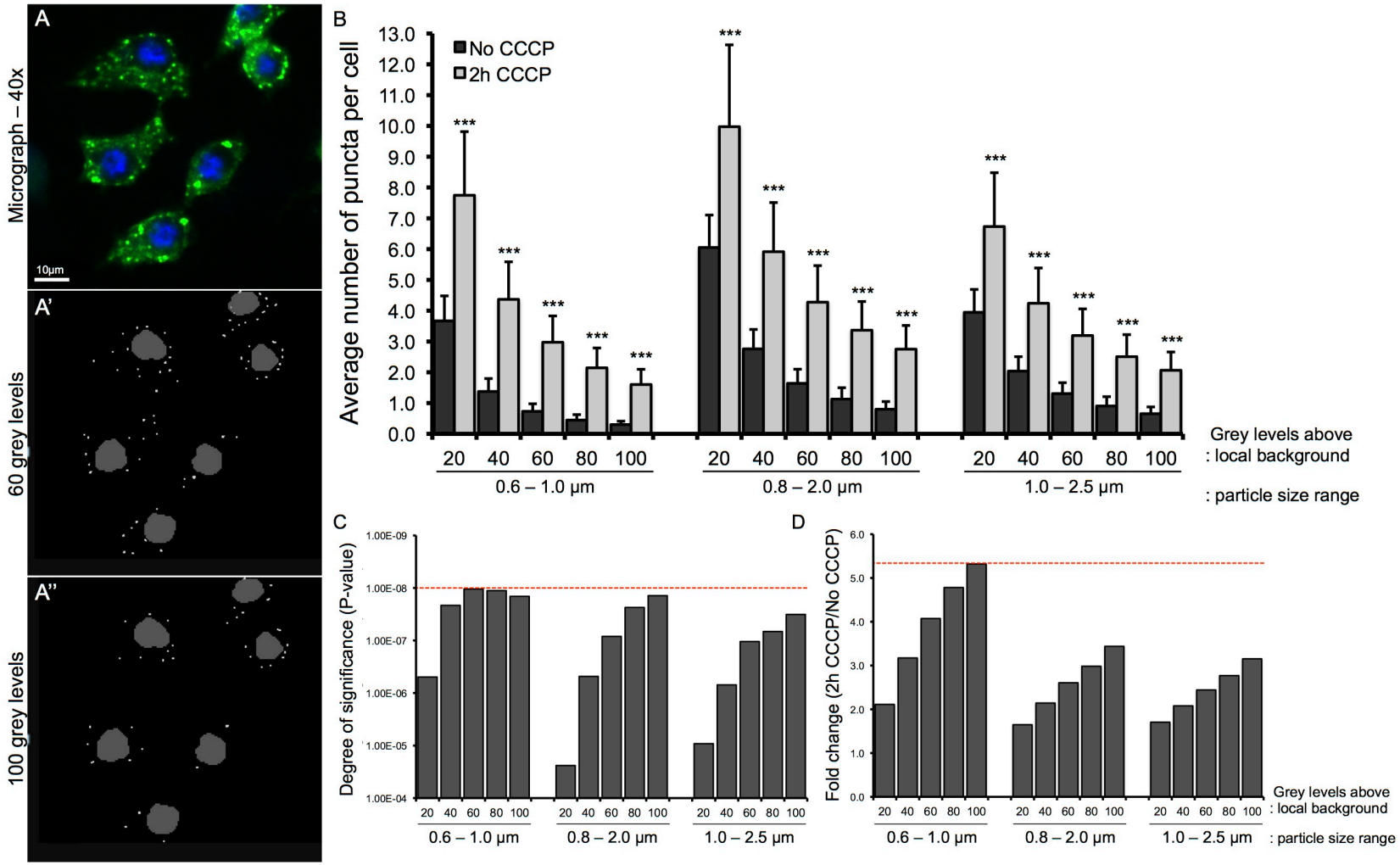

Figure 3.6. Optimisation of Transfluor parameters. (A) Example high-throughput micrograph (40x objective) with corresponding mask images for 60 (A') and 100 (A") grey levels. (B) A range of puncta sizes and intensities tested with images from vehicle- and CCCP-treated cells. As intensities increase, the sensitivity of the detection decreases, reducing noise. Each parameter was tested on 32 wells, each with 4 FOV. ***P<0.001 (Student's T-test). Error bars represent standard deviation. (C) Representation of P-values corresponding to the data in (B). (D) Representation of the 'fold change' of puncta number, corresponding to data in (B).

object sizes and intensities, all parameters analysed were able to distinguish between the two conditions (Figure 3.6 B). In order to select the most appropriate parameters, both the degree of significance (Figure 3.6 C), and the fold change in puncta number (Figure 3.6 D) between the two conditions were analysed. Using this analysis, an object size between 0.6 – 1 μm was found to produce the greatest significant difference and greatest fold change between vehicle- and CCCP-treated cells. However, the optimum 'minimum intensity' was less easily identified using this method. Having analysed the mask outputs for a range of intensities (Figure 3.6 A' and A''), '60 grey levels above background' most faithfully reproduced the micrograph data, as well as performing well in the aforementioned tests. Therefore the chosen screening parameters for automated data analyses were objects with a diameter between 0.6 μm – 1 μm, and a minimum intensity of 60 grey levels above background.

3.3.3.2 Cellular parameters

Prior to screening, a number of assay parameters required optimisation in order to achieve the greatest separation between vehicle- and CCCP-treated samples. These included the optimum number of cells per well (Figure 3.7 A, 6,000), copper induction concentration (Figure 3.7 B, 500 μM), toxin type (Figure 3.7 C, CCCP (Sigma)), and toxification duration (Figure 3.7 D, 2 hours). All chosen conditions provided a significant difference between vehicle- and CCCP-treated conditions. Additionally, the selected cell density of 6,000 cells per well produced a confluent cell population for maximum data capture. The chosen copper sulphate concentration of 500 μM lead to the most robust induction of Parkin-GFP expression, as well as producing a substantial increase in puncta number compared to lower concentrations. There were no obvious benefits to altering the CCCP manufacturer, or switching to the CCCP-analog FCCP. Therefore as in low-throughput assays, CCCP from Sigma Aldrich was used throughout screening. Finally, in mammalian cells, Parkin translocation is typically studied after a toxification of 1 - 4 hours (Geisler et al, 2010; Matsuda et al, 2010; Narendra et al, 2008; Okatsu et al, 2010; Vives-Bauza et al, 2010). In S2R+ cells, at 2 & 4 hours toxification, Parkin-GFP translocation profiles were comparable; but by 6 hours the results became highly variable. Therefore, the earliest time point of 2 hours was chosen to increase the reproducibility of the observed effect, and decrease the assay duration.

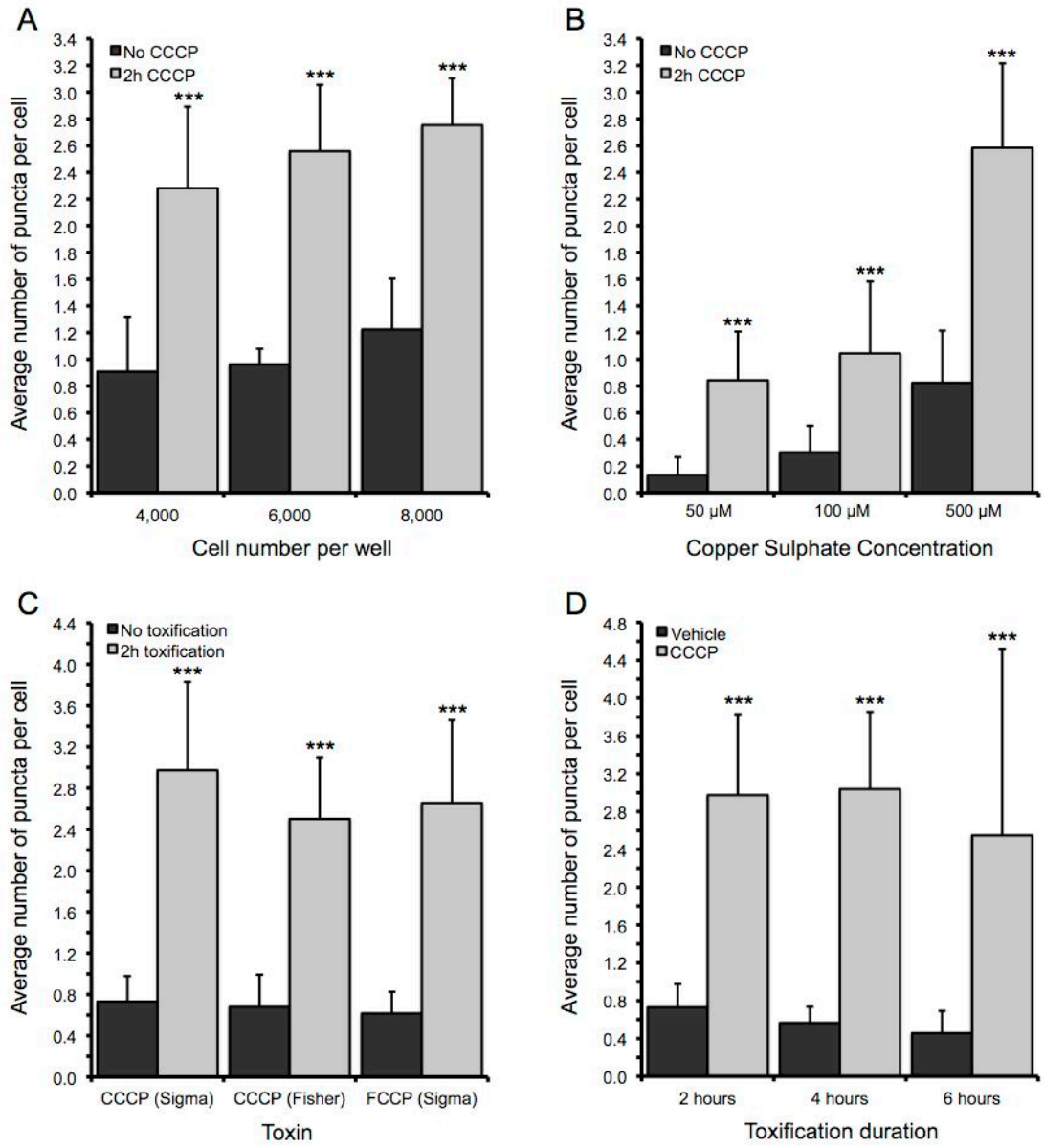

Figure 3.7. Optimisation of cellular parameters. Graphical representation of (A) cell number optimisation, (B) copper sulphate concentration titration, (C) alternate toxin source / type and (D) toxification duration time-course, in vehicle or CCCP-treated cells. All other parameters remained constant between conditions and data were analysed using the Transfluor parameters described in Figure 3.6. Error bars represent standard deviation, ***P<0.001 (Student's T-test compared to the equivalent 'No CCCP' control).

3.4 *dPINK1* SILENCING

In mammalian cells, a fundamental aspect of the PINK1/Parkin-pathway is the absolute requirement of PINK1 for both Parkin translocation and mitophagy. In contrast, knockdown of *Drosophila PINK1* (*dPINK1*) in S2R+ cells failed to prevent CCCP-induced dParkin translocation (Figure 3.8 A), despite the employment of three *dPINK1* dsRNA probes, each targeting different regions of the gene (Figure 3.8 B). Closer scrutiny revealed that each of the *dPINK1* dsRNA probes robustly reduced mRNA

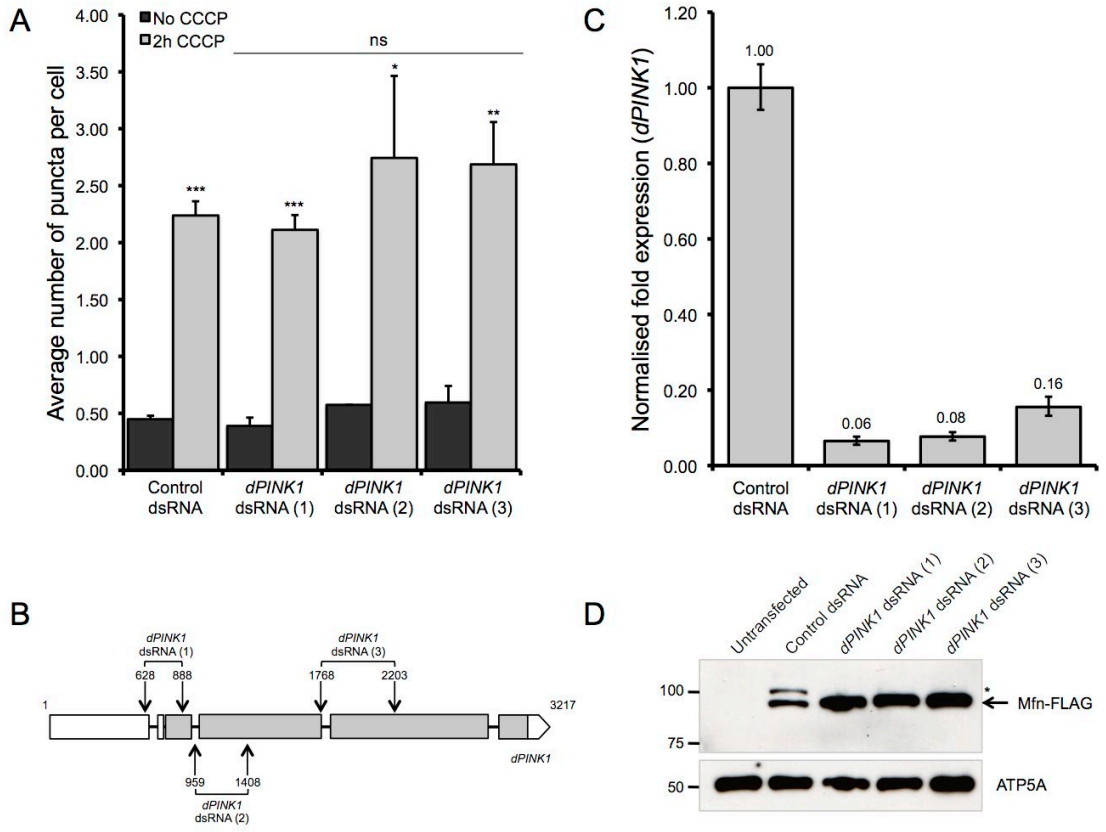

Figure 3.8. The effect of *dPINK1* knockdown on dParkin translocation and dMitofusin ubiquitination. (A) The effect of *dPINK1* or control dsRNA on dParkin translocation in S2R+ cells. At least 2 wells examined, each with 9 FOV. Error bars represent standard deviation; ***P<0.001, **P<0.01, *P<0.05 (Student's T-test). One-way ANOVA with Bonferroni's correction found no significant differences (ns) between *dPINK1* dsRNA samples and the equivalent control dsRNA samples. (B) Schematic of *dPINK1* with positions of three dsRNA probes (1-3) highlighted. (C) qRT-PCR data quantifying relative expression of *dPINK1* in control and *dPINK1* dsRNA samples following 4 days of knockdown. Data normalised to *Rpl32*; one biological repeat, 3 replicate samples per condition. Error bars represent standard deviation. (D) Western blot analysis of Mfn-FLAG following the application of control or *dPINK1* dsRNA. Lane 1 contains cell lysate with no Mfn-FLAG transfection. Lanes 2-5 contain cell lysates expressing Mfn-FLAG plus knockdown with the corresponding dsRNA. Arrow indicates unmodified steady-state Mfn-FLAG, asterisks indicates high molecular weight species. Loading control - ATP5A

levels when assessed by qRT-PCR (Figure 3.8 C), demonstrating the efficacy of gene silencing.

In the absence of a suitable dPINK1 antibody, dPINK1 activity was assessed via the analysis of steady-state levels of *Drosophila* Mitofusin (dMfn), a target of the PINK1/Parkin-pathway (Figure 3.8 D). Published data show that in S2R+ cells, dMfn is ubiquitinated in a dParkin- and dPINK1-dependent manner, producing one or more high molecular weight dMfn species. However, following *dParkin*- or *dPINK1*-knockdown, an accumulation of unmodified, steady state dMfn is observed, together with an absence of ubiquitinated forms (Ziviani et al, 2010). In agreement with published data, all three *dPINK1* dsRNAs cause an increase in steady-state dMfn-

FLAG (Figure 3.8 D, arrow), and a loss of high molecular weight isoforms (Figure 3.8 D, asterisks), compared to control dsRNA-treated S2R+ samples. These data indicate that *dPINK1* dsRNA silences dPINK1 activity, and is effective in reducing dMfn ubiquitination. Together with the qRT-PCR data (Figure 3.8 C), this suggests that all *dPINK1* dsRNA probes tested produce a significant reduction in both *dPINK1* mRNA, and ostensibly dPINK1 protein levels, yet fail to prevent dParkin translocation upon CCCP-toxification.

One conceivable explanation for a lack *dPINK1* dsRNA effect is an adaptation of S2R+ cells to no longer require dPINK1 for dParkin translocation, perhaps via an additional protein with redundant function. Alternatively, a fraction of long-lived dPINK1 protein may persist even in the event of efficient *dPINK1* mRNA knockdown, consequently maintaining the ability to promote dParkin translocation. This idea is supported by the observation that dPINK1 in S2R+ cells (Figure 3.3) and *in vivo* (Whitworth et al, 2008) exhibits differential dynamic turnover properties compared to that of mammalian PINK1 (Narendra et al, 2010b). However, the fact that *dPINK1* knockdown increases steady-state levels of dMfn, purportedly by preventing dParkin-dependent ubiquitination and degradation (a step downstream of dParkin translocation), would suggest that *dPINK1* silencing blocks dParkin activity in spite of its sustained relocalisation. Therefore I postulate that this stable fraction of dPINK1 promotes dParkin-translocation following mitochondrial damage, but is unable to activate its ubiquitin ligase domain. This idea is supported by recent evidence suggesting that the activity of Parkin depends upon its tertiary structure. Here, Parkin was found to exist in an auto-inhibitory conformation, which can be altered by a number of site-specific phosphorylation events (Trempe & Fon, 2013; Trempe et al, 2013). Importantly, PINK1-dependent phosphorylation of Parkin's ubiquitin-like (UBL) domain is suggested to relieve the auto-inhibitory effect of the UBL domain, hence leading to latent E3 ligase activation (Chaugule et al, 2011; Kondapalli et al, 2012; Shiba-Fukushima et al, 2012; Trempe et al, 2013). In the case of dParkin, it is conceivable that this dPINK1-dependent, ligase-activating phosphorylation event is absent following *dPINK1* silencing.

With the PINK1/Parkin-pathway initially being described using genetic interaction studies in *Drosophila* (Clark et al, 2006; Park et al, 2006; Yang et al, 2006), it is well defined that dPINK1 acts upstream of dParkin in the same linear pathway *in vivo*. Therefore the inability of *dPINK1* dsRNA to prevent *dParkin* translocation specifically, is likely due to an evolutionary divergence event between invertebrates and mammals, which seemingly converges again at later points in the pathway.

3.5 TEST PLATE ANALYSIS

As part of the 'assay development' phase of screening, the SRSF offer a number of small 'subset' libraries alongside the whole genome library, including single, 384-well 'test plates'. The purpose of a 'test plate' is to assess the viability of screening assays in a high-throughput context, as well as allowing screeners to become familiar with the practicalities involved. Additionally in the context of this screen, the test plate served as an exercise for screen control discovery, in the hope of identifying a novel 'positive' control gene to take the place of *dPINK1*.

The test plate consists of 275 dsRNAs arrayed across one 384-well plate. Among these are 60 random kinases arrayed in triplicate, a number of *C. elegans* negative controls, 16 empty wells for user-specific controls and a *DIAP1* plate identifier containing dsRNA against the '*Drosophila Inhibitor of Apoptosis 1*.' Every plate in the whole genome library carries its own unique 'design' of *DIAP1*-containing wells, producing a visible cell-death phenotype, and acting as a safeguard against plate barcode loss. (Figure 3.9 A).

Following data analyses using Transfluor, a significant increase in puncta number between vehicle- (Figure 3.9 B, black) and CCCP-treated (Figure 3.9 B, grey) samples is observed. *DIAP1*-induced cell death (or the loss of GFP signal) is perceived by 'Transfluor' as a 'low puncta' phenotype (Figure 3.9 B, yellow). Chosen user-specific controls included the three *dPINK1* dsRNA probes (Figure 3.8 A), all of which failed to influence CCCP-induced dParkin translocation, as discussed. Additionally, *dparkin* dsRNA was included as a measure of knockdown efficiency, where silencing largely eliminated the GFP signal, and therefore puncta number (Figure 3.9 B). This confirmed efficient dsRNA silencing of *dparkin*; an effect that can be cautiously extrapolated to all dsRNAs. Finally, *rhomboid-7* dsRNA (a *Drosophila* homolog of the intramembrane protease PARL, responsible for cleaving dPINK1 in the MIM) was included as a potential 'increaser' of puncta number. Here, it was hypothesised that the persistence of a full-length dPINK1 pool in the MIM may lead to a greater degree of dParkin translocation. Yet, despite a slight increase in dParkin translocation, this was minimal and non-significant (Figure 3.9 B, purple). However, as we now know, PINK1 stabilisation on the MOM, rather than the MIM, is crucial for dParkin translocation.

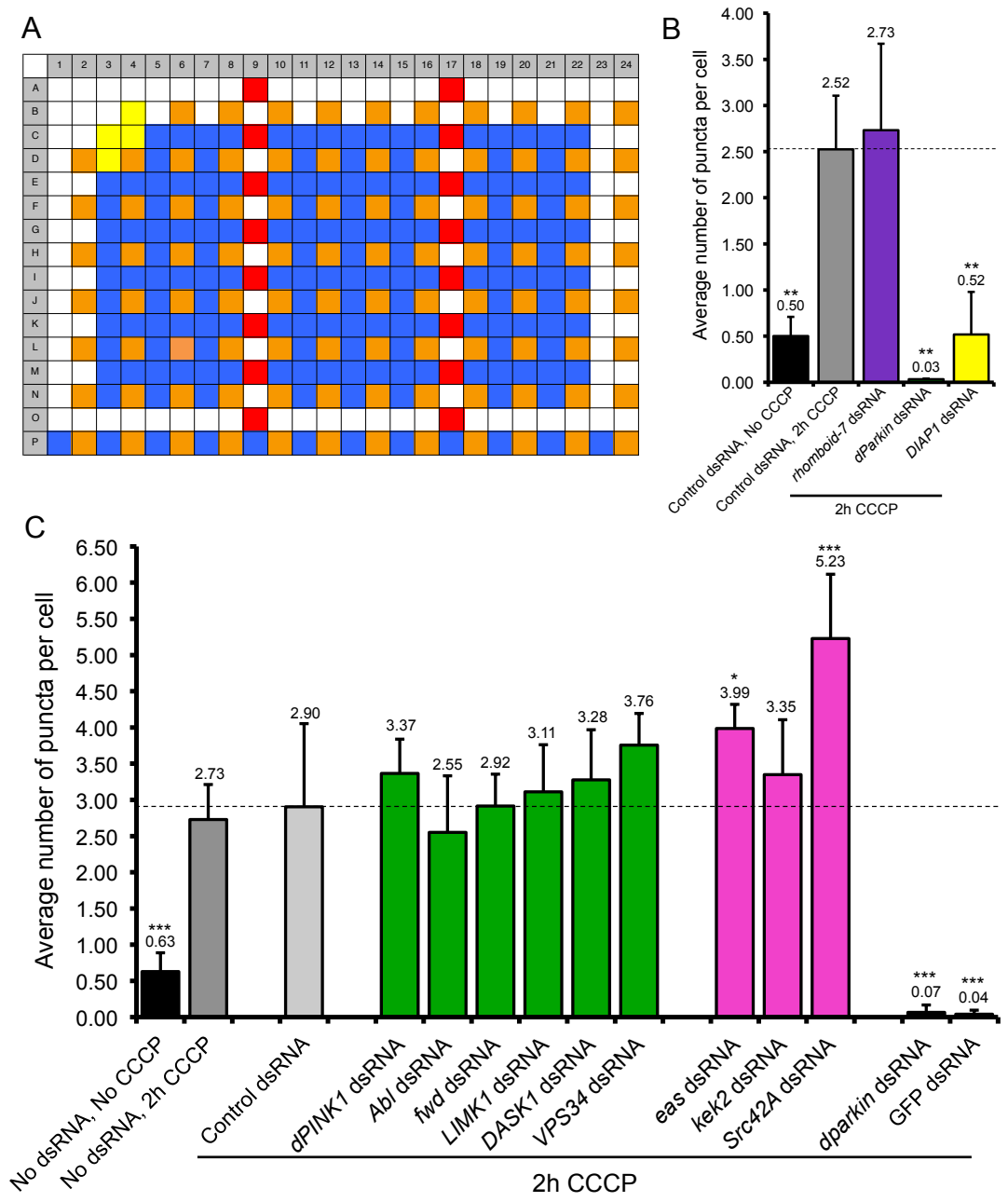

Figure 3.9. Test plate analysis and identification of putative controls. (A) Test plate layout comprising a *DIAP1* plate identifier (yellow), 60 random kinases arrayed in triplicate (blue), a selection of negative controls designed against *C.elegans* targets (orange) and two columns of 8 empty wells for the addition of user-specific controls (red). (B) Graphical representation of control data, showing a clear increase in the average number of puncta between vehicle- and CCCP-treated wells. In addition, data from the user-specific controls *rhomboid-7* and *dparkin* dsRNA are represented, together with the *DIAP1* plate identifier (lethal). Data represent at least 2 wells per condition, each comprising 9 FOV. Error bars represent standard deviation, **P<0.01 (Student's T-test, compared to 'Control dsRNA, 2h CCCP.'). (C) Graphical representation of potential screen controls, chosen following test plate analysis. Group 1 (green) represents dsRNA that decreased dParkin translocation compared to the control. Group 2 (pink) represents dsRNA that increased dParkin translocation compared to the control. Data represent at least 8 wells per condition, comprising 9 FOV per well. Error bars represent standard deviation, *P<0.05, ***P<0.001. (Student's T-test, compared to 'Control dsRNA').

3.5.1 POTENTIAL SCREEN CONTROLS

Having analysed data from the test plate, three groups of dsRNAs were identified as potential novel screen controls. First, dsRNAs targeting *Abl, fwd, LIMK1, DASK1* and *VPS34* were found to moderately reduce dParkin translocation. Second, dsRNAs targeting *eas, kek2* and *Src42a* were found to moderately increase dParkin translocation. Finally, an inbuilt test-plate control, GFP dsRNA eliminated the GFP signal giving a comparable output to that of *dparkin* dsRNA. To check the reproducibility of these observed effects, genes were systematically silenced in a number of follow-up assays (Figure 3.9 C). However, the majority of dsRNAs failed to deviate significantly from CCCP-treated control samples, rendering them unsuitable as screen controls. Despite this, GFP and *Src42A* dsRNA consistently produced a significant loss of-, or increase in translocation respectively, allowing them to be carried forward as controls for the whole genome screen.

As seen previously, *dPINK1* dsRNA continued to lack any influence on dParkin translocation (Figure 3.9 C).

3.5.2 FINALISING SCREEN CONTROLS

Together with *dparkin*, GFP dsRNA was chosen as a 'knockdown validation' control. *Src42a* dsRNA was selected as an 'increaser' of puncta number. dsRNA targeting the *C.elegans* gene '*Y39E4B.10'* was added as a negative control, chosen for its comparable phenotype to 'no dsRNA.' Finally, two copies of '*dPINK1* (2)' dsRNA were included in order to monitor the lack of effect observed during the development phase of the screen (Figure 3.10).

In the absence of a suitable dsRNA 'decreaser' of dParkin translocation, it was necessary to artificially create this phenotype by including a non-toxified ('No CCCP') area in the plate design. Fortuitously, whole genome library plates contain a quadrant of wells devoid of dsRNA (Figure 3.10, blue), originally intended as a 'no dsRNA' control. However, this provided the ideal location for the inclusion of 4 non-toxified control wells, allowing for the measurement of basal dParkin translocation. Through this, screen amplicons were assessed for their ability to reproduce this phenotype.

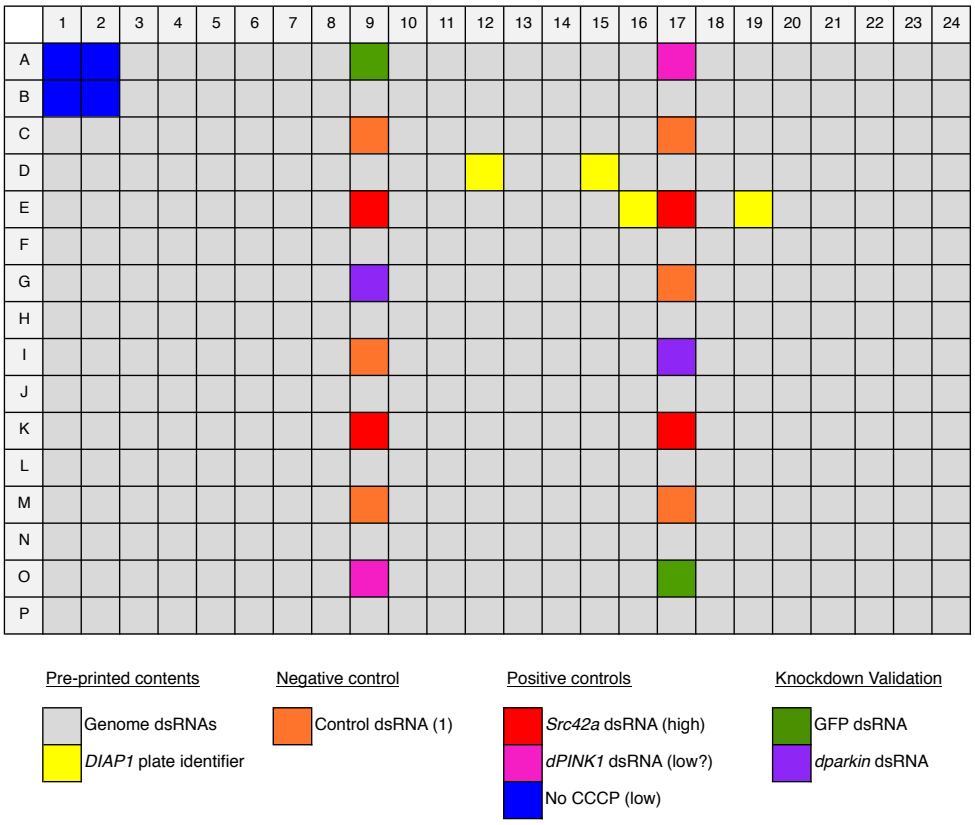

Figure 3.10. Whole genome library plate layout with controls. Schematic of the finalised plate layout for whole genome screening including positive, negative and 'knockdown validation' controls (see key).

3.6 KINOME AND PHOSPHATOME SCREEN

The kinome / phosphatome subset library comprises 1455 dsRNA arrayed over 5 plates, targeting each kinase and phosphatase in the *Drosophila* genome. The purpose of performing this subset library was to become accustomed to handling multiple plates, as well as developing a program of assay logistics in preparation for whole genome screening. This proved to be a very useful exercise as it allowed estimation of how long each assay step took to implement, and therefore how many of the 53 screening plates could be handled at once. With this, the whole genome library was split into 3 batches (18 plates, 18 plates & 17 plates), each being handled and processed at pre-defined points throughout the day.

3.7 WHOLE GENOME SCREEN

A single-assay format was adopted for whole genome screening, rather than the commonly used triplicate-assay method. The advantages of this approach are both

financial and temporal, but with the disadvantage of relying upon the success of one assay for the entirety of data capture. Because of this, the primary dataset will almost certainly contain a number of false positives and false negatives. False positives are easily identified in follow-up confirmation assays; however false negatives will be forever lost from the dataset highlighting the limits of this approach.

3.7.1 DATA ANALYSES

The whole genome screen was performed as described in section 3.3.2.4. Following completion, plates were stacked onto an 'Automate.it Scara', robotic loading system, and systematically imaged over the course of 10 days. 9 FOV per well were captured on a 40x objective, taking approximately 4 hours per plate. Once imaging was complete, automated image analysis using the optimised 'Transfluor' algorithm could proceed, averaging a further 3 hours per plate. Once all 53 plates were analysed, scrutiny of the Transfluor spreadsheet output could commence. For this, raw well data from the 9 FOV were averaged to produce one value per well, and then normalised using the median absolute deviation (see section 3.7.1.1) to produce the final dataset.

3.7.1.1 Data normalisation

In order to compare data between individual screening plates, it was necessary to 'standardise' or 'normalise' the values, converting raw puncta scores into a 'robust z-score' (Figure 3.11). Through this, each plate adopted the same central point, and comparable data spread

Data standardisation required two steps; first, normalisation on a plate-by-plate basis (Figure 3.11, steps 3 - 6); and second, normalisation across the entire genome (Figure 3.11, step 7). In this instance, the 'z-score' is calculated using the median absolute deviation (MAD); the number of absolute deviations (AD) that a value (x) is from the population median (M); where AD is the absolute difference between x and M.

Absolute deviation (AD) = $x_i - M_j$

Median absolute deviation (MAD) = $M_j\ (x_i - M_i)$ or $M_j\ (AD)$

z-score (z) = $\frac{x_i - M_j}{M_j\ (x_i - M_i)}$ or $\frac{AD}{MAD}$

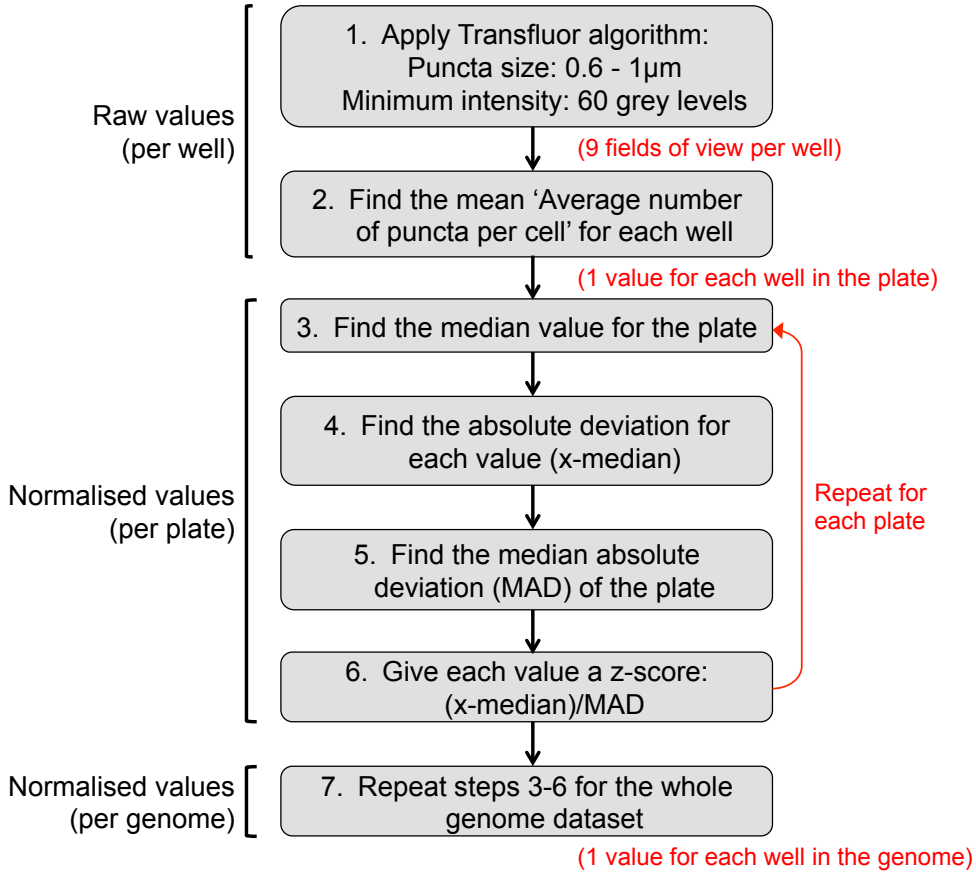

Figure 3.11. Schematic of data normalisation process. Raw values for each FOV were averaged to produce one mean value per well. Each plate was normalised individually using the MAD, before normalisation across the entire dataset.

Typically a 'z-score' represents the number of *standard* deviations (σ) ± the population *mean* ($\bar{x}$).

Deviation (*d*) = $(x_i - \bar{x})$

Standard deviation (σ) = $\sqrt{\frac{\sum(x-\bar{x})^2}{n-1}}$

z-score (z) = $\frac{(x_i-\bar{x})}{\sigma}$ or $\frac{d}{\sigma}$

However there are a number of reasons why the median absolute deviation is favoured for this type of analysis. First, the standard deviation is simply the square root of the variance; the sum of the squared deviation from the mean. The act of squaring the deviations ensures that all values of variance are positive, with the square root of the standard deviation merely reverting units back to the original. However, by squaring the

deviation, outliers are emphasised and smaller deviations from the mean can become hidden. By taking the absolute deviation, the numerical difference is returned irrespective of sign, therefore eliminating the need to square the values. In the absence of squaring, equal weight is given to every datum point, affording a greater significance to lesser changes. Second, by taking the *median* rather than the *mean* absolute deviation, the middle value is used, rather than the average. This is advantageous in a skewed dataset, as outliers with very high or very low values will have less influence on the central data point. This aspect was particularly relevant to our dataset, which exhibited a moderate skew to the right (Figure 3.14 C).

Following data normalisation, the process was validated by the observation that the negative screen control carried an average z-score of 0.2, very close to the 50th percentile (z-score = 0) (Figure 3.14 A).

3.7.1.2 Heat maps and box plots

With the final dataset complete, initial data analyses focused on the success of the assay itself, and how normalisation had affected the data as a whole. For this, both the generation of heat maps (Figure 3.12) and box-plot analysis (Figure 3.13) were found to be of use. Heat map representation for each well of every plate provides a quick visual overview of the spread of values within the dataset, particularly for those at the extremes such as controls (Figure 3.12). For example, the 'No CCCP' positive control quadrant and four 'knockdown validation' control wells (2x *dparkin* dsRNA & 2x GFP dsRNA) are clearly visible in all plates apart from plate 23, giving a crude indication that both gene silencing and dParkin translocation occurred successfully across the entire assay.

Additionally, heat maps (Figure 3.12) and box-plots (Figure 3.13) are invaluable for highlighting issues that have arisen during the screening process such as edge effects and/or equipment failure. For example, the second batch of plates has an overall lower number of puncta compared to the general plate population, likely caused by an equipment malfunction between plates 22 and 23 (Figure 3.12 A & 3.13 A i). Here the liquid handling robot crashed whilst adding the CCCP, delaying toxin application to the following plates and reducing the overall toxification duration. Additionally, the crash damaged a number of wells in plate 23, represented in the heat map by the brightest green squares. Plate 32 was dropped prior to imaging (Figure 3.12 A & 3.13 A ii) and plate 51 received a double dose of copper sulphate due to multidropper issues (Figure 3.12 A & 3.13 A iii); two events which appear to have caused a general increase in

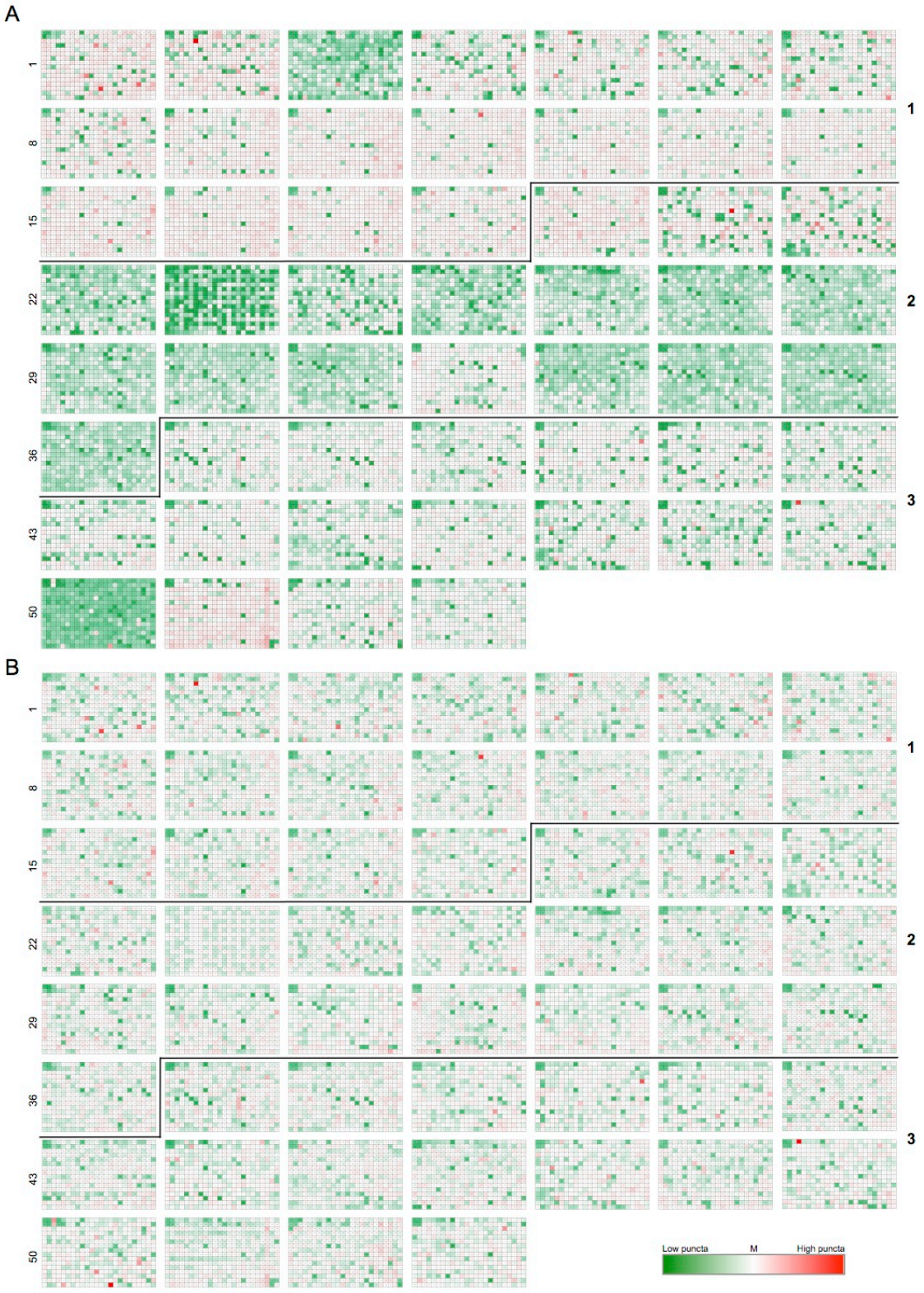

Figure 3.12. Heat map representation of the whole genome screen. 53 plates representing raw, non-normalised data (A - average number of puncta per cell) and normalised data (B - z-scores). At the extremes of the scale, green represents the lowest value, and red represents the highest value, with white being the 50th percentile or median (see scale). Numbers on the left hand side represent plate number. Black lines represent batch boundaries and bold numbers (right hand side) represent batch number.

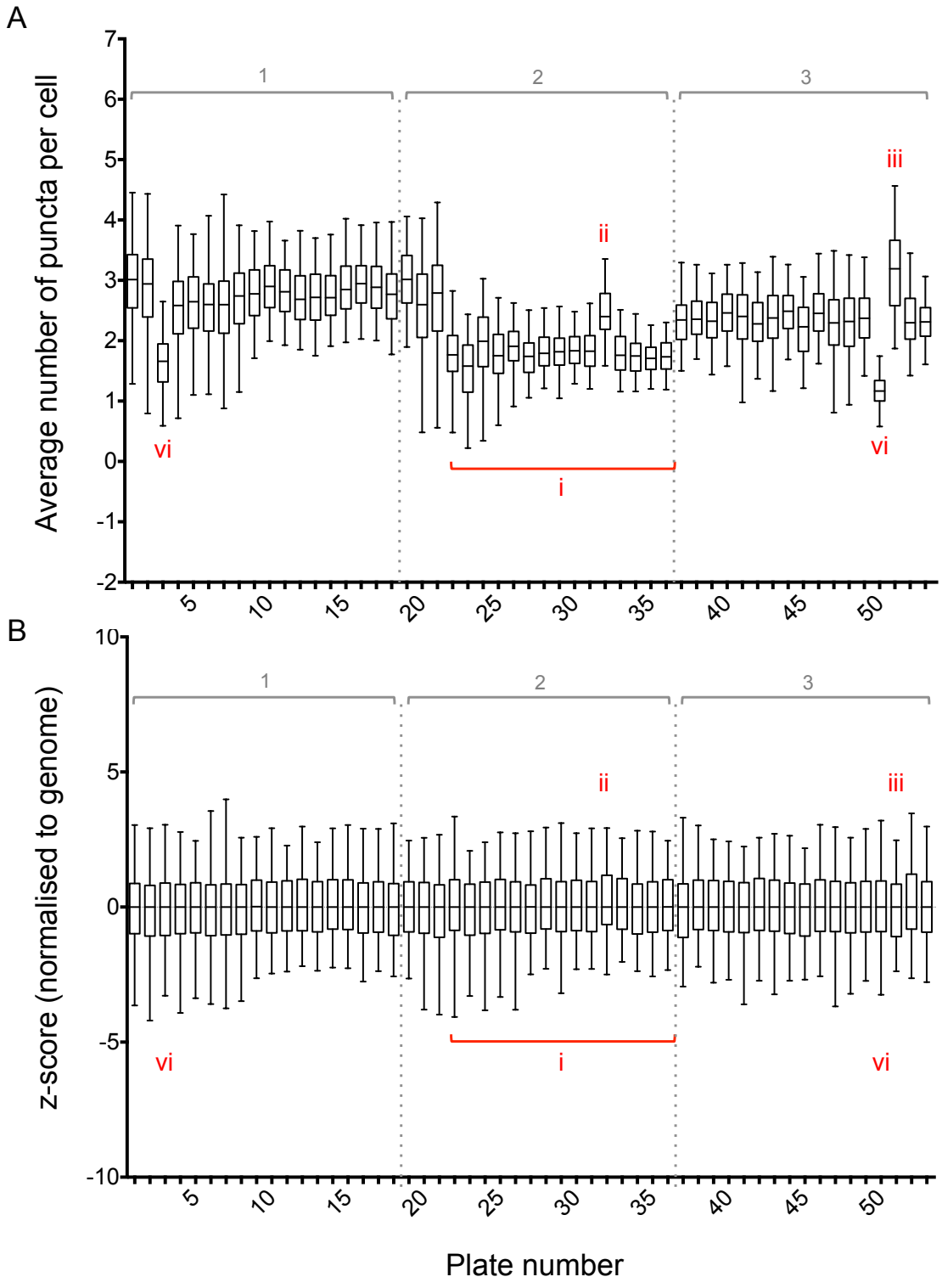

Figure 3.13. Box and whisker plots of raw and normalised plate data. Box-plot representation of raw, non-normalised screening data (A – average number of puncta per cell) and data normalised across the whole genome (B – z-score (normalised to genome)). Each box plot represents one screening plate, excluding controls (x-axis), where the box marks the 25th and 75th percentile; the central line indicates the plate median; and the whiskers represent the 5th and 95th percentile. Red labels signify events of interest during the screening process, and the grey lines and numbers demarcate the three plate batches.

puncta number. Plates 3 & 50 also have clear 'low puncta' phenotypes compared to the overall plate population, due to unknown errors during screening (Figure 3.12 A & 3.13 A iv).

3.7.1.3. Analyses of normalised data

Following data normalisation, inter-plate differences are greatly reduced, with each plate sharing a common median of 0 and a comparable data spread (Figure 3.12 B & 3.13 B). Next, screen controls were assessed in comparison to the overall performance of the genome dsRNA amplicons (Figure 3.14 A). The complete genome dataset exhibits a median of zero as a consequence of the normalisation process (Figure 3.14 A, grey). As expected, the two 'knockdown validation' controls (*dparkin* and GFP) and 'No CCCP' positive control had negative z-scores; representing values lower than the data median (Figure 3.14 A, purple, green and blue respectively). The *dPINK1* dsRNA controls (Figure 3.14 A, pink) mirrored the *C.elegans* dsRNA negative control (Figure 3.14 A, orange), with a median close to zero. This is in agreement with previous results (Figure 3.8 A). Finally, *Src42A* dsRNA (Figure 3.14 A, red) led to a positive z-score, representing values higher than the data median. Taken together, all controls behaved as expected, validating the screening assay.

Looking at the dataset in its entirety, arrayed either as a scatter plot (Figure 3.14 B) or a frequency distribution histogram (Figure 3.14 C), there is a clear skew to the right. In order to test for normality, the D'Agostino and Pearson omnibus normality test was employed, taking into account the degree of asymmetry (skewness) and the shape (kurtosis) of the frequency distribution curve. The output of such a test is a P-value of the likely deviation from normality. For an entirely symmetrical dataset, the measure of skewness is 0, with a left skew having a negative value and a right skew having a positive value. Here our dataset has a skewness value of 2.353 pulling to the right.

Additionally, when measuring the kurtosis or 'peakedness' of the data, a normal distribution will have a score of 0; with a positive score (leptokurtic) implying a curve with a sharp peak and long tails, and a negative score (platykurtic) denoting a curve with a rounded peak and short tails. Here, our dataset is leptokurtic, with a value of 33.06.

This skewness, together with the kurtosis of the data makes it a non-Gaussian dataset ($P>0.001$). The observed right skew in the dataset may be due to the limited potential for decreases in puncta number, compared to increases. For example, with a mean of

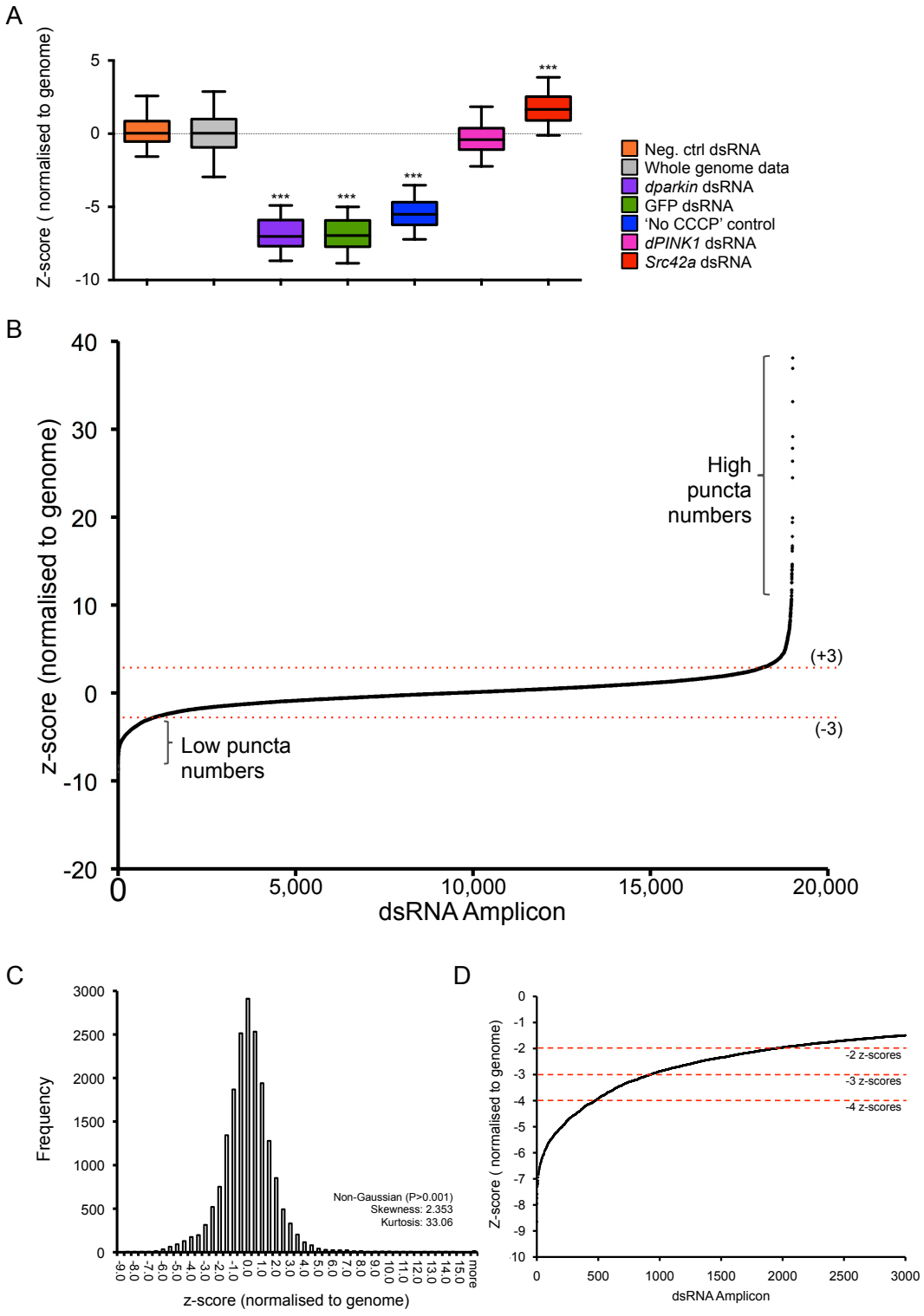

Figure 3.14. Whole genome screen data. (A) Box plot of average control z-scores (y-axis) across the genome. Box plot features as in Figure 3.13. One-way ANOVA with Bonferroni correction where ***P>0.0001 compared to 'Neg. ctrl dsRNA.' (B) Whole genome scatter graph (excluding screen controls) arranged ascending according to z-score. Red lines represent the boundary of amplicons with a z-score of ±3. The left hand tail is populated by dsRNA amplicons producing low numbers of puncta, and the right hand tail, with those producing high numbers of puncta. (C) Frequency distribution graph (histogram) of all data excluding controls. Dataset is non-normal, as surmised from D' Agostino and Pearson omnibus normality test, skewness and kurtosis (indicated). (D) Magnification of the first 3000 dsRNA amplicons, showing the left hand tail. The boundaries of -2, -3 & -4 z-scores are highlighted in red.

~2.5 puncta per cell, a complete block of translocation can take the data -2.5 to the left. However, an increase in translocation could potentially produce a limitless number of puncta - the highest being 19.9 puncta per cell in this case. This potential for large increases causes the data to have a long tail, or skew to the right.

Despite the data not being perfectly 'normal' there are very few cases in reality that fit the Gaussian ideal. The data do have some Gaussian-like properties, for example the median (2.32) and the mean (2.35) 'puncta number per cell' are very close. Additionally, the dataset has a single peak at the centre of the distribution, with tails falling away either side. For this reason, the data can be deemed 'normal' enough to prevent concern.

3.7.1.4 Defining hits

For the scope of this project, the data of interest are those dsRNA amplicons causing a *decrease* in toxin-induced Parkin translocation, as these are fewer in number and potentially more pathway-specific. Defining the cut-off for primary screen hits is largely an arbitrary task, however two factors influenced the decision; z-score values and the number of hits. Z-scores are a measure of the likelihood that the decreased dParkin translocation occurred by chance. For example, a z-score of -2 equates to a chance of 5%, where -3 equates to 0.3%. In many examples, an accepted level of significance is deemed to be a cut-off of ± 2 z-scores (Chia et al, 2010; Fisher et al, 2012; Orvedahl et al, 2011). However, this decision is also influenced by the quantity of hits falling into each of the cut-off groups. For example, if ± 2 z-scores produces an extensive hit list comprising thousands of genes, a more stringent cut-off of may be employed, and vice versa. Here, -2 z-scores provided a vast group of >2000 hit amplicons. Because of this, the stringency of the primary screen cut-off was increased to -3 z-scores, reducing the hit amplicon group to a more manageable number (Figure 3.14 D & 3.15 A).

3.7.1.5 Visual analysis of hits

Before finalising the primary genome hit list, it was apparent that a number of 'empty' wells were present within the 1004 amplicons of the -3 z-score group. These were undoubtedly false positives, and removed from the dataset.

Furthermore, dsRNA amplicons causing cell death or low levels of GFP would likely translate as a 'low puncta' phenotype, due to the absence of a signal in the green channel. In order to reduce false positives via this avenue, every FOV within the

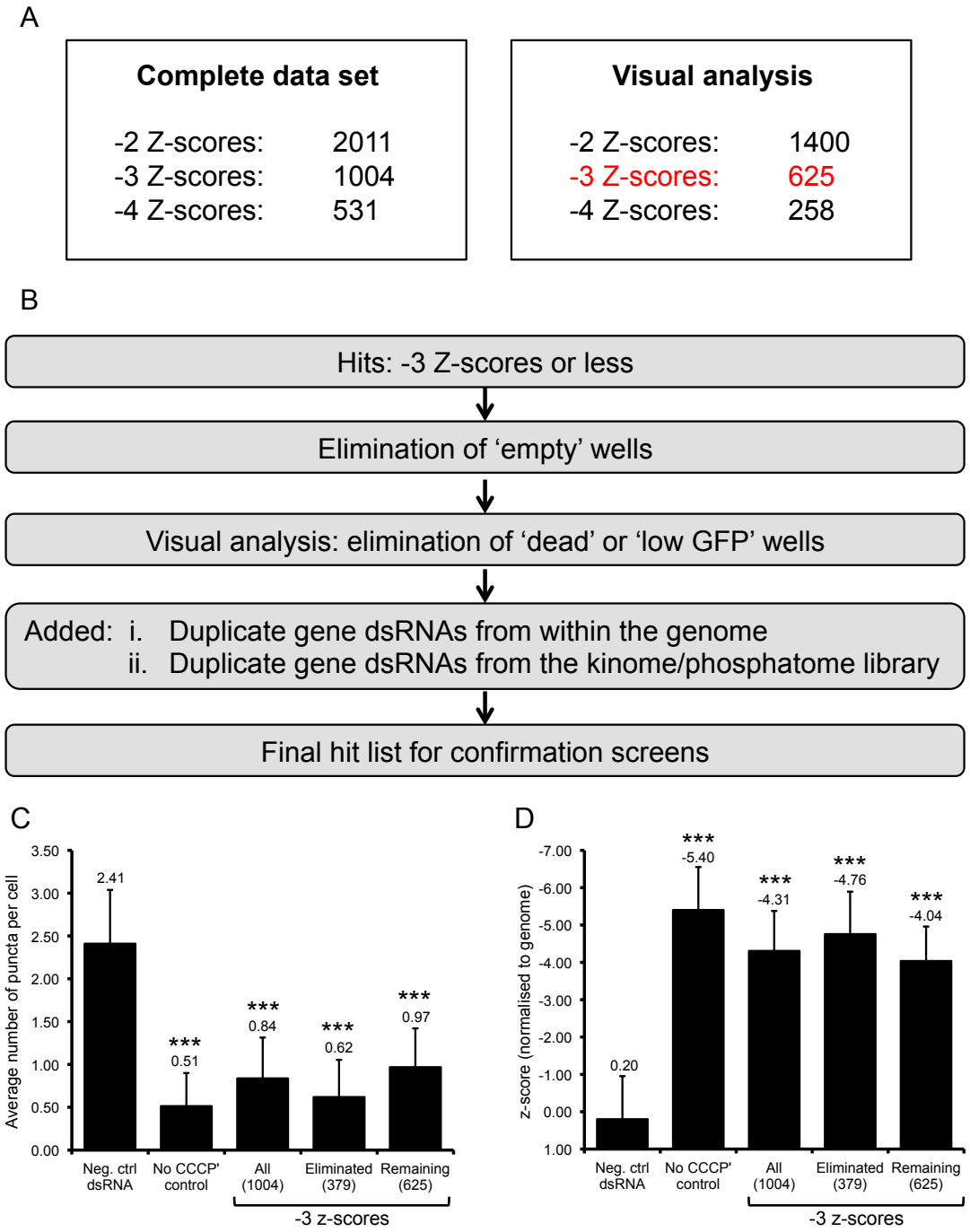

Figure 3.15. Defining primary screen hits for confirmation screens. (A) Numbers of hits depending on the chosen z-score cut-off before and after visual analysis of images. Highlighted in red is the chosen cut-off of -3 z-scores, giving a final primary screen hit list of 625 amplicons. (B) Schematic of final hit-list workflow, detailing the points of amplicon elimination and addition. (C) & (D) Graphical representation of average values (C - average raw data, D - average normalised data), of hit groups, compared to average screen controls. ***P<0.001 (one-way ANOVA with Bonferroni's correction, compared to 'Neg. ctrl dsRNA').

'-3 z-score' cut-off group underwent manual 'visual analysis,' where the viability of the phenotype was assessed. Here, wells containing 'dead,' or 'sick' looking cells were eliminated, as well as those with very low levels of GFP expression. Additionally, wells where the microscope's 'autofocus' feature had failed were eliminated in some cases,

due to the lack of puncta definition. From this, the finalised number of hit amplicons decreased from 1004 to 625 (Figure 3.15 A & B).

Prior to amplicon elimination, the average raw values and z-scores of the complete hit group (1004) were close in magnitude to the average 'No CCCP' control values (Figure 3.15 C & D). This was encouraging as it confirmed that the hit gene group mirrored the positive screen control, hence blocking dParkin translocation to basal levels. To ascertain whether amplicon elimination following visual analysis would dilute the strength of this block, data from the finalised hit group (625 genes) and the eliminated group (379) were compared (Figure 3.15 C & D). Here, slight increases in the average raw value and z-score were observed in the finalised hit group. However, this is not unexpected as many amplicons within the eliminated group caused severe phenotypes such as a complete loss of the GFP signal, and therefore a dramatic decrease in puncta number. However, despite the observed increase, the hit group continues to exhibit a clear effect on dParkin translocation compared to the negative control dsRNA.

3.8 CONFIRMING PRIMARY SCREEN HITS

In order to confirm the phenotypes observed in the primary genome screen, the 625 primary hits went through multiple rounds of re-screening. For this, a custom validation library of 3x 384-well plates was designed and printed, consisting of all 625 hits, negative and positive controls, and any additional non-hit amplicons targeting hit genes within the genome and kinome/phosphatome libraries (Figure 3.15 B). Unlike the whole genome screen, the re-screen plates were custom-designed, allowing for a larger number of inbuilt controls. Therefore, 16 wells per plate were dedicated to 'No CCCP' positive controls, and 60 wells comprised negative control dsRNA against two *C.elegans* genes. Additionally, to reduce the risk of edge effects, all outer wells remained devoid of dsRNA (Figure 3.16 A).

3.8.1 HIT PICKING AND PLATE PRINTING

Generation of the custom re-screen library involved identifying and 'picking' stock PCR templates corresponding to hit dsRNA amplicons. Due to the vast number of hit amplicons, the most efficient method was to automate the process using a liquid handling robot. Once complete, additional templates from the kinome / phosphatome subset library were hand picked and spiked into position manually. Control dsRNA templates were synthesised *de novo,* validated by gel electrophoresis, and added to

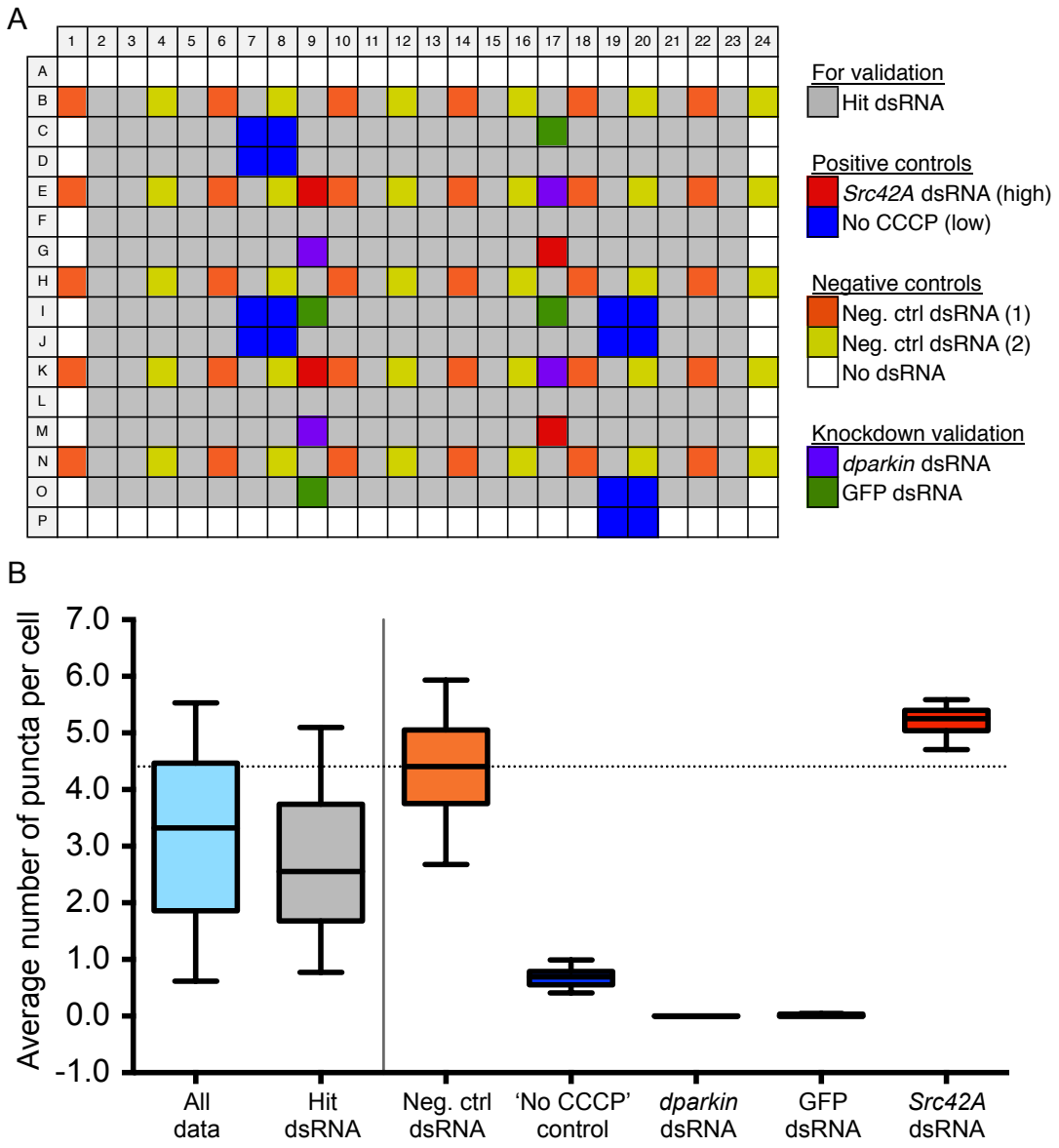

Figure 3.16 Confirmation library layout and data analyses. (A) Assay plate layout with positive and negative controls, and knockdown validation controls indicated (see key) (B) Box-plot representation of control raw data from one round of confirmation screening. Box plot features as in Figure 3.13.

the library by hand. Next, the '*in vitro* transcription' reaction mixture was added, and dsRNA synthesis could proceed. Upon completion, newly synthesised dsRNA amplicons were diluted to achieve a working concentration of 5 ng/µl, and printed at 5 µl/well (250 ng dsRNA), producing multiple copies of the re-screen library.

3.8.2 CONFIRMING PRIMARY HIT AMPLICONS

To confirm primary screen hits, four rounds of re-screening were performed using the same assay implemented in whole genome screening (section 3.3.2.4). Controls behaved as expected in each round, with 'No CCCP' positive controls producing low

numbers of puncta (Figure 3.16 B, navy), and CCCP-treated negative controls producing high numbers of puncta (Figure 3.16 B, orange). Knockdown validation controls (*dparkin* and GFP dsRNA) largely eliminated puncta, and *Src42a* dsRNA moderately increased puncta number (Figure 3.16 B, red) as anticipated. The complete dataset (Figure 3.16 B, light blue) exhibits a lower median value compared to negative control samples (Figure 3.16 B, orange) as expected, and this reduction is further accentuated by removing screen controls (Figure 3.16 B, grey).

3.8.2.1 Defining final screen hits

Unlike the whole genome screen, it was deemed unnecessary to normalise confirmation screen data, as the median and variance of the raw values were comparable between the three library plates. Per re-screen round, a hit amplicon was any dsRNA with a raw puncta score within two standard deviations (SD) of the mean of the 'No CCCP' control. Over four rounds of screening, each time a dsRNA amplicon appeared in the hit list, it achieved a score of 1, enabling an overall score (out of 4) to be calculated (Table 3.1). Additionally, if a gene had more than one dsRNA amplicon in any of the four hit lists, that gene gained an extra 'multiples score' of 0.5, enabling extra weight to be given to genes with reproducible effects. With this, the maximum screen score became 4.5.

An arbitrary confirmation hit cut-off of 2.5 was defined. Here, an amplicon would either be a hit in at least 3 out of 4 repeat screens, or 2 out of 4 screens with multiple hit amplicons. This produced a final confirmed hit list of 115 dsRNA amplicons, targeting 96 unique *Drosophila* genes (Table 3.1).

3.9 DISCUSSION

The initial aim of this chapter was to validate a *Drosophila* S2R+ cell model as an appropriate system to study the PINK1/Parkin-pathway. For this, four major pathway features, previously defined in mammalian cell systems, were assessed. These were CCCP-based dissipation of the $\Delta\Psi m$, dPINK1 MOM stabilisation, dParkin translocation and mitophagy. In the majority of cases, *Drosophila* S2R+ cells faithfully recapitulate events observed in mammalian cells. However, a small number of deviations were observed. First, dPINK1 overexpression highlighted the existence of a stable dPINK1 fraction, co-localising with the mitochondrial marker Mito-GFP, under basal conditions.

	Name	Probe ID	Score	Multiples Score
1	*Cdk9*	BKN50890	4	4.5
2	*Cdk9*	BKN50460	4	4.5
3	*Eaf*	BKN27861	4	4.5
4	*Gclm*	BKN27668	4	4.5
5	*puc*	BKN25001	4	4.5
6	*puc*	BKN46004	4	4.5
7	*sgg*	BKN50830	4	4.5
8	*tlk*	BKN28036	4	4.5
9	*CG14023*	BKN30204	4	4
10	*CG2469*	BKN21463	4	4
11	*CG3078*	BKN41059	4	4
12	*CG34449*	BKN40585	4	4
13	*CG42784*	BKN33482	4	4
14	*Cp1*	BKN27765	4	4
15	*Ctr1A*	BKN27755	4	4
16	*dco*	BKN41636	4	4
17	*Gclc*	BKN45924	4	4
18	*Hsc70-2*	BKN45569	4	4
19	*l(2)01810*	BKN23239	4	4
20	*lilli*	BKN23012	4	4
21	*MED14*	BKN22798	4	4
22	*MED19*	BKN22921	4	4
23	*MED24*	BKN20580	4	4
24	*Npc2f*	BKN31008	4	4
25	*Rpb10*	BKN29118	4	4
26	*Rpb5*	BKN20359	4	4
27	*Rpb8*	BKN29127	4	4
28	*Rrp6*	BKN20686	4	4
29	*scny*	BKN22179	4	4
30	*sec23*	BKN20755	4	4
31	*Srp54*	BKN22462	4	4
32	*Topors*	BKN23004	4	4
33	*trr*	BKN20376	4	4
34	*Cklalpha*	BKN27574	3	3.5
35	*CkIIalpha*	BKN28436	3	3.5
36	*CkIIalpha*	BKN50525	3	3.5
37	*CkIIbeta*	BKN51125	3	3.5
38	*CkIIbeta*	BKN50911	3	3.5

	Name	Probe ID	Score	Multiples Score
39	*CkIIbeta*	BKN29263	3	3.5
40	*Eaf*	BKN46090	3	3.5
41	*eIF5*	BKN45562	3	3.5
42	*Gclm*	BKN46368	3	3.5
43	*Not1*	BKN50316	3	3.5
44	*Not1*	BKN20186	3	3.5
45	*Not1*	BKN50633	3	3.5
46	*puc*	BKN60449	3	3.5
47	*Adf1*	BKN31012	3	3
48	*Arf79F*	BKN21447	3	3
49	*Arf84F*	BKN28053	3	3
50	*atl*	BKN21206	3	3
51	*atms*	BKN20176	3	3
52	*CG11198*	BKN22148	3	3
53	*CG13298*	BKN22482	3	3
54	*CG14047*	BKN29644	3	3
55	*CG14239*	BKN30730	3	3
56	*CG17660*	BKN20727	3	3
57	*CG30159*	BKN45335	3	3
58	*CG30359*	BKN22317	3	3
59	*CG3436*	BKN45977	3	3
60	*CG3975*	BKN46113	3	3
61	*CG42732*	BKN29974	3	3
62	*CG5591*	BKN27099	3	3
63	*CG9636*	BKN28345	3	3
64	*CG9883*	BKN30450	3	3
65	*cn*	BKN22004	3	3
66	*comm3*	BKN27166	3	3
67	*ctp*	BKN41267	3	3
68	*desat1*	BKN45646	3	3
69	*Dis3*	BKN21524	3	3
70	*eyg*	BKN30760	3	3
71	*Fer1HCH*	BKN30669	3	3
72	*HLH106*	BKN22813	3	3
73	*Hsc70-1*	BKN31450	3	3
74	*kto*	BKN22025	3	3
75	*lark*	BKN27711	3	3
76	*MED7*	BKN27339	3	3

	Name	Probe ID	Score	Multiples Score
77	*mod(mdg4)*	BKN41015	3	3
78	*msi*	BKN22154	3	3
79	*MtnA*	BKN32833	3	3
80	*Nlp*	BKN30946	3	3
81	*Nup75*	BKN22034	3	3
82	*pic*	BKN20655	3	3
83	*Pp1-87B*	BKN31383	3	3
84	*Prp31*	BKN22756	3	3
85	*ptip*	BKN22515	3	3
86	*pUf68*	BKN27426	3	3
87	*RpL28*	BKN45643	3	3
88	*RpL36*	BKN46193	3	3
89	*RpS14a*	BKN42019	3	3
90	*RpS6*	BKN46529	3	3
91	*Sas10*	BKN20168	3	3
92	*sl*	BKN21616	3	3
93	*srp*	BKN32327	3	3
94	*ssh*	BKN20682	3	3
95	*Syx5*	BKN21048	3	3
96	*TfIIFalpha*	BKN45044	3	3
97	*transfer RNA*	BKN40591	3	3
98	*ttk*	BKN30420	3	3
99	*Ubqn*	BKN20953	3	3
100	*vps2*	BKN22197	3	3
101	*Withdrawn*	BKN33475	3	3
102	*Withdrawn*	BKN41593	3	3
103	*CG12050*	BKN22946	2	2.5
104	*CG12050*	BKN46155	2	2.5
105	*CG2685*	BKN20517	2	2.5
106	*CG2685*	BKN46253	2	2.5
107	*CkIIalpha*	BKN50398	2	2.5
108	*eIF5*	BKN22365	2	2.5
109	*Rpb12*	BKN41948	2	2.5
110	*Rpb12*	BKN34093	2	2.5
111	*sgg*	BKN50521	2	2.5
112	*sgg*	BKN28994	2	2.5
113	*Tango6*	BKN26681	2	2.5
114	*tlk*	BKN50352	2	2.5
115	*tlk*	BKN50260	2	2.5

Table 3.1 Final hit list of confirmed dsRNA amplicons. Each row gives details of the official *Drosophila* gene name, library probe identifier (BKN), overall confirmation screen score, and multiples score. The list had been arranged by the 'multiples score' (high to low), and then alphabetically according to 'Name.' Genes highlighted in grey have more than one amplicon in the list.

On the contrary, in mammalian cells, basal PINK1 is cytoplasmic in distribution and expressed at very low levels owing to its rapid turnover. This suggests a deviation in the rate of protein turnover between *Drosophila* and mammalian systems in the absence of mitochondrial stress.

Additionally, despite an observed decrease in the mitochondrial marker ATP5A following chronic exposure to CCCP, the severity of this effect in S2R+ cells proved highly variable compared to reports in HeLa cells (Narendra et al, 2008). In S2R+ cells, high levels of cell death were frequently observed at CCCP time-points in excess of 16 hours, suggesting that these cells favour apoptosis over mitophagy. In a bid to optimise the assay, many parameters were assessed including a wide range of CCCP time points and concentrations, but to no avail. Perhaps much like mammalian systems, *Drosophila* mitophagy occurs in a cell-type specific manner, whereby nutrient source and the favoured mode of energy production dictate mitochondrial degradation under toxic conditions. Like mammalian primary neurons, S2R+ cells favour mitochondrial oxidative phosphorylation over glycolysis (Freije et al, 2012; Gusdon & Chu, 2011) suggesting that they are less likely to permit mitophagy even following widespread mitochondrial damage. In contrast, transformed HeLa cancer cells favour glycolytic, mitochondria-independent modes of energy production, perhaps explaining why they readily 'give-up' their mitochondria following damage.

Despite these deviations, S2R+ cells appear to exhibit the majority of PINK1/Parkin-pathway characteristics compared with mammalian systems, therefore providing a reliable model for pathway analysis. The next challenge was to design and optimise an assay capable of successful high-throughput application, with the objective of improving our understanding of the PINK1/Parkin-pathway in the context of mitophagy. In the absence of a robust 'mitophagy' assay (perhaps the most obvious choice for maximum data capture) our attention turned to processes upstream of mitophagy, specifically Parkin translocation. Here, Parkin translocation proved to be efficiently induced with a short, 2-hour exposure to CCCP, and easily quantified through the appearance of Parkin-GFP dots or 'puncta.' With the addition of an S2R+ cell line stably expressing Parkin-GFP, an image-based screening assay was designed looking at CCCP-induced Parkin translocation.

The assay proved to be very robust and extremely reproducible between experiments; essential attributes for high-throughput screening. However, a significant obstacle appeared in the form of our positive screen control. One of the fundamental principles of the PINK1/Parkin-pathway, at least in mammalian cell systems, is the requirement of

PINK1 for Parkin translocation and subsequent mitophagy. However, in our S2R+ system, *dPINK1* silencing had no effect on the ability of dParkin to translocate. Having verified the reduction of both *dPINK1* mRNA, and protein activity (using indirect means), the most obvious conclusion is that these cells don't rely upon dPINK1 for dParkin translocation. This is most likely due to a divergence in pathway function at the level of Parkin translocation, as downstream processes such as dMfn modification and mitochondrial perinuclear aggregation (Chapter 4) are blocked by *dPINK1* silencing. Additionally, in the whole organism, dPINK1 is known to act upstream of dParkin, with mutants sharing comparable phenotypes. I would speculate that in S2R+ cells, dParkin continues to translocate to damaged mitochondria following *dPINK1* silencing, perhaps via a long-lived MIM dPINK1 pool. However, once at the mitochondrial surface, this pool of dPINK1 is incapable of activating dParkin's latent E3-ubiquitn ligase activity (for reasons currently unknown), hence blocking pathway activation. Therefore, like mammalian systems, *dPINK1* loss in S2R+ cells appears to block the PINK1/Parkin-pathway, albeit downstream of dParkin translocation.

Rather than abandoning the entire assay based on the failings of *dPINK1*-silencing to confer the 'expected' result, an alternative means of creating a 'positive control effect' came in the form of a 'No CCCP' region within the screening plates. This acted to create an 'artificial' positive phenotype, essentially providing a measure of basal dParkin translocation levels. With the assay fully optimised, the aim of the whole genome screen was to discover novel genes acting upstream of dParkin translocation in the PINK1/Parkin-pathway. By performing the assay as a single pass, it was accepted that a number hits were likely to be missed through false negative events. These false negatives could occur for a number of reasons including experimental error with regards to equipment, and user and reagent malfunctions. Additionally, differential protein dynamics could play a role in this process, with some proteins out-living the knockdown duration, even after 72 hours of silencing. However, it is generally agreed that no whole genome RNAi screen is perfect, and despite these drawbacks, we expected to identify at least a proportion of dParkin translocation-dependent genes.

Following data analyses, a cut-off of -3 z-scores provided a substantial primary hit list of 1004 dsRNA amplicons. However, due to the nature of the 'Transfluor' algorithm, any dsRNA reducing the expression of GFP or causing cell death would be indistinguishable from genuine hits. Such genes were likely to be performing a vital housekeeping function rather than exhibiting PINK1/Parkin-pathway specificity, and were therefore considered 'false positives.' In order to deal with these 'hits,' visual

analysis of raw microscopy images was undertaken, leading to the removal of over 35% of the original primary hit group. This reduced the hit list to 625 dsRNA amplicons.

Following completion of the primary screen, rigorous hit 'confirmation screens' aimed to further eliminate false positives in the dataset. After four rounds of repeat screening, over 80% of the original 625 primary screen hits fell outside the hit criteria, producing a final validation hit list of 115 dsRNA amplicons, corresponding to 96 unique genes.

From the initial ~20,000 dsRNA targets, repeat rounds of screening have led to the identification of 96 *Drosophila* genes able to robustly and reproducibly decrease dParkin translocation following CCCP toxification. The next challenge was to take these genes, and assess their ability to influence other aspects of mitochondrial homeostasis using a range of secondary screening assays. Specifically, these assays aim to assess dParkin translocation using an alternative mode of mitochondrial damage, mitochondrial morphology alterations and toxin-induced mitochondrial perinuclear aggregation. Collating data from these secondary screens should help to build a clearer picture of the way in which hit genes influence PINK1/Parkin-mediated processes, and crucially whether this effect is specific to mitochondria and their toxin-induced degradation.

4. SECONDARY SCREENING – *DROSOPHILA* CELLS

4.1 BACKGROUND

Following completion of the primary screen, the next challenge was to assess the primary hit genes in a series of secondary assays, examining several aspects of mitochondrial homeostasis. These included analysis of mitochondrial morphology, and mitochondrial perinuclear aggregation following toxification. Collating data from these secondary screens allowed the production of a final *Drosophila* hit list, within which a number of distinct, pre-defined pathways emerged. The presence of such pathways assisted in the construction of the final hit list, allowing genes of particular interest to be included where they would have otherwise been omitted.

4.2 HYPOTHESES AND AIMS

The purpose of applying a range of secondary screens to the primary hit amplicons is to test their ability to alter processes that are distinct, but related in nature to the original screen. This is particularly useful when dealing with large datasets, where specific genes or pathways must be selected for in-depth analysis. For example, in the case of this project, the 115 confirmed hit amplicons were too great in number to take directly into an *in vivo* model, and required narrowing down further.

An additional aim of secondary screen analysis is to learn more about how these genes could play a role in the pathway of interest. For example, the three assays implemented here assess multiple points of the PINK1/Parkin-pathway including dParkin translocation, alterations in mitochondrial morphology and toxin-induced perinuclear aggregation of mitochondria prior to mitophagy (Figure 1.10).

After collating data from each of the secondary screens, and cross-referencing back to the primary screening data, final *Drosophila* screen hits were determined based on their ability to influence a range of mitochondrial homeostatic processes.

4.2.1 PARAQUAT-INDUCED PARKIN TRANSLOCATION

With respect to the primary screen, one important question to answer was whether the dParkin translocation observed was a CCCP-specific effect, or whether alternative mitochondrial insults could produce the same effect. To tackle this question, the herbicide paraquat was employed. The nature of paraquat is to increase the production of reactive oxygen species (ROS), causing oxidative damage to various cellular components. Where CCCP is able to dissipate any compartment with a differential pH

gradient, including lysosomes & peroxisomes, paraquat is suggested to act at the level of complex I of the mitochondrial ETC (Cocheme & Murphy, 2008), perhaps making this toxin more 'mitochondria-specific'.

4.2.2 MITOCHONDRIAL MORPHOLOGY ANALYSIS

A crucial mechanism for maintaining the health of the mitochondrial network is the ability of individual organelles to undergo fission and fusion. This dynamism allows damaged mitochondrial components to become segregated from the network, and removed via the mitophagy route, whilst facilitating their replacement through content mixing (Twig et al, 2008). The importance of this process is highlighted in Mitofusin (Mfn)-null MEFs, where in the absence of fusion, the fragmented network comprises a heterogeneous population of mitochondria with varying degrees of health (Narendra et al, 2010). Additionally, in conditional double knockout mice, lacking both *MFN1* and *MFN2* in muscle cells, mitochondria display a marked reduction in mtDNA content coupled with an increase in mtDNA mutation (Chen et al, 2010).

In *Drosophila* cells, the loss of *dPINK1* or *dparkin* produces a hyper-fused mitochondrial network, indicating a pro-fission or anti-fusion role for these proteins under physiological conditions. This involvement of the PINK1/Parkin-pathway in mitochondrial morphology is likely linked to the need to segregate damaged mitochondrial compartments for removal via mitophagy. Recent reports show that Mfn is ubiquitinated and degraded via the proteasome in a PINK1- and Parkin-dependent manner, preventing isolated mitochondria from re-fusing with the network (Gegg et al, 2010; Glauser et al, 2011; Poole et al, 2010; Rakovic et al, 2011; Ziviani et al, 2010). Also, PINK1 and Parkin may reduce the fusion-potential of damaged mitochondria by causing the degradation of the mitochondrial transport protein, Miro, leading to spatial isolation (Wang et al, 2011).

This secondary assay aimed to assess whether primary screen hits were able to effect mitochondrial morphology, and if so, by what means. Particular interest focused on those amplicons able to phenocopy the *dPINK1* and *dparkin* dsRNA effect; but any deviation from the wild-type scenario was deemed noteworthy.

4.2.3 MITOCHONDRIAL PERINUCLEAR AGGREGATION

One of the last stages of PINK1/Parkin-mediated mitophagy prior to degradation is the aggregation of dysfunctional mitochondria in the perinuclear region (Figure 1.10). This

organellar re-distribution is considered to increase the efficiency of the autophagy machinery, allowing degradation to progress rapidly (Okatsu et al, 2010; Vives-Bauza et al, 2010). Essentially, the manifestation of aggregated mitochondria in the perinuclear region is tantamount to the induction of mitochondrial degradation.

Using this phenomenon as a screen read-out, the aim was to ascertain which of the primary 'dParkin translocation' hits also influence the redistribution of mitochondria prior to degradation. Through this, it can be determined whether the observed dParkin translocation block was due to mitophagy-pathway inhibition, or a non-specific effect.

4.2.4 SECONDARY SCREENING LIBRARY

For secondary screening, the confirmation screen library from section 3.8 was deployed rather than generating a further custom library of confirmed screen hits. This was for a number of reasons. First, as experienced in previous rounds of hit picking, the process is both time-consuming and costly due to the vast number of dsRNA probes required. Second, confirmation dsRNA stock volumes were greatly in excess of that required for re-screening purposes, and therefore able to provide multiple surplus copies of the library. Finally, it was deemed an interesting exercise to assess if amplicons falling outside of the final hit list could influence other aspects of mitochondrial homeostasis despite a weak or inconsistent influence on dParkin translocation.

The confirmation library was made up of 3x 384 plates, comprising all 625 primary screen hits, plus user controls and an empty outside edge of wells (Figure 3.16 A). These empty wells were built into the plate design to reduce the risk of edge effects. However, here they offered the additional advantage of allowing extra screen controls to be added to the plates depending upon the assay.

4.3 PARAQUAT-INDUCED PARKIN TRANSLOCATION

Paraquat is a herbicide and oxidant known to increase the production of cellular ROS via redox cycling (Berry et al, 2010; Bonneh-Barkay et al, 2005). Due to the similarities in structure between paraquat and the parkinsonian toxin, MPP^+ it is suggested that these toxins act in an analogous fashion, via the inhibition of complex I of the electron transport chain (ETC). Whilst the exact mechanism of paraquat-related toxicity remains unclear (reviewed in Berry et al, 2010; Blesa et al, 2012; Miller, 2007), the

mitochondrial matrix, and complex I of the ETC have been identified as the principle site of paraquat action, and reduction respectively (Castello et al, 2007; Cocheme & Murphy, 2008). However, paraquat-dependent complex I inhibition is weak compared to MPP^+, and requires millimolar concentrations (Richardson et al, 2005). These data suggest that paraquat may exert its oxidative damage on targets other than mitochondrial complex I. Yet, mitochondria appear to be the principle site of paraquat action, and are therefore likely to be particularly vulnerable to the ensuing oxidative damage.

The aim of this secondary screen was to assess the effect of paraquat toxification on dParkin translocation. The reason for examining a different toxin with the same read-out as the primary screen was to verify that the observed translocation was due to mitochondrial damage caused by CCCP, and not the CCCP itself. Paraquat exposure was chosen over other cellular toxins because of its distinct mode of action compared to CCCP, as well as the suggestion that it acts directly at the level of the mitochondria. Chronic exposure to paraquat and the subsequent build-up of cellular ROS are anticipated to have analogous effects on PINK1/Parkin-pathway activation as CCCP toxification. This is due to increased mitochondrial molecular damage caused by ROS production. From a temporal point of view however, the paraquat-toxification phenotype is likely to be less severe than that observed with CCCP, due to the time taken for ROS to build up and mediate its deleterious effect. In agreement with this suggestion, Parkin translocation in HeLa cells is observed after 24 hours of paraquat toxification, compared to 1 hour of CCCP treatment (Narendra et al, 2008).

4.3.1 ASSAY DEVELOPMENT

In line with other studies, the concentration of paraquat required to produce a Parkin translocation event is in the millimolar region (Narendra et al, 2008; Narendra et al, 2010; Ziviani et al, 2010). For this reason, assay development involved the analysis of cells after the application of 10 mM paraquat. Following a toxification time-course, increasing levels of dParkin translocation were observed at 12 and 24 hours of paraquat treatment (Figure 4.1 A - C). In agreement with mammalian data, 24 hours of toxification was selected as the optimum duration (Narendra et al, 2008) as here, widespread dParkin translocation is observed compared to the non-toxified control. This time point also enabled the assay to run in parallel with mitochondrial perinuclear aggregation analysis (section 4.5), reducing the secondary screen workload.

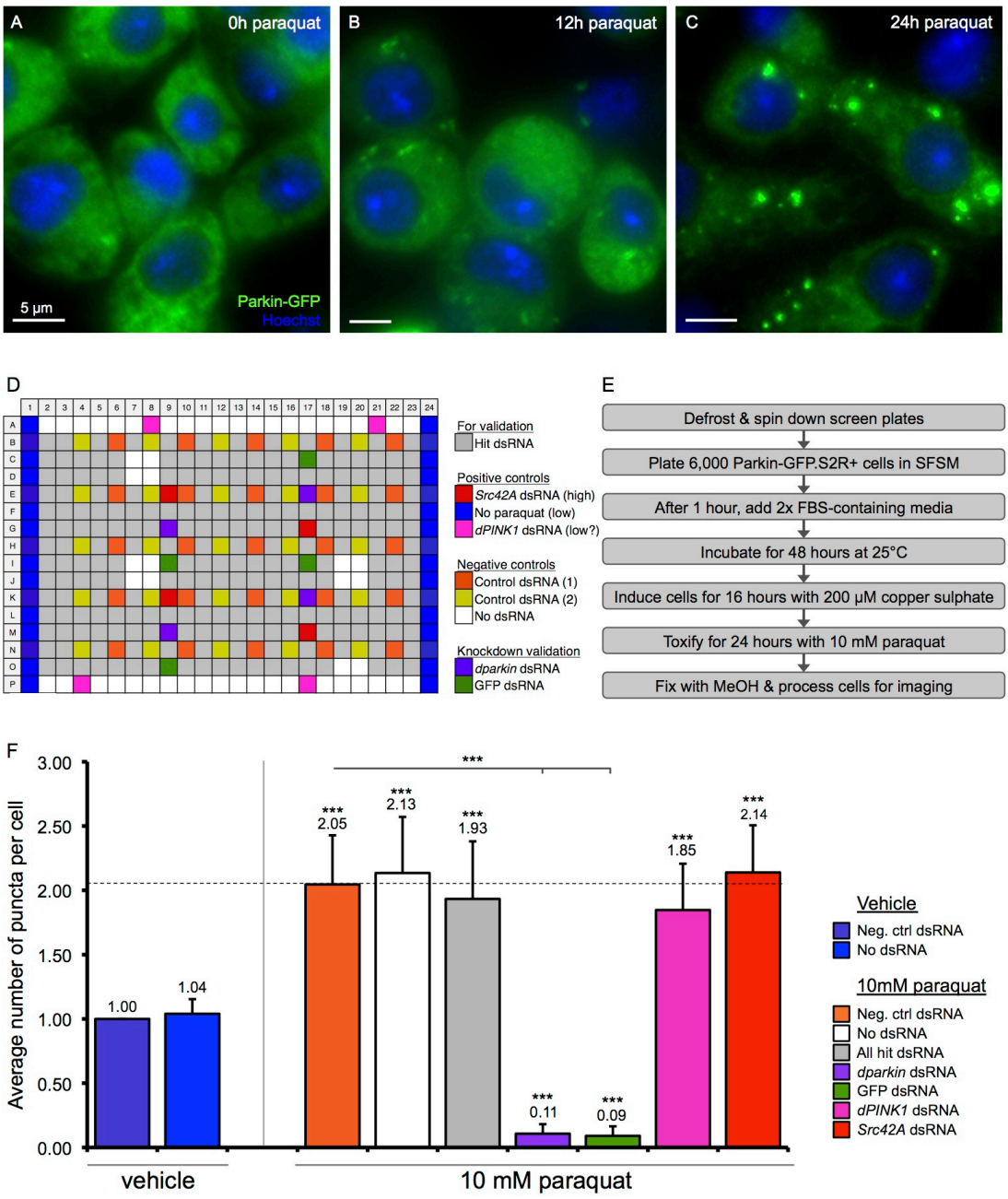

Figure 4.1 Parkin translocation following paraquat toxification. Parkin-GFP.S2R+ cells were subjected to 10 mM paraquat toxification for 0 hours (A), 12 hours (B) and 24 hours (C), after which an increase in GFP puncta formation could be observed. Scale bar: 5 µm (D) Diagram of assay plate design where colours represent different conditions (see key). Here columns 1 & 24 remain non-toxified, providing the 'no paraquat' control. Within these columns there are both 'Neg ctrl dsRNA' (indigo) and 'no dsRNA' (blue) controls. (E) Protocol workflow for paraquat-induced Parkin translocation. (F) Graphical representation of controls, normalised to 'Neg. ctrl. dsRNA' (vehicle) and averaged across the three repeat screens, Error bars represent standard deviation, ***P<0.001 (One-way ANOVA with Bonferroni's correction, compared to the vehicle-treated 'Neg. ctrl dsRNA' unless otherwise indicated).

4.3.2 PLATE LAYOUT

As previously mentioned, copies of the confirmation library (section 3.8) were ultilised for all secondary screening purposes. The similarity of this particular assay to that of the primary screen meant the availability of empty wells for extra screen controls were

largely unnecessary. However, four *dPINK1* dsRNA-containing wells were included, to test whether *dPINK1*-silencing could prevent dParkin translocation under an alternative toxification regime (Figure 4.1 D, pink). Also, like the primary screen, a 'no paraquat' or 'vehicle-treated' control was employed, providing the base level of Parkin-GFP puncta. Rather than integrate these controls into the four quadrants as in previous assays, here they populate columns 1 & 24 of the plate (Figure 4.1 D, blue), eliminating the requirement of the liquid handling robot. Where this equipment is a great time-saver when dealing with large numbers of plates, it becomes inefficient on a smaller scale due to lengthy set-up procedures.

As before, pre-printed dsRNA controls included two *C. elegans* dsRNA negative controls, two knockdown validation controls (*dparkin* & GFP dsRNA), and *Src42A* dsRNA (Figure 4.1 D).

4.3.3 PROTOCOL

The assay protocol for this screen followed largely the same steps as outlined for the primary screen. However, there were some deviations, mostly due to the fact that both this assay, and the perinuclear aggregation of mitochondria were assessed in the same plate. Because of the differing requirements of the perinuclear aggregation assay, the cells were exposed to a lower concentration of copper sulphate, for a longer duration; specifically 200 µM for 40 hours. Additionally, samples were fixed using ice-cold methanol rather than formaldehyde, allowing cellular permeabilisation for antibody application (Figure 4.1 E).

4.3.4 DATA ANALYSES

Parkin translocation assays were performed in triplicate to ensure reproducibility of the observed effect. Using the high content screening microscope, 9 FOV were captured per well using a 40x objective. As in the primary screen, data analyses were automated with the 'Transfluor' application, where objects with a size between 0.6 – 1 µm, and intensity above 60 grey levels, were counted as 'puncta'. The numerical output from this analysis was averaged over the 9 FOV, giving one value of 'average number of puncta per cell' for each dsRNA amplicon.

4.3.4.1 Controls

Having analysed the data from all three screens, average values for each of the controls could be calculated (Figure 4.1 F). This analysis showed a clear paraquat-induced increase in puncta number in both empty & negative control dsRNA-containing wells compared to vehicle-treated samples. Additionally as before, both *dparkin* & GFP dsRNA reduced the number of puncta to very low levels, confirming the silencing process. *dPINK1* dsRNA shows a slight reduction in the number of puncta per cell; and *Src42A* dsRNA shows a slight increase in the number of puncta per cell, but neither reach significance. Looking at the hit dsRNA dataset as a whole, this trends towards reducing the number of puncta per cell, as expected.

4.3.5 DEFINING HITS

Per screening round, a hit amplicon was any dsRNA with a raw puncta score within two standard deviations (SD) of the mean of the vehicle-treated negative control dsRNA (background puncta levels). Over three rounds of screening, each time an amplicon appeared in the hit list it was given a score of 1. Upon completion of the three screens, the score from each round was totaled, producing an overall 'score' for each dsRNA. For an amplicon to be deemed an overall 'hit', a minimum score of 2 was required

4.3.6 FINALISED HIT LIST

Having applied the above parameters to the screen data, a final list of 99 dsRNA hits were defined (Table 4.1). 56% of these hits were confirmed primary screen hits from section 3.8, with the remaining 44% of genes failing to qualify for this group. One such gene was *archipelago*, which achieved an overall score of 2 in the confirmation screens, hence missing out on the confirmed primary hit list. The significance of this gene will become apparent in later chapters.

Of note, this secondary screen hit list also contains two genes denoted '*withdrawn*.' This has arisen due to the *Drosophila* gene database, FlyBase continuously reviewing the status of *Drosophila* genes, removing or 'withdrawing' suspected pseudogenes from the database. Whilst these dsRNA amplicons produce an observable effect in our assays, it is unknown whether this is due to genuine gene silencing, or an off-target effect. These 'genes' possess no gene name, and have no obvious mammalian homolog, making further investigation challenging. Because of this, all 'withdrawn' genes achieving 'hit' status in this chapter are disregarded in subsequent analyses.

	Name	Probe ID	Score
1	*ago*	BKN27400	3
2	*atms*	BKN20176	3
3	*Bap55*	BKN20365	3
4	*CG14023*	BKN30204	3
5	*CG1677*	BKN23607	3
6	*CG17912*	BKN29387	3
7	*CG3078*	BKN41059	3
8	*CG40228*	BKN41643	3
9	*CG5591*	BKN27099	3
10	*Cp1*	BKN27765	3
11	*Ctr1A*	BKN27755	3
12	*Dis3*	BKN21524	3
13	*lilli*	BKN23012	3
14	*MED24*	BKN20580	3
15	*Pcaf*	BKN22042	3
16	*Pp1-87B*	BKN31383	3
17	*Pros26.4*	BKN21532	3
18	*Pros29*	BKN28002	3
19	*pUf68*	BKN27426	3
20	*Rrp6*	BKN20686	3
21	*scny*	BKN22179	3
22	*sgg*	BKN50521	3
23	*Srp54*	BKN22462	3
24	*ana1*	BKN29607	2
25	*Arc2*	BKN29801	2
26	*Arf84F*	BKN28053	2
27	*Ars2*	BKN29705	2
28	*BG4*	BKN25956	2
29	*Brd8*	BKN27830	2
30	*Cdk9*	BKN50890	2
31	*CG10267*	BKN25765	2
32	*CG1109*	BKN20307	2
33	*CG12050*	BKN22946	2
34	*CG14215*	BKN21028	2
35	*CG14239*	BKN30730	2
36	*CG16922*	BKN30892	2
37	*CG17209*	BKN20183	2
38	*CG2469*	BKN21463	2
39	*CG2685*	BKN20517	2
40	*CG34137*	BKN40629	2
41	*CG34420*	BKN29967	2
42	*CG34449*	BKN40585	2
43	*CG3975*	BKN30497	2
44	*CG4294*	BKN23609	2
45	*CG5118*	BKN25778	2
46	*CG6220*	BKN25940	2
47	*CG7886*	BKN21063	2
48	*CG8369*	BKN31376	2
49	*CG8378*	BKN20173	2
50	*CG9866*	BKN30634	2
51	*CG9883*	BKN30450	2
52	*CkIIalpha*	BKN50525	2
53	*CkIIalpha*	BKN28436	2
54	*CkIIalpha*	BKN50398	2
55	*CkIIbeta*	BKN50911	2
56	*CkIIbeta*	BKN29263	2
57	*CkIIbeta*	BKN51125	2
58	*clumsy*	BKN25605	2
59	*cn*	BKN22004	2
60	*comm3*	BKN27166	2
61	*e(y)3*	BKN32108	2
62	*Eaf*	BKN46090	2
63	*Eaf*	BKN27861	2
64	*Gclc*	BKN45924	2
65	*Gclm*	BKN27668	2
66	*l(1)G0007*	BKN22970	2
67	*l(2)01810*	BKN23239	2
68	*l(2)37Cb*	BKN20322	2
69	*MED14*	BKN22798	2
70	*MED19*	BKN22921	2
71	*MED7*	BKN27339	2
72	*MRG15*	BKN27689	2
73	*msi*	BKN22154	2
74	*Npc2f*	BKN31008	2
75	*Peritrophin-A*	BKN29878	2
76	*Pk17E*	BKN31019	2
77	*Pka-R1*	BKN22753	2
78	*Pros25*	BKN29089	2
79	*ptip*	BKN22515	2
80	*Rpb10*	BKN29118	2
81	*Rpb5*	BKN20359	2
82	*Rpb8*	BKN29127	2
83	*RpL28*	BKN45643	2
84	*sec23*	BKN20755	2
85	*Sec61alpha*	BKN45120	2
86	*sgg*	BKN50830	2
87	*SMC2*	BKN20562	2
88	*snRNP-U1-70K*	BKN45552	2
89	*srp*	BKN32327	2
90	*ssh*	BKN20682	2
91	*Sym*	BKN21288	2
92	*TfIIFalpha*	BKN45044	2
93	*TfIIFbeta*	BKN45759	2
94	*tlk*	BKN28036	2
95	*tlk*	BKN50352	2
96	*U2af38*	BKN28210	2
97	*U2af50*	BKN22886	2
98	*Withdrawn*	BKN40739	2
99	*Withdrawn*	BKN41635	2

Table 4.1 Paraquat-induced translocation of Parkin - hit table. Each row gives details of the official *Drosophila* gene name, library probe identifier (BKN), and overall secondary screen score. The list has been arranged by the 'score' (high to low), and then alphabetically according to 'Name.' Genes highlighted in grey have more than one amplicon in the hit list.

4.4. MITOCHONDRIAL MORPHOLOGY ANALYSIS

A well-documented feature of mitochondria in both mammalian and *Drosophila* systems is the highly dynamic nature of the mitochondrial network. Individual mitochondria are able to undergo rounds of fusion and fission, whereby content mixing and quality control is regulated. Under basal conditions, the mitochondrial network consists of a mixture of 'tubular' or 'fused' mitochondria, and 'dot-like' or 'fragmented' mitochondria; the make-up of which is constantly changing depending on cellular requirements. A number of core fusion and fission genes are known to be involved in this process, with *Drp1* and *Fis1* regulating fission, and *Opa1* and *Mfn1 & 2* regulating fusion.

Key studies in *Drosophila* have identified a genetic interaction between the core morphology machinery proteins, *dPINK1* and *dparkin*, suggesting a role for the PINK1/Parkin-pathway in the promotion of fission and/or inhibition of fusion (Deng et al, 2008; Poole et al, 2008; Yang et al, 2008). In support of these data, *dPINK1* or *dparkin*

silencing in *Drosophila* S2R+ cells causes a hyperfused mitochondrial network, likely due to the absence of dParkin-dependent dMfn ubiquitination (Ziviani et al, 2010). Data from mammalian studies have shown that this Mfn ubiquitination leads to its removal from the MOM, and subsequent proteasomal degradation (Glauser et al, 2011; Sarraf et al, 2013; Tanaka et al, 2010); a process believed to be important for the segregation of failing mitochondria from the network (Ziviani & Whitworth, 2010). Without this ubiquitination event, Mfn will persist on the MOM, promoting incongruous organelle fusion.

The aim of this secondary screen was to assess the effect of hit gene silencing on the morphology of the mitochondrial network. The working hypothesis was that genes causing a comparable 'fused' morphology to that of *dPINK1* and *dparkin* dsRNA, may act in the same linear pathway. Additionally, dsRNA amplicons causing a severe fusion or fragmentation phenotype were regarded as interesting, due to their ability to impact upon mitochondrial morphology as a whole.

4.4.1 ASSAY DEVELOPMENT

Before assessing mitochondrial morphology in a high-throughput setting, a number of low-throughput assays were performed to ascertain the optimal method of quantification, as well as validating potential screen controls.

4.4.1.1 Scoring system

To give a numerical value to the qualitative morphological phenotypes observed, a scoring system previously developed in the laboratory was implemented (Pogson et al., manuscript in preparation). This involved the identification of four distinct phenotypes using a scale ranging from 1 - 4 (Figure 4.2 A). Here, a score of 1 represents a 'fragmented' mitochondrial network; a score of 2 represents a 'wild-type' network; 3 represents a 'fused' network, and 4 represents a 'clumped' network.

For a network to be deemed 'fragmented,' small discrete mitochondria are present, with scant areas of fusion. In the 'wild-type' situation, a mixture of both fused and fragmented mitochondria are present. In the 'fused' state, the majority of the network comprises long, interconnected 'strings', and a 'clumped' phenotype is regarded as a severe form of fusion, with mitochondria forming a large, aggregated mass, often in perinuclear regions (Figure 4.2 A).

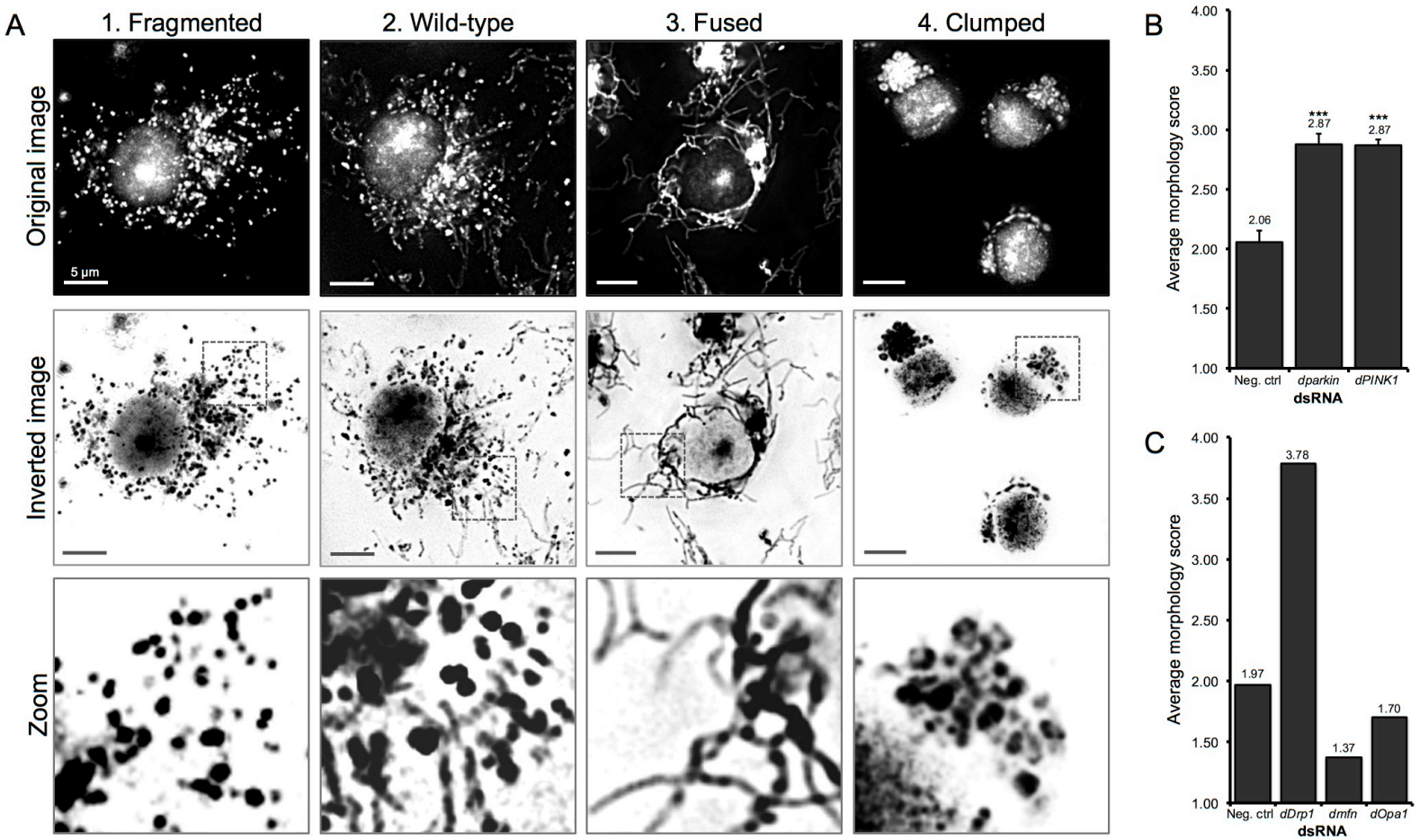

Figure 4.2 Defining a scoring system for mitochondrial morphology analysis. (A) Example images of the 4 distinct morphological phenotypes under scrutiny. A score of 1 = fragmented, 2 = wild-type, 3 = fused, 4 = clumped. Mitochondria are visualised using MTR, and counterstained with Hoechst (nuclei). 'Original images' acquired using a Deltavision RT system with a 100x objective, scale bar: 5 µm. For greater image clarity, micrographs were 'inverted' (Adobe Photoshop), boxed areas represent 'zoom'. (B & C) Manual quantification of 'Average morphology score' assessed on a cell-by-cell basis. (B) Data represents the average score from 3 independent experiments, each with a minimum of 25 cells/condition. Error bars represent standard deviation. *** P<0.001 (One-way ANOVA with Bonferroni's correction). (C) Average morphology score from one experiment, >30 cells/condition. This assay was done with the assistance of Alvaro Sanchez-Martinez.

4.4.1.2 Low-throughput analysis

Low-throughput analysis first focused on the involvement of the PINK1/Parkin-pathway in mitochondrial morphology. Previous data have shown that in the absence of *dPINK1* or *dparkin*, mitochondria adopt a hyperfused network, exhibiting an increase in the tubular appearance of the mitochondria (Ziviani et al, 2010). To quantify this effect following pathway silencing in S2R+ cells, mitochondria were imaged live using the mitochondrial dye, MitoTracker Red (MTR). This negated the need for cellular fixation; a process documented to alter mitochondrial morphology (Ziviani et al, 2010). For each condition, cells were scored manually, as in 4.4.1.1, depending on their mitochondrial network morphology.

dPINK1 and *dparkin* dsRNA have a significant and comparable influence on the mitochondrial phenotype, producing network fusion compared to the negative control dsRNA (Figure 4.2 B). Additionally, the loss of the core morphology machinery components *dDrp1*, *dOpa1* and *dmfn* also produced the expected phenotypes in S2R+ cells, with *dDrp1* dsRNA causing a severe 'clumped' phenotype; and *dOpa1* & *dmfn* dsRNA causing a fragmented phenotype (Figure 4.2 C). These data confirm that silencing the core morphology genes, as well as *dPINK1* and *dparkin* produces the expected mitochondrial morphology phenotypes in S2R+ cells. Having effectively developed the mitochondrial morphology assay in a low-throughput setting, this could then be applied to a high-throughput screening scenario.

4.4.2 PLATE LAYOUT

As with paraquat-induced dParkin translocation, plates originally designed for confirmation screening were re-used for mitochondrial morphology analysis. Here, a number of additional positive screen controls were added to the outer edge of the plate (Figure 4.3 A), including *dPINK1*, *dmfn*, *dOpa1* & *dDrp1* dsRNA, plus additional copies of *dparkin* dsRNA. These additional controls provided morphologies spanning the entire scoring range, allowing easy identification of comparable phenotypes within the dataset. Additionally, they also acted to verify the knockdown efficacy of the assay.

4.4.3 PROTOCOL

The protocol deviated substantially from previous screening assays in that wild-type S2R+ cells were used, rather than the stable Parkin-GFP.S2R+ cell line. This was due to reports that dParkin overexpression causes a significant shift in mitochondrial

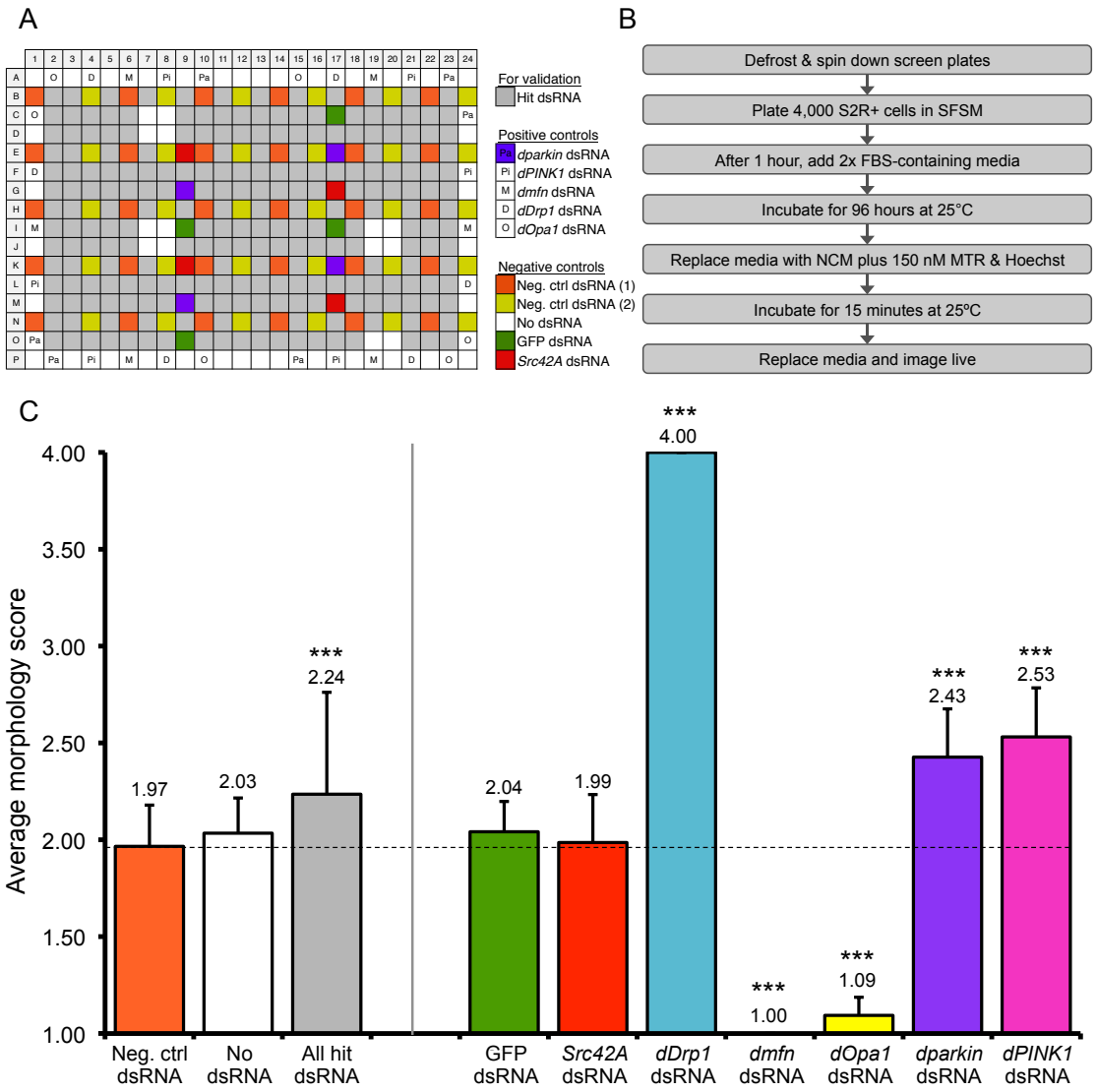

Figure 4.3 High-throughput analysis of mitochondrial morphology. (A) Diagram of assay plate design where colours represent different conditions (see key). Here, extra assay-specific controls were added to the outside edge of the plate. These comprised *dOpa1* - O, *dDrp1* – D, *dmfn* – M, *dPINK1* – Pi and *dparkin* – Pa. (B) Protocol workflow for mitochondrial morphology analysis. (C) Graphical representation of the 'average morphology score' of screen controls. Data comprises a minimum of 12 wells/condition, with 9 FOV per well. Error bars represent standard deviation, ***P<0.001 (One-way ANOVA with Bonferroni's correction, compared to the 'Neg. ctrl dsRNA').

morphology towards fission (Ziviani et al, 2010), distorting the basal morphology phenotype. Additionally, mitochondrial morphology was analysed in the absence of toxification, as CCCP has been shown to cause a mitochondrial fragmentation response, perhaps due to widespread network damage (Legros et al, 2002).

Briefly, the protocol involved plating 4,000 S2R+ cells per well in SFSM. After 1 hour, 2x FBS-containing media was added, and cells were incubated for 96 hours at 25ºC. Media was aspirated and replaced with normal culture media containing MitoTracker (150 nM) and Hoechst (2 mg/ml). After an incubation period of 15 minutes, media was

replaced, and live cells imaged immediately using the high content screening microscope (Figure 4.3 B).

4.4.4 DATA ANALYSES

Because of the complexity of the mitochondrial morphology phenotypes, it was not possible to automate data analyses of this secondary screen. Instead of automation, each image was scored manually, using the scoring system outlined in 4.4.4.1. Due to the sheer volume of data per plate, this screen was carried out as a single assay rather than in triplicate, with scoring performed per FOV, rather than on a cell-by-cell basis. The numerical values from this analysis were averaged over the 9 FOV, giving one 'average morphology score' for each dsRNA amplicon (Figure 4.3 C).

4.4.4.1 Controls

All negative controls behaved as expected, with a mean score close to the 'wild-type' value of 2 (Figure 4.3 C, Figure 4.4 C). With regards to the positive controls, *dmfn* & *dOpa1* caused a fragmented phenotype, each achieving a score of ~1 (Figure 4.3 C, Figure 4.4 A & B), and *dDrp1* dsRNA caused a clumped phenotype, achieving a score of 4 (Figure 4.3 C, Figure 4.4 F). These values are in line with data from earlier, low-throughput analyses (Figure 4.2 C). Importantly, both *dPINK1* and *dparkin* dsRNA caused a hyperfused phenotype as seen previously (Figure 4.3 C, Figure 4.4 D & E), and the dataset as a whole trended towards a more fused network, suggesting an enrichment of PINK1/Parkin-phenocopiers (Figure 4.3 C). These morphology scores closely reflect the qualitative data in example high-throughput microscopy images of control conditions (Figure 4.4 A-F).

4.4.5 DEFINING HITS

For the purposes of mitochondrial morphology screening, a hit amplicon was any dsRNA with an average morphology score outside two SD of the mean of the negative control dsRNA. Therefore any amplicon deviating from the 'wild-type' scenario, hence causing fragmentation, fusion or clumping would be deemed a hit in this screen. Despite being particularly interested in those amplicons phenocopying *dPINK1* and *dparkin* silencing, interest also lies with those producing extreme morphology changes such as fragmentation & clumping. For example, there may be some benefit in assessing which gene-types fall into each group, and whether there are common

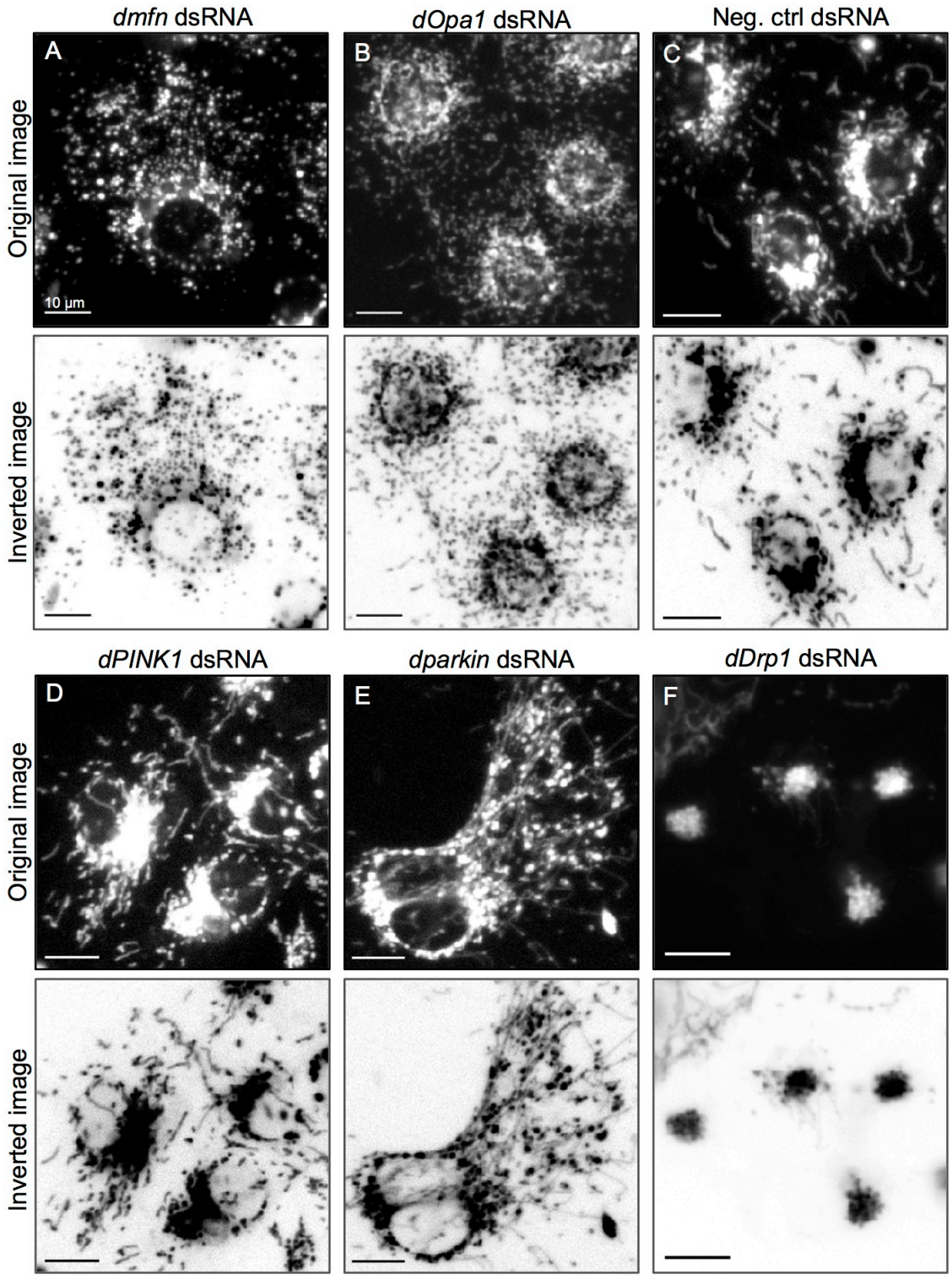

Figure 4.4 High-throughput images of screen controls. (A-F) Original micrograph images (acquired on a ImageXpress Micro widefield high content screening microscope, 40x objective), and corresponding 'inverted' images (Adobe Photoshop) of screen controls. Mitochondria are visualised using MTR, scale bar: 10 µm**.** Conditions represented comprise (A) *dmfn* and (B) *dOpa1* dsRNA - both of which cause a 'fragmented' phenotype; (C) negative control dsRNA, producing a 'wild-type' phenotype; (D) *dPINK1* and (E) *dparkin* dsRNA – causing a 'fused' phenotype; and (F) *dDrp1* dsRNA, producing a 'clumped' phenotype.

pathways involved. For example, in the 'fragmented' group, 5 genes are found to be involved in fatty acid biosynthesis, a topic that will be discussed in greater detail in later chapters.

4.4.7. FINALISED HIT LIST

Having applied the above parameters to the screening data, a final list of 161 dsRNA hits were defined (Table 4.2). This table contains hits from the confirmed primary hit group (43%), as well as dsRNAs that did not qualify for this list (57%). The majority of hits favour increases in fusion (Table 4.2, below the bold line) rather than fragmentation (Table 4.2, above the bold line), which is in agreement with them being 'phenocopiers' of *dPINK1* and *dparkin*. Compared to paraquat-induced translocation, there are substantially more hit amplicons in this list. This may be down to non-pathway related changes in morphology, such as general cellular toxicity; or because this assay was performed as one single experiment rather than in triplicate. Due to this, the potential for retaining false positives here is greater.

4.5 MITOCHONDRIAL PERINUCLEAR AGGREGATION

A phenomenon believed to occur prior to the removal of damaged mitochondria from the cell is the relocation of these mitochondria to the juxtanuclear region (Okatsu et al, 2010; Vives-Bauza et al, 2010). It is proposed that this enables efficient activation of the mitophagy process, by concentrating both substrates and autophagic machinery in the same location. For this process to occur, damaged mitochondria must be segregated from the mitochondrial network, and prevented from re-fusing (Twig et al, 2008). This is believed to occur with the help of PINK1- and Parkin-dependent ubiquitination and degradation of the pro-fusion protein, Mitofusin, and the transport protein, Miro. Here, the arrest of anterograde movement and inhibition of mitochondrial fusion is proposed to quarantine dysfunctional mitochondria, allowing them to begin retrograde movement back to the nucleus.

In the absence of a robust and reproducible mitophagy assay in *Drosophila* cells, the closest read-out for the end point of the pathway was deemed to be this perinuclear aggregation event. Despite this phenomenon being qualitatively distinct from mitophagy itself, it provided a mechanism with which to analyse processes further downstream of both Parkin translocation and mitochondrial morphology. The aims of this secondary screen were to identify dsRNA amplicons able to block the transport

	Name	Probe ID	Score	Phenotype
1	*HLH106*	BKN22813	1.00	Fragmented
2	*desat1*	BKN45646	1.00	Fragmented
3	*SCAP*	BKN22597	1.11	Fragmented
4	*Not1*	BKN50316	1.11	Fragmented
5	*Bap55*	BKN20365	1.11	Fragmented
6	*msl-2*	BKN30252	1.11	Fragmented
7	*CG2469*	BKN21463	1.22	Fragmented
8	*slp2*	BKN27657	1.22	Fragmented
9	*CG14213*	BKN29239	1.22	Fragmented
10	*CG7530*	BKN22405	1.33	Fragmented
11	*CG7065*	BKN24944	1.33	Fragmented
12	*sgg*	BKN28994	1.33	Fragmented
13	*CG30007*	BKN24788	1.33	Fragmented
14	*eyg*	BKN30760	1.33	Fragmented
15	*Not1*	BKN50633	1.38	Fragmented
16	*Pka-R1*	BKN50694	1.44	Fragmented
17	*Cdk8*	BKN27735	1.44	Fragmented
18	*atms*	BKN20176	1.44	Fragmented
19	*CG33306*	BKN26129	1.44	Fragmented
20	*Gclm*	BKN27668	1.44	Fragmented
21	*His1:CG33834*	BKN41898	1.44	Fragmented
22	*Mtr3*	BKN25095	1.56	Fragmented
23	*CG11198*	BKN22148	1.56	Fragmented
24	*Kap-alpha3*	BKN21319	1.56	Fragmented
25	*Atu*	BKN24095	1.56	Fragmented
26	*Ctr1A*	BKN27755	1.56	Fragmented
27	*CG11977*	BKN25378	2.33	Fused
28	*BG4*	BKN25956	2.33	Fused
29	*CG1737*	BKN26442	2.33	Fused
30	*MED14*	BKN22798	2.33	Fused
31	*Gclc*	BKN21658	2.33	Fused
32	*Topors*	BKN23004	2.33	Fused
33	*lilli*	BKN23012	2.33	Fused
34	*mei-S332*	BKN27238	2.33	Fused
35	*ns1*	BKN22066	2.33	Fused
36	*loco*	BKN20345	2.33	Fused
37	*scny*	BKN22179	2.33	Fused
38	*CG5800*	BKN22766	2.33	Fused
39	*CG16775*	BKN25172	2.33	Fused
40	*MED6*	BKN22010	2.33	Fused

	Name	Probe ID	Score	Phenotype
41	*CG3194*	BKN21055	2.33	Fused
42	*MED24*	BKN20580	2.44	Fused
43	*MED19*	BKN22921	2.44	Fused
44	*U2af38*	BKN28210	2.44	Fused
45	*CG42674*	BKN22652	2.44	Fused
46	*l(2)01810*	BKN23239	2.44	Fused
47	*CG13298*	BKN22482	2.44	Fused
48	*sec24*	BKN21620	2.44	Fused
49	*CG8408*	BKN22106	2.44	Fused
50	*CG9636*	BKN28345	2.44	Fused
51	*CG2556*	BKN33412	2.50	Fused
52	*CG12398*	BKN25100	2.56	Fused
53	*CG31937*	BKN20290	2.56	Fused
54	*CG30359*	BKN22317	2.56	Fused
55	*CG15888*	BKN27125	2.56	Fused
56	*Pcaf*	BKN22042	2.56	Fused
57	*pUf68*	BKN27426	2.56	Fused
58	*MED7*	BKN27339	2.56	Fused
59	*Pros25*	BKN29089	2.56	Fused
60	*RpS10a*	BKN24194	2.56	Fused
61	*CG13841*	BKN24102	2.56	Fused
62	*pic*	BKN20655	2.56	Fused
63	*mRpS10*	BKN27767	2.56	Fused
64	*Ubqn*	BKN20953	2.56	Fused
65	*Syx5*	BKN21048	2.56	Fused
66	*yellow-g*	BKN29964	2.56	Fused
67	*CG33051*	BKN32889	2.56	Fused
68	*Withdrawn*	BKN33752	2.56	Fused
69	*CG34137*	BKN40629	2.56	Fused
70	*CG30159*	BKN45335	2.56	Fused
71	*snRNP-U1-70K*	BKN45552	2.56	Fused
72	*MED10*	BKN46549	2.56	Fused
73	*Rpb12*	BKN41948	2.63	Fused
74	*Tango6*	BKN45246	2.63	Fused
75	*Cdk9*	BKN50460	2.63	Fused
76	*Doa*	BKN51136	2.67	Fused
77	*CG12050*	BKN22946	2.67	Fused
78	*cn*	BKN22004	2.67	Fused
79	*CG14023*	BKN30204	2.67	Fused
80	*CG14422*	BKN30991	2.67	Fused

	Name	Probe ID	Score	Phenotype
81	*Pk17E*	BKN31019	2.67	Fused
82	*CG8369*	BKN31376	2.67	Fused
83	*CG16885*	BKN32024	2.67	Fused
84	*CG15370*	BKN32204	2.67	Fused
85	*Doa*	BKN40396	2.67	Fused
86	*CG3078*	BKN41059	2.67	Fused
87	*kn*	BKN41716	2.67	Fused
88	*eIF5*	BKN45562	2.67	Fused
89	*CG12050*	BKN46155	2.67	Fused
90	*CG9300*	BKN23943	2.78	Fused
91	*CG6364*	BKN22328	2.78	Fused
92	*kin17*	BKN20040	2.78	Fused
93	*Sym*	BKN21288	2.78	Fused
94	*mor*	BKN22069	2.78	Fused
95	*CG17209*	BKN20183	2.78	Fused
96	*Nup75*	BKN22034	2.78	Fused
97	*CG42732*	BKN29974	2.78	Fused
98	*ab*	BKN30195	2.78	Fused
99	*CG3436*	BKN45977	2.78	Fused
100	*CG6227*	BKN28174	2.89	Fused
101	*CG5118*	BKN25778	2.89	Fused
102	*CG1109*	BKN20307	2.89	Fused
103	*PCID2*	BKN21400	2.89	Fused
104	*sl*	BKN21616	2.89	Fused
105	*tkv*	BKN22385	2.89	Fused
106	*CG12576*	BKN26430	2.89	Fused
107	*Cyp6a16Ψ*	BKN30754	2.89	Fused
108	*Withdrawn*	BKN33868	2.89	Fused
109	*Rpb12*	BKN34093	2.89	Fused
110	*CG34449*	BKN40585	2.89	Fused
111	*RpL28*	BKN45643	2.89	Fused
112	*RpS6*	BKN46529	2.89	Fused
113	*pit*	BKN26435	3.00	Fused
114	*Aats-arg*	BKN20034	3.00	Fused
115	*tlk*	BKN50352	3.00	Fused
116	*CG6712*	BKN21287	3.00	Fused
117	*CG15747*	BKN22378	3.00	Fused
118	*Rpb10*	BKN29118	3.00	Fused
119	*CG1394*	BKN29792	3.00	Fused
120	*CG34420*	BKN29967	3.00	Fused

	Name	Probe ID	Score	Phenotype
121	*CG9883*	BKN30450	3.00	Fused
122	*CG14239*	BKN30730	3.00	Fused
123	*Nlp*	BKN30946	3.00	Fused
124	*Obp56h*	BKN31996	3.00	Fused
125	*CG42784*	BKN33482	3.00	Fused
126	*transfer RNA*	BKN40591	3.00	Fused
127	*Withdrawn*	BKN40739	3.00	Fused
128	*dco*	BKN41636	3.00	Fused
129	*RpS14a*	BKN42019	3.00	Fused
130	*RpL36*	BKN46193	3.00	Fused
131	*Rpb8*	BKN29127	3.11	Fused
132	*nop5*	BKN20347	3.11	Fused
133	*Lsp1alpha*	BKN26904	3.11	Fused
134	*CG15873*	BKN29806	3.11	Fused
135	*Fer1HCH*	BKN30669	3.11	Fused
136	*CG3975*	BKN46113	3.11	Fused
137	*CkIIalpha*	BKN50525	3.14	Fused
138	*tlk*	BKN50260	3.17	Fused
139	*Rpb5*	BKN20359	3.22	Fused
140	*CG6220*	BKN25940	3.22	Fused
141	*Peritrophin-A*	BKN29878	3.22	Fused
142	*CG30156*	BKN45189	3.33	Fused
143	*Su(var)3-9*	BKN28870	3.44	Fused
144	*RpS27*	BKN28788	3.44	Fused
145	*CG12301*	BKN22878	3.44	Fused
146	*U2af50*	BKN22886	3.56	Clumped
147	*CG30156*	BKN25879	3.56	Clumped
148	*eIF5*	BKN22365	3.56	Clumped
149	*Prp31*	BKN22756	3.67	Clumped
150	*tlk*	BKN28036	3.78	Clumped
151	*Cklalpha*	BKN50737	3.89	Clumped
152	*ago*	BKN27400	4.00	Clumped
153	*Cklalpha*	BKN51078	4.00	Clumped
154	*par-1*	BKN50603	4.00	Clumped
155	*atl*	BKN21206	4.00	Clumped
156	*Trn*	BKN28990	4.00	Clumped
157	*Cklalpha*	BKN27574	4.00	Clumped
158	*Hsc70-2*	BKN29772	4.00	Clumped
159	*par-1*	BKN40395	4.00	Clumped
160	*Nacalpha*	BKN41856	4.00	Clumped
161	*Cdk9*	BKN50890	4.00	Clumped

Table 4.2 Mitochondrial morphology analysis - hit table. Each column gives details of the official *Drosophila* gene name, library probe identifier (BKN), average mitochondrial morphology score across the 9 FOV, and equivalent morphological phenotype (fragmented, fused or clumped). The list had been arranged by the 'score' (high to low), and then alphabetically according to 'Name.' Genes highlighted in grey have more than one amplicon in the hit list. Heat-map representation of the 'average morphology score' is included, with green representing low scores, red representing high scores and yellow representing the 50th percentile or median.

and aggregation of mitochondria in the perinuclear region following paraquat toxification. This blockage reflects the phenotype observed in the positive control situation, whereby *dPINK1* and *dparkin* dsRNA are able to significantly reduce perinuclear aggregation (Figure 4.6 B). Therefore, we can hypothesise that these phenocopiers are potentially acting in a common pathway with dPINK1 and dParkin.

4.5.1 ASSAY DEVELOPMENT

The ability of Parkin-GFP.S2R+ cells to undergo perinuclear aggregation following toxification was first observed when attempting to induce mitophagy. Efforts to optimise the induction of mitophagy for these cells involved testing a range of toxins, including CCCP & paraquat. Where CCCP was unable to cause perinuclear aggregation of mitochondria under the conditions tested, the application of 10 mM paraquat for 24 hours produced a clear phenotype (Figure 4.5 A). Here, under basal conditions mitochondria occupied sites throughout the cytoplasm, producing a 'diffuse' localisation. However, following paraquat toxification, mitochondria largely relocated to the perinucleus of the cell, forming an aggregated mass. Importantly, this aggregation phenotype was blocked by *dPINK1* or *dparkin* silencing (Figure 4.6 B), indicating that this phenomenon was pathway-specific.

4.5.1.1 Scoring system

To evaluate the degree of mitochondrial perinuclear aggregation, images were assessed manually using a three-point scale (Figure 4.5 B - D). Here, a score of 1 reflected a 'diffuse' mitochondrial network, and was attributed to 'vehicle'-treated samples, and paraquat-treated positive controls (Figure 4.5 B). A score of 2 reflected cellular populations with a mixture of both diffuse and aggregated mitochondria (Figure 4.5 C); and a score of 3 reflected cells where perinuclear aggregations of mitochondria were in the majority, such as with paraquat-treated negative controls (Figure 4.5 D).

4.5.2 PLATE LAYOUT

As with the previous secondary screens, plates designed for confirmation screening were re-used for mitochondrial perinuclear aggregation assessment. Because of the complementary cell-type and toxification duration, it was possible to combine mitochondrial aggregation analysis with the first secondary screen, assessing dParkin translocation. This feature provided a substantial temporal benefit, whilst still producing satisfactory screening results.

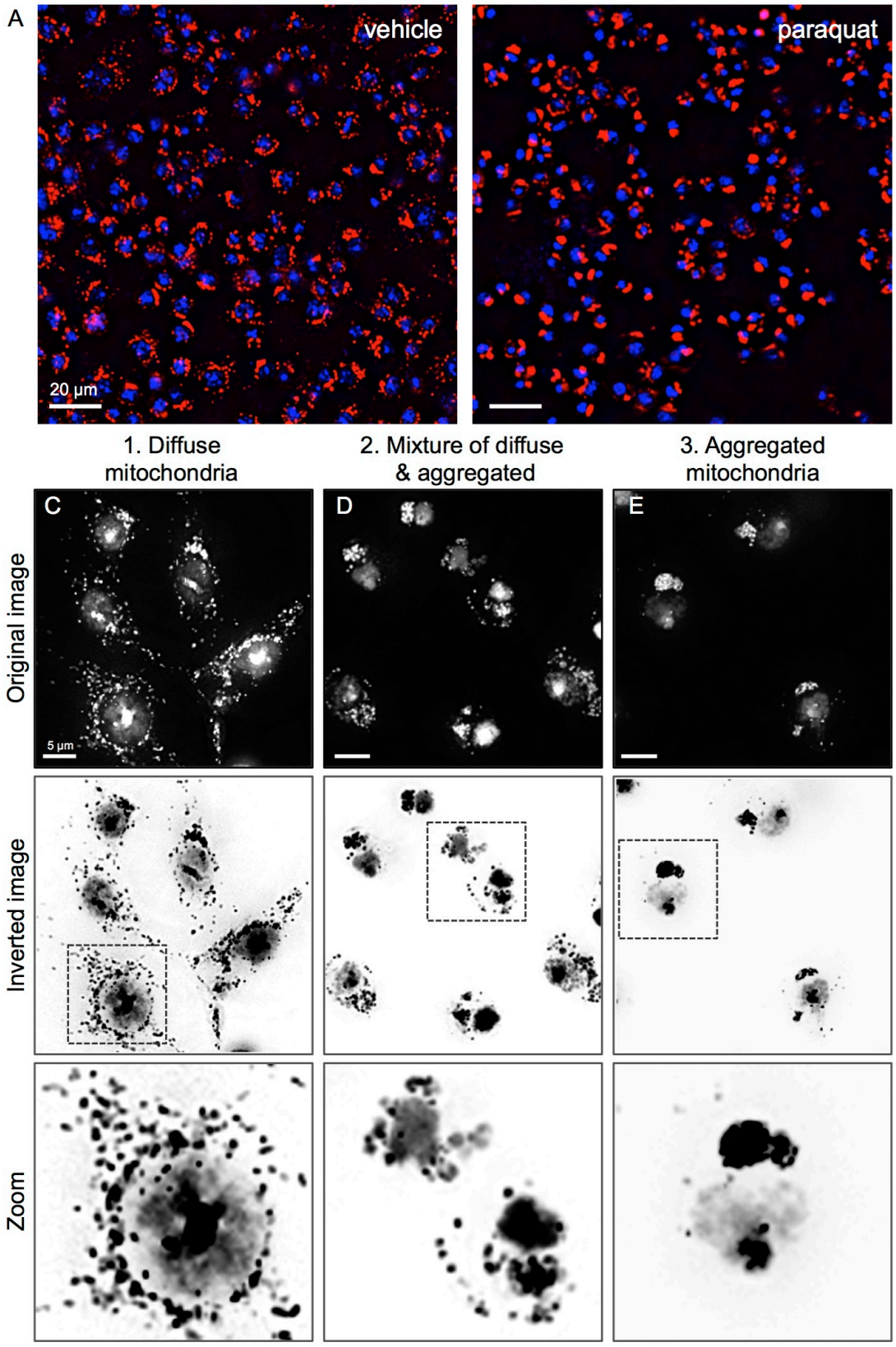

Figure 4.5 Paraquat-induced mitochondrial perinuclear aggregation. (A) Parkin-GFP.S2R+ cells were treated with vehicle or 10 mM paraquat for 24 hours. Mitochondrial localisation was assessed using a using a 20x objective, scale bar: 20 µm. Nuclei (blue – Hoechst), mitochondria (Red – ATP5A). (B - D) Example images reflecting the 3-point manual scoring system where 1 = majority diffuse mitochondria (B), 2 = a mixture of aggregated & diffuse (C), and 3 = majority aggregated mitochondria (D). Original images were acquired using a 60x objective, scale bar: 5 µm, Nuclei (Hoechst) and mitochondria (ATP5A). Corresponding inverted images were produced using Adobe Photoshop. Boxed areas represent magnification ('Zoom'). All images were acquired on a Deltavision RT system.

Together with the pre-printed controls, this secondary screen also analysed a number of additional controls, added to the outer edge of the plate (Figure 4.6 A). These included *dPINK1*, *Atg5, Atg8a* and *Atg8b* dsRNA, plus additional copies of *dparkin* dsRNA. Here, *dPINK1* and *dparkin* silencing was expected to prevent toxin-induced perinuclear aggregation through the persistence of dMfn and dMiro on the MOM, promoting network fusion and anterograde transport respectively. Additionally, autophagy genes, *Atg5, Atg8a* and *Atg8b*, involved in the synthesis of the autophagosome membrane, were predicted to cause a deviation from the control, perhaps also preventing perinuclear aggregation.

As before, a 'no paraquat' or 'vehicle-treated' control was employed, populating columns 1 & 24. Not only was this control required for assay 4.3, but also served an important purpose here, providing the base-line wild-type mitochondrial distribution phenotype. This extra control safeguarded against the risk of ineffective positive dsRNA controls.

4.5.3 PROTOCOL

The perinuclear aggregation protocol, was identical to that followed for paraquat-induced dParkin translocation (Figure 4.1 E). Here, Parkin-GFP.S2R+ cells were induced with copper sulphate for considerably longer than the primary screen, due to the prolonged toxification duration required. As a consequence, the copper sulphate concentration was lowered accordingly, to reduce the potential for toxic side-effects. Despite this, Parkin-GFP expression remained sufficient for effective data analyses.

An additional deviation from the primary screening protocol was the need to visualise mitochondria. Because of this, samples were fixed using ice-cold methanol rather than formaldehyde, allowing concurrent cellular permeabilisation (Figure 4.1 E). Application of an anti-ATP5A primary antibody and an Alexa-594 secondary antibody produced a strong MIM signal in the red channel.

4.5.4 DATA ANALYSES

Perinuclear aggregation assays were performed in triplicate to ensure reproducibility of the observed effect. Using the high content screening microscope, 4 FOV were captured per well with a 10x objective. This acquisition regime deviated from the previous screens in that fewer FOV were acquired, but at a much lower magnification. This was permissible due to the fact that the mitochondrial aggregates quantified here

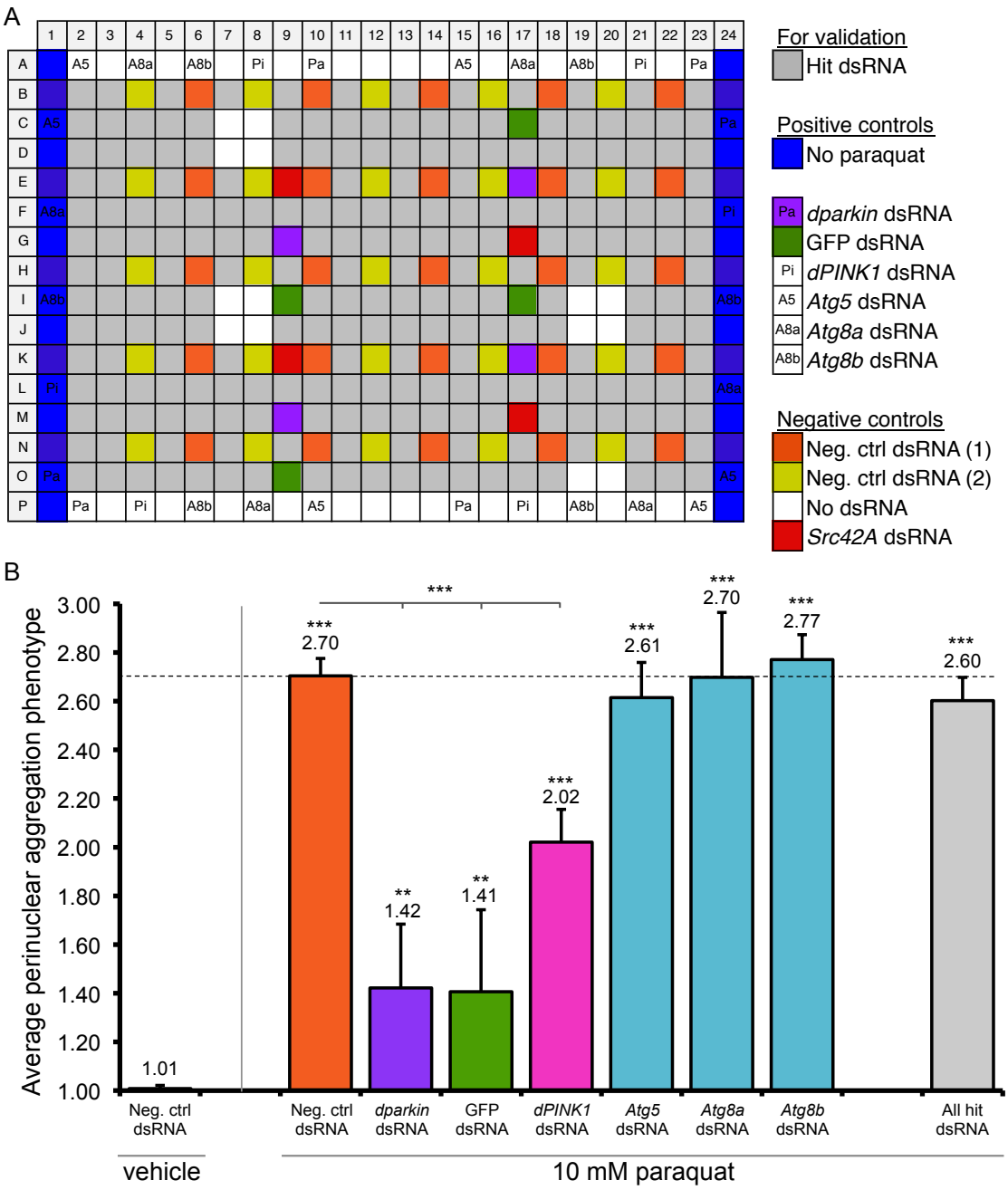

Figure 4.6 High-throughout analysis of mitochondrial perinuclear aggregation. (A) Diagram of assay plate design where colours represent different conditions (see key). Here, extra assay-specific controls were added to the outside edge of the plate. These comprised *dPINK1* – Pi, *dparkin* – Pa, *Atg5* – A5, *Atg8a* – A8a and *Atg8b* – A8b. (B) Graphical representation of the 'average perinuclear aggregation phenotype' of screen controls. Data represents average control data from three rounds of screening, with a minimum of 8 wells/condition, per screening round. Error bars represent standard deviation, ***P < 0.001, **P < 0.01, (One-way ANOVA with Bonferroni's correction, compared to the 'Neg. ctrl dsRNA', unless otherwise indicated).

could be resolved much easier than the tiny puncta and faint tubules of previous assays. Additionally with the lower magnification, a greater proportion of the cellular population was captured per FOV, compared to the 40x objective. This allowed the number of images acquired per condition to be reduced, whilst still capturing enough data to build a detailed overview.

As in the mitochondrial morphology screen, each image was scored manually using the scheme outline in section 4.5.1.1, rather than via automation (Figure 4.5 C). Original efforts concentrated on attempting to automate analysis, however, after lengthy parameter optimisation, it was deemed too unreliable. Nevertheless, due to the clear nature of the phenotype and smaller number of images per well, manual analysis was time consuming, but feasible.

4.5.4.1 Controls

Plate controls included those pre-printed within the plates, as well as additional controls spiked in around the outer edge. With regards to the dsRNAs already present in the screening plates, *Src42A* was expected to have a negligible effect on perinuclear aggregation. This was indeed the case, with an average phenotype score of 2.58 (data not shown). *dparkin* dsRNA showed a strong block of perinuclear aggregation, bringing the phenotype almost back to a wild-type, non-toxified level (Figure 4.6 B, purple). In agreement with this phenotype, GFP dsRNA also had the same affect, presumably due to the silencing of the Parkin-GFP fusion construct (Figure 4.6 B, green). This result is interesting as it suggests that dParkin overexpression is necessary for the observed perinuclear aggregation phenotype. Crucially, *dPINK1* dsRNA was able to partially block the perinuclear aggregation of mitochondria, giving a phenotype score close to 2 (Figure 4.6 B, pink). This was reassuring as it provided further evidence that *dPINK1* silencing could impact upon the mitophagy pathway in *Drosophila* S2R+ cells, as discussed in section 3.4. Finally, several dsRNAs targeting the core autophagy machinery (*Atg5, 8a* and *8b*) were added as potential controls. It was hypothesised that by playing an essential role in the formation of the autophagosome, these genes may have an influence on the aggregation phenotype. However, this was not formally tested prior to screening, and transpired to have no influence on mitochondrial aggregation (Figure 4.6 B, aqua). In retrospect, this was not unexpected, as *Atg5* (involved in autophagosome elongation) and *Atg8a/b*, (key in the formation of autophagosome membranes) are involved in degrading mitochondria, whilst this assay focuses on events just upstream of this. Perhaps a more appropriate control may have been the knockdown of the dynein motor responsible for transporting mitochondria to the perinucleus, or perhaps the application of microtubule polymerisation inhibitors such as nocodazole or colchicine (Okatsu et al, 2010)

4.5.5 DEFINING HITS

Per screening round, a hit amplicon was any dsRNA with a perinuclear aggregation score outside two SD of the mean of the paraquat-treated negative control dsRNA. Over three rounds of screening, each time an amplicon appeared in the hit list it was given a score of 1. Upon screen completion, the overall 'score' for each dsRNA was calculated. For an amplicon to be deemed an overall 'hit' in this secondary screen, a minimum score of 2 was required.

4.5.6 FINALISED HIT LIST

Having applied the above parameters to the screening data, a final list of 65 dsRNA hits were defined (Table 4.3). This list contains dsRNA from the confirmed primary hit group (52%) as well as a proportion that did not qualify for this list (48%). The number of hits in this final secondary screen is lower than that of the previous two, perhaps because the phenotype here was much easier to judge compared to the more variable nature of the morphology screen for example. Additionally, performing the assay in triplicate and screening each image by eye meant less potential for false-positive hits.

4.6 COLLATING DATA

The next challenge following secondary screening was to collate data from the three screens in order to arrive at a final *Drosophila* hit list. For this, a number of aspects had to be considered such as whether to treat each secondary screen equally or attribute greater weight to one screen over another. In addition, how to deal with secondary screen hits falling outside of the confirmed primary hit group required deliberation.

4.6.1 DEFINING HITS

To define an overall group of secondary screen hits, I decided that the mitochondrial perinuclear aggregation assay should hold greater weight over the other two secondary screens for the following reasons. First, paraquat-induced dParkin translocation was very similar in nature to the primary screen; hence, despite providing important information about the specificity of the toxification, it did not provide further insight into other aspects of mitochondrial homeostasis. Second, mitochondrial morphology; whilst

	Name	Probe ID	Score
1	*atms*	BKN20176	3
2	*CG10418*	BKN27632	3
3	*CG17912*	BKN29387	3
4	*CG2469*	BKN21463	3
5	*CG30359*	BKN22317	3
6	*CG32685*	BKN23988	3
7	*CG4294*	BKN23609	3
8	*CG7065*	BKN24944	3
9	*Cp1*	BKN27765	3
10	*Ctr1A*	BKN27755	3
11	*Dis3*	BKN21524	3
12	*l(1)G0007*	BKN22970	3
13	*lid*	BKN22841	3
14	*pic*	BKN20655	3
15	*Prp31*	BKN22756	3
16	*pUf68*	BKN27426	3
17	*rept*	BKN20068	3
18	*Rpb5*	BKN20359	3
19	*Rrp6*	BKN20686	3
20	*sec10*	BKN20533	3
21	*sgg*	BKN50521	3
22	*Srp54*	BKN22462	3
23	*tlk*	BKN28036	3
24	*ago*	BKN27400	2
25	*Art3*	BKN28748	2
26	*Atu*	BKN24095	2
27	*CG11092*	BKN25863	2
28	*CG14683*	BKN20003	2
29	*CG15459*	BKN32433	2
30	*CG2685*	BKN20517	2
31	*CG30007*	BKN24788	2
32	*CG30127*	BKN33676	2

	Name	Probe ID	Score
33	*CG33051*	BKN32889	2
34	*CG5591*	BKN27099	2
35	*CG7886*	BKN21063	2
36	*comm3*	BKN25753	2
37	*Dp1*	BKN20845	2
38	*faf*	BKN20871	2
39	*fz3*	BKN25989	2
40	*GATAe*	BKN32653	2
41	*HLH106*	BKN22813	2
42	*lilli*	BKN23012	2
43	*MED14*	BKN22798	2
44	*MED19*	BKN22921	2
45	*MED24*	BKN20580	2
46	*MED28*	BKN27691	2
47	*MED7*	BKN27339	2
48	*msl-2*	BKN30252	2
49	*Pcaf*	BKN22042	2
50	*PCID2*	BKN21400	2
51	*pont*	BKN21199	2
52	*ptip*	BKN22515	2
53	*Rpb10*	BKN29118	2
54	*Rpb8*	BKN29127	2
55	*Saf-B*	BKN20574	2
56	*Sec61alpha*	BKN22564	2
57	*sgg*	BKN28994	2
58	*Tango6*	BKN26681	2
59	*TfIIFalpha*	BKN45044	2
60	*tkv*	BKN50543	2
61	*tlk*	BKN50260	2
62	*tlk*	BKN50352	2
63	*transfer RNA*	BKN40552	2
64	*U2af50*	BKN22886	2
65	*Withdrawn*	BKN33475	2

Table 4.3 Paraquat-induced mitochondrial perinuclear aggregation - hit table. Each row gives details of the official *Drosophila* gene name, library probe identifier (BKN), and overall secondary screen score following three rounds of screening. The list has been arranged by the 'score' (high to low), and then alphabetically according to 'Name.' Genes highlighted in grey have more than one amplicon in the hit list.

probing a distinct aspect of mitochondrial homeostasis, had the potential of providing fewer mitophagy-specific hits compared to the perinuclear aggregation of mitochondria. Therefore, for a gene to be defined as a hit, it had to fall into one of the following categories (A or B):

A) A confirmed primary screen hit, AND a hit in:
   I. ≥ 2 secondary screens or
   II. mitochondrial perinuclear aggregation screen only

B) A non-confirmed primary screen hit, but an 'interesting' secondary screen hit (see below).

4.6.2. DEFINING 'INTERESTING' SECONDARY SCREEN HITS

Genes falling into category (A) were automatically considered as *Drosophila* screening hits. However, those genes falling outside of this group were able to qualify for the final screen hit group based on other 'interesting' or 'unique' attributes. These genes (category B) were not 'confirmed' primary screen hits, meaning they were selected as hits in the whole genome screen, but fell out of this group following confirmation screening. However, each of these genes featured in the hit groups of at least 2 secondary screens, or the perinuclear aggregation screen alone.

As well as satisfying the parameters defined above, these genes required additional 'interesting' attributes, ascertained through bioinformatic analysis. These included:

1) Protein-protein interactions (BioGRID/IntAct/HPRD)
2) Gene function – both *Drosophila* & human orthologs (UniProt / GO / PANTHER)
3) Protein interaction pathways (STRING)

4.6.2.1 Protein-protein interactions

Using the 'Interactions' facility in NCBI 'Gene', it was possible to establish protein-protein interactions from a number of different resources. These included the 'Biological Repository for Interaction Datasets' (BioGRID) (Stark et al, 2006), the 'Human Protein Reference Database' (HPRD) (Prasad et al, 2009) and IntAct (Kerrien et al, 2012). Each of these databases curates published and user-submitted data from both high- and low-throughput datasets, in order to build their interaction datasets. Using this facility, a number of interesting protein interactions were identified. These were based either on interactions with other genes in the hit list, as well as interactions with genes of interest outside of the list, such as those linked to Parkinson's disease. For example, some of the secondary screen genes (detailed in Table 4.4) were found to interact with the putative, PD-linked genes *LINGO1* and *GIGYF2*, as well as *parkin* itself. Additionally, links to selective autophagy via the adaptor protein SQSTM1/p62 were discovered, together with a number of inter-hit interactions (*CSNK2B* and *GSK3B*). Finally, *KAT2B* was found to interact with *RAB11A*. This is of particular interest to our lab, as Rab11-interacting proteins were found to be enriched in a previous screen looking at modifiers of dPINK1-related mitochondrial fusion.

Drosophila gene	Gene ID	Human Gene	Interaction 1	Interaction 2
ago	*CG15010*	*FBXW7*	LINGO1 (Two-hybrid)	Parkin (Affinity Capture-Western)
BAP55	*CG6546*	*ACTL6B*	CSNK2B (Two-hybrid)	GSK3B (Two-hybrid)
CG7886	*CG7886*	*CEP78*	SQSTM1 (Affinity Capture-MS)	-
Pcaf	*CG4107*	*KAT2B*	RAB11A (Two-hybrid)	-
U2af38	*CG3582*	*U2AF1L4*	GIGYF2 (Affinity Capture-MS)	-
U2af50	*CG9998*	*U2AF2*	GIGYF2 (Affinity Capture-MS)	-

Table 4.4 Protein-protein interactions. Analysis of equivalent human protein interactions between hits and relevant or interesting proteins. Brackets represent the method of analysis.

4.6.2.2 Gene function

To assess the function of the hit genes, a number of different strategies were employed including the use of Swiss-Prot; a manually annotated protein database providing functional and molecular information (UniProt, 2013); Gene Ontology (GO) which looks at cellular components, molecular functions and biological processes (Ashburner et al, 2000); and PANTHER pathways (an integral part of the GO project), which looks at the relationship between interacting molecules (Mi et al, 2013). Using the aforementioned databases, key areas of interest included stress pathways, degradation pathways (both autophagy and proteasomal), the nervous system, Parkinson's disease and mitochondria. From this, a handful of additional genes were added to the final hit list (Table 4.5).

Drosophila Gene	Gene ID	Human Gene	Gene Information
CG15459	*CG15459*	*USMG5*	**Mitochondrial inner membrane**
fz3	*CG16785*	*FZD5*	Receptor for Wnt proteins. Most of frizzled receptors are coupled to the beta-catenin canonical signaling pathway, which leads to the activation of disheveled proteins, inhibition of **GSK-3 kinase**, nuclear accumulation of beta-catenin and activation of Wnt target genes.
l(1)G0007	*CG32604*	*DHX38*	DEAD box proteins are putative RNA helicases. They are implicated in a number of cellular processes involving alteration of RNA secondary structure such as translation initiation, nuclear and **mitochondrial splicing**, and ribosome and spliceosome assembly
Pros25	*CG5266*	*PSMA2*	**Proteosome subunit** that may have a regulatory effect on another component(s) of the proteasome complex through tyrosine phosphorylation

Table 4.5 Examining gene function. Analysis of *Drosophila* and orthologous human gene function. Key details appear in a bold typeface.

4.6.2.3 Protein interaction pathways

In attempting to glean clues about how PINK1/Parkin-mediated mitophagy occurs, a useful exercise was to analyse the hit list for an enrichment of pre-defined pathways. An excellent tool for visualising protein interactions between large groups of genes is

the program ‘STRING’ (‘Search Tool for the Retrieval of Interacting Genes/Proteins’) (Jensen et al, 2009). This database collates data from known and predicted interactions, of physical (direct) and functional (indirect) associations, drawing on many of the resources mentioned in previous sections. The advantage of using STRING as an additional resource is the facility to easily visualise known protein networks, allowing the grouping of genes into individual processes or pathways.

Among the hit genes from primary and secondary screens, there is a clear enrichment of three large pathways; the Mediator Complex, the RNA polymerase II/III network and the PAF1 complex (Figure 4.7); all of which are involved in ‘housekeeping’ transcriptional processes. Here, due to the housekeeping nature of these gene groups, the PINK1/Parkin-pathway specificity of observed phenotypes may be questioned. This suggestion is strongly reinforced by the possibility that Parkin expression; essential for both Parkin translocation and perinuclear aggregation assays, may be reduced or lost as a result of impaired protein synthesis. Such events would therefore categorise these hits as ‘false positives.’ One way of dealing with these potential false positives would be to eliminate them from analysis based on their known function. However, although this is one quick method for reducing the number of hit genes, it also carries the risk of excluding genes of real interest. For example, despite their well-defined housekeeping roles, these genes may perform an alternative dual function in other processes. Additionally, genes causing a significant decrease in Parkin-GFP transcription should have been identified and removed via visual analysis in the first stages of primary screen analysis, therefore presumably safeguarding against this type of false positive. Finally, MED13, a member of the mediator complex, has been recently implicated as a risk-loci in the development of sporadic Parkinson’s disease (Lill et al, 2012), demonstrating tangible links to Parkinson’s disease pathways. Therefore, to prevent the risk of losing genuine pathway members, all hit genes linked to these large transcription networks were included in the final hit list.

4.6.3 FINAL *DROSOPHILA* HIT LIST

Having collated the above data, a final *Drosophila* screening hit list was compiled. This list contained 42 amplicons targeting 39 *Drosophila* genes from category A.I, 2 genes from A.II and a further 21 ‘interesting’ genes from category B. Together, the final hit list contains 65 dsRNA amplicons targeting 62 individual *Drosophila* genes (Table 4.6)

A The mammalian Mediator complex

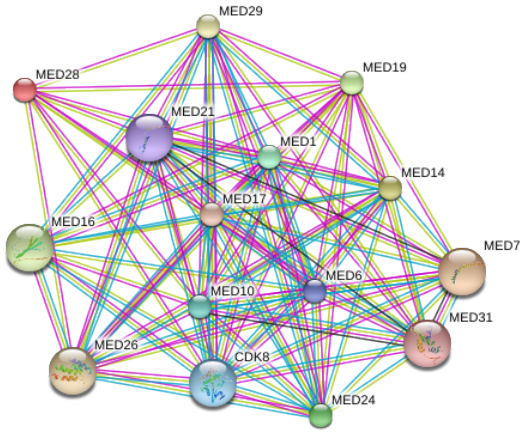

MED14, MED19, MED24, MED28, MED7

Transcriptional coactivator complex thought to be required for the expression of almost all genes. The mediator complex is recruited by transcriptional activators or nuclear receptors to induce gene expression, possibly by interacting with RNA polymerase II and promoting the formation of a transcriptional pre-initiation complex.

B RNA polymerase II/III network

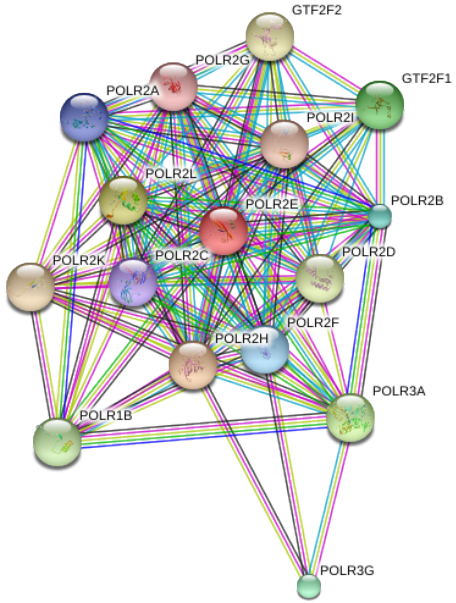

POLR2E POLR2H POLR2L POLR3A POLR3G GTF2F1

Polymerase networks responsible for synthesising messenger RNA and small RNAs.

C The mammalian PAF1 complex

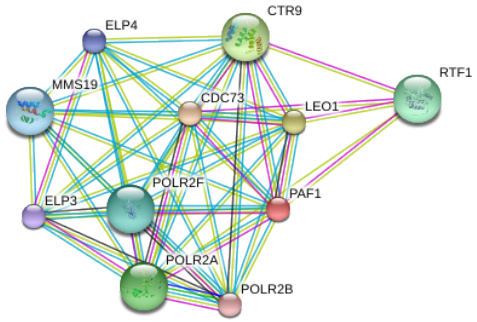

CDC73, LEO1, PAF1, CTR9

Interacts with RNA polymerase II and may be involved in initiation and elongation, and in histone methylation and RNA processing

Neighbourhood	Experiments
Gene Fusion	Databases
Co-occurrence	Textmining
Co-expression	Homology

Figure 4.7 Analysis of protein interaction pathways using STRING. Three different pathways have been identified as being 'enriched' in the secondary screen hit genes. These are the Mediator complex (A), the RNA polymerase II/III network (B) and the PAF1 complex (C). Associations between proteins in the networks are represented by a series of coloured lines (see key). These lines indicate the source of the data as detailed in the key. Below each network is a list of secondary screen hit genes found within each of the networks. At the bottom of each column is a brief description of the function of each of the pathways. Protein interaction maps were made using STRING 9.0.

	A) I.	A) II.	B)	Total
Drosophila amplicons	42	2	21	65
Drosophila genes	39	2	21	62

Table 4.6 Collating data to produce a final *Drosophila* hit list. Numbers of dsRNA amplicons and equivalent genes falling into each hit category.

After multiple rounds of primary and secondary screening, these final *Drosophila* screening hits have been found to reproducibly and robustly reduce toxin-induced dParkin translocation, as well influencing a wide range of additional mitochondria-linked processes (Table 4.7).

4.7 DISCUSSION

The aim of this part of the project was to use secondary screening methods in order to assess primary screen hits in a wider, mitochondrial context. For this, amplicons were tested for 1) an ability to influence dParkin translocation following an alternative mode of cellular toxification, 2) their effect on mitochondrial morphology and 3) their ability to prevent mitochondrial perinuclear aggregation. The reasons for looking at additional aspects of mitochondrial biology were to ascertain whether the block on dParkin translocation observed during primary screening was a stand-alone effect, or intimately linked to mitochondrial homeostasis as a whole. This was expected to go someway towards eliminating remaining false positives within the dataset. Furthermore, this process was hoped to strengthen the position of robust pathway hits, whilst reducing the overall number of *Drosophila* hits genes.

The primary screen had identified 625 dsRNA amplicons able to reduce dParkin translocation following CCCP toxification; and repeat rounds of confirmation screening brought that number down to 115 dsRNA amplicons. With secondary screening, the number of confirmed primary hits able to significantly influence paraquat-induced translocation, mitochondrial morphology and/or perinuclear aggregation fell to 44 dsRNA amplicons, more than halving the original list of confirmed hits. This list was increased to 65 hit amplicons with the inclusion of interesting, non-confirmed primary hits (Figure 4.8).

	Name	Probe ID	Score
1	*atms*	BKN20176	3
2	*CG2469*	BKN21463	3
3	*Ctr1A*	BKN27755	3
4	*Lilli*	BKN23012	3
5	*MED14*	BKN22798	3
6	*MED19*	BKN22921	3
7	*MED24*	BKN20580	3
8	*MED7*	BKN27339	3
9	*pUf68*	BKN27426	3
10	*Rpb10*	BKN29118	3
11	*Rpb5*	BKN20359	3
12	*Rpb8*	BKN29127	3
13	*tlk **	BKN28036	3
14	*tlk **	BKN50352	3
15	*Cdk9*	BKN50890	2
16	*CG12050*	BKN22946	2
17	*CG14023*	BKN30204	2
18	*CG14239*	BKN30730	2
19	*CG2685*	BKN20517	2
20	*CG34449*	BKN40585	2
21	*CG5591*	BKN27099	2
22	*CG9883*	BKN30450	2
23	*CkIIα*	BKN50525	2
24	*cn*	BKN22004	2
25	*Cp1*	BKN27765	2
26	*Dis3*	BKN21524	2
27	*Gclm*	BKN27668	2
28	*HLH106*	BKN22813	2
29	*l(2)01810*	BKN23239	2
30	*Maltase A5*	BKN22317	2
31	*pic*	BKN20655	2
32	*Prp31*	BKN22756	2

	Name	Probe ID	Score
33	*ptip*	BKN22515	2
34	*RpL28*	BKN45643	2
35	*Rrp6*	BKN20686	2
36	*scny*	BKN22179	2
37	*sgg **	BKN50521	2
38	*sgg **	BKN28994	2
39	*Srp54*	BKN22462	2
40	*TfIIFα*	BKN45044	2
41	*tlk **	BKN50260	2
42	*Withdrawn*	BKN41059	2
43	*Tango6*	BKN26681	1
44	*Withdrawn*	BKN33475	1
45	*ago*	BKN27400	3
46	*Pcaf*	BKN22042	3
47	*U2af50*	BKN22886	3
48	*ab*	BKN30195	2
49	*Atu*	BKN24095	2
50	*BAP55*	BKN20365	2
51	*CG17209*	BKN20183	2
52	*CG33051*	BKN32889	2
53	*CG6220*	BKN25940	2
54	*CG7886*	BKN21063	2
55	*l(1)G0007*	BKN22970	2
56	*Pros25*	BKN29089	2
57	*U2af38*	BKN28210	2
58	*CG15459*	BKN32433	1
59	*faf*	BKN20871	1
60	*fz3*	BKN25989	1
61	*GATAe*	BKN32653	1
62	*MED28*	BKN27691	1
63	*pont*	BKN21199	1
64	*rept*	BKN20068	1
65	*sec10*	BKN20533	1

Table 4.7 Final *Drosophila* hit list. Each row gives details of the official *Drosophila* gene name, library probe identifier (BKN), and overall secondary screen score following the collation of data from all three secondary screens. A score of 3 means that the amplicon was a hit in all three screens, a score of 2 = two screens and a score of 1 = one screen. Those amplicons shaded blue are category A) I. hits, orange are category A) II. hits and green are category B) hits. The list has been arranged by category, and then by the 'score' (high to low), and 'Name' (A to Z). The asterisks represent genes with more than one amplicon in the hit list.

Having finalised a robust list of *Drosophila* genes involved in mitochondrial homeostasis, the next logical step was to identify human orthologs of each of these hits, and re-screen them using a mammalian cell line. This provided two advantages. First, it was expected to further decrease the number of genes with a weaker influence on PINK1/Parkin-pathway processes, whilst reinforcing confidence in the stronger hits. Second, the efficacy of screen hits could be tested across species, further validating their effect in a higher organism. Given the issues that this project faced with respect to the lack of a *dPINK1*-silencing effect on dParkin translocation, it was vital to

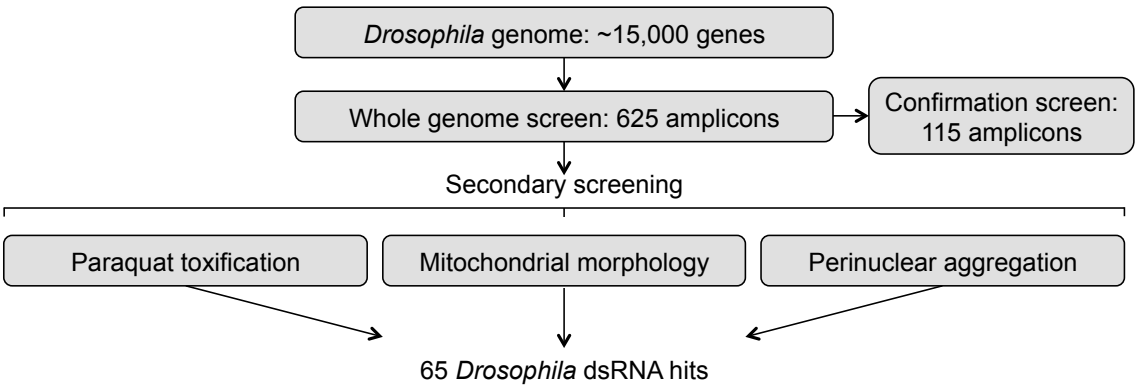

ab	*CG14239*	*CG6220*	*faf*	*Maltase A5*	*pont*	*Rpb8*	*Tango6*
ago	*CG15459*	*CG7886*	*fz3*	*MED14*	*Pros25*	*RpL28*	*TfIIFα*
atms	*CG17209*	*CG9883*	*GATAe*	*MED19*	*Prp31*	*Rrp6*	*tlk*
Atu	*CG2469*	*CkIIα*	*Gclm*	*MED24*	*ptip*	*scny*	*tlk*
BAP55	*CG2685*	*cn*	*HLH106*	*MED28*	*pUf68*	*sec10*	*tlk*
Cdk9	*CG33051*	*Cp1*	*l(1)G0007*	*MED7*	*rept*	*sgg*	*U2af38*
CG12050	*CG34449*	*Ctr1A*	*l(2)01810*	*Pcaf*	*Rpb10*	*sgg*	*U2af50*
CG14023	*CG5591*	*Dis3*	*Lilli*	*pic*	*Rpb5*	*Srp54*	*Withdrawn*
							Withdrawn

Figure 4.8 Overall *Drosophila* screening diagram. Workflow diagram representing each step of *Drosophila* cell screening. Briefly, the whole genome library was comprised of ~ 15,000 *Drosophila* genes. Following primary screening, 625 dsRNAs were found to reduce Parkin-GFP translocation following CCCP treatment. Of these, 115 dsRNAs were confirmed in 4 repeat screens. Primary hit amplicons then underwent multiple secondary screening rounds, looking at paraquat-induced dParkin translocation, mitochondrial morphology and mitochondrial perinuclear aggregation. The final *Drosophila* dsRNA hit list comprises 65 confirmed and 'interesting' non-confirmed primary amplicons with an influence on secondary screens.

demonstrate that the hits identified in our *Drosophila* system could have a comparable influence on the mammalian PINK1/Parkin-pathway. In the following chapter, two aspects of the mammalian PINK1/Parkin-pathway will be assessed, focusing on CCCP-induced Parkin translocation and mitophagy.

5. TERTIARY SCREENING – HUMAN CELLS

5.1 BACKGROUND

Following the conclusion of *Drosophila* screening, hit genes were converted into their human orthologs and re-tested in a mammalian HeLa cell system. This enabled hit validation in a more complex model, and demonstrated the relative importance of final hit genes in mammalian PINK1/Parkin-pathway processes.

The majority of the cellular work studying PINK1/Parkin-function has been performed in mammalian systems, with much of the earlier studies focusing on HeLa cells (Geisler et al, 2010a; Matsuda et al, 2010; Narendra et al, 2008; Vives-Bauza et al, 2010). HeLa cells are particularly useful for cellular studies due to their readiness for transfection, efficient gene silencing, large size facilitating imaging approaches, and ease of culturing. However, these cells also lack endogenous Parkin expression (Denison et al, 2003). Ordinarily, the expression of a major component of the studied pathway would seem like a critical requirement for a cellular model. However, in HeLa cells expressing exogenous Parkin, it has been well demonstrated that Parkin translocates to mitochondria and induces mitophagy following toxification with CCCP, analogous to that observed with endogenous Parkin in HEK293 and SH-SY5Y cells (Geisler et al, 2010a; Narendra et al, 2008). Together with the aforementioned advantages of this system, these observations make HeLa cells an attractive model for studying PINK1/Parkin-processes.

In this chapter, HeLa cells stably expressing YFP-Parkin are utilised to assess the ability of *Drosophila* hit genes to influence Parkin translocation and mitophagy. Vitally, in contrast to *Drosophila* S2R+ cells, it is well documented that HeLa cells undergo robust levels of mitophagy (Geisler et al, 2010b; Narendra et al, 2008; Tanaka et al, 2010), allowing the end point of the pathway to be assessed in this system. This feature, together with the fact that HeLa cells are derived from a human source make them a favourable candidate for use in the next stage of the screening process.

5.2 HYPOTHESES AND AIMS

The aim of this portion of the screening process was to determine which *Drosophila* hit genes have an equivalent effect on PINK1/Parkin-processes in a human cell system. Here, the use of a more complex system was hoped to demonstrate the conserved function of these genes across species, as well as reaffirming the most robust hits. For

this, two tertiary screening assays were developed looking at CCCP-induced Parkin translocation, and mitophagy,

As detailed in previous sections, Parkin translocates from a cytoplasmic location to the mitochondrial network following CCCP toxification, representing an early step in the initiation of mitophagy. At the mitochondria, a number of MOM proteins become ubiquitinated in a Parkin- and PINK1-dependent manner, preceding the degradation of those mitochondria. In this chapter, hit amplicons are assessed for their ability to phenocopy the Parkin translocation block observed following *PINK1* siRNA application, hence placing them upstream of mammalian Parkin. With this assay evaluating the same process as the primary *Drosophila* screen, the expected outcome would be an enrichment of genes causing a reduction in CCCP-induced Parkin translocation. However, one caveat with regards to mammalian genetics is the presence of greater functional redundancy of genes compared to the *Drosophila* genome, perhaps resulting in a weaker translocation block than expected in some cases.

Unlike the *Drosophila* S2R+ cell system, a wide variety of mammalian cells have been shown to undergo complete mitophagy following lengthy CCCP application, in a robust and reproducible manner (Kawajiri et al, 2010; Narendra et al, 2008; Vives-Bauza et al, 2010). This phenomenon is well documented in HeLa cells, where ~40% of cells have a reduced or eliminated mitochondrial network after 24 hours of toxification (Narendra et al, 2008). As with Parkin translocation, *PINK1* silencing leads to a block of CCCP-induced mitophagy. Utilising these observations, this aspect of tertiary screening aims to assess the ability of hits to influence the end-point of the mitophagy pathway, with screen hits expected to phenocopy the effect of *PINK1* silencing.

5.3 DESIGNING A CUSTOM siRNA LIBRARY

In order to produce a human screening library of *Drosophila* hits, orthologous human genes had to be determined, and custom library plates designed. Library synthesis was conducted by Dharmacon (Thermo Scientific Molecular Biology), who produced SMARTpool siRNA stock plates incorporating appropriate user controls.

5.3.1 FINALISING THE *DROSOPHILA* HIT LIST

Despite having finalised the *Drosophila* hit group following the conclusion of secondary screening, several additional genes were added prior to mammalian screening. These

genes originated from an earlier screening project undertaken by Joe Pogson, a postgraduate student in the Whitworth laboratory. This screen assessed the ability of genes in the *Drosophila* kinome and phosphatome to modify mitochondrial morphology, with hits being defined as those that phenocopied *dPINK1* silencing. Using a manual scoring system, hit dsRNAs had an average morphology score within 1 standard deviation of the mean of the *dPINK1* dsRNA control, therefore producing a hyper-fused network of mitochondria. Here, human orthologs of these genes were added to the human library due to their ability to mimic a major component of the PINK1/Parkin-pathway. When comparing these additional genes to the finalised *Drosophila* hit group, just one common gene was identified (*Tousled-like kinase*) out of the eleven *dPINK1* morphology phenocopiers. This perhaps reflects a propensity for non-PINK1/Parkin-pathway specific modifiers of mitochondrial morphology, such as genes affecting membrane fluidity or causing general cellular toxicity. However, with space in the tertiary human screening library, the potential for a pathway-specific effect made their inclusion worthwhile. Therefore, the *Drosophila* genes taken forward for human screening purposes encompassed the groups defined in chapter 4 (category A & B), as well as additional *Drosophila* mitochondrial morphology genes (category C):

A) A confirmed primary screen hit, AND a hit in:
   I. ≥ 2 secondary screens or
   II. perinuclear aggregation screen only

B) Non-confirmed primary screen hit, but an 'interesting' secondary screen hit.

C) *dPINK1* phenocopier hit in the mitochondrial morphology screen

These parameters produced a group of 75 hit dsRNA amplicons equating to 72 *Drosophila* genes. Of these, 10 *Drosophila* genes were added from category C (Table 5.1 and Figure 5.1, grey).

	A) I.	A) II.	B)	C)	Total
Drosophila amplicons	42	2	21	10	75
Drosophila genes	39	2	21	10	72
No human ortholog	3	1	0	0	4
Putative human orthologs	50	1	25	14	90

Table 5.1 Converting *Drosophila* hit genes into their putative human orthologs. Final quantification of *Drosophila* dsRNA amplicons and equivalent genes falling into each hit category (blue), with corresponding human genes (orange).

5.3.2 CONVERTING *DROSOPHILA* HITS INTO PUTATIVE HUMAN GENES

In order to convert *Drosophila* screen hits into their putative corresponding human orthologs, an online ortholog prediction tool from the *Drosophila* RNAi Screening Center (DRSC) was implemented. The 'DRSC Interactive Ortholog Prediction Tool or 'DIOPT', collates data from existing ortholog prediction programs (Ensembl Compara, HomoloGene, Inparanoid, Isobase, OMA, OrthoDB, orthoMCL, Phylome, RoundUp, and TreeFam), thereby producing a comprehensive list of putative orthologs for each gene (Hu et al, 2011). By inputting the 72 unique *Drosophila* hit genes, a list of 90 putative human orthologs was produced (Table 5.1 & Figure 5.1), where 4 *Drosophila* genes had no known human ortholog, and 18 *Drosophila* genes had two or more putative human orthologs.

5.3.3 HUMAN TERTIARY SCREENING LIBRARY

Having produced a list of human orthologs, the next step was to design the custom siRNA library plate layout. Here, there were a number of aspects to consider, including the most appropriate plate format and assay controls. Due to the relatively small number of human genes and the larger cell size, a 96-well plate format was chosen over the 384-well format of primary and secondary screens (Figure 5.2). This format allowed for a larger population of cells per condition, plus greater ease of manipulation with the high-throughput equipment.

PINK1 and *parkin* siRNA were included as positive screen controls, both of which were expected to produce a strong Parkin translocation and mitophagy phenotype. Additionally, two distinct 'non-targeting' siRNAs (NT1 and NT2) were included as negative controls (Figure 5.2). The plate was designed with the outer edge devoid of siRNA, to avoid edge effects. Further to this, 11 additional empty wells were integrated into the interior of the plate, acting as 'no siRNA' controls, as well as providing the facility for extra controls at a later date. With this design, the library consisted of two plates, with human gene siRNAs arranged according to their 'Ensembl gene ID.'

The silencing reagent chosen for screening was the 'siGENOME siRNA' system, in a 'SMARTpool' format (Dharmacon, Thermo Scientific Molecular Biology). siGENOME siRNA guarantees a high-efficiency reduction in gene expression of 75% or more, whilst maintaining target specificity. Each well contains a 'SMARTpool' of four siGENOME siRNA 19mers, targeting distinct regions of the mRNA - intended to increase reagent potency compared to individual siRNAs alone.

	Dmel gene	Putative Human ortholog(s)
1	*ab*	*ZBTB22, ZNF295, ZBTB37, ZBTB17, ZBTB39*
2	*ago*	*FBXW7*
3	*atms*	*PAF1*
4	*Atu*	*LEO1*
5	*BAP55*	*ACTL6A, ACTL6B*
6	*Cdk9*	*CDK9*
7	*CG12050*	*WDR75*
8	*CG14023*	*NCOA6*
9	*CG14239*	*-*
10	*CG15459*	*USMG5*
11	*CG17209*	*POLR3A*
12	*CG2469*	*CTR9*
13	*CG2685*	*WBP11*
14	*CG33051*	*POLR3G, POLR3GL*
15	*CG34449*	*ZDHHC8, ZDHHC5*
16	*CG5591*	*MLL3*
17	*CG6220*	*CDC73*
18	*CG7886*	*CEP78*
19	*CG9883*	*-*
20	*CkIIα*	*CSNK2A1, CSNK2A2*
21	*cn*	*KMO*
22	*Cp1*	*CTSL2, CTSL1, CTSS, CTSK*
23	*Ctr1A*	*SLC31A1*
24	*Dis3*	*DIS3*
25	*faf*	*USP9X, USP9Y*
26	*fz3*	*FZD5*
27	*GATAe*	*GATA4*
28	*Gclm*	*GCLM*
29	*HLH106*	*SREBF1, SREBF2*
30	*l(1)G0007*	*DHX38*
31	*l(2)01810*	*SLC17A3, SLC17A9*
32	*Lilli*	*AFF4, AFF1, AFF3, AFF2*
33	*Maltase A5*	*SLC3A1*
34	*MED14*	*MED14*
35	*MED19*	*MED19*
36	*MED24*	*MED24*

	Dmel gene	Putative Human ortholog(s)
37	*MED28*	*MED28*
38	*MED7*	*MED7*
39	*Pcaf*	*KAT2A, KAT2B*
40	*pic*	*DDB1*
41	*pont*	*RUVBL1*
42	*Pros25*	*PSMA2*
43	*Prp31*	*PRPF31*
44	*ptip*	*PAXIP1*
45	*pUf68*	*PUF60*
46	*rept*	*RUVBL2*
47	*Rpb10*	*POLR2L*
48	*Rpb5*	*POLR2E*
49	*Rpb8*	*POLR2H*
50	*RpL28*	*RPL28*
51	*Rrp6*	*EXOSC10*
52	*scny*	*USP36, USP42*
53	*sec10*	*EXOC5*
54	*sgg **	*GSK3B, GSK3A*
55	*Srp54*	*SREK1, SRSF11*
56	*Tango6*	*TMCO7*
57	*TfIIFα*	*GTF2F1*
58	*tlk **	*TLK2, TLK1*
59	*U2af38*	*U2AF1, U2AF1L4*
60	*U2af50*	*U2AF2*
61	*Withdrawn*	*-*
62	*Withdrawn*	*-*
63	*Ac78C*	*ADCY8*
64	*aPKC*	*PRKCI, PRKCZ*
65	*CG11870*	*NUAK1, NUAK2*
66	*CG2277*	*NT5DC1*
67	*Csk*	*CSK*
68	*fwd*	*PI4KB*
69	*Pka-R1*	*PRKAR1A, PRKAR1B*
70	*ND42*	*NDUFA10*
71	*Pp4-19C*	*PPP4C*
72	*Sk1*	*SPHK2, SPHK1*

Figure 5.1 Converting *Drosophila* hit genes into their putative human orthologs. Schematic of 72 final *Drosophila* (Dmel) hit genes (white) and morphology screen hits from category C (grey), with their equivalent 90 human orthologs. Gene lists are arranged alphabetically according to the official *Drosophila* gene name. Asterisks denote genes with multiple amplicons in the hit group.

The amount of stock siRNA purchased had to provide sufficient copies of the library for completion of the tertiary screen, whilst preventing wastage and unnecessary expense. Taking this into consideration, 0.1 nmol of each SMARTpool was acquired, allowing for ~30 library copies at a concentration of 25 nM.

5.4 LOW-THROUGHPUT ASSAY DEVELOPMENT

Low-throughput assay development initially focused on selecting the most appropriate cell system for screening purposes. As previously mentioned, many of the early mammalian PINK1/Parkin studies utilised a HeLa cell system for study of the pathway, and this continues to be favoured by some groups. However, given that HeLa cells are a cancer cell line with abnormal genetic make-up, they are perhaps less favorable to study than a more 'normal' cell type. This point is strongly reinforced by the fact that HeLa cells do not express the major pathway component, Parkin. Despite this, HeLa

EMPTY	EMPTY	EMPTY	EMPTY	EMPTY	EMPTY	EMPTY	EMPTY	EMPTY	EMPTY	EMPTY	EMPTY
EMPTY	EMPTY	HIT	EMPTY	HIT	HIT	EMPTY	HIT	EMPTY	HIT	EMPTY	EMPTY
EMPTY	HIT	HIT	*PINK1*	HIT	HIT	HIT	HIT	NT2	HIT	HIT	EMPTY
EMPTY	HIT	HIT	HIT	HIT	HIT	HIT	HIT	HIT	HIT	EMPTY	EMPTY
EMPTY	EMPTY	HIT	HIT	HIT	HIT	HIT	HIT	HIT	HIT	HIT	EMPTY
EMPTY	HIT	HIT	NT1	HIT	HIT	HIT	HIT	*parkin*	HIT	HIT	EMPTY
EMPTY	EMPTY	HIT	HIT	EMPTY	HIT	HIT	EMPTY	HIT	HIT	EMPTY	EMPTY
EMPTY	EMPTY	EMPTY	EMPTY	EMPTY	EMPTY	EMPTY	EMPTY	EMPTY	EMPTY	EMPTY	EMPTY

Figure 5.2 Custom siRNA library - plate layout. 96-well plates were arrayed with human siRNA SMARTpools against equivalent *Drosophila* hits (white), screen controls (coloured wells) and a quantity of empty wells (grey). Positive controls were *PINK1* siRNA (pink) and *parkin* siRNA (green), plus two negative controls (orange): non-targeting siRNA 1 (NT1) and non-targeting siRNA 2 (NT2).

cells offer many advantages over other cells lines, including a readiness for transfection and ease of culturing; attributes which are vital for high-throughput work. However, in order to diminish potential criticisms arising through the use of HeLa cells, screening of two mammalian cell types in parallel was proposed. These were HeLa cells, and human retinal pigment epithelial cells (RPE1) cells. RPE1 cells are epithelial-like adherent cells with a largely ‘normal’ genetic profile. In addition, like HeLa cells, their size makes them amenable to microscopy analyses, and they grow with relative ease in culture.

Prior to human screening, we were fortunate to be provided with HeLa- and RPE1- cell lines, stably expressing N-terminal YFP-tagged Parkin (a kind gift from the Lane lab, University of Bristol). Here, exogenous Parkin expression provided clear benefits for both screening assays, permitting easy visualisation of Parkin translocation as well as allowing mitophagy to proceed in the absence of endogenous Parkin.

5.4.1 CCCP-INDUCED PARKIN TRANSLOCATION

The first assay to establish was Parkin translocation following CCCP application. In the mammalian field, this type of analysis is typically performed between 1 and 4 hours of CCCP toxification (Geisler et al, 2010a; Matsuda et al, 2010; Narendra et al, 2008; Okatsu et al, 2010; Vives-Bauza et al, 2010). To assess the dynamics of YFP-Parkin translocation in the two stable lines, a CCCP time-course was performed over 0 - 4 hours of toxification (Figures 5.3). YFP-Parkin.HeLa cells, in the presence of the negative control siRNA show a clear increase in Parkin translocation over the time-course, with 4 hours showing almost complete mitochondrial coverage (Figure 5.3 A). In agreement, YFP-Parkin.RPE1 cells also show increased translocation, with complete mitochondrial coverage occurring a little earlier, at 3 hours of CCCP toxification (Figure 5.3 B).

Following the application of *PINK1* siRNA in YFP-Parkin.HeLa cells, Parkin translocation is almost completely absent at early CCCP time-points, and only mildly initiated after 3 and 4 hours of toxification (Figure 5.3 A). Therefore without *PINK1*, these cells no longer translocate Parkin to the MOM, making them an appropriate model for PINK1/Parkin-pathway screening. In contrast, *PINK1* silencing in YFP-Parkin.RPE1 cells failed to prevent Parkin translocation at later time-points, and caused only a mild blocking effect after 1 hour of toxification (Figure 5.3 B), This observation may indicate that RPE1 cells are inappropriate for screening purposes in the context of the PINK1/Parkin-pathway, or that gene silencing and/or toxification methodologies require further optimisation.

The second assay to establish was CCCP-induced mitophagy. This was a crucial assay to optimise, as up to this point screening has focused on upstream stages of the pathway, rather than the end-point proper. Therefore, this assay provided the opportunity to observe a complete blockage of the entire mitophagy process. Typically, mitophagy is analysed after 24 or 48 hours of CCCP treatment (Geisler et al, 2010a; Matsuda et al, 2010; Narendra et al, 2008; Tanaka et al, 2010). However, as there is currently no published data with regards to RPE1 mitophagy dynamics, a time-course of 0, 16, 24 and 48 hours of CCCP toxification was implemented. The incidence of mitophagy was observed by monitoring the loss of the mitochondrial inner membrane (MIM) protein ATP5A, both through qualitative and quantitative means. To quantify the amount of mitophagy observed in qualitative images, cells were put into three distinct categories according to their mitochondrial content - ‘full mitochondria,’ ‘reduced

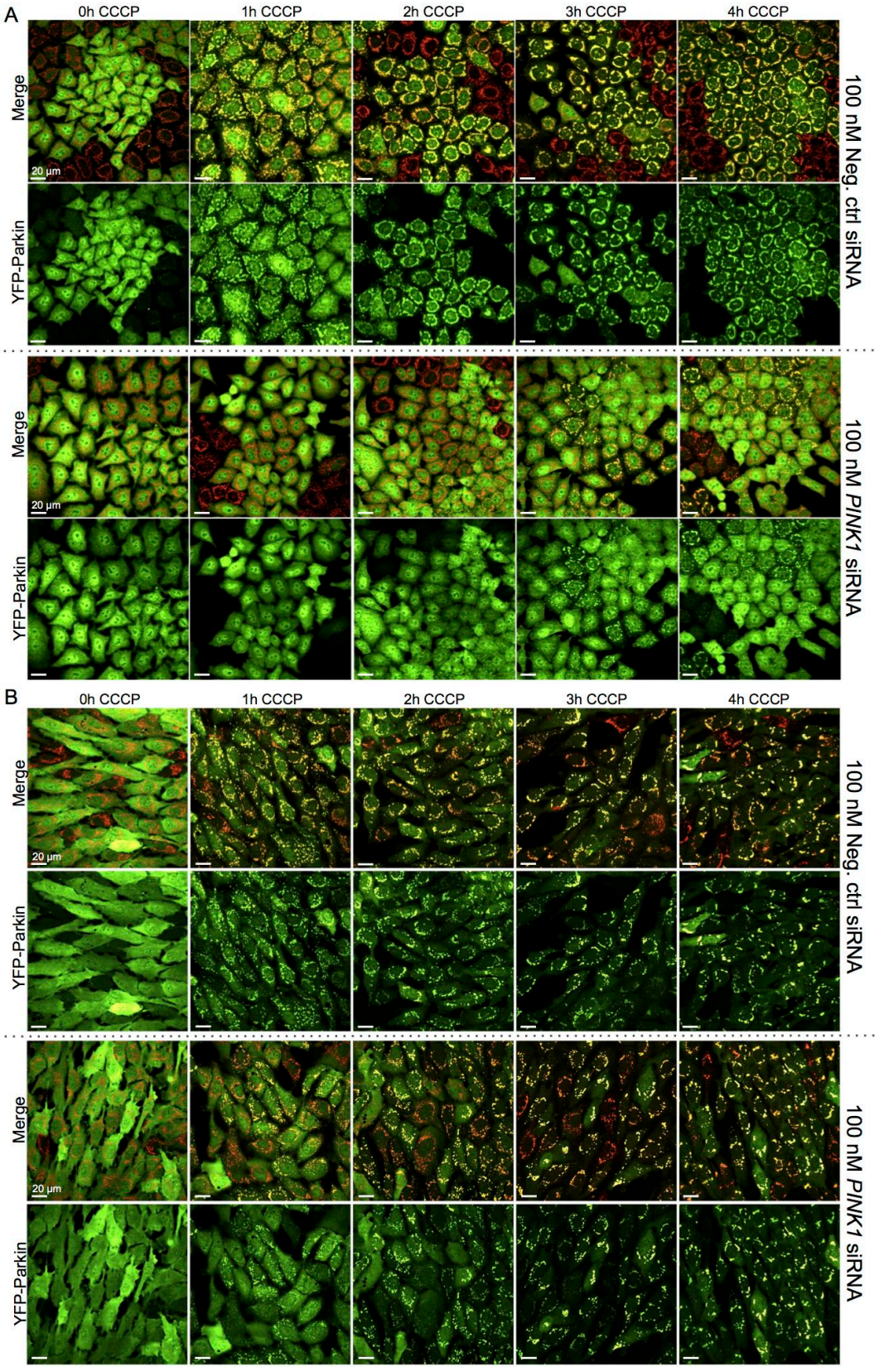

Figure 5.3 CCCP-induced Parkin translocation. YFP-Parkin.HeLa (A) and YFP-Parkin.RPE1 (B) cells were treated with 100 nM negative control or *PINK1* siRNA and toxified with 10 µM CCCP for a time-course of 0 - 4 hours as indicated. Parkin translocation was assessed by the re-distribution of YFP-Parkin (green) from the cytosol to the mitochondrial network (ATP5A – red). Scale bar: 20 µm.

mitochondria,' or 'no mitochondria' (Figure 5.4). For each condition, the percentage of cells falling into each of these categories was calculated.

5.4.2 CCCP-INDUCED MITOPHAGY

YFP-Parkin.HeLa cells, in the presence of the negative control siRNA showed a clear decrease in the number of cells with a full complement of mitochondria, and an increase in cells with 'reduced' or 'no' mitochondria after 16 and 24 hours of toxification. However, by 48 hours of toxification, much of the cell population appeared either sick or dead (Figure 5.5 A). Following quantification, a steady decrease in the number of cells with a 'full' mitochondrial network, and an increase in those with 'reduced' or 'no' mitochondria was observed over the CCCP time-course (Figure 5.5 B). Upon *PINK1* silencing, after 16 & 24 hours of CCCP treatment, many more cells retained a full complement of mitochondria compared to the negative control (Figure 5.5 C). After 48 hours of toxification, some reduction in the ATP5A signal was observed, however in contrast to the negative control, the cells look far healthier at this time-point. These data indicate that *PINK1* loss is able to block mitophagy between 16–24 hours of CCCP treatment as previously reported (Matsuda et al, 2010; Narendra et al, 2010), and reduce mitophagy after longer toxification durations. Quantification of data from microscopy images confirmed the observed maintenance of a 'full' mitochondrial network after 16 and 24 hours of CCCP treatment (Figure 5.5 D). This effect is weaker but still evident at 48 hours, in agreement with the qualitative assessment. Taken together, this confirms that the loss of *PINK1* in YFP-Parkin.HeLa cells is able to prevent mitophagy as well as Parkin translocation, supporting their use for PINK1/Parkin-pathway screening in our hands.

The observed levels of mitophagy in YFP-Parkin.RPE1 cells show a dramatic deviation from that of YFP-Parkin.HeLa cells. Here mitochondria are readily lost from almost the entire cell population by 24 hours of CCCP treatment (Figure 5.6 A & B). Even after a shorter CCCP treatment of 16 hours, cells have either a greatly reduced or absent mitochondrial network. Therefore, these cells appear to respond to CCCP toxification with a more widespread, severe induction of mitophagy. Upon *PINK1* silencing, both the qualitative and quantitative data indicate very little influence of *PINK1* loss on the amounts of mitophagy after 24 and 48 hours of CCCP treatment (Figure 5.6 C & D). However, as with Parkin translocation, *PINK1* siRNA appears to cause a modest block on mitophagy at the earliest CCCP time-point of 16 hours in these cells, showing a greater proportion of 'reduced mitochondria' phenotypes compared to 'no

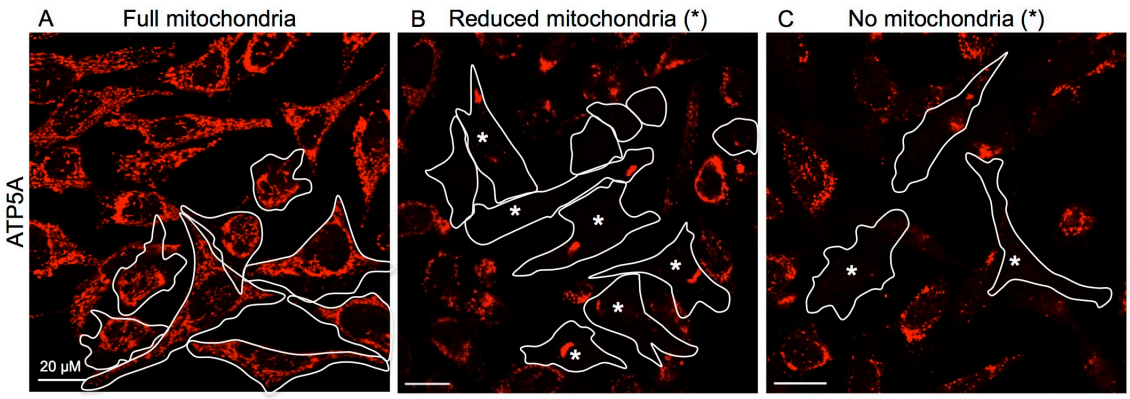

Figure 5.4 Low-throughput mitophagy quantification. To quantify mitophagy, cells are assessed on a cell-by-cell basis according to their mitochondrial content. Cells with an extensive mitochondrial network fall into the 'full mitochondria' category (A) whilst those with a reduced network fall into the 'reduced mitochondria' category. (B), asterisks). Cells that have undergone complete mitophagy, fall into the 'no mitochondria' category (C, asterisks). Mitochondrial content is assessed according to the MIM marker, ATP5A. White outlines denote YFP-Parkin-expressing cell boundaries, scale bar - 20 µm.

mitochondria.' (Figure 5.6 D). Here, the 'reduced mitochondria' appear qualitatively different in their distribution compared to the negative control, with a less aggregated, perinuclear position. However, the nature of the manual scoring system implemented does not allow distinctions to be made between these phenotypes, perhaps lessening the quantified effect at this point.

Taken together, these data again indicate that either YFP-Parkin.RPE1 cells are less sensitive to PINK1/Parkin-pathway manipulations, or that assay parameters require optimisation before the full effect of *PINK1* silencing can be observed. It may be that earlier time-points need to be assessed in order to observe a significant mitophagy block' caused by *PINK1* silencing. Alternatively, the lack of effect may be due to ineffective gene knockdown, as gene-silencing techniques often produce differential results depending on the cell type. If this is the case, poor *PINK1* siRNA silencing may explain the weak blocking effect observed. To address this issue, siRNA concentration and delivery method underwent full optimisation using qRT-PCR analysis.

5.5 DEVELOPMENT OF siRNA GENE SILENCING TECHNIQUES

In order to optimise gene silencing, quantitative real-time reverse transcription PCR (qRT-PCR) analysis of *PINK1* mRNA was undertaken. For this, a range of transfection reagents, siRNA concentrations and delivery techniques were analysed.

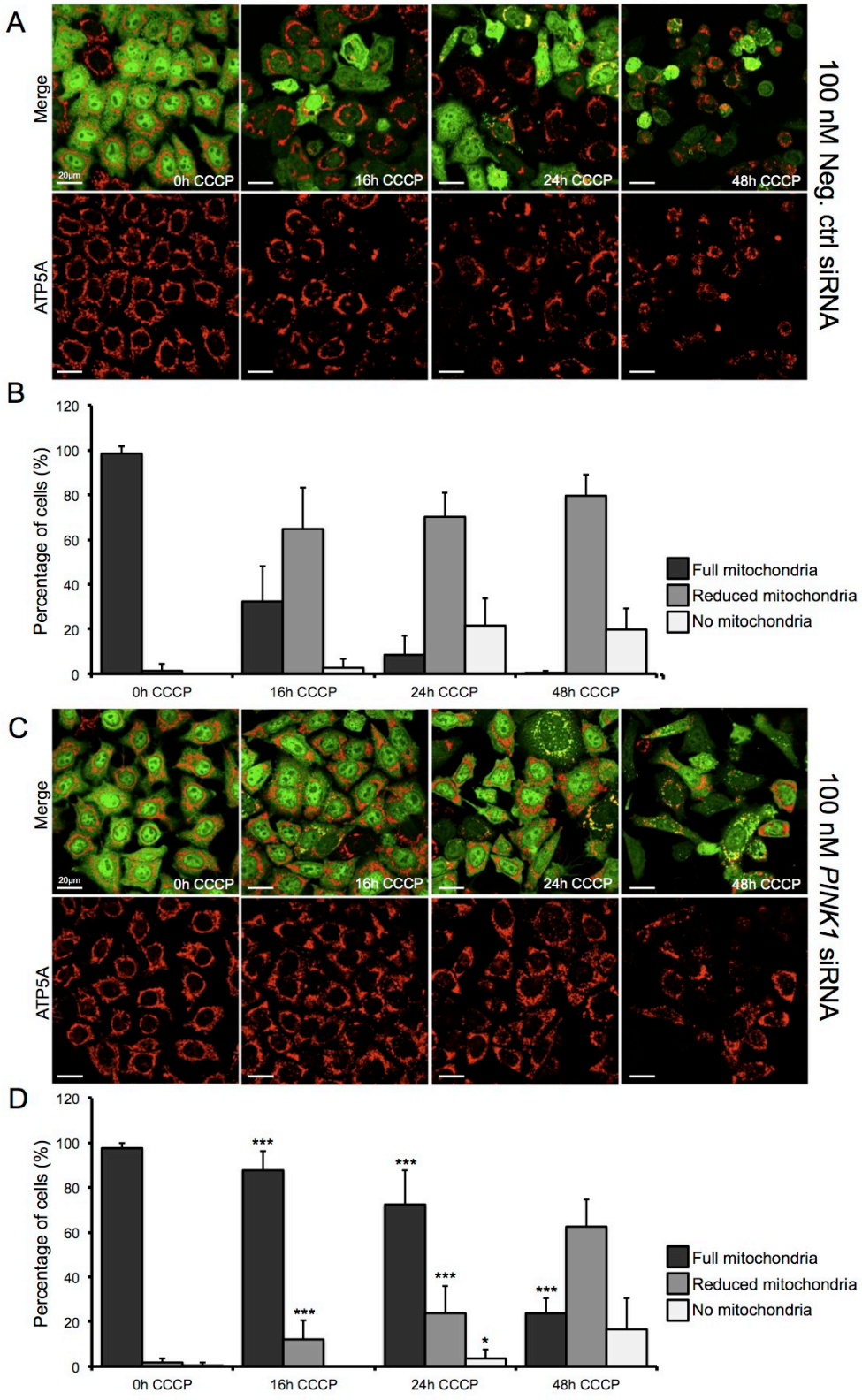

Figure 5.5 CCCP-induced mitophagy in YFP-Parkin.HeLa cells. (A & C) CCCP (10 µM) time-course over 0 - 48 hours following the application of 100 nM negative control siRNA (A) or *PINK1* siRNA (B). Mitochondria are represented by the MIM marker ATP5A (red), YFP-Parkin (green), scale bar: 20 µm. (B & D) Manual quantification of mitophagy induction in cell samples from (A) and (C) respectively. One biological repeat with at least 5 FOV per condition. Quantification based on three distinct categories; 'full mitochondria,' 'reduced mitochondria' and 'no mitochondria.' (D) *P<0.05, ***P<0.001 (Student's T-test compared to equivalent conditions in (B)

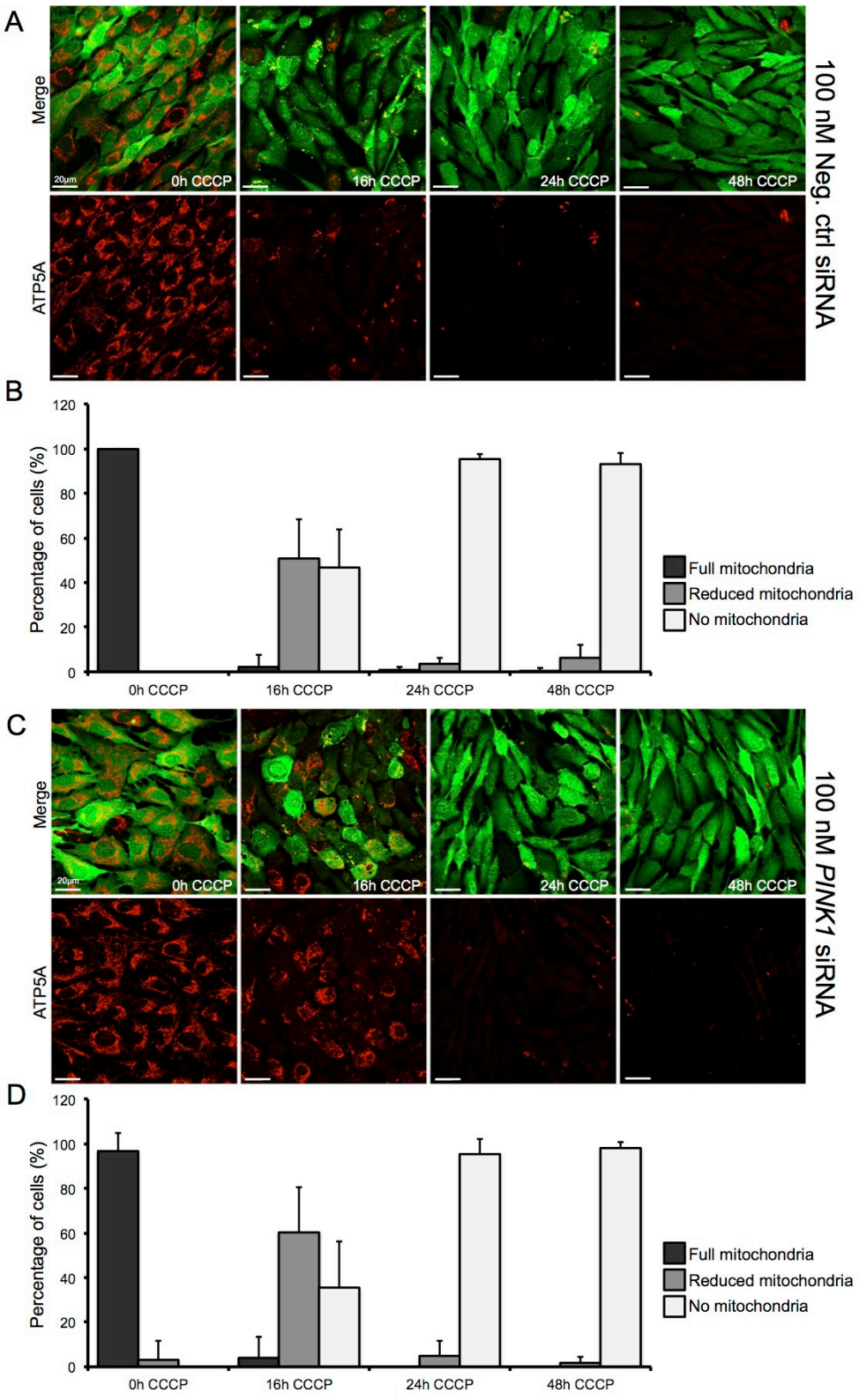

Figure 5.6 CCCP-induced mitophagy in YFP-Parkin.RPE1 cells. (A & C) CCCP (10 µM) time-course over 0 - 48 hours following the application of 100 nM negative control siRNA (A) or *PINK1* siRNA (B). Mitochondria are represented by the MIM marker ATP5A (red), YFP-Parkin (green), scale bar: 20 µm. (B & D) Manual quantification of mitophagy induction in cell samples from (A) and (C) respectively. One biological repeat with at least 5 FOV per condition. Quantification based on three distinct categories; 'full mitochondria,' 'reduced mitochondria' and 'no mitochondria.' Student's T-test comparing equivalent conditions in (B) and (D) found no significance.

5.5.1 qRT-PCR ANALYSIS OF *PINK1* SILENCING

A common issue with siRNA delivery is the cell-specific toxicity of transfection reagents used. To optimise siRNA delivery in YFP-Parkin.HeLa and YFP-Parkin.RPE1 cells, a range of reagents were tested, comprising Dharmafect 1 (Dharmacon), Effectene (Qiagen) and Lipofectamine 2000 (Invitrogen). In addition, most low-throughput silencing assays make use of a 'forward transfection' technique of siRNA delivery. This involves allowing the cells to adhere to the assay vestibule before delivering the siRNA. In contrast, high-throughput techniques tend to use a 'reverse transfection' methodology, plating cells and delivering siRNA simultaneously. This method allows siRNAs to be arrayed across the multi-well screening plates prior to assay commencement, saving a great deal of time. However, it also has the potential to reduce cell viability by increasing toxicity at the time of adherence. Under most circumstances, this reduction in cell viability and therefore cell number can be tolerated and simply overcome by increasing the starter population density.

A final aspect of siRNA delivery to consider is the optimum SMARTpool concentration for efficient gene silencing. Recommended siRNA concentrations are between 5 - 100 nM. Here, the chosen concentration should be high enough to allow efficient and long-lasting gene silencing, yet low enough to minimise siRNA-induced toxicity. The ideal siRNA concentration is largely gene-specific. However when screening large numbers of genes, optimisation of each individual siRNA would be time-consuming and costly. Therefore, the knockdown technique was optimised for the most crucial control, *PINK1*.

Initial qRT-PCR analysis used the protocol implemented in low-throughput assay development (section 5.4). This methodology involved the forward transfection of 100 nM of siRNA, delivered using Effectene transfection reagent (Figure 5.7 A). This method produced efficient *PINK1* silencing in YFP-Parkin.HeLa cells, but a poor reduction of gene expression in YFP-Parkin.RPE1 cells, perhaps explaining the lack of *PINK1* siRNA effect observed in these cells. Additionally, as the siRNA concentration used was at the high extreme of the range recommended by Dharmacon, subsequent assay optimisation focused on reducing this concentration, as well all ascertaining the optimum siRNA delivery method for both cell types. By reducing the siRNA concentration, the risk of siRNA-associated toxicity and the cost of the screen itself would be diminished.

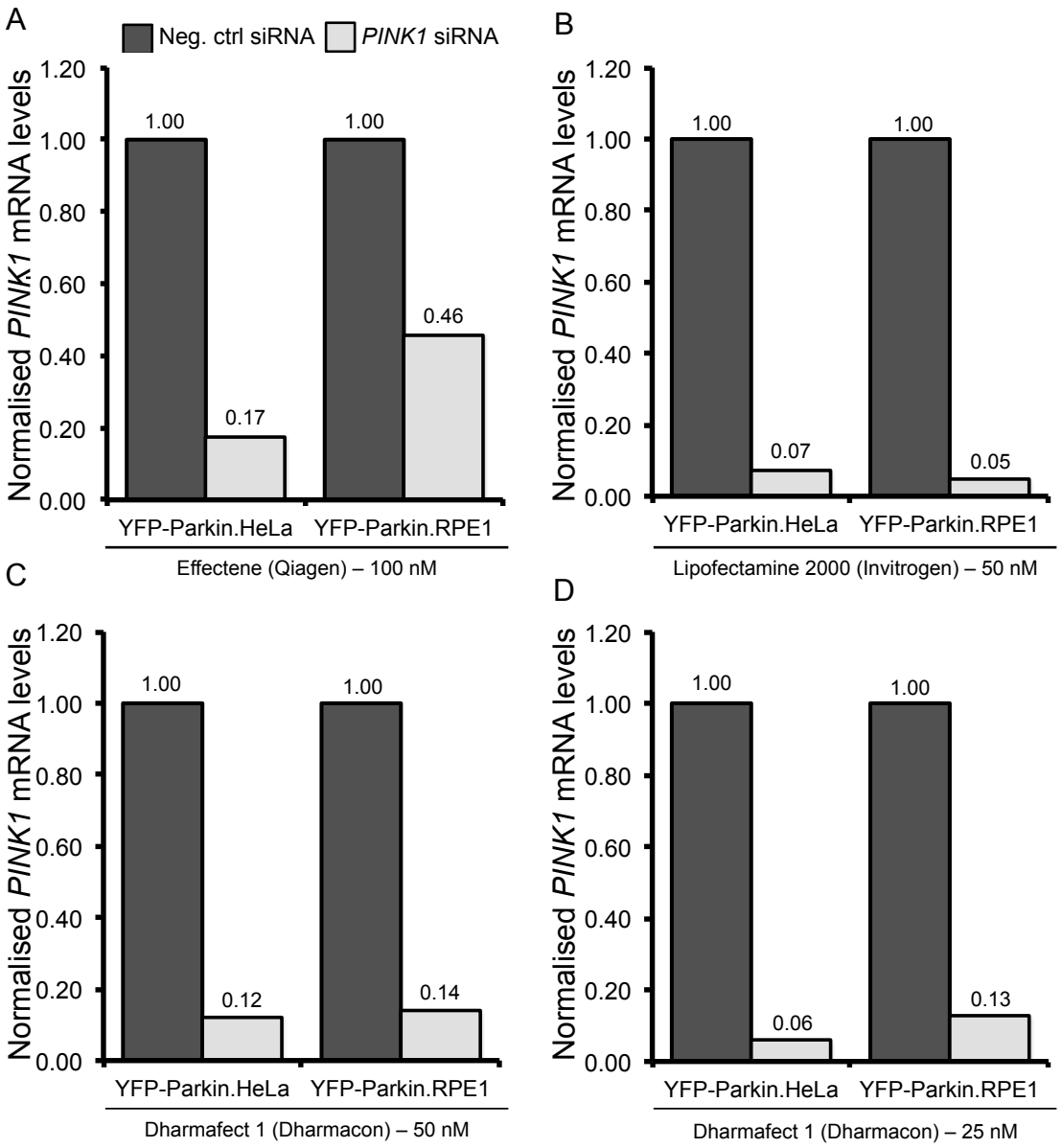

Figure 5.7 qPCR analysis of *PINK1* silencing. Analysis of optimal gene silencing conditions in YFP-Parkin.HeLa & YFP-Parkin.RPE1 cells. Cells were treated with negative control or *PINK1* siRNA at 100 nM (A), 50 nM (B & C) or 25 nM (D) concentrations for 4 days before qRT-PCR analysis of gene expression. siRNA SMARTpools were delivered using forward (A) or reverse (B-D) transfection methods, by Effectene (A), Lipofectamine 2000 (B) or Dharmafect 1 (C & D) reagents. Data averaged over three samples within one biological repeat; normalised to the housekeeping gene 18S.

The first optimisation step involved altering the method of siRNA delivery to incorporate the 'reverse transfection' of *PINK1* siRNA at the same time as cell plating (Figure 5.7 B – D). Second, two additional transfection reagents were assessed; Lipofectamine 2000 (Figure 5.7 B), and Dharmafect 1 (Figure 5.7 C & D). Third, the concentration of siRNA was reduced to 50 nM (Figure 5.7 B & C) and 25 nM (Figure 5.7 D).

Altering the delivery protocol to a 'reverse' transfection method had no obvious negative effects on gene silencing (Figure 5.7 B – D) or survival of the cell population (data not shown). Additionally, both Lipofectamine 2000 and Dharmafect 1 produced

robust gene silencing in both cell-types (Figure 5.7 B – D). However, upon cellular inspection, Lipofectamine 2000 caused an increase in cell death in the HeLa population, whereas Dharmafect 1 appeared to cause RPE1-cell toxicity (data not shown). This result indicated that optimal siRNA delivery in these two cell-types required distinct transfection reagents. Finally, the efficiency of gene silencing remained comparable following the reduction of siRNA concentration from 100 nM to 50 nM and 25 nM. Therefore, no advantage was gained by increasing the siRNA concentration beyond 25 nM for tertiary screening purposes.

Taken together, optimised conditions for gene silencing involved the reverse transfection of 25 nM siRNA, using Dharmafect 1 (YFP-Parkin.HeLa cells) or Lipofectamine 2000 (YFP-Parkin.RPE1 cells).

5.6 CCCP-INDUCED PARKIN TRANSLOCATION

Having optimised conditions for gene silencing, the next stage was to scale-up the Parkin translocation assay for use in a high-throughput format. As shown previously, YFP-Parkin.HeLa cells readily translocate YFP-Parkin to the mitochondrial network following short CCCP application. Importantly, the loss of *PINK1* is able to produce a strong translocation block, providing a valuable positive siRNA control for the assay. In contrast, whereas YFP-Parkin.RPE1 cells demonstrated efficient translocation over equivalent toxification durations, the potency of the *PINK1* siRNA translocation block was much weaker than in the HeLa cell line. As mentioned, this may have been due to suboptimal silencing methodologies. Having optimised the RPE1 silencing protocol, *PINK1* siRNA was found to substantially reduce Parkin translocation, but continued to produce a weak mitophagy block. Therefore, for the scope of this project it was decided to concentrate on screening with the YFP-Parkin.HeLa cells alone.

The aim of this assay was to identify human orthologs of *Drosophila* hit genes able to block Parkin translocation in a way analogous to *PINK1* siRNA. Within this group of genes, an overall trend towards reduced Parkin translocation was expected because of the enrichment of genes having an equivalent effect in the *Drosophila* system. However, due to a greater redundancy within the human genome, the expected effect is potentially less than that seen in S2R+ cells.

5.6.1 ASSAY DEVELOPMENT

In order to scale up the assay into 96-well plates, a number of parameters required optimisation. These included the optimum cell-density, toxification duration and data analysis method. The doubling time of a cellular population is influenced by a number of factors including the cell type, transfection reagents applied and toxification method. Having tested a range of seed densities in the 96-well plate format, an optimal density of 4,000 cells per well was established, providing a confluent population for assay analysis (data not shown). Previous, low-throughput analysis established that YFP-Parkin underwent CCCP-induced translocation between 1 and 4 hours of toxification in the stable HeLa cell-line (Figure 5.3 A). Over this time-course, translocation peaked at 4 hours of CCCP treatment; with earlier time-points maintaining clusters of partially- or non-translocated cells. Therefore, high-throughput assay development focused on Parkin translocation after 4 and 6 hours of CCCP toxification (Figure 5.8). Here, the aim was to ascertain if even greater amounts of translocation could be achieved by CCCP-applications longer than 4 hours. In the vehicle-treated negative control, no Parkin translocation is observed (Figure 5.8 A), however after 4 and 6 hours of CCCP treatment, almost the entire cell population displays a strong translocation phenotype (Figure 5.8 B & C). Following *PINK1* silencing, CCCP toxification for 4 and 6 hours failed to induce Parkin translocation, producing a phenotype comparable to that of the '0 hour' controls (Figure 5.8 D - F). This demonstrated that the silencing procedure had transferred well from the low-throughput scenario to the 96-well screening plates.

One concern with regards to the 6-hour time-point was an observed decrease in YFP-intensity compared to 4 hours of CCCP treatment in the negative control (Figure 5.8 C). This decrease may have been an issue with YFP-stability following persistent exposure to CCCP, although there is no precedent for this in the literature. Alternatively, by 6 hours of toxification, YFP-Parkin may be undergoing degradation; having already ubiquitinated targets at the MOM. Because of this, and the strength of the phenotype at earlier time-points, a 4-hour toxification period was favoured.

To quantify the observed translocation, automation using the 'Transfluor' application was attempted. Initial efforts utilised a 'puncta number' measurement, as applied in the *Drosophila* primary screen. However, the Parkin translocation phenotype observed in HeLa cells differs to that of S2R+ cells in that there are fewer discrete 'puncta' observed at this magnification and resolution, and more of a continuous 'ring' in the juxtanuclear region of the cell. This perhaps reflects the differential dynamics of these two cell types, where S2R+ cells maintain a cytoplasm-wide distribution of damaged

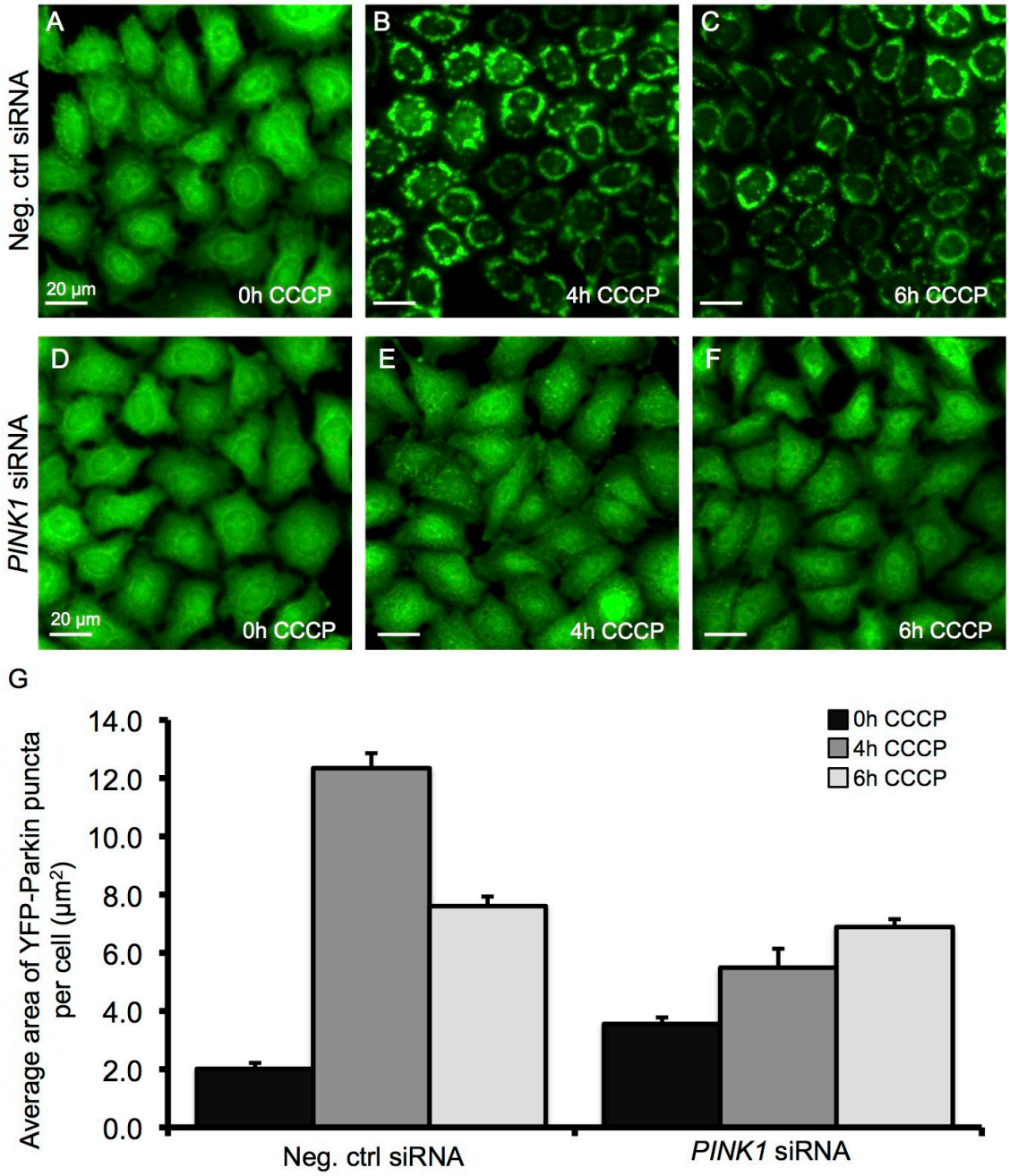

Figure 5.8 High-throughput Parkin translocation optimisation. YFP-Parkin.HeLa cells were subjected to negative control siRNA (A-C) or *PINK1* siRNA (D-F), and toxified for 0 hours (A & D), 4 hours (B & E) or 6 hours (C & F) with 10 µM CCCP. YFP-Parkin (green) translocation was assessed via qualitative data (A-F), acquired on a high content screening microscope using a 10x objective, scale bar: 20 µm. Automated quantitative data (G) was produced by the 'Transfluor' application, with a read-out of 'average area of YFP-Parkin puncta per cell (μm^2). Data acquired from one biological repeat, with a minimum of 4 wells, each with 9 FOV per condition.

mitochondria for a greater duration before transporting them to the perinucleus for degradation. In light of this observation, quantification of 'puncta number' proved difficult as the algorithm could pick up just one or two individual puncta per cell (data not shown). As an alternative, 'puncta area' was employed, quantifying the area of YFP-Parkin puncta with an intensity above the non-toxified background (Figure 5.8 G). However, where this algorithm was able to quantify a clear increase in Parkin puncta

area between vehicle-treated negative controls and those exposed to 4 hours of CCCP, this distinction was lesser after 6 hours. This assessment was not in agreement with visual image analysis, and may reflect the inability of the algorithm to detect areas of lower YFP intensity as discussed previously.

In the absence of *PINK1*, vehicle-treated conditions had a slightly higher puncta area than that of the negative control (Figure 5.8 G). However, this was not a substantial increase, and may be diminished following further biological repeats. After 4 hours of CCCP treatment, there was a slight increase in the area of YFP-Parkin puncta compared to the non-toxified control, perhaps representing low levels of Parkin translocation persisting under these conditions. Despite this, in comparison to the negative control at the equivalent time-point, a substantial block in translocation is observed. However, by 6 hours of CCCP toxification, this block is lesser, with the puncta area becoming closer in magnitude to the negative control sample. This automated assessment is in stark contrast to the qualitative data of the microscopy images (Figure 5.8 C & F), indicating failings of the algorithm to distinguish between these phenotypes. In light of these issues, manual quantification of the phenotypic data was chosen over automation.

5.6.2 PLATE LAYOUT

The human screening library consists of two 96-well plates, containing 90 siRNA SMARTpools against human orthologs of the final *Drosophila* hits (Figure 5.9 A). In addition, each plate contains positive controls against *PINK1* and *parkin*, plus two negative controls, NT1 and NT2. The outer edge of each plate is devoid of siRNA, in order to reduce the negative impact of edge effects on hit siRNA-containing wells. Additionally, this allowed for two rows of 'no CCCP' controls to be introduced, both in the absence of siRNA (empty), or in concert with the negative control, NT1 (Figure 5.9 A). This provides an additional 'positive' phenotype with which to compare screen hits. Finally, 11 'inner edge' wells were left devoid of siRNA at the time of plate design, in order to provide the facility for extra siRNA addition. Here, additional *PINK1*, *parkin* and NT1 siRNA SMARTpools were added, with two wells remaining siRNA-free (Figure 5.9 A).

5.6.3 PROTOCOL

Both of the tertiary screen assays were performed in triplicate in order to ensure the robust and reproducible nature of the overall screening hits. Before screening could take place, the custom siRNA library, supplied as dried pellets in two 96-well 'mother

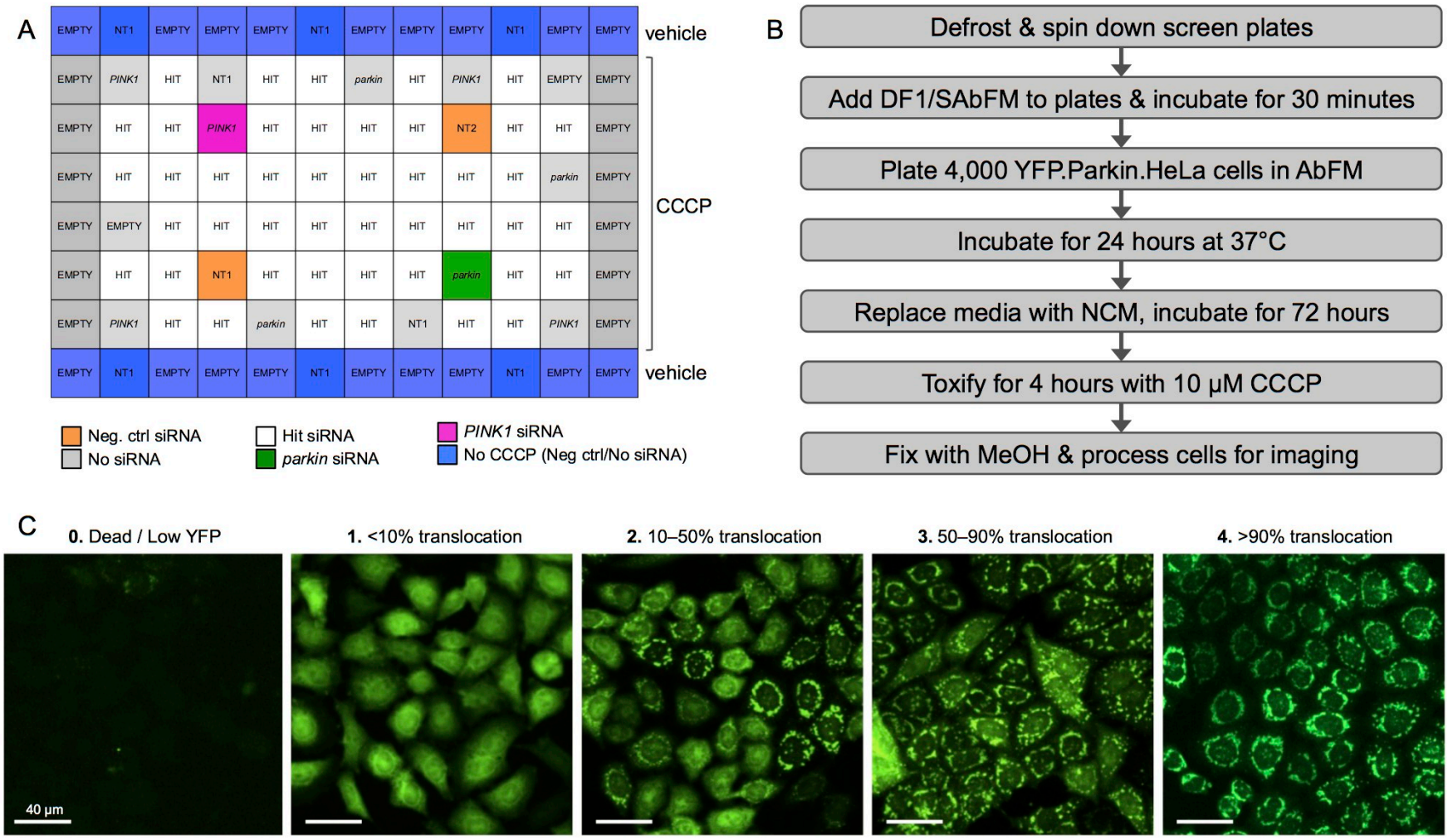

Figure 5.9 Parkin translocation assay development. (D) Diagram of assay plate design where colours represent different conditions (see key). Rows A & H remain non-toxified, and contain both 'Neg ctrl siRNA' (NT1) and 'no siRNA' (EMPTY) controls. (B) Protocol workflow for CCCP-induced Parkin translocation. (C) Example images of the 5 Parkin translocation phenotypes. Here, 0 = dead cells or low YFP expression, 1 = translocation in <10% of cells, 2 = translocation in 10 - 50% of cells, 3 = translocation in 50 - 90% of cells and 4 = translocation in >90% of cells. YFP-Parkin (green) images were captured using a high content screening microscope with a 10x objective, scale bar: 40 µm.

plates,' required resuspension in RNase-free water to a stock concentration of 2 μM. Once fully resuspended, stock siRNAs were printed into assay plates to give a final working concentration of 25 nM, and stored at -20 ºC.

For Parkin translocation analysis, plates were defrosted, and centrifuged briefly. Dharmafect 1 (DF1) diluted in serum and antibiotic-free media (SAbFM) was arrayed across the plates, and left to complex with the siRNA for 30 minutes at room temperature. Following this, 4,000 YFP-Parkin.HeLa cells in antibiotic-free media (AbFM) were added to each well, and plates incubated for 24 hours at 37ºC. To reduce transfection-reagent toxicity, media was replaced with normal culture media (NCM), and plates were incubated for a further 72 hours. Next, media was replaced with vehicle- or CCCP-containing media for 4 hours, before cellular fixation with ice-cold methanol for 10 minutes. Samples were then processed for imaging by the addition of anti-ATP5A & anti-AlexaFluor 594 (mitochondria), and Hoechst (nucleus) (Figure 5.9 B).

5.6.4 SCORING SYSTEM

Following sample processing, plates were imaged with a 10x objective at a frequency of 9 FOV per well. As automated data analysis proved both difficult and unreliable, this was performed manually using a 5-point scoring system (Figure 5.9 C). For each FOV, a score of 0, 1, 2, 3 or 4 was awarded, where 0 = extensive cell death or low YFP expression, 1= <10% of cells with Parkin translocation, 2 = between 10 - 50% of cells with Parkin translocation, 3 = between 50 - 90% of cells with Parkin translocation, and 4 = >90% of the cells with Parkin translocation (Figure 5.9 C). For each condition, the 'average Parkin translocation score' was calculated, producing one value per well.

5.6.5 CONTROLS

After visual analysis of images, vehicle-treated negative control samples consistently exhibited a diffuse, non-translocated distribution of Parkin (Figure 5.10 A). This lack of Parkin translocation is faithfully reflected in the quantification, where the 'average translocation score' is exactly '1' across all three replicate screens (Figure 5.10 B). After 4 hours of CCCP toxification, the negative control adopts a strong translocation phenotype in the majority of the cell population (Figure 5.10 A), achieving a score close to the maximum of '4' (Figure 5.10 B). In agreement, the average 'no siRNA' score also came close to '4', confirming the absence of negative effects from siRNA delivery. In contrast, *PINK1* siRNA prevented CCCP-induced translocation (Figure 5.10 A),

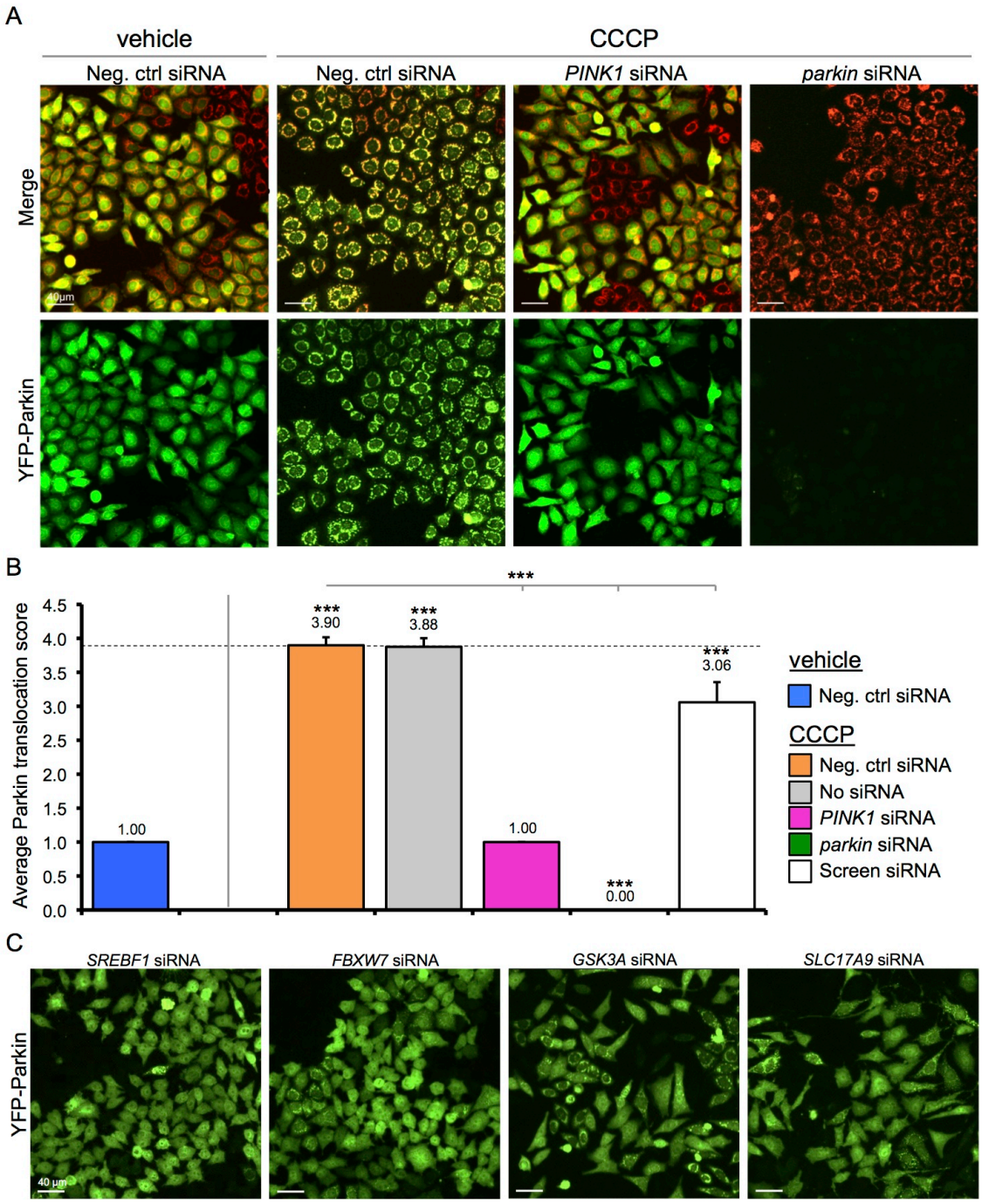

Figure 5.10 Parkin translocation screen analysis. (A) Example high-throughput images of negative control, *PINK1* and *parkin* siRNA treated cells, following the application of vehicle or CCCP for 4 hours (indicated). (B) Graphical representation of control 'average Parkin translocation scores' over three assays. Data comprises a minimum of 24 wells/condition, with 9 FOV per well. Error bars represent standard deviation, ***P<0.001 (One-way ANOVA with Bonferroni's correction, compared to the vehicle-treated 'Neg. ctrl siRNA' unless indicated). (C) Example high-throughput images of selected hit siRNAs following CCCP treatment. YFP-Parkin (green), ATP5A (red), acquired on a high content screening microscope using a 10x objective, scale bar: 40 µm.

returning the phenotype back to vehicle-treated levels (Figure 5.10 B), and *parkin* siRNA efficiently eliminated the YFP-Parkin signal confirming the success of the silencing process, and achieving a score of '0' (Figure 5.10 A & B).

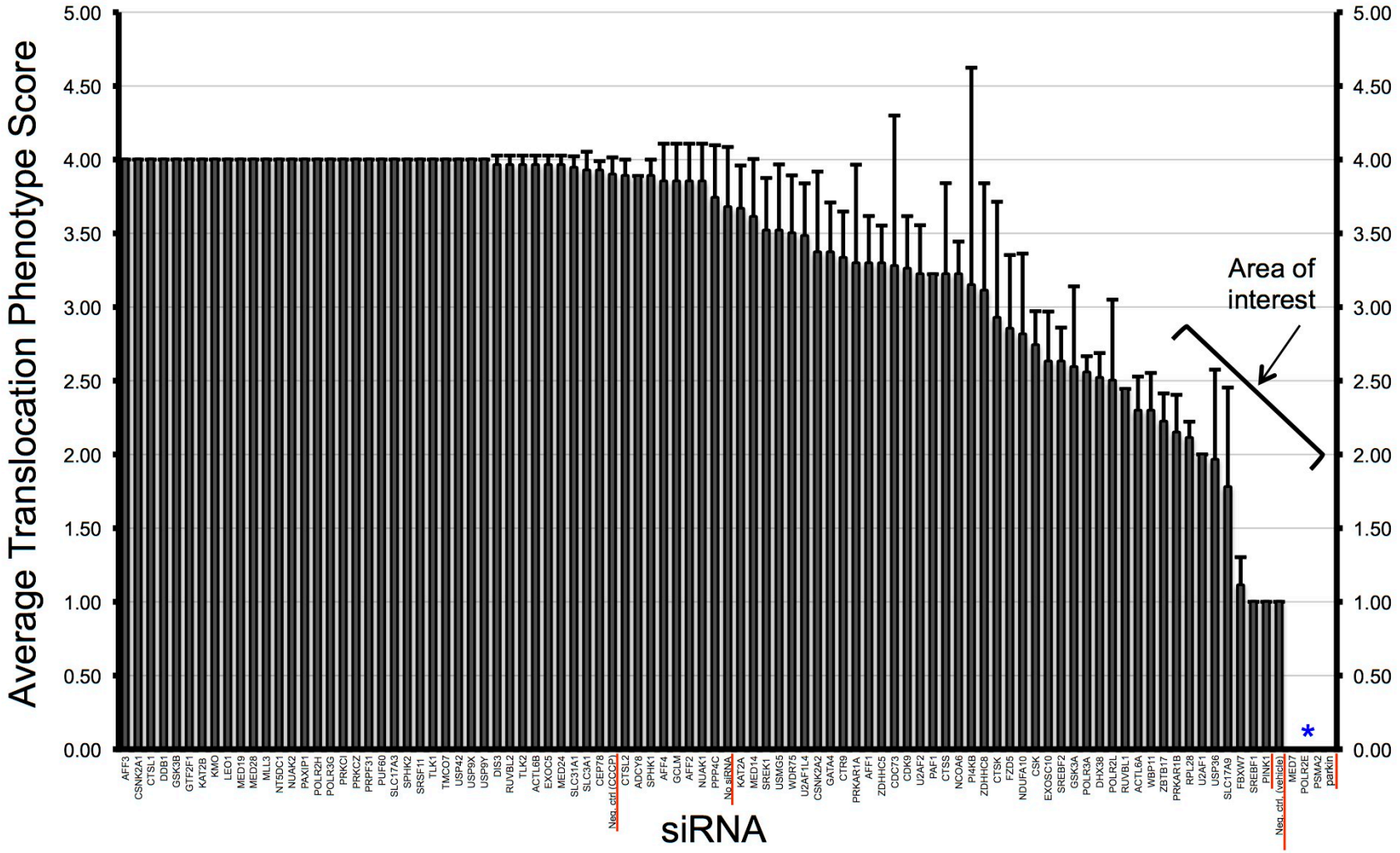

Figure 5.11 Average Parkin translocation siRNA data. Graphical representation of the 'average translocation phenotype score' of each siRNA, across three repeat screens. Data arranged according to 'average translocation score' (high to low), and gene name (A to Z), Controls are underlined in red, siRNAs producing a score of 0 (dead cells or low YFP) are indicated by the asterisk, siRNAs reducing Parkin translocation to a level comparable to *PINK1* siRNA are highlighted as the 'area of interest.' Error bars represent the standard deviation.

5.6.6 DATA ANALYSES

Visual analysis of screening images revealed a number of siRNAs producing a phenotype comparable to that of *PINK1* siRNA. Among these were siRNAs against *SREBF1, FBXW7, GSK3A* and *SLC17A9* (Figure 5.10 C and Figure 5.11, 'area of interest'), all of which produced a strong Parkin translocation block. This result was encouraging as it demonstrated the ability of *Drosophila* screen hits to influence Parkin translocation across species, hence validating S2R+ cells for use in PINK1/Parkin-pathway analysis. Despite this however, the majority of siRNAs tested had little effect on the translocation process, accumulating an 'average translocation score' of 4 or close to this (Figure 5.11). A possible reason for the widespread lack of effect is due to the presence of high levels of redundancy in the human genome, masking the outcome of gene silencing. Additionally, evolutionary divergence may have rendered some of these human orthologs obsolete in the processes studied here. Nevertheless, a small proportion of siRNAs successfully recapitulated the *PINK1* phenotype, achieving the aim of this first tertiary screen.

5.6.7 DEFINING HITS

Per screen, hits were defined as siRNAs with a Parkin translocation score outside 3 standard deviations (SD) of the mean of the CCCP-treated negative control dsRNA. For a gene to feature in the final hit group, it must have been a hit in at least 2 out of 3 screens.

5.6.8 FINALISED HIT LIST

Having applied the above parameters to the screening data, a final list of 28 siRNA hits were defined (Table 5.2); 20 of which were hits in all three screens, and 8 of which were hits in two out of three screens. Of the 14 genes added from the mitochondrial morphology screen (category C), 4 genes feature in the final mitophagy hit list (Table 5.2, grey).

5.7 CCCP-INDUCED MITOPHAGY

The second tertiary screen involved the analysis of mitophagy, through the loss of the MIM marker ATP5A. This was a key experiment as it tied together the inhibition of Parkin translocation with a block of mitochondrial degradation. By collating the

	Gene Symbol	Average Parkin Translocation score	Standard deviation	Hit frequency (out of 3 rounds)
1	*SREBF1*	1.00	0.00	3
2	*FBXW7*	1.11	0.19	3
3	*SLC17A9*	1.78	0.68	3
4	*USP36*	1.96	0.61	3
5	*U2AF1*	2.00	0.00	3
6	*RPL28*	2.11	0.11	3
7	*PRKAR1B*	2.15	0.26	3
8	*ZBTB17*	2.22	0.19	3
9	*WBP11*	2.30	0.26	3
10	*ACTL6A*	2.30	0.23	3
11	*RUVBL1*	2.44	0.00	3
12	*DHX38*	2.52	0.17	3
13	*POLR3A*	2.56	0.11	3
14	*GSK3A*	2.59	0.55	3
15	*SREBF2*	2.63	0.23	3
16	*EXOSC10*	2.63	0.34	3
17	*CSK*	2.74	0.23	3
18	*NDUFA10*	2.81	0.55	3
19	*ZDHHC8*	3.11	0.73	3
20	*U2AF2*	3.22	0.33	3
21	*POLR2L*	2.50	0.55	2
22	*FZD5*	2.85	0.50	2
23	*CTSK*	2.93	0.79	2
24	*NCOA6*	3.22	0.22	2
25	*PRKAR1A*	3.30	0.67	2
26	*CSNK2A2*	3.37	0.55	2
27	*WDR75*	3.50	0.39	2
28	*KAT2A*	3.67	0.29	2

Table 5.2 CCCP-induced Parkin translocation - hit table. Columns contain the official human gene symbol, average Parkin translocation score & standard deviation over the 3 replicate screens, and the 'hit frequency indicating the number of screens with which the siRNA was deemed a hit. Data were arranged according to the 'Hit frequency' score and then 'average translocation score' (low to high). Heat-map representation of the 'average translocation score' is included, with green representing low scores, red representing high scores and yellow representing the 50th percentile or median. Genes highlighted in grey were derived from category C hits.

mitophagy data with that from the Parkin translocation screen, a greater confidence in the PINK1/Parkin-pathway specificity of overall hits could be gained.

5.7.1 ASSAY DEVELOPMENT

Following development of the mitophagy assay in a low-throughput environment (section 5.4), the next step was to scale-up the assay into the 96-well screening format. As with Parkin translocation, the cell number, toxification duration and data analysis method required optimisation before tertiary screening was undertaken. After titrating a range of cell densities from 4,000 – 12,000 cells, a seed population of 10,000 cells per well was chosen. At this relatively high cell density, the confluency of the population

after a prolonged CCCP application was great enough to overcome increased cell death, whilst providing sufficient data for mitophagy analysis (data not shown).

Next, the optimum duration of CCCP toxification was ascertained. Here, it was important to identify the time-point causing the highest levels of mitophagy, together with the lowest levels of cell death. Following a CCCP time course of 0 – 48 hours, it was clear that after 16 and 24 hours, the ATP5A signal had greatly decreased compared to the '0 hour' control (Figure 5.12 A). However, by 48 hours, the cell density had fallen dramatically, making it difficult to judge the overall mitochondrial content of the population. Because of this, the extended toxification time of 48 hours was deemed inappropriate for screening purposes.

In an attempt to automatically quantify the observed mitophagy effect, 'Transfluor' was programmed to count the number of ATP5A-positive puncta per cell. This algorithm was able to detect a difference between toxified and non-toxified conditions, showing a steady decrease in puncta number over the CCCP time course (Figure 5.12 B). However, the detected decrease in puncta number was relatively modest, perhaps reflecting the complexity of the mitophagy phenotype. Nevertheless, taking the qualitative and quantitative data together, an optimal CCCP time-point of 24 hours was agreed.

To assess the effect of positive control siRNAs after CCCP treatment, the same algorithm was applied to samples from negative control, *PINK1* and *parkin* siRNA-treated cells (Figure 5.12 C). Again, the negative control showed a moderate decrease in ATP5A-puncta over the CCCP time-course. However, where *PINK1* and *parkin* siRNA-treated samples maintained a steady number of ATP5A-puncta throughout, overall counts are considerably lower than that of the non-toxified negative control. Because of this, the puncta quantification after 24 hours of CCCP treatment is comparable between *PINK1*, *parkin* and negative control siRNA conditions. One feasible reason for this may be due to the influence of *PINK1* and *parkin* on mitochondrial morphology, causing the algorithm to pick up fewer individual organelles. However, where the 'fused' phenotype following *Drosophila dPINK1* and *dparkin* silencing is very well defined (Ziviani et al, 2010), much controversy over their influence on mammalian mitochondrial morphology remains, with some groups even reporting fragmentation (Exner et al, 2007; Mortiboys et al, 2008; Wood-Kaczmar et al, 2008; Yang et al, 2008). Still, as the nature of the automated algorithm means that any change in mitochondrial morphology is likely to influence the output, mitophagy data were scored manually to avoid spurious results.

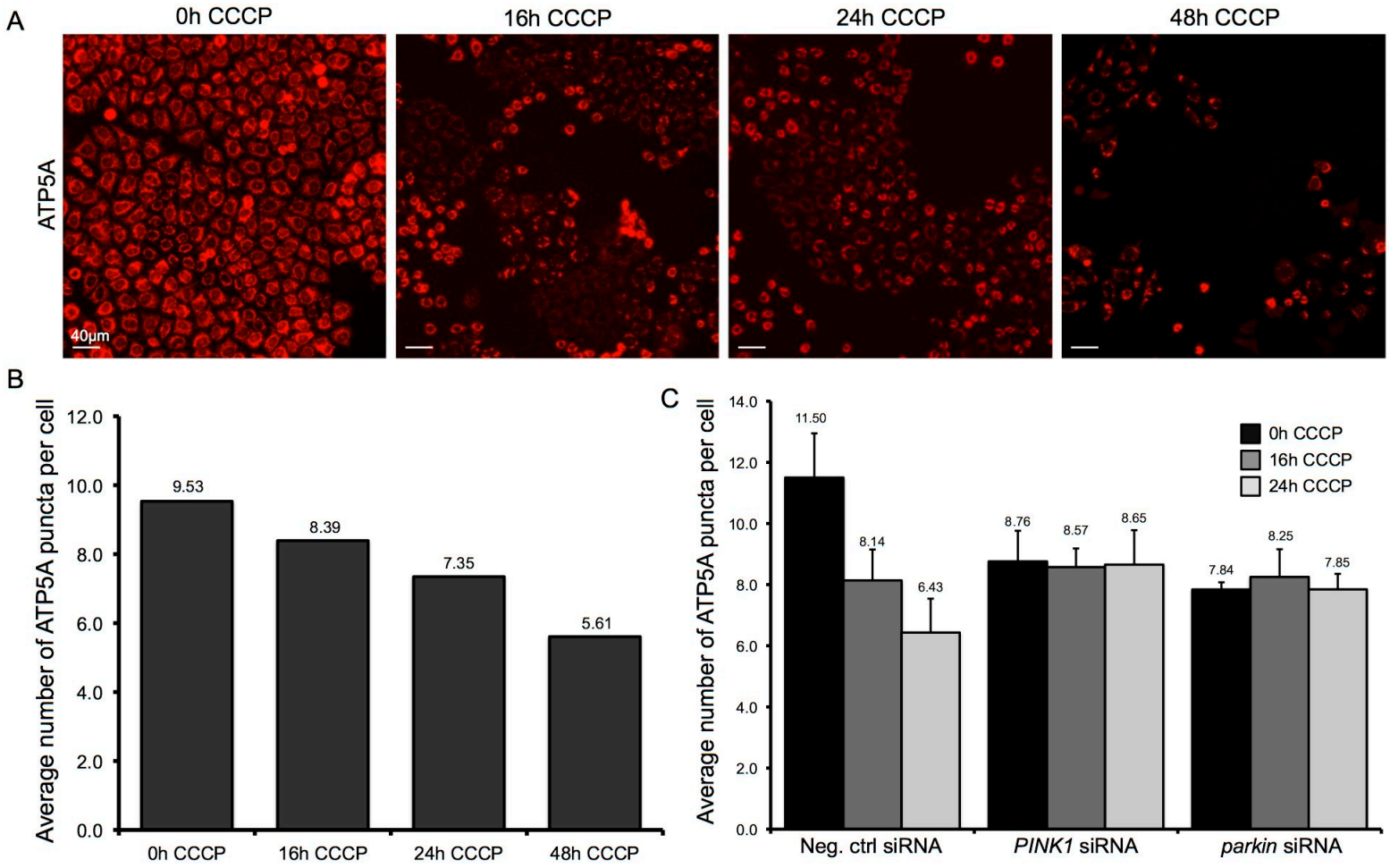

Figure 5.12 High-throughput mitophagy optimisation (A) YFP-Parkin.HeLa cells were subjected to 0, 16, 24 or 48 hours of CCCP toxification (10 µM) and assessed for mitochondrial content using the MIM marker ATP5A (red). Images acquired on a high content screening microscope, 10x objective, scale bar: 40 µm. (B) Automated quantitative data from experiment in (A), produced by 'Transfluor,' with a read-out of 'average number of ATP5A puncta per cell'. Data acquired from one well with 9 FOV per condition. (C) Automated quantitative data from negative control, *PINK1* and *parkin* siRNA-treated cells toxified for 0, 16, and 24 hours with CCCP. Data analysis as in (B). Data acquired from 4 wells, each with 9 FOV, per condition.

5.7.2 PLATE LAYOUT

Screening plates for mitophagy analysis carried the same design as those used for Parkin translocation analysis (Figure 5.9 A). These included two rows of 'no CCCP' control-wells, producing a 'basal' mitochondrial phenotype; plus a number of extra CCCP-treated controls including *PINK1*-, *parkin-,* and negative-control siRNA.

5.7.3 PROTOCOL

Like the plate design, the protocol for mitophagy analysis was similar to that used for Parkin translocation (Figure 5.9 B), with the exception of a higher cell number (10,000 cells per well), and longer toxification duration (24 hours).

5.7.4 SCORING SYSTEM

Following sample processing, 9 FOV per condition were imaged on a high content screening microscope using a 10x objective. As automated analysis produced disparate results from the qualitative data, images were analysed manually, using a 5-point scoring system (Figure 5.13). For each FOV, a score of 0, 1, 2, 3 or 4 was awarded, where 0 = extensive cell death or low YFP expression, 1 = a full complement of mitochondria, 2 = an overall reduced mitochondrial signal, 3 = a reduced mitochondrial signal, plus ~10% of cells with no mitochondria, and 4 = a reduced mitochondrial signal plus >20% of cells with no mitochondria (Figure 5.13). For each condition, the 'average mitophagy score' was calculated, producing one value per well.

5.7.5 CONTROLS

Following visual analysis of control images, under non-toxified conditions the negative control siRNA exhibited a full complement of mitochondria across the population, achieving an average mitophagy score of '1' (Figure 5.14 A & B). However, after 24 hours of CCCP toxification, a strong mitophagy induction is observed (Figure 5.14 A), producing an average score close to the maximum of '4' (Figure 5.14 B). In agreement with the negative control, the average 'no siRNA' score also came close to '4', although greater variation was observed here, indicating the possibility of edge effects. In contrast, *PINK1* siRNA prevented CCCP-induced mitophagy (Figure 5.14 A), reverting the phenotype back to non-toxified levels (Figure 5.14 B). *parkin* siRNA also produced an almost complete block of mitophagy, but achieved a score of '0' due to the lack of

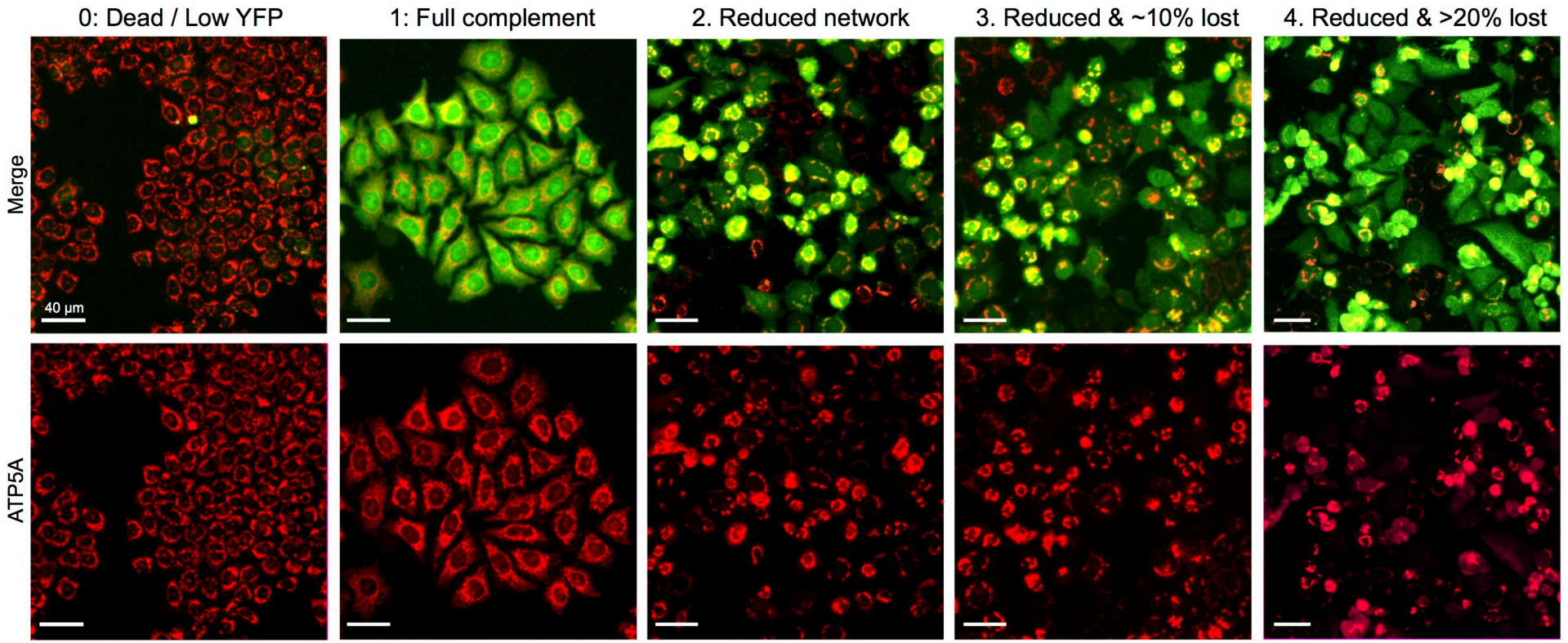

Figure 5.13 Mitophagy scoring system. Example images of the 5 'mitophagy' phenotypes under scrutiny. A score of 0 = dead cells or low YFP expression, 1 = cells with a full complement of mitochondria, 2 = cells with a predominantly reduced mitochondrial network, 3 = cells with a reduced mitochondrial network, plus approximately 10% of the population with no mitochondria, 4 = cells with a reduced network plus more than 20% of the population with no mitochondria. Images were captured using a high content screening microscope with a 10x objective, scale bar: 40 µm, YFP-Parkin (green) and ATP5A (red).

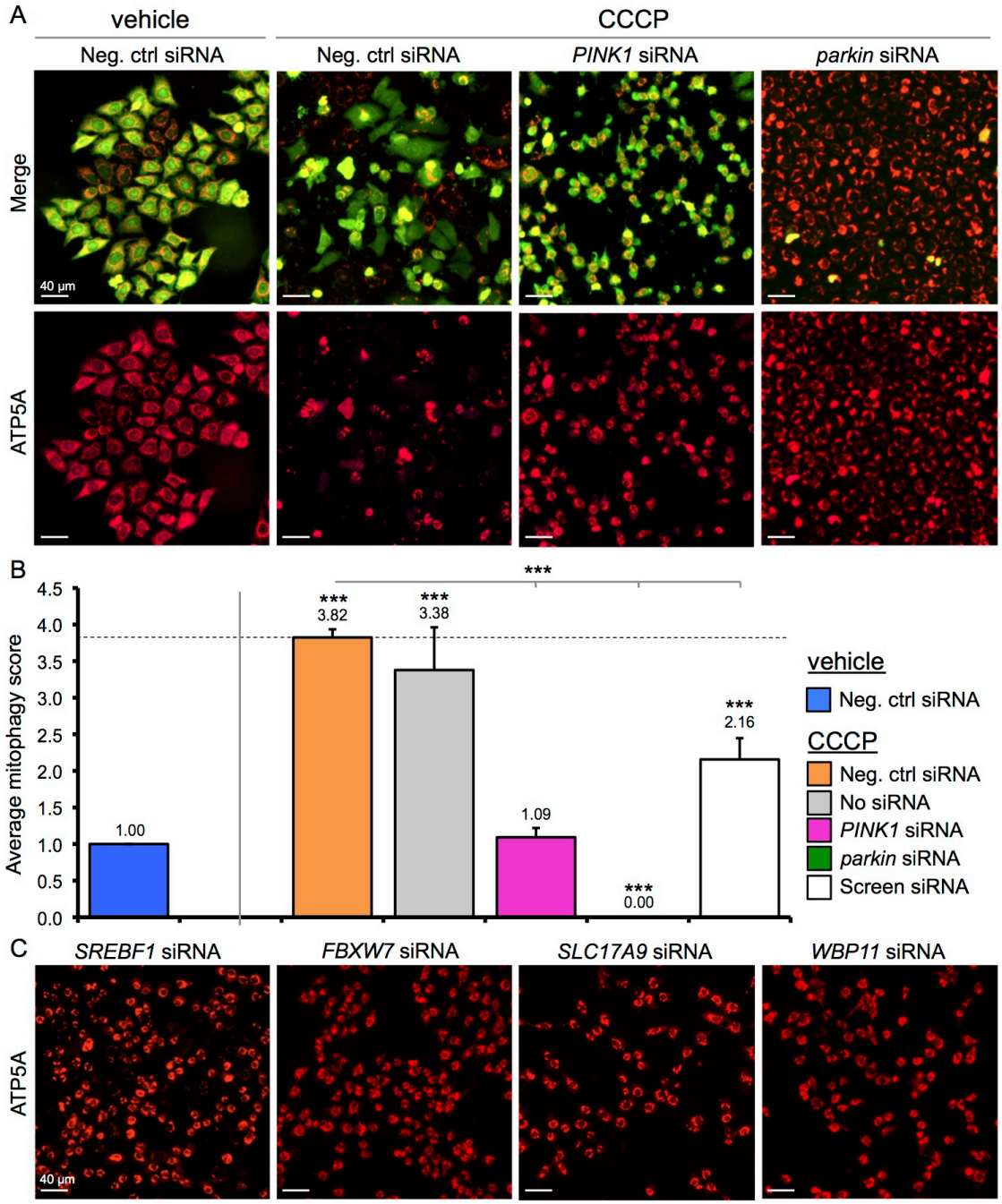

Figure 5.14 Mitophagy screen analysis. (A) Example high-throughput images of negative control, *PINK1* and *parkin* siRNA treated cells, following the application of vehicle or CCCP for 24 hours (indicated). (B) Graphical representation of control 'average mitophagy scores' over three assays. Data comprises a minimum of 24 wells/condition, with 9 FOV per well. Error bars represent standard deviation, ***P<0.001 (One-way ANOVA with Bonferroni's correction, compared to the vehicle-treated 'Neg. ctrl siRNA' unless indicated). (C) Example high-throughput images of selected hit siRNAs following CCCP treatment. YFP-Parkin (green), ATP5A (red), acquired on a high content screening microscope using a 10x objective, scale bar: 40 µm.

YFP-Parkin signal. Once again, the *parkin* control phenotype confirmed the efficacy of the silencing process (Figure 5.14 A & B).

5.7.6 DATA ANALYSES

Visual analysis of screening images revealed a number of siRNAs producing a phenotype comparable to that of *PINK1* siRNA. Among these were siRNAs against *SREBF1, FBXW7, SLC17A9* and *WBP11* (Figure 5.14 C and Figure 5.15, 'area of interest'), all of which produced a strong mitophagy block. This result was encouraging as it demonstrated the ability of these genes to block the end-point of the pathway for the first time, hence strengthening the possibility of pathway specificity. Unlike Parkin translocation, many more siRNAs had some influence on the mitophagy process (Figure 5.15), perhaps due to the complexity of the phenotype making analysis more challenging. In addition, a greater number of siRNAs achieved a score of 0 (Figure 5.15, asterisks), probably due to increased levels of CCCP-induced cell death compared with Parkin translocation assays.

5.7.7 DEFINING HITS

Per screen, hits were defined as siRNAs with a mitophagy score outside 3 SD of the mean of the CCCP-treated negative control dsRNA. For a gene to feature in the final hit group, it must have been a hit in at least 2 out of 3 screens.

5.7.8 FINALISED HIT LIST

Having applied the above parameters to the screening data, a final list of 47 siRNA hits were defined (Table 5.3), with 23 being hits in all three screens, and 24 being hits in two out of three screens. Of the 14 genes added from the aforementioned mitochondrial morphology screen (category C), 6 feature in the final mitophagy hit list (Table 5.3, grey).

5.8 COLLATING DATA

Having completed both Parkin translocation and mitophagy screens, the final task was to collate the data to produce an overall list of hits for future study. Once complete, the list could be assessed for the presence of interesting bioinformatic features including pathway enrichments. Through this, the selection of a small number of genes for further scrutiny in a low-throughput setting could be made.

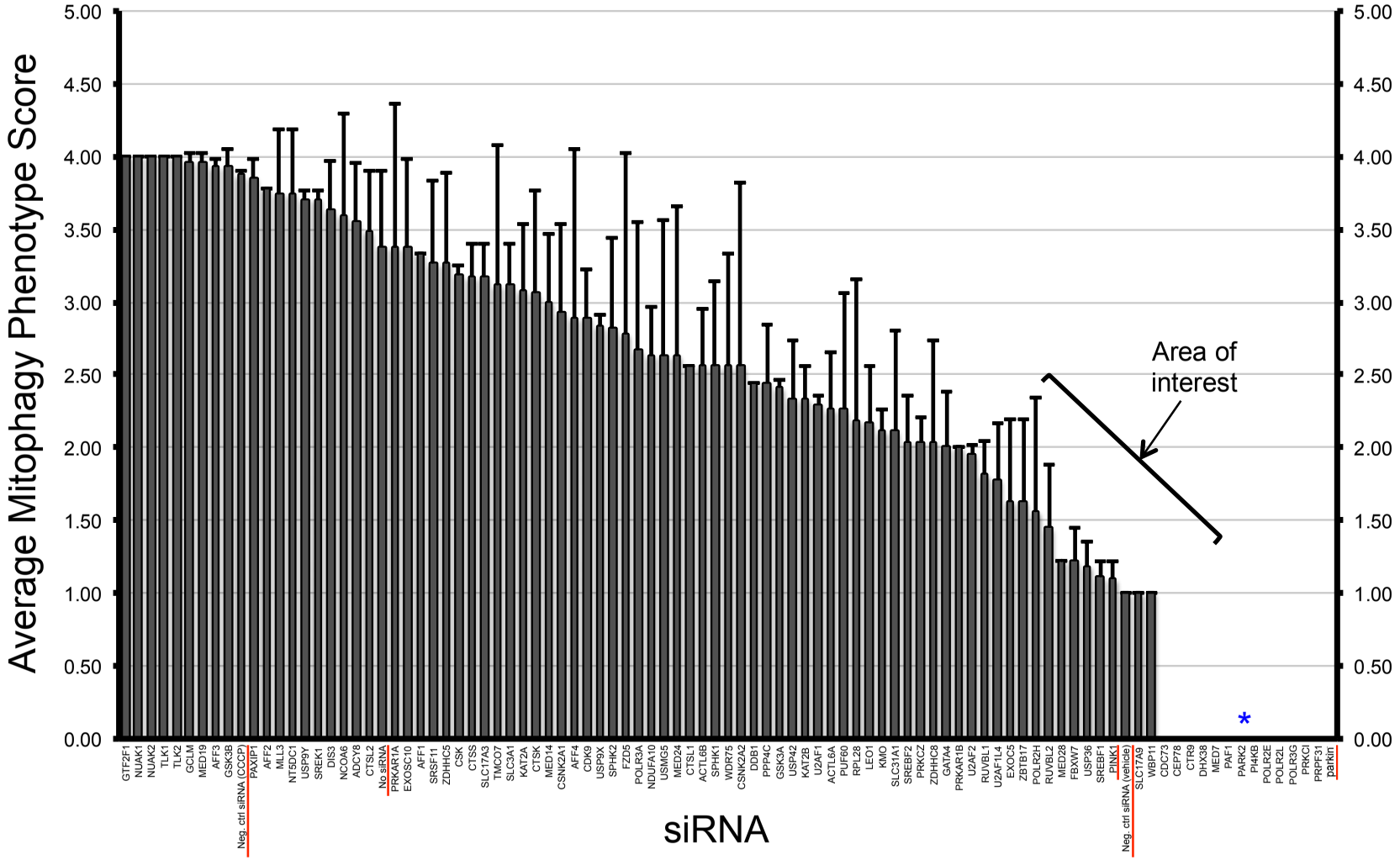

Figure 5.15 Average mitophagy siRNA data. Graphical representation of the 'average mitophagy phenotype score' of each siRNA, across three repeat screens. Data arranged according to the average mitophagy score (high to low), and then gene name (A to Z), Controls are underlined in red, siRNAs producing a score of 0 (dead cells or low YFP) are indicated (asterisk), siRNAs reducing the amount of mitophagy to a level comparable to *PINK1* siRNA are highlighted as the 'area of interest.' Error bars represent the standard deviation.

	Gene Symbol	Average Mitophagy score	Standard deviation	Hit frequency (out of 3 rounds)
1	*SLC17A9*	1.00	0.00	3
2	*WBP11*	1.00	0.00	3
3	*SREBF1*	1.11	0.11	3
4	*USP36*	1.19	0.17	3
5	*FBXW7*	1.22	0.22	3
6	*MED28*	1.22	0.00	3
7	*RUVBL2*	1.44	0.44	3
8	*EXOC5*	1.63	0.57	3
9	*ZBTB17*	1.63	0.57	3
10	*ZDHHC8*	2.04	0.71	3
11	*PRKCZ*	2.04	0.17	3
12	*RPL28*	2.19	0.97	3
13	*KAT2B*	2.33	0.22	3
14	*USP42*	2.33	0.40	3
15	*GSK3A*	2.41	0.06	3
16	*CSNK2A2*	2.56	1.26	3
17	*WDR75*	2.56	0.78	3
18	*ACTL6B*	2.56	0.40	3
19	*MED24*	2.63	1.03	3
20	*NDUFA10*	2.63	0.34	3
21	*SPHK2*	2.81	0.63	3
22	*CSNK2A1*	2.93	0.61	3
23	*KAT2A*	3.07	0.46	3
24	*POLR2H*	1.56	0.79	2
25	*U2AF1L4*	1.78	0.38	2
26	*RUVBL1*	1.81	0.23	2
27	*U2AF2*	1.94	0.08	2
28	*GATA4*	2.00	0.38	2
29	*SREBF2*	2.04	0.32	2
30	*KMO*	2.11	0.16	2
31	*SLC31A1*	2.11	0.69	2
32	*ACTL6A*	2.26	0.39	2
33	*PUF60*	2.26	0.80	2
34	*U2AF1*	2.30	0.06	2
35	*PPP4C*	2.44	0.40	2
36	*SPHK1*	2.56	0.59	2
37	*USMG5*	2.63	0.93	2
38	*POLR3A*	2.67	0.89	2
39	*FZD5*	2.78	1.25	2
40	*USP9X*	2.83	0.08	2
41	*CDK9*	2.89	0.33	2
42	*CTSK*	3.06	0.71	2
43	*SLC3A1*	3.11	0.29	2
44	*TMCO7*	3.11	0.97	2
45	*SLC17A3*	3.17	0.24	2
46	*CSK*	3.19	0.06	2
47	*SRSF11*	3.26	0.57	2

Table 5.3 CCCP-induced mitophagy - hit table. Columns contain the official human gene symbol, average mitophagy score & standard deviation over the 3 replicate screens, and the 'hit frequency indicating the number of screens with which the siRNA was deemed a hit. Data are arranged according to the 'Hit frequency' score and then 'average mitophagy score' (low to high). Heat-map representation of the 'average translocation score' is included, with green representing low scores, red representing high scores and yellow representing the 50th percentile or median. Genes highlighted in grey were derived from category C hits.

5.8.1 FINAL HUMAN HIT LIST

For a gene to be defined as a final human screen hit, it needed to appear in the hit tables of both Parkin translocation and mitophagy screens. Having collated these datasets, a final hit group of 22 human genes was determined (Table 5.4). To give the genes an order of strength, average scores from the Parkin translocation and mitophagy screens were combined, with the lowest scores towards the top, and the highest scores towards the bottom. With this, *SREBF1* became the top screening hit, followed by *FBXW7* and *SLC17A9*.

To assess whether siRNA amplicons had equivalent effects on Parkin translocation and mitophagy, datasets from all 90 human siRNAs (Figure 5.16 A) and the hit group alone (Figure 5.16 B) were plotted. To determine the strength of the association between the two variables of a linear regression, the square of Pearson's correlation coefficient (also called the 'coefficient of determination' or 'R^2') is useful. Here, an R^2 of 1 signifies perfect correlation, and an R^2 of 0 indicates no correlation. In the case of all 90 screen siRNAs (Figure 5.16 A), an R^2 of 0.275 signifies that 27.5% of mitophagy scores can be directly accounted for by the Parkin translocation score, and vice versa. This shows a significant positive relationship between Parkin translocation and mitophagy within this group of genes, albeit a relatively modest one. However, if the hit group is taken alone, the coefficient of determination increases dramatically to 0.742, meaning that 74.2% of mitophagy scores can now be directly accounted for by Parkin translocation scores, and vice versa (Figure 5.16 B). The hit group therefore contains a strong enrichment of genes having equivalent effects on both Parkin translocation and mitophagy. With regards to the linearity of the PINK1/Parkin-pathway, genes with a direct role upstream of Parkin translocation would be anticipated to affect both processes equally, confirming that the hit group follows the expected trend.

5.8.2. BIOINFORMATIC ANALYSIS

Having produced a final list of 22 hit genes, known pathway interactions and gene functions were explored. For this, the hit group together with *PINK1* and *parkin* (*PARK2*) were passed through the STRING algorithm, allowing visualisation of previously defined interactions (Figure 5.17). From this analysis, three clear groups of genes emerged, the largest of which included experimental data of a *parkin* interaction with the hit gene, *FBXW7*. Importantly, this large interaction group included the two top human hits, *SREBF1* and *FBXW7*, prompting further investigation into the functions of these proteins.

	Gene Symbol	Parkin translocation		Mitophagy		Collated
		Average score	StDev	Average score	StDev	Combined average score
1	*SREBF1*	1.000	0.00	1.111	0.11	2.111
2	*FBXW7*	1.111	0.19	1.222	0.22	2.333
3	*SLC17A9*	1.778	0.68	1.000	0.00	2.778
4	*USP36*	1.963	0.61	1.185	0.17	3.148
5	*WBP11*	2.296	0.26	1.000	0.00	3.296
6	*ZBTB17*	2.222	0.19	1.630	0.57	3.852
7	*RUVBL1*	2.444	0.00	1.815	0.23	4.259
8	*RPL28*	2.111	0.11	2.185	0.97	4.296
9	*U2AF1*	2.000	0.00	2.296	0.06	4.296
10	*ACTL6A*	2.296	0.23	2.259	0.39	4.556
11	*SREBF2*	2.630	0.23	2.037	0.32	4.667
12	*GSK3A*	2.592	0.55	2.407	0.06	5.000
13	*ZDHHC8*	3.111	0.73	2.037	0.71	5.148
14	*U2AF2*	3.222	0.33	1.944	0.08	5.167
15	*POLR3A*	2.556	0.11	2.667	0.89	5.222
16	*NDUFA10*	2.815	0.55	2.630	0.34	5.444
17	*FZD5*	2.852	0.50	2.778	1.25	5.630
18	*CSNK2A2*	3.370	0.55	2.555	1.26	5.926
19	*CSK*	2.741	0.23	3.185	0.06	5.926
20	*CTSK*	2.926	0.79	3.056	0.71	5.981
21	*WDR75*	3.500	0.39	2.555	0.78	6.056
22	*KAT2A*	3.667	0.29	3.074	0.46	6.740

Table 5.4 Final human screening hit table. Columns contain the official human gene symbol, average translocation and mitophagy score with corresponding standard deviations over 3 replicate screens, and the 'combined average score' of collated data out of a maximum score of 8. Data are arranged according to the 'combined average score' (low to high). Genes highlighted in grey were derived from category C hits.

Having drawn information from a number of sources including Uniprot and NCBI gene, the function and interacting partners of each of the hit genes were investigated (Table 5.5). Many of the hits have major roles in housekeeping processes such as transcription, DNA splicing and translation. In addition, a number of genes are also involved in metabolic processes such a lipid and glucose homeostasis; as well as links to the mitochondrial respiratory complexes. Importantly, many hit genes have been shown to physically interact with each other (Table 5.5, Interactors – black) or other genes related to the hit group (Table 5.5, Interactors – green), as well as with 'interesting' genes (Table 5.5, Interactors – orange) such as previously reported Parkinson's disease genes, *parkin (PARK2)* and *DJ-1 (PARK7).*

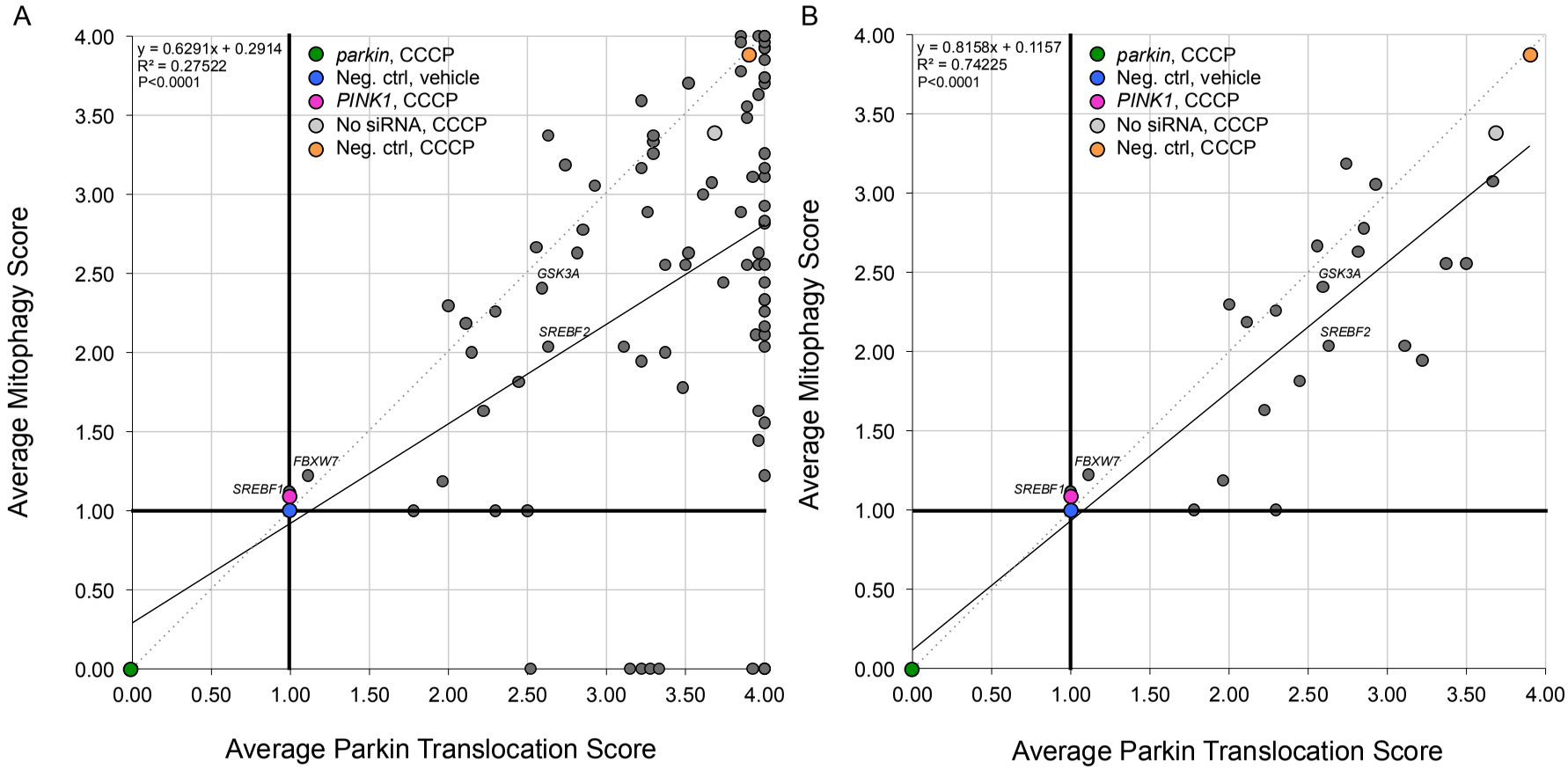

Figure 5.16 Linear regression analysis of Parkin translocation and mitophagy. Scatter graph representation of the 'average Parkin translocation score' (x-axis) against the 'average mitophagy score' (y-axis) of every screen siRNA (A) or the hit group alone (B), across three repeat screens. Coloured data points represent screen controls (see key). Solid lines represent the line of best fit and correspond to the linear regression line equation (y). Also included are 'coefficient of determination' (R^2) values, and significance of the positive data correlation (P). The solid line represents 'R^2' = 1.

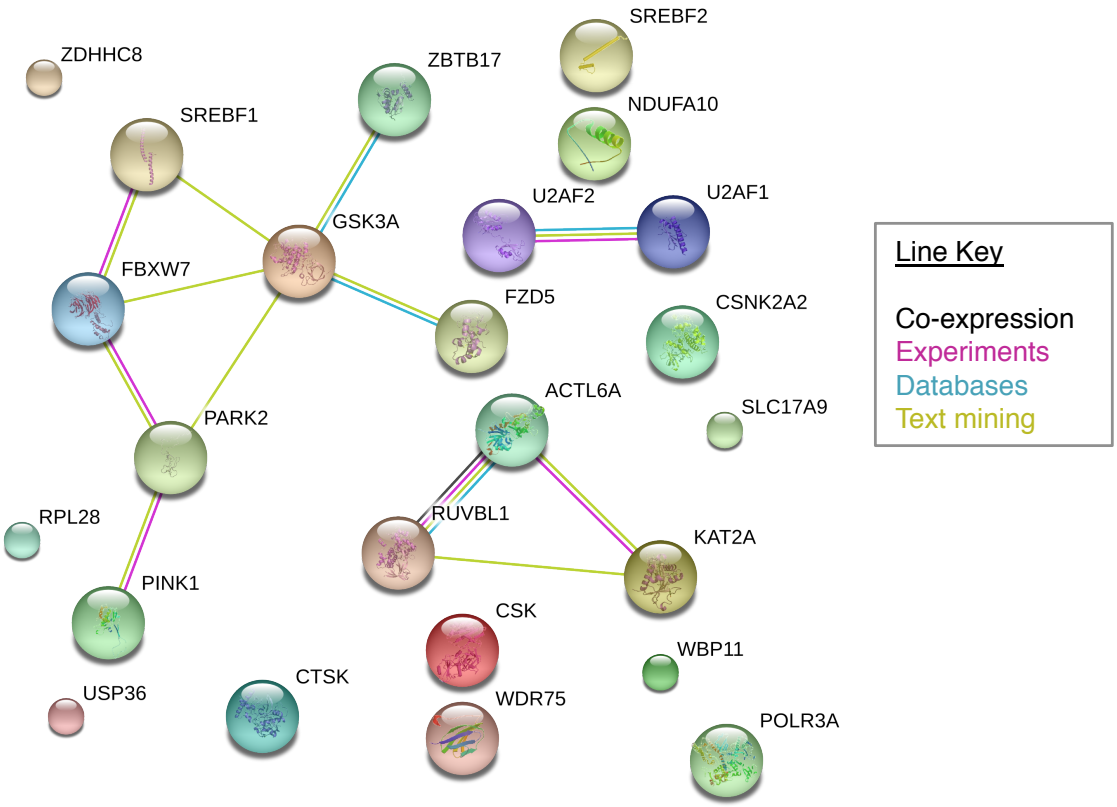

Figure 5.17 Protein interaction analysis of final human genes. Schematic representation of known and predicted protein interactions between the 22 final human hits (STRING 9.0). Nodes are joined together with coloured lines representing the type of interaction evidence used (see key).

5.8.3 GENE SELECTION FOR LOW-THROUGHPUT ANALYSIS

Following screening, the desired outcome was to identify a small number of hits for in-depth, low throughput analysis. For this, both screening data and bioinformatic information played a big part in deciding which genes to select. Taking these two data sources into account, '*sterol regulatory element binding transcription factor 1*' (*SREBF1*) and '*F-box and WD repeat domain containing E3 ubiquitin ligase*' *(FBXW7)* were selected for closer scrutiny. The reasons for selecting these two genes were due to the fact that they occupy first and second positions in the overall screening hit table, as well as forming part of a large, PINK1/Parkin-related interaction network (Figure 5.17). Additionally, *SREBF2*, a gene closely related to *SREBF1* is also found in the hit list, helping to strengthen the confidence in *SREBF1*-related pathway specificity. Finally, FBXW7 has been shown to physically interact with Parkin in an SCF-like complex (Staropoli et al, 2003), and Parkin is reported to be responsible for the proteasomal degradation of FBXW7, promoting neuronal protection (Ekholm-Reed et al, 2013).

	Gene Symbol	Gene name	Gene function - Uniprot / NCBI Gene	Interactors
1	*SREBF1*	sterol regulatory element binding transcription factor 1	Transcriptional activator required for lipid homeostasis (mainly fatty acids)	FBXW7, RUVBL1, SREBF2, KAT2A, RUVBL2, GSK3B
2	*FBXW7*	F-box and WD repeat domain containing 7, E3 ubiquitin protein ligase	Substrate recognition component of a SCF (SKP1-CUL1-F-box protein) E3 ubiquitin-protein ligase complex	SREBF1, GSK3A, LINGO1, PARK2
3	*SLC17A9*	solute carrier family 17 (vesicular nucleotide transporter), member 9	Involved in vesicular storage and exocytosis of ATP.	-
4	*USP36*	ubiquitin specific peptidase 36	Belongs to a large family of cysteine proteases that function as deubiquitinating enzymes	-
5	*WBP11*	WW domain binding protein 11	Activates pre-mRNA splicing.	GIGYF2,
6	*ZBTB17*	zinc finger and BTB domain containing 17	Plays a critical role in early lymphocyte development, where it is essential to prevent apoptosis	-
7	*RUVBL1*	RuvB-like 1	Component of the NuA4 histone acetyltransferase complex which is involved in transcriptional activation	ACTL6A, CSNK2A2, RUVBL2
8	*RPL28*	ribosomal protein L28	A component of the ribosomal 60S subunit	CSNK2A2
9	*U2AF1*	U2 small nuclear RNA auxiliary factor 1	RNA-binding protein that functions as a pre-mRNA splicing factor. Acts by enhancing the binding of U2AF2 to weak pyrimidine tracts.	U2AF2, SMURF1
10	*ACTL6A*	actin-like 6A	Component of the NuA4 histone acetyltransferase complex	RUVBL1, KAT2A, RUVBL2
11	*SREBF2*	sterol regulatory element binding transcription factor 2	Transcriptional activator required for lipid homeostasis (mainly cholesterol)	SREBF1, PARK7
12	*GSK3A*	glycogen synthase kinase 3 alpha	Constitutively active protein kinase that acts as a negative regulator in the hormonal control of glucose homeostasis	HDAC6
13	*ZDHHC8*	zinc finger, DHHC-type containing 8	Palmitoyltransferase involved in glutamatergic transmission	-
14	*U2AF2*	U2 small nuclear RNA auxiliary factor 2	Necessary for the splicing of pre-mRNA. Binds preferentially to a single-stranded structure within the polypyrimidine tract	U2AF1, GIGYF2
15	*POLR3A*	polymerase (RNA) III (DNA directed) polypeptide A	Catalytic component of RNA polymerase III, which synthesizes small RNAs	-
16	*NDUFA10*	NADH dehydrogenase (ubiquinone) 1 alpha subcomplex, 10,	Accessory subunit of the mitochondrial membrane respiratory chain NADH dehydrogenase (Complex I)	-
17	*FZD5*	frizzled family receptor 5	Believed to be the receptor for the Wnt5A ligand for beta-catenin pathway induction	GSK3B
18	*CSNK2A2*	casein kinase 2, alpha prime polypeptide	Catalytic subunit of a constitutively active serine/threonine-protein kinase complex	RUVBL1, RPL28, RUVBL2, SMURF1, HDAC6, SQSTM,
19	*CSK*	c-src tyrosine kinase	Non-receptor tyrosine-protein kinase regulating cell growth, differentiation, migration and immune response	TRAP1
20	*CTSK*	cathepsin K	Lysosomal cysteine proteinase involved in bone remodeling and resorption	-
21	*WDR75*	WD repeat domain 75	Contains 9 WD repeats.	-
22	*KAT2A*	K(lysine) acetyltransferase 2A	Functions as a histone acetyltransferase (HAT) to promote transcriptional activation.	ACTL6A, SREBF1

Table 5.5 Human hit gene function and interactors. Bioinformatic data of the 22 human screening hits, arranged in order of hit strength, displaying official gene symbol and name, a brief description of gene function, and known protein interactors. Data attained from 'Uniprot' and 'NCBI Gene' archives. Genes highlighted in grey were derived from category C hits; Interactors are colour-coded (black: hit genes, green: genes related to hits, orange: 'interesting' genes e.g. links with PD, mitophagy or mitochondria).

Following extensive literature searches, SREBP1, the transcription factor corresponding to the gene *SREBF1*, is known to be required for the transcription of enzymes for *de novo* lipid synthesis; predominantly of fatty acids, but also cholesterol (Brown & Goldstein, 1997). Importantly, SREBP1 levels are tightly regulated by the E3-ubiquitin ligase FBXW7, via the proteasomal degradation pathway (Sundqvist et al, 2005). For FBXW7-dependent ubiquitination and degradation of SREBP1 to take place, a prior phosphorylation event must occur. This phosphorylation event is performed by the serine/threonine kinase GSK3β (Kim et al, 2004; Sundqvist et al, 2005). Despite *GSK3B* itself not appearing in the hit list, the closely-related gene, *GSK3A* does feature, both of which are orthologous to *Drosophila shaggy (sgg);* a high performing gene in the *Drosophila* screen. Due to the two genes, *GSK3A* and *GSK3B*, having high amino acid homology (98% within the kinase domain) (Doble & Woodgett, 2003), and proven functional redundancy (Doble et al, 2007), *GSK3A* was also considered for low throughput analysis (Figure 5.18).

5.9 DISCUSSION

Having started the screening process with ~15,000 *Drosophila* genes, a final group of 22 human genes with a robust and reproducible effect on mammalian Parkin translocation and mitophagy have been defined. During this process, the primary *Drosophila* hits have been assessed for their ability to influence Parkin translocation under different toxification scenarios, as well as mitochondrial morphology and mitochondrial perinuclear aggregation. Taken together, this project has overseen a comprehensive screen for genes with the ability to affect PINK1/Parkin-related processes, conserved across species (Figure 5.18).

In order to select a small group of genes for further analysis, a great help came in the form of pre-defined interaction pathways, facilitated by the online interaction program, STRING. Interaction maps produced by STRING highlighted a cluster of hit genes acting in a common pathway. This pathway transpires to hold a central role in lipid homeostasis, through the maintenance of fatty acid and cholesterol levels.

One confusing aspect of this pathway is that *FBXW7*, the second hit in the final list, acts by degrading SREBP1 in the nucleus following DNA binding. This would therefore be expected to produce the opposite phenotype to that of *SREBF1* siRNA, if the observed effect is SREBP-pathway-specific. One possible explanation is that a fine balance of SREBP-pathway activation is required for efficient Parkin translocation and

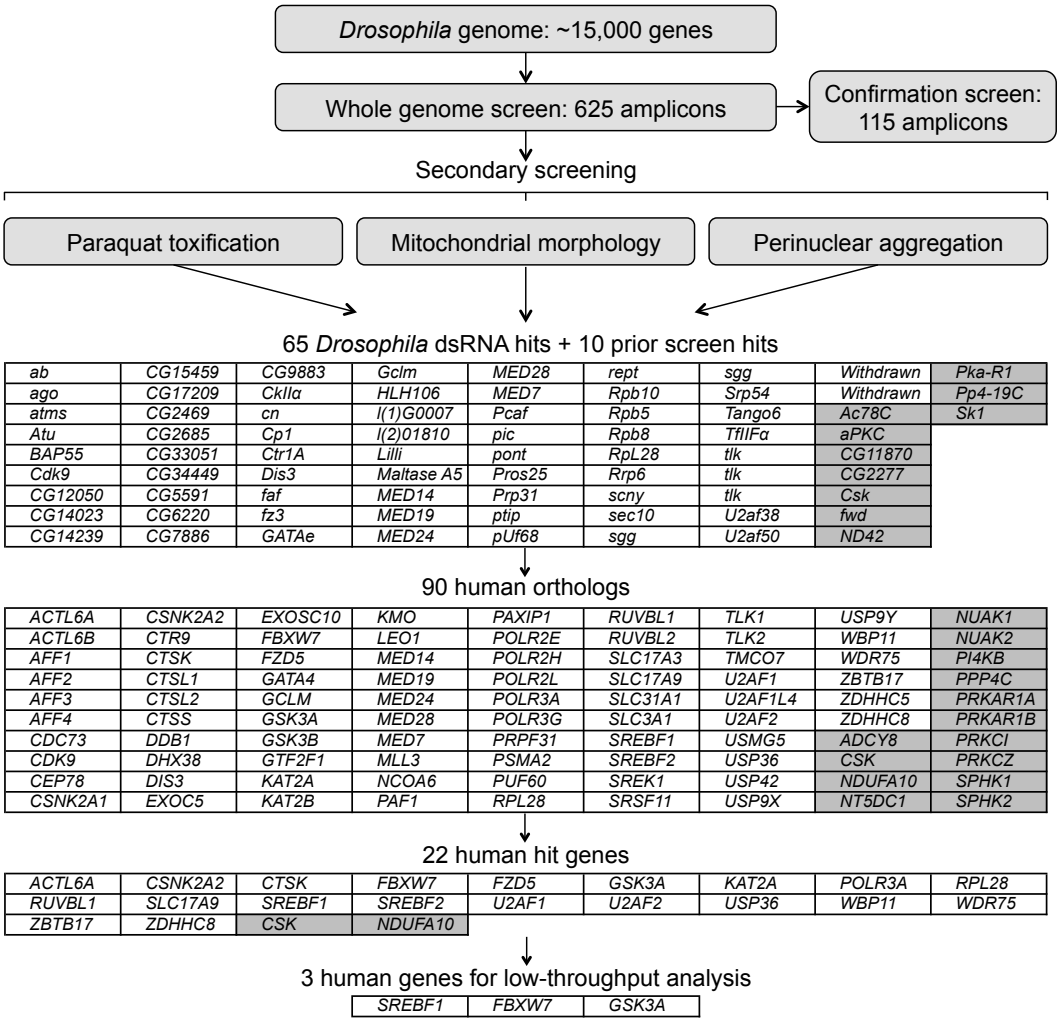

ab	*CG15459*	*CG9883*	*Gclm*	*MED28*	*rept*	*sgg*	*Withdrawn*	*Pka-R1*
ago	*CG17209*	*CkIIα*	*HLH106*	*MED7*	*Rpb10*	*Srp54*	*Withdrawn*	*Pp4-19C*
atms	*CG2469*	*cn*	*l(1)G0007*	*Pcaf*	*Rpb5*	*Tango6*	*Ac78C*	*Sk1*
Atu	*CG2685*	*Cp1*	*l(2)01810*	*pic*	*Rpb8*	*TfIIFα*	*aPKC*	
BAP55	*CG33051*	*Ctr1A*	*Lilli*	*pont*	*RpL28*	*tlk*	*CG11870*	
Cdk9	*CG34449*	*Dis3*	*Maltase A5*	*Pros25*	*Rrp6*	*tlk*	*CG2277*	
CG12050	*CG5591*	*faf*	*MED14*	*Prp31*	*scny*	*tlk*	*Csk*	
CG14023	*CG6220*	*fz3*	*MED19*	*ptip*	*sec10*	*U2af38*	*fwd*	
CG14239	*CG7886*	*GATAe*	*MED24*	*pUf68*	*sgg*	*U2af50*	*ND42*	

ACTL6A	*CSNK2A2*	*EXOSC10*	*KMO*	*PAXIP1*	*RUVBL1*	*TLK1*	*USP9Y*	*NUAK1*
ACTL6B	*CTR9*	*FBXW7*	*LEO1*	*POLR2E*	*RUVBL2*	*TLK2*	*WBP11*	*NUAK2*
AFF1	*CTSK*	*FZD5*	*MED14*	*POLR2H*	*SLC17A3*	*TMCO7*	*WDR75*	*PI4KB*
AFF2	*CTSL1*	*GATA4*	*MED19*	*POLR2L*	*SLC17A9*	*U2AF1*	*ZBTB17*	*PPP4C*
AFF3	*CTSL2*	*GCLM*	*MED24*	*POLR3A*	*SLC31A1*	*U2AF1L4*	*ZDHHC5*	*PRKAR1A*
AFF4	*CTSS*	*GSK3A*	*MED28*	*POLR3G*	*SLC3A1*	*U2AF2*	*ZDHHC8*	*PRKAR1B*
CDC73	*DDB1*	*GSK3B*	*MED7*	*PRPF31*	*SREBF1*	*USMG5*	*ADCY8*	*PRKCI*
CDK9	*DHX38*	*GTF2F1*	*MLL3*	*PSMA2*	*SREBF2*	*USP36*	*CSK*	*PRKCZ*
CEP78	*DIS3*	*KAT2A*	*NCOA6*	*PUF60*	*SREK1*	*USP42*	*NDUFA10*	*SPHK1*
CSNK2A1	*EXOC5*	*KAT2B*	*PAF1*	*RPL28*	*SRSF11*	*USP9X*	*NT5DC1*	*SPHK2*

ACTL6A	*CSNK2A2*	*CTSK*	*FBXW7*	*FZD5*	*GSK3A*	*KAT2A*	*POLR3A*	*RPL28*
RUVBL1	*SLC17A9*	*SREBF1*	*SREBF2*	*U2AF1*	*U2AF2*	*USP36*	*WBP11*	*WDR75*
ZBTB17	*ZDHHC8*	*CSK*	*NDUFA10*					

SREBF1	*FBXW7*	*GSK3A*

Figure 5.18 Overall screening workflow diagram. Workflow diagram representing each step of *Drosophila* and human cell screening. Briefly, the whole genome library was comprised of ~15,000 *Drosophila* genes. Following primary screening, 625 dsRNAs were found to reduce Parkin-GFP translocation after CCCP treatment. Of these, 115 dsRNAs were confirmed in 4 repeat screens. Primary hit amplicons then underwent multiple secondary screen assays looking at paraquat-induced Parkin translocation, mitochondrial morphology and perinuclear aggregation. Collating these data, the final *Drosophila* dsRNA hit list comprises 75 amplicons, including 10 from an earlier screen performed by Joe Pogson (grey). These *Drosophila* dsRNA amplicons equated to 90 unique human orthologs, which were tested for an ability to influence Parkin translocation and mitophagy in a human cell system, Of these 90 genes, 22 were found to robustly influence both assays, and three lipolysis-related genes were selected for closer scrutiny.

mitophagy, therefore too little or too much causes the same phenotype. This is an issue that will need addressing experimentally before we fully understand the relationship, if any, between *SREBF1*, *FBXW7* and the PINK1/Parkin-pathway.

The next stage of the project involved analysing the three 'favourite' hit genes, *SREBF1*, *FBXW7* and *GSK3A*, in a low-throughput setting. In the following chapter, the influence of these genes on several aspects of mitochondrial biology, as well as their interaction with *PINK1* and *parkin,* was assessed using cell-based and *in vivo* models. Here, the aim was to understand how these genes interact in the context of mitochondrial homeostasis.

6. LOW-THROUGHPUT ANALYSIS OF SCREEN HITS

6.1 BACKGROUND

Following screening completion, the next challenge was to select a small number of genes for follow-up analysis. The purpose of this was to ascertain whether the influence on PINK1/Parkin-related processes such as Parkin translocation and mitophagy, were pathway-specific or an artifact of a non-specific gene function e.g. general autophagy. As detailed in chapter 5, a number of top screening hits have been shown to act in a pre-defined pathway, with *de novo* lipid synthesis at its centre. These genes are *SREBF1, FBXW7* and *GSK3.* In this final results chapter, these genes will be tested for an ability to biochemically and genetically interact with the PINK1/Parkin-pathway using a range of different techniques. Analysis of these data will allow hypotheses to be offered as to how these genes may act together to promote the degradation of dysfunctional mitochondria.

6.2 THE SREBP-PATHWAY IN LIPID HOMEOSTASIS

'Sterol Regulatory Element Binding Proteins' (SREBPs) were first identified as nuclear transcription factors able to activate *low density lipoprotein receptor (LDLR)* transcription, required for cholesterol uptake from the bloodstream (Briggs et al, 1993; Wang et al, 1993). In mammals, the *SREBF*-family of genes confers three distinct basic helix-loop-helix (bHLH) transcription factors; SREBP1a, SREBP1c and SREBP2; all of which bind both E-box and sterol regulatory element (SRE) motifs in the promoter of target genes. The key role of these genes is in the regulation of global lipid synthesis by the transcription of key enzymes of fatty acid, triglyceride and cholesterol production (Brown & Goldstein, 1997). In general, SREBP1a is a potent activator of genes required for fatty acid, triglyceride and cholesterol production, whereas SREBP1c is responsible for fatty acid and triglyceride synthesis alone and SREBP2 for cholesterol synthesis. These three SREBP proteins are encoded for by two *SREBF* genes, with *SREBF1* responsible for SREBP1a and 1c, and *SREBF2* responsible for SREBP2.

SREBP family members are multidomain proteins comprising an N-terminal transactivation domain, a transcription-activating basic helix-loop-helix leucine zipper (bHLH-Zip) domain, two transmembrane domains flanking a small loop domain, and a large C-terminal regulatory domain (Figure 6.1 A, Osborne & Espenshade, 2009; Shimano, 2001). For the synthesis of SREBP1a and 1c, differential promoters within *SREBF1* are utilised, producing either a long (SREBP1a) or short (SREBP1c) transactivation sequence in the C-terminus of the protein (Hua et al, 1995)

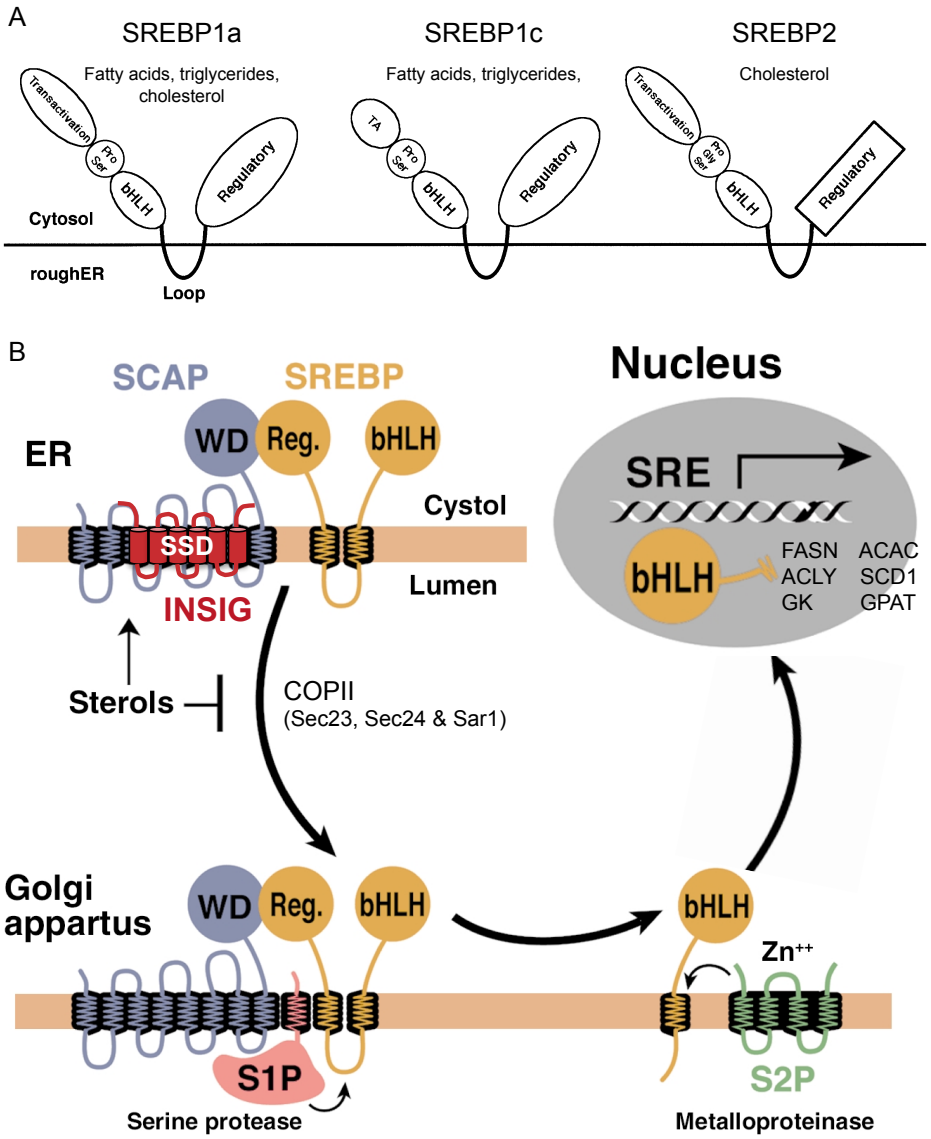

Figure 6.1 SREBP-pathway members and their regulation by sterols (A) Schematic of the functional domains, protein conformation and basal cellular localisation of the three SREBP proteins, SREBP1a, SREBP1c, and SREBP2. Pathway targets for each of the SREBP proteins are indicated. Figure adapted from Shimano (2001). (B) Schematic representation of SREBP-pathway regulation and activation by sterols. Under conditions of saturating sterols, flSREBP is retained in the ER membrane, in a hairpin conformation, with its regulatory and transcriptional domains facing the cytoplasm. Here it is in complex with the escort protein SCAP, through an interaction between the C-terminal regulatory domain of SREBP, and the N-terminal protein interacting domain (WD-40) of SCAP. To retain the SREBP-SCAP complex in the ER, the SSD domain of SCAP senses high sterol levels and allows an interaction with the retention factor INSIG. However, when sterol levels fall below the optimum, this is sensed by SCAPs SSD domain, promoting a conformational change. This leads to the dissociation of INSIG from the SREBP-SCAP complex, and allows an interaction between SCAP and the COPII coat protein Sec24. In combination with Sec23 and Sar-1, the SREBP-SCAP complex undergoes ER-to-Golgi transport via the COPII vesicular trafficking pathway. At the Golgi, two proteolytic cleavage events via the membrane-linked proteases S1P and S2P, lead to the release of the N-terminal transcriptional domain or 'mSREBP' into the cytoplasm. mSREBP1 undergoes homodimerisation before translocation to the nucleus via Importin-β. Here, it promotes target gene transcription, leading to the synthesis of fatty acids, triglycerides and cholesterol. Figure adapted from Horton et al., (2002).

.

6.2.1 SREBP-PATHWAY ACTIVATION

Activation of SREBP-target genes is tightly regulated according to the metabolic status of the cell. For example, under conditions of high intracellular cholesterol or fatty acid concentration, low metabolite availability or a lack of growth factor signaling, SREBP is inactive. However, in the event of decreased cellular cholesterol or fatty acid content, increased carbohydrate availability or signaling via the insulin pathway, SREBP becomes activated, allowing target gene transcription to commence.

Most data regarding the regulation of the SREBP-pathway have come from studies in cholesterol-dependent SREBP activation. However, although less well studied, an increasing amount of data suggest that SREBP activation is also governed by intracellular fatty acid concentration and extracellular insulin signaling. Here, whilst the mode of activation may be different, the overall activation process appears to be similar. Initially, *de novo* SREBP is transcribed and embedded in the endoplasmic reticulum (ER) membrane as an inactive full-length precursor (Figure 6.1 A and B). However, upon the receipt of activating stimuli, SREBP undergoes ER-to-Golgi transport, followed by two activating proteolytic cleavage events and subsequent release from the membrane. Activated SREBP is then able to translocate to the nucleus where transcription may begin (Figure 6.1 B). The following sections outline some of the stimulus-specific details that govern the regulation of this activation process.

6.2.1.1 SREBP-pathway activation by sterols

Sterols are part of the lipid family, and incorporate a wide range of molecules including steroid hormones and cholesterol. Of note, cholesterol is an essential component of membranes, with roles in membrane fluidity and permeability, as well as secondary messenger signaling. Sterols such as cholesterol have a well-defined role in the regulation of the SREBP pathway. Here, prior to activation by membrane-incorporated sterols, full-length SREBP (flSREBP) is embedded in the ER membrane as an inactive precursor protein (Figure 6.1 A & B). In this location, the C-terminal regulatory domain of SREBP interacts with the N-terminal WD-40 repeat domain of 'SREBP Cleavage Activating Protein' (SCAP) (Sakai et al, 1997), a SREBP escort protein required for sterol sensing via a 5-transmembrane 'sterol sensing domain' (SSD) (Hua et al, 1996). Under conditions of saturating intracellular sterol levels, the SREBP-SCAP complex is retained in the ER by an interaction between the SCAP SSD-domain and the 6-transmembrane retention factor 'Insulin Induced Gene 1/2' (INSIG-1/2) (Yabe et al,

2002; Yang et al, 2002). However, as sterol levels fall, SCAP undergoes a SSD-dependent conformational change (Brown et al, 2002; Feramisco et al, 2005), leading to the dissociation of INSIG from SCAP. Unbound INSIG-1 is unstable and undergoes rapid proteasomal degradation, coordinated by the membrane-bound ER-ubiquitin ligase Gp78, the AAA ATPase p97, and the complex-forming protein, Ubxd8 (Figure 6.2, Gong et al, 2006; Lee et al, 2006; Lee et al, 2008). The dissociation of SCAP from INSIG permits the free, cytosolic-loop 6 of SCAP to interact with the COPII vesicle coat proteins Sec23, Sec24 and Sar1 (Espenshade et al, 2002; Nohturfft et al, 2000; Sun et al, 2007). This interaction allows SCAP to mediate the translocation of SREBP from the ER to the Golgi via the COPII vesicular transport route (Sun et al, 2007).

6.2.1.2 SREBP-pathway activation by insulin

Historically, the circulating hormone insulin has been associated with the initiation of growth under nutrient rich conditions. Initial clues for an insulin involvement in the SREBP-pathway came following the observation that SREBP1c transcript levels were controlled by insulin in rat hepatocytes (Shimomura et al, 1999). Later, it was also shown that SREBP1c processing and nuclear relocation were elevated in the presence of insulin (Hegarty et al, 2005), and that insulin-dependent activation of the SREBP1c occurs via the growth-stimulating PI3K-Akt-mTOR pathway (Figure 6.3, Porstmann et al, 2009). Here, Akt phosphorylates the mTORC1-inhibitors TSC1/2, relieving the negative regulation on mTOR. This has two consequences; first it leads to the activation of mTOR-dependent protein synthesis; second it allows SREBP-pathway activation, probably via the initiation of ER-to-Golgi transport and SREBP-processing (see section 6.2.2) (Porstmann et al, 2008). Akt also regulates activated-SREBP-stabilisation in a non-mTOR dependent manner, through the inhibitory phosphorylation of GSK3, a negative regulator of the SREBP pathway (Cross et al, 1995; Porstmann et al, 2008). Together, this activation and stabilisation of SREBP promotes the lipid synthesis required for membrane expansion. Therefore, between mTOR-dependent protein synthesis and SREBP-dependent lipid synthesis, the raw materials for cellular growth are provided (Figure 6.3). Such processes rely heavily on Akt, for increased nutrient uptake (Barthel et al, 1999; Edinger & Thompson, 2002; Porstmann et al, 2008), and mitochondria, for the production of ATP and key metabolic substrates such as citrate.

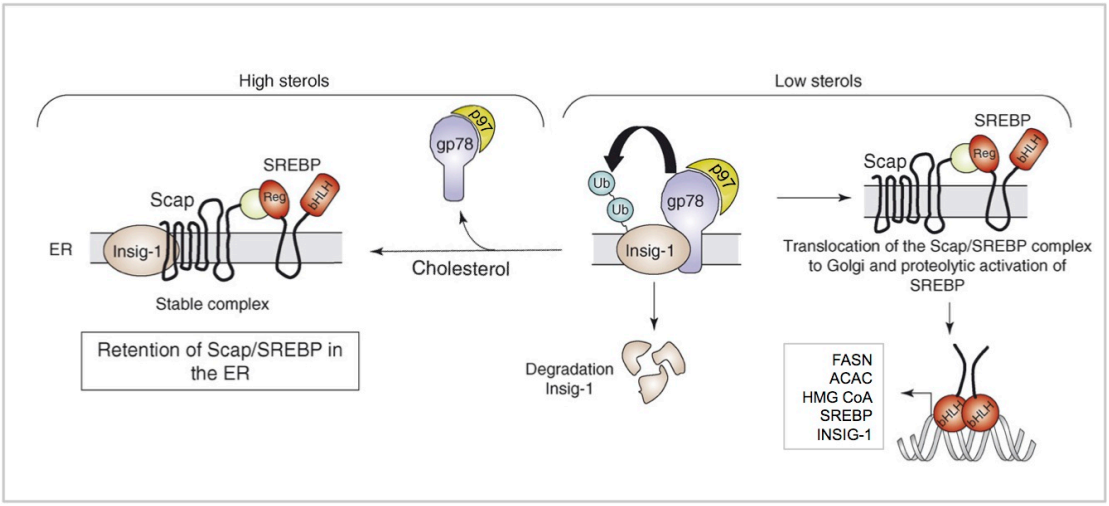

Figure 6.2 Proteasomal degradation of INSIG. Schematic representation of INSIG regulation. Here, in the presence of high sterol concentrations, INSIG retains the SREBP-SCAP complex in the ER membrane. However, in the presence of low sterol concentrations, INSIG dissociates from the SREBP-SCAP complex, becomes poly-ubiquitinated in a Gp78-dependent manner, and undergoes proteasomal degradation in a p97-dependent manner. This allows the translocation of SREBP to the nucleus and initiation of target-gene transcription. Figure adapted from Bengoechea and Ericsson (2007)

6.2.1.3 SREBP-pathway activation by fatty acids

In addition to sterol- and insulin-dependent ER-to-Golgi transport, SREBP is also regulated by fluctuations in intracellular fatty acid concentrations. Studies have shown that in the presence of elevated unsaturated fatty acids, INSIG-1 is stabilised, preventing the exit of SREBP1 from the ER (Lee et al, 2008). Interestingly, the mechanism for this stabilisation is not through the inhibition of INSIG-1 ubiquitination as with sterol sensing, but through the block of p97-dependent membrane extraction of ubiquitinated INSIG-1. Specifically, high intracellular fatty acid content prevents the interaction between INSIG-1 and the complex forming protein Ubxd8, allowing INSIG-dependent retention of SREBP-SCAP to persist in the ER membrane.

6.2.1.4 SREBP-pathway activation by ER stress

flSREBP is also activated under conditions of ER stress, arising from the build-up of unfolded proteins in the ER lumen (Osborne & Espenshade, 2009). Here flSREBP becomes activated through the depletion of INSIG-1 in thapsigargin-induced ER–stress models (Lee & Ye, 2004). Thapsigargin causes ER-stress by blocking ER-dependent calcium buffering (Lee & Ye, 2004; Lytton et al, 1991), leading to the depletion of ER calcium stores, the disruption of intra-ER protein folding, and an increase in cytosolic calcium concentration (Lee & Ye, 2004). This build-up of unfolded proteins triggers the ‘unfolded protein response’ (UPR), which coordinates the return of protein homeostasis

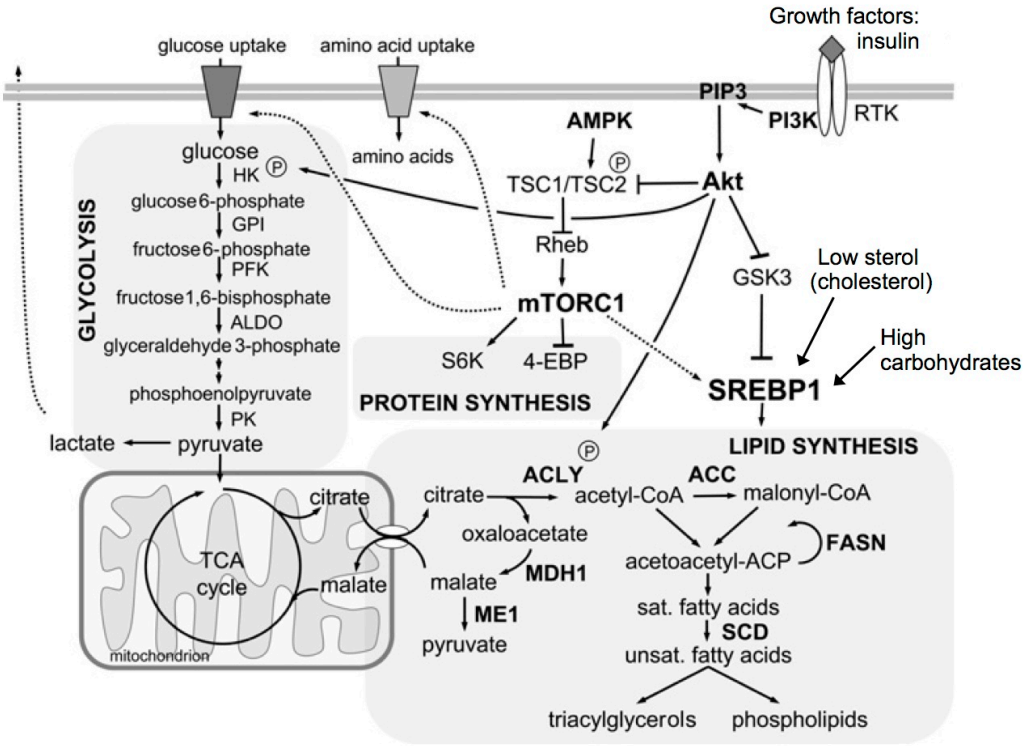

Figure 6.3 SREBP-pathway regulation by the PI3K-Akt-mTOR pathway. Schematic representation of the interplay between cellular growth and the PI3K-Akt-mTOR signaling pathway. Here, growth factors including insulin activate the PI3K-Akt pathway, which in turn relieves the negative inhibition of TSC1/2 on mTORC1. SREBP1 activation and stabilisation is coordinated by the serine/threonine kinase, Akt. Here, via the activation of mTOR, Akt stimulates SREBP-activation, and by the inhibition of the SREBP negative-regulator, GSK3, Akt promotes stabilisation. Additionally, Akt stimulates amino acid and glucose uptake, as well as stabilising HK2 for efficient glycolysis. The glycolysis pathway feeds into the mitochondrial TCA cycle, leading to ATP production and the anabolic synthesis of citrate. The availability of both energy and citrate from mitochondria is essential for SREBP-related lipid synthesis. Together, the PI3K-Akt-mTOR- and SREBP-pathways coordinate the synthesis of the building blocks required for cellular growth. Lipid synthesis abbreviations: ACLY, ATP-citrate lyase; ACC, acetyl-CoA carboxylase (also called ACAC); FASN, fatty acid synthase; SCD, stearoyl-CoA desaturase; MDH1, malate dehydrogenase 1; ME1, malic enzyme 1. Figure adapted from Porstmann et al., (2009).

by activating protein-folding chaperones and increasing protein degradation. The protein responsible for stress mediated INSIG-depletion is the stress-transducer kinase PERK, a master regulator of the UPR response. Here PERK inhibits *de novo* protein translation via the inactivating phosphorylation of 'eukaryotic translation initiation factor-2' (eIF2α) (Bobrovnikova-Marjon et al, 2008; Ron & Walter, 2007). These data show that ER-stress can promote the activation of SREBP, and hence its target genes, purportedly by reducing the inhibitory effects of INSIG-1. However, whether stress-related activation of SREBP is an accidental byproduct of a general translation block, or a functionally relevant process, (e.g. via a direct interaction between mediators of the UPR and SREBP-SCAP), is as yet unknown (Osborne & Espenshade, 2009).

6.2.2 SREBP PROCESSING AND NUCLEAR TRANSLOCATION

Regardless of the pathway stimulus, once integrated into the Golgi membrane, SREBP undergoes two proteolytic cleavage events via the membrane-integrated proteases, Site-1 Protease (S1P) and Site-2 Protease (S2P) (Figure 6.1 B, Brown & Goldstein, 1999). Here, the serine protease, S1P cleaves the intraluminal hydrophilic loop of SREBP, separating the N-terminal transcriptional domain from its C-terminal regulatory domain and associated SCAP escort (Duncan et al, 1997; Sakai et al, 1998). This is closely followed by an intramembrane cleavage within the hydrophobic transmembrane domain by the zinc metalloprotease, S2P, releasing the N-terminus of SREBP from the Golgi membrane (Rawson et al, 1997; Sakai et al, 1996). Now, the mature form of SREBP (mSREBP) is free to undergo homodimerisation, translocation to the nucleus via Importin-β, and activation of its target genes (Figure 6.1 B, Nagoshi & Yoneda, 2001). This process is dependent on SREBPs bHLH-Zip domain, and initiates the transcription of lipid-synthesis enzymes including *3-hydroxy-3-methylglutaryl-CoA synthase (HMGCS), Fatty Acid Synthase (FASN)* and *Acetyl CoA Carboxylase (ACAC)* (Brown & Goldstein, 1997). Interestingly, another transcriptional target is *LDLR*, involved in the uptake of cholesterol from the bloodstream. Therefore the SREBP pathway can regulate cholesterol levels through both *de novo* synthesis and dietary uptake.

In the nucleus, SREBP interacts with a number of cofactors, resulting in an increase in its transcriptional activity. These include P300-CBP (Ericsson & Edwards, 1998), MED15 (Yang et al, 2006a) and PGC1-β (Lin et al, 2005). Strikingly, PGC1-β is responsible for promoting the transcription of mitochondrial biogenesis genes, as well as SREBP-dependent lipid-synthesis genes, offering a link between SREBP1 and mitochondria. Thus, under nutrient-rich conditions, PGC1-β and SREBP may coordinate the synthesis of materials for membrane expansion, as well as the increased energy required for growth.

6.2.3 REGULATION OF SREBP EXPRESSION AND TURNOVER

Once in the nucleus, SREBP activity is tightly regulated on a number of levels. First, SREBP is its own transcriptional target, replenishing flSREBP levels in the ER membrane (Amemiya-Kudo et al, 2000; Sato et al, 1996). Second, INSIG-1 is also a target for SREBP-mediated transcription (Janowski, 2002), resulting in a concomitant inhibition of SREBP activation as sterol and/or fatty acid levels increase. Additionally, SREBP stability is regulated by the proteasome, via Skp1-Cullin-F-box (SCF)-mediated

proteolysis. The SCF is a multi-protein ubiquitin ligase complex, which leads to proteasomal degradation of target proteins often in a phosphorylation-dependent fashion. In the case of SREBP, a double-phosphorylation event, instigated by 'Glycogen Synthase Kinase 3 β' (GSK3β) (Kim et al, 2004; Sundqvist et al, 2005), acts as a scaffold for the interaction of the SCF-related E3 ubiquitin ligase, 'F-box and WD repeat domain containing 7' (FBXW7) with SREBP (Sundqvist et al, 2005). Here, FBXW7 ubiquitinates SREBP, initiating its rapid degradation via the ubiquitin-proteasomal system (UPS) (Figure 6.4). Importantly, DNA-binding of SREBP to target gene promoters stimulates its association with both GSK3β and FBXW7, hence upregulating SREBP turnover (Punga et al, 2006). Taken together, these data highlight the tight regulation of SREBP expression, stability and function at multiple points of the pathway. Importantly, it also highlights the need for continuous replacement of nuclear mSREBP in order to maintain persistent transcription of SREBP-target genes.

6.2.4 SREBP-PATHWAY IN *DROSOPHILA*

The *Drosophila* genome encodes orthologs of the core *SREBF*-pathway genes including one *SREBF* ortholog (also known as *HLH106*) with high homology to human *SREBF* (Seegmiller et al, 2002), *SCAP*, *S1P* and *S2P* (Dobrosotskaya et al, 2002). In contrast to mammalian SREBP, which is sensitive to both fatty acids and cholesterol, *Drosophila* SREBP is regulated by the sphingolipid pathway product, phosphatidylethanolamine (PE) (Dobrosotskaya et al, 2002). This is in part due to *Drosophila* lacking many of the enzymes required for cholesterol synthesis, making them cholesterol auxotrophs (Clark & Bloch, 1959). PE is the major phospholipid component of *Drosophila* membranes, accounting for 55% of the total composition (Jones et al, 1992), indicating that in *Drosophila,* SREBP is likely to be involved in the monitoring and maintenance of membrane phospholipid composition (Seegmiller et al, 2002). The lack of cholesterol synthesis in *Drosophila* may explain why they possess a single *SREBF* gene rather than two *SREBF* genes with distinct lipid-specific targets, as in mammals. This additional role of SREBP-dependent cholesterol homeostasis in mammalian systems is suggested to be due to a genome replication event, producing divergent pathway functions (Seegmiller et al, 2002). The absence of sterol homeostatic control in *Drosophila* may also explain the apparent lack of an obvious ortholog to mammalian INSIG, as INSIG-dependent SCAP inhibition relies largely upon sterol sensing in the ER membrane (Rawson, 2003). However, the presence of the core escort factor SCAP suggests that an unidentified *Drosophila*-specific retention factor with analogous roles to INSIG may be awaiting discovery in *Drosophila*. It is currently unknown whether *Drosophila* SCAP is responsible for the assessment of PE

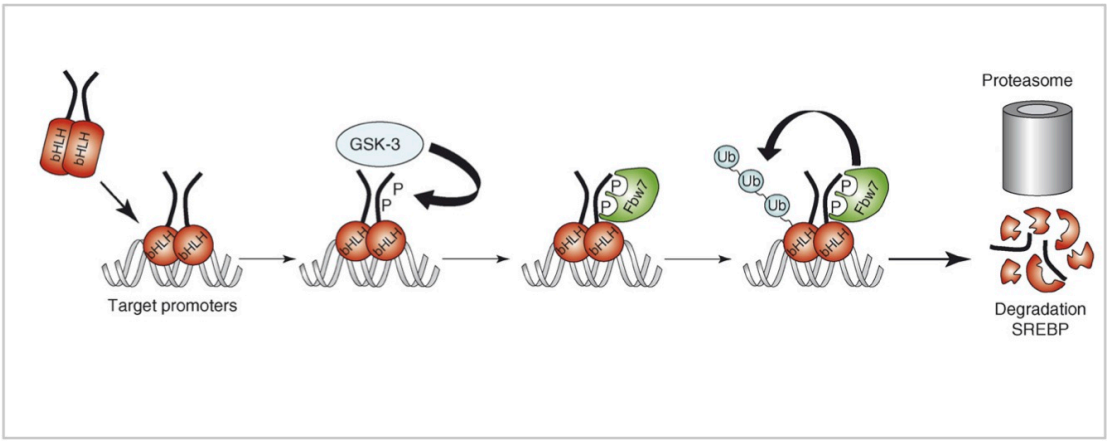

Figure 6.4 Proteasomal degradation of SREBP. Schematic representation of SREBP regulation. Here, following homodimerisation and translocation to the nucleus, mSREBP binds to target gene promoters and initiates transcription. Concomitantly, the protein kinase GSK3 phosphorylates SREBP in two locations, acting as a scaffold for the binding of the SCF-E3-ligase, FBXW7. FBXW7 promotes the polyubiquitination of SREBP, leading to its rapid turnover via the UPS. (Figure adapted from Bengoechea-Alonso and Ericsson, 2007).

membrane composition, although here, it is likely that the SSD-domain is not restricted to monitoring sterol levels, but also characteristics such as lipid composition and fluidity (Seegmiller et al, 2002).

Clues as to the global impact of *SREBF* in *Drosophila* came following analysis of null mutants and siRNA-treated animals. *SREBF*-null flies die during larval-stages indicating a crucial role in developmental processes. Mutant larval analysis showed a significant reduction in fatty acid content, with a concomitant decrease in the enzymes required for fatty acid synthesis. Additionally, mutant animals were much smaller than their heterozygous counterparts, indicating a critical role in growth (Kunte et al, 2006). In agreement, *dSREBP* siRNA-treated flies persisted to adulthood, probably due to residual SREBP expression, but exhibited much smaller body mass and size compared with control flies (Porstmann et al, 2008).

6.2.5 LIPIDS AND MITOCHONDRIA

Mitochondria play an important role in the anabolic synthesis of *de novo* fatty acids and cholesterol, as well as the release of energy from lipids via β-oxidation. Under conditions of high metabolite concentration, rather than utilising the Krebs' cycle to produce units of ATP, mitochondria release citrate into the cytoplasm for conversion into fatty acids, triglycerides and cholesterol (Figure 6.3). At the same time, malate is shuttled into mitochondria, in order to shut off the enzymes involved in fatty acid catabolism. This process provides the building blocks required for biological membrane synthesis, and allows the storage of excess energy for later use. Conversely, in the case of reduced metabolite concentration, the energy stored in fatty acids is released

in the mitochondrial matrix via fatty acid β-oxidation. This process leads to the production of NADH and H^+, which feed into the ETC, producing ATP units for the cell. Therefore, mitochondria are not only involved in the anabolic synthesis of lipids, but also fatty acid catabolism, allowing both the storage and release of energy depending upon cellular demands (Vamecq et al, 2012).

The composition of the mitochondrial membrane is unique in that it is enriched in the non-bilayer forming fatty acids, cardiolipin (CL) and phosphatidylethanolamine (PE). CL is synthesised solely in the mitochondria, whereas approximately 50% of cellular PE synthesis occurs in mitochondria (van Meer & de Kroon, 2011). Importantly, the synthesis of CL and PE relies upon SREBP-dependent transcription of lipid-synthesising enzymes including Fatty Acid Synthase (FASN) and Glycerol-3-phosphate Acyltransferase, Mitochondrial (GPAM) (Black et al, 2010; Dobrosotskaya et al, 2002), outlining the importance of SREBP in mitochondrial biosynthesis.

6.2.6 SREBP-PATHWAY COMPONANTS IN SCREEN HIT LISTS

As *SREBF1* and *2*, *FBXW7* and *GSK3A* were strong hits in the final human hit group, it seemed appropriate to assess the performance of other *SREBF*-pathway genes during the screening process (Table 6.1). Encouragingly, a large proportion of *SREBF*-related genes produced a significant effect in the primary screen. These included the chaperone *SCAP*, two members of the COPII coat complex *Sec23/24*, SREBP-target genes *FASN, ACAC* and *SCD*; and transcriptional cofactors *P300* and *MED15*. Whilst some of these genes failed to progress past the confirmation screen stage due to inconsistent effects, or aberrant cellular phenotypes (e.g. cell death), a small number proceeded to secondary screening. At this stage, many pathway genes failed to meet the criteria for advancement through to human cell screening, aside from *SREBF1 and 2, GSK3A and B* and *FBXW7,* most of which went on to populate the final human hit table. Nevertheless, these data highlight a clear enrichment for genes involved in the regulation and output of the SREBP-pathway, suggesting the involvement of lipid homeostasis in mitochondrial quality control.

6.3 ANALYSIS OF SREBP-PATHWAY COMPONENTS

Through extensive screening, key members of the SREBP-pathway have been identified as altering PINK1/Parkin-mediated mitochondrial quality control. In order to scrutinise this cross-pathway interaction, a number of approaches have been taken,

	Drosophila Screening					Mammalian Screening		
	Primary screen	Re-screen	Secondary screen			HeLa cells		
	Z-score	Hit score	Paraquat translocation	Morphology	Perinuclear Aggregation	Parkin translocation	Mitophagy	
SREBF1	-5.60	3 of 4		Fragmented				A
SREBF2	-5.60	3 of 4		Fragmented				
SCAP	-4.06	2 of 4		Fragmented				
INSIG	No known *Drosophila* ortholog							
GP78	No known *Drosophila* ortholog							
S1P	1.10							
S2P	-0.92							
Sec23	-5.16	4 of 4						B
Sec24	-4.13	1 of 4		Fused				
Sar1	Plate 23 - equipment crash (re-screened but not a hit)							
FBXW7	-3.98	2 of 4		Fused				C
GSK3A	-3.77	4 of 4		Fragmented				
GSK3B	-3.77	4 of 4		Fragmented				
FASN	-4.09	Eliminated: odd looking cells						D
ACAC	-4.37	3 of 4		Fragmented				
SCD	-4.28	3 of 4		Fragmented				
ACS	0.40							
P300	-4.81	Eliminated: sick looking cells						E
MED15	-3.38	2 of 4						
PGC-1B	0.40							

Hit
Non-hit
Not tested

A. Main pathway components
B. COPII vesicle adaptors (interact with SCAP)
C. SREBP degradation pathway
D. SREBP target genes
E. SREBP co-activators (important for SREBP-dependent transcription)

Table 6.1 Screen analysis of SREBP-pathway members. Table showing the effect of SREBP-pathway genes (left) on mitochondrial homeostasis**.** Genes in bold typeface indicate final screening hits. Their performance in *Drosophila* and mammalian screens are indicated. Green cells represent screen hits, red cells represent non-hits, and grey cells represent situations where a protein was not tested. In the primary screen, z-sores are indicated. In the re-screen, the hit frequency (out of 4) is shown. In secondary screening the mitochondrial morphology phenotype is indicated. Proteins are grouped according to their function as indicated in the key (A-E).

both biochemically and genetically. The key aims of the following experiments are to ascertain whether SREBP-related proteins play a direct role in the PINK1/Parkin-pathway, perhaps aiding in the understanding of Parkinson's disease etiology.

6.3.1 PARKIN TRANSLOCATION AND MITOPHAGY

Prior to low-throughput analysis, gene silencing efficiencies were confirmed for all siRNAs utilised in this chapter, using a qRT-PCR approach in HeLa and YFP-Parkin.HeLa cells (Appendix, Figure 9.1).

As identified in mammalian screening assays, *SREBF1* and *FBXW7* strongly influence Parkin translocation and mitophagy following CCCP toxification. In order to confirm this effect in a low-throughput setting, YFP-Parkin.HeLa cells were treated with control, *PINK1*, *SREBF1* or *FBXW7* siRNA before exposure to CCCP for 4 hours (Figure 6.5 A) or 24 hours (Figure 6.5 B). Without CCCP, Parkin translocation and mitophagy were absent in all conditions analysed. However, following 4 hours of CCCP treatment (Figure 6.5 A), control cells experienced almost complete translocation of YFP-Parkin to mitochondria. In contrast, upon *PINK1* and *SREBF1* silencing, translocation was

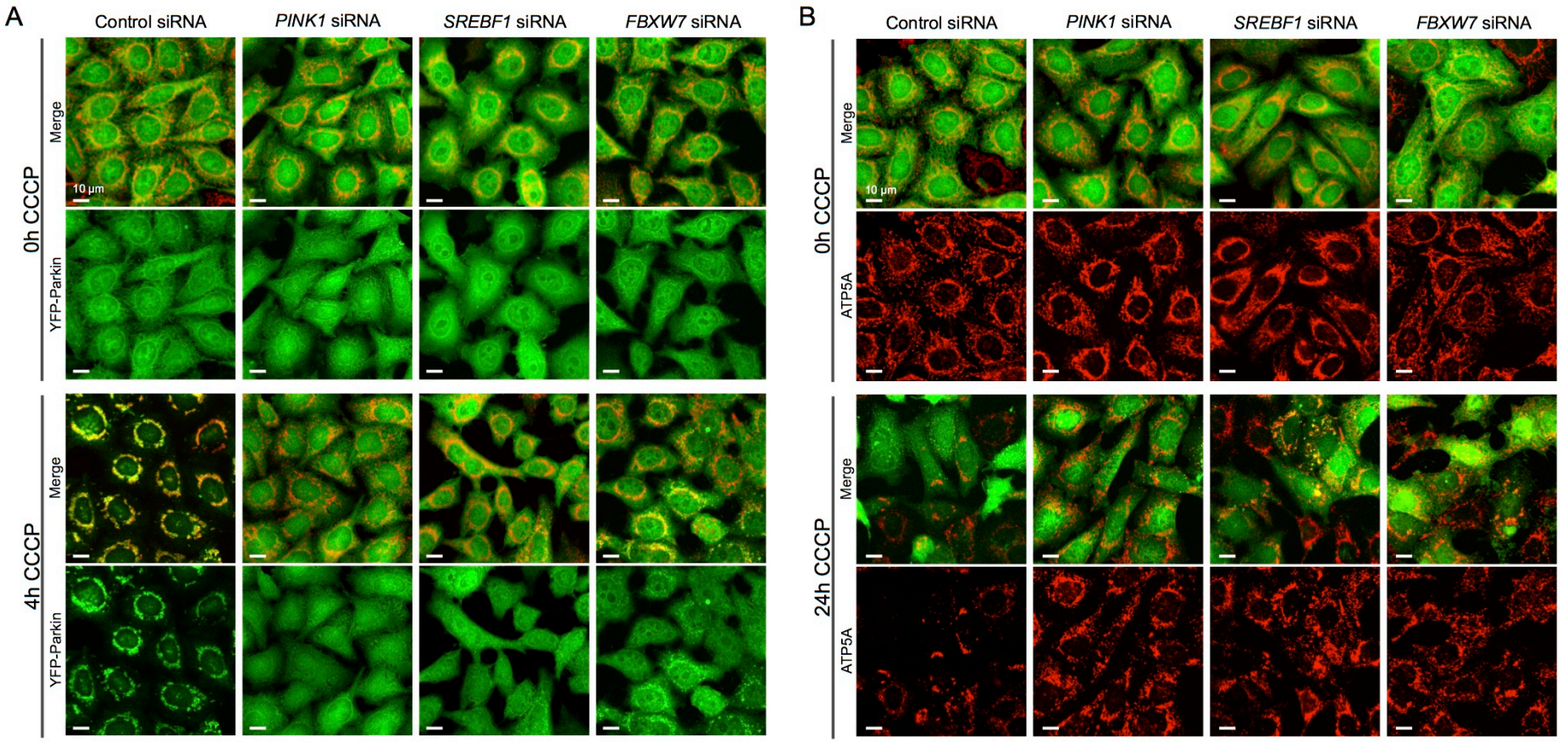

Figure 6.5 Parkin translocation and mitophagy following CCCP toxification. (A & B) YFP-Parkin.HeLa cells were exposed to 25 nM of control, *PINK1*, *SREBF1* or *FBXW7* siRNA for 4 days, prior to 4 hours (A) or 24 hours (B) of vehicle or CCCP (10 µM) treatment as indicated. (A) Parkin translocation (YFP-Parkin – green) to mitochondria (ATP5a – red) and (B) the loss of mitochondrial ATP5A signal (red) in YFP-Parkin-expressing cells (green) was assessed qualitatively by fluorescence confocal microscopy (60x objective, 2x digital zoom, scale bar: 10 µm).

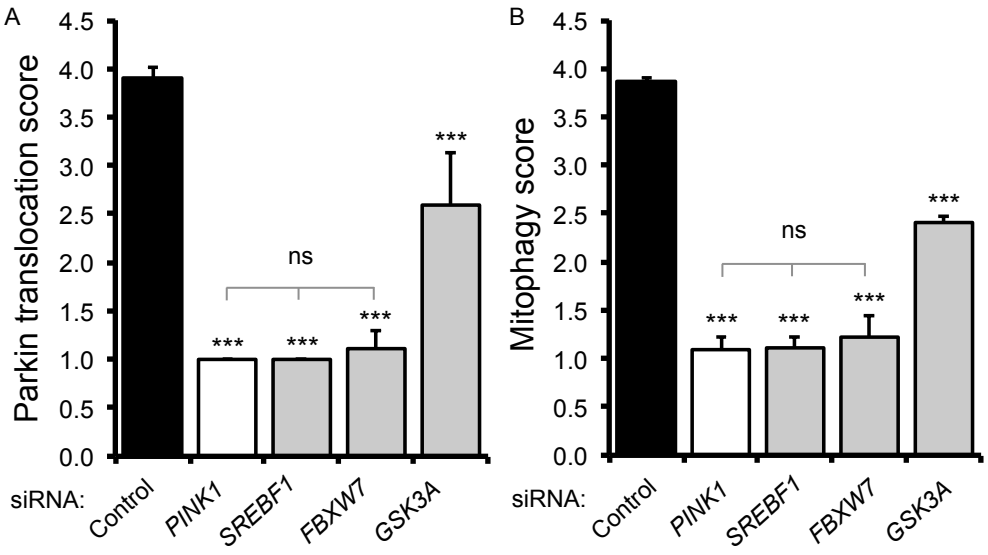

Figure 6.6 High throughput quantification of Parkin translocation and mitophagy following CCCP toxification. Graphical representation of average Parkin translocation (A) and mitophagy (B) scores following 10 μM CCCP treatment for 4 hours (A) or 24 hours (B). Data represent control, *PINK1*, *SREBF1*, *FBXW7* and *GSK3A* siRNA-treated YFP-Parkin.HeLa cells from three rounds of screening. Error bars denote the standard deviation. *** P<0.001 (One-way ANOVA with Bonferroni's correction, compared to control siRNA unless otherwise indicated).

largely absent, and upon *FBXW7* silencing, translocation was greatly reduced, with some cells displaying partial Parkin translocation phenotypes.

When CCCP-treatment was extended to 24 hours (Figure 6.5 B), a substantial proportion of control cells experienced a significant reduction or complete loss of the mitochondrial marker, ATP5A. This loss was attributed to the degradation of mitochondria via the mitophagy pathway, in agreement with published data (Narendra et al, 2008). However, upon the silencing of *PINK1*, *SREBF1* and *FBXW7*, the observed reduction in ATP5A signal was blocked.

Both Parkin translocation (Figure 6.5 A) and mitophagy (Figure 6.5 B) qualitative data are in agreement with the average quantitative high-throughput results obtained during Parkin translocation (Figure 6.6 A) and mitophagy (Figure 6.6 B) mammalian screening. Together, these data confirm that *SREBF1* and *FBXW7* are able to phenocopy *PINK1* with regards to Parkin translocation and mitophagy in cell culture.

6.3.2 ASSESSING *PINK1* TRANSCRIPT LEVELS

As CCCP-induced Parkin translocation and mitophagy require PINK1 stabilisation on the MOM, any alteration in *PINK1* expression levels may potentially alter the efficiency of both events. In an attempt to understand the mechanism with which *SREBF1* and

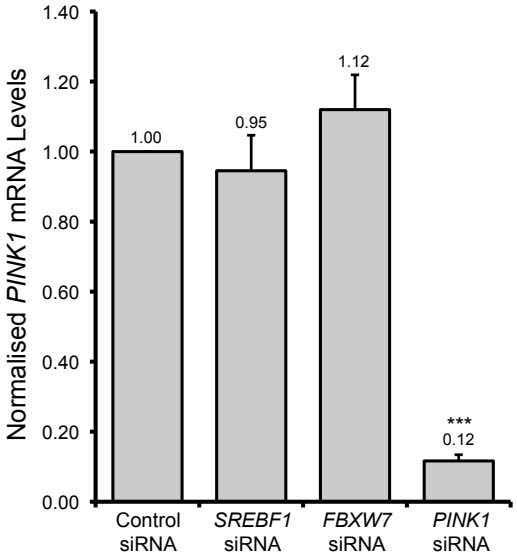

Figure 6.7 qRT-PCR analysis of *PINK1* gene expression following siRNA treatment. HeLa cells were exposed to 25 nM of control, *SREBF1*, *FBXW7* or *PINK1* siRNA for 4 days. *PINK1* expression levels were analysed using qRT-PCR against the housekeeping gene RNA18S5. Graph represents the mean of 3 biological repeats. Error bars represent the standard error. ***P<0.0001 (Student's T-test, compared to control siRNA-treated samples).

FBXW7 influence Parkin translocation and mitophagy, the effect of *SREBF1* and *FBXW7* siRNA on *PINK1* transcript levels was assessed (Figure 6.7). Here, if *SREBF1* and *FBXW7* silencing cause a concomitant downregulation of *PINK1* expression, the likely explanation for the observed block on PINK1/Parkin-pathway processes would be due to a lack of PINK1. However upon quantification of *PINK1* mRNA levels using a qRT-PCR approach, no significant differences between *PINK1* expression in control, *SREBF1* or *FBXW7* siRNA samples were found. However, *PINK1* siRNA-treated samples produced a significant decrease in transcript levels, validating the assay. These data confirm that *SREBF1* and *FBXW7* have no discernable effects on *PINK1* expression under basal conditions.

6.3.3 CHEMICAL INHIBITION OF THE SREBP-PATHWAY

In order to assess the specificity of *SREBF1* siRNA, a chemical inhibitor of the SREBP-pathway was employed. Genistein, a soy isoflavone, inhibits SREBP1 cleavage by causing the down-regulation of the activating protease, S1P. The resulting inhibition of SREBP1 activation leads to a significant decrease in the expression of SREBP1-target genes including *FASN* and *ACAC* (Shin et al, 2007). Using this approach, Parkin translocation was assessed following the application of vehicle or a range of genistein concentrations, from 10 – 100 μM (Figure 6.8). In the absence of toxification, genistein-treated cells exhibit comparable Parkin phenotypes to vehicle treated samples, maintaining a diffuse, cytoplasmic distribution (Figure 6.8 A - D). Following toxification with CCCP for 4 hours, vehicle-treated cells saw a robust initiation of Parkin translocation (Figure 6.8 E). However, in combination with genistein treatment, the observed Parkin translocation is reduced, seemingly in a dose-dependent manner

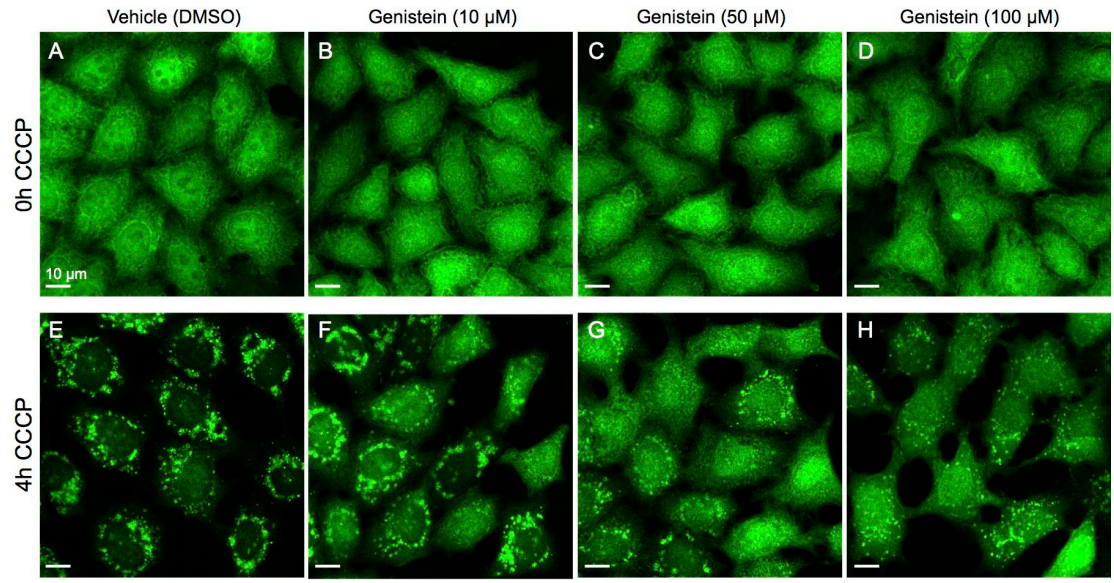

Figure 6.8 Chemical inhibition of the SREBP-pathway following Genistein treatment. YFP-Parkin.HeLa cells treated with either vehicle (A & E) or genistein (B – D, F - H) over a range of concentrations - 10 µM (B & F), 50 µM (C & G) and 100 µM (D & H), for 24 hours prior to the application of vehicle (A - D) or 10 µM CCCP (E – H) for 4 hours. Parkin translocation (YFP-Parkin – green) was assessed qualitatively by fluorescence confocal microscopy (60x objective, 2x digital zoom, scale bar: 10 µm).

(Figure 6.8 F - H). These data demonstrate a similar Parkin translocation blockage phenotype as observed with *SREBF1* silencing, hence demonstrating the specificity of the *SREBF1* siRNA effect.

6.3.4 ASSESSING STARVATION-INDUCED BULK AUTOPHAGY

Autophagy is the bulk degradation of large cellular components including mitochondria and ER, via the lysosomal pathway. Here, cargo becomes engulfed in a double membrane autophagic vesicle, known as the autophagosome, before fusing with the lysosomal compartment for hydrolytic degradation. There are a number of well-defined steps involved this process, comprising the initiation, elongation and maturation of the autophagosome; autophagosome-lysosome fusion; and content degradation (Tanida, 2011).

In an attempt to understand the interaction between PINK1/Parkin-mediated mitophagy and members of the SREBP-pathway, *SREBF1* and *FBXW7* were assessed for their influence on general autophagy (Figure 6.9). This approach aimed to ascertain whether the loss of these proteins via siRNA-gene silencing caused a general block of autophagy downstream of mitophagy initiation.

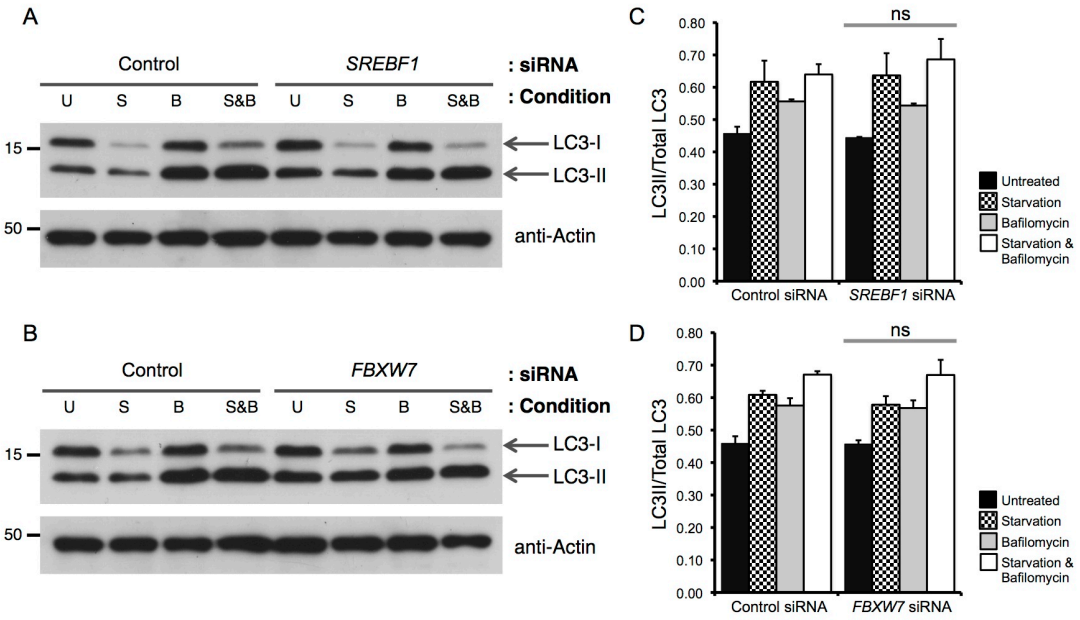

Figure 6.9 Starvation-induced autophagy. (A & B) Following control, *SREBF1* (A) or *FBXW7* (B) silencing, HeLa cells were subjected to 2 hours of control (U – untreated), starvation (S), 20 nM bafilomycin (B) or starvation with 20 nM bafilomycin (S&B) treatment. LC3 lipidation (shift from LC3-I to LC3-II) was assessed by western blot, Actin is used as a loading control. (C & D) Quantification of LC3 lipidation performed following control and *SREBF1* (C) or *FBXW7* (D) silencing. LC3 lipidation is assessed as LC3-II / total LC3 levels. Graphs represent the average of 3 assays, error bars represent standard error. Quantification was achieved using the ImageJ 'Gel' plugin. Student's T-test analysis of equivalent conditions found no significance (ns).

The SREBP-pathway has known links to autophagy, with *SREBF2* being involved in starvation-induced lipid autophagy (termed lipophagy) (Seo et al, 2011), and *Gp78* being involved in Parkin-independent mitophagy (Fu et al, 2013). In addition, the central role of the SREBP-pathway is to produce lipids required for membrane synthesis. In relation to autophagy, autophagosomes are double-membrane vesicular compartments, whose membrane is suggested to issue from organelle donors such as the ER and mitochondria (Tooze & Yoshimori, 2010). Therefore, it is conceivable that the absence of *SREBF1*-dependent membrane synthesis may cause a parallel reduction in autophagosome synthesis. The putative knock-on effect in the context of PINK1/Parkin-mediated mitophagy is a simultaneous block on mitochondrial degradation via this route. As CCCP-induced mitophagy is blocked following the loss of *SREBF1* and *FBXW7*, this may explain the observed effects.

To test the involvement of the SREBP-pathway in general autophagy, HeLa cells were subjected to starvation conditions for 2 hours (Figure 6.9 A & B). Here, nutrient depletion stimulates the cell to release stored energy and amino acids through the non-specific autophagic degradation of the cytoplasm and its contents (Mizushima, 2007). To assess the degree of starvation-induced autophagy, 'starved' samples were compared to non-starved or 'untreated' samples. Additionally, the degree of

'autophagic flux' within the system was analysed through the addition of the autophagy inhibitor, bafilomycin A_1. Here, bafilomycin A_1; a lysosomal proton pump inhibitor, causes an increase in lysosomal pH, hence preventing autophagosomal fusion with- and proteolytic degradation by the lysosome.

In order to monitor the amount of autophagy, the ubiquitin-like protein and autophagosomal marker, LC3 was examined by western blot. In the absence of autophagy, LC3-I is inactive, soluble and cytoplasmic. However, following autophagy initiation, LC3-I undergoes PE-dependent lipidation, by the E1- and E2-like enzymes ATG7 and ATG3 respectively. This lipidation event produces an active, insoluble, membrane-associated form of LC3, known as LC3-II (Tanida et al, 2004). LC3-II is a major component of the autophagosome membrane, typically used as readout for the amount of autophagy occurring within a system (Klionsky et al, 2012). Interestingly PE levels are influenced by SREBP-dependent fatty acid synthesis (Dobrosotskaya et al, 2002), further implicating the SREBP-pathway in this process.

Biochemical analysis of LC3 reveals one protein band of ~16 kDa, representing LC3-I, and an additional protein band of ~14 kDa, representing LC3-II (Figure 6.9 A & B). Following the application of control siRNA, untreated samples (U) exhibit a greater proportion of LC3-I compared to LC3-II (Figure 6.9 A & B). However, following starvation (S), the ratio shifts in favour of LC3-II, signifying the initiation of autophagy.

Of note, under starvation conditions, the total levels of LC3 are diminished compared to untreated samples. This is likely due to the autophagic degradation of LC3-II on the intra-autophagosomal surface by lysosomal cathepsins (Tanida, 2011); an occurrence that represents 'autophagic flux'. To assess the degree of autophagic flux, bafilomycin A_1 can be employed. In this situation, the autophagy pathway continues to produce autophagosomes, but their lysosomal degradation is inhibited, leading to an autophagosomal build-up. Under basal conditions in control siRNA-treated cells, the application of bafilomycin A_1 alone (B) leads to a significant increase in the amount of LC3-II, but has little effect on the amount of LC3-I (Figure 6.9 A & B). However, under starvation conditions, the simultaneous application of bafilomycin A_1 (S&B) causes the ratio of LC3-I to LC3-II to shift dramatically in favour of autophagosome-associated LC3-II.

Together, these data demonstrate first that starvation stimulates autophagy (U:S and B:S&B), and second, that there is a small amount of flux in the system (U:B and S:S&B). In order to quantify this effect, the amount of LC3-II was compared to the total

LC3 levels (LC3-I + LC3-II) (Figure 6.9 C & D, Klionsky et al, 2012). This calculation reflected the biochemical data whereby an increase in the proportion of LC3-II (and therefore autophagy) was observed following starvation, and low levels of autophagic flux were detected with the addition of bafilomycin A_1.

When comparing control siRNA-treated samples (Figure 6.9 A - D), with *SREBF1* siRNA (Figure 6.9 A & C), and *FBXW7* siRNA (Figure 6.9 B & D) treated samples, no significant difference is observed under any conditions. These data indicate that the silencing of *SREBF1* and *FBXW7* has no detectable influence of the initiation of general autophagy after 2 hours of starvation. This result would suggest that *SREBF1* and *FBXW7* are acting in a CCCP-induced mitophagy-specific fashion.

6.3.5 MITOCHONDRIAL MEMBRANE POTENTIAL ANALYSIS

Another possible explanation for the observed Parkin translocation and subsequent mitophagy block following *SREBF1* and *FBXW7* silencing is via the reversal of the mitochondrial transmembrane complex, ATP-synthase. ATP-synthase utilises the MIM proton gradient to drive the production of ATP, as H^+ ions flow from the IMS to the matrix though its F_o proton pore. This proton flow catalyses the phosphorylation of ADP to ATP in an ATP-synthase dependent manner. However, ATP-synthase can also function in reverse, by hydrolysing ATP in order to pump H^+ ions out of the matrix and into the IMS. Through this, ATP-synthase has the ability to repolarise the $\Delta\Psi m$ when the proton-motive force is reduced. Whether ATP-synthase acts to synthesise or hydrolyse ATP depends on the energy requirements of the cell and steepness of the proton gradient across the MIM (Alberts et al, 1994).

In the case of *SREBF1* and *FBXW7*, if their silencing leads to a reversal of ATP-synthase, PINK1 is unlikely to become stabilised on the MOM even in the presence of CCCP, leading to a loss of Parkin translocation and mitophagy. In support of this event, a recent genome-wide RNAi screen reported that the loss of *ATPase inhibitory factor 1* (*ATPIF1*) blocked Parkin translocation following CCCP-treatment due to ATP-Synthase reversal and subsequent maintenance of $\Delta\Psi m$ (Lefebvre et al, 2013). In order to assess whether ATP-synthase reversal is occurring under these conditions, the $\Delta\Psi m$ was assessed using the mitochondrial membrane potential indicator dye, tetramethylrhodamine methyl ester (TMRM). TMRM is a lipophilic, cationic dye that easily traverses biological membranes, and accumulates in the most negatively charged compartments within the cell - primarily mitochondria (Scaduto & Grotyohann, 1999). Hyperpolarised mitochondria with a negatively charged matrix accumulate more

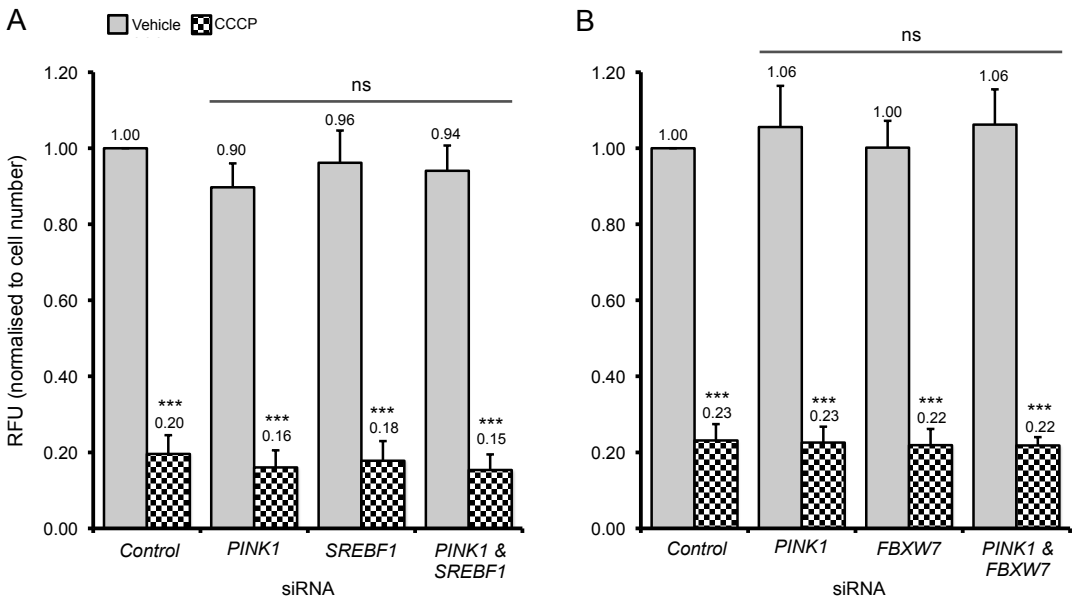

Figure 6.10 Mitochondrial membrane potential analysis. HeLa cells were treated with control or *PINK1* siRNA (A & B), *SREBF1* siRNA (A), *FBXW7* siRNA (B) or a combination of *PINK1* & *SREBF1* siRNA (A) or *PINK1* & *FBXW7* siRNA (B) for 2 days before the addition of either vehicle or 10 μM CCCP for 1 hour as indicated. ΔΨm was assessed by the application of the potentiometric dye, TMRM (50 nM) for 30 minutes. Cells were washed with either vehicle or 10 μM CCCP-containing assay buffer before fluorescence quantification by a microplate reader, providing the output as relative fluorescence units (RFU). TMRM fluorescence was normalised to cell number through the application of the DNA-binding dye, CyQuant for 1 hour. Nuclear count was assessed using a microplate reader. Data represent four biological repeats; error bars denote the standard error. Student's t-test was performed between vehicle and CCCP-treated pairs, ***P<0.001. One-way ANOVA with Bonferroni's correction was applied across vehicle-treated and CCCP-treated groups, and compared to control siRNA-treated samples. No significance (ns) was found within any of the groups.

TMRM dye than hypopolarised mitochondria, producing bright red/orange fluorescence.

To test whether *SREBF1* and *FBXW7* loss leads to the maintenance of the ΔΨm, HeLa cells were exposed to *SREBF1* and *FBXW7* siRNA, before the application of either vehicle or CCCP for 1 hour. Following this, cells were bathed in TMRM-containing buffer before further washes in either vehicle or CCCP-containing buffer. TMRM fluorescence was determined using a microplate reader, and normalised to cell number (Figure 6.10).

SREBF1 and *FBXW7* siRNA-treated samples were compared to control and *PINK1* siRNA-treated samples, as well as a double knockdown situation, where *PINK1* was silenced in combination with ether *SREBF1* or *FBXW7*. As expected, control siRNA-treated samples showed intense TMRM fluorescence following vehicle treatment, with a robust fall in fluorescence after the application of the ΔΨm uncoupler, CCCP (Figure 6.10 A & B). When comparing control siRNA treated cells to those treated with *PINK1* (Figure 6.10 A & B), *SREBF1* (Figure 6.10 A), *FBXW7* (Figure 6.10 B) or a combination

(Figure 6.10 A & B) of siRNAs, no significant difference was observed. These data indicate that *SREBF1* and *FBXW7* silencing does not block Parkin translocation and mitophagy through the maintenance of the $\Delta\Psi m$.

Of note, in contrast to the residual TMRM staining observed here after CCCP treatment (~20%), preparation of isolated rat heart mitochondria treated with CCCP results in the complete loss of TMRM staining (Scaduto & Grotyohann, 1999). One possible reason for the observed 'background' TMRM fluorescence is the $\Delta\Psi m$-independent binding of TMRM to mitochondria in this assay, albeit at low levels (Perry et al, 2011). Alternatively, despite CCCP-induced loss of TMRM from the mitochondrial matrix, the dye may still remain trapped in the cytosol, perhaps accounting for some low background fluorescence. Despite this residual staining, the outcome of the assay remains clear, and the overall conclusions unaffected.

6.3.6 PARKIN TRANSLOCATION RESCUE WITH LIPIDS

To assess whether the block on Parkin translocation following *SREBF1* siRNA is a consequence of a decrease in SREBP-induced lipid synthesis, Parkin translocation was assessed following the application of cholesterol, fatty acids or a combination of the two (Figure 6.11). Here, YFP-Parkin.HeLa cells were exposed to control or *SREBF1* siRNA before being 'primed' for 24 hours with vehicle- (Figure 6.11 A - D), cholesterol- (Figure 6.11 E, I & J - high concentrations, Figure 6.11 F, K & L, low concentrations) or fatty acid- (Figure 6.11 F, K & L - high concentration, Figure 6.12 G, J & L - low concentration) containing media. In the absence of fatty acids and cholesterol, control siRNA-treated cells exhibited a lack of Parkin translocation in the absence of CCCP (Figure 6.11 A), and a robust translocation phenotype following 4 hours of CCCP treatment (Figure 6.11 B). As previously demonstrated, *SREBF1* siRNA results in a lack of Parkin translocation in the absence of CCCP (Figure 6.11 C), and a substantial reduction following 4 hours of CCCP (Figure 6.11 D). However, following the addition of fatty acids and/or cholesterol, a partial restoration of Parkin translocation was observed in most cases (Figure 6.11 E - L). This effect was quantified manually, demonstrating a general trend in all conditions towards increased Parkin translocation, with four of these conditions reaching significance (Figure 6.11 M). Importantly, the application of exogenous fatty acids and cholesterol had no effect on Parkin translocation in non-toxified control and *SREBF1* siRNA samples (Appendix, Figure 9.2 A), consistent with the absence of general toxicity. Additionally, no effect of fatty acid and cholesterol application was observed in CCCP-treated control siRNA samples, demonstrating the specificity of the rescue (Appendix, Figure 9.2 B).

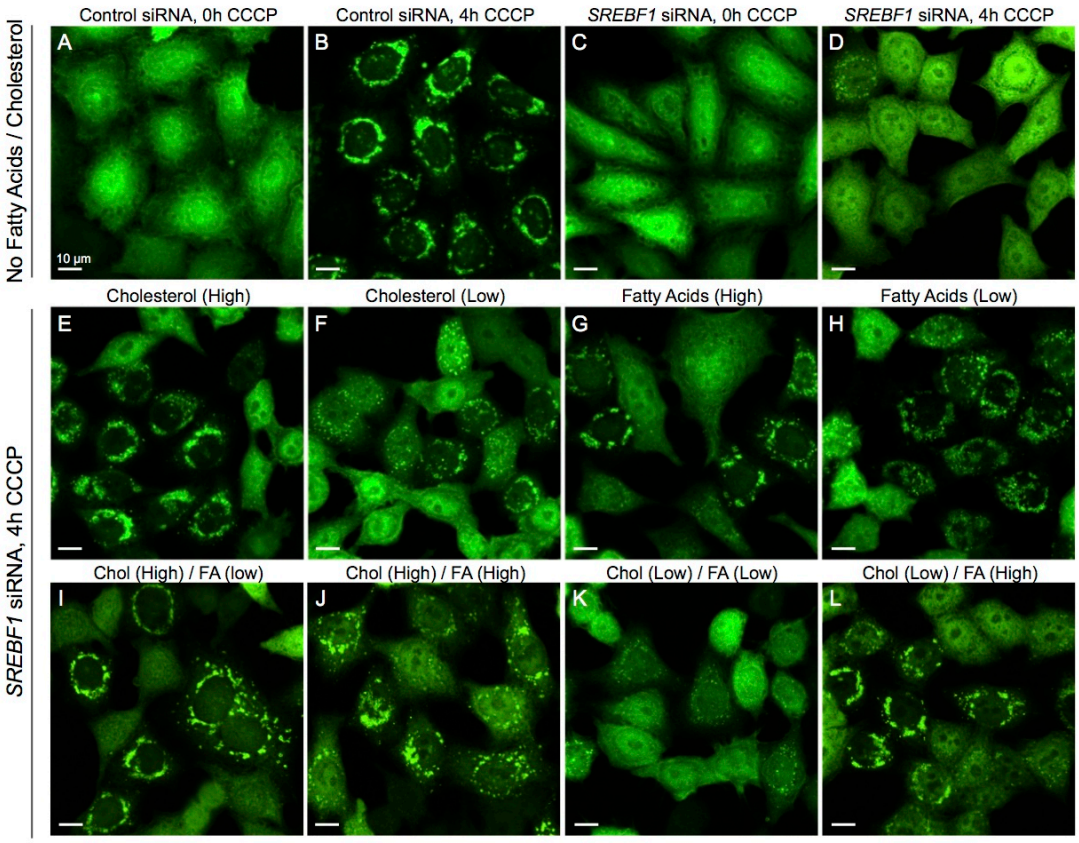
Control siRNA, 0h CCCP
Control siRNA, 4h CCCP
SREBF1 siRNA, 0h CCCP
SREBF1 siRNA, 4h CCCP
No Fatty Acids / Cholesterol
A
B
C
D
10 µm
Cholesterol (High)
Cholesterol (Low)
Fatty Acids (High)
Fatty Acids (Low)
SREBF1 siRNA, 4h CCCP
E
F
G
H
Chol (High) / FA (low)
Chol (High) / FA (High)
Chol (Low) / FA (Low)
Chol (Low) / FA (High)
I
J
K
L

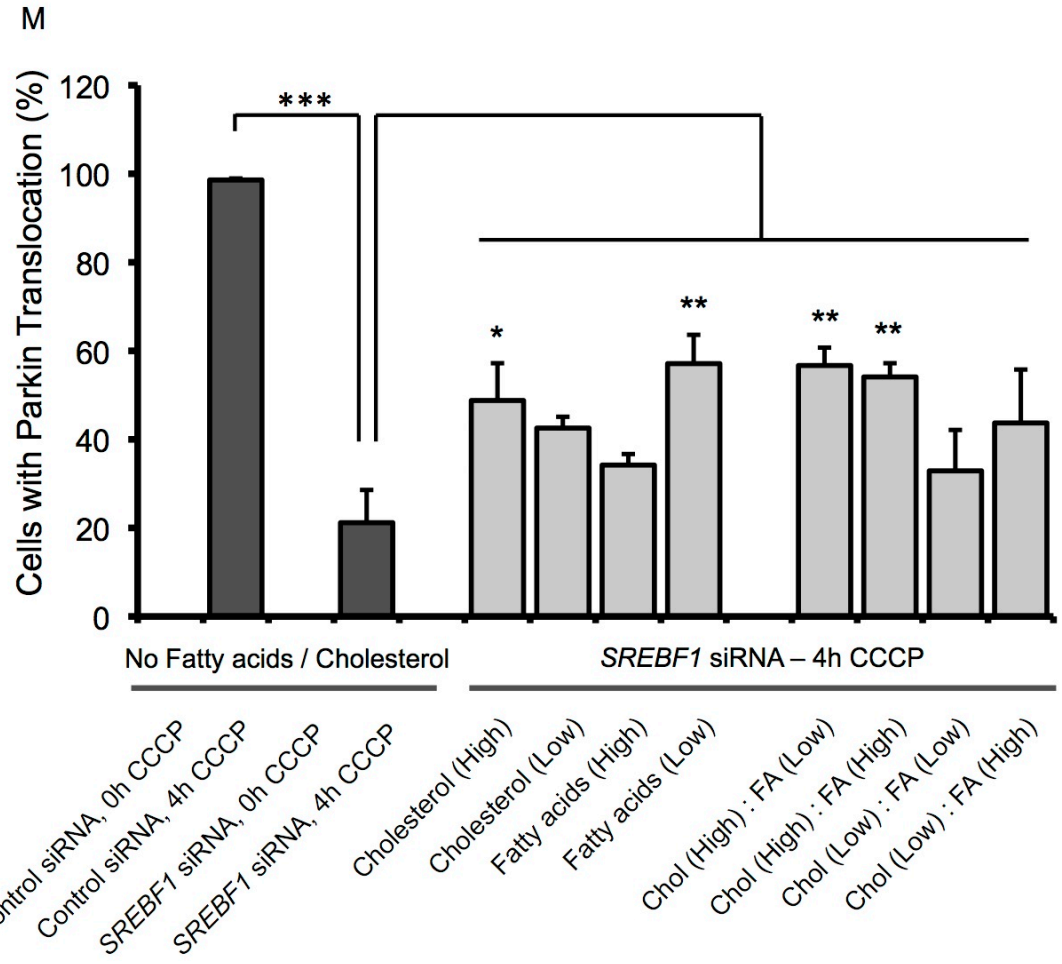
M
Cells with Parkin Translocation (%)
120
100
80
60
40
20
0
***
*
**
**
**
No Fatty acids / Cholesterol
SREBF1 siRNA – 4h CCCP
Control siRNA, 0h CCCP
Control siRNA, 4h CCCP
SREBF1 siRNA, 0h CCCP
SREBF1 siRNA, 4h CCCP
Cholesterol (High)
Cholesterol (Low)
Fatty acids (High)
Fatty acids (Low)
Chol (High) : FA (Low)
Chol (High) : FA (High)
Chol (Low) : FA (Low)
Chol (Low) : FA (High)

Figure 6.11 Rescuing SREBP1-dependent Parkin translocation with fatty acids and cholesterol. YFP-Parkin.HeLa cells were treated with control or *SREBF1* siRNA for 4 days before the addition of either vehicle (A - D), cholesterol (E & F), fatty acids (G & H) or a combination of cholesterol and fatty acids (I-L) for 24 hours. Samples were then treated with either vehicle (A & C) or 10 µM CCCP (B, D, E - L) for 4 hours. Parkin translocation (YFP-Parkin – green) was assessed qualitatively (A - L) by fluorescence confocal microscopy (60x objective, 2x digital zoom, scale bar: 10 µm) and quantitatively as the percentage of cells with Parkin translocation (M). (M) Graphical representation of Parkin translocation quantification following the application of conditions A - L. Data represent 3 biological repeats, each with 5 FOV per condition, per assay. Error bars represent standard error. **P<0.01, *P<0.05 (one-way ANOVA with Bonferroni's correction, compared to *SREBF1* siRNA, 4h CCCP). FA - fatty acids; Chol – cholesterol. High – high concentration; Low – low concentration.

Interestingly, both cholesterol and fatty acids were able to overcome the *SREBF1*-dependent block on Parkin translocation, indicating a potential role for both lipid groups in mitophagy initiation. Seemingly higher concentrations of cholesterol and lower concentrations of fatty acids were required for a significant rescue of Parkin translocation. Additionally, some combinations of fatty acids and cholesterol together produced a significant translocation recue, which relied upon the presence of high cholesterol levels. Taken together, these data suggest that SREBP-dependent lipid synthesis is key to Parkin translocation, rather than an alternative pathway output.

The next step was to assess whether the application of fatty acids and/or cholesterol was able to overcome *PINK1* siRNA-dependent inhibition of Parkin translocation. For this, three of the strongest translocation rescue conditions from the previous assay were employed, together with an additional condition, combining low fatty acid concentrations with 'very high' cholesterol concentrations. Here, control siRNA samples behaved as in Figure 6.11 (Figure 6.12 A, E & I). Following PINK1 siRNA treatment, almost a complete lack of Parkin translocation was observed in vehicle- (Figure 6.12 C & I) and CCCP-treated (Figure 6.12 D & I) conditions. However, under these conditions, the application of cholesterol and/or fatty acids prior to toxification produced no rescue of the Parkin translocation block (Figure 6.12 E - I). These data show that *PINK1* siRNA phenotypes are not rescued by the application of SREBP-related lipids, at least at the concentrations tested. Hence this suggests that SREBP1-dependent lipid production acts upstream of PINK1 in the PINK1/Parkin-pathway.

As discussed, mitochondria exhibit a distinct lipid profile, with the majority of the membrane comprising the non-bilayer forming lipids cardiolipin (CL) and phosphatidylethanolamine (PE). As *SREBF1* siRNA leads to a block of mitophagy, the next logical step was to test whether exogenous application of these mitochondrial lipids could rescue Parkin translocation (Figure 6.13). Here, following control (Figure 6.13 A – E) or *SREBF1* (Figure 6.13 F – J) siRNA application, YFP-Parkin.HeLa cells

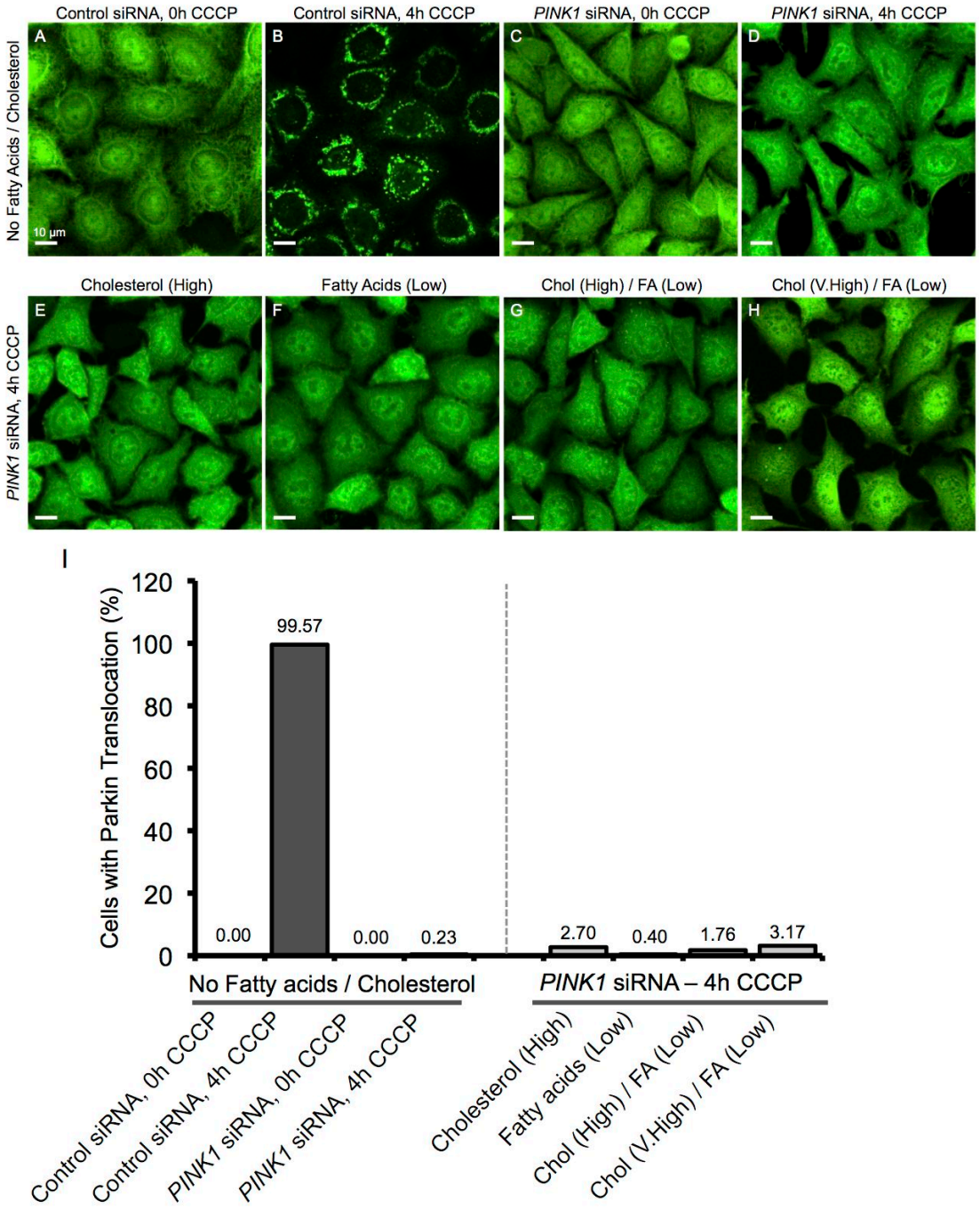

Figure 6.12 Rescuing PINK1-dependent Parkin translocation with fatty acids and cholesterol. YFP-Parkin.HeLa cells were treated with control or *PINK1* siRNA for 4 days before the addition of either vehicle (A - D), cholesterol (E), fatty acids (F) or a combination of cholesterol and fatty acids (G & H) for 24 hours. Samples were then treated with either vehicle (A & C) or 10 µM CCCP (B, D, E - H) for 4 hours. Parkin translocation (YFP-Parkin – green) was assessed qualitatively (A - H) by fluorescence confocal microscopy (60x objective, 2x digital zoom, scale bar: 10 µm) and quantitatively as the percentage of cells with Parkin translocation (I). (I) Graphical representation of Parkin translocation quantification following the application of conditions A - H. Data represent 1 biological repeat with 5 FOV per condition. FA - fatty acids; Chol – cholesterol. High – high concentration; Low – low concentration; V.High – very high concentration.

were primed with vehicle (Figure 6.13 A, C, F & H), cardiolipin (Figure 6.13 B & G), PE (Figure 6.13 D & I) or a combination of cardiolipin and PE (Figure 6.13 E & J) for 24 hours. Following this, cells were treated with either vehicle or CCCP for 4 hours, as

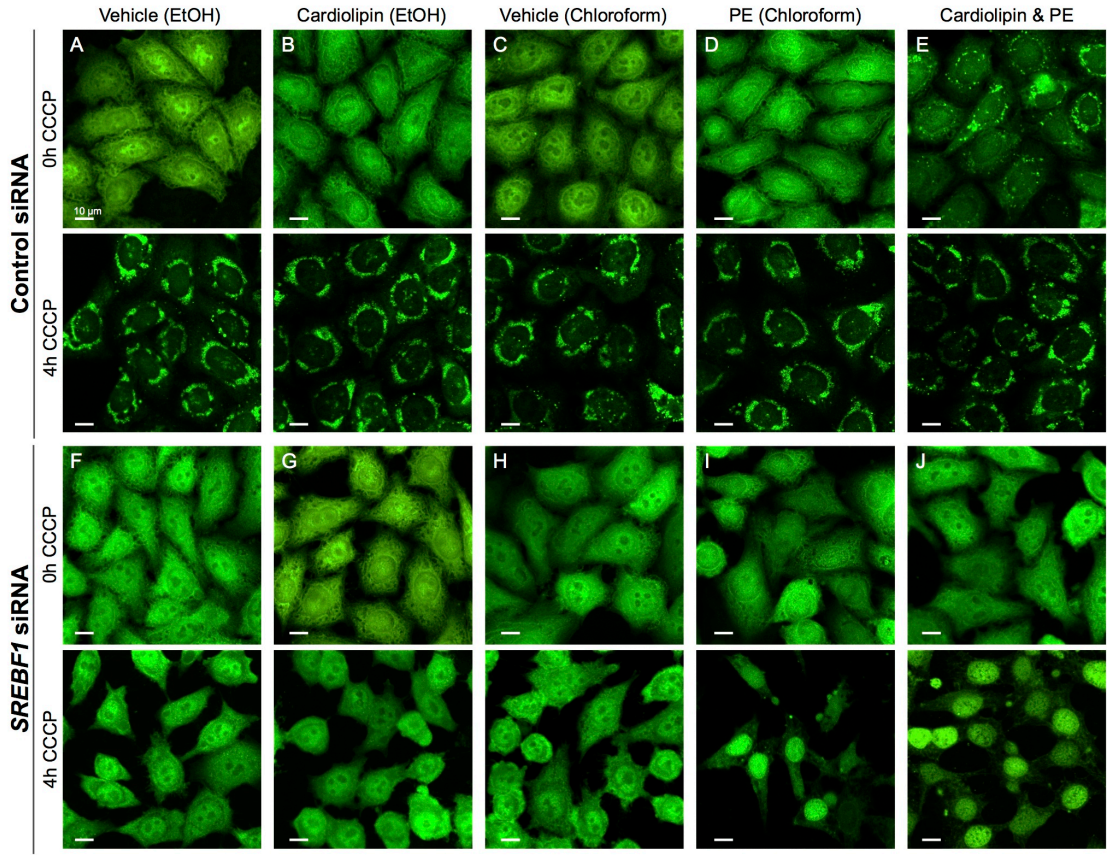

Figure 6.13 Rescuing SREBP1-dependent Parkin translocation with cardiolipin and PE. YFP-Parkin.HeLa cells were treated with control or *SREBF1* siRNA for 4 days before the addition of either vehicle (A, F, C & H), cardiolipin (B & G), PE (D & I) or a combination of cardiolipin and PE (E & J) for 24 hours. Samples were then treated with either vehicle or 10 µM CCCP for 4 hours as indicated. Parkin translocation (YFP-Parkin – green) was assessed qualitatively by fluorescence confocal microscopy (60x objective, 2x digital zoom, scale bar: 10 µm).

indicated. As shown previously, control siRNA-treated cells primed with 'vehicle' displayed no Parkin translocation in the absence of toxification, and a strong Parkin translocation phenotype upon CCCP application (Figure 6.13 A & C); as seen upon the application of cardiolipin (Figure 6.13 B) or PE (Figure 6.13 D).

As before, *SREBF1* siRNA showed a lack of Parkin translocation both in the absence and presence of CCCP toxification (Figure 6.13 F & H). However, following the exogenous application of cardiolipin (Figure 6.13 G), PE (Figure 6.13 I), or cardiolipin and PE (Figure 6.13 J), the inhibition of Parkin translocation persisted both with and without CCCP. These data indicate that at these concentrations, Parkin translocation is not rescued by exogenous application of cardiolipin or PE.

Interestingly in control samples, following the application of cardiolipin and PE together, non-toxified cells exhibited a partial translocation phenotype (Figure 6.13 E '0h CCCP'). In contrast, the same condition failed to induce translocation after *SREBF1* siRNA treatment (Figure 6.13 J, '0h CCCP'). The reason for this is currently unknown.

However, perhaps under control conditions, the observed Parkin translocation is triggered by increased toxicity caused by the combined presence of both lipids - an event that requires *SREBF1*. Alternatively, the combined treatment of CL and PE may alter the composition and behaviour of the mitochondrial membrane, perhaps preventing the mitochondrial import of PINK1. Here, full-length PINK1 stabilisation on the MOM would prompt Parkin to translocate even in the absence of CCCP. However, due to time constraints, this hypothesis remains to be tested.

In addition, following *SREBF1* silencing, PE, or the combined treatment of cardiolipin and PE caused a redistribution of Parkin to the nucleus after CCCP treatment (Figure 6.13 I & J, '4h CCCP'). This observation suggests that excess PE results in a CCCP-dependent redistribution of Parkin to the nucleus only in the absence of SREBP1. Currently, this observation cannot be adequately explained. However, it may be that in the absence of SREBP1, the combination of PE and CCCP stimulates the redistribution of Parkin to the nucleus for the degradation of Parkin target proteins. Indeed, following DNA damage, Parkin has previously been shown to translocate to the nucleus and promote DNA repair (Kao, 2009), setting a precedence for nuclear localisation under certain stress conditions.

6.3.7 PINK1 STABILISATION FOLLOWING CCCP

As mentioned, recent studies have shown that PINK1 is stabilised on the outer membrane of damaged mitochondria in a $\Delta\Psi$m-dependent manner, leading to the translocation of Parkin from the cytoplasm (Matsuda et al, 2010; Narendra et al, 2010). Under basal conditions, healthy mitochondria exert a hyperpolarised membrane, leading to the import of full-length PINK1 through the translocase complexes TOM and TIM23. At the MIM, PINK1 undergoes rapid cleavage by MPP (Greene et al, 2012; Jin et al, 2010) and PARL (Deas et al, 2011; Jin et al, 2010) and subsequent release into the cytosol for proteasomal degradation by the N-end rule pathway (Yamano & Youle, 2013). However, in the event of reduced $\Delta\Psi$m, such as following CCCP treatment, full-length PINK1 is no longer imported into the mitochondria. Instead, it decorates the MOM, promoting the relocation of Parkin to the mitochondria, activation of latent Parkin E3-ligase activity, ubiquitination of mitochondrial Parkin substrates, and the removal of damaged mitochondria via mitophagy (Matsuda et al, 2010; Narendra et al, 2008; Narendra et al, 2010). If PINK1 fails to stabilise on the MOM, even in the presence of CCCP Parkin no longer receives the signal to undergo translocation, hence blocking PINK1/Parkin-mediated mitophagy (Matsuda et al, 2010; Narendra et al, 2010).

To further our understanding of the influence of *SREBF1* and *FBXW7* on the PINK1/Parkin-pathway, PINK1 redistribution to mitochondria following CCCP was analysed (Figure 6.14). Here, HeLa cells were treated with control, *FBXW7* or *SREBF1* siRNA, prior to transient transfection of PINK1-GFP. Following this, cells were subjected to vehicle- (Figure 6.14 A) or CCCP-treatment (Figure 6.14 B) for 1 hour. The co-localisation of PINK1-GFP with the mitochondrial marker, ATP5A was assessed via fluorescence microscopy (Figure 6.14 A & B), and manually quantified as the percentage of cells exhibiting no-, partial- or complete colocalisation of PINK1-GFP with ATP5A (Figure 6.14 C).

In the absence of toxification, control siRNA-treated cells exhibited a diffuse, cytoplasmic PINK1-GFP distribution, with almost no mitochondrial colocalisation (Figure 6.14 A). However, following CCCP toxification, the majority of control cells displayed almost complete PINK1-GFP colocalisation with ATP5A (Figure 6.14 B). *FBXW7* siRNA mirrored the data obtained with control siRNA application. However, where *SREBF1* siRNA treatment produces a comparable PINK1-GFP distribution in the absence of CCCP (Figure 6.14 A), following CCCP treatment, a partial block on PINK1-GFP colocalisation with ATP5A is observed, with many more cells displaying either ‘no colocalisation’ or a ‘partial colocalisation’ phenotype (Figure 6.14 B).

These data infer that whilst *FBXW7* appears to have no influence upon the stabilisation of PINK1 following CCCP application, *SREBF1* silencing causes a partial block of PINK1 stabilisation. This partial block may be due to changes in the lipid composition of the mitochondrial membrane, causing alterations in characteristics such as membrane fluidity and thickness. Such events may reduce the efficiency with which PINK1 associates with- and remains held upon- the MOM. In this respect, it may be interesting to assess if basal PINK1 is able to undergo mitochondrial import and cleavage following *SREBF1* silencing, or whether this manipulation prevents a general association between PINK1 and mitochondria.

Nevertheless, this assay suggests that *SREBF1* is acting upstream, and *FBXW7* is acting downstream, of PINK1 stabilisation in the PINK1/Parkin-pathway. However, whether the *SREBF1*-dependent partial block of PINK1 stabilisation is sufficient to cause the robust block on Parkin translocation, is yet to be determined. For example, it may be that *SREBF1* plays a more complex, dual role in the PINK1/Parkin-pathway. This question could be tackled in part by overexpressing a non-cleavable form of full-length PINK1 in combination with *SREBF1* siRNA. Here, if Parkin translocation continues to be reduced, it would indicate that *SREBF1* also has a part to play

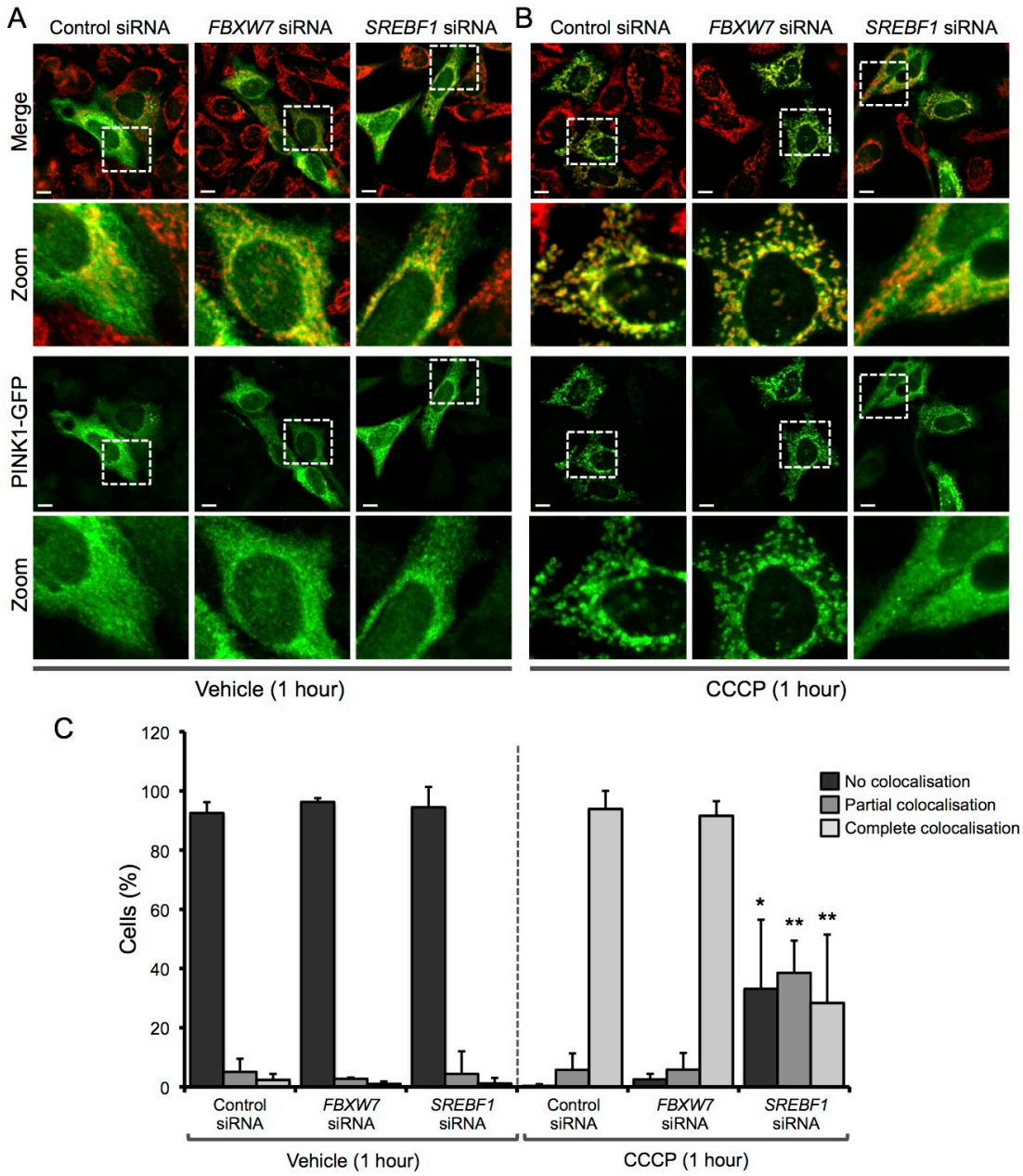

Figure 6.14 PINK1 redistribution following CCCP treatment. HeLa cells were treated with control, *FBXW7* or *SREBF1* siRNA for 3 days before the transient transfection of PINK1-GFP (green) for 16 hours. Cells were subjected to either vehicle (A) or 10 μM CCCP (B) for 1 hour, before being assessed for PINK1-GFP colocalisation with the mitochondrial network (ATP5A – red) by fluorescence confocal microscopy (60x objective, 2x digital zoom, scale bar: 10 μm). Confocal microscopy data were analysed manually as the percentage of cells with no PINK1-GFP colocalisation, partial PINK1-GFP colocalisation or complete PINK1-GFP colocalisation with ATP5A (C). Graphical data represent 3 biological repeats, each with 10 FOV per condition, per assay. Error bars represent standard deviation. * P<0.05, **P<0.01 (one-way ANOVA with Bonferroni's correction, compared with the equivalent control siRNA conditions).

downstream of PINK1 stabilisation. Additionally, it would be interesting to establish whether the *SREBF1*-dependent reduction in PINK1 stabilisation can be rescued by adding fatty acids and cholesterol back into the system as observed with Parkin translocation (section 6.3.6).

6.3.8 ANALYSIS OF SREBP1 PROTEIN LEVELS

In order to gain a more complete picture of the interaction between the PINK1/Parkin-pathway and SREBP-pathway, SREBP1 protein levels were assessed using western blot, in the presence of control, *PINK1* or *parkin* siRNA (Figure 6.15 A). In the control situation, a CCCP time-course between 0 – 6 hours resulted in the gradual decrease of flSREBP1 (Figure 6.15 A & B), suggesting the possibility of induced SREBP1 activation. One explanation for this proposed activation is that CCCP is known to cause both mitochondrial and ER-related stress (Bouman et al, 2011). Under these conditions, the ER unfolded protein response (UPR) is triggered, an event known to cause PERK-activation and a consequent decrease in the translation of INSIG-1. In the absence of INSIG, the SREBP-SCAP complex is no longer retained in the ER, and may undergo ER-to-Golgi translocation and activation.

Upon *PINK1* silencing, the same gradual decrease in flSREBP1 protein levels was observed. However, in contrast, silencing of *parkin* prevented this CCCP-dependent decrease in flSREBP1 levels, leading to a slight, but variable increase in flSREBP1 over time. Why *parkin* siRNA leads to a block of this process is currently unknown. It could be that in the event of ER-stress, Parkin is somehow required for flSREBP1 exit from the ER, or in mediating the branch of the UPR responsible for flSREBP1 activation. This theory has some support from the recent observation that Parkin expression is upregulated by the UPR following ER stress. Here, Parkin expression is activated by ATF4, a transcription factor downstream of PERK, which leads to a reduction in ER-stress-induced apoptosis (Bouman et al, 2011). Perhaps interaction analyses using an immunoprecipitation approach between Parkin, SREBP and its pathway interactors would go some way to elucidate the relationship between these proteins following CCCP treatment.

In order to understand fully the way with which CCCP and the PINK1/Parkin-pathway regulates SREBP1 protein levels, both isoforms of SREBP1 must be assessed. The SREBP1 antibody used in figure 6.15 is raised against an epitope able to detect both flSREBP1 (125 kDa) and mSREBP1 (68 kDa) (Appendix, Figure 9.3 A). However, despite this, the detection of mSREBP1 in this assay remained elusive (Appendix, Figure 9.3 B). These data indicate that either the antibody is unable to recognise mSREBP1, suggesting specificity issues, or that mSREBP1 was absent from the protein preparations.

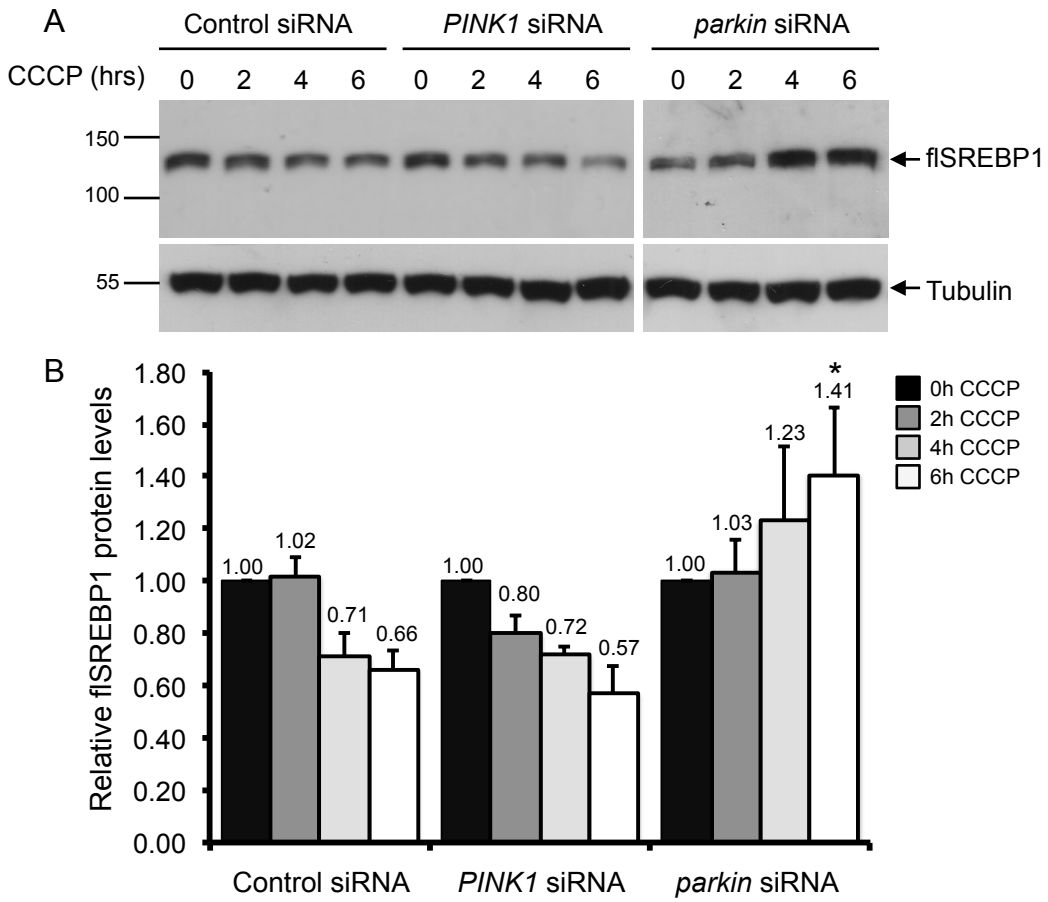

Figure 6.15 SREBP1 protein analysis following CCCP treatment. YFP-Parkin.HeLa cells were treated with control, *PINK1* or *parkin* siRNA for 4 days before being subjected to 0, 2, 4, or 6 hours of 10 µM CCCP. Full length SREBP1 (flSREBP1) protein levels (125 kDa) were assessed via western blot using anti-SREBP1 (2A4) antibody (Santa Cruz) (A). Average protein levels from 4 biological repeats were analysed using the ImageJ plugin, 'Gels,' (B). In each case, the relative protein levels were normalised to the tubulin loading control, and then '0 hours CCCP' for each siRNA condition. Error bars represent the standard deviation. *P<0.05 (one-way ANOVA with Bonferroni's correction, compared to equivalent 'Control siRNA' conditions).

To test the specificity of the antibody, YFP-Parkin.HeLa cells treated with either control or *SREBF1* siRNA were assessed (Appendix, Figure 9.3 B). Compared to control siRNA samples, *SREBF1* siRNA caused a robust reduction in the high molecular weight band, representing flSREBP1 (125 kDa). This established that the antibody was specific to SREBP1, as well as confirming the efficiency of *SREBF1* silencing following siRNA treatment. Next, the stability of activated mSREBP1 was tested through the application of the proteasomal inhibitor MG-132 (Appendix, Figure 9.3 C). Under these conditions, a low molecular weight band of ~68 kDa appeared, representing mSREBP1. These data indicated that the absence of the processed form of SREBP1 was due to its instability. As we know, mSREBP1 undergoes rapid proteasomal turnover in the nucleus (Wang et al, 1994), in a GSK3 and FBXW7-dependent manner (Kim et al, 2004; Punga et al, 2006; Sundqvist et al, 2005). To test whether the E3-ubiquitin ligase, FBXW7 was responsible for the observed turnover of mSREBP1,

FBXW7 was silenced (Appendix, Figure 9.3 D). As with MG-132 application, under these conditions, mSREBP1 was once again detectable.

Having established that the lack of mSREBP1 detection was due to its proteasomal turnover, analysis of the literature revealed that many groups working on the SREBP-family apply ALLN, a cysteine protease and proteasome inhibitor, prior to mSREBP1 analysis (Hegarty et al, 2005; Porstmann et al, 2008; Seegmiller et al, 2002; Sun et al, 2007; Wang et al, 1994). Through this adaption to the protocol, together with alternative sourcing of the SREBP1 (2A4) antibody and the loading of more protein per lane, mSREBP1 could be easily detected as a band of the correct size (Figure 6.16 A).

The effect of ALLN on YFP-Parkin.HeLa cells was tested in the presence or absence of CCCP treatment over a time-course of 6 hours (Figure 6.16). In the absence of CCCP, ALLN causes a gradual increase in the amount of both flSREBP1 (Figure 6.16 A & B) and mSREBP1 (Figure 6.16 A & C). This is likely due to mSREBP1 stabilisation, and a concomitant increase in flSREBP1 transcription, by persisting mSREBP1 activity. As observed in the absence of ALLN (Figure 6.15), flSREBP1 sees a gradual decrease over time in the presence of ALLN and CCCP (Figure 6.16 A & B). This is supposedly due to the activation of SREBP1 in the presence of CCCP-induced ER-stress. However, if CCCP is causing flSREBP1 activation, the expected outcome for mSREBP1, when comparing 'ALLN' to 'ALLN and CCCP' treated conditions would be a build-up of mSREBP1 levels in the nucleus. In contrast, CCCP induces a sharp decrease in mSREBP1 even when the proteasome is blocked by ALLN. These data would suggest that either in the presence of CCCP, the ALLN-dependent proteasome block is insufficient to prevent a proteasomal-dependent degradation, or that mSREBP1 is undergoing degradation via an alternative route such as autophagy. Alternatively, perhaps flSREBP1 itself may be being degraded rather than activated following CCCP treatment. In this circumstance, it is unlikely that degradation is occurring via the proteasomal route, as levels decrease robustly in the presence of ALLN. Therefore again, flSREBP1 may be being degraded via the autophagy route.

To test whether autophagy is playing a role in SREBP1 degradation in the presence of CCCP, combinations of ALLN, the autophagy inhibitor bafilomycin A_1 and CCCP were applied to YFP-Parkin.HeLa cells for 2 hours (Figure 6.17). As seen in Figure 6.16, large decreases in flSREBP1 (Figure 6.17 A & B, dark grey), and mSREBP1 (Figure 6.17 A & C, dark grey) were observed between 'ALLN' and 'ALLN and CCCP' treated conditions. If autophagy is involved in causing the degradation of either flSREBP1 or mSREBP1 following CCCP toxification, we would expect to see the maintenance of

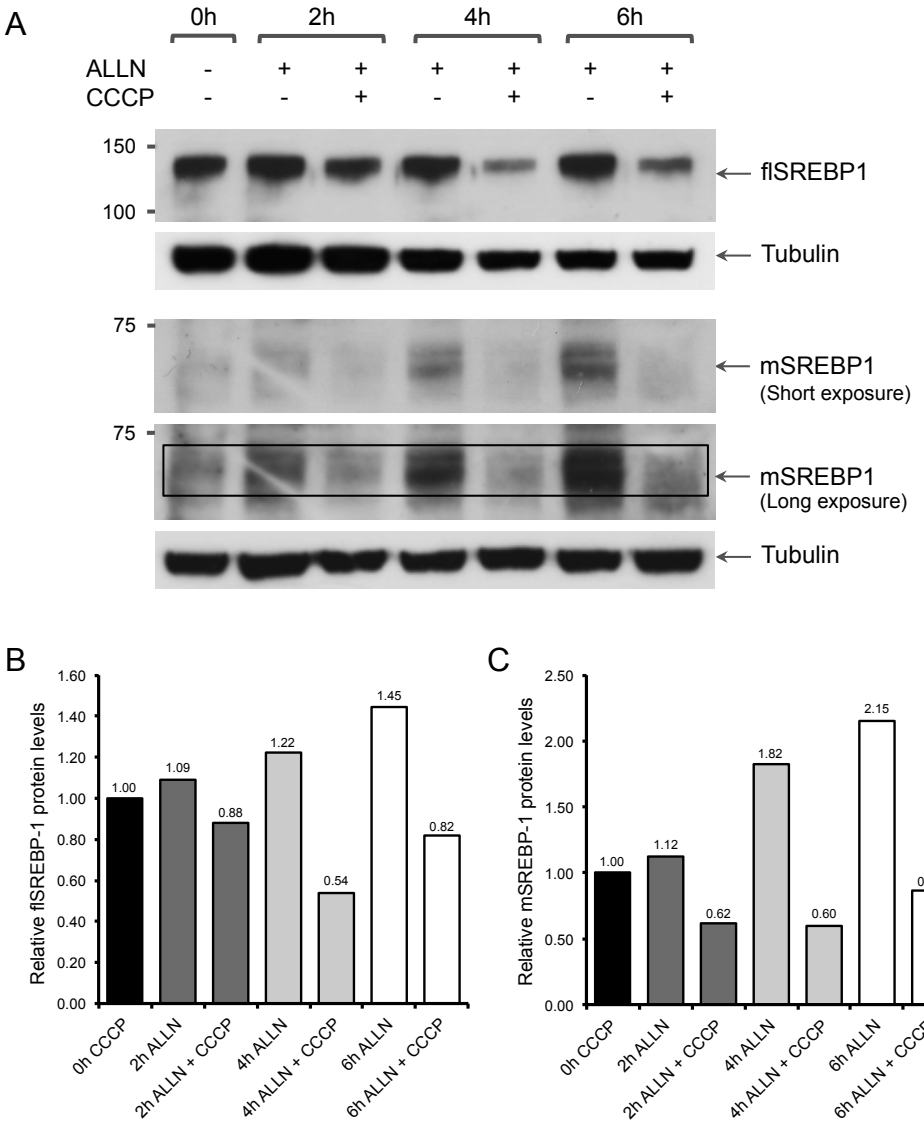

Figure 6.16 SREBP1 protein analysis following ALLN and CCCP treatment. YFP-Parkin.HeLa cells were subjected to 0, 2, 4, or 6 hours of 10 μM CCCP, in the absence or presence of 25 μg/ml ALLN as indicated. (A) flSREBP1 (125 kDa) and mSREBP1 (68 kDa) protein levels were assessed via western blot using anti-SREBP1 (2A4) antibody (BD Biosciences). Loading control – anti-tubulin. (B and C) Protein levels from 1 biological repeat were analysed using the ImageJ plugin, 'Gels,' In each case, the relative protein levels were normalised to the tubulin loading control, and then '0h CCCP.'

SREBP1 levels in 'bafilomycin and CCCP' treated conditions compared to 'bafilomycin' treated cells alone. However, there is a CCCP-dependent decrease in both flSREBP1 (Figure 6.17 A & B, light grey) and mSREBP1 (Figure 6.17 A & C, light grey), indicating that SREBP1 is not degraded by the autophagy route under these conditions. Interestingly, bafilomycin treatment alone causes a general decrease in flSREBP1 levels compared to untreated cells (Figure 6.17 A & B, black vs. light grey). This may be due to the fact that defective autophagy, as caused by bafilomycin treatment, causes increased ER-stress, therefore leading to the activation of flSREBP1 (Schonthal, 2012; Yin et al, 2012). This suggestion is supported by the slight increase

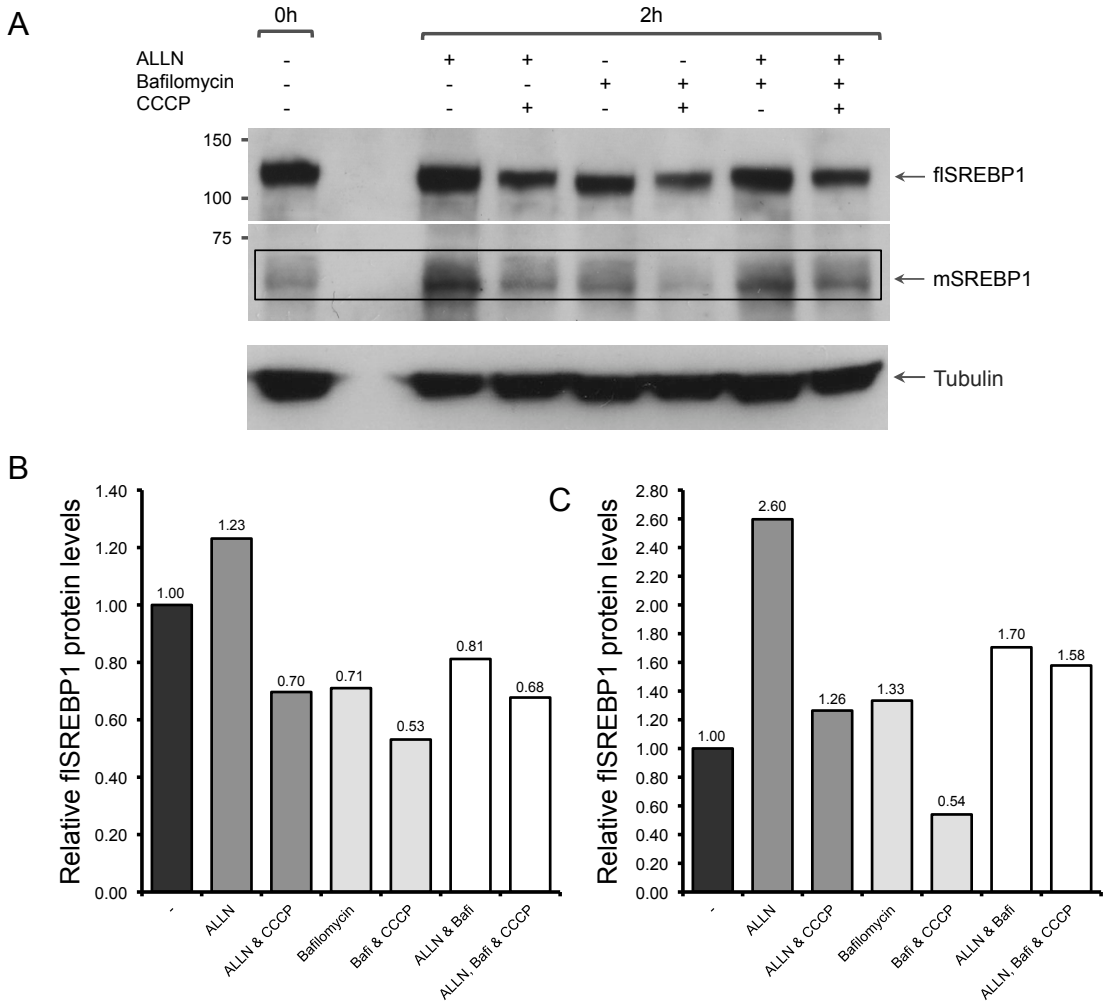

Figure 6.17 SREBP-1 protein analysis following ALLN, bafilomycin A_1 and CCCP treatment. YFP-Parkin.HeLa cells were treated subjected to 2 hours (2h) of 10 µM CCCP, in the absence or presence of 25 µg/ml ALLN and/or 20 nM bafilomycin as indicated. (A) flSREBP1 (125 kDa) and mSREBP1 (68 kDa) protein levels were assessed via western blot using anti-SREBP-1 (2A4) antibody (BD Biosciences). Loading control – anti-tubulin. (B and C) Protein levels from 1 biological repeat were analysed using the ImageJ plugin, 'Gels,' In each case, the relative protein levels were normalised to the tubulin loading control, and then to 'untreated' (-).

in mSREBP1 levels observed under the same conditions (Figure 6.17 A & C, black vs. light grey).

Finally, in order to determine whether SREBP1 protein levels are controlled by a combination of proteasomal and autophagic degradation, the combined inhibition of these routes by 'ALLN and bafilomycin' was analysed. Here, compared to 'ALLN' treatment alone, flSREBP1 is decreased in the absence of CCCP, indicating again that bafilomycin-induced ER-stress causes SREBP1 activation (Figure 6.17 A & B, dark grey vs. white). The levels of flSREBP1 are slightly higher than those seen with bafilomycin alone, suggesting that the additional proteasomal block leads to increased transcription of flSREBP1 (Figure 6.17 A & B, light grey vs. white). Following CCCP-treatment, only a small decrease in flSREBP1 levels is observed (Figure 6.17 A & B,

white). This suggests either that only a small additional increase in SREBP1 activation occurs by the addition of CCCP in combination with bafilomycin, or that a combination of proteasomal and autophagic degradation is responsible for the observed flSREBP1 decrease after ALLN or bafilomycin-treatment alone.

With regards to mSREBP1 in the presence of ALLN and bafilomycin, there is an increase in levels compared to untreated cells before CCCP-treatment, likely reflecting the activation of flSREBP1 by bafilomycin treatment, together with the inhibition of the proteasome by ALLN (Figure 6.17 A & C, black vs. white). However, following CCCP treatment, the levels of mSREBP1 change very little compared to non-CCCP treated conditions (Figure 6.17 A & C, white). This may be again, because the additional CCCP insult causes only a minor additional activation of SREBP1. Alternatively, it could indicate that following CCCP treatment; mSREBP1 is degraded in a proteasomal and autophagic–dependent manner.

In order to understand these data fully, first the observed effects would require confirmation via repeat analysis. However, overall, it may suggest that SREBP1 undergoes both autophagic and proteasomal degradation. This is perhaps understandable, as ER-stress activates the autophagy pathway, causing the engulfment of parts of the ER-network by autophagosomes (Bernales et al, 2006; Ding et al, 2007; Ogata et al, 2006). This may lead to the autophagic degradation of at least flSREBP1, which would reduce the amount of activated mSREBP1 available for translocation to the nucleus.

Despite failing to elucidate exactly what happens to SREBP1 isoforms following CCCP treatment, the application of ALLN, together with a new source of SREBP1 antibody and increased protein amounts has enabled the analysis of mSREBP1 levels. Hence, SREBP1 isoforms were again analysed following the application control, *PINK1* or *parkin* siRNA, in the presence or absence of ALLN and/or CCCP (Figure 6.18). First looking at flSREBP1, there is a clear decrease in levels following the application of CCCP in both control and *PINK1* siRNA-treated cells (Figure 6.18 A, B & D). However, as observed in figure 6.15, the dynamics of flSREBP1 following *parkin* siRNA application deviate from that seen with control siRNA (Figure 6.18 C & D). Here, despite an initial decrease in flSREBP1 after 2 hours of CCCP treatment, flSREBP1 levels begin to increase after 4 and 6 hours of CCCP.

Second, as shown in Figure 6.16, control conditions also produce a decrease in mSREBP1 levels over the CCCP time-course (Figure 6.18 A & E). This same pattern is

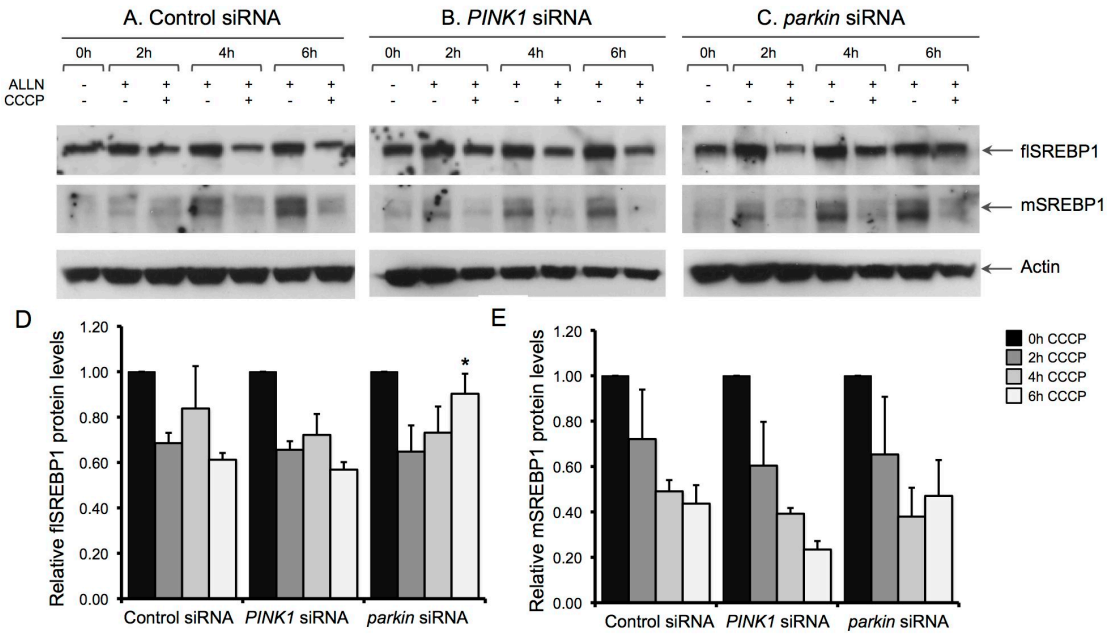

Figure 6.18 Analysis of SREBP1 isoforms following PINK1/Parkin-pathway silencing. YFP-Parkin.HeLa cells were treated with control (A), *PINK1* (B) or *parkin* (C) siRNA for 4 days before being subjected to 0, 2, 4, or 6 hours of ALLN (25 µg/ml) and/or CCCP (10 µM) as indicated. flSREBP1 (125 kDa) and mSREBP1 (68 kDa) protein levels were assessed via western blot using anti-SREBP1 (2A4) antibody (BD Bioscience) (A - C). Average flSREBP1 (D) and mSREBP1 (E) protein levels from 3 biological repeats were analysed using the ImageJ plugin, 'Gels.' In each case, the relative protein levels were normalised to the actin loading control, and then '0h CCCP'. Error bars represent the standard error. Equivalent conditions were analysed by one-way ANOVA with Bonferroni's correction. *P<0.05.

observed following the application of *PINK1* and *parkin* siRNA (Figure 6.18 B, C & E), indicating that the loss of these genes has no effect on mSREBP1 levels.

Taken together, these data suggest that CCCP promotes the gradual reduction of both flSREBP1 and mSREBP1 levels over a duration of 6 hours. This reduction in SREBP1 protein levels may be due to ER-stress caused by CCCP application. One of the consequences of the UPR is a temporary block of *de novo* translation until cellular homeostasis is restored. Therefore, CCCP may promote the conversion of flSREBP1 into mSREBP1, but block the translation of *de novo* protein for ER-replenishment. How these changes in SREBP1 protein levels are related to PINK1/Parkin-mediated mitophagy are currently unknown. However, interestingly, the loss of *parkin* alters the dynamics of flSREBP1, suggesting a feedback system between these two proteins. As ER-stress leads to increases in SREBP1-dependent lipid synthesis, and CCCP causes both mitochondrial and ER stress, it is conceivable that the PINK1/Parkin-pathway utilises SREBP-dependent lipids for the execution of mitophagy. In support of this, Parkin is a known lipid sensor (Kim et al, 2011), whose expression levels are enhanced upon CCCP treatment (Bouman et al, 2011). Following *SREBF1* siRNA treatment, the reduction in free lipid concentration, and hence the ability to undergo mitophagy may be sensed by Parkin, blocking it from translocating to damaged mitochondria. Why free

lipids are required for mitophagy is not yet understood. However, as lipids are essential for mitochondrial biogenesis, it may be that the cost of losing mitochondria, coupled with the lack of resources required to replenish those lost, cause the cell to block mitophagy initiation.

6.3.9 *DROSOPHILA IN VIVO* ANALYSIS

Currently, *in vivo* genetic interaction analyses between the SREBP-pathway and PINK1/Parkin-pathway are in the preliminary stages. However, there are a plethora of tools available to allow for a future in-depth assessment. In *Drosophila*, there is one *SREBF* ortholog, known as *helix loop helix protein 106 (HLH106)* and one *FBXW7* ortholog known as *archipelago (ago)*. Additionally, *Drosophila* also possess a single ortholog of *GSK3*, known as *shaggy (sgg).* Available stocks for each of these genes include overexpression, null-mutant and RNAi lines, allowing a wide scope for experimentation. The initial question to be addressed was whether the loss of SREBP-pathway genes cause phenotypes similar to *PINK1* (*PINK1^{B9}) and parkin* (*park^{25})* null-mutants. Following this assessment, key experiments begun to address whether overexpression or loss of SREBP-pathway genes were able to modify the *parkin* or *PINK1*-null phenotypes. Importantly, as described in section 1.6, both *parkin* and *PINK1* mutant flies exhibit almost identical phenotypes including male sterility, locomotor defects, mitochondrial swelling, DA neuron loss and muscle wasting. These phenotypes can be easily assessed in an experimental setting, with the simplest tests addressing locomotor defects by way of established climbing and flight assays. Here, *parkin* and *PINK1*-null mutants, and *PINK1* RNAi lines exhibit drastically reduced climbing and flight abilities (Clark et al, 2006; Greene et al, 2003; Park et al, 2006; Yang et al, 2006b). These simple phenotypes were employed in preliminary analyses, to assess the presence of genetic interactions between PINK1/Parkin- and SREBP-pathway members. Here, genetic combinations causing amelioration or exacerbation of the locomotor phenotypes were of interest.

6.3.9.1 Gene silencing with RNAi

Initial SREBP-pathway assessment involved climbing and flight analysis following the application of *HLH106* RNAi (Figure 6.19 A & B), *ago* RNAi (Figure 6.19 C & D) and *sgg* RNAi (Figure 6.19 E & F). Following *HLH106* silencing using two different RNAi lines, significant defects in both climbing and flight were observed, with *HLH106* RNAi line 2 producing the strongest phenotype in both cases (Figure 6.19 A & B). This may be because of greater knockdown efficiency in this RNAi line, or perhaps a higher

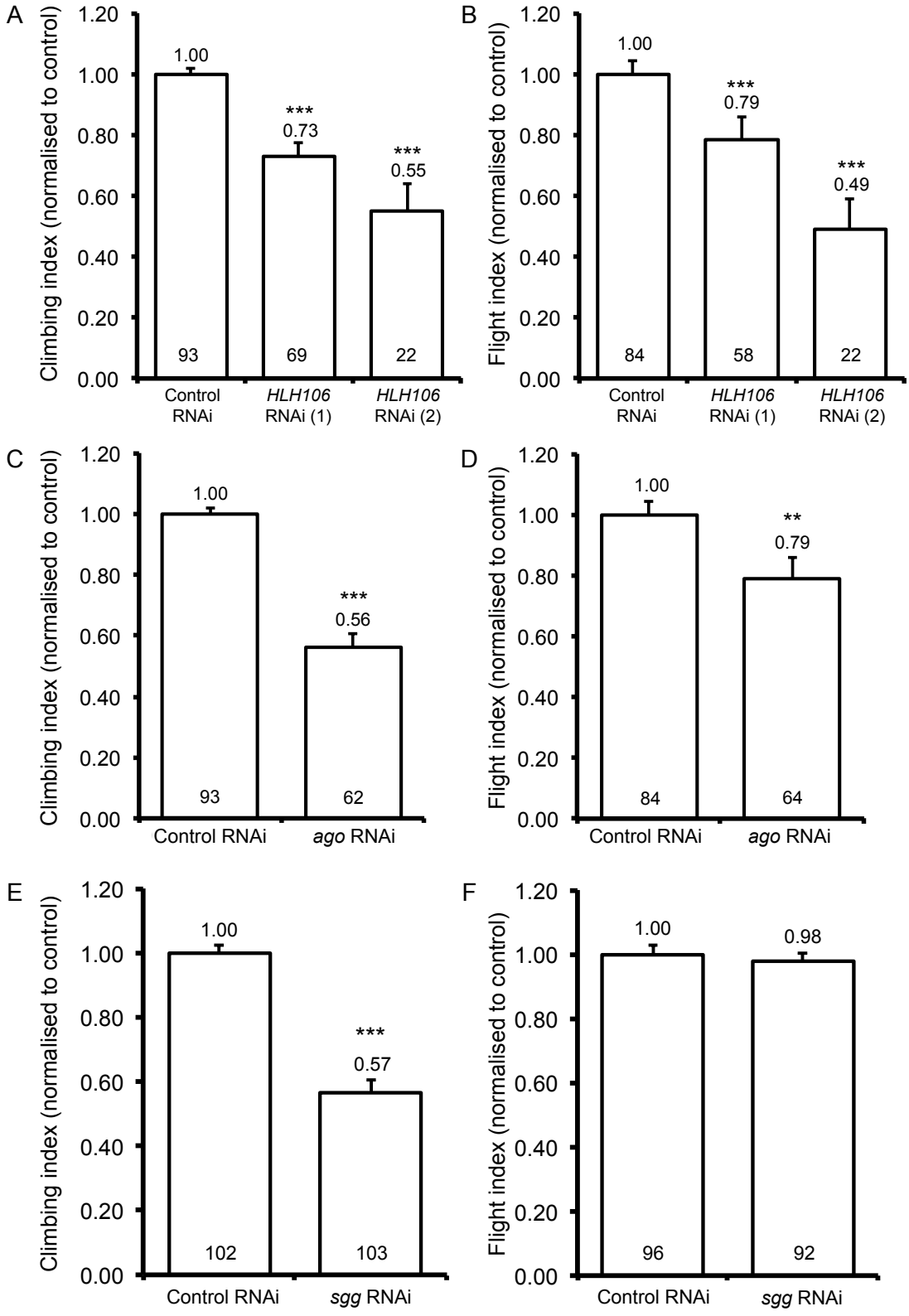

Figure 6.19 Locomotor responses in SREBP-pathway RNAi-treated *Drosophila*. *Drosophila* expressing RNAi against *HLH106* (A & B), *ago* (C & D) and *sgg* (E & F) via the GAL4-UAS system were assessed for their ability to climb (A, C & E) and fly (B, D & F). *HLH106* and *ago* RNAi was driven with the strong ubiquitous driver, daughterless, whereas *sgg* RNAi was driven using the weaker ubiquitous driver, Act5C. Error bars represent standard error. Figures within columns represent the number of animals tested per condition. Data were tested using either one-way ANOVA with Bonferroni's correction (A & B) or Student's t-test (C - F). **P<0.01, ***P<0.001.

degree of toxicity. One way to address this would be via qRT-PCR analysis of transcript levels, enabling the quantification of gene expression in these flies. In the case of *ago* RNAi, both climbing and flight are significantly reduced following gene silencing, with a stronger decrease observed in the climbing assay compared to the flight assay (Figure 6.19 C & D). This may be to do with tissue- and system-specificity, as the climbing assay tests both coordination and muscle strength, whereas the flight assay tests the reflex action of the indirect flight muscles. Typically, the climbing assay is a more sensitive test of locomotion, and is often less variable than the flight assay. Therefore, subtle defects may be detected in the climbing assay, but missed in the flight assay. Finally, *sgg* RNAi causes a climbing defect but not a flight defect (Figure 6.19 E & F). This again may be due to tissue- or system-specific effects of *sgg* silencing. Interestingly, *sgg* siRNA follows the same pattern as *ago* RNAi, which is in agreement with these two proteins having a shared function of *HLH106* proteasomal degradation. Overall these data are encouraging, as all SREBP-pathway components analysed phenocopy the loss of *PINK1* and *parkin* to some extent with regards to locomotor difficulties.

6.3.9.2 Genetic interaction analysis

Of particular interest is the possibility of a genetic interaction between the PINK1/Parkin-pathway and the SREBP-pathway. To test this possibility, initial efforts focused on the upregulation and/or downregulation of *HLH106* and *ago* in a $park^{25}$ mutant background (Figures 6.20 and 6.21 respectively). Here, the upregulation of wild-type *HLH106* in a $park^{25}$ mutant background produced lethality (Figure 6.20 A & B). This observation is intriguing as upregulation of *HLH106* in a wild-type background is viable (Figure 6.20 A & B). This could indicate a genetic interaction between *parkin* and *HLH106*, whereby increased *HLH106*-expression exacerbates *parkin*-null phenotypes.

A constitutively active (CA) variant of *HLH106*, missing its regulatory C-terminus (ΔC) was viable in both a wild-type and $park^{25}$ background, but failed to significantly alter the reduced climbing and flight observed in $park^{25}$ mutants (Figure 6.20 A & B). However, whilst this genetic combination produces live progeny, the flies are weak and completely unable to climb (Figure 6.20 A), despite performing moderately in the flight assay (Figure 6.20 B). These data suggest that again, overexpression of a CA form of *HLH106* produces tissue and/or system-specific effects, affecting co-ordination and leg strength, rather than indirect flight muscle reflexes. Intriguingly, the CA form of *HLH106* appeared less noxious than the wild-type form in both wild-type and $park^{25}$

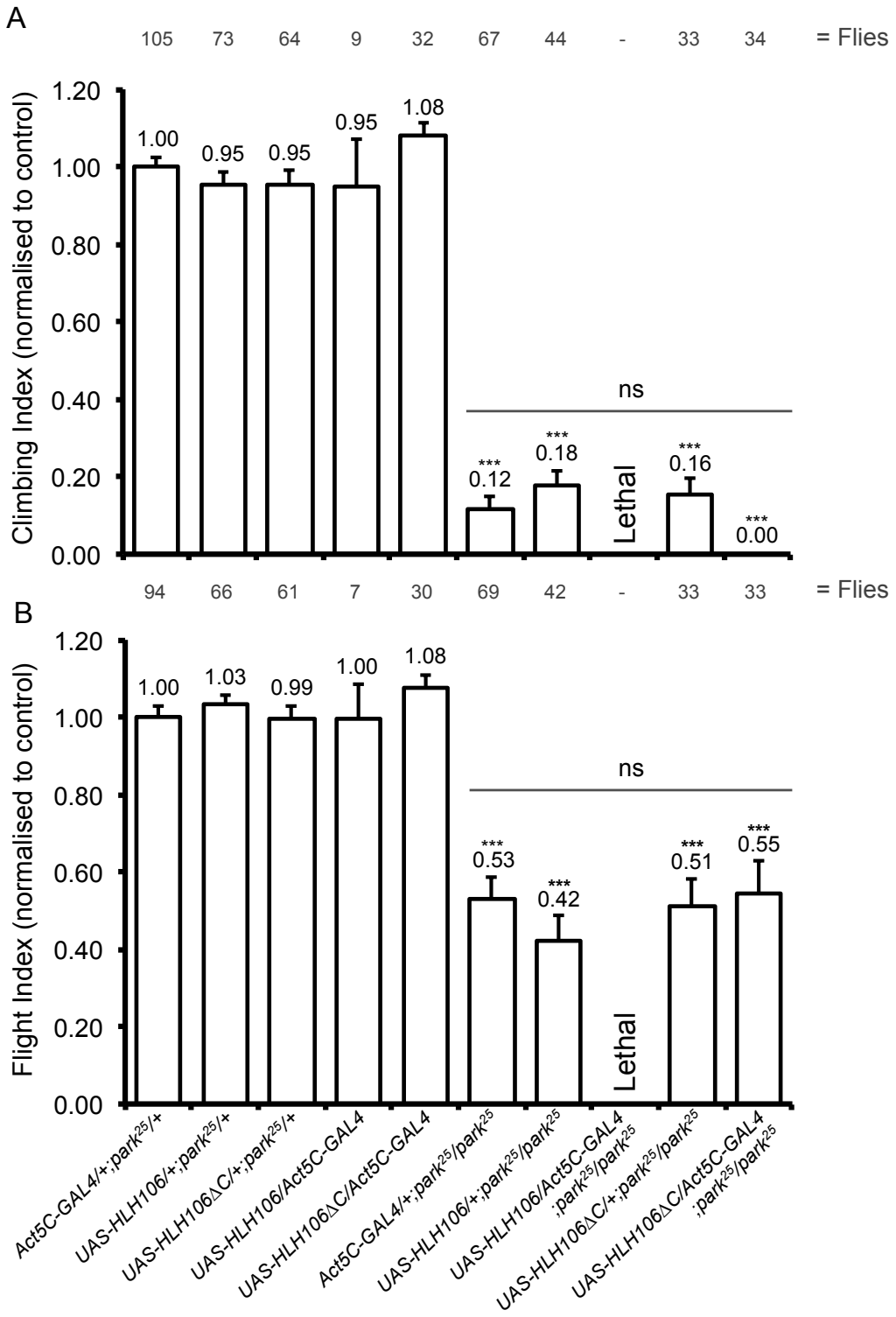

Figure 6.20 Locomotor responses in *park[25]* *Drosophila* following upregulation of HLH106 levels. *parkin*-null *Drosophila* (*park[25]*) were assessed for their ability to climb (A) and fly (B) following the overexpression of wild-type *HLH106* or constitutively active *HLH106ΔC* (*HLH106* without its regulatory C-terminus). *HLH106 overexpression* was driven by Act5C-GAL4. Assay controls were *park[25]* heterozygotes (wild-type) or homozygotes (mutant) in the presence of either *UAS-HLH106*, *UAS-HLH106ΔC* or the Act5C-GAL4 driver and *UAS-HLH106* and *UAS-HLH106ΔC driven by* .Act5C-GAL4. Error bars represent standard error. Figures above columns represent the number of animals tested per condition. Data were tested using one-way ANOVA with Bonferroni's correction compared to Act5C-GAL4/+;*park[25]*/+, ***P<0.001

backgrounds. The deleterious effect of wild type *HLH106* may be due to off-target toxicity, or perhaps the fact that wild-type *HLH106* is trapped in the ER, whilst CA *HLH106* freely activates its target genes.

The upregulation of wild-type *ago*, or a dominant negative *ago* transgene lacking its core F-box domain (*ago*Δ*F*) (Mortimer & Moberg, 2007), failed to modify the reduced climbing and flight phenotypes of the $park^{25}$ mutant (Figure 6.21 A & B). Additionally, a reduction in ago expression, with the employment of two mutant alleles, ago^{1} or ago^{3} (Moberg et al, 2001), also failed to modify the $park^{25}$ phenotypes (Figure 6.21 C & D). Here, flies were heterozygous for the *ago* mutant alleles, as complete deletion of *ago* is embryonic lethal (Data not shown, Mortimer & Moberg, 2007).

Altogether, these data suggest that overexpression of *HLH106* may exacerbate, but does not rescue locomotor phenotypes caused by the absence of *parkin*. However, alterations in *ago* expression levels have no obvious effect on the *parkin*-null phenotypes assessed. These data would therefore place *HLH106* and *ago* upstream of *parkin* in the PINK1/Parkin pathway. Next, it will be interesting to assess whether the overexpression or loss of these genes in a *PINK1*-null background are able to modify *PINK1*-associated locomotor defects, perhaps giving a clearer idea of how these genes interact. However, in the context of *SREBF1* at least, a rescue under these circumstances is perhaps unlikely, as data from cellular analyses suggest that *SREBF1* is upstream of *PINK1*.

6.4 DISCUSSION

In this chapter, I have outlined initial efforts made to understand the relationship between the SREBP-pathway and PINK1/Parkin-mediated mitophagy. Whilst the story is incomplete, these data have gone some way to suggest ways in which these pathways interact at a number of different levels, to coordinate mitochondrial quality control. Specifically, I have used genistein, the SREBP-pathway inhibitor, to show that the PINK1/Parkin-pathway effects observed following SREBP1 silencing are SREBP1-specific. Additionally, I have eliminated the possibility that the observed decreases in Parkin translocation are due to reduced *PINK1* expression levels, general autophagy blockage or the maintenance of the $\Delta\Psi$m under CCCP-treated conditions. Importantly, I have shown that fatty acids and cholesterol, the output of the SREBP-pathway, are able to rescue Parkin-translocation following *SREBF1* silencing, highlighting the importance of the maintenance of intracellular lipid levels for mitophagy induction. Interestingly, the application of fatty acids and cholesterol were insufficient to rescue

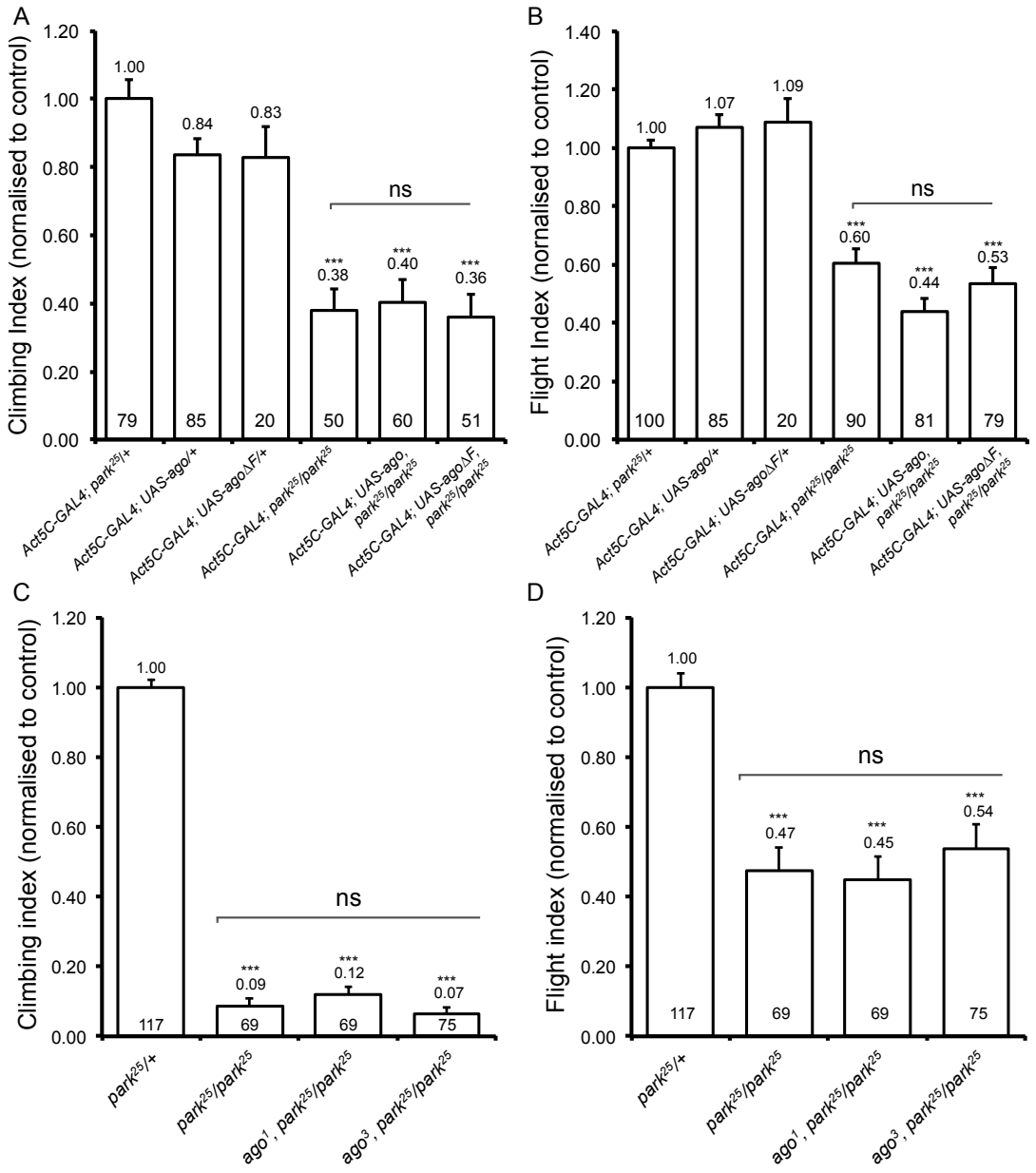

Figure 6.21 Locomotor responses in *park*^{25} *Drosophila* following altered *ago* levels. (A & B) *parkin*-null *Drosophila* (*park*^{25}) were assessed for their ability to climb (A) and fly (B) following the overexpression of wild-type *ago* or dominant negative *ago*Δ*F*. (*ago* without its F-box domain). *ago* overexpression was driven by Act5C-GAL4. (C & D) *park*^{25} *Drosophila* were assessed for their ability to climb (C) and fly (D) following reduced *ago* expression (the loss of one copy of *ago* - *ago*^{1} and *ago*^{3}). In all cases, assay controls were *park*^{25} heterozygotes (wild-type) and homozygotes (mutant). Error bars represent standard error. Figures within columns represent the number of animals tested per condition. Data were tested using one-way ANOVA with Bonferroni's correction, ***P<0.001.

the block on Parkin translocation observed under *PINK1* siRNA conditions, indicating that SREBP1 and lipid synthesis is upstream of PINK1 stabilisation. With regards to this, PINK1 stabilisation is partially compromised following *SREBF1* silencing, suggesting that SREBP1 and/or SREBP-dependent lipid synthesis plays a role in stabilising PINK1 on the outer mitochondrial membrane. Again, this observation would suggest that SREBP1 acts upstream of PINK1.

SREBP1 protein analysis has revealed a dynamic change in protein levels in the presence of CCCP. This may be due to flSREBP1 activation and the increased transcription of lipid-related genes. This would tie in with the suggestion that mitophagy will proceed only in a lipid-rich environment where degraded mitochondria may be replaced by increased mitochondrial biogenesis. Interestingly, *parkin* siRNA produces a change in SREBP-dynamics following CCCP, leading to the maintenance of flSREBP1 protein levels rather than the observed decrease seen under control siRNA conditions. This may indicate a feedback mechanism between Parkin and SREBP1, whereby under CCCP toxification, Parkin assesses the lipid-content of the cell, and if appropriate, initiates mitophagy, and the activation of SREBP1.

In vivo analysis of *Drosophila SREBP*, *FBXW7* and *GSK3* homologs showed that a reduction in gene expression by the application of RNAi caused a reduction in locomotor abilities, as is the case with *PINK1* and *Parkin* loss. However, no clear genetic interaction between these genes could be observed in preliminary experiments. This may suggest that these genes do not interact with each other. However, in combination with cellular data, these observations are consistent with the SREBP-pathway acting upstream of PINK1 and Parkin. An interesting avenue of exploration would be to assess the mitochondrial and dopaminergic neuron status of SREBP-pathway mutants and siRNA-treated flies, in order to assess similarities between SREBP- and PINK1/Parkin-phenotypes. Of note, both *dSREBP* RNAi-treated flies and *parkin*-null flies show a reduced body size and weight (Pesah et al, 2004; Porstmann et al, 2008). Additionally, *parkin*- and *PINK1*-null flies exhibit an abnormal wing posture, with wings being ‘held up’ in some instances (Clark et al, 2006; Yang et al, 2006a). A similar phenotype has also been observed following a reduction in *ago* expression (data not shown), which will warrant future investigation and quantification.

7. DISCUSSION

7.1 SUMMARY

Despite several years of intense study, a number of mechanistic questions remain regarding the process of PINK1/Parkin-mediated mitophagy. These include the manner in which mitochondria are damaged, and how these mitochondria are identified for degradation, the stimulus for PINK1 stabilisation on the MOM, and the mode of Parkin translocation. In a bid to resolve some of these remaining questions, the aim of this study was to perform a genome-wide RNAi screen in *Drosophila* S2R+ cells to identify novel promoters of PINK1/Parkin-mediated mitophagy. Here, Parkin redistribution from the cytoplasm to dysfunctional mitochondria was assessed, thereby providing the potential for gene discovery upstream of Parkin translocation. The desired outcome from this screen was to identify novel genes acting in the PINK1/Parkin-pathway, to promote mitochondrial degradation.

7.2 RNAi SCREENING

The initial stages of *Drosophila* S2R+ cell screening focused on assay development and optimisation, and included undertaking a number of small, subset screens. After finalising the best conditions for Parkin translocation assessment, a *Drosophila* whole genome primary screen was performed, where ~18,000 dsRNA amplicons were tested for their ability to alter the degree of Parkin translocation following CCCP toxification. Here ~1,000 dsRNA amplicons were found to produce an inhibitory effect on Parkin translocation. After visual analysis of images, this group was reduced to 625, through the removal of amplicons causing low levels of GFP, or cellular toxicity. Of these 625 primary hits, 115 were found to have a robust and reproducible effect following four rounds of confirmation screening. To test the ability of these hits to influence other aspects of mitochondrial biology, a series of secondary screens analysed three aspects of PINK1/Parkin-mediated mitochondrial homeostasis. These included an alternative method of toxin-induced Parkin translocation, mitochondrial morphology changes and toxin-induced mitochondrial aggregation in the juxtanuclear region. Having collated data from these screens, 65 dsRNA amplicons equating to 62 unique *Drosophila* genes were found to influence a range of PINK1/Parkin-related mitochondrial processes.

To assess the functional conservation of *Drosophila* hit genes across species, human orthologs corresponding to the final *Drosophila* hit list were identified, and re-tested for their ability to alter Parkin translocation and mitophagy in a human HeLa cell system.

Out of 90 human genes, 22 were found to reproducibility influence both processes, demonstrating cross-species conservation of gene function. Using bioinformatic analysis, a clear pathway emerged within this group, containing several members of a well-defined lipogenesis pathway. This group included the two strongest hit genes, together with a predefined functional link with Parkin. Because of this, the SREBP lipogenesis pathway was selected for follow-up study in a low-throughput setting.

7.2.1 EVALUATION OF SCREENING

Each step of the screening process presented challenges that had to be overcome. However the identification of a small group of genes with reproducible effects on PINK1/Parkin-pathway processes provides a marker for screen success.

The first major challenge to overcome was that silencing *dPINK1* in *Drosophila* S2R+ cells has little effect on CCCP-induced dParkin translocation. This was unexpected, as both *dPINK1* mRNA levels, via qRT-PCR analysis, and dPINK1 activity, via the assessment of dMfn steady state levels, followed the expected trend. In order to rationalise this, the assessment of dPINK1 protein distribution in S2R+ cells under basal conditions revealed a deviation from the situation reported in mammalian systems. In mammalian cells, due to its rapid turnover by the N-end rule pathway (Yamano and Youle, 2013), PINK1 protein levels are very low, with diffuse cytoplasmic distribution under basal conditions (Narendra et al., 2010). However in S2R+ cells, a substantial proportion of dPINK1 was found to co-localise with the mitochondrial marker, Mito-GFP (Figure 3.3). This observation is consistent with *Drosophila in vivo* data, whereby a fraction of cleaved dPINK1 is readily detectable under control conditions (Whitworth et al., 2008). These data suggest the presence of a stable fraction of cleaved dPINK1, perhaps explaining how Parkin translocation persists following *dPINK1* dsRNA application. Here, I posit that even following *dPINK1* mRNA silencing, this stable fraction of dPINK1 continues to produce a translocation event. However, despite continued translocation of Parkin, intriguingly both dMfn ubiquitination and perinuclear aggregation of damaged mitochondria are reduced in *PINK1* dsRNA-treated samples (Figures 3.8 D and 4.6 B). These data would suggest that cleaved dPINK1 can stimulate the redistribution of Parkin to the mitochondria, but is unable to activate latent Parkin E3-ligase activity, hence blocking the pathway at the level of Parkin target proteins. This is in agreement with recent published data that suggest that Parkin exists in an auto-inhibited state, where its tertiary structure occludes its E3-ligase domain (Trempe et al., 2013). However, following Parkin phosphorylation by PINK1 (Kondapalli et al., 2012), Parkin undergoes a conformational

change, activating its latent E3-ligase activity and allowing stable accumulation on the MOM (Lazarou et al., 2013), and interaction with target substrates.

In the light of the proposed divergence of PINK1 function between *Drosophila* and mammalian systems, the choices for proceeding were either to re-think the primary assay in order to develop a screening scenario with a suitable positive control, or continue developing the Parkin translocation screen in the absence of a positive control. Because S2R+ cells faithfully recapitulate many of the well-defined stages of the mitophagy pathway, including robust Parkin translocation upon CCCP-toxification, our decision was to continue focusing on this step, employing a 'no CCCP' control in the place of *dPINK1* dsRNA. Whilst this was a risk, the assay was still expected to identify genes involved in the translocation event and processes upstream of this, even in the absence of a *dPINK1* dsRNA effect.

Because of the issues with the *dPINK1* in the primary screen, the secondary screens proved extremely valuable, as they provided clues as to the specificity of the observed effects with regards to PINK1/Parkin-mediated mitophagy. First, paraquat, the redox cycling oxidative stressor, was employed to induce Parkin translocation. This assay demonstrated that the observed Parkin distributions were likely caused by mitochondrial dysfunction rather than a CCCP-specific effect. Second, the effect of gene silencing on mitochondrial morphology was assessed. This assay was particularly relevant to the PINK1/Parkin-pathway, as *PINK1* and *parkin* are known to promote fragmentation, with their RNAi producing a hyper-fused phenotype. Here, dsRNA amplicons causing a deviation from the wild-type morphology, particularly in the direction of *PINK1* and *parkin* dsRNA, were of interest. Third, a later stage of the mitophagy pathway was assessed, looking at the perinuclear aggregation of mitochondria following prolonged toxification. This aspect of screening was particularly important as it tested the mitophagy-specific effects of hit genes downstream of Parkin translocation. Here, mitochondrial perinuclear aggregation occurs prior to mitophagy proper (Okatsu et al., 2010; Vives-Bauza et al., 2010). Conspicuously, the obvious assay to implement here would have been the analysis of mitophagy itself. However, where reductions in the MIM marker ATP5A, are observed following prolonged toxification, this effect proved variable (Figure 3.4 C & D). The reasons for this are unknown, but may be a cell-specific effect, due to the mode of energy production in S2R+ cells. For example, cells reliant on oxidative respiration such as neurons are less likely to undergo widespread mitophagy compared to cells favouring glycolytic ATP-producing pathways such as HeLa cells (Gusdon and Chu, 2011). Therefore this would suggest that S2R+ cells favour oxidative phosphorylation, thus rely too heavily on their

mitochondrial population to degrade them. In agreement, *Drosophila* S2 cells have been reported to favour a predominantly mitochondria-dependent oxidative respiratory state (Freije et al., 2012). Crucially however, a recent *in vivo* study in *Drosophila* successfully demonstrated the occurrence of PINK1/Parkin-related mitophagy in a physiological setting, confirming the existence of this process in the whole *Drosophila* organism, and supporting the notion of cell-type specificity (Vincow et al., 2013). The study of mitophagy in *Drosophila* cell culture may be possible using alternative *Drosophila*-derived cell lines, although many of these are difficult to culture and small in size, making them less amenable to image-based experimentation.

Switching to a human cell system following the conclusion of *Drosophila* screening provided a number of clear benefits. These included the opportunity to confirm hit gene involvement in PINK1/Parkin-related processes across species, demonstrating conserved pathway function. Additionally, the use of HeLa cells allowed the assessment of Parkin translocation and mitophagy in the presence of a strong *PINK1* siRNA-dependent pathway block. Here, *PINK1* silencing virtually eliminated both processes. Notably, a small number of tested siRNAs were able to phenocopy the *PINK1* siRNA effect (Figures 5.11 and 5.15), demonstrating that in spite of aforementioned disparities, clear functional conservation between *Drosophila* and human PINK1/Parkin-processes exist. Critically, when assessing mitophagy proper for the first time, the majority of siRNA probes causing a strong Parkin translocation block also produced a robust mitophagy block (Figure 5.16 B), highlighting the pathway specificity of the observed effects.

Initial development of human screening techniques involved analysis of both HeLa and RPE1 cells. The aim was to screen both cell types in order to assess similarities and differences in pathway regulation between these two systems. Here, HeLa cells are a cancer cell line with abnormal genetic makeup, whereas RPE1 cells are an epithelial cell line with a relatively normal genetic profile. Comparisons in a low-throughput setting found that both cell lines undergo efficient Parkin translocation following short periods of CCCP toxification. However, where HeLa cells undergo moderate levels of mitophagy after 24 hours of CCCP treatment, RPE1 cells exhibit almost complete loss of their mitochondria by this time point (section 5.4). These data suggest differences in the readiness of these cells to lose their mitochondria, perhaps again due to the mode of energy synthesis favoured. However, another disparity was observed following *PINK1* silencing. In HeLa cells, *PINK1* loss completely blocks Parkin translocation and mitophagy (section 5.4). However, in RPE1 cells, whilst optimisation of *PINK1* siRNA silencing (Figure 5.7) resulted in a moderate *PINK1*-dependent block on Parkin

translocation, mitophagy continued to occur at levels comparable to control siRNA-treated samples (data not shown). The reasons for this lack of effect are currently unknown, but may be due to the expression of a functionally redundant mitophagy-promoting pathway in RPE1 cells. In support of this, a recent study in COS-7 cells reported that the endoplasmic reticulum (ER) E3-ubiquitin ligase, Gp78 ubiquitinates the fusion protein Mitofusin at mitochondria-associated ER-membrane sites (MAMs) following CCCP, promoting mitophagy in a Parkin-independent manner (Fu et al., 2013). Nevertheless, whilst the differences between HeLa and RPE1 cells raise many interesting questions that warrant further investigation, for the scope of this project HeLa cells alone were selected for screening, as here, PINK1/Parkin-processes are well defined in the literature.

Post-screening, the identification of several components of the SREBP1 pathway within the 22 final human hits was an exciting occurrence, particularly as the pathway member, FBXW7 had previously been found to act in an SCF-like complex with Parkin (Staropoli et al., 2003), as well as undergoing Parkin-dependent degradation (Ekholm-Reed et al., 2013). Importantly this pathway, with a central role in lipid homeostasis, contained the two strongest screen hits; therefore supporting its selection for further investigation. This decision was greatly influenced by the utilisation of the online protein interaction program, STRING (Jensen et al., 2009), which allowed easy visualisation of experimental and predicted interactions between hit genes (Figure 5.17). However, a cautionary note is that where the 'strongest' interactions are documented here, independent investigation using BioGRID, IntAct and HPRD highlighted protein interactions between hit genes that were absent from the STRING output (Table 5.5). Such findings highlight the limits of using bioinformatic tools, and outline the benefits of manual bioinformatic investigation.

Other pathway enrichments in the hit group included genes involved in histone acetyltransferase transcriptional activation and pre-mRNA splicing (Figure 5.17). However, these contained fewer pathway members, produced a weaker block on PINK1/Parkin-related processes compared to *SREBF1* and *FBXW7*, and lacked previous links to *parkin, PINK1* or associated pathway genes. On this basis, this group of genes was not considered for closer scrutiny in the context of this project. However, these, and other genes in the hit list still represent attractive candidates for PINK1/Parkin-mediated mitophagy regulation. Future work may therefore investigate pathway interactions between the remaining hits, *PINK1* and *parkin* in a low-throughput setting.

Comparing our whole genome screen to recently published whole genome RNAi data, it is clear that whilst there are some common trends, the overall outcomes are quite different. For example, a screen originally looking at the autophagic degradation of viral proteins, and later at CCCP-induced Parkin-dependent mitophagy, identified *SMURF1* as a promoter of these processes (Orvedahl et al., 2011). In our screen, *dSMURF1* has a z-score of -3.1, hence being included in the hit group. However, this gene failed to achieve hit status in confirmation and secondary screens. Additionally, two genome-wide RNAi screens specifically looking at Parkin translocation identified *Hexokinase 2* (*HK2*) (McCoy et al., 2013) and *ATPIF1* (Lefebvre et al., 2013) as promoters of Parkin translocation. Where *dHK2* only achieved a z-score of -0.7 in our screen, two *Drosophila* orthologs of *ATPIF1*, *CG13551* and *CG34423* each achieved a z-score of -2.6, trending in the right direction. It's worth noting that whilst the top hits from these screens deviated somewhat from our final hit list, these screens were all carried out in human cells, with some looking at slightly different aspects of mitochondrial biology. Because of this, it is perhaps unsurprising that the outcomes are different. Additionally, in many cases, full screening datasets are not published, with most groups only reporting on 'favourite' genes. This therefore does not rule out the inclusion of SREBP-pathway components within the hit lists of these screens.

7.3 THE SREBP-PATHWAY

The SREBP-pathway plays a central role in the regulation of cellular fatty acid, triglyceride and cholesterol synthesis and uptake. The core members of the pathway are the transcription factors, SREBP1 and 2, master regulators of the pathway, SCAP - a SREBP-escort, INSIG - a negative regulator of the pathway, S1P and S2P - proteases involved in SREBP activation, and GSK3 and FBXW7 – a serine threonine kinase and SCF-ubiquitin ligase complex member respectively, who coordinate SREBP turnover. Within the human hit list of 22 genes, *SREBF1/2*, as well as *FBXW7* and *GSK3A* were present. This signifies a clear enrichment of genes involved in the SREBP pathway.

The SREBP pathway can be activated by a number of stimuli including reductions in intracellular cholesterol and fatty acids, increases in carbohydrate availability and growth hormones, and ER stress. With this, inactive, full-length SREBP (flSREBP) undergoes ER-to-Golgi transport via the COPII-coated vesicular transport route, together with the escort protein, SCAP. Here, SREBP is proteolytically activated by S1P/S2P, releasing the active N-terminal bHLH domain into the cytoplasm. From here,

active or ‘mature’ SREBP (mSREBP) translocates to the nucleus, where transcription of target genes begins (Figure 6.1 B).

Importantly, activation of mSREBP target genes is tightly regulated on a number of levels. First, coactivators such as P300, PGC-1β and MED15 associate with mSREBP to enhance its transcriptional activity. Second, both SREBP and INSIG are transcriptional targets of mSREBP, allowing replacement of ER-localised flSREBP, as well as its negative regulator. Finally, the binding of mSREBP to its target promoters stimulates its phosphorylation by GSK3, leading to FBXW7-dependent ubiquitination and proteasomal degradation (Figure 6.4). Through this, sustained activation of the SREBP-pathway requires a continuous supply of mSREBP in the nucleus.

7.4 PINK1, PARKIN AND THE SREBP-PATHWAY

7.4.1 SREBP-PATHWAY GENES AND PARKIN TRANSLOCATION

Following the discovery of SREBP-pathway enrichment in the final human hit group, a germane question to pose was how other SREBP-related genes performed in whole genome screening. To answer this, *Drosophila* orthologs of the main pathway members were identified, and their behaviour over the screening process assessed. Encouragingly, many SREBP-pathway members produced a significant reduction in Parkin translocation in the primary screen (Table 6.1). These included the SREBP escort *dSCAP*, essential for SREBP activation (Rawson, 2003), the COPII coat elements, *dSec23* and *dSec24*, required for ER-to-Golgi transport, and the transcriptional coactivators *dP300* and *dMED15*. Importantly, the major SREBP transcriptional targets, *acetyl CoA carboxylase* (*dACAC*), *fatty acid synthase* (*dFASN*) and *stearoyl-CoA desaturase (dSCD)*, also produced a reduction in Parkin translocation. This implied that the canonical lipid-synthesis role of the SREBP pathway was important for Parkin translocation.

All of the aforementioned genes are positive regulators of the SREBP-pathway, therefore predicted to produce an equivalent phenotype to *SREBF1* silencing, Intriguingly, two negative regulators of the pathway, *dFBXW7* and *dGSK3* also produced a robust decrease in Parkin translocation, whilst having the opposite effect on lipid synthesis. The reasons for this unexpected occurrence are unclear, but possible explanations are discussed in detail in later sections.

SREBP-pathway genes failing to influence Parkin translocation included *dS1P* and *dS2P* proteases. This was a surprising result as the proteolytic activation of SREBP by S1P and S2P is essential for the transcription of SREBP-targets in mammals (Rawson, 2003). However, it may be that under screening conditions (i.e. CCCP-treatment), or in a *Drosophila* system, SREBP is activated via an alternative proteolytic route. Alternatively, S1P and S2P cleavage may be unnecessary for Parkin translocation or exhibit functional redundancy with other genes. Finally, the stability of these proteins may exceed the knockdown period, preventing manifestation of a phenotype.

The SREBP-coactivator *dPGC-1B*, involved in mitochondrial biogenesis, also failed to influence Parkin translocation. This may be because PGC-1β enhances the transcription of non-mitophagy-related SREBP genes, or that genes required for *PGC-1B*-dependent mitochondrial biogenesis are activated downstream of PINK1/Parkin-pathway activation.

Finally, the SREBP-target gene, *Acetyl CoA Synthetase (ACS*) was unable to inhibit Parkin translocation, despite target genes *ACAC, FASN* and *SCD* producing a strong block. During lipogenesis, ACS catalyses the conversion of acetate to acetyl CoA - the major substrate of the lipid synthesis pathway. However, whilst acetyl CoA is essential for lipid synthesis, ACS-dependent acetyl CoA production is not the sole source. Rather, citrate from the Kreb's cycle also supplies the lipid synthesis pathway with acetyl CoA via the action of ATP-citrate lyase (ACLY) (Hynes and Murray, 2010). With this, it is perhaps not surprising that the loss of *ACS* has a negligible effect on Parkin translocation. In contrast, ACAC, FASN and SCD are absolutely required for the conversion of acetyl CoA into lipids (Figure 6.3, Porstmann et al., 2009), explaining the robust block on translocation here.

7.4.2 NOVEL EVIDENCE FOR SREBP-PATHWAY INVOLVEMENT IN PD

The final results chapter in this study performed an in-depth analysis of SREBP1 and FBXW7 in the context of the PINK1/Parkin-pathway. Here the effects of *SREBF1* and *FBXW7* silencing on Parkin translocation and mitophagy were confirmed in a low-throughput setting (Figure 6.5). In order to elucidate the mechanism behind this pathway block, a number of approaches were taken. First, *PINK1* transcript levels were assessed, as any reduction in *PINK1* mRNA expression levels would likely influence the degree with which pathway processes were initiated. However, qRT-PCR analysis confirmed the maintenance of *PINK1* expression after downregulation of these genes (Figure 6.7). Next, the effect of reduced *SREBF1* and *FBXW7* expression on general

autophagy was analysed. Here the hypothesis proposed that a block in general autophagy might lead to the pathway phenotypes observed, due to saturation of the autophagy degradation route. In support of this hypothesis, evidence from the literature highlights a number of SREBP-pathway links with autophagy. First, phosphatidylethanolamine (PE) required for the lipidation of the autophagosome membrane component LC3, requires the SREBP-pathway for its synthesis (Dobrosotskaya et al., 2002). Second, SREBP2 has been linked to the regulation of starvation-induced autophagy, associating with promoters of autophagy-related genes including *ATG8* and *ATG4*, both involved in autophagosome biogenesis (Seo et al., 2011). Third, the E3-ligase Gp78, involved in SREBP-pathway activation, has been shown to induce mitophagy in a Parkin-independent manner (Fu et al., 2013). However, when general starvation-induced autophagy was assessed in the absence of *SREBF1* and *FBXW7*, the pattern of LC3 isoforms recapitulated that seen in control siRNA-treated conditions (Figure 6.9). Therefore, under the conditions tested the SREBP-pathway does not cause a general autophagy block.

Next, the effect of SREBP-pathway members on $\Delta\Psi$m was assessed. Here if gene silencing produced a reversal of ATP-synthase, the PINK1/Parkin-pathway would fail to be activated due to the maintenance of the $\Delta\Psi$m, and consequent absence of PINK1 stabilisation on the MOM. In the literature, there are some grounds for this theory, as a recent whole genome RNAi screen identified *ATPIF1* as producing this effect (Lefebvre et al., 2013). However, using the potentiometric dye, TMRM, no difference was observed between experimental and control siRNA-treated samples (Figure 6.10).

Having disregarded the above hypotheses, the next question was whether the canonical, lipid synthesising function of the SREBP-pathway was important for PINK1/Parkin-processes. For this, fatty acids and cholesterol in varying concentrations and combinations were added to *SREBF1* siRNA-treated cells prior to CCCP application (Figure 6.11). Indeed, certain combinations - specifically high concentrations of cholesterol and low concentrations of fatty acids, were able to partially rescue Parkin translocation. This result indicated that SREBP-pathway lipid synthesis was important for PINK1/Parkin-pathway activation. Interestingly, the addition of fatty acids and cholesterol in a *PINK1* siRNA-background was unable to rescue Parkin translocation defects (Figure 6.12), suggesting that SREBP-pathway lipids act upstream of PINK1 in the pathway. In support of this, *SREBF1* siRNA partially blocks PINK1 stabilisation on the MOM, suggesting a role for SREBP or SREBP-dependent lipid synthesis in PINK1 activation (Figure 6.14). Here it will be important to ascertain whether the application of exogenous lipids is able to rescue the reduction in

PINK1-stabilisation, hence confirming a role for lipids in this process. In contrast, *FBXW7* siRNA does not affect PINK1 stabilisation, suggesting that FBXW7 acts downstream of PINK1 in the PINK1/Parkin pathway.

Biochemical analysis of SREBP following CCCP toxification revealed a reduction in inactive flSREBP1 in a time-dependent manner, suggesting a CCCP-dependent activation event (Figure 6.15). Intriguingly, this decrease in flSREBP1 was blocked by *parkin* siRNA treatment, indicating a feedback loop, whereby Parkin is involved in stimulating flSREBP1 activation and consequent lipid synthesis. However, whilst this is an attractive proposition, data from mSREBP1 analysis under the same conditions also produced a marked decrease over time even in the presence of a proteasome inhibitor. The reason for this is currently unknown, but may be due to insufficient proteasomal blockage or degradation via an alternative route.

Finally, *in vivo* analysis of *dSREBF*, *dFBXW7* and *dGSK3* revealed climbing and flight defects in RNAi-treated animals comparable to those seen in *dPINK1* and *dparkin*-deficient animals (Figure 5.19). Whilst these data are encouraging and suggest defects in locomotion, without performing genetic interaction analyses it would be difficult to claim that these effects were PINK1/Parkin-pathway specific. Preliminary efforts to assess genetic interactions between *dSREBF*, *dFBXW7* and the PINK1/Parkin pathway focused on altering expression levels in a *dparkin*-null background. However, with the combinations tested, no obvious interactions were observed apart from increased lethality when overexpressing wild-type *dSREBF* in a *dparkin*-null background (Figure 6.20). This result ties in nicely with the suggestion that Parkin is involved in the activation of SREBP, as a constitutively active form of SREBP is viable in the absence of *dparkin*. Here, the next logical step is to test if *dSREBF* and *dFBXW7* overexpression are able to rescue *dPINK1* mutant phenotypes. However, as cellular data indicate that *dSREBF* acts upstream of PINK1, the expected outcome here would be negative. However, the same may not be true for *dFBXW7*, as discussed below (Section 7.4.3.1).

7.4.3 CLUES FROM THE LITERATURE

Currently, there are no reports in the literature of a direct interaction between SREBP and PINK1 or Parkin. Despite this, a recent GWAS study has identified a *SREBF1*-containing locus as a risk factor in the development of sporadic Parkinson's disease (Do et al., 2011). This report is of great significance to this study as it provides a clear link between *SREBF1*, our top screening hit, and sporadic PD. Not only has this gone

some way towards validating the screening process, it has also highlighted the possibility of a link between sporadic risk variants and familial causes of PD, with mitochondrial turnover a central theme.

Of the other SREBP-pathway genes included in the final hit group, FBXW7 has been found to physically and functionally interact with Parkin. First, FBXW7 was reported to act in a multi-protein, SCF-like complex with Parkin and Cullin-1, where the WD-repeat domain of FBXW7 interacts with the carboxy-terminus of Parkin in the region of the RING domains (Staropoli et al., 2003). This interaction mediates the proteasomal degradation of Cyclin E, a protein involved in apoptosis initiation following excitotoxicity in neurons, hence preventing cell death. Second, a recent study found that FBXW7 is degraded in a Parkin-dependent manner in primary neurons, allowing regulation of the SCF-complex (Ekholm-Reed et al., 2013). The outcome of this degradation event was the stabilisation of the MOM anti-apoptotic factor, Mcl-1. Together these data provide evidence that Parkin exerts cytoprotection by directly interacting with a SREBP-pathway member, strengthening the suggestion that these two pathways are functionally related.

More evidence for a common pathway function comes from the observation that both *dSREBF* RNAi expressing *Drosophila* and *parkin*-null *Drosophila* have a reduced body mass and wing size (Pesah et al., 2004; Porstmann et al., 2008) and *parkin*-null mice exhibit significantly lower weight-gain compared to control animals (Palacino et al, 2004). These phenotypic similarities suggest a role for these two proteins in cellular growth. In agreement with this, the SREBP pathway is activated following elevated growth hormone signaling and consequent activation of the Akt/mTOR pathway (Porstmann et al., 2009). Additionally, Parkin regulates cellular uptake of fatty acids via the stabilisation of the fatty acid transporter CD36 (Kim et al., 2011). Together these data suggest that SREBP and Parkin promote cell growth via increases in intracellular lipids.

7.4.3.1 Opposing actions of SREBP1, FBXW7 and GSK3A

SREBP-pathway analysis reveals that SREBP promotes lipid synthesis and organism growth, whilst GSK3A and FBXW7 switch off the SREBP-pathway by promoting mSREBP proteasomal turnover. These opposing roles suggest that *SREBF1* loss should produce opposite phenotypes to that of *GSK3A* and *FBXW7*. Indeed, mitochondrial morphology analysis revealed that *dSREBF* dsRNA causes a fragmented phenotype, whilst *dFBXW7* causes a fused phenotype (Table 6.1).

Additionally, in contrast to the growth-promoting effects of SREBP, FBXW7 is a known tumour suppressor (Mao et al., 2004), which inhibits cell proliferation via the degradation of Cyclin E and Myc (Moberg et al., 2001; Mortimer and Moberg, 2007). However, in the context of the PINK1/Parkin-pathway, all three genes produce a pathway block, to varying degrees. Why this is the case is currently unknown, however it may be that a tightly controlled balance of lipid levels within the cell is required for PINK1/Parkin-pathway activation. In support of this, epidemiology studies in sporadic Parkinson's disease have identified a correlation between decreased dietary fatty acids and cholesterol, and increased risk of developing PD (de Lau et al., 2005; de Lau et al., 2006; Huang et al., 2008). Conversely, the accumulation of free lipids in cells can also produce lipotoxicity leading to ER and mitochondrial stress. Particularly relevant to mitochondria, elevated saturated fatty acids lead to increased ROS production and a fall in $\Delta\Psi m$, ultimately causing cell death (Rial et al., 2010). Additionally, in the brains of PD patients, elevated polyunsaturated fatty acids have been detected (Sharon et al., 2003). These data highlight the importance of maintaining homeostatic lipid levels; where tipping the balance in either direction can have pathological consequences.

Further to the above, reduced cellular cholesterol via the administration of Simvastatin in cardiomyocytes inhibited the Akt/mTOR pathway and evoked Parkin translocation, and mitophagy, providing cardioprotection (Andres et al., 2013). This result contrasts with our data, where *SREBF1* silencing, and a presumed concomitant decrease in intracellular lipids leads to a block in Parkin translocation and mitophagy. However, while these results appear to contradict each other, they may help to explain why *FBXW7*, a negative regulator of the SREBP pathway produces the same phenotype as the loss of *SREBF1* itself. Intriguingly, in our study the application of exogenous cardiolipin and phosphatidylethanolamine produced a Parkin translocation phenotype in control, but not *SREBF1* siRNA-treated samples (Figure 6.13 E and J), suggesting that excess lipids can activate the PINK1/Parkin pathway.

Another possible explanation for the equivalent effects of *SREBF* and *FBXW7* siRNA could be that the persistence of mSREBP in the nucleus in the absence of proteasomal turnover leads to the hyper-activation of SREBP target genes, one of which is the negative pathway regulator INSIG. Here, over a silencing period of 4 days, INSIG levels may rise so high that SREBP becomes 'locked' in the ER despite the metabolic- or toxification- status of the cell. Under these circumstances, the loss of *FBXW7* may produce phenotypes equal to the loss of *SREBF* itself. One way to test this hypothesis would be to analyse the cellular lipid profile after silencing these two genes. Here, the prediction would be a decrease in free lipids under both conditions.

However, a more attractive explanation for the corresponding phenotypes of *SREBF1* and *FBXW7* is the occurrence of a non-SREBP related function of FBXW7. With regards to the degradation of FBXW7, Parkin was found to specifically target a cytosolic isoform of FBXW7, called FBXW7β, for proteasomal degradation (Ekholm-Reed et al., 2013). Here, FBXW7β degradation was shown to be required for cell survival following the application of oxidative stressors such as CCCP and tertiary-butyl hydroperoxide (tBHP). The purpose of this degradation was the resulting stabilisation of the pro-survival, anti-apoptotic MOM protein, Mcl-1 (Ekholm-Reed et al., 2013). Interestingly, FBXW7-dependent degradation of Mcl-1 requires prior phosphorylation of Mcl-1 by GSK3. Taking these data together, I speculate that the trigger for Parkin translocation is the requirement for Mcl-1 stabilisation on the MOM. Therefore, in the absence of Mcl-1 degradation through *FBXW7* and *GSK3* silencing, a stable fraction of Mcl-1 persists, eliminating Parkin translocation and subsequent mitophagy. In support of this study, it has been shown that upregulation of *Drosophila* Bcl-2 (*Buffy*), an anti-apoptotic MOM protein related to mammalian Mcl-1, can rescue $PINK1^{B9}$ mitochondrial dysfunction *in vivo* (Park et al., 2006), highlighting a clear relationship between anti-apoptotic mitochondrial proteins and the PINK1/Parkin-pathway.

In contrast to the predicted lack of rescue of *Drosophila dPINK1*-null phenotypes following *dSREBF* overexpression (section 7.4.2), if FBXW7 is responsible for Parkin translocation downstream of PINK1, *dFBXW7* overexpression may rescue the associated phenotypes. However, if Parkin translocation requires both PINK1 stabilisation and FBXW7, *dFBXW7* overexpression would have no effect on the PINK1-null phenotypes. Alternatively, if *dFBXW7* overexpression leads to potent *Buffy* degradation, the outcome may be widespread apoptosis and a resulting reduction in viability. Unfortunately this scenario was not tested due to time restrictions.

GSK3A, a gene with very close homology and functional redundancy to the more widely studied *GSK3B* (Doble et al., 2007; Doble and Woodgett, 2003) was also present in the final human hit list. Interestingly, where GSK3β is known to co-ordinate the regulation of SREBP-stability together with FBXW7, it was found to have no effect on the PINK1/Parkin-processes tested. However, the loss of *GSK3A* produced a moderate Parkin translocation and mitophagy block. The reasons for this are unknown, however, it may be that like GSK3β, GSK3α can phosphorylate SREBP, leading to its degradation. This would make GSK3α a negative regulator of the SREBP-pathway. However, this is yet to be formally tested. To address this, the stability of mSREBP following *GSK3A* and *GSK3B* silencing could be analysed, as *GSK3B* loss causes an increase in mSREBP protein levels (Bengoechea-Alonso and Ericsson, 2009;

Sundqvist et al., 2005). An alternative explanation is that *GSK3A* is a known transcriptional target of SREBP (Reed et al., 2008). Therefore loss of *SREBF* and *GSK3A* could produce equivalent phenotypes. However, as mentioned above, together with FBXW7β, GSK3 is known to be involved in Mcl-1 degradation, highlighting yet another role for GSK3.

Taken together, the preferred explanation for the equivalent pathway effects are as follows: 1) SREBP1 acts upstream of PINK1, where lipid synthesis is required for efficient stabilisation of PINK1 and translocation of Parkin to mitochondria. 2) FBXW7β and GSK3 act downstream of PINK1, with a role in degrading the anti-apoptotic mitochondrial factor, Mcl-1. Here, for mitophagy to proceed without the release of pro-apoptotic mitochondrial factors, Parkin must degrade FBXW7β at the MOM, hence promoting Mcl-1 stabilisation and cell-protection. Here, Parkin translocation may be triggered by the GSK3/FBXW7β-dependent reduction in Mcl-1 levels.

Presumably, FBXW7 siRNA targets the cytosolic β isoform, as well as the nuclear α and γ isoforms. However, the predicted increase in lipid synthesis resulting from FBXW7α/γ silencing and subsequent stabilisation of mSREBP is unlikely to override the loss of FBXW7β, as this is anticipated to act further downstream in the PINK1/Parkin-pathway.

7.5 MODEL

Despite a number of unresolved questions regarding the interaction between the PINK1/Parkin- and SREBP-pathways, a general picture of how these proteins interact to co-ordinate PINK1/Parkin-mediated mitophagy is beginning to emerge (Figure 7.1). First, increased cellular stress by CCCP toxification affects both the mitochondrial network (Figure 7.1 A) and the endoplasmic reticulum (Figure 7.1 B) (Bouman et al., 2011). In the context of the endoplasmic reticulum, CCCP is known to activate the unfolded protein response (UPR), involved in degrading misfolded proteins. A master regulator of this process is the stress-transducer kinase PERK. PERK acts by temporarily inhibiting *de novo* protein translation via the inactivating phosphorylation of eukaryotic translation initiation factor-2 (eIF2α) (Bobrovnikova-Marjon et al., 2008; Ron and Walter, 2007). Importantly, a known effect of this translation inhibition is the depletion of the SREBP-negative regulator INSIG (Lee and Ye, 2004). Therefore ER-stress, caused by CCCP, can promote the activation of SREBP and hence its target genes, purportedly by reducing the inhibitory effects of INSIG1. Interestingly, the

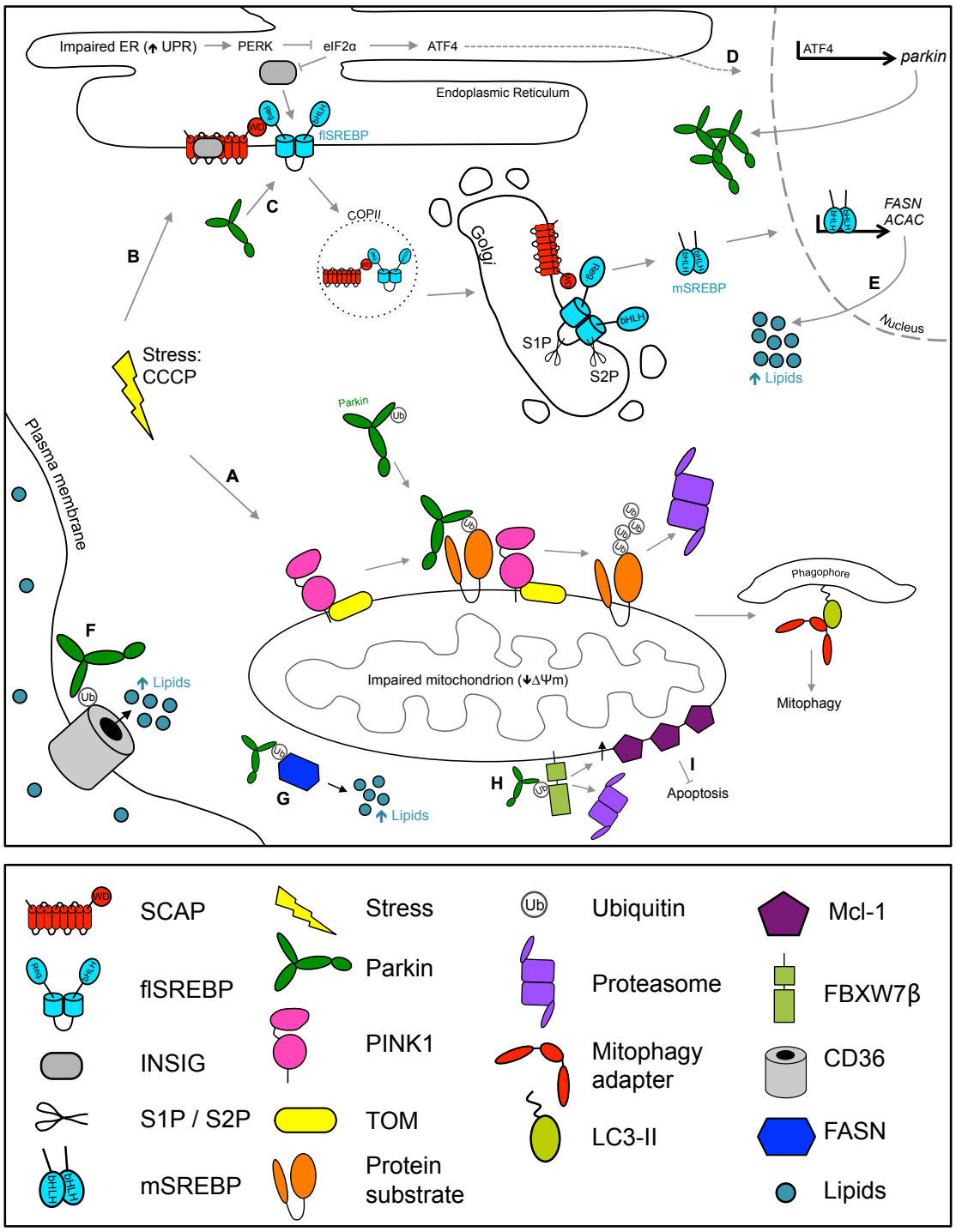

Figure 7.1 Model of novel interactions between the PINK1/Parkin-pathway, SREBP and FBXW7. Schematic of the proposed interaction between PINK1/Parkin-mediated mitophagy, SREBP in the endoplasmic reticulum and FBXW7 on the mitochondrial outer member. In brief, Parkin-dependent SREBP pathway activation, and CD36 & FASN stabilisation following cellular stress produces an increase in the lipid content of the cell. If this reaches a permissive level, Parkin undergoes translocation in an FBXW7-dependent manner, in order to prevent apoptosis and induce mitophagy. For cell survival, mitochondrial biogenesis replaces lost mitochondria via the utilisation of free lipids.

CCCP-dependent decrease in inactive flSREBP1 is blocked by the loss of Parkin (Figure 6.15), suggesting that Parkin is involved in the activation of SREBP1, conceivably via the ubiquitination and degradation of the existing INSIG pool (Figure 7.1 C).

Another outcome of the CCCP-induced UPR is the upregulation of *parkin* expression by the PERK-activated transcription factor ATF4 (Figure 7.1 D, Bouman et al., 2011), demonstrating a putative positive feedback loop, sustaining the activation of SREBP by Parkin. The outcome of SREBP-pathway activation is the upregulation of lipogenesis-pathway enzymes leading to increased lipid synthesis (Figure 7.1 E). This elevation in *de novo* lipid synthesis is proposed to be necessary for the initiation of PINK1/Parkin-mediated mitophagy. In support of this, Parkin can produce a local increase in cellular fatty acid content by ubiquitinating and stabilising the fatty acid transporter, CD36 (Figure 7.1 F). Additionally, upon CCCP, Parkin ubiquitinates and stabilises the essential lipid synthesis enzyme, FASN (Sarraf et al., 2013), two events presumably leading to an increase in intracellular lipid content (Figure 7.1 G). With this, the potential to generate replacement mitochondria is anticipated to be a permissive event, allowing mitophagy to proceed.

In the event of low intracellular lipids, such is the case following *SREBF* silencing; this model would predict a block of PINK1/Parkin-mediated mitophagy, upstream of PINK1 stabilisation. Conversely, in the case of 'permissive' lipid content, PINK1 is stabilised on the MOM (Figure 7.1 A), Parkin is recruited, Parkin substrates are ubiquitinated and mitophagy can proceed. Here, Parkin translocation may be dependent on steady-state Mcl-1 levels, which are regulated by FBXW7β (Figure 7.1 H). In this scenario, a CCCP-dependent reduction in Mcl-1 levels through the coordinated action of GSK3 and FBXW7β could trigger Parkin relocation. Consequently at the MOM, Parkin ubiquitinates FBXW7β leading to its removal by the proteasome, thus preventing initiation of apoptosis (Figure 7.1 I).

7.5.1 REVISED PINK1/PARKIN PATHWAY

If the proposed model is correct, this study has achieved its original aim of identifying novel members of the PINK1/Parkin-pathway. Here, I surmise that the role of the pathway is not only in the degradation of dysfunctional mitochondria, but also in the prevention of toxin-induced apoptosis via Mcl-1 stabilisation, and the increase in cellular lipid content for mitochondrial biogenesis. Support for the latter function of the PINK/Parkin-pathway comes from a study showing that Parkin promotes mitochondrial biogenesis by causing the degradation of PARIS - a transcriptional repressor of the mitochondrial biogenesis gene, *PGC-1A* (Shin et al., 2011). Additionally, high levels of dietary fat cause an increase in *parkin* expression (Kim et al., 2011), suggesting that excess cellular lipids may permit basal degradation and replacement of failing mitochondria. Finally, CD36 has been found on the MOM (Smith et al., 2011),

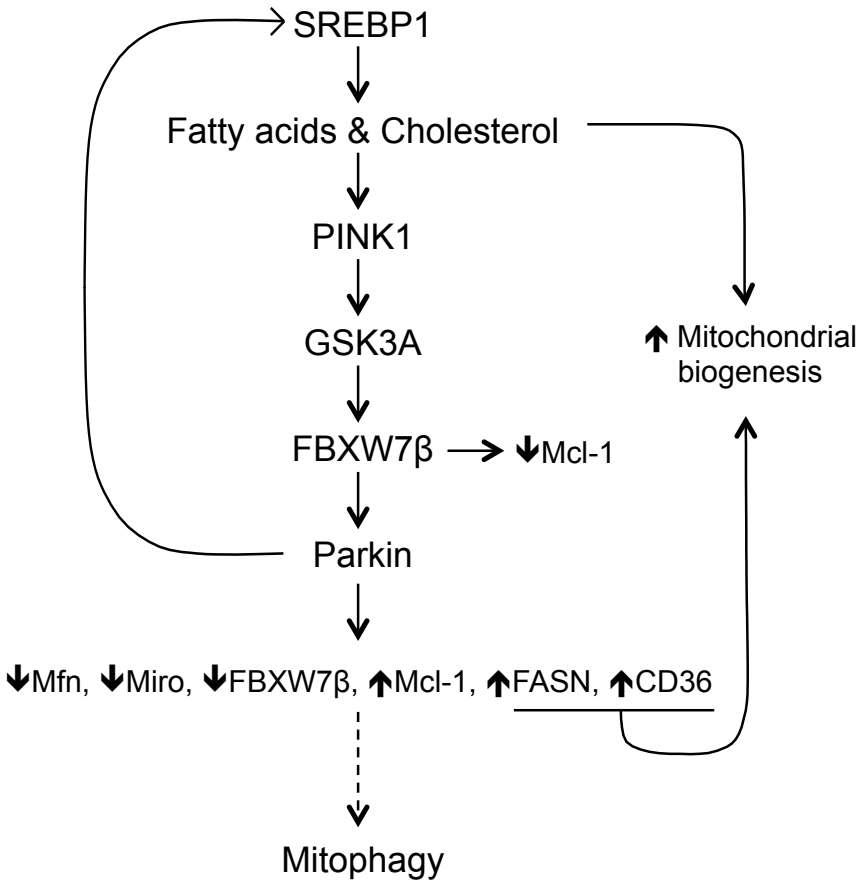

Figure 7.2 Revised PINK1/Parkin pathway containing SREBP, GSK3A and FBXW7. Schematic of the revised PINK1/Parkin pathway showing SREBP1 and SREBP1-depedent lipid synthesis upstream of PINK1; and GSK3A and cytoplasmic FBXW7 (FBXW7β) downstream of PINK1. Here, GSK3A and FBXW7β co-ordinate the removal of the pro-apoptotic factor, Mcl-1 from mitochondria following toxification. Parkin translocates to the nucleus and degrades FBXW7β, promoting the stabilisation of Mcl-1 and survival of the cell. Mfn and Miro are also degraded in a Parkin-dependent manner, leading the sequestering and isolation of damaged mitochondria. Finally, Parkin ubiquitinates and stabilises FASN and CD36 causing a local increase in lipid levels. Together with SREBP1-dependent lipogenesis, mitochondrial biogenesis can proceed.

suggesting that Parkin may also regulate the uptake of fatty acids into mitochondria for the initiation of mitochondrial biogenesis.

In summary, I have identified two novel promoters of PINK1/Parkin-mediated mitophagy upstream of Parkin translocation. Here, SREBP and SREBP-dependent lipid synthesis act upstream of PINK1 stabilisation, and FBXW7 acts downstream of PINK1 stabilisation (Figure 7.2). Despite a lack of full understanding of the regulatory mechanisms involved in these processes, this screen has identified a novel interaction between two well-studied pathways, the PINK1/Parkin-pathway, and the SREBP-pathway, both of which have been genetically linked to Parkinson's disease. This demonstrates a significant advance in our understanding of the way that mitochondrial turnover is regulated, and also highlights the possibility of a common, mitochondrial etiology for both familial and sporadic forms of Parkinson's disease.

8. REFERENCES

Adams MD, Celniker SE, Holt RA, Evans CA, Gocayne JD, et al. (2000) The genome sequence of Drosophila melanogaster. *Science* **287:** 2185-2195

Ahn TB, Kim SY, Kim JY, Park SS, Lee DS, Min HJ, Kim YK, Kim SE, Kim JM, Kim HJ, Cho J, Jeon BS (2008) alpha-Synuclein gene duplication is present in sporadic Parkinson disease. *Neurology* **70:** 43-49

Alberts B, Bray D, Lewis J, al. e (1994) The Respiratory Chain and ATP Synthase. *Molecular Biology of the Cell* **3rd edition**

Alegre-Abarrategui J, Christian H, Lufino MM, Mutihac R, Venda LL, Ansorge O, Wade-Martins R (2009) LRRK2 regulates autophagic activity and localizes to specific membrane microdomains in a novel human genomic reporter cellular model. *Human molecular genetics* **18:** 4022-4034

Allam MF, Campbell MJ, Hofman A, Del Castillo AS, Fernandez-Crehuet Navajas R (2004) Smoking and Parkinson's disease: systematic review of prospective studies. *Mov Disord* **19:** 614-621

Amati-Bonneau P, Valentino ML, Reynier P, Gallardo ME, Bornstein B, Boissiere A, Campos Y, Rivera H, et al. (2008) OPA1 mutations induce mitochondrial DNA instability and optic atrophy 'plus' phenotypes. *Brain* **131:** 338-351

Amemiya-Kudo M, Shimano H, Yoshikawa T, Yahagi N, Hasty AH, Okazaki H, Tamura Y, Shionoiri F, et al. (2000) Promoter analysis of the mouse sterol regulatory element-binding protein-1c gene. *J Biol Chem* **275:** 31078-31085

Andres AM, Hernandez G, Lee P, Huang C, Ratliff EP, Sin J, Thornton CA, Damasco MV, Gottlieb RA (2013) Mitophagy is required for acute cardioprotection by simvastatin. *Antioxid Redox Signal*

Ascherio A, Weisskopf MG, O'Reilly EJ, McCullough ML, Calle EE, Rodriguez C, Thun MJ (2004) Coffee consumption, gender, and Parkinson's disease mortality in the cancer prevention study II cohort: the modifying effects of estrogen. *Am J Epidemiol* **160:** 977-984

Ashburner M, Ball CA, Blake JA, Botstein D, Butler H, Cherry JM, Davis AP, Dolinski K, et al. (2000) Gene ontology: tool for the unification of biology. The Gene Ontology Consortium. *Nat Genet* **25:** 25-29

Bandopadhyay R, Kingsbury AE, Cookson MR, Reid AR, Evans IM, Hope AD, Pittman AM, Lashley T, Canet-Aviles R, Miller DW, McLendon C, Strand C, Leonard AJ, Abou-Sleiman PM, Healy DG, Ariga H, Wood NW, de Silva R, Revesz T, Hardy JA, Lees AJ (2004) The expression of DJ-1 (PARK7) in normal human CNS and idiopathic Parkinson's disease. *Brain : a journal of neurology* **127:** 420-430

Barthel A, Okino ST, Liao J, Nakatani K, Li J, Whitlock JP, Jr., Roth RA (1999) Regulation of GLUT1 gene transcription by the serine/threonine kinase Akt1. *The Journal of biological chemistry* **274:** 20281-20286

Beasley SA, Hristova VA, Shaw GS (2007) Structure of the Parkin in-between-ring domain provides insights for E3-ligase dysfunction in autosomal recessive Parkinson's disease. *Proceedings of the National Academy of Sciences of the United States of America* **104:** 3095-3100

Beckingham KM, Armstrong JD, Texada MJ, Munjaal R, Baker DA (2005) Drosophila melanogaster--the model organism of choice for the complex biology of multi-cellular organisms. *Gravit Space Biol Bull* **18:** 17-29

Beilina A, Van Der Brug M, Ahmad R, Kesavapany S, Miller DW, Petsko GA, Cookson MR (2005) Mutations in PTEN-induced putative kinase 1 associated with recessive parkinsonism

have differential effects on protein stability. *Proceedings of the National Academy of Sciences of the United States of America* **102:** 5703-5708

Bellani S, Sousa VL, Ronzitti G, Valtorta F, Meldolesi J, Chieregatti E (2010) The regulation of synaptic function by alpha-synuclein. *Commun Integr Biol* **3:** 106-109

Bellen HJ, Tong C, Tsuda H (2010) 100 years of Drosophila research and its impact on vertebrate neuroscience: a history lesson for the future. *Nat Rev Neurosci* **11:** 514-522

Bender A, Krishnan KJ, Morris CM, Taylor GA, Reeve AK, Perry RH, Jaros E, Hersheson JS, Betts J, Klopstock T, Taylor RW, Turnbull DM (2006) High levels of mitochondrial DNA deletions in substantia nigra neurons in aging and Parkinson disease. *Nat Genet* **38:** 515-517

Bengoechea-Alonso MT, Ericsson J (2007) SREBP in signal transduction: cholesterol metabolism and beyond. *Current opinion in cell biology* **19:** 215-222

Bengoechea-Alonso MT, Ericsson J (2009) A phosphorylation cascade controls the degradation of active SREBP1. *The Journal of biological chemistry* **284:** 5885-5895

Berg D, Niwar M, Maass S, Zimprich A, Moller JC, Wuellner U, et al. (2005) Alpha-synuclein and Parkinson's disease: implications from the screening of more than 1,900 patients. *Mov Disord* **20:** 1191-1194

Bernales S, McDonald KL, Walter P (2006) Autophagy counterbalances endoplasmic reticulum expansion during the unfolded protein response. *PLoS biology* **4:** e423

Berry C, La Vecchia C, Nicotera P (2010) Paraquat and Parkinson's disease. *Cell Death Differ* **17:** 1115-1125

Bertoncini CW, Fernandez CO, Griesinger C, Jovin TM, Zweckstetter M (2005) Familial mutants of alpha-synuclein with increased neurotoxicity have a destabilized conformation. *The Journal of biological chemistry* **280:** 30649-30652

Betarbet R, Sherer TB, MacKenzie G, Garcia-Osuna M, Panov AV, Greenamyre JT (2000) Chronic systemic pesticide exposure reproduces features of Parkinson's disease. *Nature neuroscience* **3:** 1301-1306

Biskup S, Moore DJ, Celsi F, Higashi S, West AB, Andrabi SA, Kurkinen K, Yu SW, Savitt JM, Waldvogel HJ, Faull RL, Emson PC, Torp R, Ottersen OP, Dawson TM, Dawson VL (2006) Localization of LRRK2 to membranous and vesicular structures in mammalian brain. *Annals of neurology* **60:** 557-569

Black SM, Schott ME, Batdorf BH, Benson BA, Rutherford MS, Levay-Young BK, Dalmasso AP (2010) IL-4 induces protection of vascular endothelial cells against killing by complement and melittin through lipid biosynthesis. *Eur J Immunol* **40:** 803-812

Blesa J, Phani S, Jackson-Lewis V, Przedborski S (2012) Classic and new animal models of Parkinson's disease. *J Biomed Biotechnol* **2012:** 845618

Bobrovnikova-Marjon E, Hatzivassiliou G, Grigoriadou C, Romero M, Cavener DR, Thompson CB, Diehl JA (2008) PERK-dependent regulation of lipogenesis during mouse mammary gland development and adipocyte differentiation. *Proceedings of the National Academy of Sciences of the United States of America* **105:** 16314-16319

Bonifati V (2007) LRRK2 low-penetrance mutations (Gly2019Ser) and risk alleles (Gly2385Arg)-linking familial and sporadic Parkinson's disease. *Neurochem Res* **32:** 1700-1708

Bonifati V, Rizzu P, Squitieri F, Krieger E, Vanacore N, van Swieten JC, Brice A, van Duijn CM, Oostra B, Meco G, Heutink P (2003a) DJ-1(PARK7), a novel gene for autosomal recessive, early onset parkinsonism. *Neurol Sci* **24:** 159-160

Bonifati V, Rizzu P, van Baren MJ, Schaap O, Breedveld GJ, Krieger E, et al. (2003b) Mutations in the DJ-1 gene associated with autosomal recessive early-onset parkinsonism. *Science* **299:** 256-259

Bonneh-Barkay D, Reaney SH, Langston WJ, Di Monte DA (2005) Redox cycling of the herbicide paraquat in microglial cultures. *Brain Res Mol Brain Res* **134:** 52-56

Bouman L, Schlierf A, Lutz AK, Shan J, Deinlein A, et al. (2011) Parkin is transcriptionally regulated by ATF4: evidence for an interconnection between mitochondrial stress and ER stress. *Cell Death Differ* **18:** 769-782

Boutros M, Kiger AA, Armknecht S, Kerr K, Hild M, Koch B, Haas SA, Paro R, Perrimon N (2004) Genome-wide RNAi analysis of growth and viability in Drosophila cells. *Science* **303:** 832-835

Bower JH, Maraganore DM, McDonnell SK, Rocca WA (1999) Incidence and distribution of parkinsonism in Olmsted County, Minnesota, 1976-1990. *Neurology* **52:** 1214-1220

Braak H, Del Tredici K, Rub U, de Vos RA, Jansen Steur EN, Braak E (2003) Staging of brain pathology related to sporadic Parkinson's disease. *Neurobiol Aging* **24:** 197-211

Braak H, Ghebremedhin E, Rub U, Bratzke H, Del Tredici K (2004) Stages in the development of Parkinson's disease-related pathology. *Cell Tissue Res* **318:** 121-134

Brand AH, Perrimon N (1993) Targeted gene expression as a means of altering cell fates and generating dominant phenotypes. *Development* **118:** 401-415

Briggs MR, Yokoyama C, Wang X, Brown MS, Goldstein JL (1993) Nuclear protein that binds sterol regulatory element of low density lipoprotein receptor promoter. I. Identification of the protein and delineation of its target nucleotide sequence. *The Journal of biological chemistry* **268:** 14490-14496

Brown AJ, Sun L, Feramisco JD, Brown MS, Goldstein JL (2002) Cholesterol addition to ER membranes alters conformation of SCAP, the SREBP escort protein that regulates cholesterol metabolism. *Mol Cell* **10:** 237-245

Brown MS, Goldstein JL (1997) The SREBP pathway: regulation of cholesterol metabolism by proteolysis of a membrane-bound transcription factor. *Cell* **89:** 331-340

Brown MS, Goldstein JL (1999) A proteolytic pathway that controls the cholesterol content of membranes, cells, and blood. *Proceedings of the National Academy of Sciences of the United States of America* **96:** 11041-11048

Burchell VS, Nelson DE, Sanchez-Martinez A, Delgado-Camprubi M, Ivatt RM, Pogson JH, Randle SJ, Wray S, Lewis PA, Houlden H, Abramov AY, Hardy J, Wood NW, Whitworth AJ, Laman H, Plun-Favreau H (2013) The Parkinson's disease-linked proteins Fbxo7 and Parkin interact to mediate mitophagy. *Nature neuroscience*

Canet-Aviles RM, Wilson MA, Miller DW, Ahmad R, McLendon C, Bandyopadhyay S, Baptista MJ, Ringe D, Petsko GA, Cookson MR (2004) The Parkinson's disease protein DJ-1 is neuroprotective due to cysteine-sulfinic acid-driven mitochondrial localization. *Proceedings of the National Academy of Sciences of the United States of America* **101:** 9103-9108

Castello PR, Drechsel DA, Patel M (2007) Mitochondria are a major source of paraquat-induced reactive oxygen species production in the brain. *The Journal of biological chemistry* **282:** 14186-14193

Chan CS, Gertler TS, Surmeier DJ (2009) Calcium homeostasis, selective vulnerability and Parkinson's disease. *Trends Neurosci* **32:** 249-256

Chan NC, Salazar AM, Pham AH, Sweredoski MJ, Kolawa NJ, Graham RL, Hess S, Chan DC (2011) Broad activation of the ubiquitin-proteasome system by Parkin is critical for mitophagy. *Human molecular genetics* **20:** 1726-1737

Chartier-Harlin MC, Dachsel JC, Vilarino-Guell C, Lincoln SJ, Lepretre F, Hulihan MM, Kachergus J, Milnerwood AJ, et al. (2011) Translation initiator EIF4G1 mutations in familial Parkinson disease. *Am J Hum Genet* **89:** 398-406

Chaudhuri KR, Healy DG, Schapira AH (2006) Non-motor symptoms of Parkinson's disease: diagnosis and management. *Lancet Neurol* **5:** 235-245

Chaugule VK, Burchell L, Barber KR, Sidhu A, Leslie SJ, Shaw GS, Walden H (2011) Autoregulation of Parkin activity through its ubiquitin-like domain. *Embo J* **30:** 2853-2867

Chen D, Gao F, Li B, Wang H, Xu Y, Zhu C, Wang G (2010a) Parkin mono-ubiquitinates Bcl-2 and regulates autophagy. *J Biol Chem* **285:** 38214-38223

Chen H, Chomyn A, Chan DC (2005) Disruption of fusion results in mitochondrial heterogeneity and dysfunction. *The Journal of biological chemistry* **280:** 26185-26192

Chen H, Vermulst M, Wang YE, Chomyn A, Prolla TA, McCaffery JM, Chan DC (2010b) Mitochondrial fusion is required for mtDNA stability in skeletal muscle and tolerance of mtDNA mutations. *Cell* **141:** 280-289

Chen Y, Dorn GW, 2nd (2013) PINK1-phosphorylated mitofusin 2 is a Parkin receptor for culling damaged mitochondria. *Science* **340:** 471-475

Chia NY, Chan YS, Feng B, Lu X, Orlov YL, Moreau D, Kumar P, Yang L, Jiang J, Lau MS, Huss M, Soh BS, Kraus P, Li P, Lufkin T, Lim B, Clarke ND, Bard F, Ng HH (2010) A genome-wide RNAi screen reveals determinants of human embryonic stem cell identity. *Nature* **468:** 316-320

Chinta SJ, Andersen JK (2005) Dopaminergic neurons. *The international journal of biochemistry & cell biology* **37:** 942-946

Choi J, Sullards MC, Olzmann JA, Rees HD, Weintraub ST, Bostwick DE, Gearing M, Levey AI, Chin LS, Li L (2006) Oxidative damage of DJ-1 is linked to sporadic Parkinson and Alzheimer diseases. *The Journal of biological chemistry* **281:** 10816-10824

Choi P, Snyder H, Petrucelli L, Theisler C, Chong M, Zhang Y, Lim K, Chung KK, Kehoe K, D'Adamio L, Lee JM, Cochran E, Bowser R, Dawson TM, Wolozin B (2003) SEPT5_v2 is a parkin-binding protein. *Brain research Molecular brain research* **117:** 179-189

Chung KK, Zhang Y, Lim KL, Tanaka Y, Huang H, Gao J, Ross CA, Dawson VL, Dawson TM (2001) Parkin ubiquitinates the alpha-synuclein-interacting protein, synphilin-1: implications for Lewy-body formation in Parkinson disease. *Nat Med* **7:** 1144-1150

Clark AJ, Bloch K (1959) The absence of sterol synthesis in insects. *The Journal of biological chemistry* **234:** 2578-2582

Clark IE, Dodson MW, Jiang C, Cao JH, Huh JR, Seol JH, Yoo SJ, Hay BA, Guo M (2006) Drosophila pink1 is required for mitochondrial function and interacts genetically with parkin. *Nature* **441:** 1162-1166

Clark SL, Jr. (1957) Cellular differentiation in the kidneys of newborn mice studies with the electron microscope. *J Biophys Biochem Cytol* **3:** 349-362

Clemens JC, Worby CA, Simonson-Leff N, Muda M, Maehama T, Hemmings BA, Dixon JE (2000) Use of double-stranded RNA interference in Drosophila cell lines to dissect signal

transduction pathways. *Proceedings of the National Academy of Sciences of the United States of America* **97:** 6499-6503

Cocheme HM, Murphy MP (2008) Complex I is the major site of mitochondrial superoxide production by paraquat. *The Journal of biological chemistry* **283:** 1786-1798

Conway KA, Lee SJ, Rochet JC, Ding TT, Williamson RE, Lansbury PT, Jr. (2000) Acceleration of oligomerization, not fibrillization, is a shared property of both alpha-synuclein mutations linked to early-onset Parkinson's disease: implications for pathogenesis and therapy. *Proceedings of the National Academy of Sciences of the United States of America* **97:** 571-576

Conway KA, Rochet JC, Bieganski RM, Lansbury PT, Jr. (2001) Kinetic stabilization of the alpha-synuclein protofibril by a dopamine-alpha-synuclein adduct. *Science* **294:** 1346-1349

Corti O, Hampe C, Koutnikova H, Darios F, Jacquier S, Prigent A, Robinson JC, Pradier L, Ruberg M, Mirande M, Hirsch E, Rooney T, Fournier A, Brice A (2003) The p38 subunit of the aminoacyl-tRNA synthetase complex is a Parkin substrate: linking protein biosynthesis and neurodegeneration. *Hum Mol Genet* **12:** 1427-1437

Corti O, Lesage S, Brice A (2011) What genetics tells us about the causes and mechanisms of Parkinson's disease. *Physiol Rev* **91:** 1161-1218

Costello S, Cockburn M, Bronstein J, Zhang X, Ritz B (2009) Parkinson's disease and residential exposure to maneb and paraquat from agricultural applications in the central valley of California. *Am J Epidemiol* **169:** 919-926

Cross DA, Alessi DR, Cohen P, Andjelkovich M, Hemmings BA (1995) Inhibition of glycogen synthase kinase-3 by insulin mediated by protein kinase B. *Nature* **378:** 785-789

Dagda RK, Cherra SJ, 3rd, Kulich SM, Tandon A, Park D, Chu CT (2009) Loss of PINK1 function promotes mitophagy through effects on oxidative stress and mitochondrial fission. *J Biol Chem* **284:** 13843-13855

Darios F, Corti O, Lucking CB, Hampe C, Muriel MP, Abbas N, Gu WJ, Hirsch EC, Rooney T, Ruberg M, Brice A (2003) Parkin prevents mitochondrial swelling and cytochrome c release in mitochondria-dependent cell death. *Hum Mol Genet* **12:** 517-526

Dauer W, Przedborski S (2003) Parkinson's disease: mechanisms and models. *Neuron* **39:** 889-909

Dawson TM, Ko HS, Dawson VL (2010) Genetic animal models of Parkinson's disease. *Neuron* **66:** 646-661

de Lau LM, Bornebroek M, Witteman JC, Hofman A, Koudstaal PJ, Breteler MM (2005) Dietary fatty acids and the risk of Parkinson disease: the Rotterdam study. *Neurology* **64:** 2040-2045

de Lau LM, Koudstaal PJ, Hofman A, Breteler MM (2006) Serum cholesterol levels and the risk of Parkinson's disease. *Am J Epidemiol* **164:** 998-1002

Deas E, Plun-Favreau H, Gandhi S, Desmond H, Kjaer S, Loh SH, Renton AE, Harvey RJ, Whitworth AJ, Martins LM, Abramov AY, Wood NW (2011) PINK1 cleavage at position A103 by the mitochondrial protease PARL. *Human molecular genetics* **20:** 867-879

Delettre C, Lenaers G, Griffoin JM, Gigarel N, Lorenzo C, et al. (2000) Nuclear gene OPA1, encoding a mitochondrial dynamin-related protein, is mutated in dominant optic atrophy. *Nat Genet* **26:** 207-210

Deng H, Dodson MW, Huang H, Guo M (2008) The Parkinson's disease genes pink1 and parkin promote mitochondrial fission and/or inhibit fusion in Drosophila. *Proc Natl Acad Sci U S A* **105:** 14503-14508

Deng H, Jankovic J, Guo Y, Xie W, Le W (2005) Small interfering RNA targeting the PINK1 induces apoptosis in dopaminergic cells SH-SY5Y. *Biochemical and biophysical research communications* **337:** 1133-1138

Denison SR, Wang F, Becker NA, Schule B, Kock N, Phillips LA, Klein C, Smith DI (2003) Alterations in the common fragile site gene Parkin in ovarian and other cancers. *Oncogene* **22:** 8370-8378

Dietzl G, Chen D, Schnorrer F, Su KC, Barinova Y, Fellner M, Gasser B, Kinsey K, Oppel S, Scheiblauer S, Couto A, Marra V, Keleman K, Dickson BJ (2007) A genome-wide transgenic RNAi library for conditional gene inactivation in Drosophila. *Nature* **448:** 151-156

Ding WX, Ni HM, Gao W, Hou YF, Melan MA, Chen X, Stolz DB, Shao ZM, Yin XM (2007) Differential effects of endoplasmic reticulum stress-induced autophagy on cell survival. *The Journal of biological chemistry* **282:** 4702-4710

Do CB, Tung JY, Dorfman E, Kiefer AK, Drabant EM, Francke U, Mountain JL, Goldman SM, Tanner CM, Langston JW, Wojcicki A, Eriksson N (2011) Web-based genome-wide association study identifies two novel loci and a substantial genetic component for Parkinson's disease. *PLoS Genet* **7:** e1002141

Doble BW, Patel S, Wood GA, Kockeritz LK, Woodgett JR (2007) Functional redundancy of GSK-3alpha and GSK-3beta in Wnt/beta-catenin signaling shown by using an allelic series of embryonic stem cell lines. *Dev Cell* **12:** 957-971

Doble BW, Woodgett JR (2003) GSK-3: tricks of the trade for a multi-tasking kinase. *Journal of cell science* **116:** 1175-1186

Dobrosotskaya IY, Seegmiller AC, Brown MS, Goldstein JL, Rawson RB (2002) Regulation of SREBP processing and membrane lipid production by phospholipids in Drosophila. *Science* **296:** 879-883

Duncan EA, Brown MS, Goldstein JL, Sakai J (1997) Cleavage site for sterol-regulated protease localized to a leu-Ser bond in the lumenal loop of sterol regulatory element-binding protein-2. *The Journal of biological chemistry* **272:** 12778-12785

Edinger AL, Thompson CB (2002) Akt maintains cell size and survival by increasing mTOR-dependent nutrient uptake. *Molecular biology of the cell* **13:** 2276-2288

Ekholm-Reed S, Goldberg MS, Schlossmacher MG, Reed SI (2013) Parkin-dependent degradation of the f-box protein fbw7beta promotes neuronal survival in response to oxidative stress by stabilizing mcl-1. *Mol Cell Biol* **33:** 3627-3643

Elbashir SM, Harborth J, Lendeckel W, Yalcin A, Weber K, Tuschl T (2001) Duplexes of 21-nucleotide RNAs mediate RNA interference in cultured mammalian cells. *Nature* **411:** 494-498

Ericsson J, Edwards PA (1998) CBP is required for sterol-regulated and sterol regulatory element-binding protein-regulated transcription. *The Journal of biological chemistry* **273:** 17865-17870

Espenshade PJ, Li WP, Yabe D (2002) Sterols block binding of COPII proteins to SCAP, thereby controlling SCAP sorting in ER. *Proceedings of the National Academy of Sciences of the United States of America* **99:** 11694-11699

Exner N, Treske B, Paquet D, Holmstrom K, Schiesling C, Gispert S, Carballo-Carbajal I, Berg D, et al. (2007) Loss-of-function of human PINK1 results in mitochondrial pathology and can be rescued by parkin. *J Neurosci* **27:** 12413-12418

Fahn S, Oakes D, Shoulson I, Kieburtz K, Rudolph A, Lang A, Olanow CW, Tanner C, Marek K (2004) Levodopa and the progression of Parkinson's disease. *N Engl J Med* **351:** 2498-2508

Fallon L, Belanger CM, Corera AT, Kontogiannea M, Regan-Klapisz E, Moreau F, Voortman J, Haber M, Rouleau G, Thorarinsdottir T, Brice A, van Bergen En Henegouwen PM, Fon EA (2006) A regulated interaction with the UIM protein Eps15 implicates parkin in EGF receptor trafficking and PI(3)K-Akt signalling. *Nat Cell Biol* **8:** 834-842

Farrer M, Chan P, Chen R, Tan L, Lincoln S, Hernandez D, Forno L, Gwinn-Hardy K, Petrucelli L, Hussey J, Singleton A, Tanner C, Hardy J, Langston JW (2001) Lewy bodies and parkinsonism in families with parkin mutations. *Annals of neurology* **50:** 293-300

Farrer M, Gwinn-Hardy K, Muenter M, DeVrieze FW, Crook R, Perez-Tur J, Lincoln S, Maraganore D, Adler C, Newman S, MacElwee K, McCarthy P, Miller C, Waters C, Hardy J (1999) A chromosome 4p haplotype segregating with Parkinson's disease and postural tremor. *Human molecular genetics* **8:** 81-85

Feramisco JD, Radhakrishnan A, Ikeda Y, Reitz J, Brown MS, Goldstein JL (2005) Intramembrane aspartic acid in SCAP protein governs cholesterol-induced conformational change. *Proceedings of the National Academy of Sciences of the United States of America* **102:** 3242-3247

Fisher KH, Wright VM, Taylor A, Zeidler MP, Brown S (2012) Advances in genome-wide RNAi cellular screens: a case study using the Drosophila JAK/STAT pathway. *BMC Genomics* **13:** 506

Freije WA, Mandal S, Banerjee U (2012) Expression profiling of attenuated mitochondrial function identifies retrograde signals in Drosophila. *G3 (Bethesda)* **2:** 843-851

Fu M, St-Pierre P, Shankar J, Wang PT, Joshi B, Nabi IR (2013) Regulation of mitophagy by the Gp78 E3 ubiquitin ligase. *Mol Biol Cell* **24:** 1153-1162

Fuchs J, Nilsson C, Kachergus J, Munz M, Larsson EM, Schule B, Langston JW, Middleton FA, Ross OA, Hulihan M, Gasser T, Farrer MJ (2007) Phenotypic variation in a large Swedish pedigree due to SNCA duplication and triplication. *Neurology* **68:** 916-922

Fukae J, Sato S, Shiba K, Sato K, Mori H, Sharp PA, Mizuno Y, Hattori N (2009) Programmed cell death-2 isoform1 is ubiquitinated by parkin and increased in the substantia nigra of patients with autosomal recessive Parkinson's disease. *FEBS Lett* **583:** 521-525

Funayama M, Hasegawa K, Kowa H, Saito M, Tsuji S, Obata F (2002) A new locus for Parkinson's disease (PARK8) maps to chromosome 12p11.2-q13.1. *Annals of neurology* **51:** 296-301

Gasser T, Hardy J, Mizuno Y (2011) Milestones in PD genetics. *Mov Disord* **26:** 1042-1048

Gautier CA, Kitada T, Shen J (2008) Loss of PINK1 causes mitochondrial functional defects and increased sensitivity to oxidative stress. *Proceedings of the National Academy of Sciences of the United States of America* **105:** 11364-11369

Gegg ME, Cooper JM, Chau KY, Rojo M, Schapira AH, Taanman JW (2010) Mitofusin 1 and mitofusin 2 are ubiquitinated in a PINK1/parkin-dependent manner upon induction of mitophagy. *Human molecular genetics* **19:** 4861-4870

Geisler S, Holmstrom KM, Skujat D, Fiesel FC, Rothfuss OC, Kahle PJ, Springer W (2010a) PINK1/Parkin-mediated mitophagy is dependent on VDAC1 and p62/SQSTM1. *Nature cell biology* **12:** 119-131

Geisler S, Holmstrom KM, Treis A, Skujat D, Weber SS, Fiesel FC, Kahle PJ, Springer W (2010b) The PINK1/Parkin-mediated mitophagy is compromised by PD-associated mutations. *Autophagy* **6:** 871-878

George JM (2002) The synucleins. *Genome Biol* **3:** REVIEWS3002

George JM, Jin H, Woods WS, Clayton DF (1995) Characterization of a novel protein regulated during the critical period for song learning in the zebra finch. *Neuron* **15:** 361-372

Gispert S, Ricciardi F, Kurz A, Azizov M, Hoepken HH, Becker D, Voos W, Leuner K, Muller WE, Kudin AP, et al. (2009) Parkinson phenotype in aged PINK1-deficient mice is accompanied by progressive mitochondrial dysfunction in absence of neurodegeneration. *PLoS One* **4:** e5777

Glater EE, Megeath LJ, Stowers RS, Schwarz TL (2006) Axonal transport of mitochondria requires milton to recruit kinesin heavy chain and is light chain independent. *J Cell Biol* **173:** 545-557

Glauser L, Sonnay S, Stafa K, Moore DJ (2011) Parkin promotes the ubiquitination and degradation of the mitochondrial fusion factor mitofusin 1. *Journal of neurochemistry* **118:** 636-645

Goker-Alpan O, Schiffmann R, LaMarca ME, Nussbaum RL, McInerney-Leo A, Sidransky E (2004) Parkinsonism among Gaucher disease carriers. *J Med Genet* **41:** 937-940

Golbe LI, Lazzarini AM, Spychala JR, Johnson WG, Stenroos ES, Mark MH, Sage JI (2001) The tau A0 allele in Parkinson's disease. *Mov Disord* **16:** 442-447

Goldberg MS, Fleming SM, Palacino JJ, Cepeda C, Lam HA, Bhatnagar A, Meloni EG, Wu N, Ackerson LC, Klapstein GJ, Gajendiran M, Roth BL, Chesselet MF, Maidment NT, Levine MS, Shen J (2003) Parkin-deficient mice exhibit nigrostriatal deficits but not loss of dopaminergic neurons. *The Journal of biological chemistry* **278:** 43628-43635

Gong Y, Lee JN, Lee PC, Goldstein JL, Brown MS, Ye J (2006) Sterol-regulated ubiquitination and degradation of Insig-1 creates a convergent mechanism for feedback control of cholesterol synthesis and uptake. *Cell Metab* **3:** 15-24

Gorell JM, Johnson CC, Rybicki BA, Peterson EL, Richardson RJ (1998) The risk of Parkinson's disease with exposure to pesticides, farming, well water, and rural living. *Neurology* **50:** 1346-1350

Grace AA, Bunney BS (1983) Intracellular and extracellular electrophysiology of nigral dopaminergic neurons--2. Action potential generating mechanisms and morphological correlates. *Neuroscience* **10:** 317-331

Greene AW, Grenier K, Aguileta MA, Muise S, Farazifard R, Haque ME, McBride HM, Park DS, Fon EA (2012) Mitochondrial processing peptidase regulates PINK1 processing, import and Parkin recruitment. *EMBO Rep* **13:** 378-385

Greene JC, Whitworth AJ, Kuo I, Andrews LA, Feany MB, Pallanck LJ (2003) Mitochondrial pathology and apoptotic muscle degeneration in Drosophila parkin mutants. *Proc Natl Acad Sci U S A* **100:** 4078-4083

Guo M (2012) Drosophila as a model to study mitochondrial dysfunction in Parkinson's disease. *Cold Spring Harb Perspect Med* **2**

Guo X, Macleod GT, Wellington A, Hu F, Panchumarthi S, Schoenfield M, Marin L, Charlton MP, Atwood HL, Zinsmaier KE (2005) The GTPase dMiro is required for axonal transport of mitochondria to Drosophila synapses. *Neuron* **47:** 379-393

Gusdon AM, Chu CT (2011) To eat or not to eat: neuronal metabolism, mitophagy, and Parkinson's disease. *Antioxid Redox Signal* **14:** 1979-1987

Hampe C, Ardila-Osorio H, Fournier M, Brice A, Corti O (2006) Biochemical analysis of Parkinson's disease-causing variants of Parkin, an E3 ubiquitin-protein ligase with monoubiquitylation capacity. *Human molecular genetics* **15:** 2059-2075

Hancock DB, Martin ER, Mayhew GM, Stajich JM, Jewett R, Stacy MA, Scott BL, Vance JM, Scott WK (2008) Pesticide exposure and risk of Parkinson's disease: a family-based case-control study. *BMC Neurol* **8:** 6

Hannon GJ, Rossi JJ (2004) Unlocking the potential of the human genome with RNA interference. *Nature* **431:** 371-378

Hao LY, Giasson BI, Bonini NM (2010) DJ-1 is critical for mitochondrial function and rescues PINK1 loss of function. *Proceedings of the National Academy of Sciences of the United States of America* **107:** 9747-9752

Haque ME, Thomas KJ, D'Souza C, Callaghan S, Kitada T, Slack RS, Fraser P, Cookson MR, Tandon A, Park DS (2008) Cytoplasmic Pink1 activity protects neurons from dopaminergic neurotoxin MPTP. *Proc Natl Acad Sci U S A* **105:** 1716-1721

Hardy J (2010) Genetic analysis of pathways to Parkinson disease. *Neuron* **68:** 201-206

Hardy J, Cai H, Cookson MR, Gwinn-Hardy K, Singleton A (2006) Genetics of Parkinson's disease and parkinsonism. *Annals of neurology* **60:** 389-398

Hardy J, Singleton A (2009) Genomewide association studies and human disease. *N Engl J Med* **360:** 1759-1768

Hatano Y, Li Y, Sato K, Asakawa S, Yamamura Y, Tomiyama H, Yoshino H, Asahina M, Kobayashi S, Hassin-Baer S, Lu CS, Ng AR, Rosales RL, Shimizu N, Toda T, Mizuno Y, Hattori N (2004) Novel PINK1 mutations in early-onset parkinsonism. *Annals of neurology* **56:** 424-427

Healy DG, Abou-Sleiman PM, Lees AJ, Casas JP, Quinn N, Bhatia K, Hingorani AD, Wood NW (2004) Tau gene and Parkinson's disease: a case-control study and meta-analysis. *J Neurol Neurosurg Psychiatry* **75:** 962-965

Healy DG, Falchi M, O'Sullivan SS, Bonifati V, Durr A, Bressman S, Brice A, et al. (2008) Phenotype, genotype, and worldwide genetic penetrance of LRRK2-associated Parkinson's disease: a case-control study. *Lancet Neurol* **7:** 583-590

Hegarty BD, Bobard A, Hainault I, Ferre P, Bossard P, Foufelle F (2005) Distinct roles of insulin and liver X receptor in the induction and cleavage of sterol regulatory element-binding protein-1c. *Proceedings of the National Academy of Sciences of the United States of America* **102:** 791-796

Henn IH, Bouman L, Schlehe JS, Schlierf A, Schramm JE, Wegener E, Nakaso K, Culmsee C, Berninger B, Krappmann D, Tatzelt J, Winklhofer KF (2007) Parkin mediates neuroprotection through activation of IkappaB kinase/nuclear factor-kappaB signaling. *J Neurosci* **27:** 1868-1878

Hernan MA, Takkouche B, Caamano-Isorna F, Gestal-Otero JJ (2002) A meta-analysis of coffee drinking, cigarette smoking, and the risk of Parkinson's disease. *Annals of neurology* **52:** 276-284

Hernan MA, Zhang SM, Rueda-deCastro AM, Colditz GA, Speizer FE, Ascherio A (2001) Cigarette smoking and the incidence of Parkinson's disease in two prospective studies. *Annals of neurology* **50:** 780-786

Hoepken HH, Gispert S, Morales B, Wingerter O, Del Turco D, Mulsch A, Nussbaum RL, Muller K, Drose S, Brandt U, Deller T, Wirth B, Kudin AP, Kunz WS, Auburger G (2007) Mitochondrial dysfunction, peroxidation damage and changes in glutathione metabolism in PARK6. *Neurobiol Dis* **25:** 401-411

Horn T, Sandmann T, Boutros M (2010) Design and evaluation of genome-wide libraries for RNA interference screens. *Genome Biol* **11:** R61

Horton JD, Goldstein JL, Brown MS (2002) SREBPs: activators of the complete program of cholesterol and fatty acid synthesis in the liver. *J Clin Invest* **109:** 1125-1131

Hristova VA, Beasley SA, Rylett RJ, Shaw GS (2009) Identification of a novel Zn2+-binding domain in the autosomal recessive juvenile Parkinson-related E3 ligase parkin. *The Journal of biological chemistry* **284:** 14978-14986

Hu Y, Flockhart I, Vinayagam A, Bergwitz C, Berger B, Perrimon N, Mohr SE (2011) An integrative approach to ortholog prediction for disease-focused and other functional studies. *BMC Bioinformatics* **12:** 357

Hua X, Nohturfft A, Goldstein JL, Brown MS (1996) Sterol resistance in CHO cells traced to point mutation in SREBP cleavage-activating protein. *Cell* **87:** 415-426

Hua X, Wu J, Goldstein JL, Brown MS, Hobbs HH (1995) Structure of the human gene encoding sterol regulatory element binding protein-1 (SREBF1) and localization of SREBF1 and SREBF2 to chromosomes 17p11.2 and 22q13. *Genomics* **25:** 667-673

Huang X, Abbott RD, Petrovitch H, Mailman RB, Ross GW (2008) Low LDL cholesterol and increased risk of Parkinson's disease: prospective results from Honolulu-Asia Aging Study. *Mov Disord* **23:** 1013-1018

Hudson G, Amati-Bonneau P, Blakely EL, Stewart JD, He L, Schaefer AM, Griffiths PG, Ahlqvist K, Suomalainen A, Reynier P, McFarland R, Turnbull DM, Chinnery PF, Taylor RW (2008) Mutation of OPA1 causes dominant optic atrophy with external ophthalmoplegia, ataxia, deafness and multiple mitochondrial DNA deletions: a novel disorder of mtDNA maintenance. *Brain : a journal of neurology* **131:** 329-337

Huynh DP, Scoles DR, Nguyen D, Pulst SM (2003) The autosomal recessive juvenile Parkinson disease gene product, parkin, interacts with and ubiquitinates synaptotagmin XI. *Hum Mol Genet* **12:** 2587-2597

Hynes MJ, Murray SL (2010) ATP-citrate lyase is required for production of cytosolic acetyl coenzyme A and development in Aspergillus nidulans. *Eukaryot Cell* **9:** 1039-1048

Ibanez P, Bonnet AM, Debarges B, Lohmann E, Tison F, Pollak P, Agid Y, Durr A, Brice A (2004) Causal relation between alpha-synuclein gene duplication and familial Parkinson's disease. *Lancet* **364:** 1169-1171

Imai Y, Soda M, Inoue H, Hattori N, Mizuno Y, Takahashi R (2001) An unfolded putative transmembrane polypeptide, which can lead to endoplasmic reticulum stress, is a substrate of Parkin. *Cell* **105:** 891-902

Ishihara N, Jofuku A, Eura Y, Mihara K (2003) Regulation of mitochondrial morphology by membrane potential, and DRP1-dependent division and FZO1-dependent fusion reaction in mammalian cells. *Biochemical and biophysical research communications* **301:** 891-898

Ishihara N, Nomura M, Jofuku A, Kato H, Suzuki SO, Masuda K, Otera H, Nakanishi Y, Nonaka I, Goto Y, Taguchi N, Morinaga H, Maeda M, Takayanagi R, Yokota S, Mihara K (2009) Mitochondrial fission factor Drp1 is essential for embryonic development and synapse formation in mice. *Nature cell biology* **11:** 958-966

Janetzky B, Hauck S, Youdim MB, Riederer P, Jellinger K, Pantucek F, Zochling R, Boissl KW, Reichmann H (1994) Unaltered aconitase activity, but decreased complex I activity in substantia nigra pars compacta of patients with Parkinson's disease. *Neuroscience letters* **169:** 126-128

Janowski BA (2002) The hypocholesterolemic agent LY295427 up-regulates INSIG-1, identifying the INSIG-1 protein as a mediator of cholesterol homeostasis through SREBP. *Proceedings of the National Academy of Sciences of the United States of America* **99:** 12675-12680

Jeibmann A, Paulus W (2009) Drosophila melanogaster as a model organism of brain diseases. *Int J Mol Sci* **10:** 407-440

Jenner P, Dexter DT, Sian J, Schapira AH, Marsden CD (1992) Oxidative stress as a cause of nigral cell death in Parkinson's disease and incidental Lewy body disease. The Royal Kings and Queens Parkinson's Disease Research Group. *Annals of neurology* **32 Suppl:** S82-87

Jensen LJ, Kuhn M, Stark M, Chaffron S, Creevey C, Muller J, Doerks T, Julien P, Roth A, Simonovic M, Bork P, von Mering C (2009) STRING 8--a global view on proteins and their functional interactions in 630 organisms. *Nucleic Acids Res* **37:** D412-416

Jiang H, Jiang Q, Feng J (2004) Parkin increases dopamine uptake by enhancing the cell surface expression of dopamine transporter. *J Biol Chem* **279:** 54380-54386

Jin SM, Lazarou M, Wang C, Kane LA, Narendra DP, Youle RJ (2010) Mitochondrial membrane potential regulates PINK1 import and proteolytic destabilization by PARL. *The Journal of cell biology* **191:** 933-942

Jin SM, Youle RJ (2012) PINK1- and Parkin-mediated mitophagy at a glance. *Journal of cell science* **125:** 795-799

Joch M, Ase AR, Chen CX, MacDonald PA, Kontogiannea M, Corera AT, Brice A, Seguela P, Fon EA (2007) Parkin-mediated monoubiquitination of the PDZ protein PICK1 regulates the activity of acid-sensing ion channels. *Mol Biol Cell* **18:** 3105-3118

Jones HE, Harwood JL, Bowen ID, Griffiths G (1992) Lipid composition of subcellular membranes from larvae and prepupae of Drosophila melanogaster. *Lipids* **27:** 984-987

Kanki T (2010) Nix, a receptor protein for mitophagy in mammals. *Autophagy* **6:** 433-435

Kanki T, Klionsky DJ, Okamoto K (2011) Mitochondria autophagy in yeast. *Antioxid Redox Signal* **14:** 1989-2001

Kanki T, Wang K, Baba M, Bartholomew CR, Lynch-Day MA, Du Z, Geng J, Mao K, Yang Z, Yen WL, Klionsky DJ (2009a) A genomic screen for yeast mutants defective in selective mitochondria autophagy. *Molecular biology of the cell* **20:** 4730-4738

Kanki T, Wang K, Cao Y, Baba M, Klionsky DJ (2009b) Atg32 is a mitochondrial protein that confers selectivity during mitophagy. *Dev Cell* **17:** 98-109

Kao SY (2009) DNA damage induces nuclear translocation of parkin. *J Biomed Sci* **16:** 67

Kawajiri S, Saiki S, Sato S, Sato F, Hatano T, Eguchi H, Hattori N (2010) PINK1 is recruited to mitochondria with parkin and associates with LC3 in mitophagy. *FEBS letters* **584:** 1073-1079

Kerrien S, Aranda B, Breuza L, Bridge A, Broackes-Carter F, Chen C, Duesbury M, Dumousseau M, et al. (2012) The IntAct molecular interaction database in 2012. *Nucleic Acids Res* **40:** D841-846

Kieburtz K, Wunderle KB (2013) Parkinson's disease: evidence for environmental risk factors. *Mov Disord* **28:** 8-13

Kim KH, Song MJ, Yoo EJ, Choe SS, Park SD, Kim JB (2004) Regulatory role of glycogen synthase kinase 3 for transcriptional activity of ADD1/SREBP1c. *The Journal of biological chemistry* **279:** 51999-52006

Kim KY, Stevens MV, Akter MH, Rusk SE, Huang RJ, Cohen A, Noguchi A, Springer D, Bocharov AV, Eggerman TL, Suen DF, Youle RJ, Amar M, Remaley AT, Sack MN (2011) Parkin is a lipid-responsive regulator of fat uptake in mice and mutant human cells. *J Clin Invest* **121:** 3701-3712

Kim RH, Smith PD, Aleyasin H, Hayley S, Mount MP, Pownall S, Wakeham A, You-Ten AJ, Kalia SK, Horne P, Westaway D, Lozano AM, Anisman H, Park DS, Mak TW (2005) Hypersensitivity of DJ-1-deficient mice to 1-methyl-4-phenyl-1,2,3,6-tetrahydropyrindine (MPTP) and oxidative stress. *Proc Natl Acad Sci U S A* **102:** 5215-5220

Kitada T, Asakawa S, Hattori N, Matsumine H, Yamamura Y, Minoshima S, Yokochi M, Mizuno Y, Shimizu N (1998) Mutations in the parkin gene cause autosomal recessive juvenile parkinsonism. *Nature* **392:** 605-608

Kitada T, Pisani A, Porter DR, Yamaguchi H, Tscherter A, Martella G, Bonsi P, Zhang C, Pothos EN, Shen J (2007) Impaired dopamine release and synaptic plasticity in the striatum of PINK1-deficient mice. *Proceedings of the National Academy of Sciences of the United States of America* **104:** 11441-11446

Klein C, Lohmann-Hedrich K, Rogaeva E, Schlossmacher MG, Lang AE (2007) Deciphering the role of heterozygous mutations in genes associated with parkinsonism. *Lancet Neurol* **6:** 652-662

Klein C, Westenberger A (2012) Genetics of Parkinson's disease. *Cold Spring Harb Perspect Med* **2:** a008888

Klionsky DJ, Abdalla FC, Abeliovich H, Abraham RT, Acevedo-Arozena A, Adeli K AL, et al. (2012) Guidelines for the use and interpretation of assays for monitoring autophagy. *Autophagy* **8:** 445-544

Ko HS, Kim SW, Sriram SR, Dawson VL, Dawson TM (2006) Identification of far upstream element-binding protein-1 as an authentic Parkin substrate. *J Biol Chem* **281:** 16193-16196

Ko HS, von Coelln R, Sriram SR, Kim SW, Chung KK, Pletnikova O, Troncoso J, Johnson B, Saffary R, Goh EL, Song H, Park BJ, Kim MJ, Kim S, Dawson VL, Dawson TM (2005) Accumulation of the authentic parkin substrate aminoacyl-tRNA synthetase cofactor, p38/JTV-1, leads to catecholaminergic cell death. *J Neurosci* **25:** 7968-7978

Kondapalli C, Kazlauskaite A, Zhang N, Woodroof HI, Campbell DG, Gourlay R, Burchell L, Walden H, Macartney TJ, Deak M, Knebel A, Alessi DR, Muqit MM (2012) PINK1 is activated by mitochondrial membrane potential depolarization and stimulates Parkin E3 ligase activity by phosphorylating Serine 65. *Open Biol* **2:** 120080

Kordower JH, Chu Y, Hauser RA, Freeman TB, Olanow CW (2008) Lewy body-like pathology in long-term embryonic nigral transplants in Parkinson's disease. *Nat Med* **14:** 504-506

Kruger R, Vieira-Saecker AM, Kuhn W, Berg D, Muller T, Kuhnl N, Fuchs GA, Storch A, Hungs M, Woitalla D, Przuntek H, Epplen JT, Schols L, Riess O (1999) Increased susceptibility to sporadic Parkinson's disease by a certain combined alpha-synuclein/apolipoprotein E genotype. *Annals of neurology* **45:** 611-617

Kumar A, Cookson MR (2011) Role of LRRK2 kinase dysfunction in Parkinson disease. *Expert reviews in molecular medicine* **13:** e20

Kunte AS, Matthews KA, Rawson RB (2006) Fatty acid auxotrophy in Drosophila larvae lacking SREBP. *Cell Metab* **3:** 439-448

Langston JW, Ballard P, Tetrud JW, Irwin I (1983) Chronic Parkinsonism in humans due to a product of meperidine-analog synthesis. *Science* **219:** 979-980

Langston JW, Forno LS, Rebert CS, Irwin I (1984) Selective nigral toxicity after systemic administration of 1-methyl-4-phenyl-1,2,5,6-tetrahydropyrine (MPTP) in the squirrel monkey. *Brain Res* **292:** 390-394

Lashuel HA, Hartley D, Petre BM, Walz T, Lansbury PT, Jr. (2002) Neurodegenerative disease: amyloid pores from pathogenic mutations. *Nature* **418:** 291

Lazarou M, Jin SM, Kane LA, Youle RJ (2012) Role of PINK1 binding to the TOM complex and alternate intracellular membranes in recruitment and activation of the E3 ligase Parkin. *Dev Cell* **22:** 320-333

Lazarou M, Narendra DP, Jin SM, Tekle E, Banerjee S, Youle RJ (2013) PINK1 drives Parkin self-association and HECT-like E3 activity upstream of mitochondrial binding. *The Journal of cell biology* **200:** 163-172

Lee HJ, Patel S, Lee SJ (2005) Intravesicular localization and exocytosis of alpha-synuclein and its aggregates. *The Journal of neuroscience : the official journal of the Society for Neuroscience* **25:** 6016-6024

Lee JN, Song B, DeBose-Boyd RA, Ye J (2006) Sterol-regulated degradation of Insig-1 mediated by the membrane-bound ubiquitin ligase gp78. *The Journal of biological chemistry* **281:** 39308-39315

Lee JN, Ye J (2004) Proteolytic activation of sterol regulatory element-binding protein induced by cellular stress through depletion of Insig-1. *The Journal of biological chemistry* **279:** 45257-45265

Lee JN, Zhang X, Feramisco JD, Gong Y, Ye J (2008) Unsaturated fatty acids inhibit proteasomal degradation of Insig-1 at a postubiquitination step. *The Journal of biological chemistry* **283:** 33772-33783

Lee JY, Nagano Y, Taylor JP, Lim KL, Yao TP (2010) Disease-causing mutations in parkin impair mitochondrial ubiquitination, aggregation, and HDAC6-dependent mitophagy. *The Journal of cell biology* **189:** 671-679

Lees AJ, Hardy J, Revesz T (2009) Parkinson's disease. *Lancet* **373:** 2055-2066

Lefebvre V, Du Q, Baird S, Ng AC, Nascimento M, Campanella M, McBride HM, Screaton RA (2013) Genome-wide RNAi screen identifies ATPase inhibitory factor 1 (ATPIF1) as essential for PARK2 recruitment and mitophagy. *Autophagy* **9:** 1770-1779

Legros F, Lombes A, Frachon P, Rojo M (2002) Mitochondrial fusion in human cells is efficient, requires the inner membrane potential, and is mediated by mitofusins. *Molecular biology of the cell* **13:** 4343-4354

Lesage S, Anheim M, Condroyer C, Pollak P, Durif F, Dupuits C, Viallet F, Lohmann E, Corvol JC, Honore A, Rivaud S, Vidailhet M, Durr A, Brice A (2011) Large-scale screening of the Gaucher's disease-related glucocerebrosidase gene in Europeans with Parkinson's disease. *Human molecular genetics* **20:** 202-210

Lesage S, Brice A (2009) Parkinson's disease: from monogenic forms to genetic susceptibility factors. *Human molecular genetics* **18:** R48-59

Lesage S, Brice A (2012) Role of mendelian genes in "sporadic" Parkinson's disease. *Parkinsonism Relat Disord* **18 Suppl 1:** S66-70

Li HM, Niki T, Taira T, Iguchi-Ariga SM, Ariga H (2005) Association of DJ-1 with chaperones and enhanced association and colocalization with mitochondrial Hsp70 by oxidative stress. *Free radical research* **39:** 1091-1099

Li JY, Englund E, Holton JL, Soulet D, Hagell P, Lees AJ, Lashley T, Quinn NP, Rehncrona S, Bjorklund A, Widner H, Revesz T, Lindvall O, Brundin P (2008) Lewy bodies in grafted neurons in subjects with Parkinson's disease suggest host-to-graft disease propagation. *Nat Med* **14:** 501-503

Lill CM, Roehr JT, McQueen MB, Kavvoura FK, Bagade S, Schjeide BM, Schjeide LM, Meissner E, Zauft U, et al. (2012) Comprehensive research synopsis and systematic meta-analyses in Parkinson's disease genetics: The PDGene database. *PLoS Genet* **8:** e1002548

Lim KL, Chew KC, Tan JM, Wang C, Chung KK, Zhang Y, Tanaka Y, Smith W, Engelender S, Ross CA, Dawson VL, Dawson TM (2005) Parkin mediates nonclassical, proteasomal-independent ubiquitination of synphilin-1: implications for Lewy body formation. *J Neurosci* **25:** 2002-2009

Lin J, Yang R, Tarr PT, Wu PH, Handschin C, Li S, Yang W, Pei L, Uldry M, Tontonoz P, Newgard CB, Spiegelman BM (2005) Hyperlipidemic effects of dietary saturated fats mediated through PGC-1beta coactivation of SREBP. *Cell* **120:** 261-273

Lin W, Kang UJ (2010) Structural determinants of PINK1 topology and dual subcellular distribution. *BMC Cell Biol* **11:** 90

Lipsky NG, Pedersen PL (1981) Mitochondrial turnover in animal cells. Half-lives of mitochondria and mitochondrial subfractions of rat liver based on [14C]bicarbonate incorporation. *The Journal of biological chemistry* **256:** 8652-8657

Liu S, Sawada T, Lee S, Yu W, Silverio G, Alapatt P, Millan I, Shen A, Saxton W, Kanao T, Takahashi R, Hattori N, Imai Y, Lu B (2012) Parkinson's disease-associated kinase PINK1 regulates Miro protein level and axonal transport of mitochondria. *PLoS Genet* **8:** e1002537

Liu X, Cheng R, Verbitsky M, Kisselev S, Browne A, Mejia-Sanatana H, Louis ED, Cote LJ, Andrews H, Waters C, Ford B, Frucht S, Fahn S, Marder K, Clark LN, Lee JH (2011) Genome-wide association study identifies candidate genes for Parkinson's disease in an Ashkenazi Jewish population. *BMC Med Genet* **12:** 104

Liu X, Weaver D, Shirihai O, Hajnoczky G (2009) Mitochondrial 'kiss-and-run': interplay between mitochondrial motility and fusion-fission dynamics. *Embo J* **28:** 3074-3089

Livak KJ, Schmittgen TD (2001) Analysis of relative gene expression data using real-time quantitative PCR and the 2(-Delta Delta C(T)) Method. *Methods* **25:** 402-408

Lucking CB, Durr A, Bonifati V, Vaughan J, De Michele G, Gasser T, Harhangi BS, Meco G, Denefle P, Wood NW, Agid Y, Brice A (2000) Association between early-onset Parkinson's disease and mutations in the parkin gene. *N Engl J Med* **342:** 1560-1567

Lytton J, Westlin M, Hanley MR (1991) Thapsigargin inhibits the sarcoplasmic or endoplasmic reticulum Ca-ATPase family of calcium pumps. *The Journal of biological chemistry* **266:** 17067-17071

Mann VM, Cooper JM, Krige D, Daniel SE, Schapira AH, Marsden CD (1992) Brain, skeletal muscle and platelet homogenate mitochondrial function in Parkinson's disease. *Brain : a journal of neurology* **115 (Pt 2):** 333-342

Mao JH, Perez-Losada J, Wu D, Delrosario R, Tsunematsu R, Nakayama KI, Brown K, Bryson S, Balmain A (2004) Fbxw7/Cdc4 is a p53-dependent, haploinsufficient tumour suppressor gene. *Nature* **432:** 775-779

Mata IF, Kachergus JM, Taylor JP, Lincoln S, Aasly J, Lynch T, Hulihan MM, Cobb SA, Wu RM, Lu CS, Lahoz C, Wszolek ZK, Farrer MJ (2005) Lrrk2 pathogenic substitutions in Parkinson's disease. *Neurogenetics* **6:** 171-177

Mata IF, Wedemeyer WJ, Farrer MJ, Taylor JP, Gallo KA (2006) LRRK2 in Parkinson's disease: protein domains and functional insights. *Trends in neurosciences* **29:** 286-293

Matsuda N, Sato S, Shiba K, Okatsu K, Saisho K, Gautier CA, Sou YS, Saiki S, Kawajiri S, Sato F, Kimura M, Komatsu M, Hattori N, Tanaka K (2010) PINK1 stabilized by mitochondrial depolarization recruits Parkin to damaged mitochondria and activates latent Parkin for mitophagy. *The Journal of cell biology* **189:** 211-221

Matsumine H, Saito M, Shimoda-Matsubayashi S, Tanaka H, Ishikawa A, Nakagawa-Hattori Y, Yokochi M, et al. (1997) Localization of a gene for an autosomal recessive form of juvenile Parkinsonism to chromosome 6q25.2-27. *Am J Hum Genet* **60:** 588-596

Matsushima-Nishiu M, Unoki M, Ono K, Tsunoda T, Minaguchi T, Kuramoto H, Nishida M, Satoh T, Tanaka T, Nakamura Y (2001) Growth and gene expression profile analyses of endometrial cancer cells expressing exogenous PTEN. *Cancer Res* **61:** 3741-3749

McCoy MK, Kaganovich A, Rudenko IN, Ding J, Cookson MR (2013) Hexokinase activity is required for recruitment of parkin to depolarized mitochondria. *Human molecular genetics*

Meissner C, Lorenz H, Weihofen A, Selkoe DJ, Lemberg MK (2011) The mitochondrial intramembrane protease PARL cleaves human Pink1 to regulate Pink1 trafficking. *Journal of neurochemistry* **117:** 856-867

Mi H, Muruganujan A, Thomas PD (2013) PANTHER in 2013: modeling the evolution of gene function, and other gene attributes, in the context of phylogenetic trees. *Nucleic Acids Res* **41:** D377-386

Miller DW, Ahmad R, Hague S, Baptista MJ, Canet-Aviles R, McLendon C, Carter DM, Zhu PP, Stadler J, Chandran J, Klinefelter GR, Blackstone C, Cookson MR (2003) L166P mutant DJ-1, causative for recessive Parkinson's disease, is degraded through the ubiquitin-proteasome system. *The Journal of biological chemistry* **278:** 36588-36595

Miller GW (2007) Paraquat: the red herring of Parkinson's disease research. *Toxicol Sci* **100:** 1-2

Miller KE, Sheetz MP (2004) Axonal mitochondrial transport and potential are correlated. *Journal of cell science* **117:** 2791-2804

Misko A, Jiang S, Wegorzewska I, Milbrandt J, Baloh RH (2010) Mitofusin 2 is necessary for transport of axonal mitochondria and interacts with the Miro/Milton complex. *The Journal of neuroscience : the official journal of the Society for Neuroscience* **30:** 4232-4240

Mitsumoto A, Nakagawa Y (2001) DJ-1 is an indicator for endogenous reactive oxygen species elicited by endotoxin. *Free Radic Res* **35:** 885-893

Mizuno Y, Ohta S, Tanaka M, Takamiya S, Suzuki K, Sato T, Oya H, Ozawa T, Kagawa Y (1989) Deficiencies in complex I subunits of the respiratory chain in Parkinson's disease. *Biochemical and biophysical research communications* **163:** 1450-1455

Mizushima N (2007) Autophagy: process and function. *Genes Dev* **21:** 2861-2873

Moberg KH, Bell DW, Wahrer DC, Haber DA, Hariharan IK (2001) Archipelago regulates Cyclin E levels in Drosophila and is mutated in human cancer cell lines. *Nature* **413:** 311-316

Moore DJ, West AB, Dikeman DA, Dawson VL, Dawson TM (2008) Parkin mediates the degradation-independent ubiquitination of Hsp70. *Journal of neurochemistry* **105:** 1806-1819

Morais VA, Verstreken P, Roethig A, Smet J, Snellinx A, Vanbrabant M, Haddad D, Frezza C, Mandemakers W, Vogt-Weisenhorn D, Van Coster R, Wurst W, Scorrano L, De Strooper B (2009) Parkinson's disease mutations in PINK1 result in decreased Complex I activity and deficient synaptic function. *EMBO Mol Med* **1:** 99-111

Mortiboys H, Thomas KJ, Koopman WJ, Klaffke S, Abou-Sleiman P, Olpin S, Wood NW, Willems PH, Smeitink JA, Cookson MR, Bandmann O (2008) Mitochondrial function and morphology are impaired in parkin-mutant fibroblasts. *Annals of neurology* **64:** 555-565

Mortimer NT, Moberg KH (2007) The Drosophila F-box protein Archipelago controls levels of the Trachealess transcription factor in the embryonic tracheal system. *Dev Biol* **312:** 560-571

Nagakubo D, Taira T, Kitaura H, Ikeda M, Tamai K, Iguchi-Ariga SM, Ariga H (1997) DJ-1, a novel oncogene which transforms mouse NIH3T3 cells in cooperation with ras. *Biochemical and biophysical research communications* **231:** 509-513

Nagoshi E, Yoneda Y (2001) Dimerization of sterol regulatory element-binding protein 2 via the helix-loop-helix-leucine zipper domain is a prerequisite for its nuclear localization mediated by importin beta. *Mol Cell Biol* **21:** 2779-2789

Nakajima A, Kataoka K, Hong M, Sakaguchi M, Huh NH (2003) BRPK, a novel protein kinase showing increased expression in mouse cancer cell lines with higher metastatic potential. *Cancer Lett* **201:** 195-201

Nalls MA, Plagnol V, Hernandez DG, Sharma M, Sheerin UM, Saad M, Simon-Sanchez J, et al. (2011) Imputation of sequence variants for identification of genetic risks for Parkinson's disease: a meta-analysis of genome-wide association studies. *Lancet* **377:** 641-649

Narendra D, Kane LA, Hauser DN, Fearnley IM, Youle RJ (2010a) p62/SQSTM1 is required for Parkin-induced mitochondrial clustering but not mitophagy; VDAC1 is dispensable for both. *Autophagy* **6:** 1090-1106

Narendra D, Tanaka A, Suen DF, Youle RJ (2008) Parkin is recruited selectively to impaired mitochondria and promotes their autophagy. *J Cell Biol* **183:** 795-803

Narendra D, Walker JE, Youle R (2012) Mitochondrial quality control mediated by PINK1 and Parkin: links to parkinsonism. *Cold Spring Harb Perspect Biol* **4**

Narendra DP, Jin SM, Tanaka A, Suen DF, Gautier CA, Shen J, Cookson MR, Youle RJ (2010b) PINK1 Is Selectively Stabilized on Impaired Mitochondria to Activate Parkin. *PLoS Biol* **8:** e1000298

Neupert W, Herrmann JM (2007) Translocation of proteins into mitochondria. *Annu Rev Biochem* **76:** 723-749

Neuspiel M, Schauss AC, Braschi E, Zunino R, Rippstein P, Rachubinski RA, Andrade-Navarro MA, McBride HM (2008) Cargo-selected transport from the mitochondria to peroxisomes is mediated by vesicular carriers. *Current biology : CB* **18:** 102-108

Ni JQ, Liu LP, Binari R, Hardy R, Shim HS, Cavallaro A, Booker M, Pfeiffer BD, Markstein M, Wang H, Villalta C, Laverty TR, Perkins LA, Perrimon N (2009) A Drosophila resource of transgenic RNAi lines for neurogenetics. *Genetics* **182:** 1089-1100

Nohturfft A, Yabe D, Goldstein JL, Brown MS, Espenshade PJ (2000) Regulated step in cholesterol feedback localized to budding of SCAP from ER membranes. *Cell* **102:** 315-323

Norris EH, Uryu K, Leight S, Giasson BI, Trojanowski JQ, Lee VM (2007) Pesticide exposure exacerbates alpha-synucleinopathy in an A53T transgenic mouse model. *Am J Pathol* **170:** 658-666

Novak I, Kirkin V, McEwan DG, Zhang J, Wild P, Rozenknop A, Rogov V, Lohr F, Popovic D, Occhipinti A, Reichert AS, Terzic J, Dotsch V, Ney PA, Dikic I (2010) Nix is a selective autophagy receptor for mitochondrial clearance. *EMBO Rep* **11:** 45-51

Ogata M, Hino S, Saito A, Morikawa K, Kondo S, Kanemoto S, Murakami T, Taniguchi M, Tanii I, Yoshinaga K, Shiosaka S, Hammarback JA, Urano F, Imaizumi K (2006) Autophagy is activated for cell survival after endoplasmic reticulum stress. *Mol Cell Biol* **26:** 9220-9231

Okamoto K, Kondo-Okamoto N, Ohsumi Y (2009) Mitochondria-anchored receptor Atg32 mediates degradation of mitochondria via selective autophagy. *Dev Cell* **17:** 87-97

Okatsu K, Oka T, Iguchi M, Imamura K, Kosako H, Tani N, Kimura M, Go E, Koyano F, Funayama M, Shiba-Fukushima K, et al. (2012) PINK1 autophosphorylation upon membrane potential dissipation is essential for Parkin recruitment to damaged mitochondria. *Nat Commun* **3:** 1016

Okatsu K, Saisho K, Shimanuki M, Nakada K, Shitara H, Sou YS, Kimura M, Sato S, Hattori N, Komatsu M, Tanaka K, Matsuda N (2010) p62/SQSTM1 cooperates with Parkin for perinuclear clustering of depolarized mitochondria. *Genes Cells* **15:** 887-900

Okui M, Yamaki A, Takayanagi A, Kudoh J, Shimizu N, Shimizu Y (2005) Transcription factor single-minded 2 (SIM2) is ubiquitinated by the RING-IBR-RING-type E3 ubiquitin ligases. *Exp Cell Res* **309:** 220-228

Olzmann JA, Li L, Chudaev MV, Chen J, Perez FA, Palmiter RD, Chin LS (2007) Parkin-mediated K63-linked polyubiquitination targets misfolded DJ-1 to aggresomes via binding to HDAC6. *The Journal of cell biology* **178:** 1025-1038

Orvedahl A, Sumpter R, Jr., Xiao G, Ng A, Zou Z, Tang Y, Narimatsu M, Gilpin C, Sun Q, Roth M, Forst CV, Wrana JL, Zhang YE, Luby-Phelps K, Xavier RJ, Xie Y, Levine B (2011) Image-based genome-wide siRNA screen identifies selective autophagy factors. *Nature* **480:** 113-117

Osborne TF, Espenshade PJ (2009) Evolutionary conservation and adaptation in the mechanism that regulates SREBP action: what a long, strange tRIP it's been. *Genes Dev* **23:** 2578-2591

Paisan-Ruiz C, Jain S, Evans EW, Gilks WP, Simon J, van der Brug M, Lopez de Munain A, Aparicio S, Gil AM, Khan N, et al. (2004) Cloning of the gene containing mutations that cause PARK8-linked Parkinson's disease. *Neuron* **44:** 595-600

Paisan-Ruiz C, Nath P, Washecka N, Gibbs JR, Singleton AB (2008) Comprehensive analysis of LRRK2 in publicly available Parkinson's disease cases and neurologically normal controls. *Hum Mutat* **29:** 485-490

Palacino JJ, Sagi D, Goldberg MS, Krauss S, Motz C, Wacker M, Klose J, Shen J (2004) Mitochondrial dysfunction and oxidative damage in parkin-deficient mice. *J Biol Chem* **279:** 18614-18622

Pankratz N, Pauciulo MW, Elsaesser VE, Marek DK, Halter CA, Wojcieszek J, Rudolph A, Shults CW, Foroud T, Nichols WC (2006) Mutations in DJ-1 are rare in familial Parkinson disease. *Neuroscience letters* **408:** 209-213

Park J, Lee SB, Lee S, Kim Y, Song S, Kim S, Bae E, Kim J, Shong M, Kim JM, Chung J (2006) Mitochondrial dysfunction in Drosophila PINK1 mutants is complemented by parkin. *Nature* **441:** 1157-1161

Parker WD, Jr., Boyson SJ, Parks JK (1989) Abnormalities of the electron transport chain in idiopathic Parkinson's disease. *Annals of neurology* **26:** 719-723

Parkinson J (2002) An essay on the shaking palsy. 1817. *J Neuropsychiatry Clin Neurosci* **14:** 223-236; discussion 222

Perry SW, Norman JP, Barbieri J, Brown EB, Gelbard HA (2011) Mitochondrial membrane potential probes and the proton gradient: a practical usage guide. *Biotechniques* **50:** 98-115

Pesah Y, Pham T, Burgess H, Middlebrooks B, Verstreken P, Zhou Y, Harding M, Bellen H, Mardon G (2004) Drosophila parkin mutants have decreased mass and cell size and increased sensitivity to oxygen radical stress. *Development* **131:** 2183-2194

Petit A, Kawarai T, Paitel E, Sanjo N, Maj M, Scheid M, Chen F, Gu Y, et al. (2005) Wild-type PINK1 prevents basal and induced neuronal apoptosis, a protective effect abrogated by Parkinson disease-related mutations. *J Biol Chem* **280:** 34025-34032

Pickart CM, Fushman D (2004) Polyubiquitin chains: polymeric protein signals. *Curr Opin Chem Biol* **8:** 610-616

Plun-Favreau H, Klupsch K, Moisoi N, Gandhi S, Kjaer S, Frith D, Harvey K, Deas E, Harvey RJ, McDonald N, Wood NW, Martins LM, Downward J (2007) The mitochondrial protease HtrA2 is regulated by Parkinson's disease-associated kinase PINK1. *Nature cell biology* **9:** 1243-1252

Polymeropoulos MH, Higgins JJ, Golbe LI, Johnson WG, Ide SE, Di Iorio G, Sanges G, Stenroos ES, Pho LT, Schaffer AA, Lazzarini AM, Nussbaum RL, Duvoisin RC (1996) Mapping of a gene for Parkinson's disease to chromosome 4q21-q23. *Science* **274:** 1197-1199

Polymeropoulos MH, Lavedan C, Leroy E, Ide SE, Dehejia A, Dutra A, Pike B, Root H, Rubenstein J, et al. (1997) Mutation in the alpha-synuclein gene identified in families with Parkinson's disease. *Science* **276:** 2045-2047

Poole AC, Thomas RE, Andrews LA, McBride HM, Whitworth AJ, Pallanck LJ (2008) The PINK1/Parkin pathway regulates mitochondrial morphology. *Proc Natl Acad Sci U S A* **105:** 1638-1643

Poole AC, Thomas RE, Yu S, Vincow ES, Pallanck L (2010) The mitochondrial fusion-promoting factor mitofusin is a substrate of the PINK1/parkin pathway. *PLoS One* **5:** e10054

Porstmann T, Santos CR, Griffiths B, Cully M, Wu M, Leevers S, Griffiths JR, Chung YL, Schulze A (2008) SREBP activity is regulated by mTORC1 and contributes to Akt-dependent cell growth. *Cell Metab* **8:** 224-236

Porstmann T, Santos CR, Lewis C, Griffiths B, Schulze A (2009) A new player in the orchestra of cell growth: SREBP activity is regulated by mTORC1 and contributes to the regulation of cell and organ size. *Biochem Soc Trans* **37:** 278-283

Pramstaller PP, Schlossmacher MG, Jacques TS, Scaravilli F, Eskelson C, Pepivani I, Hedrich K, Adel S, Gonzales-McNeal M, Hilker R, Kramer PL, Klein C (2005) Lewy body Parkinson's disease in a large pedigree with 77 Parkin mutation carriers. *Annals of neurology* **58:** 411-422

Prasad TS, Kandasamy K, Pandey A (2009) Human Protein Reference Database and Human Proteinpedia as discovery tools for systems biology. *Methods Mol Biol* **577:** 67-79

Pridgeon JW, Olzmann JA, Chin LS, Li L (2007) PINK1 protects against oxidative stress by phosphorylating mitochondrial chaperone TRAP1. *PLoS Biol* **5:** e172

Proukakis C, Dudzik CG, Brier T, MacKay DS, Cooper JM, Millhauser GL, Houlden H, Schapira AH (2013) A novel alpha-synuclein missense mutation in Parkinson disease. *Neurology* **80:** 1062-1064

Punga T, Bengoechea-Alonso MT, Ericsson J (2006) Phosphorylation and ubiquitination of the transcription factor sterol regulatory element-binding protein-1 in response to DNA binding. *The Journal of biological chemistry* **281:** 25278-25286

Rakovic A, Grunewald A, Kottwitz J, Bruggemann N, Pramstaller PP, Lohmann K, Klein C (2011) Mutations in PINK1 and Parkin impair ubiquitination of Mitofusins in human fibroblasts. *PLoS One* **6:** e16746

Ramirez A, Heimbach A, Grundemann J, Stiller B, Hampshire D, Cid LP, Goebel I, Mubaidin AF, Wriekat AL, Roeper J, Al-Din A, Hillmer AM, Karsak M, Liss B, Woods CG, Behrens MI, Kubisch C (2006) Hereditary parkinsonism with dementia is caused by mutations in ATP13A2, encoding a lysosomal type 5 P-type ATPase. *Nat Genet* **38:** 1184-1191

Rascol O, Lozano A, Stern M, Poewe W (2011) Milestones in Parkinson's disease therapeutics. *Mov Disord* **26:** 1072-1082

Rawson RB (2003) The SREBP pathway--insights from Insigs and insects. *Nat Rev Mol Cell Biol* **4:** 631-640

Rawson RB, Zelenski NG, Nijhawan D, Ye J, Sakai J, Hasan MT, Chang TY, Brown MS, Goldstein JL (1997) Complementation cloning of S2P, a gene encoding a putative metalloprotease required for intramembrane cleavage of SREBPs. *Mol Cell* **1:** 47-57

Reed BD, Charos AE, Szekely AM, Weissman SM, Snyder M (2008) Genome-wide occupancy of SREBP1 and its partners NFY and SP1 reveals novel functional roles and combinatorial regulation of distinct classes of genes. *PLoS Genet* **4:** e1000133

Reis K, Fransson A, Aspenstrom P (2009) The Miro GTPases: at the heart of the mitochondrial transport machinery. *FEBS letters* **583:** 1391-1398

Ren Y, Zhao J, Feng J (2003) Parkin binds to alpha/beta tubulin and increases their ubiquitination and degradation. *J Neurosci* **23:** 3316-3324

Rial E, Rodriguez-Sanchez L, Gallardo-Vara E, Zaragoza P, Moyano E, Gonzalez-Barroso MM (2010) Lipotoxicity, fatty acid uncoupling and mitochondrial carrier function. *Biochimica et biophysica acta* **1797:** 800-806

Richardson JR, Quan Y, Sherer TB, Greenamyre JT, Miller GW (2005) Paraquat neurotoxicity is distinct from that of MPTP and rotenone. *Toxicol Sci* **88:** 193-201

Ron D, Walter P (2007) Signal integration in the endoplasmic reticulum unfolded protein response. *Nat Rev Mol Cell Biol* **8:** 519-529

Rubin GM, Yandell MD, Wortman JR, Gabor Miklos GL, Nelson CR, Hariharan IK, Fortini ME, Li PW, Apweiler R, et al. (2000) Comparative genomics of the eukaryotes. *Science* **287:** 2204-2215

Sakai J, Duncan EA, Rawson RB, Hua X, Brown MS, Goldstein JL (1996) Sterol-regulated release of SREBP-2 from cell membranes requires two sequential cleavages, one within a transmembrane segment. *Cell* **85:** 1037-1046

Sakai J, Nohturfft A, Cheng D, Ho YK, Brown MS, Goldstein JL (1997) Identification of complexes between the COOH-terminal domains of sterol regulatory element-binding proteins (SREBPs) and SREBP cleavage-activating protein. *The Journal of biological chemistry* **272:** 20213-20221

Sakai J, Rawson RB, Espenshade PJ, Cheng D, Seegmiller AC, Goldstein JL, Brown MS (1998) Molecular identification of the sterol-regulated luminal protease that cleaves SREBPs and controls lipid composition of animal cells. *Mol Cell* **2:** 505-514

Sandoval H, Thiagarajan P, Dasgupta SK, Schumacher A, Prchal JT, Chen M, Wang J (2008) Essential role for Nix in autophagic maturation of erythroid cells. *Nature* **454:** 232-235

Sarraf SA, Raman M, Guarani-Pereira V, Sowa ME, Huttlin EL, Gygi SP, Harper JW (2013) Landscape of the PARKIN-dependent ubiquitylome in response to mitochondrial depolarization. *Nature* **496:** 372-376

Satake W, Nakabayashi Y, Mizuta I, Hirota Y, Ito C, Kubo M, Kawaguchi T, Tsunoda T, Watanabe M, et al. (2009) Genome-wide association study identifies common variants at four loci as genetic risk factors for Parkinson's disease. *Nat Genet* **41:** 1303-1307

Sato R, Inoue J, Kawabe Y, Kodama T, Takano T, Maeda M (1996) Sterol-dependent transcriptional regulation of sterol regulatory element-binding protein-2. *The Journal of biological chemistry* **271:** 26461-26464

Sato R, Yang J, Wang X, Evans MJ, Ho YK, Goldstein JL, Brown MS (1994) Assignment of the membrane attachment, DNA binding, and transcriptional activation domains of sterol regulatory element-binding protein-1 (SREBP-1). *The Journal of biological chemistry* **269:** 17267-17273

Scaduto RC, Jr., Grotyohann LW (1999) Measurement of mitochondrial membrane potential using fluorescent rhodamine derivatives. *Biophys J* **76:** 469-477

Schapira AH, Cooper JM, Dexter D, Clark JB, Jenner P, Marsden CD (1990) Mitochondrial complex I deficiency in Parkinson's disease. *J Neurochem* **54:** 823-827

Schneider I (1972) Cell lines derived from late embryonic stages of Drosophila melanogaster. *J Embryol Exp Morphol* **27:** 353-365

Schonthal AH (2012) Targeting endoplasmic reticulum stress for cancer therapy. *Front Biosci (Schol Ed)* **4:** 412-431

Schwarz TL (2013) Mitochondrial trafficking in neurons. *Cold Spring Harb Perspect Biol* **5**

Schweers RL, Zhang J, Randall MS, Loyd MR, Li W, Dorsey FC, Kundu M, Opferman JT, Cleveland JL, Miller JL, Ney PA (2007) NIX is required for programmed mitochondrial clearance during reticulocyte maturation. *Proceedings of the National Academy of Sciences of the United States of America* **104:** 19500-19505

Seegmiller AC, Dobrosotskaya I, Goldstein JL, Ho YK, Brown MS, Rawson RB (2002) The SREBP pathway in Drosophila: regulation by palmitate, not sterols. *Dev Cell* **2:** 229-238

Seo YK, Jeon TI, Chong HK, Biesinger J, Xie X, Osborne TF (2011) Genome-wide localization of SREBP-2 in hepatic chromatin predicts a role in autophagy. *Cell Metab* **13:** 367-375

Sharon R, Bar-Joseph I, Mirick GE, Serhan CN, Selkoe DJ (2003) Altered fatty acid composition of dopaminergic neurons expressing alpha-synuclein and human brains with alpha-synucleinopathies. *The Journal of biological chemistry* **278:** 49874-49881

Shiba-Fukushima K, Imai Y, Yoshida S, Ishihama Y, Kanao T, Sato S, Hattori N (2012) PINK1-mediated phosphorylation of the Parkin ubiquitin-like domain primes mitochondrial translocation of Parkin and regulates mitophagy. *Sci Rep* **2:** 1002

Shimano H (2001) Sterol regulatory element-binding proteins (SREBPs): transcriptional regulators of lipid synthetic genes. *Prog Lipid Res* **40:** 439-452

Shimomura I, Bashmakov Y, Ikemoto S, Horton JD, Brown MS, Goldstein JL (1999) Insulin selectively increases SREBP-1c mRNA in the livers of rats with streptozotocin-induced diabetes. *Proceedings of the National Academy of Sciences of the United States of America* **96:** 13656-13661

Shimura H, Hattori N, Kubo S, Mizuno Y, Asakawa S, Minoshima S, Shimizu N, Iwai K, Chiba T, Tanaka K, Suzuki T (2000) Familial Parkinson disease gene product, parkin, is a ubiquitin-protein ligase. *Nat Genet* **25:** 302-305

Shimura H, Schlossmacher MG, Hattori N, Frosch MP, Trockenbacher A, Schneider R, Mizuno Y, Kosik KS, Selkoe DJ (2001) Ubiquitination of a new form of alpha-synuclein by parkin from human brain: implications for Parkinson's disease. *Science* **293:** 263-269

Shin ES, Lee HH, Cho SY, Park HW, Lee SJ, Lee TR (2007) Genistein downregulates SREBP-1 regulated gene expression by inhibiting site-1 protease expression in HepG2 cells. *J Nutr* **137:** 1127-1131

Shin JH, Ko HS, Kang H, Lee Y, Lee YI, Pletinkova O, Troconso JC, Dawson VL, Dawson TM (2011) PARIS (ZNF746) repression of PGC-1alpha contributes to neurodegeneration in Parkinson's disease. *Cell* **144:** 689-702

Sidransky E, Lopez G (2012) The link between the GBA gene and parkinsonism. *Lancet Neurol* **11:** 986-998

Sidransky E, Nalls MA, Aasly JO, Aharon-Peretz J, Annesi G, Barbosa ER, Bar-Shira A, Berg D, Bras J, Brice A, Chen CM, et al. (2009) Multicenter analysis of glucocerebrosidase mutations in Parkinson's disease. *N Engl J Med* **361:** 1651-1661

Silvestri L, Caputo V, Bellacchio E, Atorino L, Dallapiccola B, Valente EM, Casari G (2005) Mitochondrial import and enzymatic activity of PINK1 mutants associated to recessive parkinsonism. *Hum Mol Genet* **14:** 3477-3492

Sim CH, Lio DS, Mok SS, Masters CL, Hill AF, Culvenor JG, Cheng HC (2006) C-terminal truncation and Parkinson's disease-associated mutations down-regulate the protein serine/threonine kinase activity of PTEN-induced kinase-1. *Human molecular genetics* **15:** 3251-3262

Simon-Sanchez J, Schulte C, Bras JM, Sharma M, Gibbs JR, Berg D, Paisan-Ruiz C, Lichtner P, Scholz SW, et al. (2009) Genome-wide association study reveals genetic risk underlying Parkinson's disease. *Nat Genet* **41:** 1308-1312

Simon-Sanchez J, Singleton AB (2008) Sequencing analysis of OMI/HTRA2 shows previously reported pathogenic mutations in neurologically normal controls. *Human molecular genetics* **17:** 1988-1993

Singleton AB, Farrer M, Johnson J, Singleton A, Hague S, Kachergus J, Hulihan M, Peuralinna T, Dutra A, Nussbaum R, Lincoln S, Crawley A, Hanson M, Maraganore D, Adler C, Cookson MR, Muenter M, Baptista M, Miller D, Blancato J, Hardy J, Gwinn-Hardy K (2003) alpha-Synuclein locus triplication causes Parkinson's disease. *Science* **302:** 841

Siskind LJ (2005) Mitochondrial ceramide and the induction of apoptosis. *Journal of bioenergetics and biomembranes* **37:** 143-153

Smith BK, Jain SS, Rimbaud S, Dam A, Quadrilatero J, Ventura-Clapier R, Bonen A, Holloway GP (2011) FAT/CD36 is located on the outer mitochondrial membrane, upstream of long-chain acyl-CoA synthetase, and regulates palmitate oxidation. *Biochem J* **437:** 125-134

Soubannier V, McLelland GL, Zunino R, Braschi E, Rippstein P, Fon EA, McBride HM (2012) A vesicular transport pathway shuttles cargo from mitochondria to lysosomes. *Current biology : CB* **22:** 135-141

Spillantini MG, Schmidt ML, Lee VM, Trojanowski JQ, Jakes R, Goedert M (1997) Alpha-synuclein in Lewy bodies. *Nature* **388:** 839-840

Sriram SM, Kim BY, Kwon YT (2011) The N-end rule pathway: emerging functions and molecular principles of substrate recognition. *Nat Rev Mol Cell Biol* **12:** 735-747

Stark C, Breitkreutz BJ, Reguly T, Boucher L, Breitkreutz A, Tyers M (2006) BioGRID: a general repository for interaction datasets. *Nucleic Acids Res* **34:** D535-539

Staropoli JF, McDermott C, Martinat C, Schulman B, Demireva E, Abeliovich A (2003) Parkin is a component of an SCF-like ubiquitin ligase complex and protects postmitotic neurons from kainate excitotoxicity. *Neuron* **37:** 735-749

Stowers RS, Megeath LJ, Gorska-Andrzejak J, Meinertzhagen IA, Schwarz TL (2002) Axonal transport of mitochondria to synapses depends on milton, a novel Drosophila protein. *Neuron* **36:** 1063-1077

Strauss KM, Martins LM, Plun-Favreau H, Marx FP, Kautzmann S, Berg D, Gasser T, Wszolek Z, Muller T, Bornemann A, Wolburg H, Downward J, Riess O, Schulz JB, Kruger R (2005) Loss of function mutations in the gene encoding Omi/HtrA2 in Parkinson's disease. *Hum Mol Genet* **14:** 2099-2111

Sulzer D (2007) Multiple hit hypotheses for dopamine neuron loss in Parkinson's disease. *Trends in neurosciences* **30:** 244-250

Sulzer D, Zecca L (2000) Intraneuronal dopamine-quinone synthesis: a review. *Neurotox Res* **1:** 181-195

Sun LP, Seemann J, Goldstein JL, Brown MS (2007) Sterol-regulated transport of SREBPs from endoplasmic reticulum to Golgi: Insig renders sorting signal in Scap inaccessible to COPII proteins. *Proceedings of the National Academy of Sciences of the United States of America* **104:** 6519-6526

Sundqvist A, Bengoechea-Alonso MT, Ye X, Lukiyanchuk V, Jin J, Harper JW, Ericsson J (2005) Control of lipid metabolism by phosphorylation-dependent degradation of the SREBP family of transcription factors by SCF(Fbw7). *Cell Metab* **1:** 379-391

Surmeier DJ, Guzman JN, Sanchez-Padilla J (2010) Calcium, cellular aging, and selective neuronal vulnerability in Parkinson's disease. *Cell Calcium* **47:** 175-182

Sutoo D, Akiyama K, Geffard M (1989) Central dopamine-synthesis regulation by the calcium-calmodulin-dependent system. *Brain Res Bull* **22:** 565-569

Suzuki Y, Imai Y, Nakayama H, Takahashi K, Takio K, Takahashi R (2001) A serine protease, HtrA2, is released from the mitochondria and interacts with XIAP, inducing cell death. *Mol Cell* **8:** 613-621

Taira T, Saito Y, Niki T, Iguchi-Ariga SM, Takahashi K, Ariga H (2004) DJ-1 has a role in antioxidative stress to prevent cell death. *EMBO Rep* **5:** 213-218

Takahashi H, Ohama E, Suzuki S, Horikawa Y, Ishikawa A, Morita T, Tsuji S, Ikuta F (1994) Familial juvenile parkinsonism: clinical and pathologic study in a family. *Neurology* **44:** 437-441

Tan EK, Chai A, Teo YY, Zhao Y, Tan C, Shen H, Chandran VR, Teoh ML, Yih Y, Pavanni R, Wong MC, Puvan K, Lo YL, Yap E (2004) Alpha-synuclein haplotypes implicated in risk of Parkinson's disease. *Neurology* **62:** 128-131

Tanaka A, Cleland MM, Xu S, Narendra DP, Suen DF, Karbowski M, Youle RJ (2010) Proteasome and p97 mediate mitophagy and degradation of mitofusins induced by Parkin. *The Journal of cell biology* **191:** 1367-1380

Tanaka Y, Kanai Y, Okada Y, Nonaka S, Takeda S, Harada A, Hirokawa N (1998) Targeted disruption of mouse conventional kinesin heavy chain, kif5B, results in abnormal perinuclear clustering of mitochondria. *Cell* **93:** 1147-1158

Tang B, Xiong H, Sun P, Zhang Y, Wang D, Hu Z, Zhu Z, Ma H, Pan Q, Xia JH, Xia K, Zhang Z (2006) Association of PINK1 and DJ-1 confers digenic inheritance of early-onset Parkinson's disease. *Human molecular genetics* **15:** 1816-1825

Tanida I (2011) Autophagy basics. *Microbiol Immunol* **55:** 1-11

Tanida I, Ueno T, Kominami E (2004) LC3 conjugation system in mammalian autophagy. *The international journal of biochemistry & cell biology* **36:** 2503-2518

Tanner CM, Kamel F, Ross GW, Hoppin JA, Goldman SM, Korell M, Marras C, Bhudhikanok GS, et al. (2011) Rotenone, paraquat, and Parkinson's disease. *Environ Health Perspect* **119:** 866-872

Tayebi N, Walker J, Stubblefield B, Orvisky E, LaMarca ME, Wong K, Rosenbaum H, Schiffmann R, Bembi B, Sidransky E (2003) Gaucher disease with parkinsonian manifestations: does glucocerebrosidase deficiency contribute to a vulnerability to parkinsonism? *Mol Genet Metab* **79:** 104-109

Thiruchelvam M, McCormack A, Richfield EK, Baggs RB, Tank AW, Di Monte DA, Cory-Slechta DA (2003) Age-related irreversible progressive nigrostriatal dopaminergic neurotoxicity in the paraquat and maneb model of the Parkinson's disease phenotype. *Eur J Neurosci* **18:** 589-600

Thomas B, Beal MF (2007) Parkinson's disease. *Human molecular genetics* **16 Spec No. 2:** R183-194

Tooze SA, Yoshimori T (2010) The origin of the autophagosomal membrane. *Nature cell biology* **12:** 831-835

Trempe JF, Fon EA (2013) Structure and Function of Parkin, PINK1, and DJ-1, the Three Musketeers of Neuroprotection. *Front Neurol* **4:** 38

Trempe JF, Sauve V, Grenier K, Seirafi M, Tang MY, Menade M, Al-Abdul-Wahid S, Krett J, Wong K, Kozlov G, Nagar B, Fon EA, Gehring K (2013) Structure of parkin reveals mechanisms for ubiquitin ligase activation. *Science* **340:** 1451-1455

Troiano AR, Cazeneuve C, Le Ber I, Bonnet AM, Lesage S, Brice A (2008) Re: Alpha-synuclein gene duplication is present in sporadic Parkinson disease. *Neurology* **71:** 1295; author reply 1295

Tsai YC, Fishman PS, Thakor NV, Oyler GA (2003) Parkin facilitates the elimination of expanded polyglutamine proteins and leads to preservation of proteasome function. *J Biol Chem* **278:** 22044-22055

Twig G, Elorza A, Molina AJ, Mohamed H, Wikstrom JD, Walzer G, Stiles L, Haigh SE, Katz S, Las G, Alroy J, Wu M, Py BF, Yuan J, Deeney JT, Corkey BE, Shirihai OS (2008a) Fission and selective fusion govern mitochondrial segregation and elimination by autophagy. *Embo J* **27:** 433-446

Twig G, Hyde B, Shirihai OS (2008b) Mitochondrial fusion, fission and autophagy as a quality control axis: the bioenergetic view. *Biochim Biophys Acta* **1777:** 1092-1097

Um JW, Min DS, Rhim H, Kim J, Paik SR, Chung KC (2006) Parkin ubiquitinates and promotes the degradation of RanBP2. *J Biol Chem* **281:** 3595-3603

UniProt C (2013) Update on activities at the Universal Protein Resource (UniProt) in 2013. *Nucleic Acids Res* **41:** D43-47

Unoki M, Nakamura Y (2001) Growth-suppressive effects of BPOZ and EGR2, two genes involved in the PTEN signaling pathway. *Oncogene* **20:** 4457-4465

Valente EM, Abou-Sleiman PM, Caputo V, Muqit MM, Harvey K, Gispert S, Ali Z, Del Turco D, Bentivoglio AR, et al. (2004a) Hereditary early-onset Parkinson's disease caused by mutations in PINK1. *Science* **304:** 1158-1160

Valente EM, Bentivoglio AR, Dixon PH, Ferraris A, Ialongo T, Frontali M, Albanese A, Wood NW (2001) Localization of a novel locus for autosomal recessive early-onset parkinsonism, PARK6, on human chromosome 1p35-p36. *Am J Hum Genet* **68:** 895-900

Valente EM, Salvi S, Ialongo T, Marongiu R, Elia AE, Caputo V, Romito L, Albanese A, Dallapiccola B, Bentivoglio AR (2004b) PINK1 mutations are associated with sporadic early-onset parkinsonism. *Annals of neurology* **56:** 336-341

Vamecq J, Dessein AF, Fontaine M, Briand G, Porchet N, Latruffe N, Andreolotti P, Cherkaoui-Malki M (2012) Mitochondrial dysfunction and lipid homeostasis. *Curr Drug Metab* **13:** 1388-1400

Van Den Eeden SK, Tanner CM, Bernstein AL, Fross RD, Leimpeter A, Bloch DA, Nelson LM (2003) Incidence of Parkinson's disease: variation by age, gender, and race/ethnicity. *Am J Epidemiol* **157:** 1015-1022

van Duijn CM, Dekker MC, Bonifati V, Galjaard RJ, Houwing-Duistermaat JJ, Snijders PJ, Testers L, Breedveld GJ, Horstink M, Sandkuijl LA, van Swieten JC, Oostra BA, Heutink P (2001) Park7, a novel locus for autosomal recessive early-onset parkinsonism, on chromosome 1p36. *American journal of human genetics* **69:** 629-634

Van Laar VS, Arnold B, Cassady SJ, Chu CT, Burton EA, Berman SB (2011) Bioenergetics of neurons inhibit the translocation response of Parkin following rapid mitochondrial depolarization. *Human molecular genetics* **20:** 927-940

van Meer G, de Kroon AIPM (2011) Lipid map of the mammalian cell. *Journal of Cell Science* **124:** 5-8

van Spronsen M, Mikhaylova M, Lipka J, Schlager MA, van den Heuvel DJ, Kuijpers M, Wulf PS, et al. (2013) TRAK/Milton motor-adaptor proteins steer mitochondrial trafficking to axons and dendrites. *Neuron* **77:** 485-502

Vilarino-Guell C, Wider C, Ross OA, Dachsel JC, Kachergus JM, Lincoln SJ, Soto-Ortolaza AI, Cobb SA, Wilhoite GJ, Bacon JA, et al. (2011) VPS35 mutations in Parkinson disease. *Am J Hum Genet* **89:** 162-167

Vincow ES, Merrihew G, Thomas RE, Shulman NJ, Beyer RP, MacCoss MJ, Pallanck LJ (2013) The PINK1-Parkin pathway promotes both mitophagy and selective respiratory chain turnover in vivo. *Proceedings of the National Academy of Sciences of the United States of America* **110:** 6400-6405

Vives-Bauza C, Zhou C, Huang Y, Cui M, de Vries RL, Kim J, May J, Tocilescu MA, Liu W, Ko HS, Magrane J, Moore DJ, Dawson VL, Grailhe R, Dawson TM, Li C, Tieu K, Przedborski S (2010) PINK1-dependent recruitment of Parkin to mitochondria in mitophagy. *Proceedings of the National Academy of Sciences of the United States of America* **107:** 378-383

Volles MJ, Lansbury PT, Jr. (2002) Vesicle permeabilization by protofibrillar alpha-synuclein is sensitive to Parkinson's disease-linked mutations and occurs by a pore-like mechanism. *Biochemistry* **41:** 4595-4602

Volles MJ, Lansbury PT, Jr. (2003) Zeroing in on the pathogenic form of alpha-synuclein and its mechanism of neurotoxicity in Parkinson's disease. *Biochemistry* **42:** 7871-7878

Volpicelli-Daley LA, Luk KC, Patel TP, Tanik SA, Riddle DM, Stieber A, Meaney DF, Trojanowski JQ, Lee VM (2011) Exogenous alpha-synuclein fibrils induce Lewy body pathology leading to synaptic dysfunction and neuron death. *Neuron* **72:** 57-71

Walden H, Martinez-Torres RJ (2012) Regulation of Parkin E3 ubiquitin ligase activity. *Cell Mol Life Sci* **69:** 3053-3067

Wang X, Briggs MR, Hua X, Yokoyama C, Goldstein JL, Brown MS (1993) Nuclear protein that binds sterol regulatory element of low density lipoprotein receptor promoter. II. Purification and characterization. *The Journal of biological chemistry* **268:** 14497-14504

Wang X, Sato R, Brown MS, Hua X, Goldstein JL (1994) SREBP-1, a membrane-bound transcription factor released by sterol-regulated proteolysis. *Cell* **77:** 53-62

Wang X, Schwarz TL (2009) The mechanism of Ca2+ -dependent regulation of kinesin-mediated mitochondrial motility. *Cell* **136:** 163-174

Wang X, Winter D, Ashrafi G, Schlehe J, Wong YL, Selkoe D, Rice S, Steen J, LaVoie MJ, Schwarz TL (2011) PINK1 and Parkin target Miro for phosphorylation and degradation to arrest mitochondrial motility. *Cell* **147:** 893-906

Waterham HR, Koster J, van Roermund CW, Mooyer PA, Wanders RJ, Leonard JV (2007) A lethal defect of mitochondrial and peroxisomal fission. *N Engl J Med* **356:** 1736-1741

Weihofen A, Thomas KJ, Ostaszewski BL, Cookson MR, Selkoe DJ (2009) Pink1 forms a multiprotein complex with Miro and Milton, linking Pink1 function to mitochondrial trafficking. *Biochemistry* **48:** 2045-2052

Wenzel DM, Lissounov A, Brzovic PS, Klevit RE (2011) UBCH7 reactivity profile reveals parkin and HHARI to be RING/HECT hybrids. *Nature* **474:** 105-108

West A, Periquet M, Lincoln S, Lucking CB, Nicholl D, Bonifati V, Rawal N, Gasser T, Lohmann E, Deleuze JF, Maraganore D, Levey A, Wood N, Durr A, Hardy J, Brice A, Farrer M (2002) Complex relationship between Parkin mutations and Parkinson disease. *Am J Med Genet* **114:** 584-591

Westermann B (2010) Mitochondrial fusion and fission in cell life and death. *Nat Rev Mol Cell Biol* **11:** 872-884

Whitworth AJ, Lee JR, Ho VM, Flick R, Chowdhury R, McQuibban GA (2008) Rhomboid-7 and HtrA2/Omi act in a common pathway with the Parkinson's disease factors Pink1 and Parkin. *Dis Model Mech* **1:** 168-174; discussion 173

Whitworth AJ, Theodore DA, Greene JC, Benes H, Wes PD, Pallanck LJ (2005) Increased glutathione S-transferase activity rescues dopaminergic neuron loss in a Drosophila model of Parkinson's disease. *Proceedings of the National Academy of Sciences of the United States of America* **102:** 8024-8029

Wood-Kaczmar A, Gandhi S, Yao Z, Abramov AY, Miljan EA, Keen G, Stanyer L, Hargreaves I, Klupsch K, Deas E, et al. (2008) PINK1 is necessary for long term survival and mitochondrial function in human dopaminergic neurons. *PLoS One* **3:** e2455

Xiong Y, Dawson VL, Dawson TM (2012) LRRK2 GTPase dysfunction in the pathogenesis of Parkinson's disease. *Biochem Soc Trans* **40:** 1074-1079

Yabe D, Brown MS, Goldstein JL (2002) Insig-2, a second endoplasmic reticulum protein that binds SCAP and blocks export of sterol regulatory element-binding proteins. *Proceedings of the National Academy of Sciences of the United States of America* **99:** 12753-12758

Yamano K, Youle RJ (2013) PINK1 is degraded through the N-end rule pathway. *Autophagy* **9**

Yanagawa S, Lee JS, Ishimoto A (1998) Identification and characterization of a novel line of Drosophila Schneider S2 cells that respond to wingless signaling. *J Biol Chem* **273:** 32353-32359

Yang F, Vought BW, Satterlee JS, Walker AK, Jim Sun ZY, Watts JL, DeBeaumont R, Saito RM, Hyberts SG, Yang S, Macol C, Iyer L, Tjian R, van den Heuvel S, Hart AC, Wagner G, Naar AM (2006a) An ARC/Mediator subunit required for SREBP control of cholesterol and lipid homeostasis. *Nature* **442:** 700-704

Yang T, Espenshade PJ, Wright ME, Yabe D, Gong Y, Aebersold R, Goldstein JL, Brown MS (2002) Crucial step in cholesterol homeostasis: sterols promote binding of SCAP to INSIG-1, a membrane protein that facilitates retention of SREBPs in ER. *Cell* **110:** 489-500

Yang Y, Gehrke S, Imai Y, Huang Z, Ouyang Y, Wang JW, Yang L, Beal MF, Vogel H, Lu B (2006b) Mitochondrial pathology and muscle and dopaminergic neuron degeneration caused by inactivation of Drosophila Pink1 is rescued by Parkin. *Proceedings of the National Academy of Sciences of the United States of America* **103:** 10793-10798

Yang Y, Nishimura I, Imai Y, Takahashi R, Lu B (2003) Parkin suppresses dopaminergic neuron-selective neurotoxicity induced by Pael-R in Drosophila. *Neuron* **37:** 911-924

Yang Y, Ouyang Y, Yang L, Beal MF, McQuibban A, Vogel H, Lu B (2008) Pink1 regulates mitochondrial dynamics through interaction with the fission/fusion machinery. *Proc Natl Acad Sci U S A* **105:** 7070-7075

Yin JJ, Li YB, Wang Y, Liu GD, Wang J, Zhu XO, Pan SH (2012) The role of autophagy in endoplasmic reticulum stress-induced pancreatic beta cell death. *Autophagy* **8:** 158-164

Youle RJ, van der Bliek AM (2012) Mitochondrial fission, fusion, and stress. *Science* **337:** 1062-1065

Yu W, Sun Y, Guo S, Lu B (2011) The PINK1/Parkin pathway regulates mitochondrial dynamics and function in mammalian hippocampal and dopaminergic neurons. *Human molecular genetics* **20:** 3227-3240

Zhang Y, Gao J, Chung KK, Huang H, Dawson VL, Dawson TM (2000) Parkin functions as an E2-dependent ubiquitin- protein ligase and promotes the degradation of the synaptic vesicle-associated protein, CDCrel-1. *Proceedings of the National Academy of Sciences of the United States of America* **97:** 13354-13359

Zhou C, Huang Y, Shao Y, May J, Prou D, Perier C, Dauer W, Schon EA, Przedborski S (2008) The kinase domain of mitochondrial PINK1 faces the cytoplasm. *Proc Natl Acad Sci U S A* **105:** 12022-12027

Zimprich A, Benet-Pages A, Struhal W, Graf E, Eck SH, Offman MN, Haubenberger D, Spielberger S, Schulte EC, et al. (2011) A mutation in VPS35, encoding a subunit of the retromer complex, causes late-onset Parkinson disease. *Am J Hum Genet* **89:** 168-175

Zimprich A, Biskup S, Leitner P, Lichtner P, Farrer M, Lincoln S, Kachergus J, Hulihan M, Uitti RJ, Calne DB, Stoessl AJ, Pfeiffer RF, Patenge N, Carbajal IC, Vieregge P, Asmus F, Muller-Myhsok B, Dickson DW, Meitinger T, Strom TM, Wszolek ZK, Gasser T (2004) Mutations in

LRRK2 cause autosomal-dominant parkinsonism with pleomorphic pathology. *Neuron* **44:** 601-607

Ziviani E, Tao RN, Whitworth AJ (2010) Drosophila parkin requires PINK1 for mitochondrial translocation and ubiquitinates mitofusin. *Proceedings of the National Academy of Sciences of the United States of America* **107:** 5018-5023

Ziviani E, Whitworth AJ (2010) How could Parkin-mediated ubiquitination of mitofusin promote mitophagy? *Autophagy* **6:** 660-662

Zuchner S, Mersiyanova IV, Muglia M, Bissar-Tadmouri N, Rochelle J, Dadali EL, Zappia M, Nelis E, Patitucci A, Senderek J, Parman Y, Evgrafov O, Jonghe PD, Takahashi Y, Tsuji S, Pericak-Vance MA, Quattrone A, Battaloglu E, Polyakov AV, Timmerman V, Schroder JM, Vance JM (2004) Mutations in the mitochondrial GTPase mitofusin 2 cause Charcot-Marie-Tooth neuropathy type 2A. *Nat Genet* **36:** 449-451

9. APPENDIX

9.1 ASSESSING siRNA SILENCING

In order to understand the relationship between SREBP- and PINK1/Parkin-pathways, both cellular and *in vivo* approaches were utilised. From a cellular point of view, the main tool at our disposal was the transient silencing of pathway genes using siRNA. In Chapter 6, low-throughout analysis of screen hits utilised HeLa and YFP-Parkin.HeLa cell lines in combination with *PINK1*, *parkin*, *FBXW7* and *SREBF1* siRNAs. To assess the efficiency of gene silencing qRT-PCR methods were employed (Figure 9.1). These data demonstrate the efficient knockdown of all genes tested in both HeLa cells (Figure 9.1 A-D), and YFP-Parkin.HeLa cells (Figure 9.1 E-H). Importantly, in agreement with published data, HeLa cells lack detectable levels of endogenous *parkin* (Figure 9.1 B), hence the requirement for Parkin overexpression when utilising these cells in pathway analysis (Denison et al, 2003).

9.2 PARKIN TRANSLOCATION RESCUE WITH LIPIDS

As outlined in section 6.3.6, Parkin translocation following *SREBF1* siRNA treatment could be rescued by the addition of exogenous cholesterol and/or fatty acids. Here, Figure 9.2 represents accompanying control data, demonstrating an absence of effect on Parkin translocation following the application of fatty acids and cholesterol in non-toxified control and *SREBF1* siRNA samples (Figure 9.2 A). These data confirm that cholesterol and fatty acids are unable to trigger Parkin translocation in the absence of CCCP, suggesting a lack of general toxicity conferred by their presence. Additionally, there was an absence of effect following fatty acid and/or cholesterol application in CCCP-treated control siRNA samples (Figure 9.2 B). Together, these control assays suggest that the observed rescue of Parkin translocation in *SREBF1*-silenced cells following CCCP (Figure 6.11) is specific to the reinstatement of *SREBF1* pathway products, and not due to general cellular or mitochondrial toxicity.

9.3 SREBP1 (2A4) ANTIBODY ANALYSIS

The SREBP-pathway has been studied in great detail since its discovery in 1993 (Briggs et al, 1993; Wang et al, 1993). As a consequence, many antibodies for SREBP protein analysis are available. One of the most widely used SREBP1 antibodies originates from the lab of Goldstein and Brown, raised against an epitope known as

2A4 (Figure 9.3 A, Sato et al, 1994). This epitope is available from a number of different companies, and recognises both flSREBP1a and c, and mSREBP1a and c. In order to test the specificity of the antibody, YFP-Parkin.HeLa cells were treated with either control or *SREBF1* siRNA. Under control conditions, only flSREBP1 was visible, forming a band at ~125 kDa (Figure 9.3 B). Following *SREBF1* siRNA treatment, this high molecular weight band greatly reduced in strength, indicating that the antibody specifically recognised flSREBP1. To ascertain why the activated mSREBP1 form was not visible, cells were treated with control siRNA plus the proteasomal inhibitor MG-132 (Figure 9.3 C). Here, as nuclear mSREBP1 is known to be rapidly turned over by the proteasome, a block at this level should reveal a lower molecular weight band of ~68 kDa. Indeed, a relatively faint band of this weight was now visible, demonstrating that prior experiments probably failed to detect mSREBP1 due to its instability. Another way to inhibit mSREBP1 turnover was to silence *FBXW7* – a SCF-complex protein involved in its turnover in the nucleus (Figure 9.3 D). Once again, a lower molecular weight band of ~68 kDa was visible, albeit at even lower levels than that observed with MG-132 treatment. This may have been due to incomplete silencing of *FBXW7*, as qRT-PCR data suggests that *FBXW7* knockdown reduces expression to ~30% (Figure 9.1 H), indicating residual FBXW7 activity within the cell.

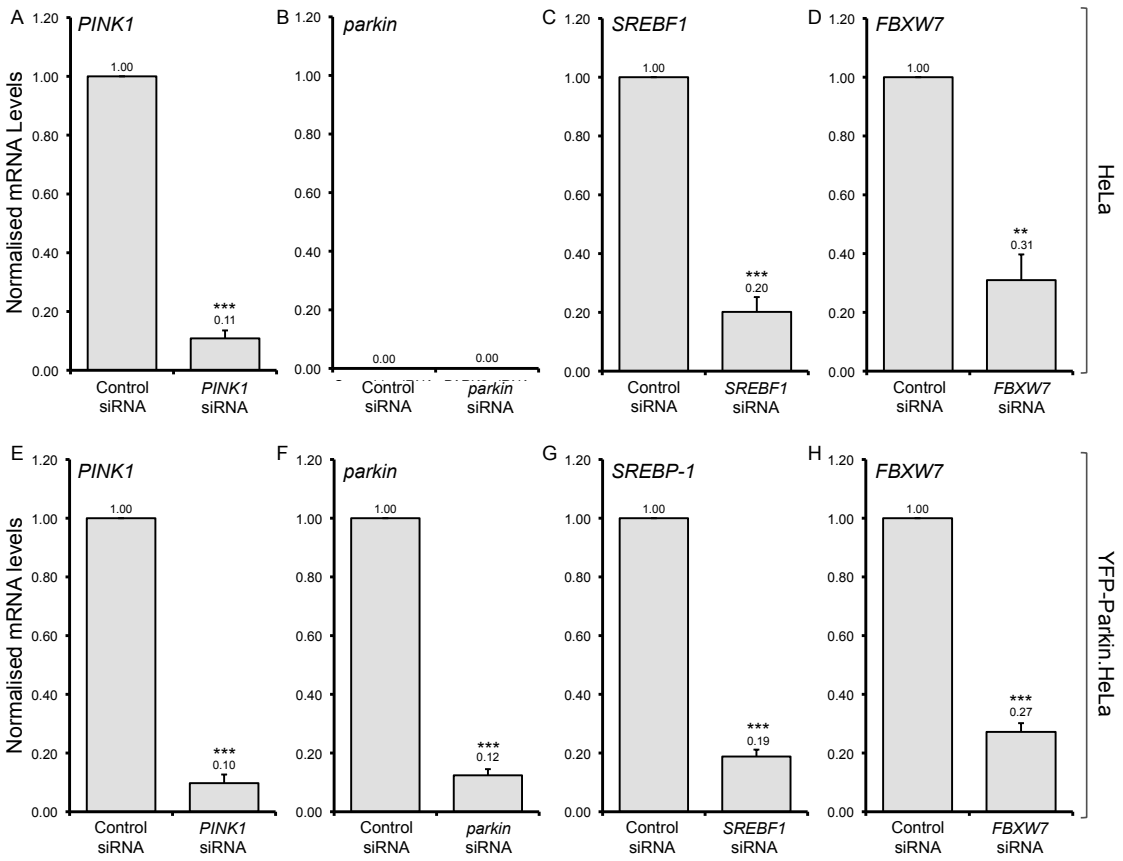

Figure 9.1 qRT-PCR analysis of gene expression following siRNA treatment. HeLa cells (A - D) or YFP-Parkin.HeLa cells (E-H) were exposed to 25 nM of control (A - H), *PINK1* (A & E), *parkin* (B & F), *FBXW7* (C & G) or *SREBF1* (D & H) siRNA for 4 days. Gene expression levels were analysed using qRT-PCR against the housekeeping gene RNA18S5. Graphs represent the mean of 3 biological repeats. Error bars represent the standard deviation. **P<0.01, ***P<0.0001 (Student's T-test).

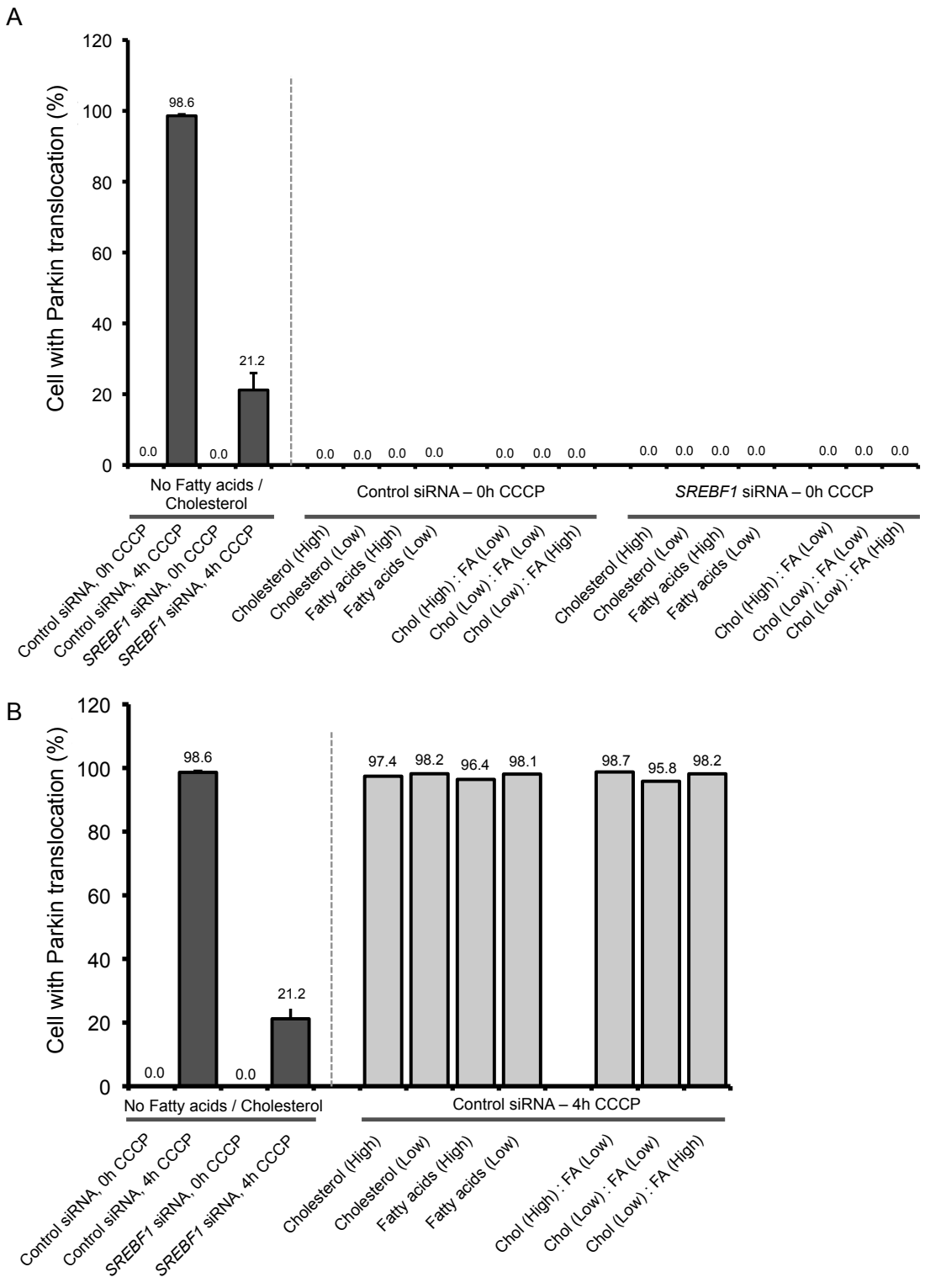

Figure 9.2 Parkin translocation with fatty acids and cholesterol – controls analysis. Assay performed as in Figure 6.12. (A) Graphical representation of Parkin translocation following control or *SREBF1* siRNA application in the absence of CCCP. (B) Graphical representation of Parkin translocation following control siRNA application after CCCP toxification for 4 hours. Data represent 1 biological repeat with 5 FOV per condition. FA - fatty acids; Chol – cholesterol. High – high concentration; Low – low concentration.

A

Protein sequence – SREBP1a

MDEPPFSEAALEQALGEPCDLDAALLTDIEDMLQLINNQDSDFPGLFDPPYAGSGA
GGTDPASPDTSSPGSLSPPPATLSSSLEAFLSGPQAAPSPLSPPQPAPTPLKMYPS
MPAFSPGPGIKEESVPLSILQTPTPQPLPGALLPQSFPAPAPPQFSSTPVLGYPSPP
GGFSTGSPPGNTQQPLPGLPLASPPGVPPVSLHTQVQSVVPQQLLTVTAAPTAAP
VTTTVTSQIQQVPVLLQPHFIKADSLLLTAMKTDGATVKAAGLSPLVSGTTVQTGPL
PTLVSGGTILATVPLVVDAEKLPINRLAAGSKAPASAQSRGEKRTAHNAIEKRYRSSI
NDKIIELKDLVVGTEAKLNKSAVLRKAIDYIRFLQHSNQKLKQENLSLRTAVHKSKSL
KDLVSACGSGGNTDVLMEGVKTEVEDTLTPPPSDAGSPFQSSPLSLGSRGSGSGG
SGSDSEPDSPVFEDSKAKPEQRPSLHSRGMLDRSRLALCTLVFLCLSCNPLASLLG
ARGLPSPSDTTSVYHSPGRNVLGTESRDGPGWAQWLLPPVVWLLNGLLVLVSLVL
LFVYGEPVTRPHSGPAVYFWRHRKQADLDLARGDFAQAAQQLWLALRALGRPLPT
SHLDLACSLLWNLIRHLLQRLWVGRWLAGRAGGLQQDCALRVDASASARDAALVY
HKLHQLHTMGKHTGGHLTATNLALSALNLAECAGDAVSVATLAEIYVAAALRVKTSL
PRALHFLTRFFLSSARQACLAQSGSVPPAMQWLCHPVGHRFFVDGDWSVLSTPW
ESLYSLAGNPVDPLAQVTQLFREHLLERALNCVTQPNPSPGSADGDKEFSDALGYL
QLLNSCSDAAGAPAYSFSISSSMATTTGVDPVAKWWASLTAVVIHWLRRDEEAAER
LCPLVEHLPRVLQESERPLPRAALHSFKAARALLGCAKAESGPASLTICEKASGYLQ
DSLATTPASSSIDKAVQLFLCDLLLVVRTSLWRQQQPPAPAPAAQGTSSRPQASAL
ELRGFQRDLSSLRRLAQSFRPAMRRVFLHEATARLMAGASPTRTHQLLDRSLRRR
AGPGGKGGAVAELEPRPTRREHAEALLLASCYLPPGFLSAPGQRVGMLAEAARTL
EKLGDRRLLHDCQQMLMRLGGGTTVTSS

flSREBP1 (125 kDa)
mSREBP1 (68 kDa)
SREBP1 (2A4) antibody epitope

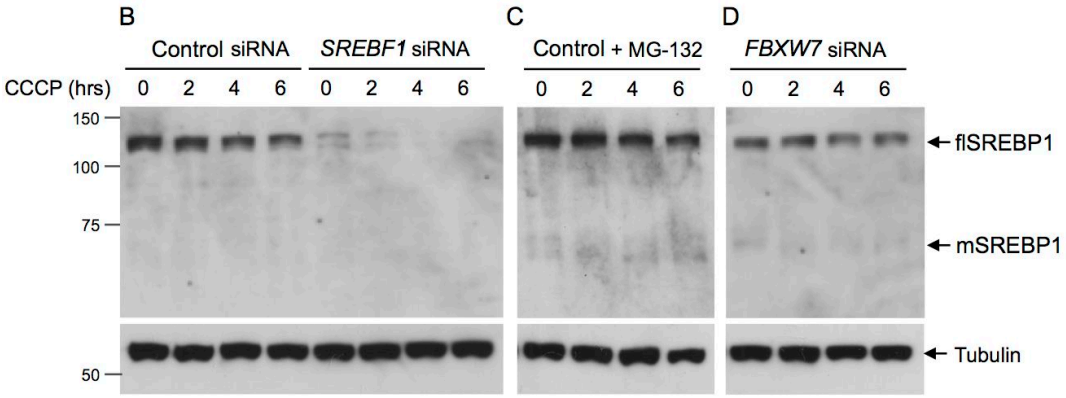

Figure 9.3 SREBP1 (2A4) antibody analysis. (A) Protein sequence of SREBP1a, with flSREBP1 (whole sequence including black, green and red), mSREBP1c (green and red) and the SREBP1 (2A4) epitope (red) highlighted. The SREBP1 (2A4) epitope also recognises flSREBP1c, and mSREBP1c (data not shown). (B) Western blot analysis of SREBP1 protein levels in YFP-Parkin.HeLa cell samples exposed to control or *SREBF1* siRNA, and 10 μM CCCP for 0 - 6 hours. In this assay, SREBP1 is visualised using the SREBP1 (2A4) antibody in (A) from Santa Cruz. (C) Analysis of SREBP1 protein levels in the presence of the proteasome inhibitor MG-132 (25 μM). (D) Analysis of SREBP1 protein levels in the presence of *FBXW7* siRNA. (B – D) loading control – tubulin.